

## General Aviation Propulsion

**G3/07**

**NASA**





**NASA Conference Publication 2126**

# **General Aviation Propulsion**

Proceedings of a conference held at  
NASA Lewis Research Center  
Cleveland, Ohio  
November 28-29, 1979



National Aeronautics  
and Space Administration

**Scientific and Technical  
Information Branch**

1980



## **FOREWORD**

The National Aeronautics and Space Administration is actively involved in the quest for improved general aviation aircraft. Programs exploring and demonstrating new technologies in general aviation propulsion are being conducted at the Lewis Research Center and by industrial contractors and university grantees. These programs are the Quiet, Clean, General Aviation Turbofan (QCGAT) program; the General Aviation Turbine Engine (GATE) study program; the general aviation propeller technology program; and the advanced rotary, diesel, and reciprocating engine programs. A two-day conference was held in November of 1979 to provide representatives from government, industry, and universities with the latest findings of these programs. This publication contains all the papers presented at that conference.

Gilbert K. Sievers  
NASA Lewis Research Center  
Conference chairman

**PRECEDING PAGE BLANK NOT FILMED**



## CONTENTS

	Page
FOREWORD. . . . .	iii
OVERVIEW OF NASA QCGAT PROGRAM	
Gilbert K. Sievers. . . . .	1
AIRESEARCH QCGAT ENGINE, AIRPLANE, AND NACELLE DESIGN FEATURES	
Roger W. Heldenbrand. . . . .	11
AIRESEARCH QCGAT ENGINE PERFORMANCE AND EMISSIONS TESTS	
William M. Norgren. . . . .	45
AIRESEARCH QCGAT ENGINE - ACOUSTIC TEST RESULTS	
Larry S. Kisner . . . . .	65
QCGAT AIRCRAFT/ENGINE DESIGN FOR REDUCED NOISE AND EMISSIONS	
Leonard I'Anson and Kenneth M. Terrill. . . . .	101
AVCO LYCOMING QCGAT PROGRAM DESIGN CYCLE, DEMONSTRATED PERFORMANCE AND EMISSIONS	
Phil Fogel and Angelo Koschier. . . . .	135
AVCO LYCOMING QUIET CLEAN GENERAL AVIATION TURBOFAN ENGINE	
Craig A. Wilson . . . . .	155
SUMMARY OF NASA QCGAT PROGRAM	
Gilbert K. Sievers. . . . .	189
NEW OPPORTUNITIES FOR FUTURE, SMALL, GENERAL-AVIATION TURBINE ENGINES (GATE)	
William C. Strack . . . . .	195
AN OVERVIEW OF NASA RESEARCH ON POSITIVE DISPLACEMENT GENERAL-AVIATION ENGINES	
Erwin E. Kempke, Jr. . . . .	221
THE SPARK-IGNITION AIRCRAFT PISTON ENGINE OF THE FUTURE	
Kenneth J. Stuckas. . . . .	231
LIGHTWEIGHT DIESEL AIRCRAFT ENGINES FOR GENERAL AVIATION	
Steven G. Berenyi and Alex P. Brouwers. . . . .	247
ADVANCED ROTARY ENGINE STUDIES	
Charles Jones . . . . .	287
POSITIVE DISPLACEMENT TYPE GENERAL-AVIATION ENGINES: SUMMARY AND CONCLUDING REMARKS	
Erwin E. Kempke, Jr. . . . .	313

	Page
NASA PROPELLER TECHNOLOGY PROGRAM	
Daniel C. Mikkelsen . . . . .	315
LOW SPEED PROPELLERS - IMPACT OF ADVANCED TECHNOLOGIES	
Ira D. Keiter . . . . .	327
ADVANCED TURBOPROP POTENTIAL FOR HIGH SPEED	
Bernard S. Gatzen . . . . .	345
HIGH-SPEED-PROPELLER WIND-TURBINE AEROACOUSTIC RESULTS	
Robert J. Jeracki and James H. Dittmar. . . . .	361
ADVANCED PROPELLER AERODYNAMIC ANALYSES	
Lawrence J. Bober . . . . .	375
PROPELLER AEROACOUSTIC METHODOLOGIES	
Kenneth D. Korkan and Gerald M. Gregorek. . . . .	387
NASA PROPELLER NOISE RESEARCH	
George C. Greene. . . . .	405
PROPELLER DYNAMIC AND AEROELASTIC EFFECTS	
Barnes W. McCormick . . . . .	421

OMITTED  
P. 11

## OVERVIEW OF NASA QCGAT PROGRAM

Gilbert K. Sievers  
National Aeronautics and Space Administration  
Lewis Research Center

Today, the turbofan-powered general aviation fleet is growing at a greater percentage rate than the rest of the general aviation fleet. Jet powered general-aviation aircraft numbered over 2100 in 1978 with annual sales of about 250 in 1978. Annual sales are expected to be over 400 by 1985.

Jet powered general-aviation aircraft utilize all of the approximately 400 commercial airports in the United States, plus a significant number of general-aviation airports located in suburban areas. There are approximately 14 100 of these suburban airports, most of which are located in small communities with no industrial buffer zones and with people living nearby. Therefore, general aviation has the potential for greater community reaction to noise and pollution than commercial and large transport aircraft.

The QCGAT program seeks to improve the environmental characteristics of civil aircraft in the vicinity of airports. In the past, NASA has concentrated its efforts in engine research toward the commercial or large aircraft field. Now with the QCGAT program, NASA has applied this large engine technology to small engines in the general-aviation or small-engine field.

### PROGRAM OBJECTIVES

The program was conducted in two phases, a study phase and an experimental phase. The objectives for the study phase were to examine the applicability of current large turbofan technology to small engines, to do a preliminary design of the QCGAT engine, and to develop the requirements and a program plan for the experimental phase.

The objective of the experimental phase was to demonstrate that the application of large-turbofan-engine technology to small, general-aviation turbofan engines can result in less noise, lower emissions, and acceptable fuel consumption. While low emissions and acceptable fuel consumption are important, the program was primarily directed toward low noise.

Figure 1 shows some of the NASA programs that have contributed to the current status of large turbofan engine technology. These include the QCSEE program, the Quiet Engine program, the Quiet Nacelle programs, the Refan program, and the Clean Combustor program.

## PROGRAM APPROACH

As was mentioned previously, the program was conducted in two phases. The study phase helped define the experimental phase. It was started in April of 1975 and lasted about 6 months. Three contractors were involved in the study phase: Garrett AiResearch, Avco Lycoming, and the General Electric Co.

The experimental phase was a competitive procurement. Two bids were received, and contracts were awarded to both bidders, AiResearch and Avco Lycoming. The experimental phase consisted of a demonstration program in which each contractor was to design, fabricate, and test a QCGAT engine. Each engine was then delivered to NASA Lewis for further testing.

The technical approach for each contractor was to use an existing modern gas generator or engine core to save development time and money. The engine was to develop less than 5000 pounds of static thrust, and all rotating parts were to be flightworthy. A boilerplate rather than a flightworthy nacelle was acceptable. However, the internal aerodynamic contours and the acoustic treatment for the nacelle had to be of flight design.

Goals were set for noise, emissions, and fuel consumption. The emissions goals selected were the now abandoned 1979 EPA emission goals for class T1 engines. NASA generated its own noise goals. Since existing gas generators were being used, drastic reductions in fuel consumption could not be expected. However, fuel consumption should not suffer at the expense of reducing noise and pollutant emissions. Therefore, a fuel-consumption goal equal to or better than existing engines was set.

Since the flight-noise calculations require a flight profile, each contractor was asked to synthesize an aircraft for their engine. A twin-engine aircraft was selected for consistency in noise calculations.

Finally, the engines were to be delivered to NASA Lewis for further experimental testing.

## PROGRAM GOALS

The NASA generated noise goals at the FAR-36 measuring stations are shown in figures 2 to 4. Figure 2 is for takeoff. The goal and the FAR 36 requirements are expressed in EPNdB as a function of aircraft takeoff gross weight. The noise certification levels for four twin-engine aircraft are also shown. These aircraft are considered to be among the quietest turbofan-powered aircraft in the fleet today. As can be seen, the NASA goal is 8 to 12 EPNdB below any general-aviation aircraft flying today. In the range of aircraft gross weight used in the QCGAT program, the NASA goal is 16 to 19 EPNdB below the current 1977 FAA rule.

Figures 3 and 4 show the sideline and approach goals. The plots are similar to that shown for takeoff. Again, the NASA goals are well below existing quiet general-aviation aircraft and the 1977 FAA rule.



These goals were set to insure the inclusion of existing low-noise technology in the QCGAT engine designs. Achievement of these goals will result in aircraft noise levels that are perceived to be 45 to 55 percent less noisy than the levels of the quietest current business jets.

Another way of illustrating the effect of achieving these goals is by using noise footprint areas. A noise footprint is the ground area below the aircraft which is subject to a noise level greater than a given level during takeoff and landing. The footprint area for an aircraft using the QCGAT engines is predicted to be one-tenth that of the quietest current business jets. A comparison of the footprints is shown in figure 5. Similar reductions were achieved between the Lear 35 and the AiResearch QCGAT powered airplane and between the Citation and the Avco-Beech QCGAT powered airplane. Also, little variation in percent reduction of footprint area exists for levels between 70 and 90 EPNdB.

Achievement of the stringent QCGAT noise goals should eliminate noise as a major constraint on the future growth of the turbofan-powered, general aviation fleet.

The QCGAT emissions goals are shown in table I. These goals were the 1979 EPA emission goals for class T1 engines. EPA has since abandoned these goals as being too stringent for this time frame. However, these goals were kept for the QCGAT program.

The QCGAT performance goals are given in table II. The goals are based on the results from the study phase and are considered to be achievable goals with fuel consumption equal to or better than existing engines.

#### QCGAT ENGINES

Artists' versions of the QCGAT engines are shown in figures 6 and 7. Design details of both engines, except those of the mixer nozzles, will be discussed in following papers. The details of the mixer nozzles are under the NASA Early Domestic Dissemination or FEDD clause. Contractor reports on the mixers have been distributed to U.S. companies.

The reasons that two engines rather than one were selected for the QCGAT program, are evident in table II. The AiResearch engine is a higher thrust machine and is designed for an aircraft that cruises at high speed and altitude and has a long range. The Avco engine is a low-thrust machine designed for an aircraft that cruises lower, slower, and has an intermediate range.

#### QCGAT AIRCRAFT

An artist's version of the aircraft synthesized by Beech Aircraft for the Avco QCGAT engine is shown in figure 8. The AiResearch synthesized aircraft is a stretched version of the Learjet 35. A photograph of Learjet 35 is shown in figure 9. The AiResearch QCGAT engine powered version appears to be very simi-

lar. The major changes to the outward appearance are larger nacelles and a longer fuselage.

A comparison of the QCGAT aircraft with similar existing aircraft is given in table III. The Avco QCGAT powered aircraft performs a similar mission to that of the Citation I, and, even though it is a much lighter aircraft, it has both a higher maximum payload capability and a lower fuel consumption at comparable cruise conditions. The AiResearch QCGAT aircraft has a larger passenger or payload capability than the Learjet 35 and also has lower fuel consumption at comparable cruise conditions.

Keeping in mind the lower noise and lower pollutant emissions of the QCGAT powered aircraft while making these comparisons, the QCGAT advantages are apparent.

#### QCGAT SCHEDULE

A bar chart showing the schedule for the major items in the QCGAT experimental phase are shown in figure 10. The experimental phase started about the end of 1976. The engine design, fabrication, and testing were accomplished within the time frames shown in the figure. The AiResearch QCGAT engine was delivered to Lewis in February 1979, and the Avco engine in October 1979. Final contractor reports covering the development of these engines will be available and distributed in the near future.

TABLE I. - QCGAT EMISSIONS GOALS - INSTALLED

Emission	Contract goal	
	g/kN sec	lb/1000 lb thrust-hr/cycle
Carbon monoxide	0.266	9.4
Unburned hydrocarbons	.045	1.6
Oxides of nitrogen	.105	3.7

TABLE II. - QCGAT PERFORMANCE GOALS  
[Standard day; installed]

		Avco	AiResearch
Sea level takeoff	Thrust, N(lb)	7166 (1611)	17312 (3892)
	SFC, kg/hr-N (lb/hr-lb)	0.0370 (0.363)	0.0431 (0.423)
Design cruise M = 0.6 7600 m (25 000 ft)	Thrust, N (lb)	2157 (485)	-----
	SFC, kg/hr-N (lb/hr-lb)	0.0610 (0.628)	-----
Design cruise M = 0.8 12 200 m (40 000 ft)	Thrust, N (lb)	-----	4017 (903)
	SFC, kg/hr-N (lb/hr-lb)	-----	0.0759 (0.744)

TABLE III. - AIRCRAFT COMPARISON

	Avco	Citation I	AiResearch	Learjet 35
Takeoff gross weight, kg (lb)	3538 (7800)	5375 (11 850)	8674 (19 122)	7711 (17 000)
Number of seats	6	7	14	10
Maximum payload, kg (lb)	1134 (2500)	816 (1800)	1231 (2714)	862 (1900)
Maximum range at maximum payload, km (mi)	1408 (769)	1732 (935)	3456 (1866)	3926 (2120)
Passenger km/kg-fuel (passenger miles/lb-fuel)	13.8 (3.90)	7.56 (2.13)	16.4 (4.62)	14.0 (3.90)
Maximum cruise speed, m/sec (knots)	185 (359)	183 (355)	236 (459)	239 (464)
Maximum cruise mach number	0.626	0.607	0.801	0.810
Ceiling, m (ft)	12 340 (40 500)	12 500 (41 000)	13 720 (45 000)	13 720 (45 000)

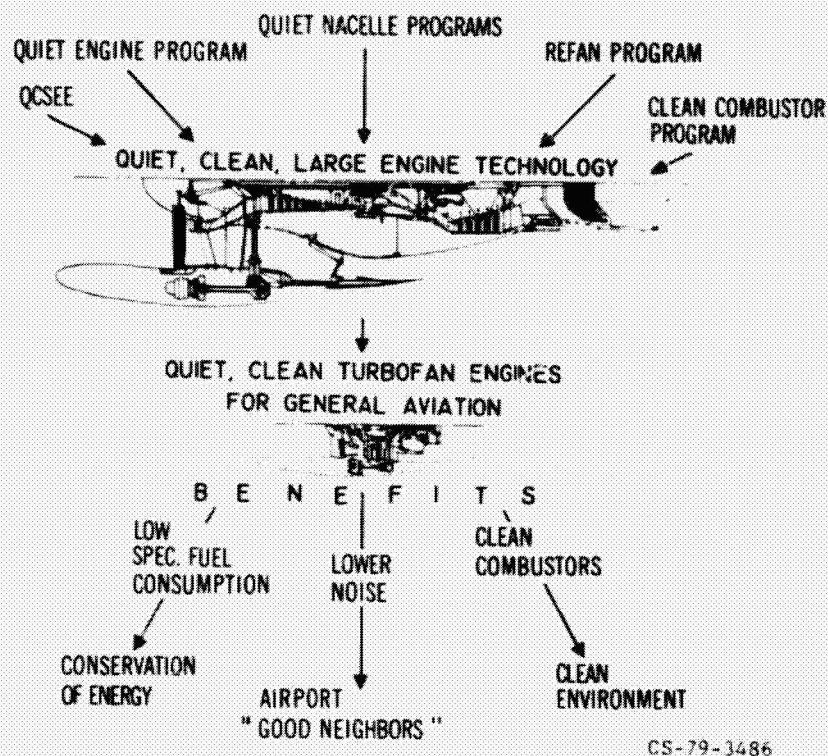


Figure 1

## TAKEOFF NOISE GOAL

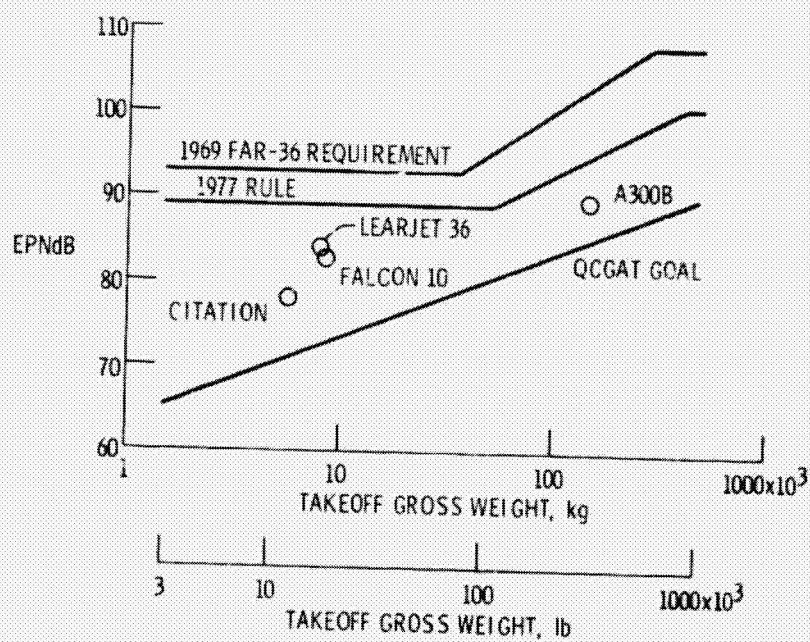


Figure 2

## SIDELINE NOISE GOAL

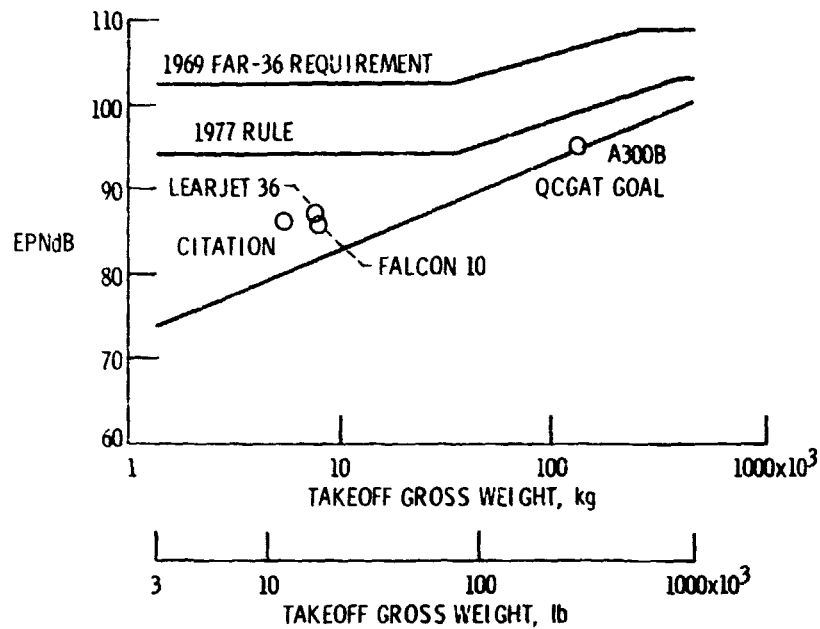


Figure 3

## APPROACH NOISE GOAL

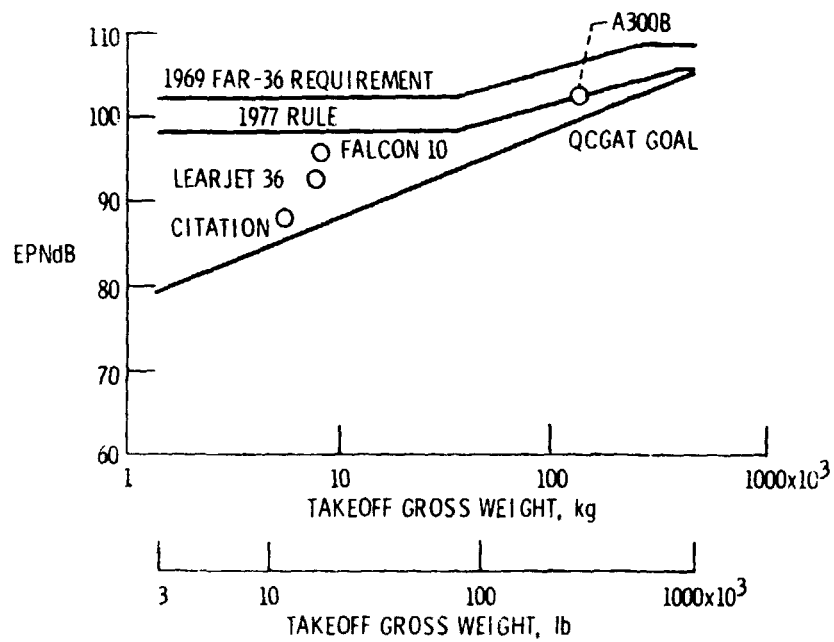
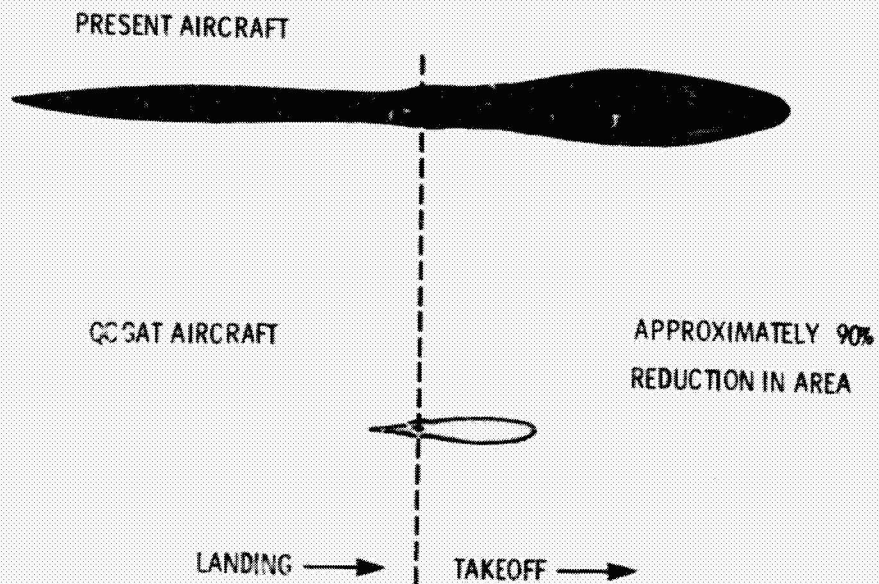


Figure 4

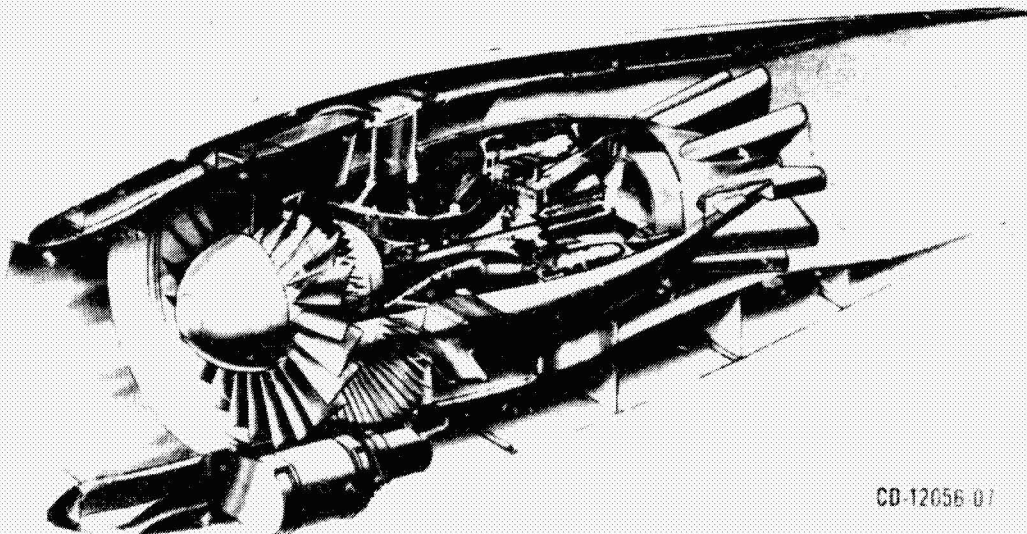
## COMPARATIVE FOOTPRINTS



CS-79-3627

Figure 5

## AVCO LYCOMING QCGAT ENGINE

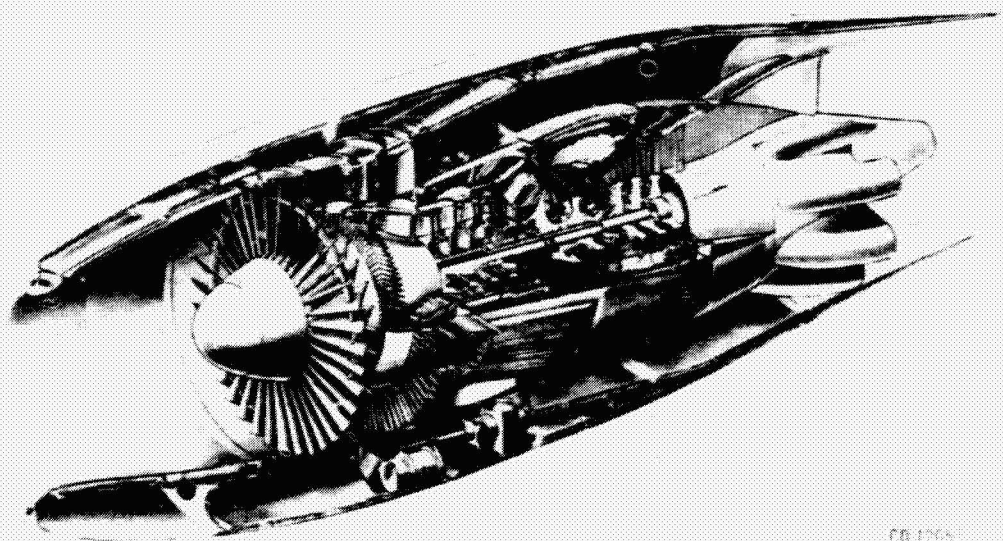


CD-12056 07

CS-79-1206

Figure 6

## **GARRETT AIRESEARCH QCGAT ENGINE**



CD 17651

CS-79-1207

Figure 7

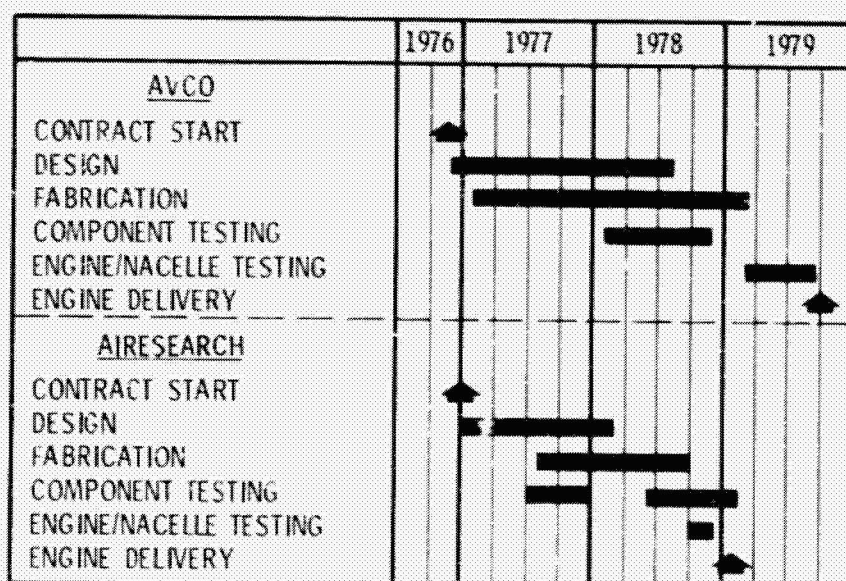


Figure 8



Figure 9

QCGAT SCHEDULE  
EXPERIMENTAL PHASE



CS-700-177-1

Figure 10



9,  
N80-22323

## **AIRESEARCH QCGAT ENGINE, AIRPLANE, AND NACELLE DESIGN FEATURES**

**Roger W. Heldenbrand  
AiResearch Manufacturing Company of Arizona  
A Division of The Garrett Corporation**

### **SUMMARY**

The Quiet, Clean, General Aviation Turbofan (QCGAT) engine and nacelle system was designed and tested by the AiResearch Manufacturing Company of Arizona under Contract to NASA Lewis Research Center. The engine utilized the core of the AiResearch Model TFE731-3 engine and incorporated several unique noise- and emissions-reduction features. Major performance, emissions, and noise goals were demonstrated, and the engine and nacelle were delivered to NASA Lewis Research Center for additional testing.

### **INTRODUCTION**

The design features of the QCGAT engine, airplane and nacelle are described in this paper. Test programs and results of the engine performance, emissions, and noise tests are discussed in subsequent papers.

An isometric cutaway of the QCGAT engine in a flight-type nacelle is shown in figure 1. The engine was designed around the core of the AiResearch Model TFE731-3 turbofan engine. This engine is a production unit used in several domestic and foreign business jets. The engine consists of the TFE731-3 high-pressure (HP) spool and low-pressure (LP) compressor, plus several unique and new components including a low-speed fan, a fan gearbox, associated ducts and structure, a reduced-emissions combustion system, and an LP turbine.

An airplane design, synthesized by Garrett in order to evaluate the QCGAT Engine, was selected to be similar to business jets using Model TFE731 Engines, but somewhat larger, thus taking advantage of the higher thrust level.

Two nacelles were designed for the program:

- o A production flight-weight nacelle featuring integral acoustic treatment
- o A 'workhorse' nacelle, fabricated especially for this test program and featuring replaceable inlets, acoustic panels, and a special mixer compound nozzle.

An overall task schedule is shown in figure 2. The QCGAT Phase II experimental program was divided into ten major tasks. These culminated with delivery of an engine, associated test support equipment, and spares at the end of 25 months. As experienced with most hardware-oriented programs, difficulties and delays were experienced with design iterations and fabrication schedules. However, the test program was accelerated, and the engine was shipped on schedule.

The technical goals for the program are listed in table 1. Performance goals represented a TSFC improvement of approximately 9 percent over other turbofan engines. The noise goals were 10- to 15-EPNdB below the Federal Aviation Administration's FAR Part 36 requirements. The emissions goals were identical to the EPA 1979 standards for T-1 class engines. (The EPA subsequently determined that general aviation was not a significant source of air pollution and therefore did not impose these standards).

## ENGINE DESIGN

The principal program objective was to demonstrate the application of large turbofan noise- and emissions-reduction technology to small general aviation turbofans. To do this, a number of unique features were incorporated in the basic design of the QCGAT engine in order to reduce the emissions and noise levels below those of the already quiet TFE731 engine. This work was initiated in 1975 during the QCGAT Phase I study. Twelve candidate engine configurations were screened. Many parameters were considered, including:

- o Fan pressure ratios at takeoff and cruise
- o Thrust
- o TSFC
- o Lapse rate
- o Fan diameter
- o Installed weight
- o Noise
- o Nacelle drag
- o Acoustic shielding
- o Cost.

The engine cycle selected for the program represented a practical engine from the standpoints of cost, weight, airplane/nacelle interference drag, and cruise propulsion efficiency. The engine also exhibited high potential for reduction of turbomachinery and jet noise, and reduction of chemical and visible exhaust emissions. The design point for the engine (typical for most modern business jets) and principal engine cycle parameters are listed in table 2.

Figure 3 is a cross-section of the overall QCGAT engine design. The QCGAT engine is based on the core of TFE731-3, but

incorporates a fan used in the AiResearch Model ATF3 engine. The fan is driven by a new low-pressure turbine via a newly designed five star-gear gearbox. The low-pressure compressor is driven directly by the low-pressure turbine. The HP spool consists of a centrifugal compressor driven by a cooled axial turbine. The combustor is an adaptation of a production TFE731 combustor that was designed for low smoke. Accessories and the fuel control are driven by the HP spool through a tower shaft. A finned heat exchanger in the fan bypass duct cools the oil for the fan gearbox and engine lubrication system. The flange-to-flange length of the engine is 143.15 cm (56.36 in.) and the fan diameter is 77.47 cm (30.5 in.). When fully instrumented and wet, the test engine weighs approximately 426.38 kg, (940 lb). Figure 4 shows the engine in the test cell prior to initial calibration.

The major acoustic design features of the QCGAT engine and nacelle system are shown in figure 5 and outlined below:

- o No inlet guide vanes
- o High inlet throat Mach number
- o Low tip speed, single-stage fan (36 blades)
- o Phased inlet acoustic treatment
- o Optimized fan blade-to-stator vane count
- o 2.12 rotor-chord, fan-to-stator spacing
- o Phased fan bypass duct acoustic treatment
- o Low fan jet velocity

- o Reverse-flow annular combustor
- o High-work, low-pressure turbine with low core-exhaust velocity
- o 12-lobe mixer compound nozzle.

With the possible exception of the reverse-flow combustor and the mixer compound nozzle, each of these features above is based on work done with large engines and is a direct application of that technology.

#### COMPONENT DESIGNS

The QCGAT fan (fig. 6) is a 36-blade design derived from the fan used on the AiResearch Model ATF3 Turbofan engine. The principal design features are given on table 3 with the design point at 12,192 m (40,000 ft), standard day at a flight Mach number of 0.8. This fan is approximately 10-percent larger in diameter than the TFE731 fan, and rotates at 17-percent slower speed. Thus, fan turbomachinery component noise levels are lower. The fan-stage flow path (fig. 7) was designed to minimize the core-flow Mach number and to prevent large accelerations in the strut regions. Absolute local Mach numbers, and blade and vane counts are also shown. The bypass stator location is slightly more than two rotor-chord lengths downstream. The vane counts of both stators were selected to minimize rotor and stator noise interaction. The bypass performance map (fig. 8) shows the engine operating lines for co-annular nozzle and mixer compound exhaust nozzle from idle through takeoff. Slightly greater surge margin was achieved with the mixer compound nozzle. A fan component rig test was not conducted. However, adequate data was available from the Model ATF3 fan rig tests,

and actual QCGAT engine operation to define the QCGAT fan for the engine performance model.

The fan gearbox (fig. 9) is similar to that of the TFE731. However, the overall gear ratio was changed from 0.5559 to 0.4634 to match lower fan speed. Resilient mounts were incorporated on the star gears to maintain gear alignment during high-torque loads. The star-gear shafts were precision ground to form the bearing inner race, and the star gears were counterphased and nonfactored. The gear reduction system transmits in excess of the 2.74 MW (3675 hp) required for the QCGAT engine, and has been designed for life greater than 5000 hours at higher power.

The fan support structure (fig. 10) includes the fan support housing, intermediate case, and the engine support housing (main engine mount), as well as the fan gearbox and fan itself. These components were designed to survive a 1.8-kg (4-lb) bird strike at a velocity of 250 knots and the loss of two adjacent fan blades (but not simultaneously). Finite-element stress analyses were performed on the major structural pieces for the loads listed in table 4. Stress isopleths and displacements are shown in figure 11.

The low-pressure compressor, high-pressure compressor, and high-pressure turbine are standard components of the TFE731-3 engine and were used without design changes. The design-point characteristics of these components are listed given on table 5.

The LP turbine, which drives the fan, and the low-pressure compressor, is a 3-stage shrouded axial design. The QCGAT engine design-point operating conditions are given in table 6. Several critical constraints were imposed on the design of the turbine. Since the QCGAT engine was based on the TFE731 core, the overriding ground rule was to minimize changes to existing TFE731 hardware.

Because the QCGAT low-pressure turbine is larger in diameter and axially longer than that of the TFE731, it was necessary to design a gas flow path that would not cause disruption of airflow distribution in the combustor plenum. Location of the TFE731 aft turbine bearing was retained. The unusual shape of the third-stage disk (fig. 12) was the result of this latter constraint. Since LP spool speed is fixed by the TFE731 LP compressor, the larger turbine represented a major design challenge from the standpoints of stress, vibration, blade flutter, life, and materials. In addition, use of the 12-lobe compound mixer nozzle required low exit swirl angles. Total-to-total efficiency goal was set at 90 percent. As a result of these constraints, numerous compromises were necessary during design. Although it is not feasible to include the detailed results of all aerodynamic, thermodynamic, and mechanical design analyses in this report, all constraints were satisfied, including that of efficiency.

It was originally intended to use only a hydromechanical control system for the QCGAT engine. However, because the hydromechanical unit is considered a backup system on the TFE731, it was decided to use a production TFE731 electronic control system as the primary control. The control (fig. 13) is a full-authority system providing speed control, overtemperature, and overspeed protection under all operating conditions. These include start, transient, and steady state. A comparison of QCGAT engine characteristics and the TFE731-3 was made to determine if modifications were necessary to the existing computer. This comparison showed that the basic logic was satisfactory, and the adjustment ranges were adequate.

The QCGAT combustor (fig. 14) is a version of the TFE731 burner in production at the initiation of the program. In-house modifications for the TFE731 engine, which consisted of hole-pattern variations for smoke reduction, were incorporated in the

QCGAT engine. During engine testing, emissions were controlled with a system adapted from the NASA/AiResearch T1 Pollution Reduction Technology Program. Air was supplied to the secondary fuel nozzles at the taxi-idle power setting only. This aided the fuel atomization process (see fig. 15). At all power settings except taxi-idle condition, the fuel was reconnected to the secondary fuel circuit. An air-assist system was not used. (This system is discussed in a subsequent paper.)

Accessories for engines like QCGAT and the TFE731 normally consist of customer-furnished equipment. The accessory drive gearbox, shown at the bottom of the engine in figure 16, provides mounting pads and drives on the forward side of the gearbox for a hydraulic pump or similar equipment. These items not normally required for airplane service were not supplied with the QCGAT engine. A starter-generator was furnished, and although not shown in figure 16, mounts on the pad occupied by the laboratory air-turbine starter.

#### QCGAT AIRPLANE DESIGN

The airplane synthesized for the engine was based primarily on the Learjet 35/36, although it also had minor features found on other business airplane using TFE731 engines. The major differences between the AiResearch QCGAT airplane (fig. 17) and the Learjet 35/36 are the elongated fuselage to increase payload (passenger) capacity, a slightly higher wing loading, and the relocation of the horizontal tail. The increased payload was possible because of the higher-thrust engines. The increased wing loading was the consequence of the combined wing and flap configuration. The horizontal tail was moved to avoid engine exhaust. The airplane definition had two principal objectives: First, to provide an airplane that



utilized the installed thrust of the QCGAT engine to produce take-off and approach flight profiles for which noise estimates could be computed for sideline, takeoff, and approach FAR Part 36 measurement locations shown in figure 18. Without a well-defined airplane configuration, it would not have been possible to make realistic and consistent comparisons of in-flight noise levels. The second objective was to represent a viable airplane with respect to its ability to transport passengers and cargo with a fuel efficiency comparable to current business-jet airplane. At maximum takeoff gross weight of 8,674 kg (19,122 lb), the 12-passenger AiResearch QCGAT airplane takes full advantage of the higher thrust of the QCGAT engine, yet meets the noise goals at all three FAR Part 36 measurement locations.

Table 7 gives the principal airplane design parameters. As listed in this table, the wing incorporates double-slotted flaps for good low-speed performance. The relatively high wing loading of  $354.5 \text{ kg/m}^2$  ( $72.6 \text{ lb/ft}^2$ ) assures a smooth ride comparable to commercial jets.

The takeoff profile presented in figure 19 shows lift-off after a takeoff roll of 914 m (3000 ft) and, at 6.48 km (3.5 nmi) from brake release, an altitude of more than 1,067 m (3500 ft) with thrust cutback and approximately 1158 m (3800 ft) with full thrust. As indicated on the payload-range chart, (fig. 20), the QCGAT airplane with a maximum payload of 1231 kg (2714 lb) has a maximum range of 3445 km (1860 nmi). This would allow the airplane to fly non-stop from Phoenix to New York City at an altitude of 1524 m (5000 ft) with more than 30 minutes reserve fuel.

## NACELLES

During preliminary design tasks, two nacelle designs were selected; a flight nacelle and a workhorse nacelle. Only the workhorse nacelle was carried through to detail design and fabrication. The flight nacelle was used primarily to look at airplane installation characteristics and weight estimates.

The flight nacelle (fig. 21) incorporated integrally phased acoustic treatment in the inlet barrel, the inner and outer bypass duct, and the aft fan duct. It also incorporated the extra nozzle mixing length for the core exhaust mixer. The workhorse nacelle essentially duplicated the internal aerodynamic design and acoustical treatment of the flight nacelle except for a section in the area immediately aft of the fan that had no acoustic treatment in the flight nacelle. The weight of the flight nacelle was estimated at 134 kg (295 lb). The total installed propulsion system weight was estimated at 513 kg (1130 lb).

A cross section of the workhorse nacelle is shown with the engine in figure 22. This nacelle was designed to provide maximum test configuration versatility for the QCGAT engine. Figure 22 also shows the basic component arrangements. The principal components include the inlet barrel, that accommodates a flight-simulator lip, a conventionally shaped nacelle lip, the inner and outer bypass ducts located opposite the engine hot section, the aft barrel, the core mixer, and the nozzle.

The inlet barrel (fig. 23) incorporates two sets of interchangeable duct liners--one set of acoustic-treatment panels and one set of hardwall panels, as well as the two different inlet lips. The flight-simulator lip (fig. 23) is designed to control and direct the inlet airflow, thus simulating actual flight conditions. The conventional nacelle lip is installed on the engine as

shown in figure 24. The inlet barrel was designed for high-inlet recovery at a relatively high-throat Mach number of 0.79 at cruise (fig. 25). When the inlet barrel is removed, a reference bellmouth assembly can be installed directly on the engine inlet flange. Detailed performance tests were conducted with the bellmouth and will be discussed later.

The inner and outer bypass duct section (fig. 26) also incorporated two sets of duct liners--acoustical-treatment and hardwall panels. As in the inlet barrel, these replaceable panels were in 180-degree sections and were radially adjustable so that the flow-path continuity could be controlled. The outer bypass duct contained a faired service strut that provided for extensive pressure and temperature instrumentation, as well as support of the aft section of the engine. The aft flange of the outer bypass duct was common to two nozzle schemes--the mixer compound nozzle and the coannular nozzle. Figure 27 shows half the outer bypass duct section removed. The service strut is visible, and the core section of the coannular nozzle is installed.

A 12-lobe core mixer (fig. 28) was designed for the AiResearch QCGAT engine to improve both performance and takeoff noise. With the mixer compound nozzle, a 1-percent TSFC improvement in sea-level performance was demonstrated. A 3.2-percent TSFC improvement at cruise was estimated based on mixer model and engine tests. A 3- to 5-EPNdB reduction in takeoff noise from the coannular configuration was achieved with the mixer compound nozzle. As shown in figure 29, smoke traces on the mixer centerbody indicated that the mixer compound nozzle was performing as predicted. Similar smoke traces were observed in the nozzle section downstream of the mixer.

The final sections of the workhorse nacelle assembly (fig. 30) are the aft barrel, which has hardwall and acoustic panels, and the

nozzle. These sections are used only when the mixer is installed. They are removed when the coannular nozzle system is used.

The complete workhorse nacelle assembly is shown in figures 31 and 32. These figures show the engine mounted on the test stand at AiResearch's remote desert test facility in the San Tan mountains, southeast of Phoenix.

### CONCLUSION

The following points summarize the design of the AiResearch QCGAT engine and nacelle system:

- o An existing turbofan engine core was utilized for an experimental demonstrator engine. This was a requirement of the original problem statement and was particularly important with respect to minimizing costs and maximizing reliability.
- o Several unique components were successfully adapted to this core: fan, gearbox, combustor, low-pressure turbine, and associated structure. These components formed the basis for meeting the main program objective demonstrating the application of large turbofan engine design, emissions, and noise technology in small general aviation turbofans.
- o A highly versatile workhorse nacelle incorporating interchangeable acoustic and hardwall duct liners, showed that large-engine attenuation technology could be applied to small propulsion engines. The application of the mixer compound nozzle demonstrated both performance and noise advantages on the engine.

The QCGAT program made several significant contributions to general aviation propulsion:

- o Application of exhaust-emissions reduction techniques.
  - 1. Hydrocarbon and carbon monoxide goals were met.
  - 2. Nitrogen oxides were greatly reduced.
- o With the aid of NASA, improved small engine noise-analysis techniques, including core noise and static-to-flight correlations, were developed.
- o Major noise reduction, beyond that of an already quiet engine, was obtained. The AiResearch QCGAT engine is significantly quieter than any other business jet engine.

TABLE 1. AIRESEARCH QCGAT ENGINE, TECHNICAL GOALS.

		Thrust N (lbf)	TSFC kg/N.h (lbm/hr/lbf)
A. Performance			
Takeoff (SLS,ISA)			
o Uninstalled		17,512 (3,937)	0.0426 (0.418)
o Installed		17,312 (3,892)	0.0431 (0.423)
Cruise [12,192 m (40,000 ft), M = 0.8]			
o Uninstalled		3,954 (889)	0.0775 (0.760)
o Installed (with mixer nozzle)		4,017 (903)	0.0759 (0.744)
B. Noise (FAR Part 36)			EPNdB
Takeoff			73.3
Sideline			82.3
Approach			87.3
C. Emissions (EPA 1979 Standards T-1)			EPAP
Hydrocarbon (HC)			1.6
Carbon Monoxide (CO)			9.4
Oxides of Nitrogen (NO <sub>x</sub> )			3.7
Smoke Number			38.0
D. Weight		E. Life	
kg (lbm)		hr	
377 (832)		10,000	

TABLE 2. QCGAT CYCLE PARAMETERS.

Design point . . . . .	12,192 m (40,000 ft), M = 0.8, ISA
Thrust . . . . .	4,017 N (902 lbf)- installed
TSFC . . . . .	0.0759 kg/N.h (0.744 lbm/hr/lbf)
Bypass ratio . . . . .	3.71
Fan pressure ratio . . . . .	1.62
Cycle pressure ratio . . . . .	17.7
Turbine inlet temperature . . . . .	1,266K (1,820°F)
Corrected fan airflow . . . . .	77.8 kg/s (171.6 lb/s-c)
Corrected core airflow . . . . .	11.5 kg/s (25.4 lb/sec)

TABLE 3. QCGAT FAN DESIGN FEATURES.

At Design Point--12,192 m (40,000 ft, C.8M, ISA).	
Diameter . . . . .	77.5 cm (30.5 in.)
Radius ratio . . . . .	0.46
Inlet corrected airflow . . . . .	77.8 kg/s (171.6 lbm/sec)
Bypass ratio . . . . .	3.7
Bypass pressure ratio . . . . .	1.62
Core pressure ratio . . . . .	1.55
Inlet tip relative Mach No. . . . .	1.39
Inlet corrected tip speed . . . . .	6.985 m/s (1375 ft/sec)

TABLE 4. QCGAT DESIGN LOADS.

Item Description	Radial Load N (lbf)	Moment Load J (lbf-in.)	Fan Thrust N (lbf)	Bird Strike Torque J (lbf-in.)
Fan support	289,134 (65,000)	-- --	14,679 (3,300)	-- --
Intermediate case	289,134 (65,000)	832,473 (614,000)	14,679 (3,300)	454,199 (335,000)
Engine support housing (main engine mount)	289,134 (65,000)	1,128,041 (832,000)	14,679 (3,300)	454,199 (335,000)

TABLE 5. MODEL TFE731-3 ENGINE COMPONENTS,  
DESIGN POINT CHARACTERISTICS.



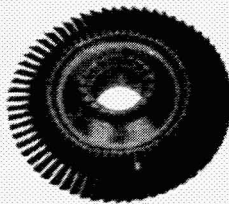
Design Point Parameters	Low-Pressure Compressor	High-Pressure Compressor	High-Pressure Turbine
Type	Four-stage axial	Single-stage centrifugal	Single-stage cooled axial
N/	2,094 rad/s (20,000 rpm)	2,295 rad/s (21,917 rpm)	1,406 rad/s (13,431 rpm)
P/P	4.27	2.57	1.832
W /	11.11 kg/s (24.5 lb/sec)	2.99 kg/s (6.60 lb/sec)	2.129 kg/s (4.693 lb/sec)
T <sub>inlet</sub>	--	--	1,329K (1,933°F)
			



TABLE 6. QCGAT LOW-PRESSURE TURBINE.

Engine Operating Conditions at Design Point: Cruise Mach No. 0.8 at 12,192 m (40,000 ft), ISA	
Pressure ratio (total-to-total rating) -	5.707
Efficiency (total-to-total rating) -	90.2%
Max flow rate - - - - -	5.055 Kg/s (11.145 lbm/sec)
Speed - - - - -	2,118.0 rad/s (20,229 rpm)
Specific work - - - - -	406.515 kJ/kg (174.77 Btu/lbm)

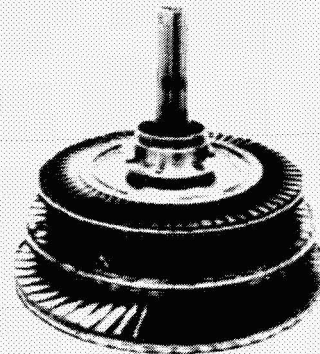


TABLE 7. AIRESEARCH QCGAT AIRPLANE PARAMETERS.

Wing area . . . . .	24.49 m <sup>2</sup> (263.6 ft <sup>2</sup> )
Sea level static thrust (Installed-ISA + 283.15K (273.15°C)) . . . . .	16,845 N (3,787 lbf)
Flaps . . . . .	Double-slotted
Flap span/wing span . . . . .	0.700
Sea level static thrust/takeoff gross weight [ISA + 283.15K (273.15°C)] . . . . .	0.396
Takeoff gross weight with respect to wing area . .	107.97 Kg/m <sup>2</sup> (72.55 lbm/ft <sup>2</sup> )
Capacity (crew + passengers) . . . . .	2 + 12
Operating weight empty . . . . .	4,808 Kg (10,599 lbm)
Takeoff gross weight . . . . .	8,674 Kg (19,122 lbm)
Maximum ramp weight. . . . .	8,787 Kg (19,372 lbm)
Maximum fuel weight. . . . .	3,152 Kg (6,948 lbm)
Maximum useable fuel . . . . .	3,140 Kg (6,922 lbm)
Maximum payload. . . . .	1,231 Kg (2,714 lbm)
Maximum landing wiehgt . . . . .	6,775 Kg (14,936 lbm)
Zero fuel weight with maximum payload . . . . .	6,021 Kg (13,273 lbm)
Fuel weight with maximum payload . . . . .	2,766 Kg (6,099 lbm)
Payload with maximum fuel . . . . .	846 Kg (1,865 lbm)

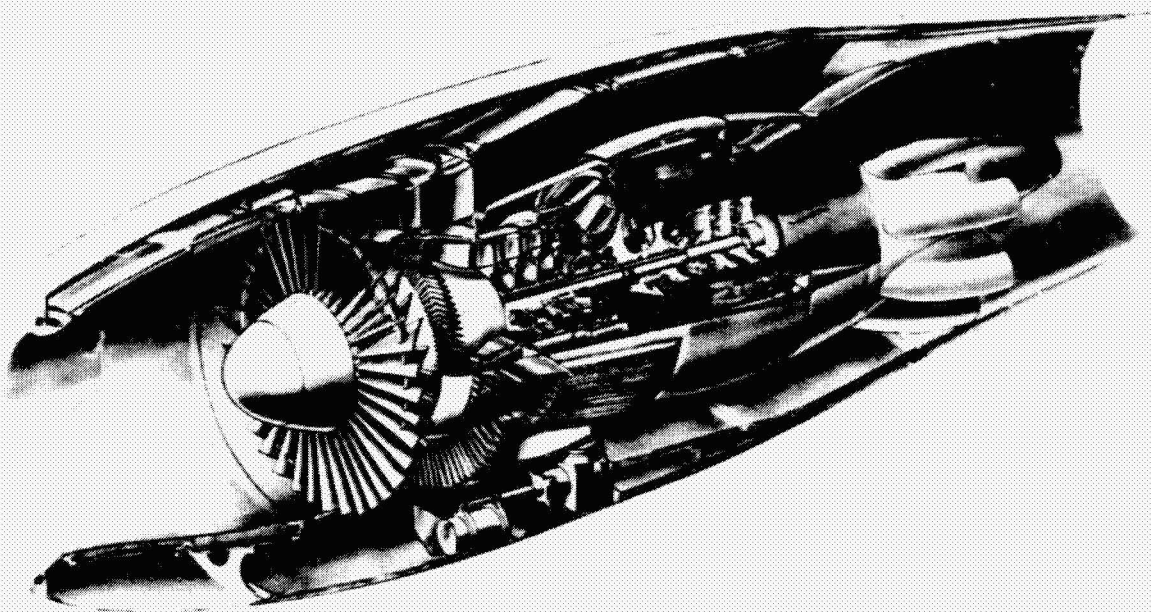


Figure 1. AiResearch QCGAT Engine.

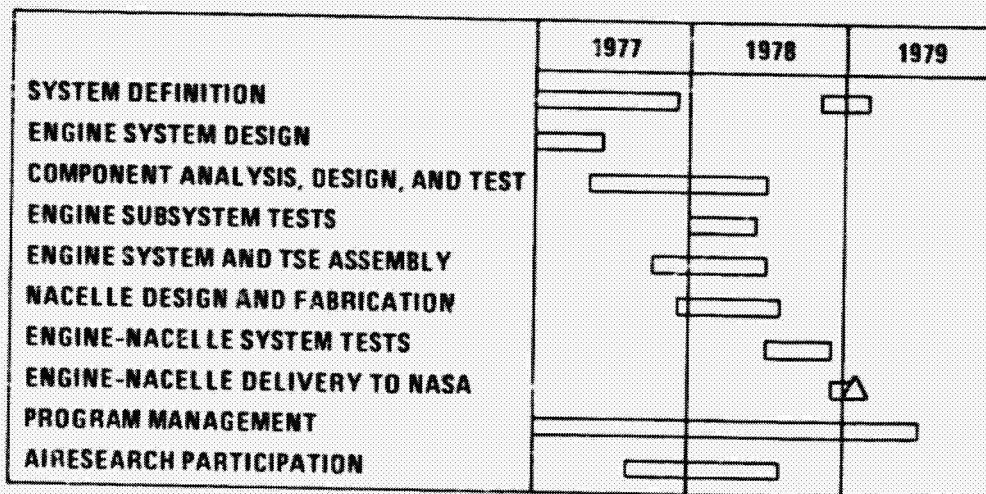
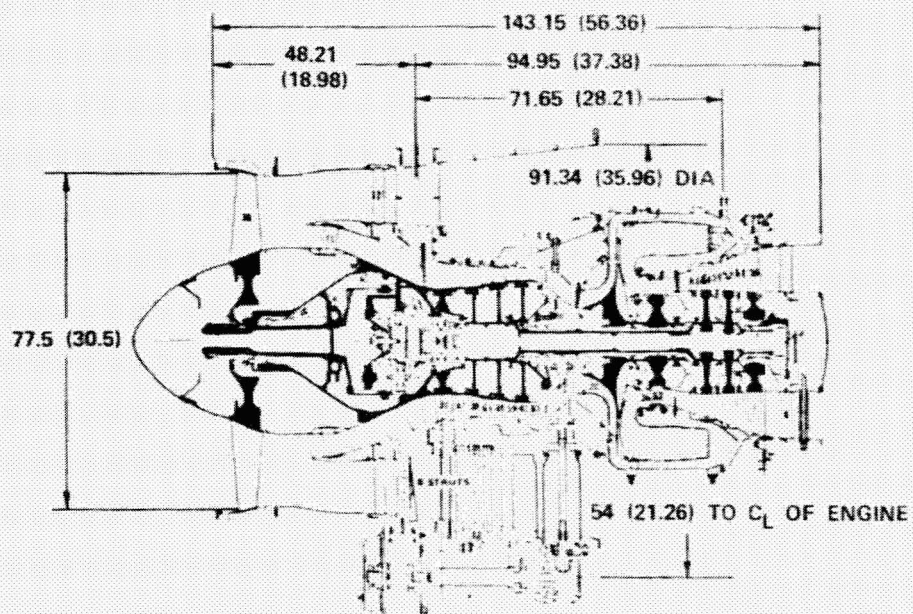


Figure 2. AiResearch QCGAT Schedule.





NOTE: DIMENSIONS ARE IN CENTIMETERS WITH INCHES GIVEN IN PARENTHESES.

Figure 3. Cross Section of AiResearch QCGAT Engine.

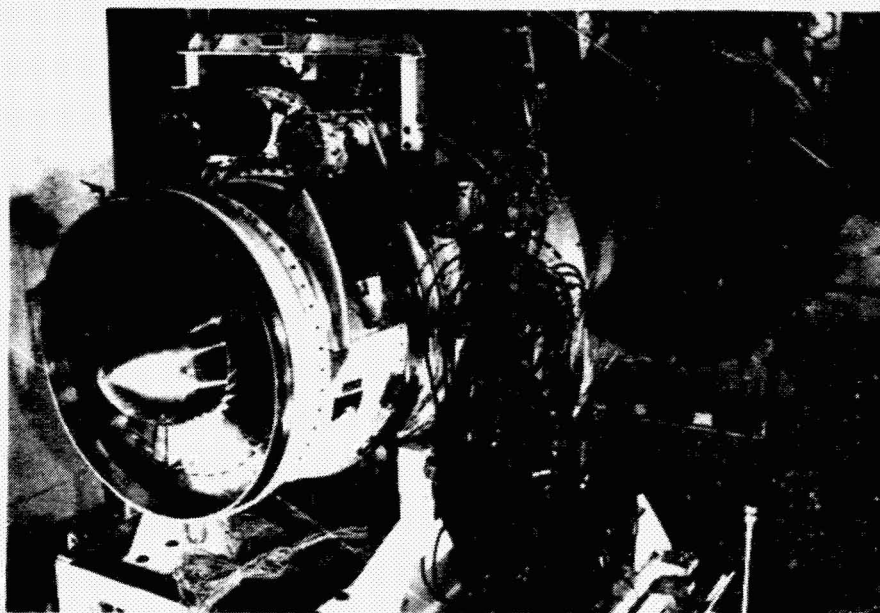


Figure 4. AiResearch QCGAT Engine.

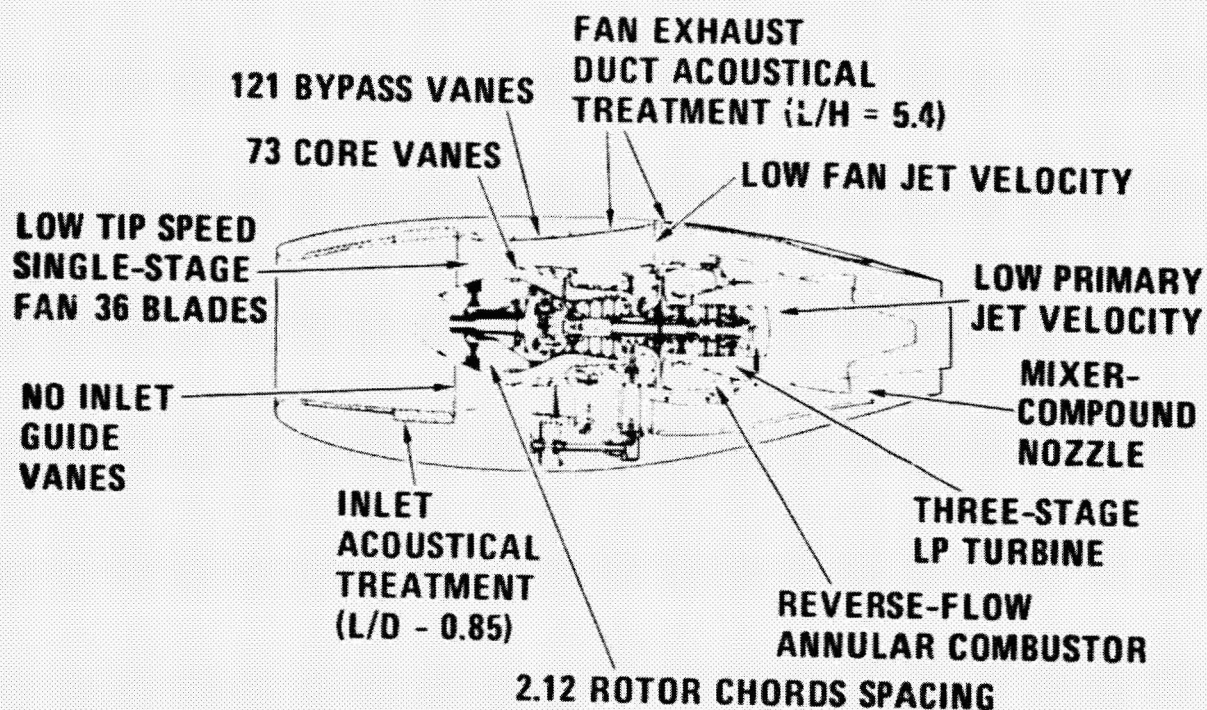


Figure 5. Major Acoustic Design Features of the QCGAT Engine Nacelle.

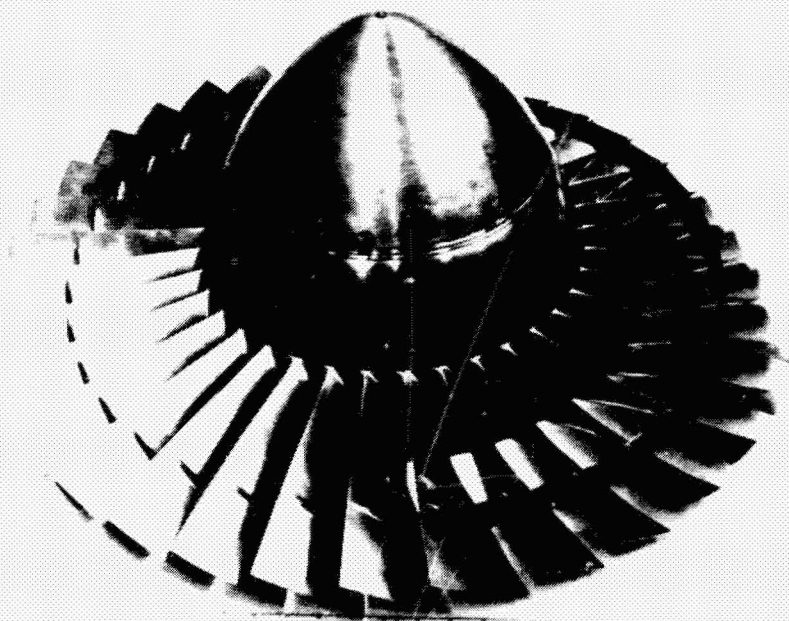


Figure 6. QCGAT Fan Rotor.



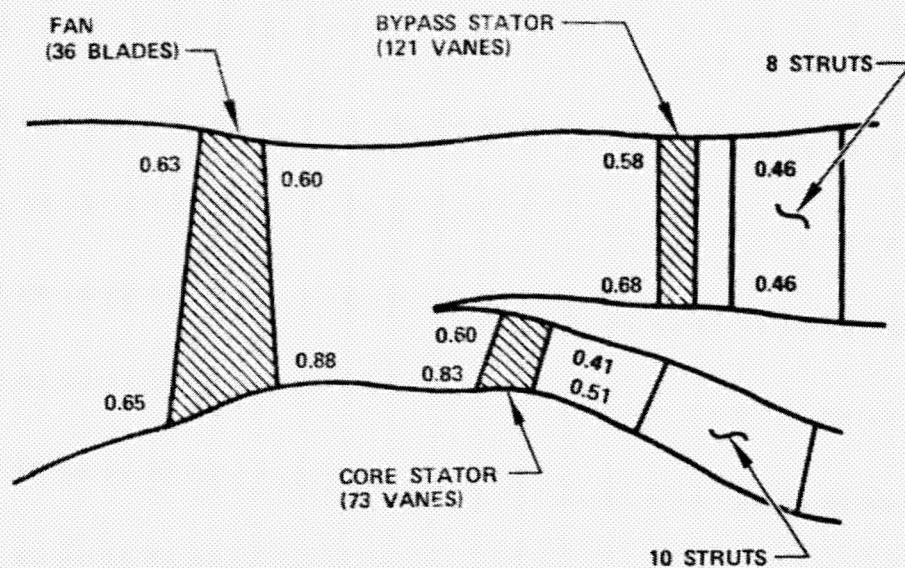
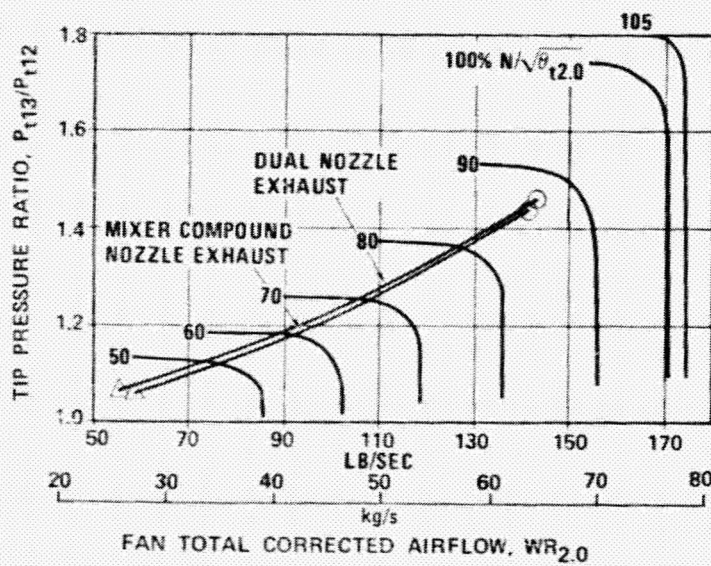


Figure 7. Mach Numbers (Absolute) for Fan Stage and Transition Ducts.



- NOTES: 1.  $100\% N/\sqrt{\theta_{t2.0}} = 1058.6 \text{ rad/s (10,111 RPM)}$   
 2.  $\triangle$  INDICATES AIRFLOW AT IDLE  
 3.  $\circ$  INDICATES AIRFLOW AT TAKEOFF

Figure 8. Estimated Performance of AiResearch QCGAT Engine.



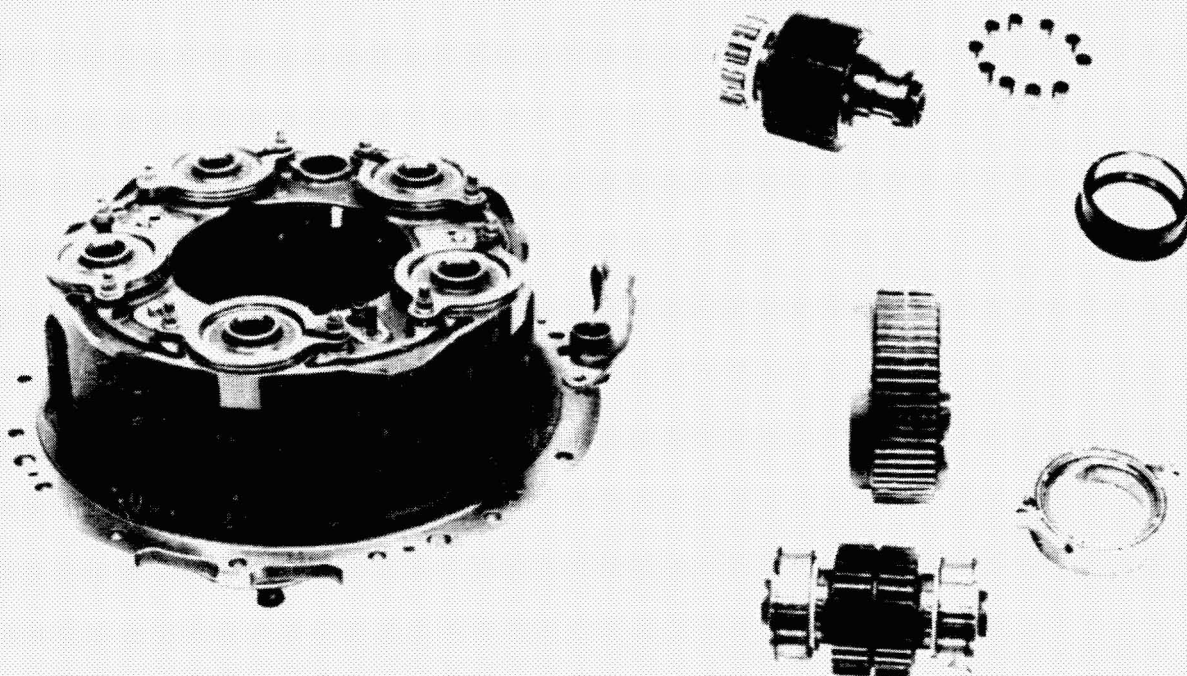


Figure 9. QCGAT Fan Gearbox.

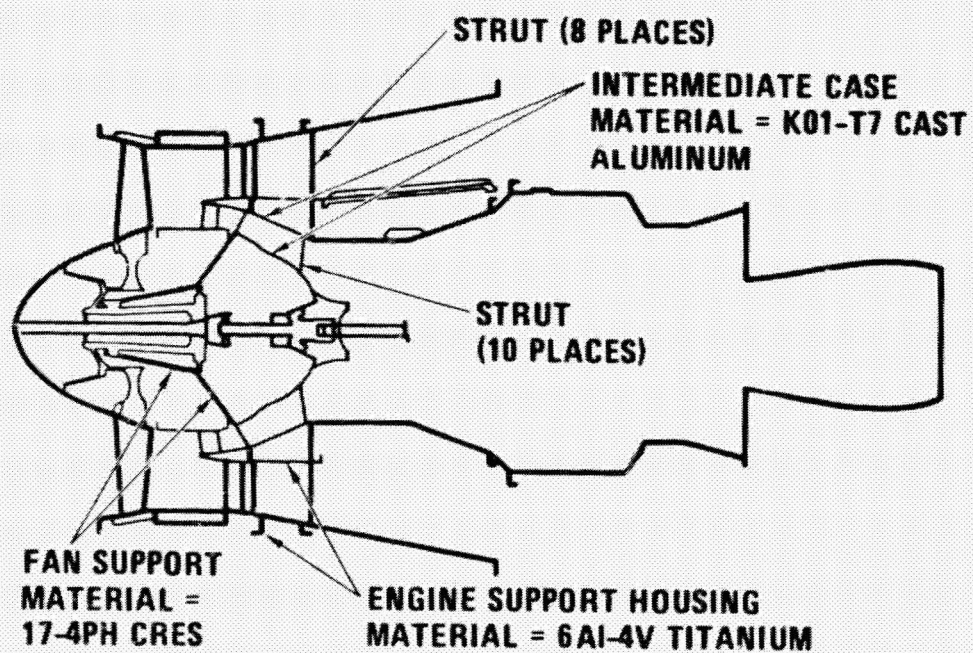


Figure 10. QCGAT Fan Support Structure.

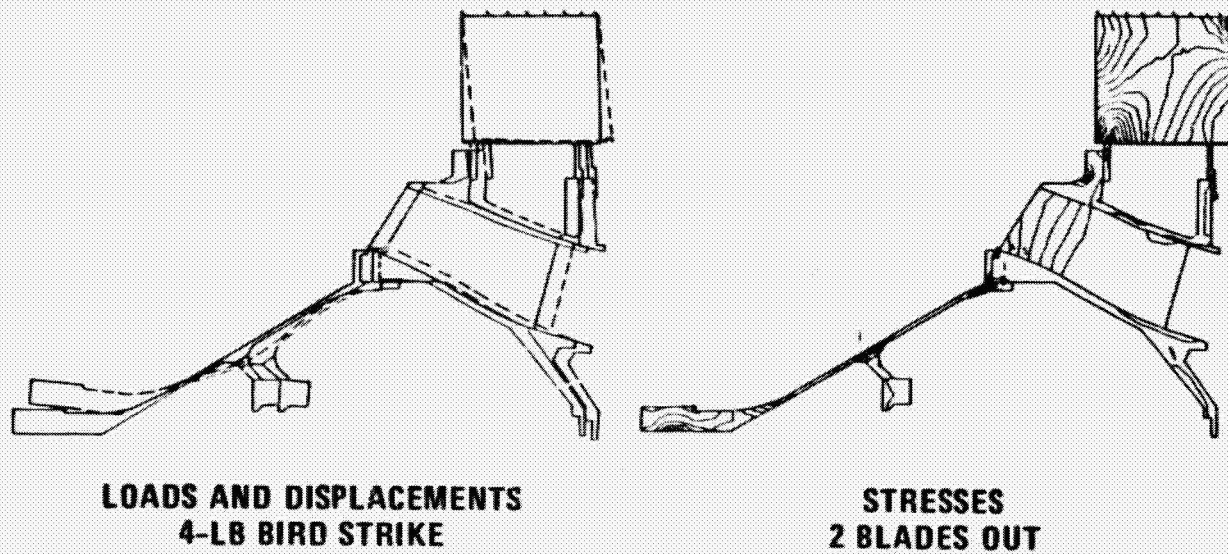


Figure 11. Fan Support Structure Stress and Loads.

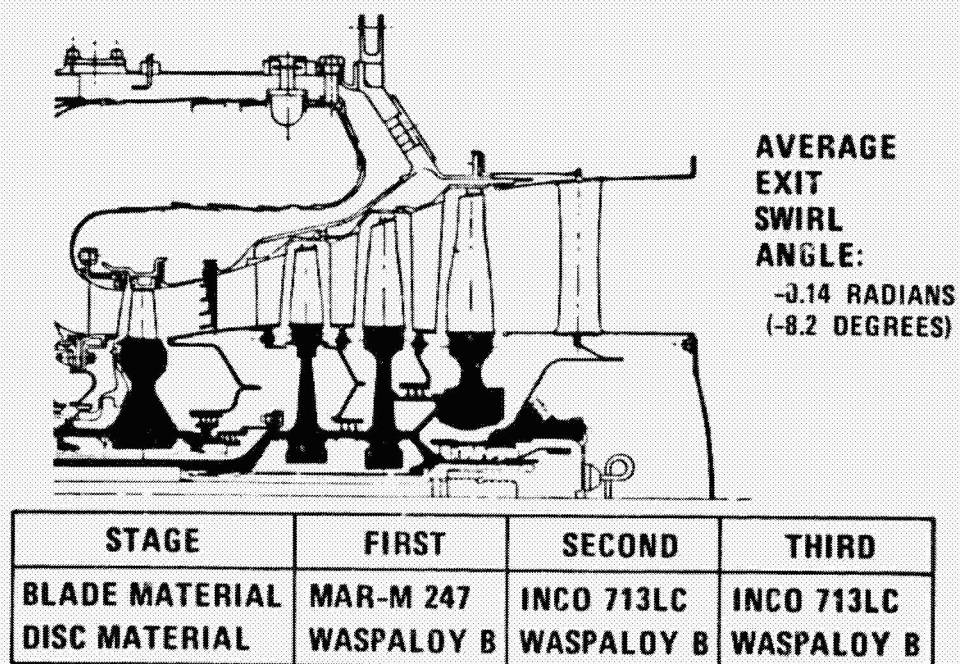


Figure 12. QCGAT Low-Pressure Turbine.



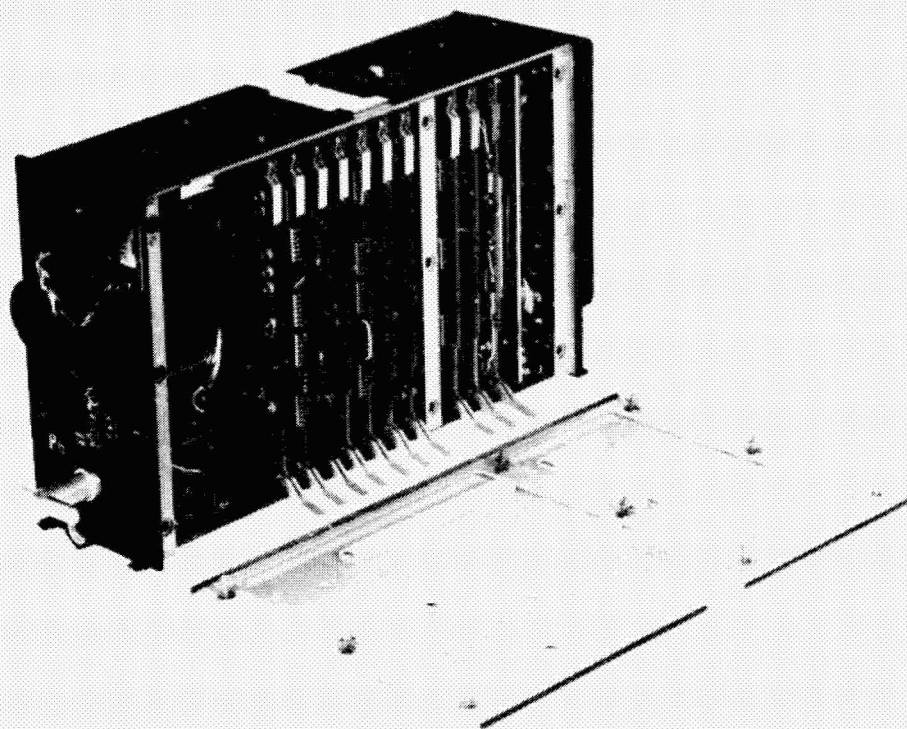


Figure 13. Electronic Fuel Control Computer.



Figure 14. QCGAT Combustor.



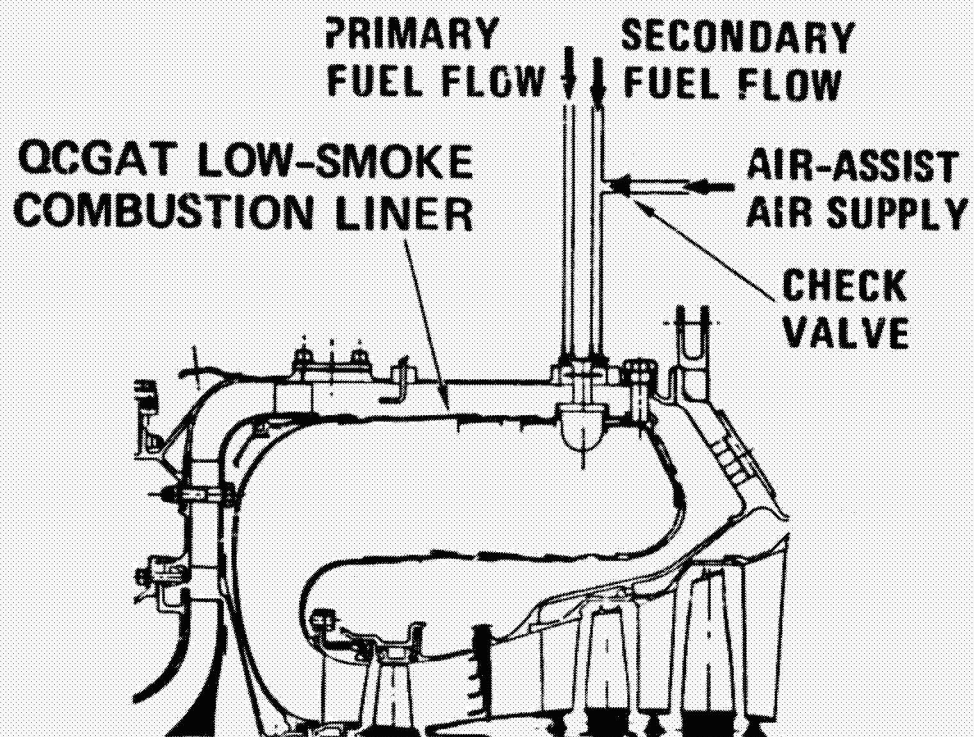


Figure 15. QCGAT Combustor Air Assist System.

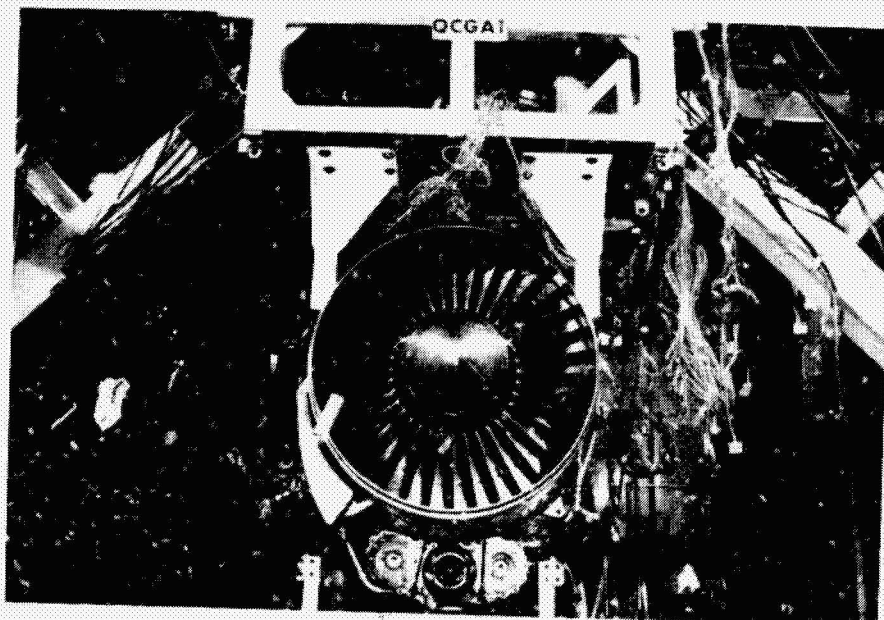


Figure 16. Front View of QCGAT Engine.

THIS PAGE IS  
OF POOR QUALITY

LENGTH	17.60 m (57.75 FT)
WING SPAN	12.95 m (42.5 FT)
HEIGHT	4.12 m (13.5 FT)
WING AREA	24.49 m <sup>2</sup> (263.6 FT <sup>2</sup> )
MAX T.O.G.W.	8,673.6 kg (19,122 LB)
MAX PAYLOAD	1,231.0 kg (2,714 LB)

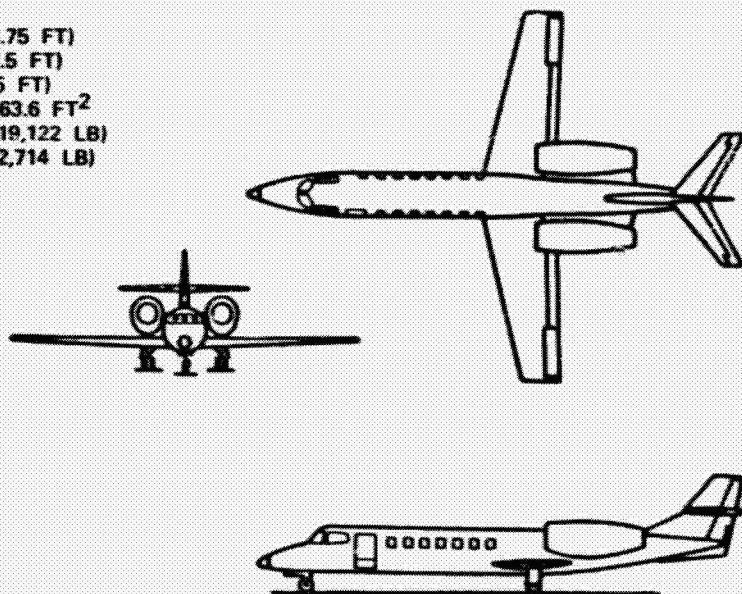


Figure 17. AiResearch QCGAT Airplane.

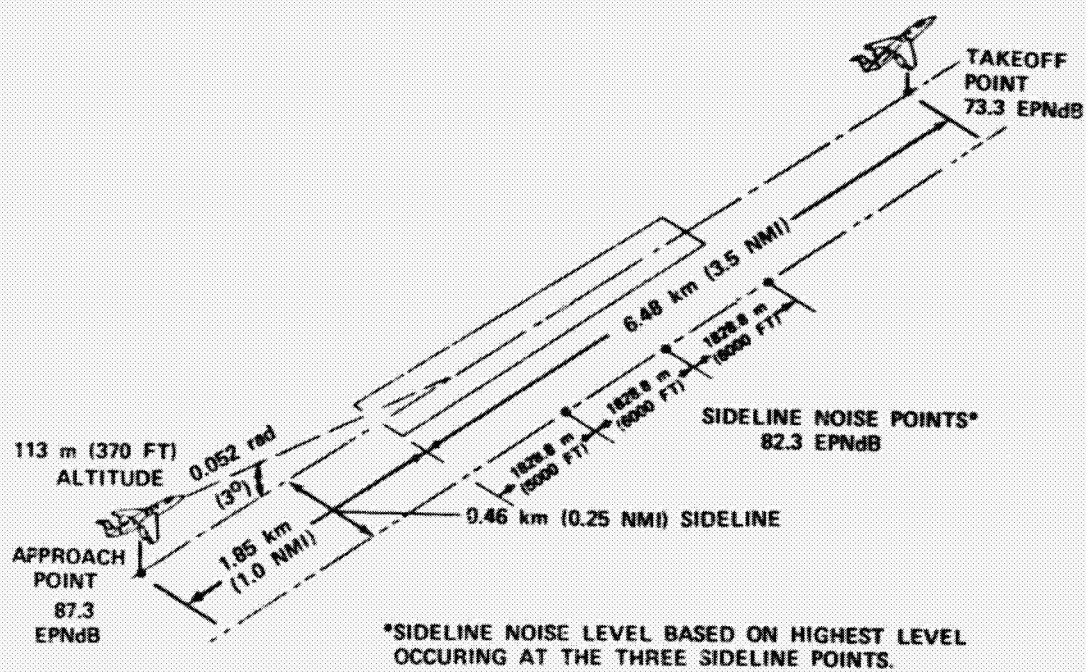


Figure 18. QCGAT Airplane Noise Goals.

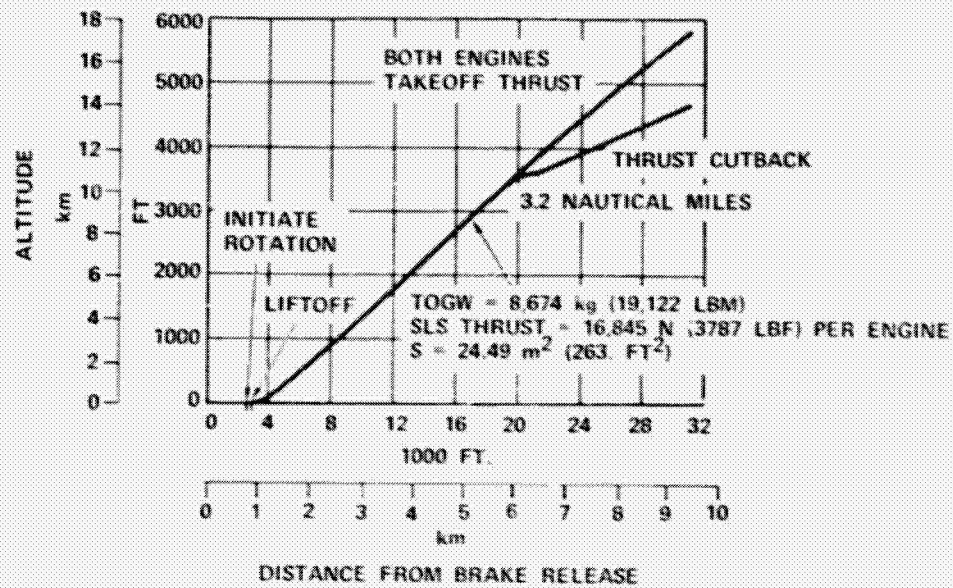


Figure 19. AiResearch QCGAT Airplane Takeoff Profile.

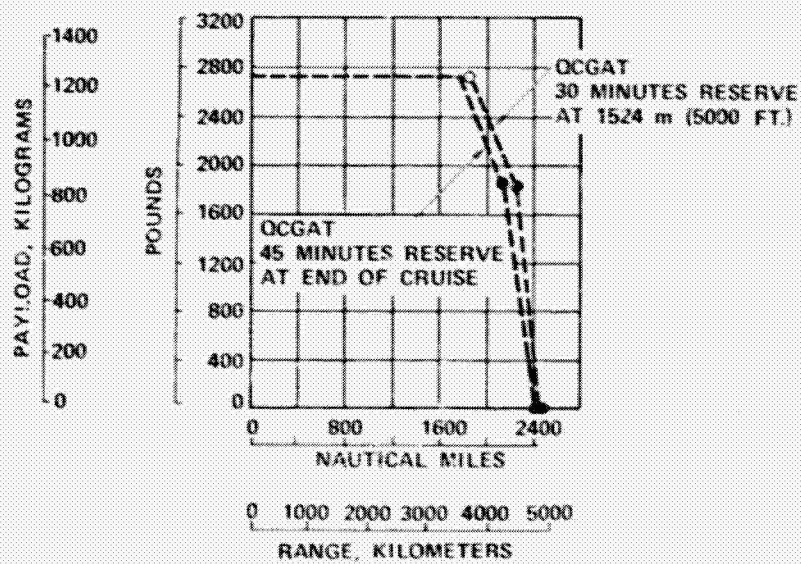


Figure 20. AiResearch QCGAT Airplane Payload versus Range.

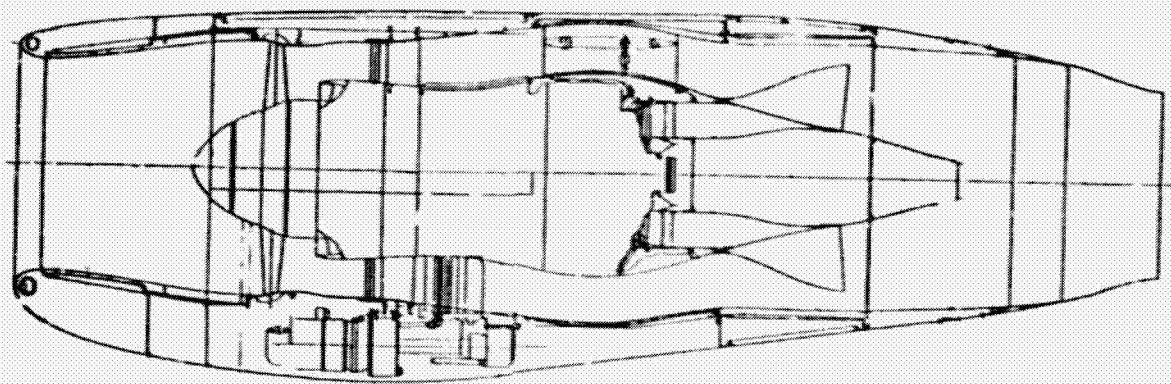


Figure 21. QCGAT Flight Nacelle.

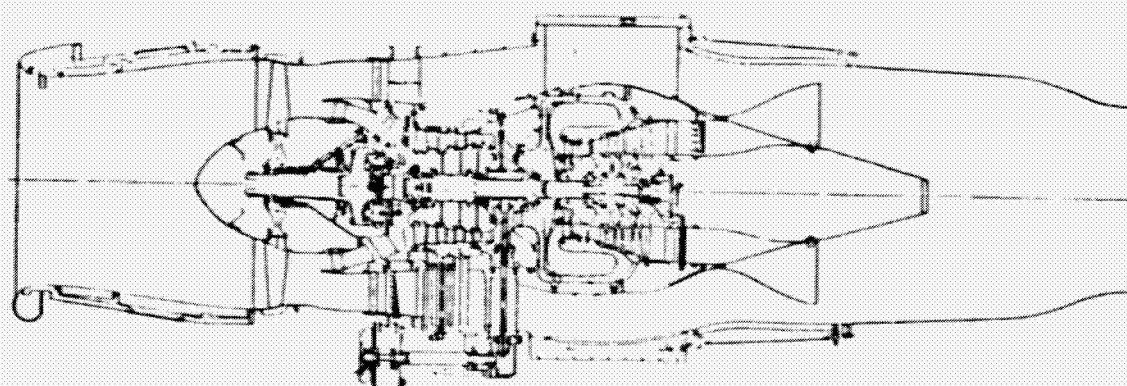


Figure 22. QCGAT Workhorse Nacelle.

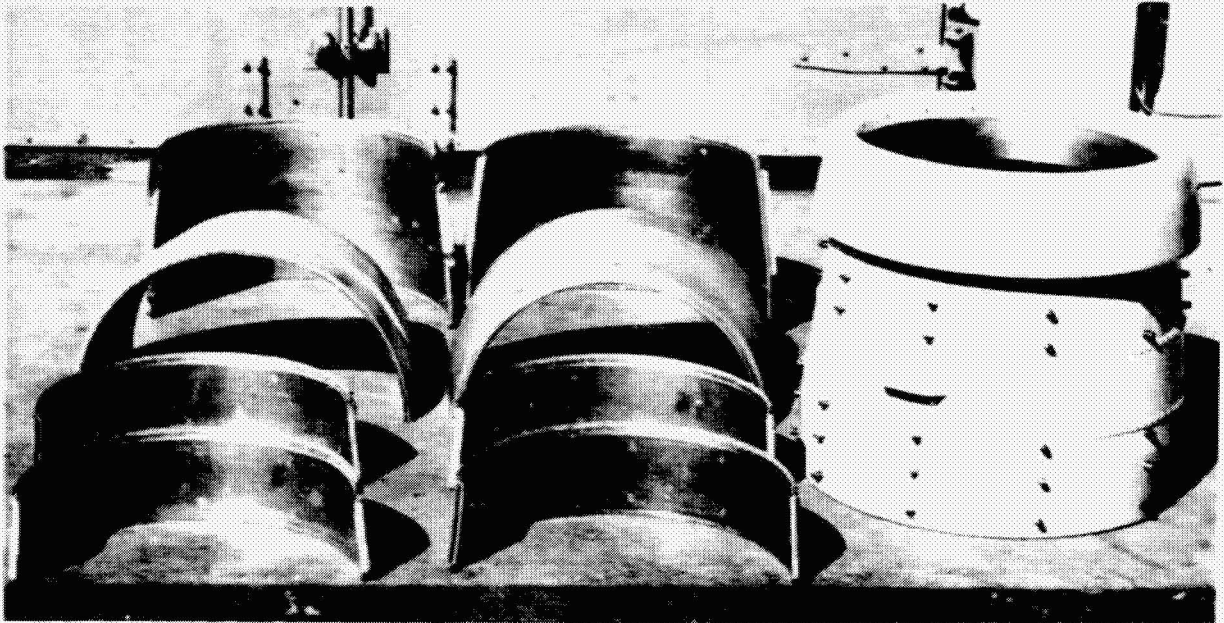


Figure 23. Inlet Barrel.

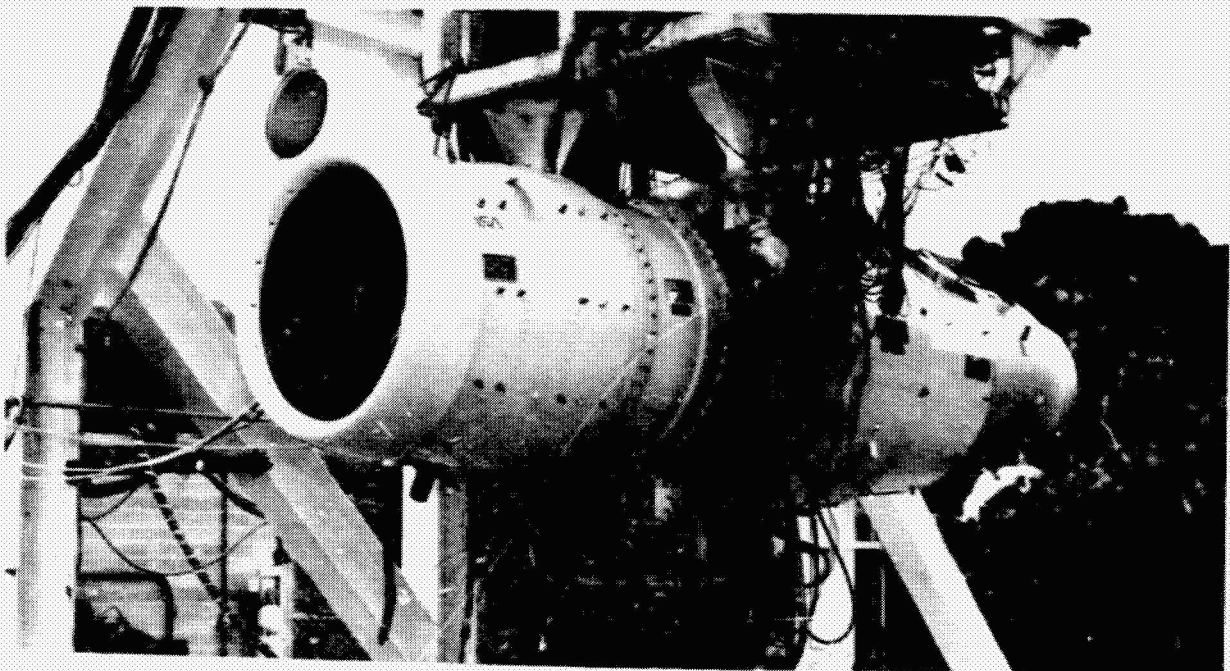


Figure 24. QCGAT Engine with Nacelle Inlet Lip.



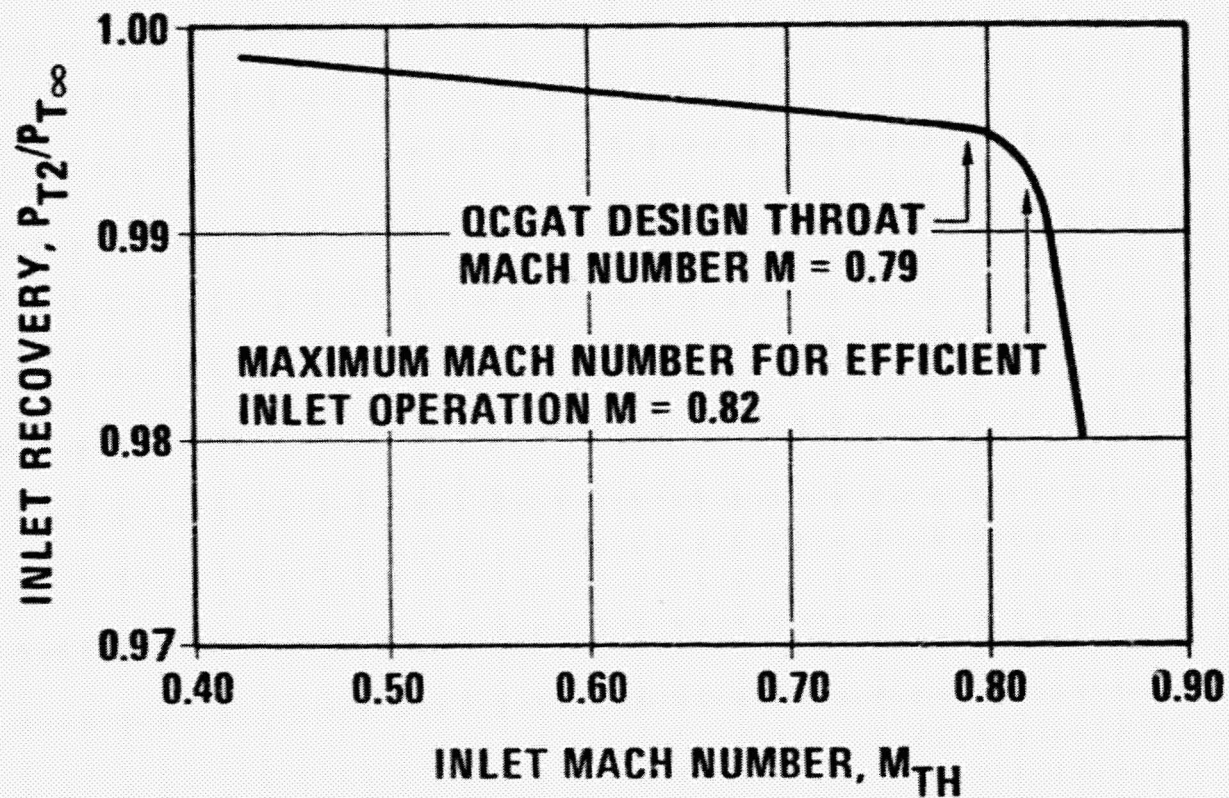


Figure 25. QCGAT Inlet Recovery Characteristics.

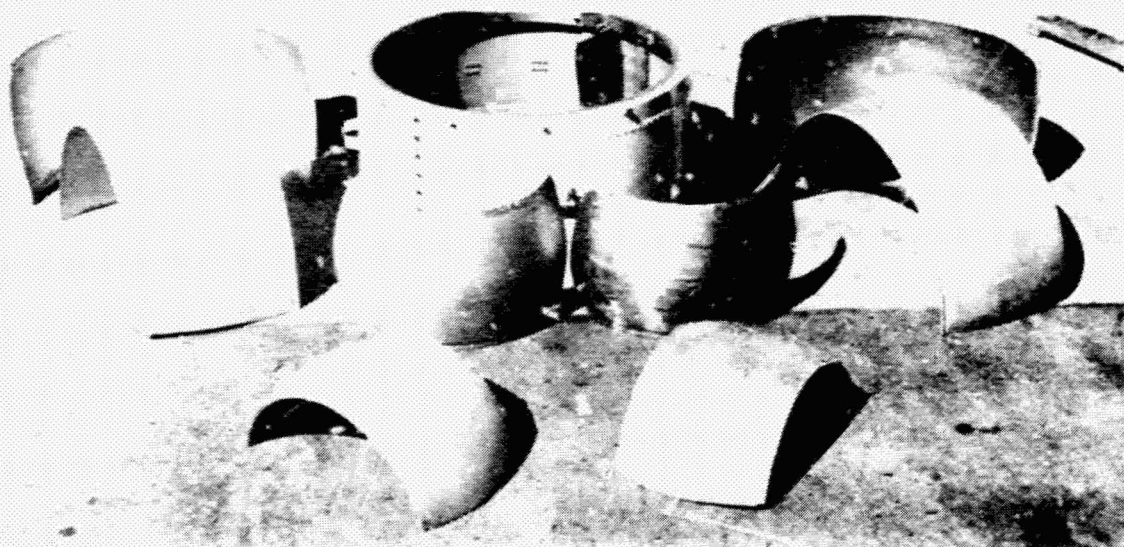


Figure 26. Workhorse Nacelle Inner and Outer Bypass Duct.

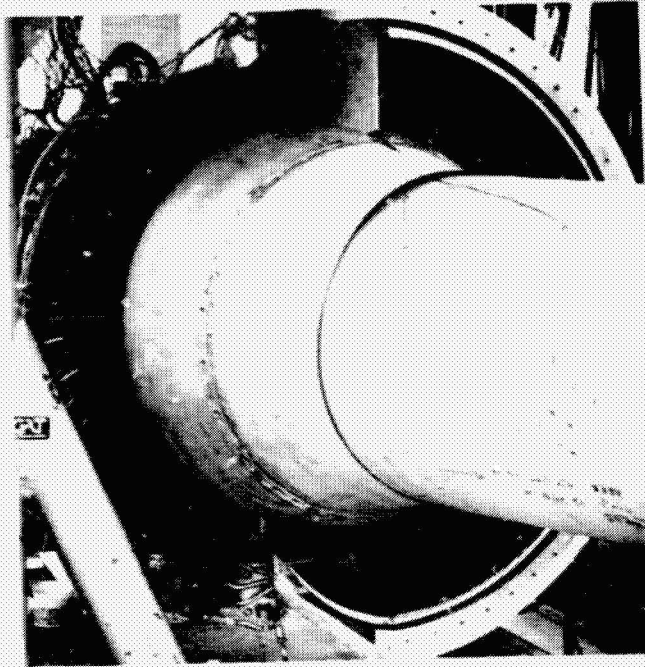


Figure 27. Workhorse Nacelle--Service Strut.

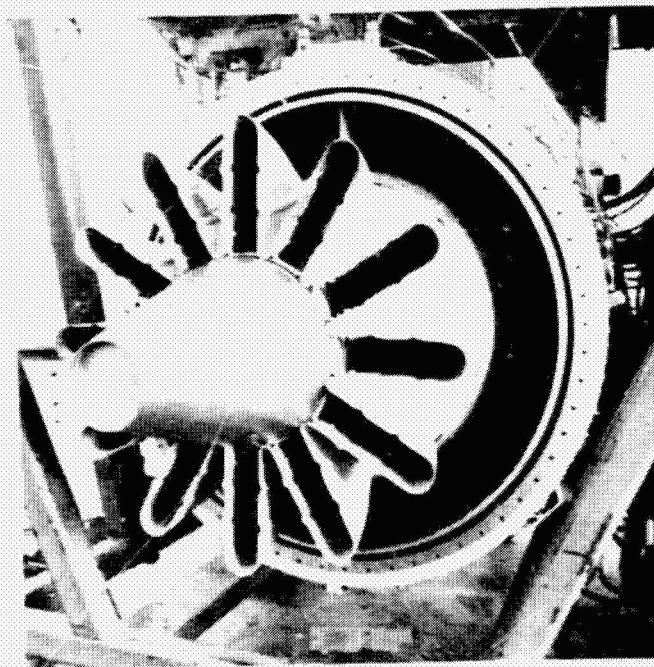


Figure 28. QCGAT Mixer Nozzle.



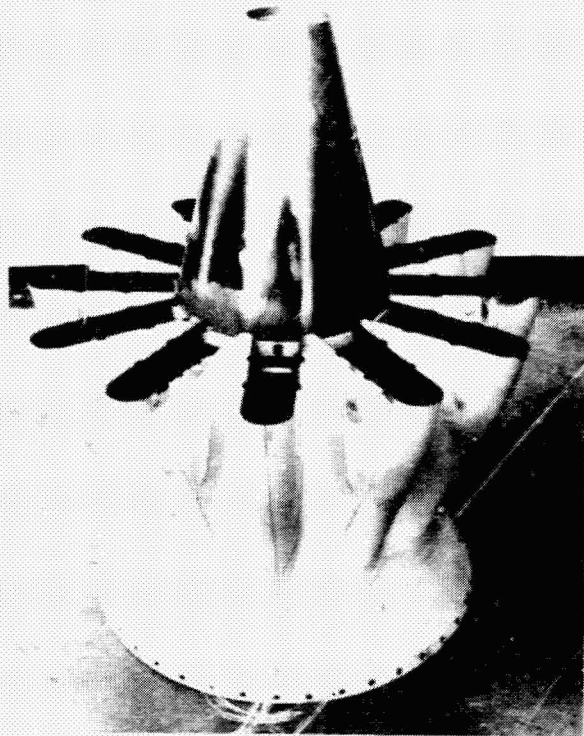


Figure 29. QCGAT Mixer Nozzle.

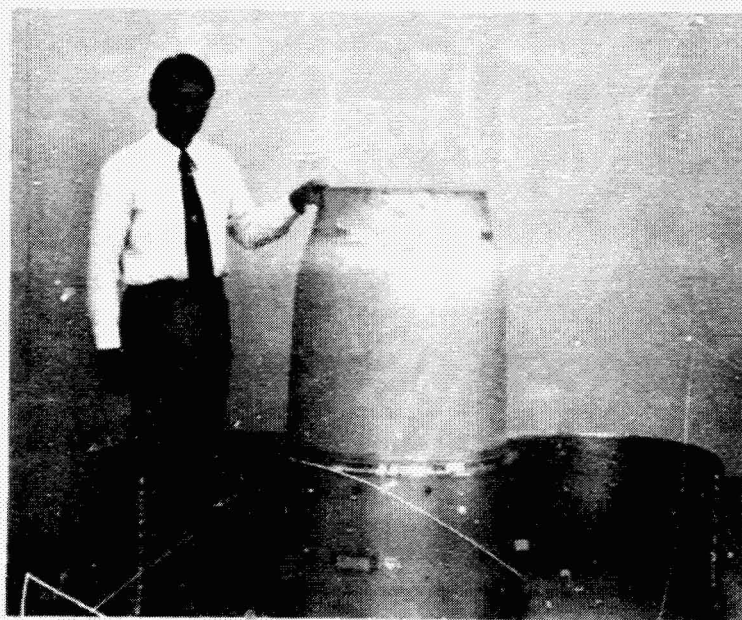


Figure 30. QCGAT Nacelle Aft Barrel and Nozzle.



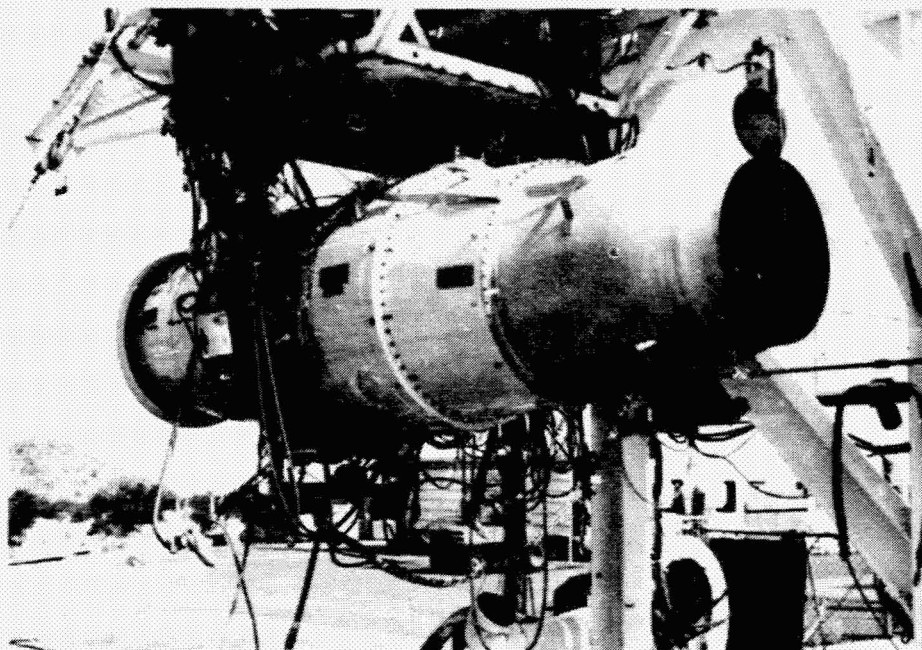


Figure 31. QCGAT Nacelle Assembly Fully  
Installed in Test Stand  
(Side View Looking Forward).

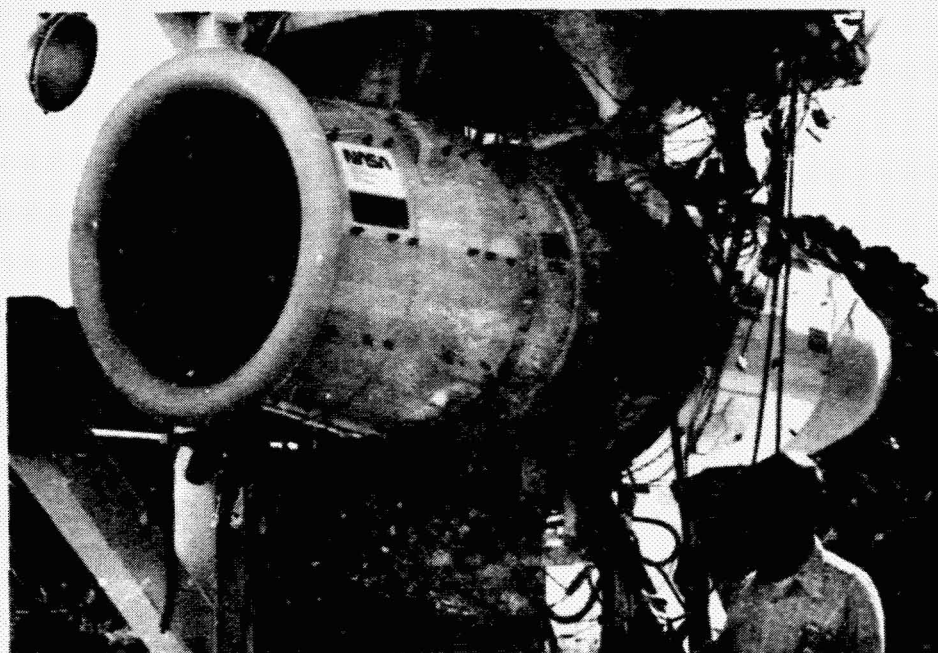


Figure 32. QCGAT Nacelle Assembly Fully  
Installed in Test Stand  
(Side View Looking Aft).

D2

N 80-22329

## AIRESEARCH QCGAT ENGINE PERFORMANCE AND EMISSIONS TESTS

William M. Norgren  
AiResearch Manufacturing Company of Arizona  
A Division of The Garrett Corporation

### SUMMARY

A Quiet, Clean, General Aviation Turbofan (QCGAT) engine and nacelle system was designed and tested by the AiResearch Manufacturing Company of Arizona under Contract to the NASA Lewis Research Center. The engine utilized the core of AiResearch Model TFE731-3 engine and incorporated numerous noise and emissions reduction features. Endurance, performance, and emissions tests were conducted on the engine prior to the acoustic test sequence. Test results proved that the engine met most of the design goals, and a teardown inspection of the engine following the tests showed the unit to be in excellent condition.

### INTRODUCTION

Performance and emission tests were conducted on a specially designed AiResearch QCGAT engine in the 17,793-N (4,000-lb) thrust class. Testing included aerodynamic performance, emission testing, and acoustic tests. This paper discusses the performance and emissions tests and inspection results of those tests.

Due to the requirement to perform a complex series of acoustic tests, as well as performance and emissions tests, two separate test areas were used. Most of the fully instrumented performance testing was conducted in the Phoenix development and qualification test cells shown in figure 1. Another series of performance comparisons were run at the AiResearch San Tan remote test site (fig. 2) to establish a baseline for the subsequent acoustic tests.

The test sequence was set up to ensure the structural integrity of the engine and to obtain baseline performance in both acoustic and hardwall installation configurations. By working around the clock, the testing phase was compressed into six weeks. The engine was subsequently refurbished, acceptance tested, and delivered on schedule. Figure 3 outlines the AiResearch test schedule. Scheduled dates were met with the cooperation of the weather, but more significantly, with the excellent support and response AiResearch received from the NASA engineering staff.

The first run of any new airplane engine is referred to as a "green run". A green run is a preliminary test to determine how well the unit runs, and to determine potential problem areas. It also establishes normal values for vibration, oil pressure, temperatures, etc. On completion of the QCGAT green run, the engine was completely disassembled, inspected, reassembled, and cycled into a 40-hour endurance test prior to beginning performance and acoustic testing.

The endurance cycle (table 1) was intended to duplicate the conditions of a jet cycle while wearing in the engine. Approximately 40 hours were run to wear in the seals, bearings, etc. This provided performance and engine conditions representative of a typical engine.

#### TEST OBJECTIVES

The primary objectives of the QCGAT test program were to demonstrate the engine capabilities required to meet the program goals, to prove the structural integrity, and to measure engine performance, emission, and acoustic characteristics. The series of tests included operation with various combinations of inlets, thrust nozzles, and acoustic treatments. Table 2 lists the performance goals for the QCGAT engine.

The 1979 emission goals set by the EPA in 1973 for the class T1 engines are listed in table 3. These standards have since been dropped by the EPA, but were maintained as QCGAT program goals. The EPA parameter (EPAP) is determined from emissions measurements made at four power settings and then added together. The time weighing factor (table 4) used in this calculation is derived from the time established by EPA as being the typical time spent in each operating mode for an airplane with T1 Class engines.

The smoke standard is established as a function of rated engine power and approximately represents the threshold for visible smoke from an engine exhaust. The standard is expressed as Smoke Number (SN), and is a function of the amount of light reflected from a sample of particulate collected on a piece of filter paper exposed to the engine exhaust. The higher the SN, the greater the amount of particulates; hence, the greater the smoke visibility. Smoke measurements were made at the same four power settings as the gaseous emission test. The highest SN of the four power settings was considered the smoke number for the engine.

#### AERODYNAMIC PERFORMANCE

A fully instrumented engine was installed in the Phoenix development and qualification test cell. Figure 4 shows the engine without the inlet attached. Figure 5 shows the engine with a calibrated bellmouth. The first tests were run with a coannular nozzle (fig. 6) to establish baseline performance against which the mixer compound nozzle (fig. 7) could be compared. In total, seven performance calibrations were made (table 5). As the test sequence progressed, the coannular nozzle was replaced with the mixer compound nozzle. The subsequent combinations calibrated the flight simulator lip and nacelle lip to the coannular nozzle and mixer compound nozzles, respectively. Before final calibration, the engine was removed from the test cell, and the hardwall fan duct was replaced with the acoustic fan duct. Since the fan duct contains

most of the accessories and plumbing, this became a relatively major change. The engine was reinstalled and final performance calibration was run.

Acoustic testing and final acceptance tests were then begun on the engine. As measured, engine performance was found to be close to what had been expected. With the exception of the fan, the new components met or exceeded their estimated performance. As anticipated, the mixer compound nozzle provided a significant improvement to the engine. Table 6 shows the results of four of the configurations compared at a constant low-pressure rotor speed ( $N_1$ ) of 1938 rad/s (18,510 rpm).

Performance Calibration 2 - Using the mixer compound nozzle, this calibration resulted in a significant increase in airflow and thrust at a constant  $N_1$ . The mixer compound nozzle has a bypass stream area that is effectively much larger than the coannular nozzle. This provided a rematch of the fan to a higher efficiency and flow. The core stream area is effectively smaller than the coannular nozzle and caused a greater low-pressure (LP) turbine discharge pressure. The engine had a greater high-pressure (HP) turbine discharge temperature because of the increased total airflow, thus requiring more power from the LP turbine. This increased power was supplied by increasing the turbine-inlet temperature, resulting in a higher HP rotor speed ( $N_2$ ) and compressor discharge pressure ( $P_{t3}$ ). The increased thrust resulted principally from the increased airflow.

Performance Calibration 5 - Using the nacelle-lip inlet with the mixer compound nozzle, the engine performance (i.e., thrust, TSFC, etc.) was similar to performance calibration 2, which also used the mixer compound nozzle.

Performance Calibration 7 - Using the nacelle-lip inlet, the mixer compound nozzle, and full acoustic treatment in the bypass duct, the acoustic treatment had little effect on the performance

of the engine as compared to calibration 5. Similar tests confirmed this conclusion.

Table 7 shows two engine configurations compared with the pre-test analytical model. Thrust, airflow, and a high-rotor speed approximated the model parameters; however, fuel flow, TSFC, and turbine discharge temperature ( $T_{t4.2}$ ) were discrepant. Analysis of this and other data showed that at maximum sea level static thrust, the fan was lower than predicted in efficiency and in airflow. This characteristic is typical of most fans in this size class wherein compromises in aerodynamic configurations imposed by design for bird strike cause unfavorable airfoil loadings with consequent decrease in efficiency and airflow capacity.

#### COMPARISON TO AERODYNAMIC GOALS

Table 8 is a comparison of the tested engine performance to the QCGAT program goals. The largest difference occurred on the uninstalled engine where the fan performance, as well as a one percent lower than estimated thrust coefficient for the coannular nozzle, resulted in a specific fuel consumption slightly over the estimate.

When the nacelle was installed, including the mixer nozzle, the sea level static TSFC is seen to be 1.4 percent over the goal. In this case, a comparison of the engine tested performance versus the analytical model showed that the mixer nozzle exceeded the estimate, while the fan performance was below the estimate.

Extrapolation of the tested data to the altitude cruise condition shows that the cruise TSFC would be below the estimated level. Since the majority of the mission fuel is consumed at cruise, it is concluded that the program fuel consumption goals were achieved and that QCGAT has demonstrated a significant advancement in engine efficiency.

## EMISSIONS TEST

Work on the combustion system design of the AiResearch QCGAT engine was conducted under separate contract for the T-1 combustor, initially selected for the program. However, schedule incompatibilities prevented direct incorporation of the T-1 combustor in the program and an interim design was used.

The combustor liner used in the QCGAT tests (fig. 8) was a modification of the production TFE731 burner. These modifications consisted of several variations, and included punched versus pierced holes. Different hole locations and sizes were incorporated for smoke number reduction. The actual burner used in the test was an experimental interim design. As a result, the temperature pattern factor was higher than desired during early testing. This condition was corrected on later burners.

Control of the gaseous emissions at idle was accomplished by supplying air to the secondary atomizers of the fuel nozzles. This air improved emissions two ways: It caused all of the fuel to pass through the primary nozzle instead of allowing a small portion of fuel to flow out of the secondaries. The air also improved the vaporization of the fuel coming out of the primary atomizer.

Figure 9 depicts the combustor air assist system. Air for the assist system was provided from a laboratory system that approximated the characteristics of engine supply air. The air was provided at a pressure and temperature that simulated compressor bleed air, and was cooled with a simple air-to-air heat exchanger in the fan duct.

The air was supplied from a laboratory compressed-air source with a supply pressure of 14.4 kPa (300 psig). After passing through a 20-micron filter, the air was heated by an electric heater to between 366K (200°F) and 422K (300°F). This simulated an air assist system where the discharge temperature from the heat of

compression for the assist air would be similar to air extracted from the boost compressor. The air then passed through a flow measuring section and was introduced to the secondary fuel line. For this test, the line was disconnected from the flow divider and the flow divider path capped. A schematic of this system is shown in figure 10.

Emissions were collected for measurement with a 24-element probe similar to the one shown in figure 11. Measurements were taken only with the coannular nozzle since there was no standard technique of measuring established for the mixer compound nozzle.

The HC and CO goals were met by using an air assist inlet pressure of 5.027 kPa (105 psid) and a temperature of 389K (240°F) at taxi idle. The results are presented in table 9. This pressure and temperature is relatively easy to obtain with a boost compressor on an aircraft engine. Lower air-assist pressure would have resulted in higher emission index values (i.e., g/kg fuel) for both HC and CO. Since more than 90 percent of the HC and CO EPAP values are contributed by the taxi-idle terms, small changes in HC and CO emission index values at that power setting resulted in significant changes in the overall EPAP values for the two pollutants.

The CO and HC emissions met the goals and  $\text{NO}_x$  was significantly reduced, but slightly above goal. The smoke number was also above goal. However, the engine showed no sign of visible smoke while operating at the test point in several tests.

#### TEARDOWN INSPECTION

After completion of all tests, the engine was completely disassembled, inspected, and refurbished prior to shipment to NASA. With almost 70 accumulated hours of testing including 70 starts, the majority of parts were in excellent condition and only three components showed any unusual signs of wear. A single sun-gear



tooth had developed a small pit as shown by the arrow under magnification in figure 12. This was later found to be the result of a flaw in the basic material from which the part was constructed. The wear pattern was judged to be good and commensurate with the time and load on the gear system.

The second discrepancy was microscopic surface cracks radiating from a couple of the special instrumentation bosses (see arrow) of the turbine plenum shown in figure 13. These were the results of torch brazing the HP compressor discharge total-pressure probes into the plenum after the part had completed the normal stress-relieving process. This is a problem that is unique to the highly instrumented test engine and would not appear on production-type plenums.

The third problem noted was a crack in the surface of one HP turbine cooled stator vane (figure 14). This crack resulted from a single hot streak in the engine. This was the result of using the experimental low-smoke combustion liner that had not been sufficiently developed at the time this test was run. This characteristic was subsequently corrected, and later production low-smoke combustor liners did not exhibit a hot streak.

All three of the problems found during teardown inspection were determined to be the result of outside factors and not the result of design deficiency. The basic engine design fulfilled design requirements. All AiResearch QCGAT engine discrepancies were removed prior to shipment to NASA.

#### TECHNICAL ACCOMPLISHMENTS

The technical accomplishments demonstrated by the AiResearch QCGAT test program are numerous. Most important is the fact that the engine met the design goals in almost every case (i.e., thrust, TSFC, emissions, etc.). Performance was slightly better than predicted for the installed configuration with the mixer compound

nozzle at the design point of 12,192 m (40,000 ft), 0.8 Mach number.

Performance of the AiResearch QCGAT engine was excellent throughout all testing. No serious mechanical malfunctions were encountered, and no significant test time was lost due to engine-related problems. Emissions were drastically reduced over similar engines, and the engine exhibited good smoke performance.

The testing of the AiResearch QCGAT engine provided evidence of the engine reliability and performance. After 82 hours and 77 starts the unit remained trouble-free. The few problems encountered were mostly associated with laboratory or cell equipment. Engine performance remained satisfactory with very little degradation as the unit accumulated time.

Though the LP turbine did not have the benefit of rig testing, it proved to meet design goals for the engine. Similarly, the full-scale mixer compound nozzle was found to perform better than anticipated.

#### CONCLUSION

As shown by the test program, the AiResearch QCGAT engine met almost all of the program goals. This is graphic evidence that the application of large engine acoustic technology to small engines as well as the application of specialized small engine technologies can result in low-noise, low-emissions, and reduced fuel consumption general aviation turbofan engines.

**TABLE 1. QCGAT ENDURANCE TEST CYCLE.**

Condition	Cycle Time (min.)
Start	-
Idle	5
Takeoff	5
Max. Continuous	10
Max. Cruise	45
Idle	5
75% Max. Cruise	5
Idle	5
Approach	5
Idle	5
Shutdown	15
Total 1 hr 45 min.	
23 Cycles = total run time of 34.5 hr	

**TABLE 2. ENGINE PERFORMANCE GOALS.**

Condition	Goals	
	Thrust N (lbf)	TSFC kg/N·h (lbm/hr/lbf)
<u>Takeoff, Sea Level Static, Standard Day:</u>		
o Uninstalled	17,513 (3,937)	0.0426 (0.418)
o With ground test nacelle and acoustic treatment and mixer compound nozzle	17,312 (3,892)	0.0431 (0.423)
<u>Design Cruise, 12,192-m (40,000-ft) Altitude, 0.8 Mach Number:</u>		
o Uninstalled	3,954 (889)	0.0775 (0.760)
o With ground test nacelle and acoustic treatment and mixer compound nozzle	4,017 (903)	0.0759 (0.744)

TABLE 3. EMISSIONS PROGRAM GOALS.

Pollutant	EPAPS Program Goal, kg/4448 N-h/cycle (lbm/1000 lbf-hr/cycle)
Unburned Hydrocarbon (HC)	0.73 (1.6)
Carbon Monoxide (CO)	4.26 (9.4)
Oxides of Nitrogen (NO <sub>x</sub> )	1.68 (3.7)
Smoke	38*

\*EPA smoke number.

TABLE 4. EMISSIONS CYCLE.

Mode	Percent Rated Power	Time Minutes
Taxi-out	Taxi-idle	19.0
Takeoff	100	.5
Climbout	90	2.5
Approach	30	4.5
Taxi-in	Taxi-idle	7.0
Total		33.5

TABLE 5. PERFORMANCE CALIBRATIONS AND  
ENGINE CONFIGURATIONS.

Calibration No.	Description
1	Bell mouth and Coannular Nozzle
2	Bell mouth and Mixer Compound Nozzle
3	Flight-Simulator Lip and Coannular Nozzle
4	Nacelle Lip and Coannular Nozzle
5	Nacelle Lip and Mixer Compound Nozzle
6	Flight-Simulator Lip and Mixer Compound Nozzle
7	Flight-Simulator Lip, Mixer Compound Nozzle and Acoustically Treated Ducts

TABLE 6. QCGAT TEST RESULTS.

Parameter	Configuration/Result by Test Number			
	1	2	5	7
Acoustic Treatment	Hardwall	Hardwall	Hardwall	Acoustic Panel
Inlet Configuration	Bellmouth	Bellmouth	Nacelle	Simulator
Exhaust Configuration	Coannular	Mixer	Mixer	Mixer
Test Parameter				
o Thrust, N(lbf)	15,413 (3,465)	16,525 (3,715)	16,903 (3,800)	16,792 (3,775)
o TSFC, kg/N-h (lbm/hr/lbf)	0.0457 (0.448)	0.0443 (0.434)	0.0437 (0.429)	0.0438 (0.430)
o High rotor speed $N_2$ , rad/s (rpm)	3,011 (28,760)	3,024 (28,880)	3,033 (28,970)	3,035 (28,990)
o HP turbine discharge temperature $T_{t4.2}$ K(°F)	1,105 (1,530)	1,119 (1,555)	1,125 (1,566)	1,119 (1,554)
o Total airflow, kg/s (lbm/sec)	60.87 (134.2)	63.55 (140.1)	-	-

TABLE 7. TEST RESULTS COMPARED TO ANALYTICAL MODEL.

Parameter	Coannular Nozzles		Mixer Compound Nozzle	
	Model	Test	Model	Test
Thrust, N(lbf)	18,055 (4,059)	18,038 (4,055)	15,813 (3,555)	16,503 (3,710)
TSFC, kg/N-h (lbm/hr/lbf)	0.0443 (0.434)	0.0457 (0.448)	0.0432 (0.424)	0.0443 (0.434)
High Rotor Speed $N_2$ , rad/s (rpm)	3,024 (28,887)	3,061 (29,240)	2,970 (29,364)	3,024 (28,880)
Low Rotor Speed $N_1$ , rad/s (rpm)	2,042 (19,500)	2,042 (19,500)	1,937 (18,500)	1,937 (18,500)
HP Disc Temperature $T_{t4.2}$ , K(°F)	1,123 (1,562)	1,141 (1,594)	1,083 (1,490)	1,119 (1,554)
Fan Nozzle Inlet Temperature $T_{t17}$ , K(°F)	327 (129.6)	330 (135.0)	322 (119.6)	324 (124.0)
Fan Nozzle Total Pressure $P_{t17}$ , N/cm <sup>2</sup> (psi)	14.58 (21.15)	14.60 (21.18)	14.38 (20.85)	14.08 (20.42)
Engine Total Airflow $\dot{W}_{AT}$ , kg/s (lb/sec)	65.6 (144.6)	65.3 (143.9)	62.3 (137.4)	63.5 (140.1)

TABLE 8. QCGAT TEST RESULTS VERSUS PERFORMANCE GOALS.

Flight Condition	THRUST, N (lbf)		%	TSFC, kg/N-h (lbm/hr/lbf)		%
	Goal	Test		Goal	Test	
Sea level, static, standard day, uninstalled (Bellmouth and Coannular Nozzle)	17,513 (3,937)	17,513 (3,937)	0	0.0426 (0.418)	0.0459 (0.450)	+7.7
Sea level, static, standard day, installed (nacelle lip and mixer compound nozzle)	17,312 (3,892)	17,312 (3,892)	0	0.0431 (0.423)	0.0437 (0.429)	+1.4
Design cruise (extrapolated from static data), Mach 0.8, 12,192m, (40,000 ft), installed (nacelle lip and mixer compound nozzle)	5,016 (903)	4,016 (903)	0	0.0759 (0.744)	0.0756 (0.741)	-0.4

TABLE 9. EMISSIONS TEST RESULTS VERSUS PROGRAM GOALS.

Pollutant	EPAPS, kg/4448 N-h/cycle (lbm/1000 lbf-hr/cycle)	
	Program Goal	Test Result
Unburned Hydrocarbon (HC)	0.73 (1.6)	0.73 (1.6)
Carbon Monoxide (C))	4.26 (9.4)	3.63 (8.0)
Oxides of Nitrogen (NO <sub>x</sub> )	1.68 (3.7)	2.09 (4.6)
Smoke	38*	42*
*EPA Smoke number.		

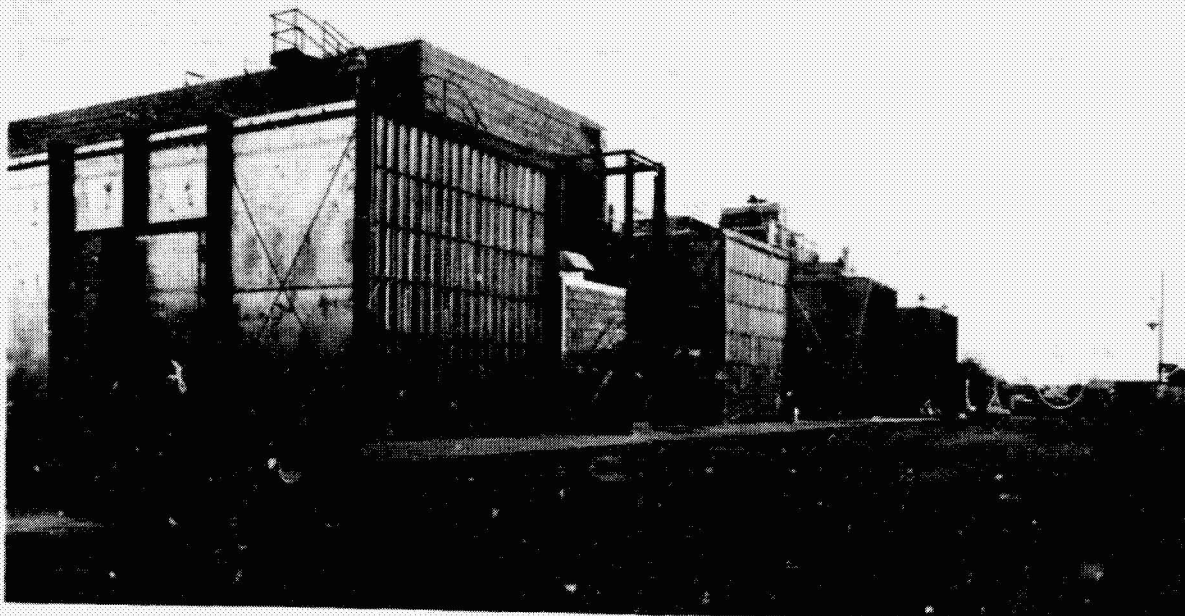


Figure 1. Development and Qualification Test Area.

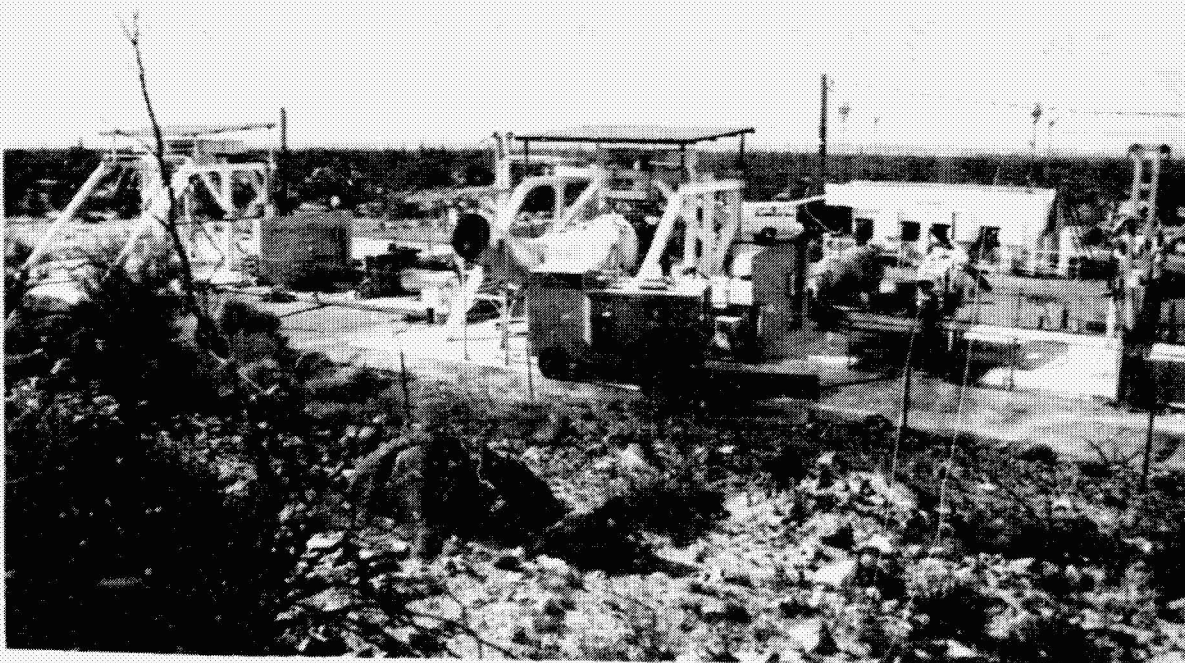


Figure 2. San Tan Test Center.

	OCT	NOV	DEC	JAN
GREEN RUN	■			
ENDURANCE	■			
PERFORMANCE		■		
ACOUSTIC		■		
ACCEPTANCE TEST				■

Figure 3. QCGAT Engine Test Schedule.

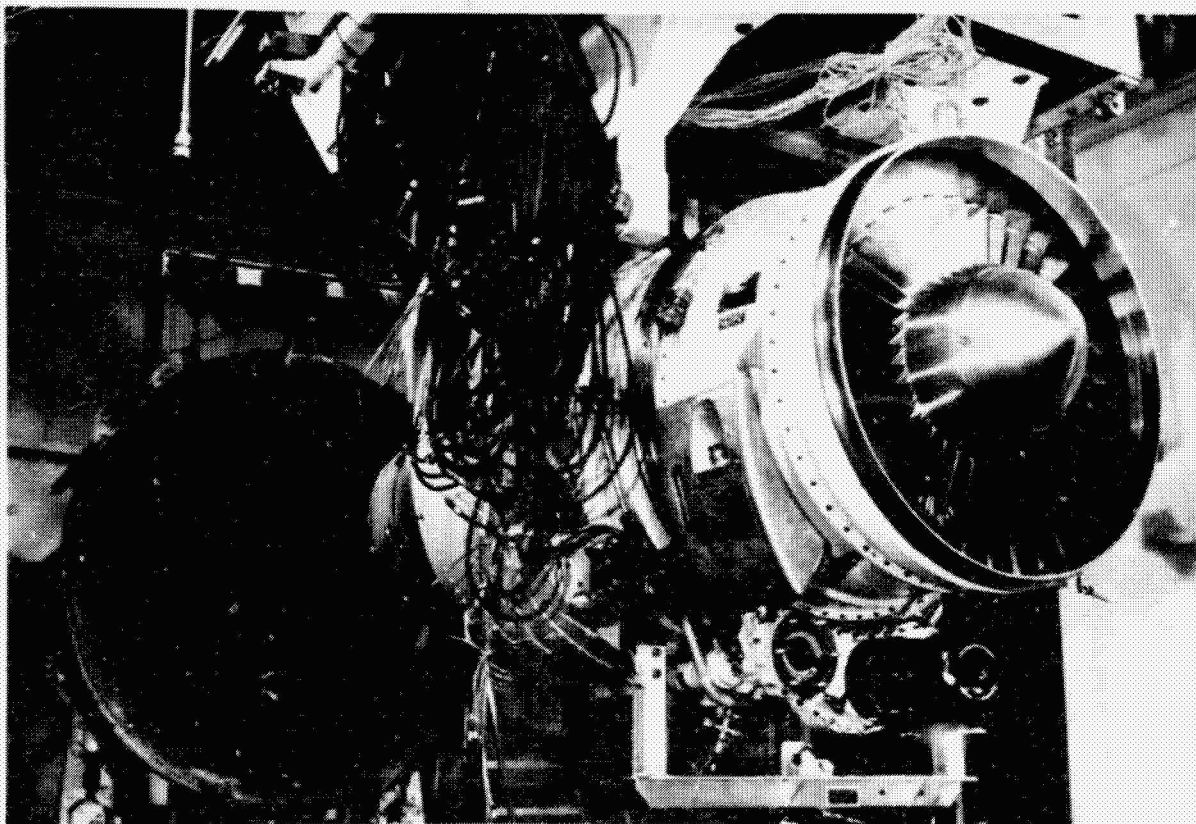


Figure 4. Instrumented QCGAT Engine.



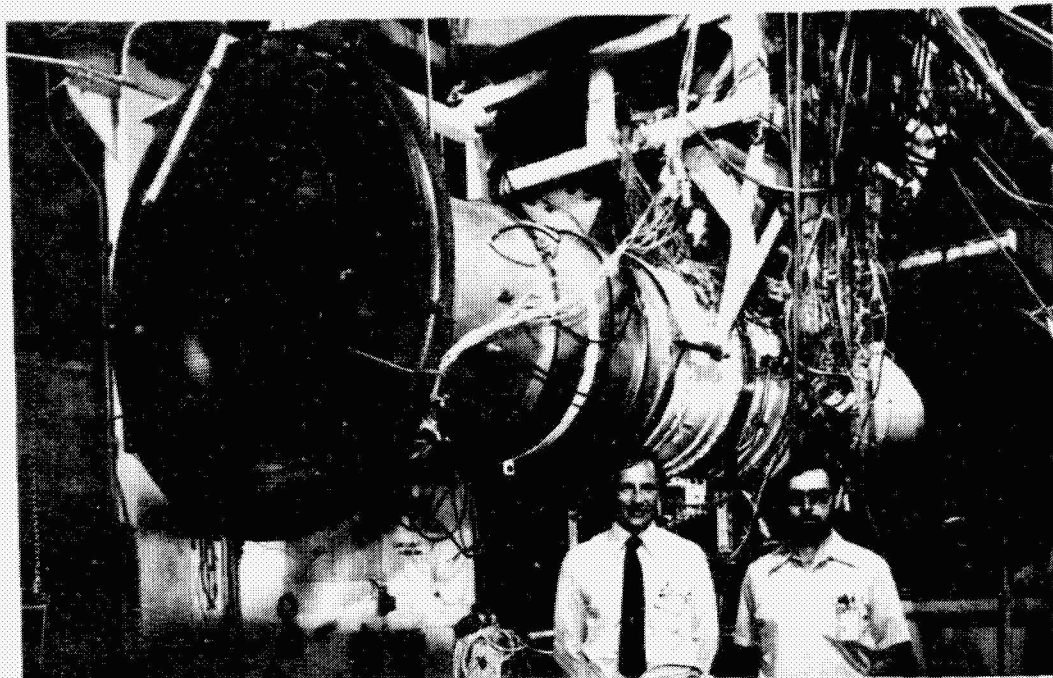


Figure 5. Engine with Calibrated Bellmouth.

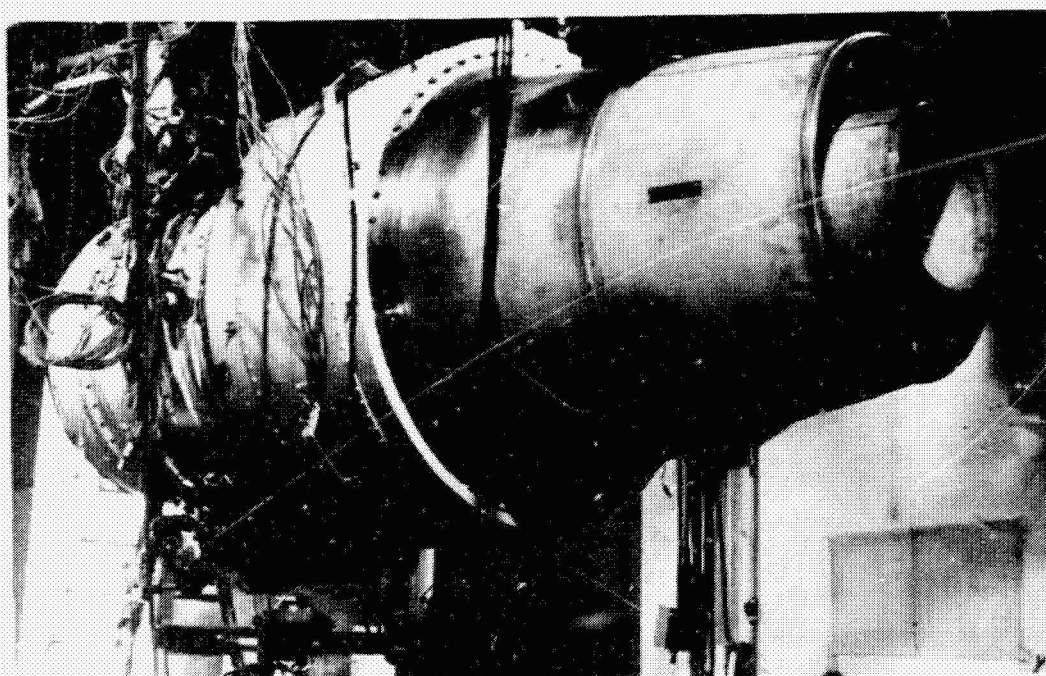


Figure 6. Engine with Coannular Nozzle.

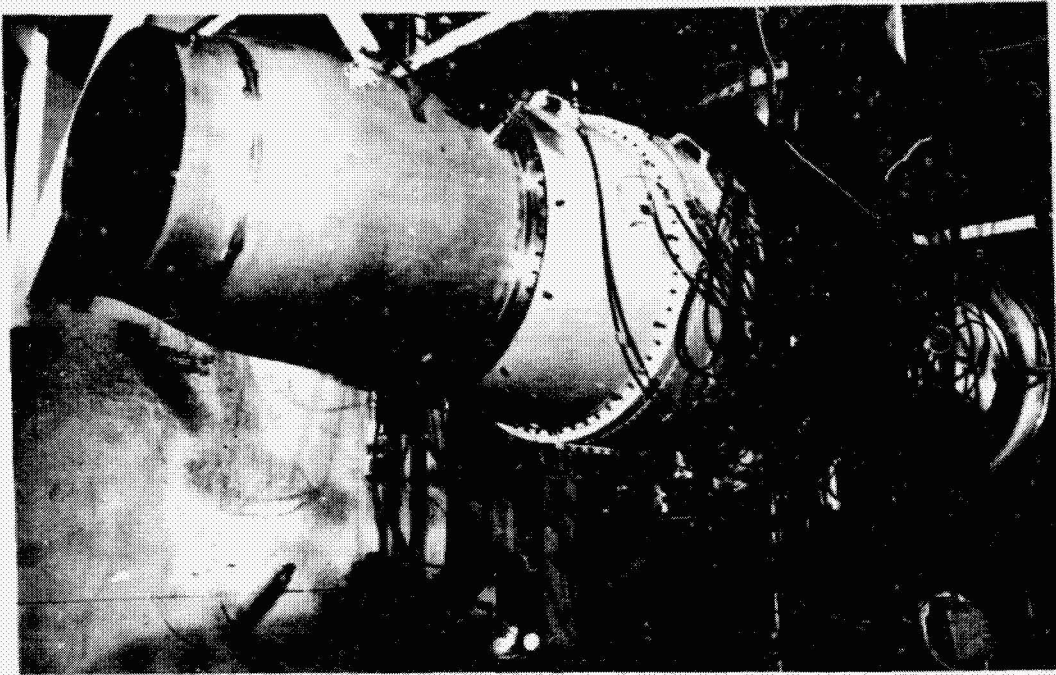


Figure 7. Engine with Mixer Compound Nozzle.



Figure 8. QCGAT Combustor.

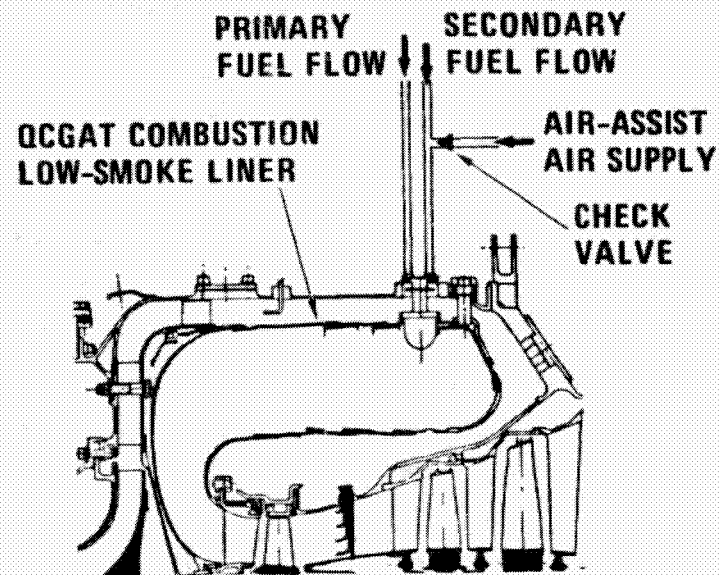


Figure 9. QCGAT Combustor Air Assist System.

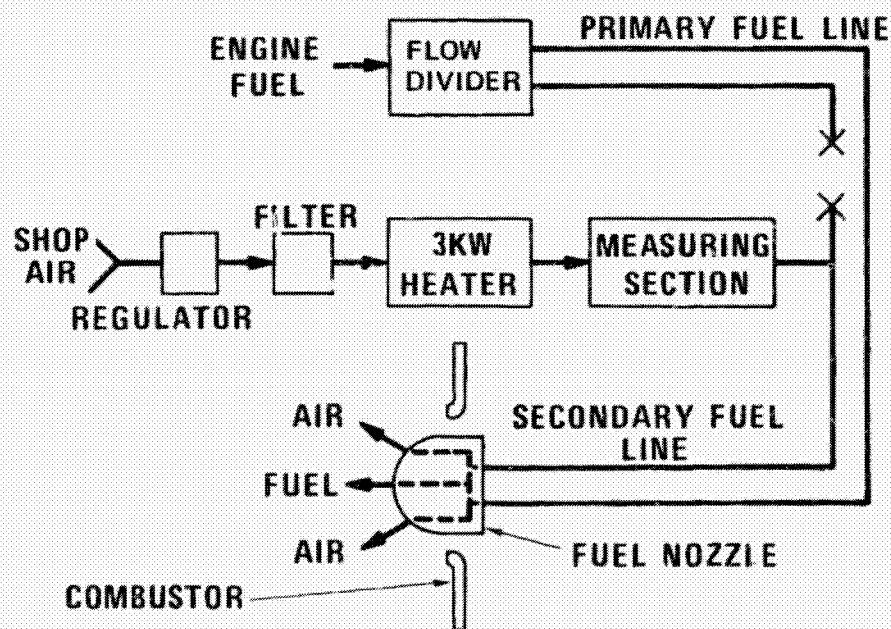


Figure 10. Air Assist System Schematic.

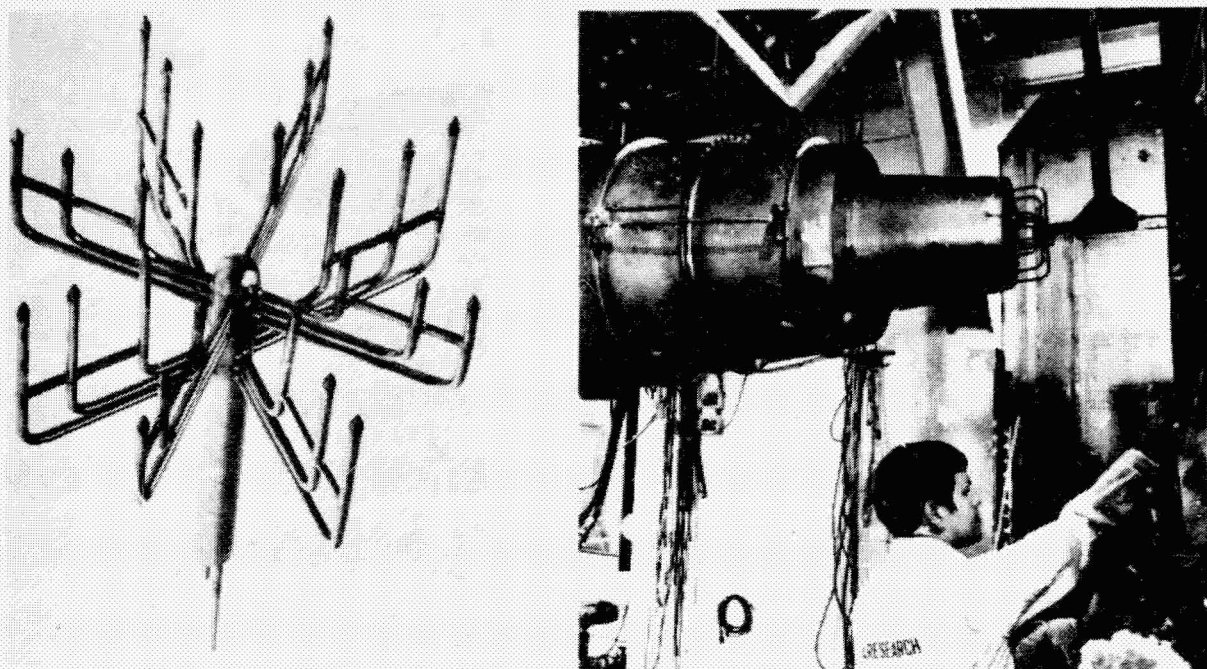


Figure 11. Emissions Probe

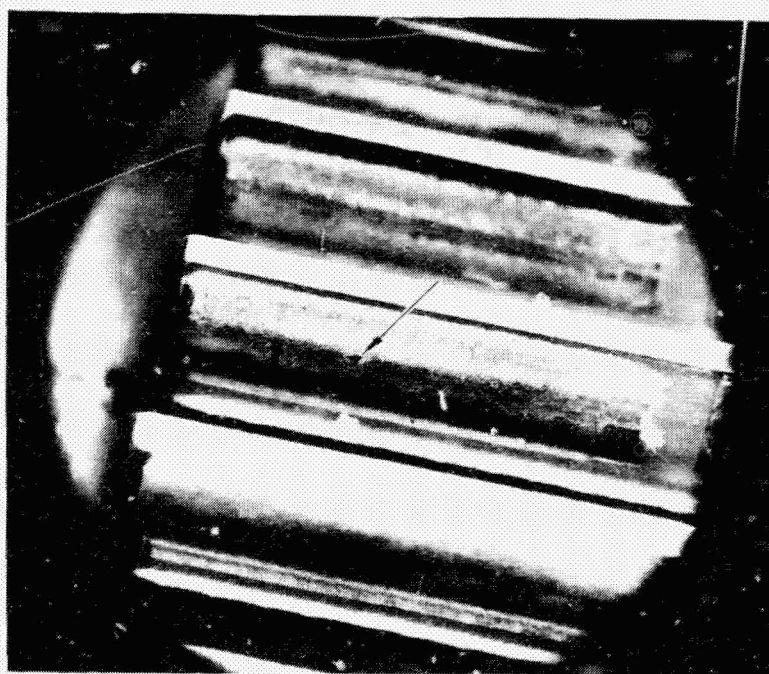


Figure 12. Sun Gear Tooth Wear.





Figure 13. Turbine Plenum and Special Instrumentation.

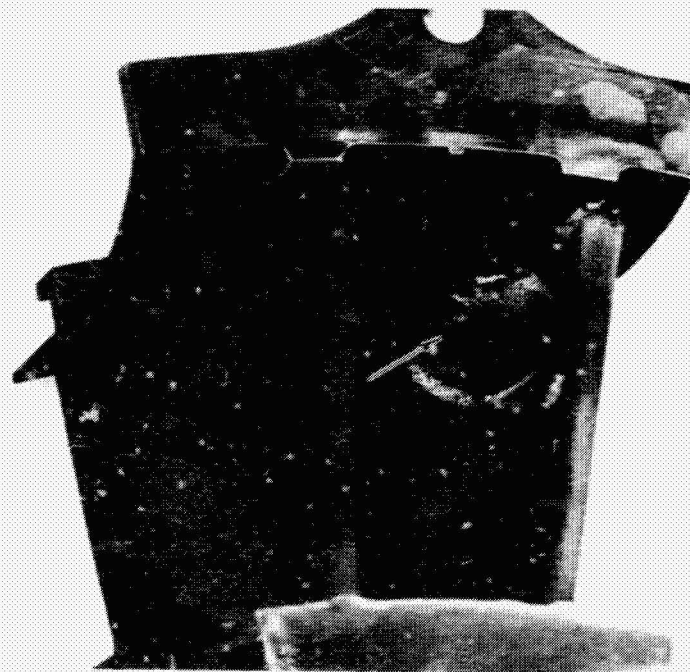


Figure 14. HP Turbine Stator Segment.

1 N80-22330

## AIRESEARCH QCGAT ENGINE - ACOUSTIC TEST RESULTS

Larry S. Kisner  
AiResearch Manufacturing Company of Arizona  
A Division of The Garrett Corporation

### SUMMARY

The noise levels of the AiResearch Quiet, Clean, General Aviation Turbofan (QCGAT) engine were measured in ground static noise tests. The static noise levels were found to be markedly lower than the demonstrably quiet AiResearch Model TFE731 engine. The measured QCGAT noise levels were correlated with analytical noise-source predictions to derive free-field component noise predictions. These component noise sources were used to predict the QCGAT flyover noise levels at FAR Part 36 conditions. The predicted flyover noise levels are about 10 decibels lower than the current quietest business jets.

### INTRODUCTION

This paper describes the acoustic design, static noise test results, noise source correlation analyses, and flyover noise predictions for the AiResearch QCGAT engine.

### NOISE GOALS

NASA specified goals for the QCGAT engine at the FAR Part 36 sideline, takeoff, and approach conditions as a function of maximum takeoff gross weight. The noise goals for the twin-engine airplane postulated in this program are shown in figure 1. The maximum takeoff gross weight for the airplane defined by AiResearch is 8674 kg (19,122 lb). The specific noise goals at the FAR Part 36 conditions are:

Takeoff (without cutback):	73.3 EPNdB
Sideline (1500 ft):	82.3 EPNdB
Approach:	87.3 EPNdB

These levels are significantly below the existing FAR Part 36 Stage 3 noise limits.

#### NOISE OBJECTIVES

To achieve the program noise objectives, large turbofan engine noise-reduction technology was applied to the smaller AiResearch general aviation engine. The objectives accomplished during the program were as follows:

- o The engine was defined, and the cycle conditions were determined to provide low noise-generation features.
- o An acoustically treated nacelle was designed and fabricated.
- o The ground static engine noise levels were measured for several configurations, establishing an engine baseline and demonstrating the effectiveness of the acoustical design features.
- o Static noise-source correlations were developed, and component noise spectra with adjustments for flight effects were used to estimate flyover noise levels in compliance with QCGAT noise goals.

#### ACOUSTIC DESIGN FEATURES

The acoustic design effort emphasized minimizing noise generation at the source and maximizing noise reduction achieved through



judicious application of nacelle acoustic treatment in the fan inlet and exhaust ducts. Acoustic duct liner configurations were designed to balance the noise suppression at takeoff, sideline, and approach condition, providing the broadest possible attenuation bandwidth without sacrificing significant attenuation from optimum at any one of the three operating conditions.

The major acoustic features of the QCGAT engine are illustrated in figure 2. Noise-reduction technology was applied to the two major noise sources, the fan and the jet. The fan noise-source reduction features included the following: elimination of inlet guide vanes, low tip speed and pressure ratio, single-stage fan, a large rotor to stator spacing of 2.12 rotor chords, and a large number of bypass and core stators to cut-off rotor-stator interaction tones. The jet noise-reduction features included low fan discharge and primary jet-exhaust velocities, and a 12-lobe mixer compound exhaust nozzle.

The nacelle acoustic treatment design selected for the QCGAT engine consisted of a single-cavity system used in series with different cavity depths in the axial direction and where possible equivalent depths on opposing walls. A broadband resonator was constructed from aluminum perforated sheet bonded to a 0.95-cm (3/8-in.) all-aluminum honeycomb backing because of its structural ruggedness, low cost, and known acoustic performance.

A schematic of the acoustic liner installation is shown in figure 3. The inlet-wall treatments--sections  $A_1$ ,  $A_2$ , and B--were tuned to provide primary suppression at the FAR Part 36 sideline condition with a length equal to 2.16-cm (0.85-in.) mean inlet diameter. The fan discharge duct treatments--sections 1, 2, and 3--were tuned to provide balanced attenuation between sideline and approach conditions, and have an effective total length equal to 5.4 times the average duct height.

Final optimization of the engine and nacelle exhaust liner design was completed using a computer program based upon the axisymmetric mode theory of Minner and Rice (ref. 1). To achieve optimum attenuation, the required cavity depths and face sheet open areas were computed.

The design procedure for the inlet liners was based upon the recent multimodal duct treatment analysis developed at NASA-Lewis by Rice (ref. 2 through 5). The inlet liners were tuned to attenuate modes that radiate energy at larger angles from the inlet axis, thus reducing sideline noise radiation.

The major design characteristics of the inlet and exhaust liners are shown in table 1. The inlet sections  $A_1$ ,  $A_2$ , and B have backing depths of 1.83 cm (0.72 in.), 2.8 cm (1.1 in.), and 1.35 cm (0.53 in.), respectively. Open areas range from 5.8 to 14.2 percent. The inlet liners are tuned for the sideline condition in the 1000- to 2500-Hz range. The total length of the inlet treatment is 59.9 cm (23.6 in.). The exhaust liner configuration is 123.7-cm (48.7-in.) long and was tuned for approach conditions where fan exhaust noise is dominant in the 2000- to 4000-Hz frequency range.

#### ENGINE NOISE TESTS

The QCGAT engine was installed at the AiResearch San Tan test facility (fig. 4) for acoustical measurements. Noise data was taken at specified engine load conditions from ground idle to take-off power to determine the untreated engine noise levels, the noise reduction attained with various combinations of acoustic treatments, and the noise reduction achieved with a mixer compound exhaust nozzle. This data was used to determine the static noise levels for use in predicting flyover noise levels.

A schematic of the acoustic test setup at San Tan is shown in figure 5. Data was taken on a 30.4-meter (100-foot) radius at every 10 degrees, from 10 degrees to 160 degrees, for each configuration and load condition. The microphones are B&K, 1.270-cm (0.5-in.) diameter, Type 4133, mounted for normal incidence of the direct sound field and were located 1.5 meters (5 ft) above the ground.

In addition to the 16 far-field microphone locations, 6 internal noise measurements were made with three 0.3175-cm (0.125-in.) condensor microphones and three 0.6350-cm (0.25-in.) condensor infinite tube systems (fig. 6). Two 0.3175-cm (0.125-in.) microphones were installed flush mounted with the duct surface in the fan inlet nacelle, one near the fan tip, the other near the nacelle inlet. Another 0.32-cm (0.125-in.) microphone was located in the exhaust duct near the mixer exit plane. The 0.6350-cm (0.25-in.) infinite tube systems were located in the low-pressure (LP) turbine rear-bearing support area aft of the LP turbine, near the mixer exit plane, and near the exhaust nozzle exit plane. The internal noise measurements were recorded simultaneously with the far-field measurements. This data was recorded for 2 minutes at each condition to allow coherence analysis between the internal and far-field noise.

All tests were conducted within the recommended environmental limits of wind speed, temperature, and relative humidity. The tests were conducted in November 1978 from midnight to 6 a.m. when the wind was calm and ambient noise levels were low. The temperature ranged from 280K (44°F) to 286K (56°F) and the relative humidity ranged from 70 to 85 percent during the tests.

The key acoustic parameters for the simulated static takeoff and approach conditions are shown in table 2. At takeoff, the engine operates at 16,098 N (3619 lb) of thrust with a fan pressure

ratio of 1.41. The fan relative tip Mach number is supersonic at 1.17, and the mixer exhaust velocity is only 258 m/s (846 ft/sec). The fan-blade passing frequency is 5236 Hz, in a low annoyance range.

At approach, the fan operates subsonically at a relative tip Mach number of 0.79. The fan pressure ratio is 1.18, and the fan-blade passing frequency is 3638 Hz. The thrust level at approach, static condition, is 7019 N (1578 lb) with a lower mixer exhaust velocity of 166 m/s (545 ft/sec).

Table 3 shows the same key acoustic parameters of the FAR Part 36 flight conditions of takeoff, sideline, and approach. Tables 2 and 3 show a comparison between static and flight fan relative tip Mach numbers and jet velocities. At takeoff, the QCGAT airplane reaches an altitude of 1151 m (3776 ft) above measurement location. At this altitude, thrust is at 12,869 N (2893 lb), with a fan pressure ratio of 1.44. The fan relative tip Mach number is 1.22, and blade passing frequency is 5495 Hz. Mixer exhaust velocity is 285 m/s (936 ft/sec). At approach, the fan relative tip Mach number is 0.78, the fan pressure ratio is 1.16, and the blade passing frequency is 3677 Hz. At a thrust level of 4639 N (1043 lb), the mixer exhaust velocity is 176 m/s (577 ft/sec). Sideline acoustic parameters are essentially the same as takeoff acoustic parameters.

Acoustic data was taken for the seven test configurations listed in table 4. The fully treated engine was tested first with both mixer compound and coannular exhaust nozzle systems (configurations 1 and 2). With the mixer nozzle installed, acoustic panels were systematically replaced with hardwall panels in configurations 3 and 4 until the fully hardwall configuration 5 was attained. Configuration 6 was the hardwall engine with the nacelle lip instead of the flight-simulator lip. The final configuration, configuration 7, consisted of the hardwall nacelle, flight-simulator lip, and coannular nozzle. Comparisons were made between

the treated and hardwall with mixer compound nozzle (configuration 1 versus 5), treated and hardwall with coannular nozzle (configuration 2 versus 7), mixer compound versus coannular nozzle with treated nacelle (configuration 1 versus 2), and mixer compound versus coannular nozzle with hardwall nacelle (configuration 5 versus 7).

#### GROUND REFLECTION ANALYSIS

Before the ground static acoustic data can be compared or used to predict flyover noise levels, the data must be corrected for FAA 248K (77°F) and 70-percent relative humidity, and for ground reflection. The ground reflection problem is illustrated in figure 7. A wave reflected from the ground interferes with the direct sound wave at the receiver. Depending on ground acoustic impedance, the reflected wave can diminish or enhance the sound intensity at the microphone due to a phase-angle shift. The type of soil at the San Tan site consists of a random combination of hard-packed clay, sand, and decomposed granite particles; no known data exists on the impedance of this soil.

The terrain around San Tan Cell No. 5 slopes downward from the engine pad so that the ground locations upon which the microphones were pole-mounted are at an average elevation of 1.13 m (3.7 ft) below that of the engine pad. Thus, the QCGAT engine, which was mounted 2.29 m (7.5-ft) above the engine pad was, on the average, 3.41 m (11.2-ft) above the ground, relative to the microphone locations.

The impedance correlation procedure, based upon references 6 through 13, is outlined as follows:

1. Measured data at takeoff condition at all three microphone heights and all 16 array angles were used to obtain final AiResearch San Tan soil impedance estimates.

2. Using previously published data, an initial normalized impedance array was assumed ( $R/\rho c$  and  $X/\rho c$  versus frequency).
3. The excess attenuation,  $A_e$ , was computed for each microphone height, and corrected sound pressure level ( $SPL_c$ ) spectra was determined.
4. A 3-way difference scheme was used to calculate the differences between the three corrected spectra at each 1/3-octave band.
5. Iterations were performed on the values of  $R/\rho c$  and  $X/\rho c$  until all differences approached zero (steps 3 and 4, above). The convergence criteria was based upon the values of average differences at each 1/3-octave band. When reasonable values of impedance failed to provide convergence at a 1/3-octave band, the two microphone heights having a frequency furthest away from a null frequency were used and convergence was obtained.
6. Inasmuch as convergence criteria was based on average differences, observations of individual differences were then made, and minor adjustments to the normalized impedance were performed, thus establishing the final impedance values given in figure 8.
7. Excess attenuation 1/3-octave band spectra was computed for the three microphone heights, based on final ground impedance estimates.
8.  $A_e$  spectra was then applied to the measured data for all three microphone heights. Comparison plots were prepared at representative array angles.

9. Acoustic measurements were also made at the three microphone heights for approach. To check the relative validity of the ground-reflection correction procedure, the  $A_e$  spectra was applied to the approach data and comparisons of the corrected data again were made. The correlation of the approach corrected data was consistent with that of the takeoff corrected data.

An example of the 'as measured' spectra from each microphone is shown in figure 9. Large differences between the pole-mounted and ground microphones were observed from 200 to 4000 Hz. Figure 10 shows the same data with the excess attenuation corrections applied. Overall, good agreement was obtained for all microphones and all 1/3-octave band frequencies.

An example of the final result of applying the ground correction is shown in figure 11. The free-field levels were reduced in the low frequency range, and the ground dip in the 400- through 500-Hz range was decreased, resulting in a smooth spectral curve. Little or no change occurred at the high frequencies.

#### ACOUSTIC COMPARISONS OF STATIC DATA

The corrected data for each acoustic configuration tested was compared to establish trends and illustrate the level comparisons with the equivalent Model TFE731-3 takeoff and approach static data. A comparison between the hardwall coannular configuration--the loudest QCGAT configuration--with the Model TFE731-3 at takeoff condition is shown in figure 12. The QCGAT tone-corrected perceived noise levels (PNLT) are considerably lower than the Model TFE731-3 primarily because of the lower exhaust velocity, even though the QCGAT engine produces 8-percent more thrust. This difference is shown more vividly in the 1/3-octave spectral plot at 150 degrees from the inlet axis (fig. 13). This shows clearly a



reduction in jet noise, as well as in the high frequency fan tone. Similar reductions were achieved at approach.

Further reductions in noise were achieved with the QCGAT mixer compound nozzle as shown in figure 14. At the same 150-degree angle, the QCGAT coannular and mixer compound nozzle configurations are compared at takeoff static condition. At 200 Hz, the mixer is about 7 dB quieter than the coannular nozzle. Note, however, that there are peaks at 1600 and 2500 Hz with the mixer being 2- to 3-dB higher at these frequencies. The source of these tones were investigated in detail, including some cross-correlation analysis at NASA. The results revealed a high correlation between internal core noise and the far-field noise levels at certain discrete frequencies, primarily centered about 200 Hz and 2500 Hz. This led to the development of a new noise-source correlation attributing this excess noise to core noise.

Final reductions in noise were attained with the acoustically treated mixer configuration as shown in figure 15. Also shown in figure 15 is the treated versus hardwall mixer data at approach condition and at 50 degrees from the fan inlet. A broad range of frequencies from 630 Hz to 6300 Hz are attenuated due to the inlet treatment. The same configurations are compared at 120 degrees in the aft quadrant in figure 16. Here, larger attenuations approaching 10 dB are observed, but in a narrower frequency band. The actual attenuations in the lower frequencies cannot be observed because of the masking by jet and core noise sources.

The treatment was effective in reducing the sideline noise levels as shown in figure 17. The treated versus hardwall coannular configurations at 90 degrees and at approach condition are shown. The blade passing tone at 4000 Hz is attenuated nearly 7 dB.

In summarizing ground static data comparisons, the AiResearch QCGAT engine demonstrated significantly quieter noise levels than the currently quiet Model TFE731 business-jet engine, and showed that application of noise reduction technology, such as a mixer compound exhaust system and acoustically treated fan inlet and exhaust nacelles, achieved even lower noise levels.

#### NOISE SOURCE CORRELATIONS

A primary objective of the QCGAT acoustic program was to determine flyover noise levels based on static engine data, and to demonstrate that these noise levels meet the program goals, which are set well below current technology airplane. To accomplish this objective, a methodology was derived to predict the major component noise sources, adjust the individual sources from static to flight conditions, and predict the noise source flyover levels.

The analytical tools used by AiResearch to predict QCGAT engine noise sources are presented in table 5. The prediction procedures for fan noise, jet noise, and core noise were based upon the NASA Aircraft Noise Prediction Program (ANOPP) recommended procedures with empirical modifications based upon previous AiResearch experience.

A comparison of predicted noise sources based upon these prediction procedures and measured data is shown in figure 18. The fan noise prediction agrees well with the measured data with a slight overprediction of the blade passing harmonic. However, the measured low-frequency noise, particularly from 160 Hz to 2500 Hz, is higher than predicted jet and core noise. In order to account for this, it is necessary to make assumptions for the apportionment of the jet and core to the total noise signature. Two approaches were used and are shown in table 6: The first model attributed the difference between predicted and measured noise in the 50- to

2500-Hz frequency range to the jet. Jet noise was adjusted accordingly on an average delta basis. The second model assumed jet noise predictions were valid, and adjusted the core noise to exactly match the measured data. Both models adjusted the fan and turbine noise to exactly match the measured levels in the appropriate frequency range.

Figure 19 shows an example of the jet-noise-dominated correlation for the softwall mixer at 120 degrees and at takeoff condition. The average difference from 50 to 2000 Hz is applied at each frequency to produce a modified jet noise prediction that fits through the data. In this model, core noise is predicted to be well below the jet noise at the takeoff condition. Above 2000 Hz, the fan noise is adjusted to fit the data. Turbine noise contributions were unimportant except at frequencies above 12,500 Hz, which was out of the range of interest for flyover noise calculations. Similar correlations were made for each far-field angle from 10 to 160 degrees.

The same set of acoustic data is shown in figure 20, with the core-noise-dominated model predictions. The jet noise prediction is considerably below the measured data. The fan noise was determined to be the difference between the measured total and the predicted sum of jet, core, and turbine noise in the 3150- to 10,000-Hz bands. The total of all the noise sources exactly matched the measured data.

#### FLYOVER PREDICTION PROCEDURE

Calculated flyover noise levels for the QCGAT engine were based upon the adjusted noise sources obtained from correlating the predicted and measured static noise data. A block diagram of this procedure is given in figure 21. The measured corrected static noise data and the predicted noise sources are fed into a program

called NASADELTA. The program compares and computes difference spectra for each noise source at each engine operating condition. The noise source prediction program is again used to predict the noise levels at the FAR Part 36 flyover conditions. These predictions are adjusted by applying the appropriate correction spectra determined from the static data.

The adjusted noise sources are taken to flight conditions with corrections for distance, atmospheric attenuation, jet relative velocity and dynamic amplification effects, fan inlet cleanup, doppler effects, wing shielding, and ground effects. The adjusted sources are "flown" along a prescribed flight path using the GTENFLY program.

For each flyover condition -- takeoff, sideline, and approach-- the SPL, PNL, and PNL<sup>T</sup> were calculated for each 1/2 second of the flight trajectory. The duration time, duration correction, effective perceived noise level (EPNL) for each source, and the total EPNL were calculated in accordance to FAR Part 36 procedures.

#### FLYOVER NOISE CALIBRATION WITH MEASURED LEARJET DATA

Based upon static data comparisons, the QCGAT engine demonstrated substantial reductions in noise levels compared to the quiet AiResearch Model TFE731-2 engine that powers the Learjet 35/36 airplane. This airplane is certified to be 5 EPNdB below the FAR Part 36 Stage 3 noise limits. However, the initial flyover predictions, based upon the previously described methodology, yielded QCGAT noise levels comparable to measured Learjet flyover noise levels. This methodology was thus used to predict the Learjet flyover noise levels to determine its validity.

A comparison of the predicted and measured in-flight spectra for the Learjet 35/36 based upon the excess jet noise model, is

shown in figure 22. Although the static noise predictions for the TFE731 engine were adjusted to match measured static noise levels, when taken to flight, the predictions are higher than the measured flyover levels. The overprediction occurs primarily in the low frequency, jet-dominated range. At the takeoff condition, the predicted flyover EPNL is 88.7 EPNdB compared to a measured value of 84 EPNdB. Similar differences between predicted and measured flyover noise levels were observed at approach and sideline conditions.

A second set of flyover predictions for the Learjet certification tests were made based upon the core noise dominated model, as shown in figure 23. The predicted levels are even higher than those based upon the previous model. This is primarily due to the assumed dominance of core noise to which beneficial in-flight reductions are not applied.

Table 7 compares the predicted and measured total EPNL for takeoff and approach conditions for both prediction models. The individual noise sources cannot be compared directly because the flight-path position for which the maximum tone-corrected perceived noise level occurs is not the same, resulting in a different composition of noise sources. This shift in location of the maximum PNLT prevents the use of an in-flight spectral difference array to match the measured flyover data. The spectral correction model was abandoned in favor of a single EPNL correction delta applied to each source. An outline of this calibration procedure used to match the measured Learjet data and to predict the QCGAT flyover noise levels is shown in figure 24. The final QCGAT flyover noise levels reflect measured flyover data and are thus considered realistic.

## QCGAT FLYOVER NOISE PREDICTIONS

The unadjusted and adjusted flyover noise predictions for the QCGAT engine are given in table 8. Each method, with appropriate adjustments for differences between predicted and measured Learjet levels yielded similar results, indicating that the QCGAT engine is 2.0 EPNdB below the sideline noise goal, 4.6 to 5.4 EPNdB below the approach noise goal, and from 0.2 EPNdB below to 1.4 EPNdB above the takeoff noise goal.

## ACOUSTIC ANALYSIS SUMMARY

A summary of the acoustic analysis performed in the QCGAT program is outlined below:

- o A ground reflection analysis was developed to correct the measured static noise levels to free-field.
- o Flyover noise predictions were made based upon two separate noise source correlation models: One assumed jet noise to be the dominant generating mechanism; the other assumed core noise to be responsible for excess noise above the known jet noise levels.
- o Both prediction models were applied to the TFE731-2-powered Learjet and were found to overpredict the measured in-flight levels, although the ground static data was used to calibrate the predictions.
- o The overpredictions occurred primarily in the low-frequency range where both jet and core noise are expected to be important.

- o Final flyover predictions were made with adjustments for the differences between predicted and measured Learjet noise levels.

#### SUMMARY OF ACOUSTIC RESULTS

The noise reduction technology demonstrated in the QCGAT Program is summarized below:

- o The QCGAT softwall nacelle/mixer configuration demonstrated a 9.3 EPNdB reduction in flyover noise at takeoff condition, a 10.3 EPNdB reduction at approach, and a 7.7 EPNdB reduction at sideline condition compared to the TFE731-2-powered Learjet.
- o The QCGAT hardwall nacelle coannular nozzle configuration was shown to be 4.2 EPNdB quieter than the Learjet at takeoff condition, although the QCGAT airplane takeoff gross weight is 963 kg (2122 lb) greater than the Learjet.
- o The QCGAT hardwall nacelle/mixer was 3.5 EPNdB quieter at takeoff and 4.3 EPNdB quieter at approach than the QCGAT hardwall nacelle/coannular nozzle.
- o The QCGAT softwall nacelle/mixer was quieter than the QCGAT hardwall nacelle/mixer by 2.6 EPNdB and 1.3 EPNdB at approach and takeoff conditions, respectively.

The final QCGAT flyover noise levels based upon the excess core noise model are shown in figures 25 through 27, compared with the FAR Part 36 noise limits, the QCGAT noise goals, and the measured Learjet flyover levels.



## CONCLUSIONS

The measured static noise levels of the AiResearch QCGAT engine were markedly lower than the demonstrably quiet TFE731 engine. The following conclusions were made:

- o Based on the excess jet noise correlation model, the QCGAT engine met or bettered the program noise goals.
- o Based on the excess core noise correlation, the QCGAT engine met or bettered the program noise goals both for hardwall and softwall nacelle configurations at sideline and approach conditions, and was slightly above the take-off noise goal.

The AiResearch QCGAT program has demonstrated that it is possible to design quiet engines for general aviation aircraft.

## REFERENCES

1. Minner, G.L. and Rice, E.J., "Computer Method for Design of Acoustic Liners for Turbofan Engines," NASA TM X-3317, 1976.
2. Rice, E.J., "Acoustic Liner Optimum Impedance for Spinning Modes with Mode Cut-Off Ratio as the Design Criterion," AIAA Paper 76-516, Palo Alto, CA., 1976.
3. Rice, E.J., "Inlet Noise Suppressor Design Method Based Upon the Distribution of Acoustic Power with Mode Cut-Off Ratio," Paper Presented at the Thirteenth Annual Meeting of the Society of Engineering Science, Inc., George Washington University, 1976.
4. Rice, E.J., "Multimodal Far-Field Acoustic Radiation Pattern - An Approximate Equation," AIAA Paper 77-1281, presented in Atlanta Georgia, October, 1977.
5. Rice, E.J., "Attenuation of Sound in Ducts with Acoustic Treatment - A Generalized Approximate Equation," NASA TMX-71830.
6. Pao, S.F., A.R. Wenzel, and P.B. Oncely, "Prediction of Ground Effects on Aircraft Noise," NASA-TP-1104, 1978.
7. Zorumski, W.E., "Prediction of Aircraft Sideline Noise Attenuation," NASA-TM-78717, 1978.
8. Chessell, C.I., "Propagation of Noise Along a Finite Impedance Boundary," J. Acoust. Soc. America, Vol. 62, No. 4, October 1977, pp. 825-834.
9. Chessell, C.I., "Meteorological and Ground Effects on the Propagation of Aircraft Noise Close to the Earth's Surface," J. of Sound and Vib., Vol. 60, No. 2, 1978, pp. 251-266.
10. Embleton, T.F.W., J.E. Piercy, and N. Olson, "Outdoor Sound Propagation Over Ground of Finite Impedance," J. Acoust. Soc. Am., Vol. 59, No. 2, February 1976, pp. 267-277.
11. Daigle, G.A., Effects of Atmospheric Turbulence on the Interface of Sound Waves Above a Finite Impedance Boundary," J. Acoust. Soc. Am., Vol. 65, No. 1, January 1979, pp. 45-49.
12. Putnam, T.W., "Review of Aircraft Noise Propagation," NASA-TMX-56033, September, 1975.
13. Oncely, P.B., "Propagation of Jet Engine Noise Near a Porous Surface," J. Sound Vib., Vol. 13, No. 1, 1970, pp. 27-35.

**TABLE 1. QCGAT NACELLE ATTENUATOR DESIGN CHARACTERISTICS.**

Liner Section	Tuned Freq, Hz	Operating Condition Tuned for	Liner Length, cm (in.)	Face Sheet Open Area, %	Cavity Depth, cm (in.)	Honeycomb Cell Size, $\phi$ cm (in.)
A <sub>1</sub>	1000	Sideline	17.5 (6.9)	5.8	18.83 (0.72)	1.905 (0.75)
A <sub>2</sub>	1000	Sideline	27.2 (10.7)	8.6	2.79 (1.10)	1.905 (0.75)
B	2500	Sideline	15.2 (6.0)	14.2	1.32 (0.52)	0.953 (0.375)
1	2500	Approach	32.0 (12.6)	7.0	1.42 (0.56)	0.953 (0.375)
2	1000	Approach	38.9 (15.3)	8.6	0.91 (0.36)	0.953 (0.375)
3	2000	Approach	52.8 (20.8)	6.8	1.96 (0.77)	1.905 (0.75)

**TABLE 2. QCGAT ENGINE KEY ACOUSTIC PARAMETERS FOR SIMULATED STATIC TEST CONDITION.**

Engine Parameter	Simulated Static Test Condition, 282K (48°F)	
	Takeoff	Approach
Engine net thrust	16,098 N (3,619 lbf)	7,019 N (1,578 lbf)
Fan rotor speed	913 rad/s (8,726 rpm)	634.8 rad/s (6,063 rpm)
Fan pressure ratio, tip	1.41	1.18
Fan tip relative Mach No.	1.17	0.79
Fan blade passing frequency	5,236 Hz	3,638 Hz
Fan airflow	61.7 kg/s (136.1 lbm/sec)	42.4 kg/s (93.5 lbm/sec)
Core airflow	11.6 kg/s (25.5 lbm/sec)	6.2 kg/s (13.6 lbm/sec)
Mixer exhaust velocity	257.9 m/s (846 ft/sec)	166.1 m/s (545 ft/sec)
Mixer exhaust total temperature	406.8K (732.3°R)	365.9K (658.6°R)
LP turbine rotor speed	1,941.5 rad/s (18,543 rpm)	1,348.9 rad/s (12,883 rpm)
Turbine last stage relative tip Mach No.	0.472	0.349
Turbine last stage pressure ratio (total to static)	1.61	1.22

**TABLE 3. QCGAT ENGINE KEY ACOUSTIC PARAMETERS  
FOR FLYOVER NOISE CONDITION.**

Engine Parameter	FAR PART 36 CERTIFICATION CONDITION		
	Takeoff	Sideline	Approach
Engine net thrust	12,869 N (2,893 lbf)	13,318 N (2,994 lbf)	4,639 N (1,043 lbf)
Fan rotor speed	958.9 rad/s (9,159 rpm)	954.8 rad/s (9,119 rpm)	641.4 rad/s (6,126 rpm)
Fan pressure ratio, tip	1.44	1.43	1.16
Fan tip relative Mach No.	1.22	1.20	0.78
Fan blade passing frequency	5,495 Hz	5,471 Hz	3,677 Hz
Fan airflow	60.1 kg/s (132.4 lbm/sec)	62.4 kg/s (137.6 lbm/sec)	44.8 kg/s (98.7 lbm/sec)
Core airflow	11.4 kg/s (25.2 lbm/sec)	11.9 kg/s (26.3 lbm/sec)	6.2 kg/s (13.7 lbm/sec)
Mixer exhaust velocity	285.3 m/s (936 ft/sec)	284.3 m/s (933 ft/sec)	175.9 m/s (577 ft/sec)
Mixer exhaust total temperature	429.1K (772.3°R)	433.8K (780.8°R)	381.5K (686.7°R)
LP turbine rotor speed	2,037.8 rad/s (19,463 rpm)	2,028.9 rad/s (19,378 rpm)	1,363.3 rad/s (13,021 rpm)
Turbine last stage relative tip Mach No.	0.467	0.465	0.356
Turbine last stage pressure ratio (total to static)	1.70	1.69	1.26

**TABLE 4. ACOUSTIC TEST CONFIGURATIONS.**

Acoustic Configuration Number	Description
1	Fully treated engine with mixer compound nozzle
2	Fully treated engine with coannular nozzle
3 & 4	Partially treated with mixer compound nozzle
5	Hardwall engine with mixer compound nozzle
6	Hardwall engine with nacelle lip, mixer nozzle
7	Hardwall engine with coannular nozzle

**TABLE 5. QCGAT ENGINE NOISE PREDICTION PROCEDURE.**

Major Component Noise Sources Predicted	Prediction Method
Fan inlet noise - Discrete, broadband Buzz saw	NASA TMX-71763* FAA-RD-71-73*
Fan discharge noise - Discrete, broadband	NASA TMX-71763*
Jet noise	NASA TMX-73552
Combustion noise	NASA TMS-71627
Turbine noise	AIAA 75-449
Total noise	Sum of individual component noise levels
<p>NOTE: One-third octave spectra from 50 to 16,000 Hertz directivity angles from 0.17 to 2.79 radians (10 to 160 degrees) from inlet centerline.</p> <p>*Modified by AiResearch</p>	

**TABLE 6. NOISE PREDICTION METHODOLOGY COMPARISON.**

Excess Jet Model	Excess Core Model
Jet noise based on NASA method adjusted to fair through low-frequency data	Jet noise based on NASA method
Core noise based on NASA method	Core noise defined as difference between measured and predicted sum of jet, fan, turbine in 50-250 Hz frequency bands
re. discrete, broadband, and buzz saw adjusted to 731 data	Fan inlet and fan discharge defined as difference between measured and predicted sum of jet, core, turbine in 3150-10,000 Hz bands
GE turbine noise method	GE turbine noise method

**TABLE 7. TFE731-2/LEAR 36 FLYOVER NOISE COMPARISON.**

	EPNL, EPNdB		
	Predicted		Measured
	Excess Jet Model	Excess Core Model	
Takeoff	88.7 (+4.7)	90.8 (+6.8)	84.0
Approach	95.9 (+3.7)	98.6 (+6.4)	92.2

**TABLE 8. QCGAT FLYOVER NOISE SUMMARY.**

Configuration	EPNL, EPNdB				QCGAT Goal
	Excess Jet Prediction Method		Excess Core Prediction Method		
	Unadjusted	With Learning	Unadjusted	With Learning	
Hardwall mixer takeoff	79.3	74.6	83.1	76.0	73.3
Softwall mixer takeoff	77.8	73.1 (-0.2) *	81.7	74.7 (+1.4) *	
Hardwall mixer approach	88.2	84.5	91.0	84.5	87.3
Softwall mixer approach	86.4	82.7 (-4.6) *	88.5	81.9 (-5.4) *	
Hardwall mixer sideline	85.7	81.7	89.0	81.7	82.3
Softwall mixer sideline	84.3	80.3 (-2.0) *	87.6	80.3 (-2.0) *	
*Indicates difference between goal and predicted EPNL.					

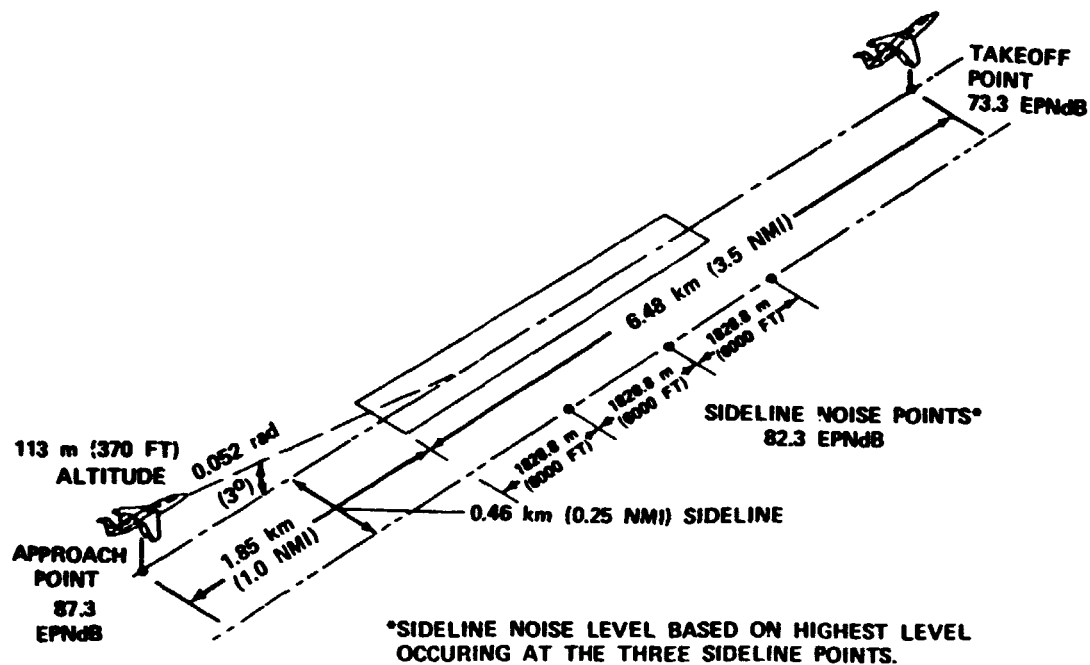


Figure 1. QCGAT Airplane Noise Goals.

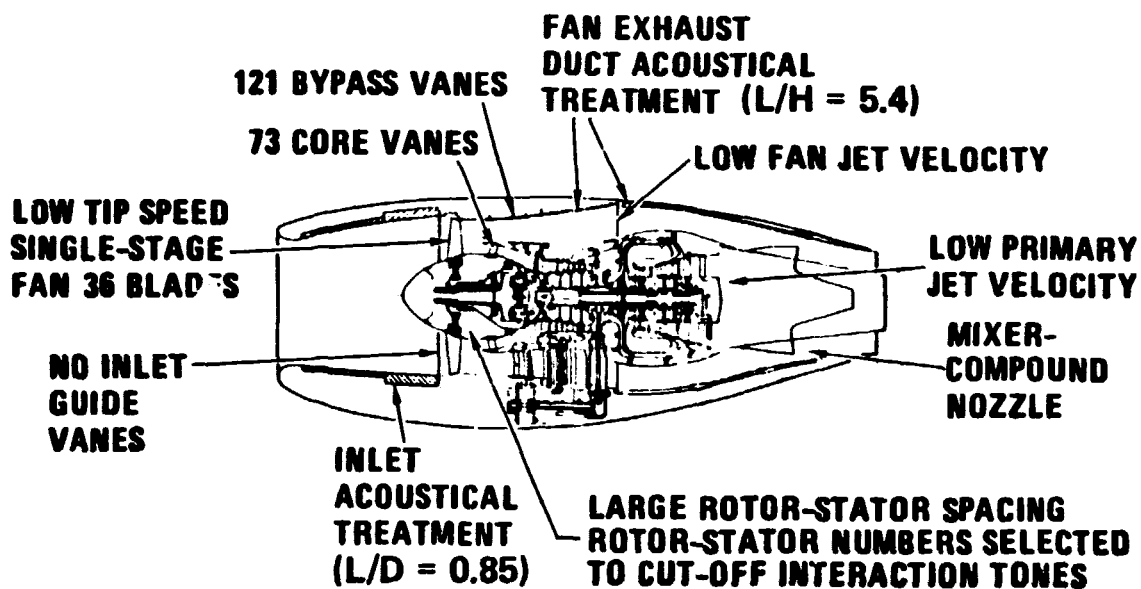
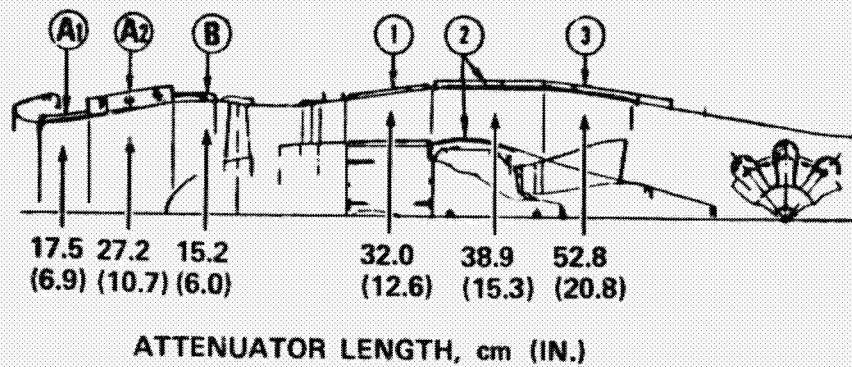


Figure 2. QCGAT Acoustic Design Features.





**NOTE:**

○ DENOTES SECTION NUMBER USED IN ATTENUATION ANALYSIS

Figure 3. Nacelle Acoustic Treatment.



Figure 4. San Tan Acoustic Test Site.

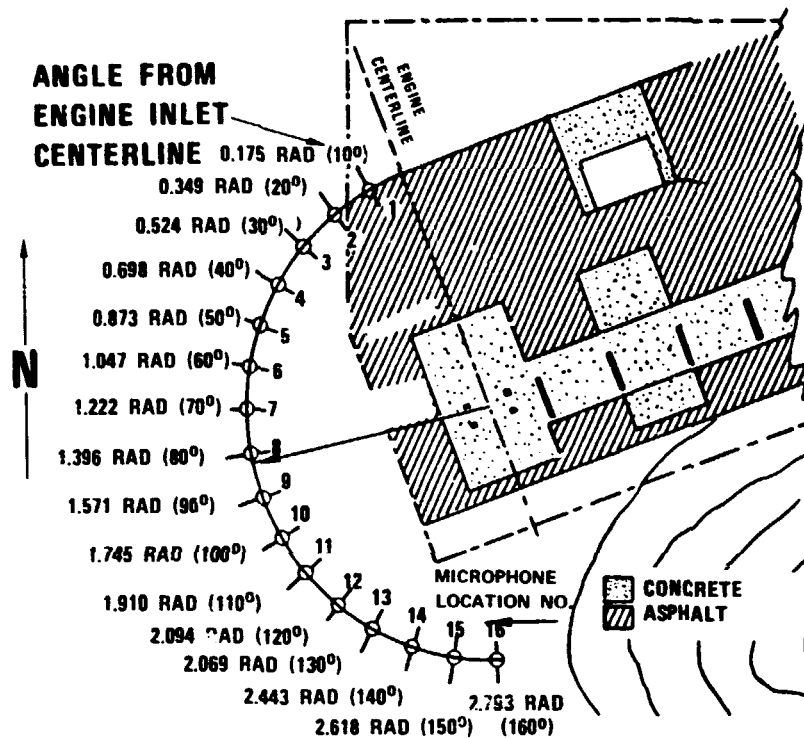
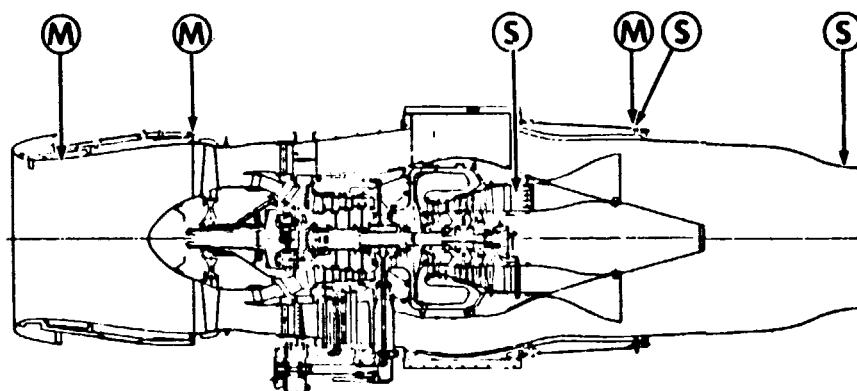


Figure 5. Acoustic Test Setup.



- (M) DENOTES 0.3175-cm (1/8-IN.) MICROPHONE  
(S) DENOTES 0.635-cm (1/4-IN.) SEMI-INFINITE TUBE

Figure 6. Internal Acoustic Instrumentation.

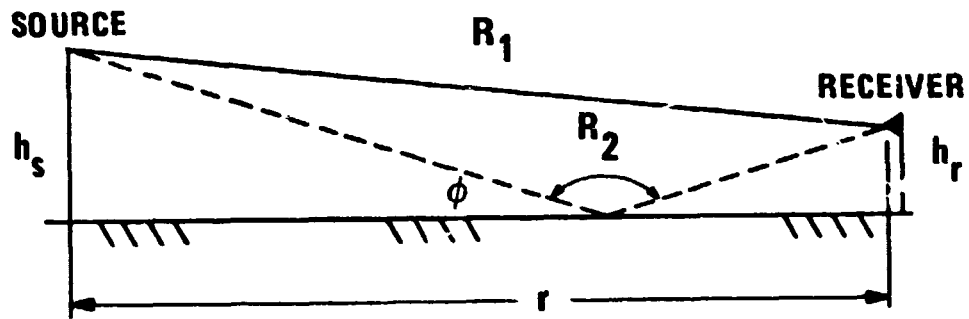


Figure 7. Ground Reflection Correction Model.

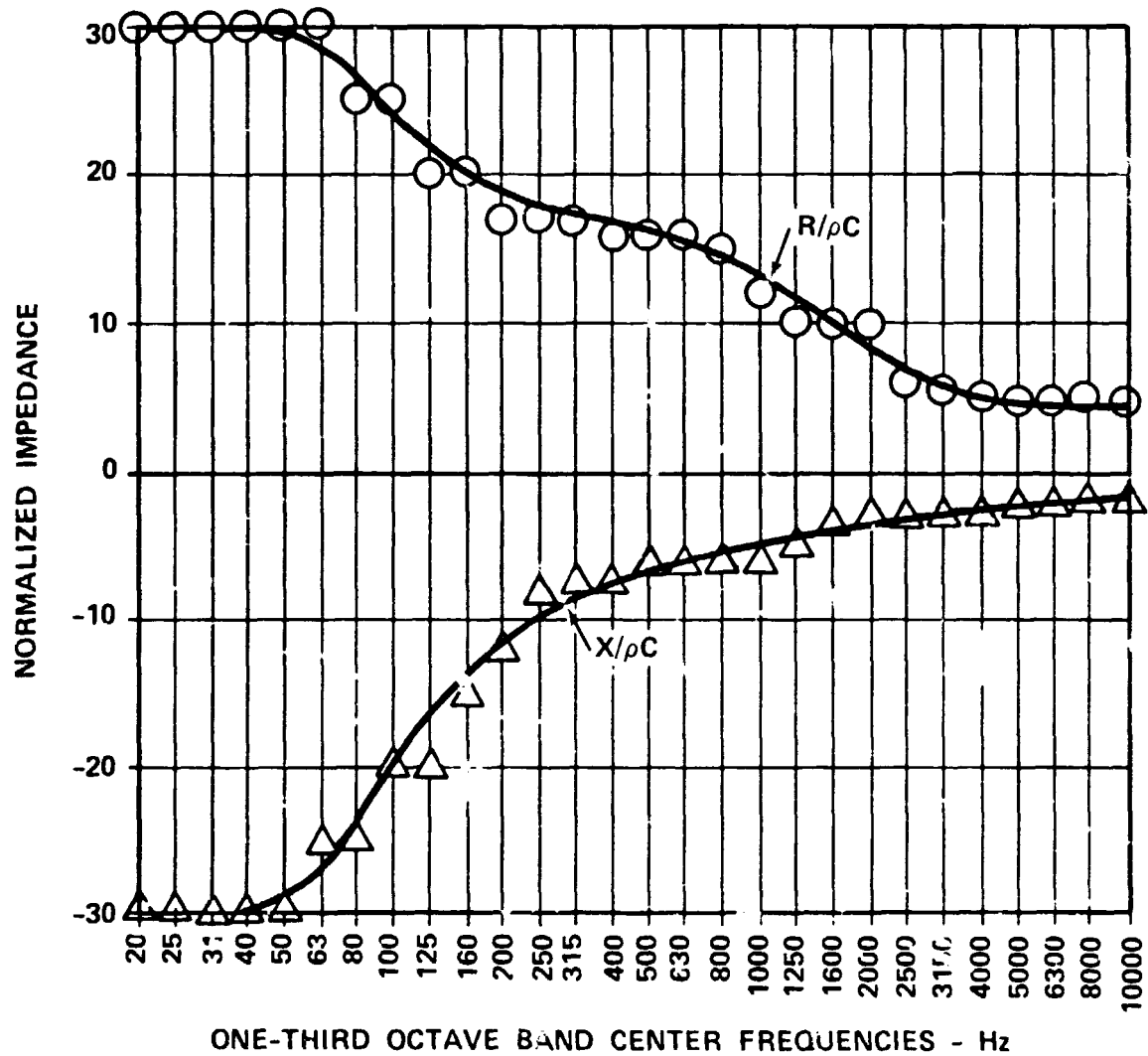


Figure 8. Correlated Acoustic Impedance for Desert Soil at San Tan (AiResearch).

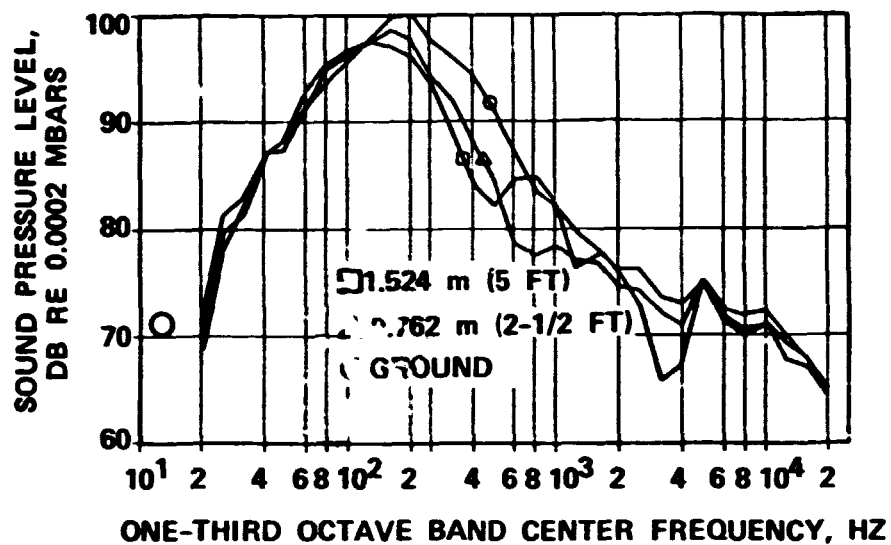


Figure 9. Measured Data for Acoustic Configuration No. 2 at 2.62 Radian (150-Degree) Position.

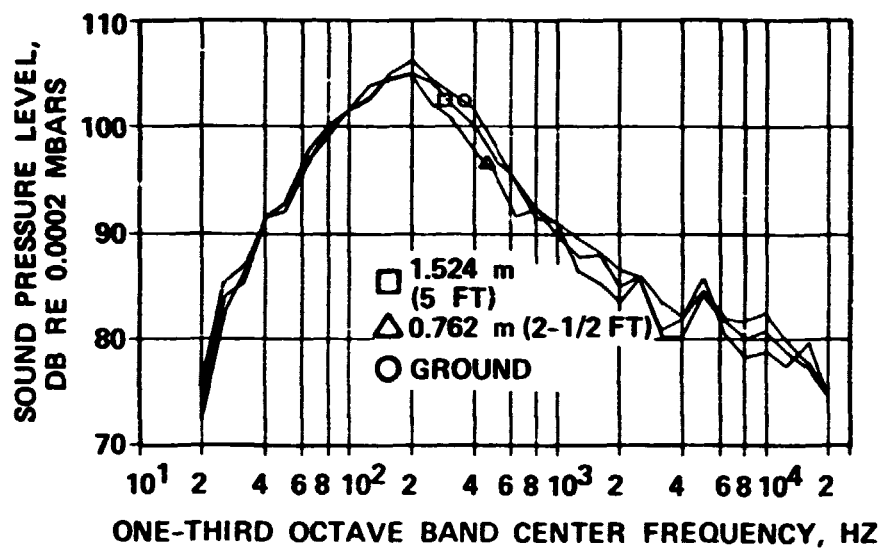


Figure 10. Corrected Data for Acoustic Configuration No. 2 at 2.62 Radian (150-Degree) Position.

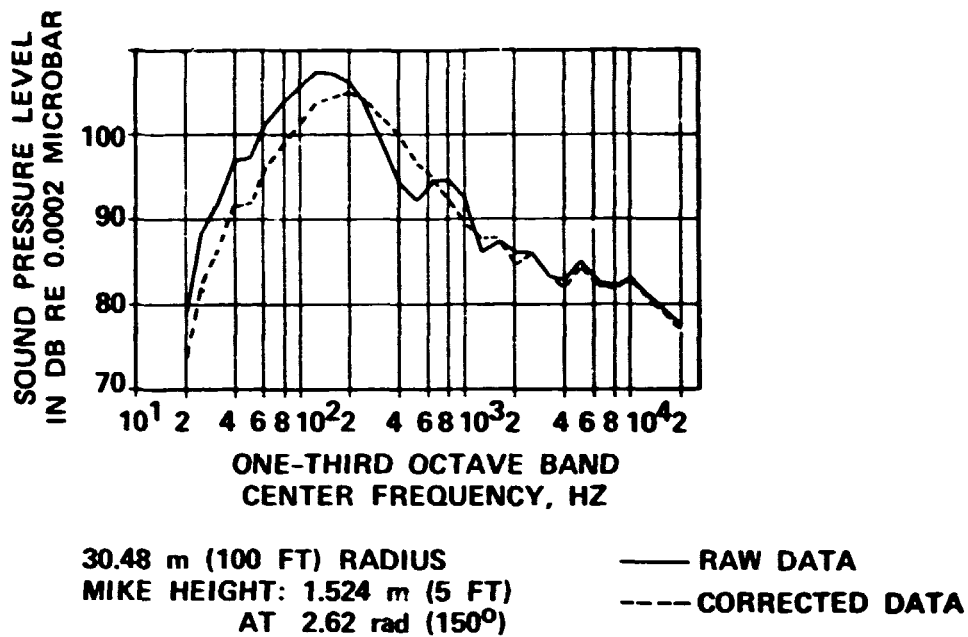


Figure 11. Raw Data versus Ground Corrected Data.

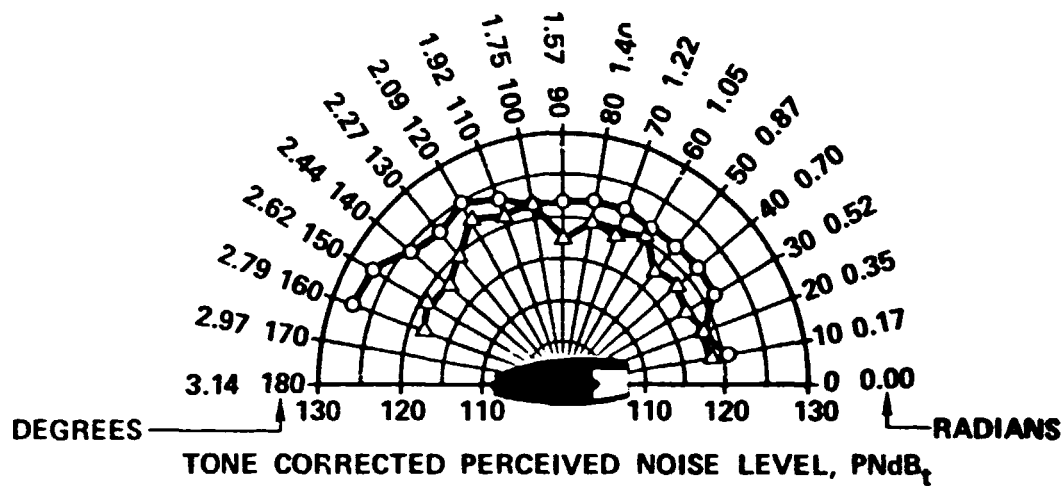


Figure 12. Static Comparison at Takeoff of Model TFE731-3 and QCGAT Coannular Nozzle Configurations.

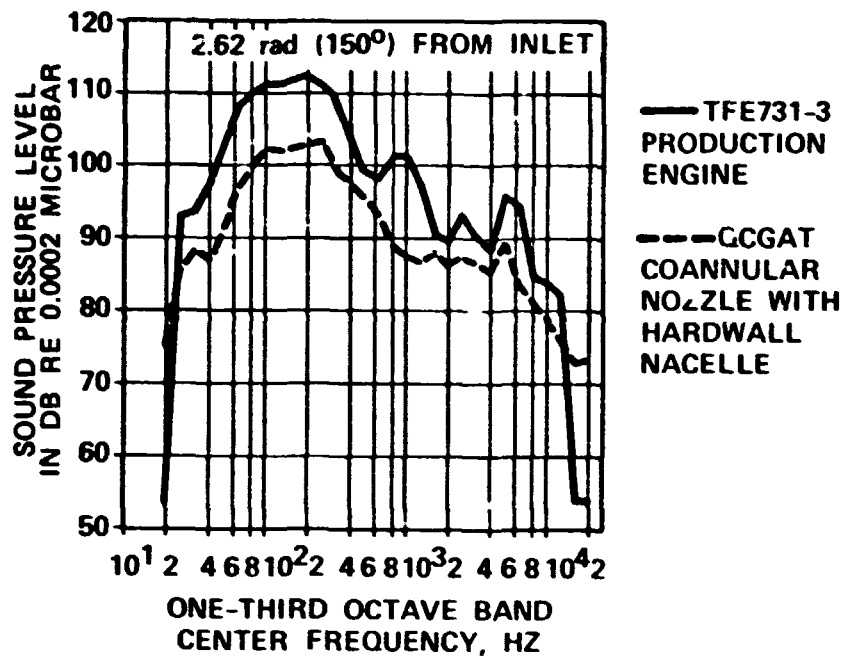


Figure 13. Noise Level Comparison at Takeoff of Model TFE731 and QCGAT Coannular Nozzle Configurations.

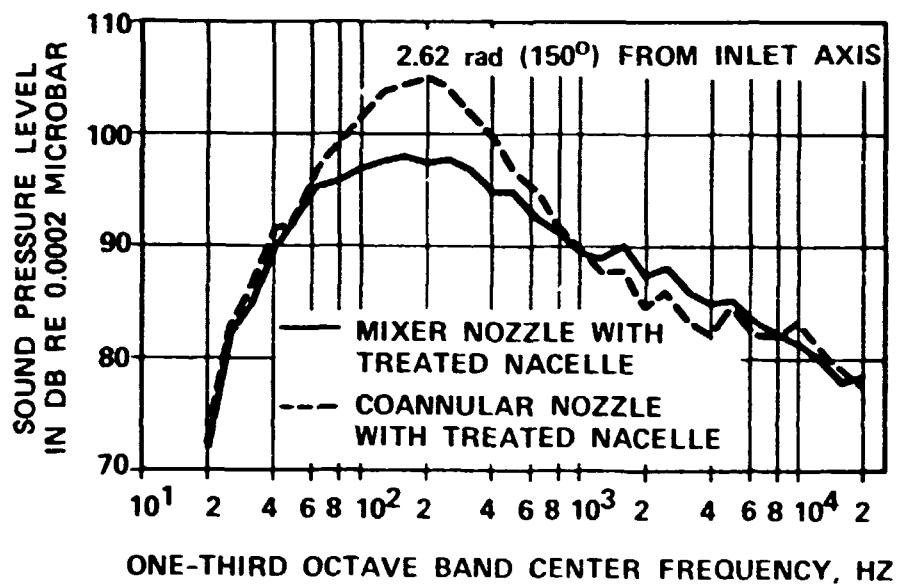


Figure 14. Noise Level Comparison at Takeoff of QCGAT Mixer Compound and Coannular Nozzle Configurations.

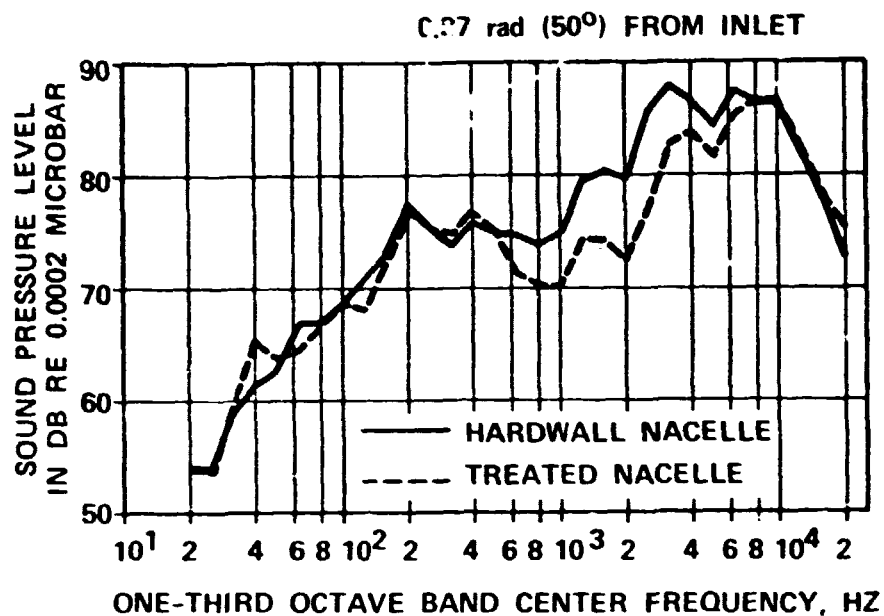


Figure 15. Approach Noise Level Comparison of Hardwall versus Treated Acoustic Panels at 0.87 rad (50°) from Engine Inlet Centerline for the Mixer Compound Nozzle Configuration.

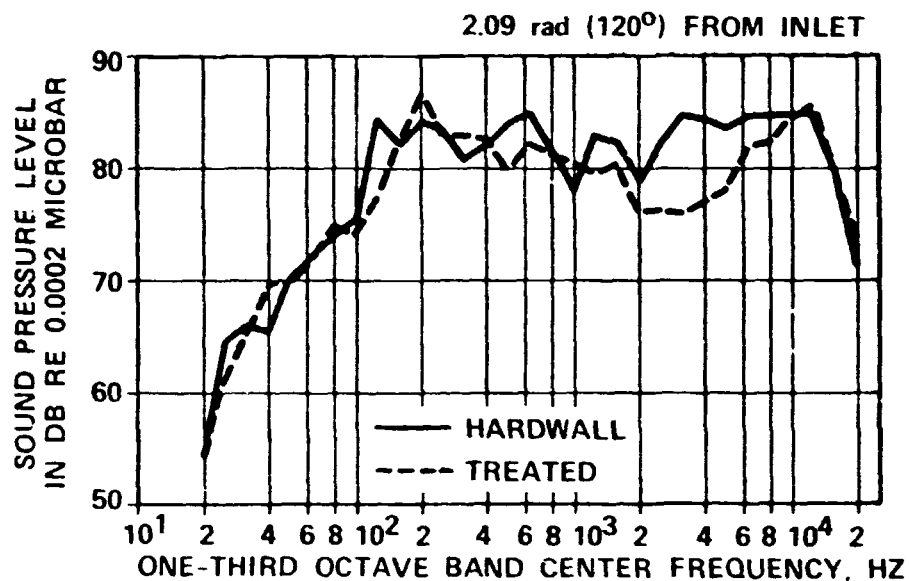


Figure 16. Approach Noise Level Comparison of Hardwall versus Treated Acoustic Panels at 2.09 rad (120°) from Engine Inlet Centerline for the Mixer Compound Nozzle Configuration.



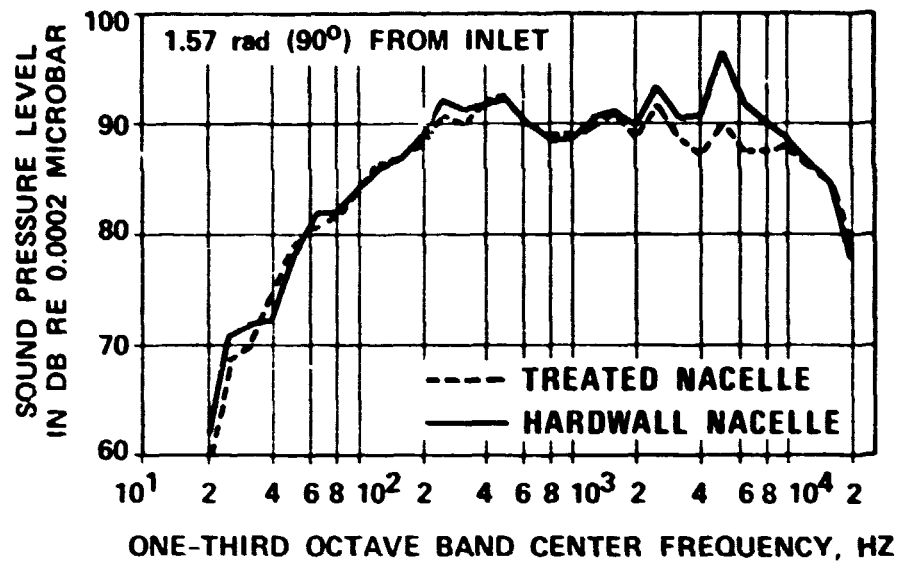


Figure 17. Takeoff Noise Level Comparison of Hardwall versus Treated Acoustic Panels at 1.57 rad (90°) from Engine Inlet Centerline for the Coannular Nozzle Configuration.

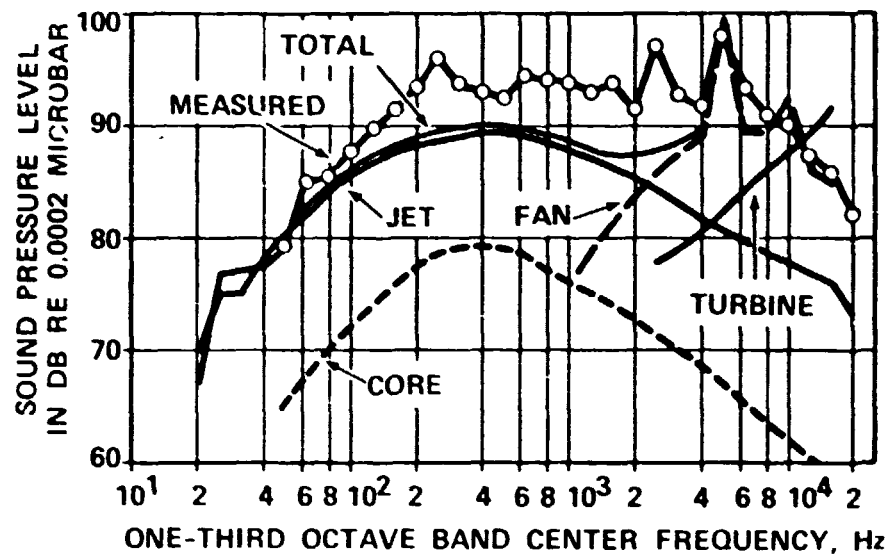


Figure 18. Comparison of Measured and Predicted Noise Levels Before Correlation.

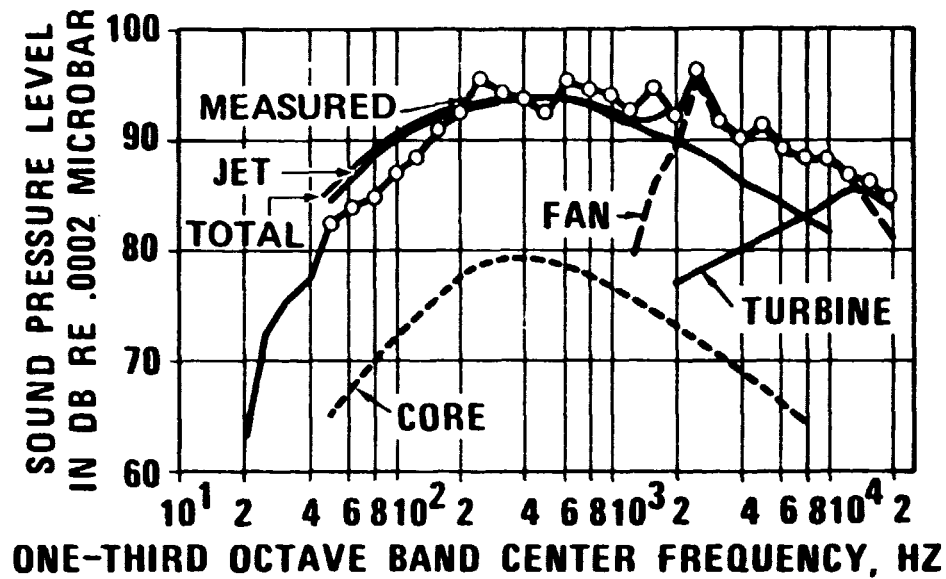


Figure 19. Data Correlation, Excess Jet Model, Softwall Mixer, 2.09-Radian (120-Degree) Position.

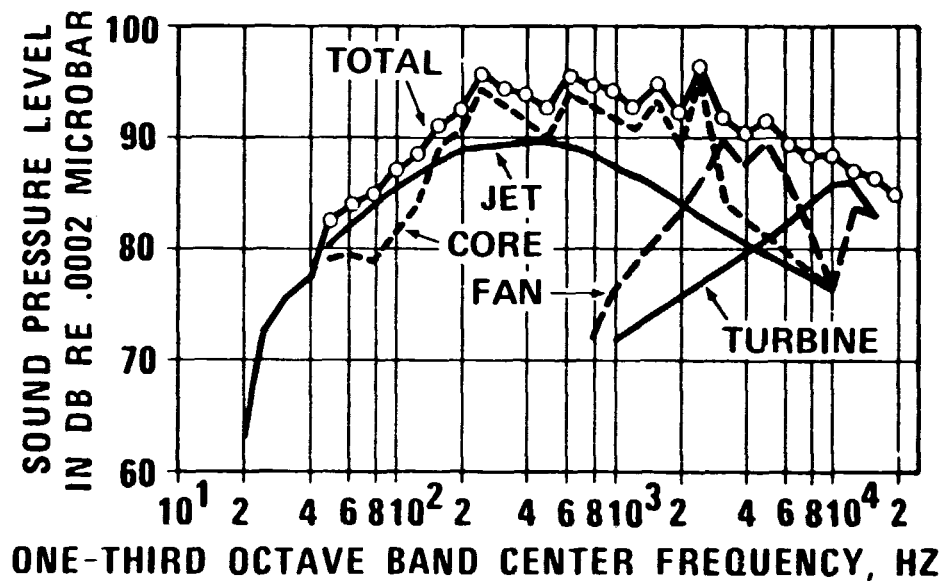


Figure 20. Data Correlation, Excess Core Model, Softwall Mixer, 2.09-Radian (120-Degree) Position.

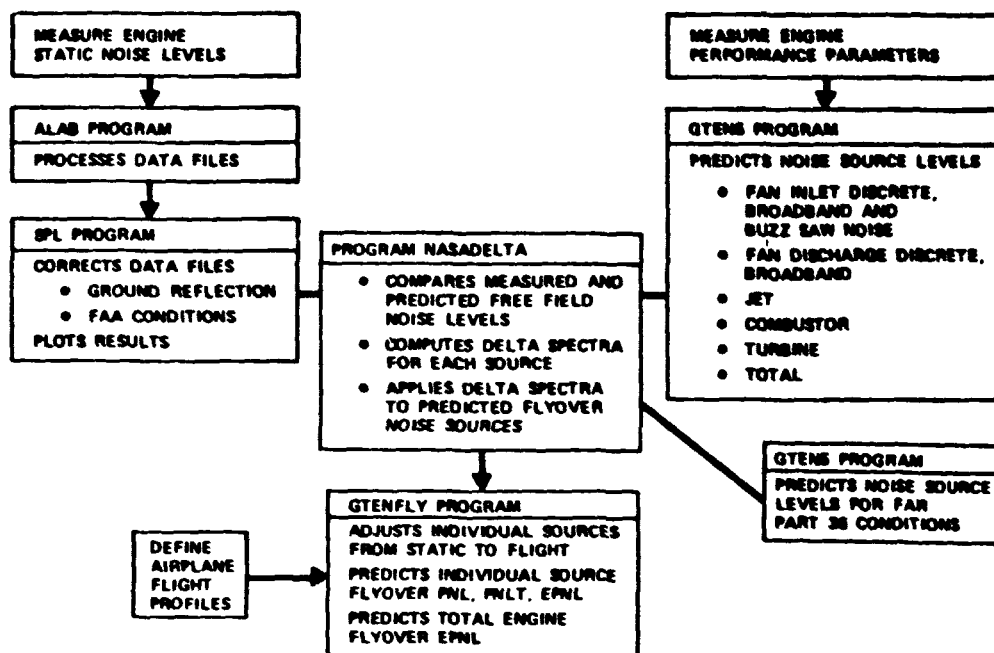


Figure 21. Flyover Noise Prediction from Static Data.

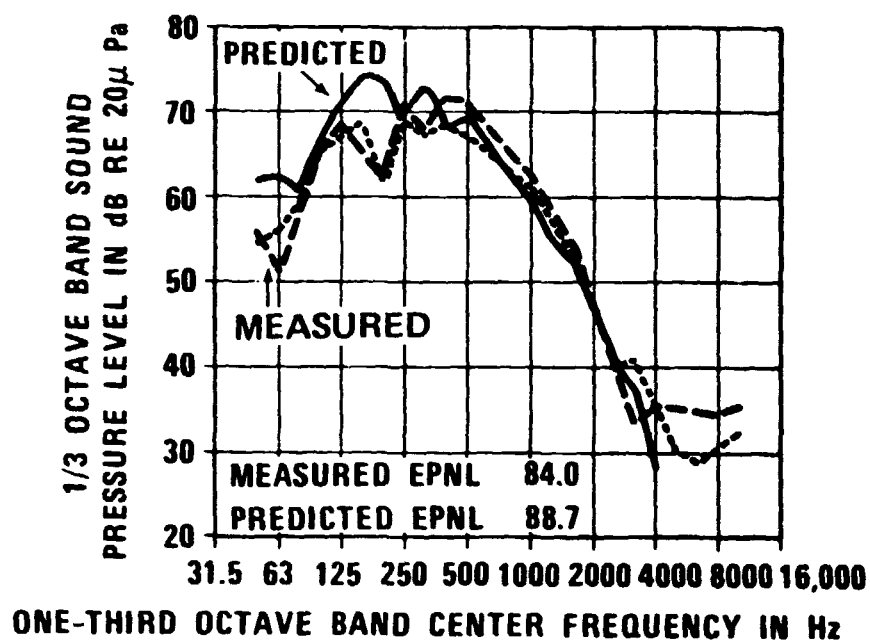


Figure 22. Measured Learjet 35/36 versus Predicted Excess Jet Model.

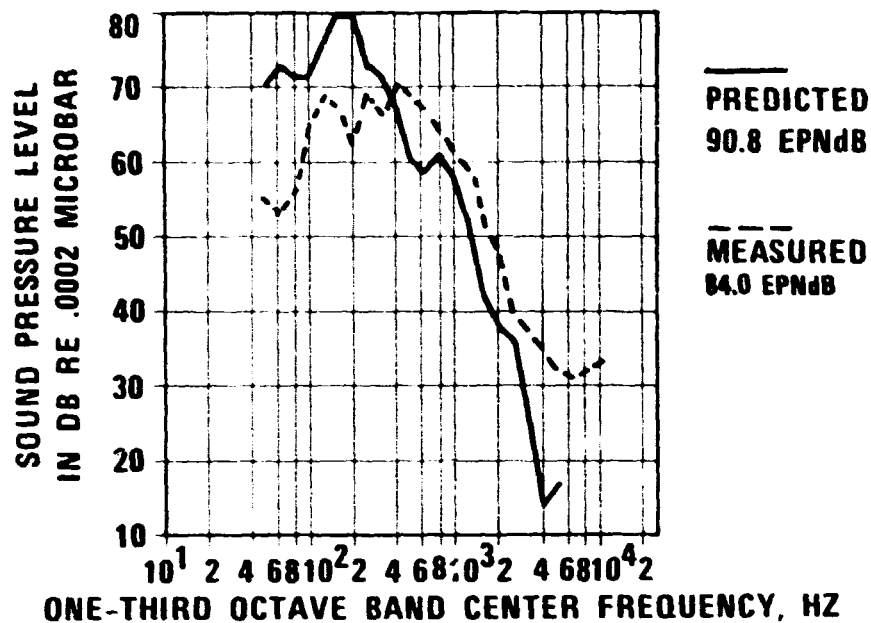


Figure 23. Measured Learjet 35/36 versus Predicted Excess Core Model.

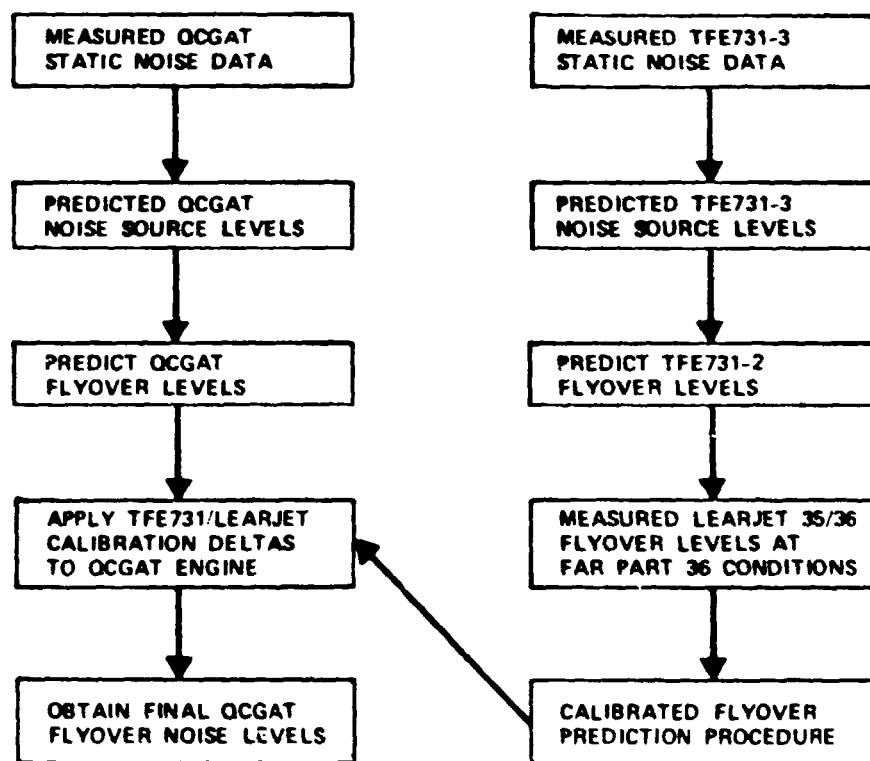


Figure 24. Flyover Noise Calibration Procedure.

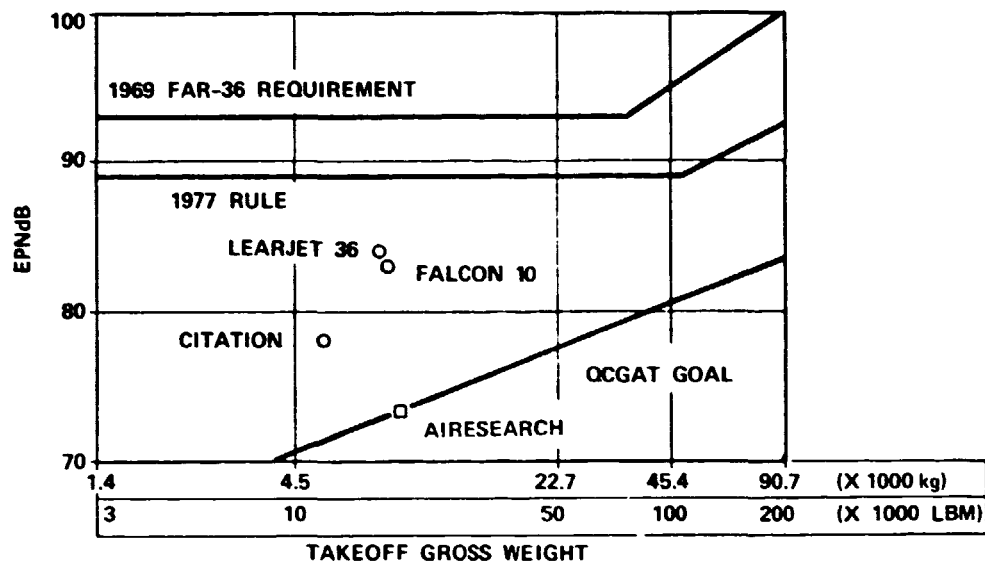


Figure 25. Takeoff Noise Summary.

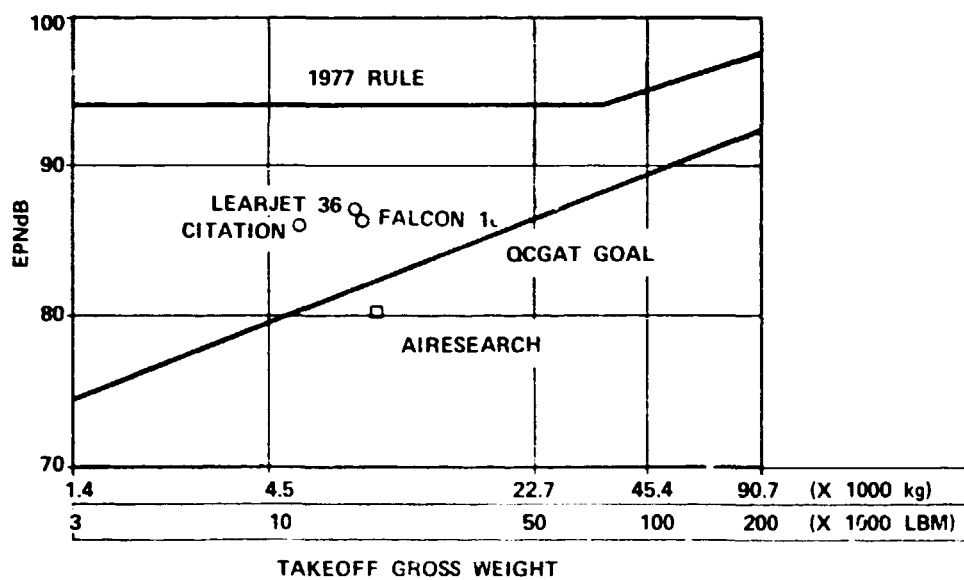


Figure 26. Sideline Noise Summary.

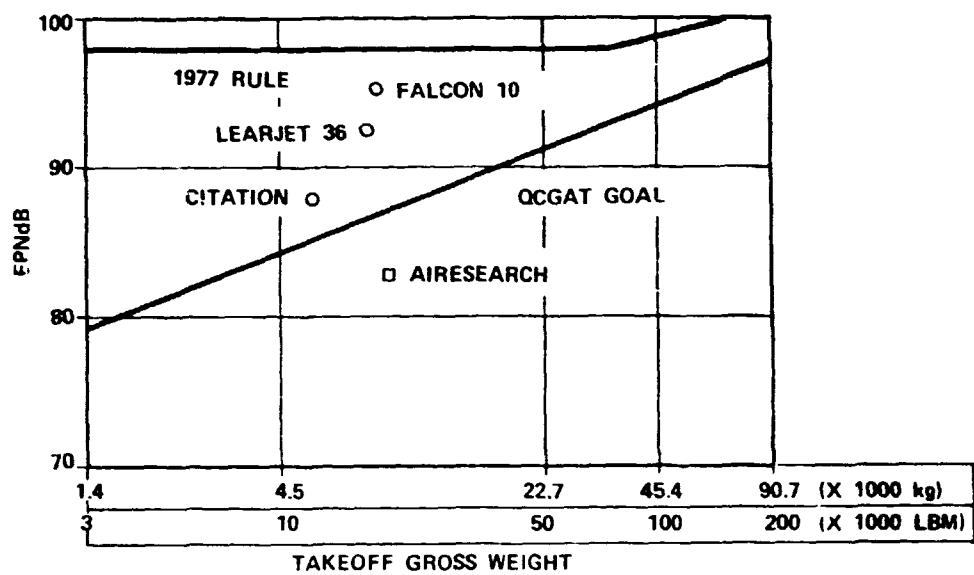


Figure 27. Approach Noise Summary.

**1 N80-22331**

**QCGAT AIRCRAFT/ENGINE DESIGN FOR REDUCED  
NOISE AND EMISSIONS**

**Leonard I'Anson and Kenneth M. Terrill  
Avco Lycoming Division**

**INTRODUCTION**

The multi-engine general aviation fleet size is expected to increase by 70 percent in the decade of the 1980's according to the General Aviation Manufacturers Association (GAMA). These general aviation aircraft typically use suburban airports that are unprotected by commercial buffer zones. Consequently, there is the potential for general aviation to create more widespread adverse community reaction to noise and pollution than that experienced with commercial air carrier aircraft. Recognizing this, NASA let contracts to apply large engine quieting and emissions reduction technology to smaller engines and to develop new and more suitable technology where required. These resulting "Quiet, Clean, General Aviation Turbofan" (QCGAT) contracts required delivery of a turbofan engine and nacelle demonstrator, as well as preliminary definition of an appropriate general aviation aircraft system, that could use the engine as propulsion.

This paper describes the resulting aircraft/nacelle/engine designs created under the Avco Lycoming contract. These designs reflect the technical expertise of the following subcontractors:

Aircraft Design - Beech Aircraft Corporation  
Nacelle Mechanical Design - Avco Aerostructures  
Nacelle Acoustic Treatment - Lockheed Aircraft Corporation

**AIRCRAFT PRELIMINARY DESIGN**

To guide the aircraft system design, five primary objectives were established:

1. Practical, direct application of technology without significant scaling was very important. This required selection of aircraft and engine sizes which would be appropriate for an appreciable segment of general aviation.
2. The aircraft must also offer attractive range, fuel economy, and flight speed. A target of 2593 kilometers (1400 nautical miles) was established. This exceeds the range of most current small business aircraft. It also provides non-stop travel between opposite extremes of high density traffic areas.



3. A cruise Mach Number of 0.62 was chosen as an optimum compromise between time and fuel economy. It provides 40 percent higher cruise speed than a turboprop, with a 30 percent improvement in fuel economy over operation at 0.8 Mach Number.
4. A balanced field length of 762 meters (2500 feet) was desired because it permits safe operation from 70 percent of all U.S. airports which are open to the public, including airports with sod runways.
5. Ecological characteristics of an aircraft system are likely to become primary competitive parameters for general aviation in the 1980 decade. Therefore, they deserve close attention in design selections.

The initial step in aircraft preliminary design was the selection of appropriate size and design. The vast majority of general aviation aircraft operating from airfields located in suburban communities are in the size class below 5433 kg (12,000 lb) gross weight. In the lower extremity of the gross weight spectrum, small private aircraft in the range below 1814 kg (4,000 lb) are generally powered by single-piston engines. It is expected that market constraints for very low-cost aircraft in this class will dictate continued usage of piston engines for the foreseeable future. It, therefore, follows that the greatest public ecological benefits can be realized by introduction of a quiet, clean aircraft system in the 1814 - 5433 kg (4,000 - 12,000 lb) gross weight class. Figure 1 shows the projected market volume for various sizes of general aviation aircraft.

As with the passenger car trend towards smaller and more sophisticated cars to perform the same function, it is expected that the decade of 1980's will see a similar general aviation trend towards reduced aircraft weight and smaller engine size for the same mission. Because noise, emissions, and fuel consumption reduce with engine size, subsequent improvement in ecological characteristics can be anticipated. Utilizing technologies such as turbofan propulsion, high aspect ratio super critical wing and lightweight composite structures, it is expected that a new class of small general aviation aircraft will emerge in the eighties. A target of 30 percent weight reduction was considered achievable.

For aircraft size selection, our target was the largest segment of general aviation aircraft where cost of turbofan propulsion does not preclude its introduction.

Figure 1 presents a composite plot of aircraft gross weight versus both "The Number of New Aircraft to be Built" and "The Current Estimated Nominal Aircraft Cost". The number of aircraft is based on General Aviation Manufacturers Association data. The expected trend toward lighter weight and higher cost for the same mission has not been reflected to ensure conservative engine sizing. The range of 3175 - 4536 kg (7,000 to 10,000 lb) gross weight appeared attractive, with 3629 kg (8,000 lb) selected as our goal.

With the defined aircraft goals and Lycoming estimates for engine performance, Beech Aircraft Corporation conducted parametric studies to optimize the aircraft preliminary design.

The aircraft which evolved is depicted in figure 2. It is a sleek, advanced design, six-place aircraft with 3538 kg (7,800 lb) maximum gross weight. It offers a 2778 kilometer (1500 nautical mile) range with cruise speed of 0.5 Mach Number and will take-off and land on the vast majority of general aviation airfields. Advanced features include broad application of composite materials and a supercritical wing design with winglets. Full-span fowler flaps have been introduced to improve landing capability. Engines are fuselage-mounted with inlets over the wing to provide shielding of fan noise by the wing surfaces.

The high bypass ratio QCGAT engine plays an important role in shaping the aircraft design. It offers a dramatic reduction in specific fuel consumption compared with current pure jets and low-to-moderate bypass ratio turbofans. Figure 3 provides this comparison, reflecting a 22 percent improvement in fuel economy.

This lower fuel consumption may be used in either of two ways or in combination:

It can substantially reduce aircraft gross weight for the same range. The reduced weight provides compound interest on the fuel economy. It also requires lower thrust favoring reduction of noise and emissions.

If preferred, the lower fuel consumption can be translated into longer range for the original gross weight.

We chose to reduce gross weight and favor ecological characteristics.

Composite structures have been used extensively in the aircraft preliminary design to further reduce gross weight. Areas selected by Beech for the application of composite materials are shown in figure 4. Kevlar graphite composites were used for aircraft weight estimates. Further potential for weight savings exists in the engine nacelles. Conventional design was used to reflect the low-risk, low-cost test nacelle. Critical load carrying members such as the wing spar are conventional aluminum construction.

Approximately 40 percent of the structure is fiber epoxy or honeycomb-bonded structure. The use of composite structure in aircraft design provides a decreasing rate of benefit as the application of composites becomes more widespread in the design. Initial selection of applications is in noncritical areas. As the stress in selected areas increases, the design safety factor also increases to compensate for uncertainties resulting from the youth of the composite application. Beech cautions that, while these composite applications are technically feasible, development beyond the scope normally undertaken by industry would be required to assure success.

Structural design is in accordance with Federal Aviation Regulation Part 23 airworthiness standards for normal category airplanes.

A 17 percent thickness-to-chord ratio supercritical wing shape was selected because it offers a number of advantages over the conventional 12 percent NACA shape. These advantages are summarized in figure 5.

From the cross sectional comparison shown here, it can be concluded that the supercritical wing provides larger volume for fuel storage for the same chord width. The thickness increase has the supplementary benefit of higher section modulus, permitting lighter construction for equivalent bending loads.

The two shapes have comparable drag characteristics in the cruise mode. Increase in the NACA airfoil thickness in an attempt to achieve similar volume is impractical, because it results in a significant reduction in useful flight speed combined with an overall drag increase at lower speeds.

Iterative design studies show a 25 percent increase in fuel capacity combined with a 3 percent decrease in aircraft gross weight. These savings are for an equivalent aspect ratio of 10 and a design wing loading of  $2250 \text{ N/m}^2$  (47 lb/sq ft) of wing area.

Prior test data have shown an appreciable increase in lift capability as depicted in this comparison. This promises a more forgiving aircraft for variations in angle of attack, enhancing safety. For equivalent sophistication of flap systems, reduced landing speeds are achievable resulting in shorter landing field length capability.

The airfoil selected by Beech is similar to the NASA GA (W) - 1 airfoil, but is tailored specifically for the high-speed, high fuel volume and the high-lift requirements of the QCGAT configuration. The pressure distribution used to guide the design tailoring would identify it as a BAC Sonic Plateau airfoil with a 17 percent thickness ratio.

Full-span fowler flaps and spoilers have been introduced to achieve the desired 762 meter (2500 feet) take-off field length and landing distances with reduced wing area. Winglets have also been added to reduce actual span and wing structural weight, while maintaining high effective aspect ratio.

Major lift parameters are summarized below. Establishing optimum flap settings was beyond the scope of this study. However, experience indicates that a full flap deflection of 40 degrees for landing and take-off flap setting of 40 percent of full deflection are appropriate for fowler flap design. These values of  $C_{l_{\max}}$  represent available state-of-the-art with advanced airfoils.

Flap Positions	$C_L$ $\alpha = 0$	$\frac{d C_L}{d \alpha}$	$C_{L_{max}}$
Up	.132	.088	1.6
40% (Take-Off)	.98	.088	2.35
Down	2.13	.088	3.45

Many drag influencing design details of the QCGAT airplane are not established at this time, because the airplane is as yet a preliminary design study. For drag analysis, ambitious estimates were made for the various items. Achievement of total airplane drag coefficients will require exacting effort in the practical development of the airplane. The resulting QCGAT aircraft drag compares with that of the Learjet Model 24, which is an extremely clean airplane. Allowances have been made for differences in wing thickness, component sizes, etc. Drag coefficients used are summarized below:

Total $C_{Dp}$ , Flaps and gear up	.02661, .02534 cruise
Incremental $C_{Dp}$ for landing gear	.0164
Incremental $C_{Dp}$ for full flap	.04066
Incremental $C_{Dp}$ for T.O. flap	.0163
Incremental $C_{Dp}$ for one engine out	.01209

Four major airplane variables were considered in the parametric study to optimize the wing configuration. They are:

1. Wing area
2. Wing aspect ratio
3. Fuel weight
4. Take-off weight

In the study, for each performance goal, the limiting aspect ratio versus wing area is plotted for several take-off weights, including the effects of wing geometry on wing weight. These limits for each of the performance goals are then summarized on a graph so that the best compromise can be selected. A design point of 15.33 square meter (165 square feet) wing area and an effective aspect ratio of 10 were selected.

Table I summarizes the expected weights for fuel, structure-plus-propulsion, and complete aircraft with payload for both conventional and QCGAT aircraft designs.

The first line represents a hypothetical aircraft of current vintage design with low bypass turbofan propulsion. Introduction of a QCGAT high bypass turbofan reduces fuel consumption by 22 percent. When this savings is iterated through the aircraft design, structure and gross weight reduce, provid-

ing an additional 5.5 percent in fuel economy. Similar iterations with weight savings from composite materials and supercritical wing result in an additional 4.4% savings in fuel. The combination of engine and aircraft changes provide 32% better fuel economy. The 22% reduction in gross weight permits the use of a smaller engine with 22% lower thrust and, therefore, lower absolute emissions and noise.

Our aircraft study projected the maximum ranges shown in figure 6 for various payloads. While 1134 kg (2500 lb) is depicted as maximum payload for the aircraft, only 753 kg (1660 lb) is required to accommodate six people with their baggage. At this payload, the achievable range is in excess of 2963 kilometers (1600 nautical miles). Flight conditions are 10058 meters (33,000 feet) and an average flight speed of approximately 0.5 Mach Number.

In our QCGAT aircraft study, landing distance, rather than take-off capability, set the minimum usable airfield length. Introduction of full-span fowler flaps with moderate wing loading results in a very low "landing configuration" stall speed. The 32 meters/sec (62 knots) stall speed compares with 41 - 46 meters/sec (80 - 90 knots) for current typical jet and turboprop aircraft. Since landing distance is proportional to stall speed squared, this low landing speed provides an attractive sea level FAR landing field length of 811 meters (2660 feet).

Figure 7 shows a representative sample of general aviation airfields plotted on coordinates of field elevation and field length. The Beech QCGAT aircraft with full useful payloads has a landing capability consistent with the majority of these fields.

The expected stall speeds promise a very forgiving airplane in the take-off and landing mode where most accidents occur.

The aircraft preliminary design was conducted to establish realistic criteria for noise measurement. Figure 8 depicts the locations for noise measurement, as well as the aircraft and engine conditions at the point of measurement.

Approach noise is measured directly below the flight path 1852 meters (one nautical mile) prior to the beginning of the runway. Approach aircraft glide slope is fixed at three degrees. Take-off sideline consists of multiple measurements 463 meters (0.25 nautical miles) to one side of the take-off flight path. Take-off flyover condition is measured 6482 meters (3.5 nautical miles) from brake release, directly below the flight path.

Looking at the tabulation of aircraft and engine conditions, the approach conditions are quoted for 40-degree wing flap angle. This gives the shortest landing distance and the highest noise level. Where increase runway length is available, 16 degrees flaps could be used. Velocity would increase to 55.6 meters/sec (108 knots) and thrust would reduce to 818.47 n (184 lb)/engine providing further reduction in noise.

Where take-off sideline noise is measured at multiple locations, the altitude of 262 m (860 ft) produces the highest estimated noise. Conditions are summarized for this altitude.

Climb rate of the QCGAT aircraft approximates current aircraft of similar mission. It attains an altitude of 106 m (3630 ft) at the take-off flyover measurement point.

#### ENGINE DESIGN

This portion of the paper will touch on design objectives, noise, and emission considerations, engine cycle and engine description, and conclude with specific design features.

Before proceeding into the details of the engine design, a brief review of the design objectives is in order.

The ecological characteristics of an aircraft system are a direct reflection of the engine design. Careful attention to engine design details which impact noise and emissions is required to produce an engine that will become a welcome resident in a suburban community.

Appeal of turbofans is indisputable. They swept virtually the entire commercial carrier market in a period of twenty years. The same trend has started in general aviation with the larger size aircraft. The rate of turbofan penetration into the smaller general aviation aircraft size is a function of the engine cost. This cost generally equates to simplicity of engine configuration. The result is basic; to be successful, it must be simple in configuration. Take-off thrust should be sufficient to permit operation from the majority of general aviation airfields.

The mechanical design life goal should reflect the anticipated aircraft mission. Beech projected a useful aircraft life of 12,000 hours with an average flight cycle lasting 90 minutes. Our design goal was to match this life without replacement of major parts.

Despite the best intentions of the designer, parts do break and it is desirable to be able to replace them conveniently. Modular engine construction achieves this goal.

A 12.191-meter (40,000-foot) flight envelope is attractive for avoidance of traffic and bad weather.

The need for fuel economy goes without saying.

The larger engines for commercial carrier aircraft have demonstrated substantial advances in the technology of noise reduction. They have provided the recipe for quiet engine design which was used for QCGAT and is summarized in figure 9.

Blend low fan blade tip speed and low fan pressure ratio with high fan bypass ratio.

The fan stator should be set at least two fan blade chord lengths aft from the blade trailing edge. The quantity of fan stator vanes should exceed two times the number of fan blades to avoid interaction of fan blade wakes with the stator vanes. Canted stator vanes are preferred.

Exhaust noise reduces with exhaust velocity, and turbine blade-pass frequency should exceed the audible range.

During the iterations which optimize an engine performance cycle, continuous attention is required to avoid adverse impact on emissions characteristics. Table II summarizes the primary causes for emissions along with the engine parameters which have a beneficial influence on emissions.

Unburned hydrocarbons and carbon monoxide emissions are primarily a reflection of poor combustor efficiency at idle. Low combustor inlet temperature at idle aggravates the carbon monoxide emissions. To reduce these two constituents, one would strive for very high combustor efficiency at idle combined with elevated combustor inlet temperature. To achieve the higher inlet temperature, a compressor with poor efficiency at low speed if desired. This compressor should then be run as fast as idle thrust constraints will permit, and then bleed air to achieve even higher speed for the same thrust.

Whereas idle conditions have the primary influence on UHC and CO, take-off conditions predominate in the creation of NO<sub>x</sub>. Generally, the higher the combustor inlet temperature at take-off, the more difficult the problem with NO<sub>x</sub>. Another important axiom, NO<sub>x</sub> and CO can usually be traded through combustor design modification. Either emission can be improved at the expense of the other to achieve the desired combination.

Comments, so far, have ignored engine bypass ratio. Emissions are produced exclusively in the core engine. The higher the bypass ratio, the lower the emissions for a given thrust rating.



A high-pressure compressor pressure ratio of approximately 10/1 under cruise conditions was selected as being achievable without compromise in configuration simplicity. Demonstrated component technology indicated two transonic axial stages combined with a single centrifugal stage would be sufficient. Modest work input requirements for this compressor permit selection of a single-stage air-cooled turbine drive.

An  $\text{NO}_x$  emission goal was considered the most difficult to achieve, with high-pressure ratio engines requiring a complex combustor configuration. Because  $\text{NO}_x$  emissions increase with pressure ratio, this 10/1 pressure ratio selection also favored combustor configuration simplicity.

Figure 10 shows the results of one of many parametric performance studies conducted during the cycle selection phase. This particular study was conducted for 7620 meters (25,000 feet) cruise at 0.6 Mach Number. Engine performance is plotted two ways for comparison. The chart on the left provides bare engine performance as it would be measured in an altitude test chamber. The righthand chart modified the SFC coordinate to reflect installed specific fuel consumption. Here, losses associated with nacelle drag and weight are factored in as the nacelle size varies with engine bypass ratio.

Performance for a variety of fan bypass ratios are plotted on coordinates of specific fuel consumption and fan pressure ratio. In both figures, specific fuel consumption is seen to reduce with increasing fan bypass ratio up to a ratio of 10/1. Optimum fan pressure ratio decreases with increasing bypass ratio.

A fan bypass ratio of 9.6/1 at cruise was selected to limit required input work to the capability of a single-stage fan drive turbine. The corresponding fan pressure ratio was set at 1.35.

The engine was sized to produce in excess of 7117 N (1600 lb) of thrust under sea level static operating conditions. Sea level and altitude performance are summarized in table III. This performance compares favorably with even larger, more sophisticated engines currently in use.

Figure 11 schematically shows the engine configuration we selected. The gas generator section was not funded by the NASA QCGAT Program. The engine has only six rotating cascades in total, and only two in the hot section where maintenance costs normally accrue. As such, it achieves the simplicity necessary to penetrate the medium aircraft size general aviation cost barrier.

The configuration is a high-bypass turbofan composed of a single-stage fan, a gas generator section, and a single-stage, low-pressure, fan-drive turbine.

Initial compression is provided by the fan stage with the majority of the air bypassing the gas generator section to produce thrust directly, much as a small propeller would. Air flowing through the hub of the fan enters the gas generator and is further compressed by the high-pressure compressor.

A reverse-flow annular atomizing combustor accommodated fuel burning and energy release. Hot gases take a second 180 degree turn before flowing through the high-pressure compressor-drive turbine.

These gases then continue axially aft through the fan-drive turbine. Power from this turbine is transmitted forward by a shaft that is concentric within the hollow gas generator shaft. Rotational speed is reduced by a reduction gear to match the optimum fan engine.

The advantages of the selected configuration are numerous. Initial studies projected attractive specific fuel consumption while maintaining the desired simplicity of only six rotating cascades. Compliance with the recipe for low noise and emissions has been achieved. The reverse-flow combustor permits packaging the gas generator turbine inside the combustor to achieve a short coupled engine, thus avoiding difficulties of casing deformation and shaft natural frequencies. The resulting engine center-of-gravity is close to the axial plane of the main engine mounts, simplifying installation requirements.

Use of the reduction gear permits individual speed optimization to achieve the best efficiency for the fan and the single-stage low-pressure turbine. Also, the low-pressure turbine may then operate at higher rotational speeds where blade pass frequencies, a common noise source, are outside the audible tone spectrum even under low-speed aircraft approach conditions.

Overall, engine configuration is shown cross sectionally in figure 12. External dimensions are approximately 610 mm X 910 mm (2 feet X 3 feet), not including the accessory gearbox.

Helical reduction gearing introduces an axial mechanical load which opposes aerodynamic loads on both the fan and the low-pressure turbine. This provides a significant reduction in thrust loads on the ball bearings in both the fan and low-pressure turbine rotor systems.

The accessory gearbox is chin-mounted at the bottom of the main frame for ease of maintenance without core cowl removal. Accessory drive is provided from the high-pressure rotor spool via a conventional bevel gear mesh and through-shaft with intermediate bearing support.

Figure 13 shows the modular maintenance features of the engine. The engine disassembles into four basic modules, as shown. The fan module includes fan, stators, reduction gear, and main engine frame. The core module contains the high-pressure compressor, its drive turbine, and the combustor.

Separation of the gas generator and low-pressure turbine modules allows visual inspection of all the hot-section components. Full disassembly of both modules was demonstrated to NASA representatives during the short period of a coffee break at one of our coordination meetings.

On the wing maintenance is virtually unlimited by engine configuration. Hot-section inspection, fan blade accessory replacements, gas generators and low-pressure turbine module exchanges are but a few of the options available to the operator.

The QCGAT engine fan module is depicted in figure 14. The fan blade tip diameter is approximately 559 mm (22 in.) with a modest tip speed of 335 meter/second (1100 feet/second) at take-off conditions. The ratio of stator vanes to fan blades is 2.46 for acoustic considerations. The distance between the fan blade trailing edge and the fan stator vane leading edge has been maintained at 2.1 fan blade chord lengths to minimize noise from rotating blade wakes. The fan stator is canted aft to maximize this distance for a given engine length.

The reduction gear permits high turbine rotational speed producing a blade-pass frequency which is above the audible range, even under reduced power approach conditions.

Fan blade containment capability has been provided in the fan shroud design. Imbalance resulting from blade loss, has been a design criteria for the supporting structure.

Hot oil sprayed into the hub of the spinner provides continuous anti-icing and additional oil cooling.

Figure 15 shows an assembled fan wheel. There are 24 rugged long-chord fan blades which are designed to withstand bird impact without the support of a mid-span shroud. Fewer, long-chord blades were selected as being preferable to a higher quantity of short-chord blades incorporating midspan dampers. This reduces wheel cost and avoids the performance penalties associated with midspan shrouds.

Figure 16 depicts the fan bypass stator assembly. In this design, the stator vanes are manually inserted into potted boots retained in the inner and outer shrouds. This feature permits individual vane replacement rather than returning the entire assembly for overhaul repair in the event of foreign object damage.

The QCGAT main structural frame is shown in figure 17. The frame is integrally cast of aluminum. Four engine mounting bosses are provided to permit selection by the airframe designer for top, side, or bottom engine mounting.

A cross-section of the QCGAT core engine is shown in figure 18. The compressor and turbine stages are mounted on a hollow shaft which acts as a throughbolt furnishing the necessary clamping force for the rotor system.

The compressor rotor thrust load is carried by a ball bearing at the front end. A spring-loaded ball bearing at the end of the shaft permits expansion while maintaining radial position. Accessory drive is taken from this rotor by means of a bevel gear drive.

Two ball bearings, supporting the fan-drive turbine rotor, are contained in the same housing which supports the aft high-pressure rotor bearing. This avoids the cost of lubricating and sealing individual packages. A concentric drive shaft through the high-pressure rotor delivers the fan-drive turbine power to the fan module.

All rotating cascades for both the high-compressor and low-pressure turbine rotors are integrally cast to reduce cost. Air cooling is confined to the high-pressure turbine.

Blade loss containment is provided throughout.

The combustor is a folded annular atomizing burner.

In a conventional atomizing combustor, an axial vortex is generated around each atomizer by swirling the air with vanes. In the QCGAT size combustor, sixteen atomizers and swirlers would have been required to attain even, circumferential, temperature distribution.

Figure 19 shows the "circumferentially stirred" configuration which was selected in preference to the conventional combustor. Primary air is admitted through slots in the liner header producing flow circulation in a circumferentially oriented vortex. Secondary air jets, called "folding jets", enter the inner wall directly downstream of each atomizer and force the circumferential vortex into a horseshoe shape as it flows downstream. In this manner, two downstream vortexes are created for each atomizer, and the required number of atomizers is cut by one-half, to eight.

Prior testing has shown this configuration to be superior to conventional combustors in emissions characteristics. It also demonstrated significant margin in UHC and CO but was initially somewhat above QCGAT NO<sub>x</sub> goals. This permitted the trade-off of CO for NO<sub>x</sub> mentioned previously to assure achievement of NO<sub>x</sub> goals.

As a result of this intensive design effort, the first QCGAT engine was assembled in October 1978. In figure 20, the core engine module is shown being connected to the fan module. Figure 21 is a front 3/4 view of the basic engine fully assembled. The addition of the test inlet bellmouth, plus the core engine cowling, is depicted in figure 22.

Figure 23 shows the birth of a new engine model installed in the test cell just prior to its initial test run. Figure 24 is an enlarged view of the engine installed. The first engine run was in October 1978. A 30-hour mechanical verification test was completed in April 1979. May and June were devoted to damping an undesirable resonance in the ring gear. Emission tests were conducted in July.

Figure 25 shows the engine at the acoustic test site during the acoustic testing phase of the program, which was completed in August. The demonstrator engine was then inspected, acceptance tested, and delivered to NASA in October 1979.

## NACELLE DESIGN

A preliminary design in the flight nacelle was defined to establish a realistic baseline from which a ground test nacelle could duplicate the important features at reduced program cost. Only the ground test nacelle was fabricated.

An artist's conception of the flight nacelle is shown in figure 26. The nacelle is composed of the following sections:

1. An inlet duct to provide uniform flow into the engine
2. A fan outer duct and core cowl to guide the bypass air around the engine
3. A mixer assembly to force the mixing of hot, higher velocity core engine exhaust with the cooler, low velocity fan stream
4. A confluent mixing chamber preceding the final nacelle exit nozzle
5. An aerodynamically shaped outer skin, designed to minimize drag at the higher flight speeds.

A mixed-flow confluent exhaust system was selected because it reduces the peak exit velocity, improves propulsive efficiency, and reduces jet noise.

Noise attenuation treatment in the form of perforated acoustic panels has been introduced in the air intake section and in the fan duct outer wall.

Figure 27 shows the engine/nacelle mounting and maintenance access panels. The engine is designed to carry the nacelle aerodynamic and "G" loads. An airframe or nacelle yoke attaches to two points on the engine main frame plus an aft steady link. The entire nacelle is then carried by the appropriate engine flanges. Four access panels are provided for ease of maintenance.

The nacelle aerodynamic contours, summarized in figure 28, are optimized for low drag at 0.65 Mach Number, 10688-meter (35,000-foot) cruise conditions. The intake is designed for high cruise efficiency with modest compromises for static 20.6 meters/sec (40-knot) crosswind tolerance and pressure recovery at low-speed take-off conditions. A NASA/McDonnell-Douglas computer program for three dimensional flow calculations has been used for predicting inlet cowl flow conditions. This program computes flow over axisymmetric bodies at various flow angles of attack. Inlet and fan duct flow velocities are generally below 0.4 Mach Number.

The nacelle is circular in cross-section except for the bottom portion which expands into an elliptical section to house the engine accessories. Boat tail angles vary from 14 to 18 degrees.

The QCGAT ground test nacelle which was used to explore noise and emissions reduction is shown in figure 29. The internal flow lines, flight inlet lip, and the exhaust nozzle are identical to the flight nacelle. External skin was eliminated to reduce program cost.

Flight-worthy hardwall and noise attenuation panels can be readily exchanged as desired.

Three inlet lip configurations (figure 30) which were tested with the QCGAT engine are as follows:

1. An inlet bellmouth for loss-free baseline calibration
2. An exact replica of the flight nacelle lip
3. A lip designed to simulate landing approach inflow conditions.

The flight lip and the inlet bellmouth are compared in figure 31.

Figure 32 shows two views of the mixer nozzle. Studies showed seven lobes to be the optimum for our engine. We selected six, with a very minor performance penalty, to avoid any possible seventh-order upstream excitation of turbine blading. Both shaker tests and engine strain gage testing showed satisfactory dynamic characteristics.

#### CONCLUSIONS

Challenging objectives were set for the QCGAT aircraft preliminary design to respond to our assessment of general aviation needs for the 1980 decade. The aircraft design achieves these objectives to provide six-place, long-distance flight which will be attractive to both the user and the suburban community.

Flight characteristics of this aircraft have been computed to define realistic criteria for measurement of ecological characteristics.

Reflecting on the engine and nacelle designs, the primary objectives of the QCGAT Program have been fulfilled. Large engine noise reduction technology has been successfully employed to the general aviation size engine. The QCGAT Program culminated in demonstration of QCGAT acoustic goals with margin.

A simplified approach to emissions was conceived in response to this program, and the QCGAT goals for emissions were very nearly achieved. Considerable margin was demonstrated for both CO and UHC emissions and NO<sub>x</sub> was within 1 percent of the goal.

QCGAT has given birth to a new engine which is designed to serve the needs of general aviation in the 1980's. While still in its infancy, it has demonstrated attractive performance by current standards. Further development tuning will be required to achieve its full potential which is reflected in

the QCGAT performance goals. Component tests have verified the long term objectives. However, turbine rematch is required to recoup the inherent configuration performance.

Versatile ground test nacelles were created to investigate ecological design parameters. Acoustic panels versus hardwall and mixed exhaust versus split streams were tested under this program.

**TABLE I**  
**BENEFITS FROM ADVANCED**  
**AIRCRAFT DESIGN**

AIRCRAFT CONFIGURATION	FUEL WEIGHT, Kg (LBS)	STRUCTURE AND PROPULSION WEIGHT, Kg (LBS)	GROSS WEIGHT, Kg (LBS)
Current Aircraft	1,368 (3,016)	2,518 (5,551)	4,518 (9,960)
Introduce QCGAT Engine	992 (2,186)	2,390 (5,268)	4,013 (8,848)
Use Composites and Supercritical Wing	931 (2,053)	1,978 (4,360)	3,538 (7,800)
SAVINGS	32%	23%	22%

**TABLE II**  
**DESIGN CONSIDERATIONS FOR EMISSIONS**

EMISSION	CAUSE
Unburned Hydrocarbons	Combustion inefficiency
Carbon Monoxide	Inadequate: Residence Time, Temperature, Efficiency
NO <sub>x</sub>	High Residence Time/Temperature
Smoke	Local Rich Zones

• Beneficial Engine Characteristics:

High Combustion Efficiency at Idle

High Combustor Inlet Temperature at Idle  
(High Speed, Low Compressor Efficiency, Bleed)



TABLE III  
**PROPOSED QCGAT ENGINE PERFORMANCE**

PARAMETER	FLIGHT CONDITION	
	TAKEOFF Sea Level, Static	MAX CRUISE 0.6 M, 7315 M (25,000 FT)
Thrust	7206 N (1622 lbs)	2162 N (486 lbs)
Specific Fuel Consumption	0.0367 Kg/N/hr (0.360 lb/lb hr)	0.063 (Kg/N hr) (0.626 lb/lb hr)

### NEW GENERAL AVIATION AIRCRAFT FOR THE 1980 DECADE

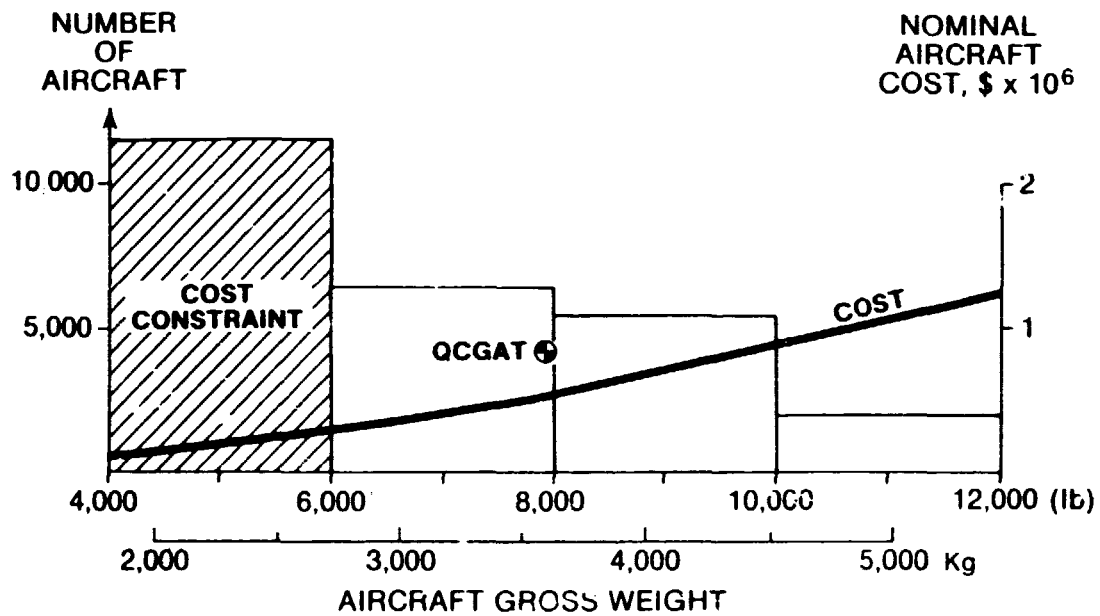


Figure 1

## QCGAT AIRCRAFT DESIGN

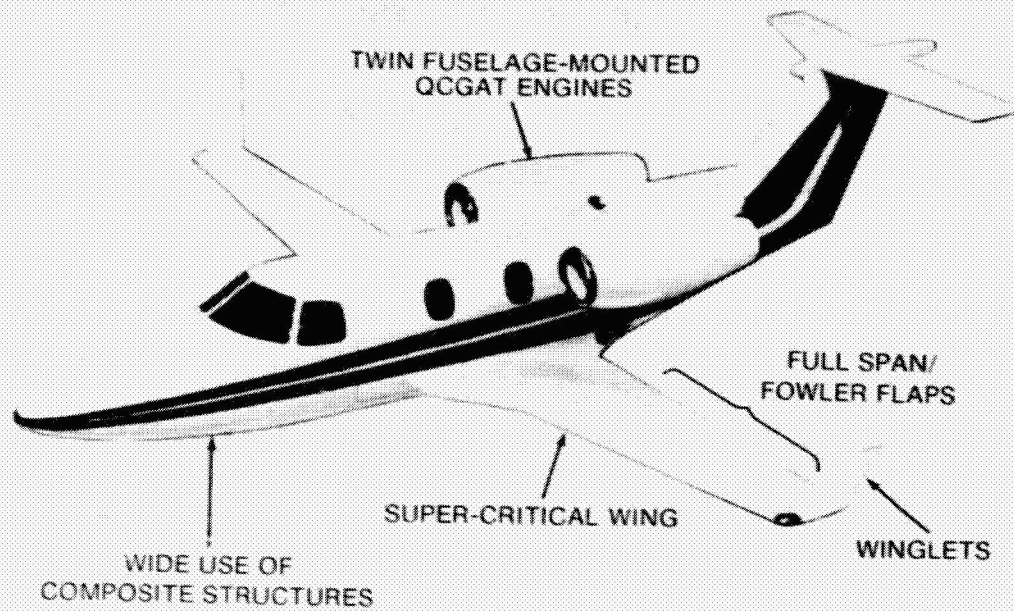


Figure 2

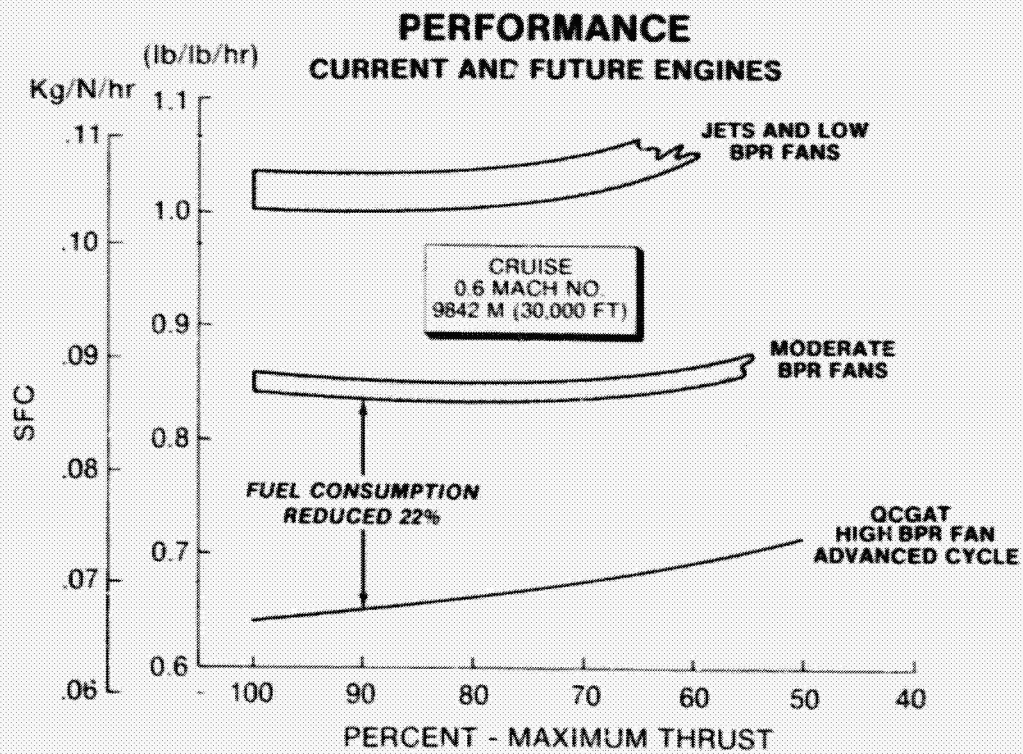


Figure 3

## DESIGN AREAS SELECTED FOR COMPOSITE STRUCTURES

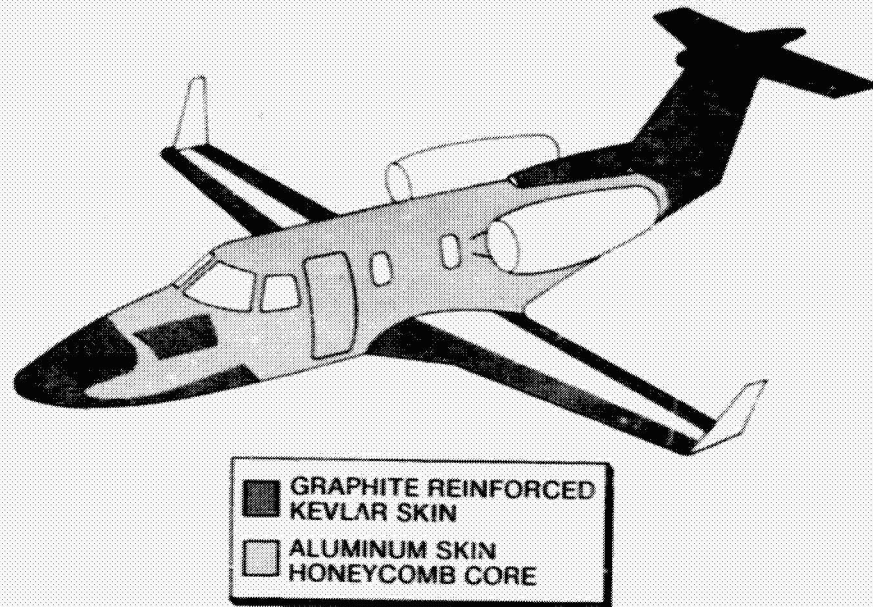


Figure 4

## WING SELECTION

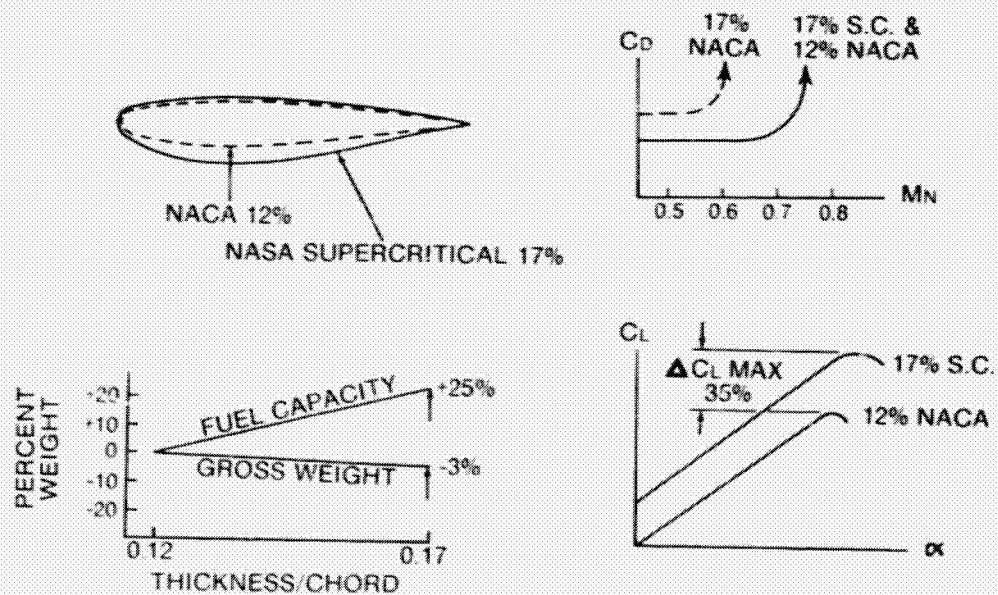


Figure 5

## BEST RANGE vs PAYLOAD

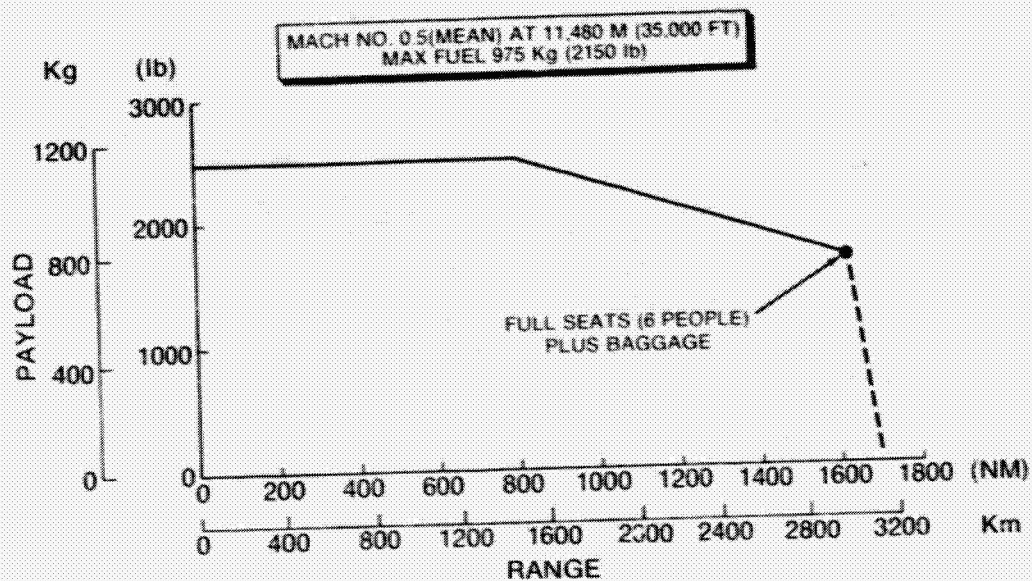


Figure 6

## AIRCRAFT STALL SPEED AND FIELD CAPABILITY

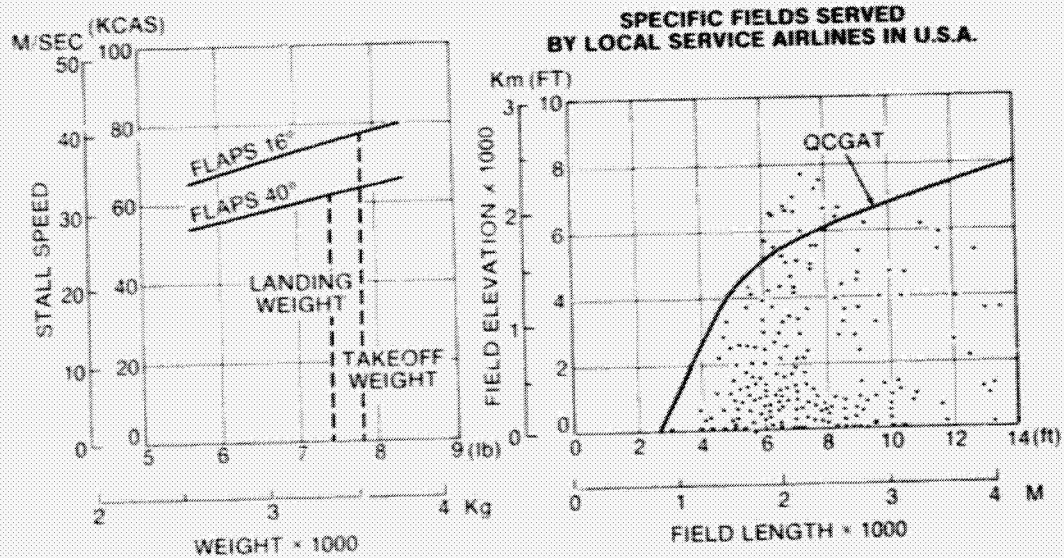


Figure 7

## AIRCRAFT NOISE MEASUREMENT CONDITION

CONDITION	ALTITUDE M (FT)	VELOCITY M/SEC (KTS)	THRUST/ENGINE N (LB)	FLAP ANGLE
Approach	113 (370)	46.85 (91)	1157 (260)	40°
Takeoff Sideline	262 (860)	53.02 (103)	4880 (1097)	16°
Takeoff Flyover	1106 (3630)	53.02 (103)	4644 (1044)	16°

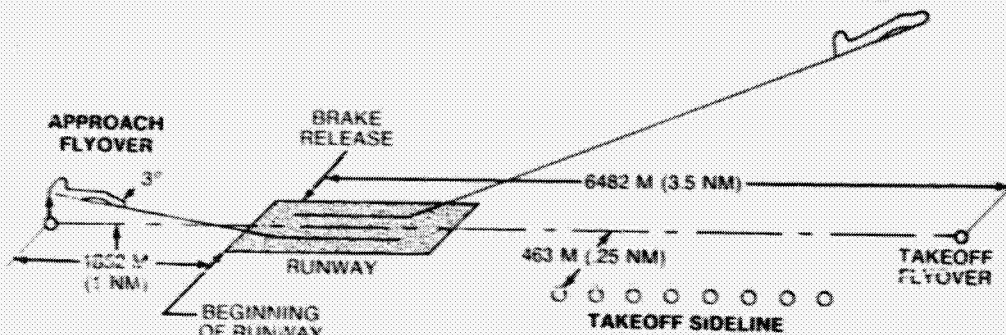


Figure 8

## DESIGN CONSIDERATIONS FOR REDUCED NOISE

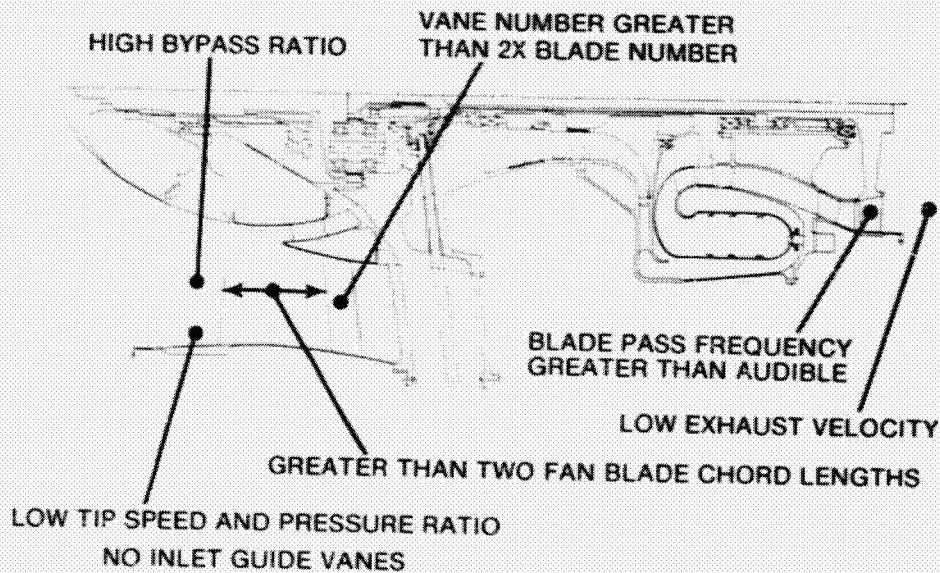


Figure 9

## DESIGN STUDY

### SAMPLE OF OPTIMIZATION TO DEFINE FAN PRESSURE RATIO

CONSTANT COMPONENT EFFICIENCY  
CRUISE AT 0.6 MACH NO. 7315 M (25,000 FT)  
ENGINES SIZED FOR CRITICAL OEI  
CLIMB OUT AT 0.15 MACH NO.  
CYCLE PRESSURE RATIO 10.2

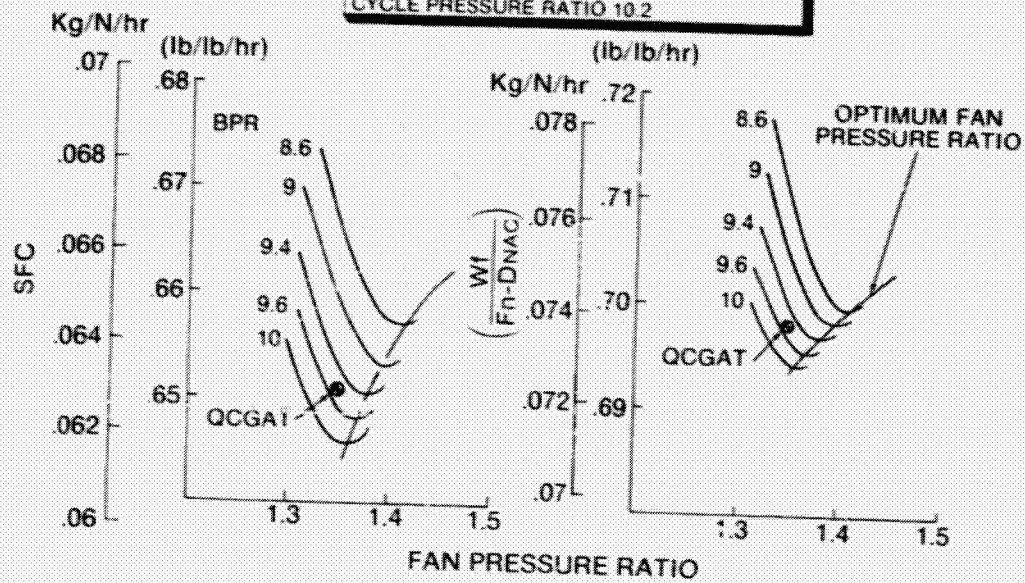
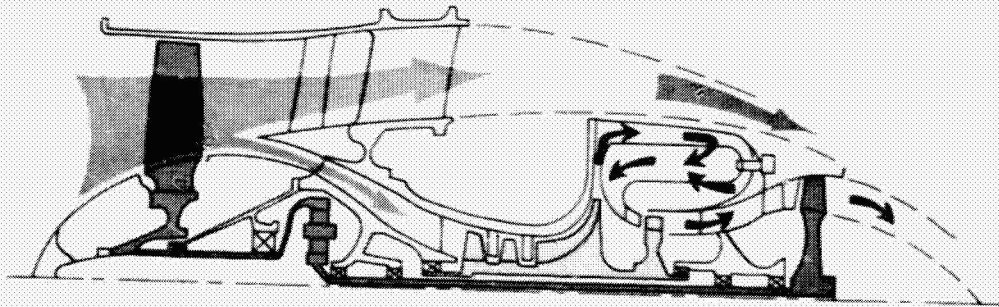


Figure 10

### SELECTED QCGAT ENGINE CONFIGURATION



- Configuration Simplicity
  - Six Rotating Cascades
- Superior Performance
- "GOOD NEIGHBOR" Design

Figure 11



## QCGAT ENGINE CROSS SECTION

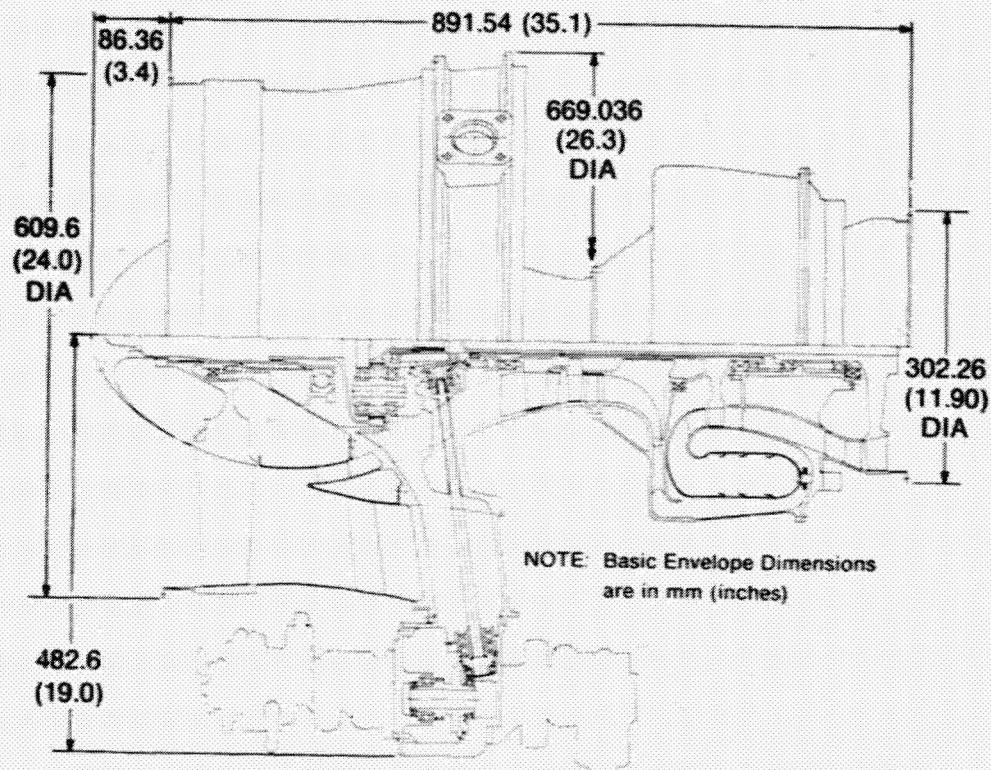


Figure 12

## QCGAT ENGINE MODULES

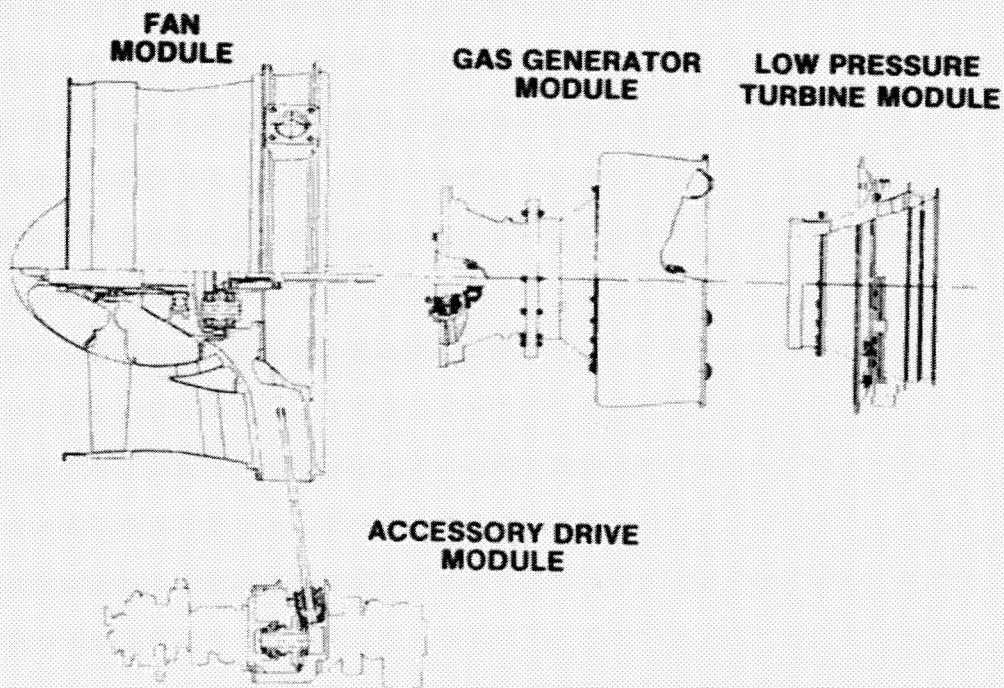


Figure 13

## QCGAT FAN MODULE

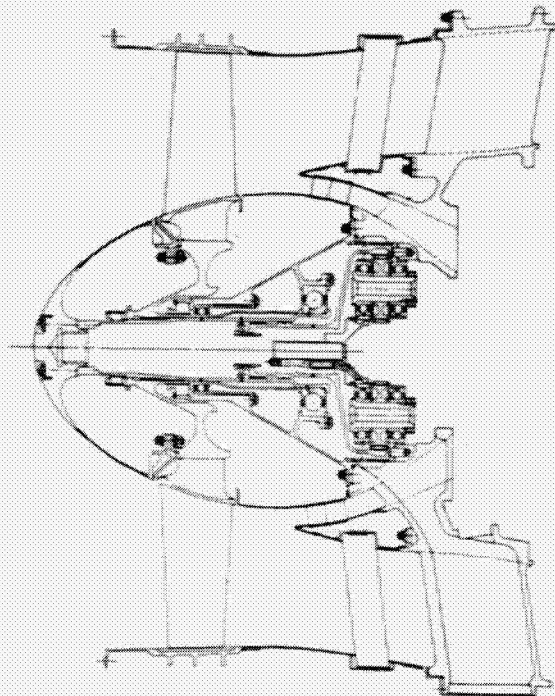


Figure 14

## QCGAT FAN WHEEL ASSEMBLY

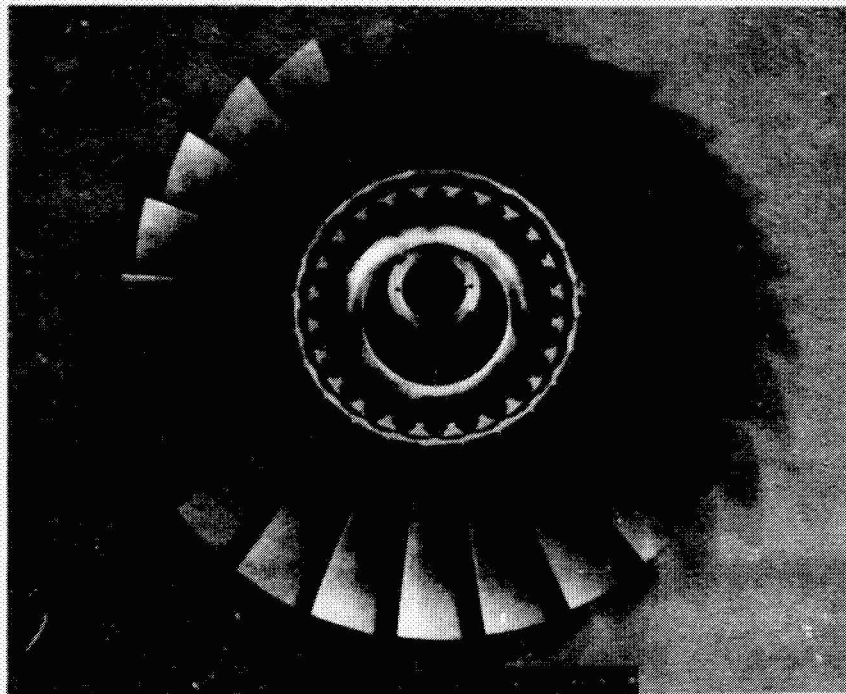


Figure 15



### **QCGAT REPLACEABLE VANE FAN STATOR**

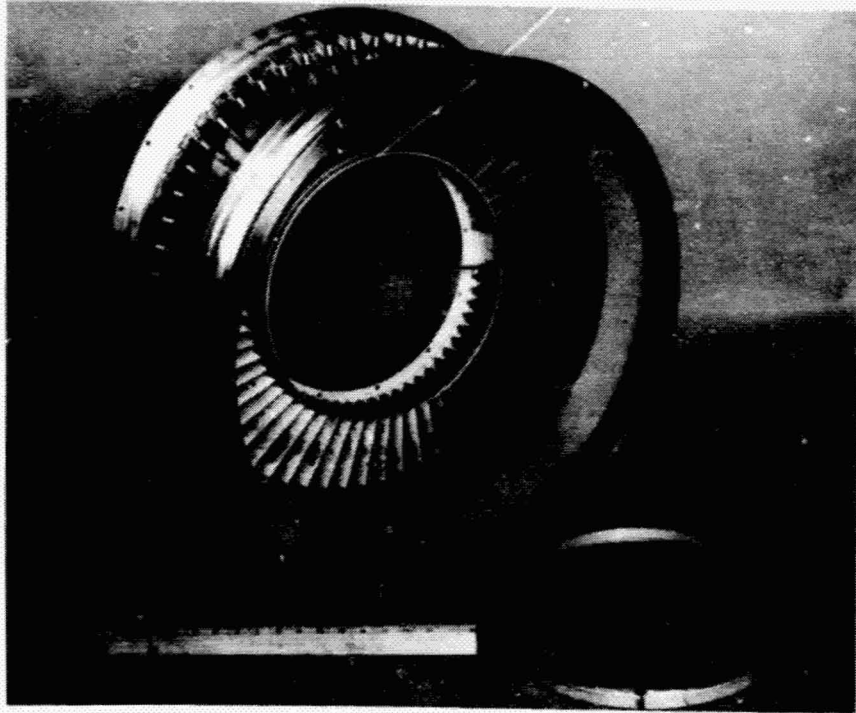


Figure 16

### **QCGAT ENGINE MAIN FRONT FRAME**

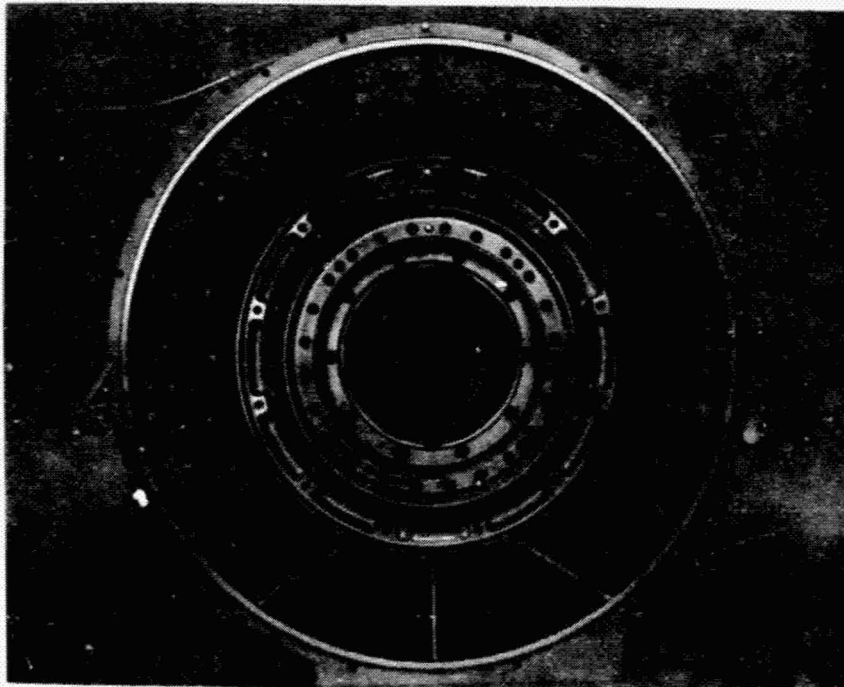


Figure 17

## QCGAT CORE ENGINE

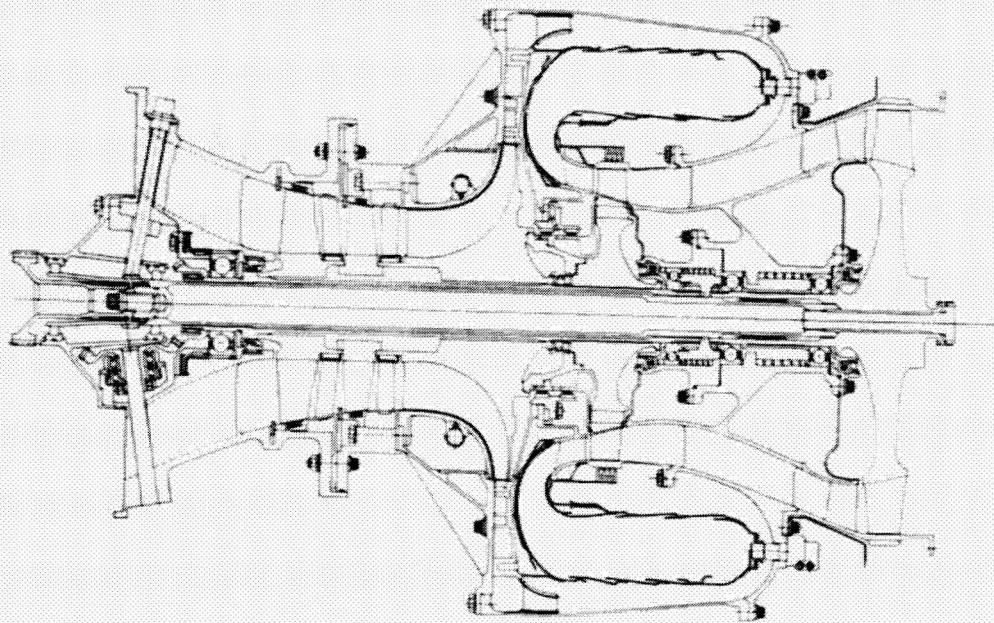


Figure 18

## QCGAT COMBUSTOR

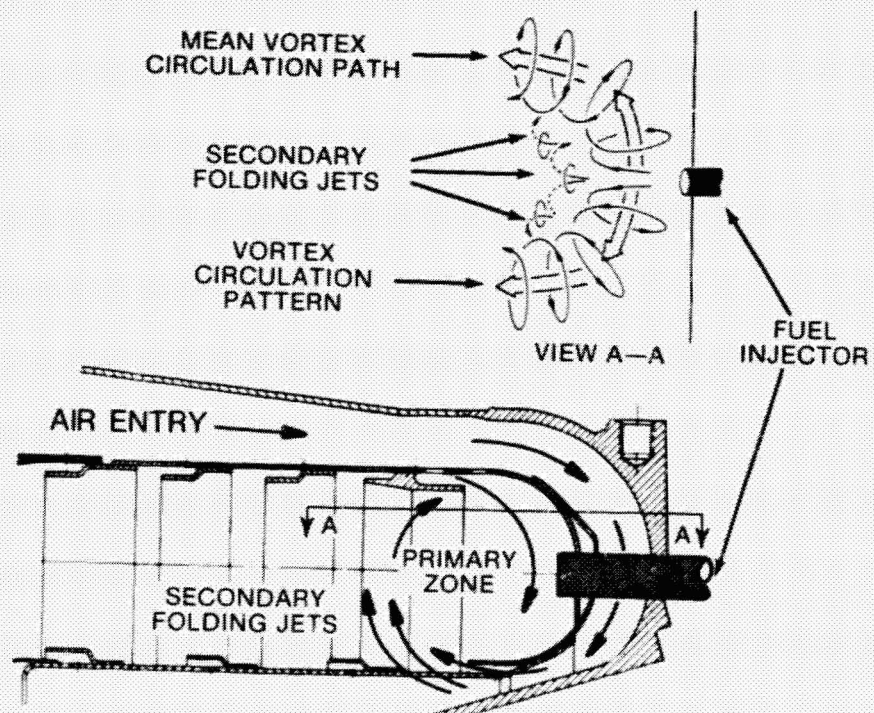


Figure 19



## QCGAT ENGINE ASSEMBLY

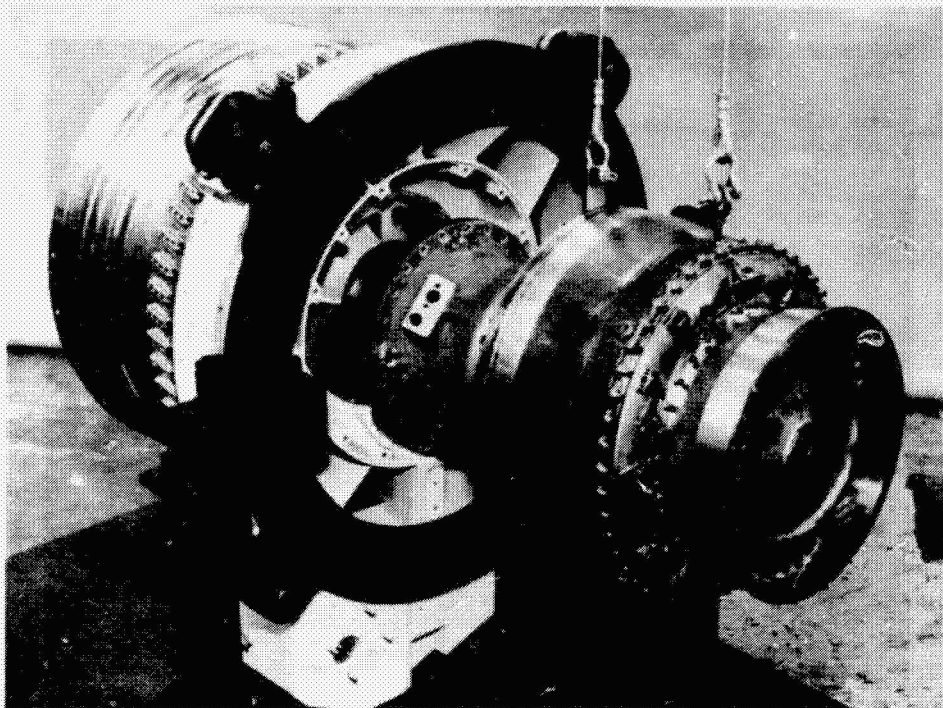


Figure 20

## QCGAT ENGINE

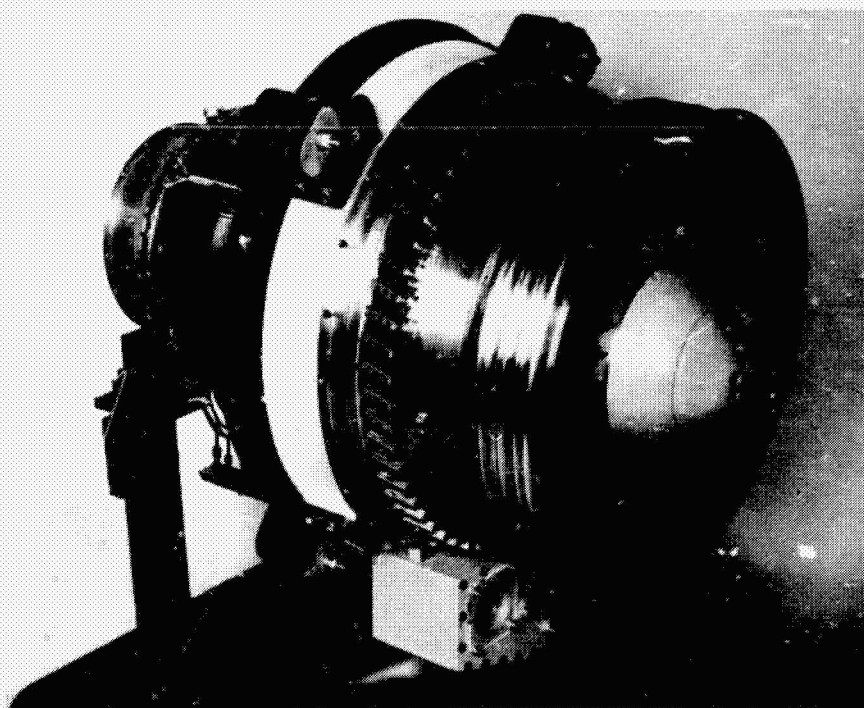


Figure 21

**QCGAT ENGINE WITH BELLMOUTH  
AND CORE COWL**

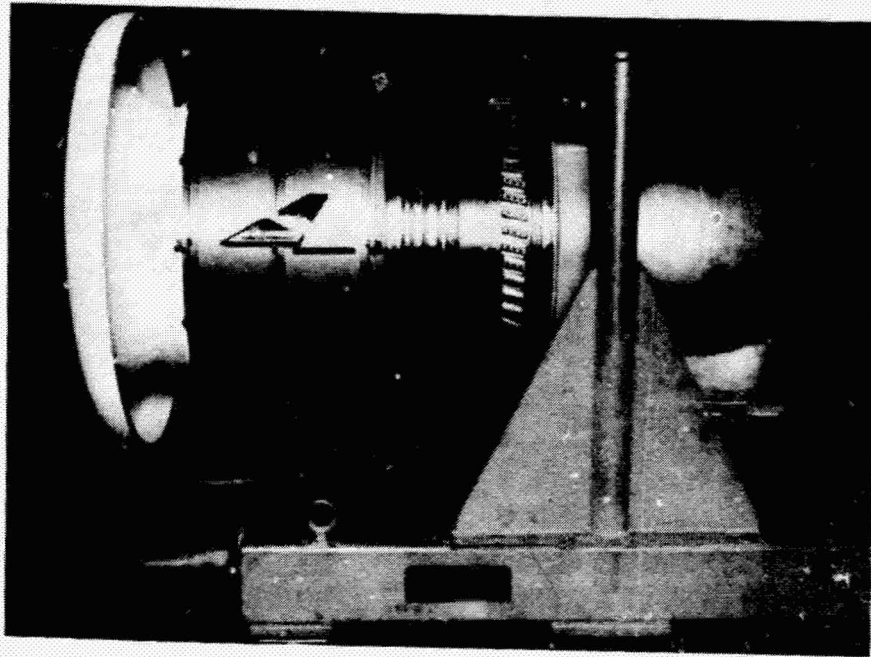


Figure 22

**QCGAT ENGINE IN DEVELOPMENT TEST CELL**

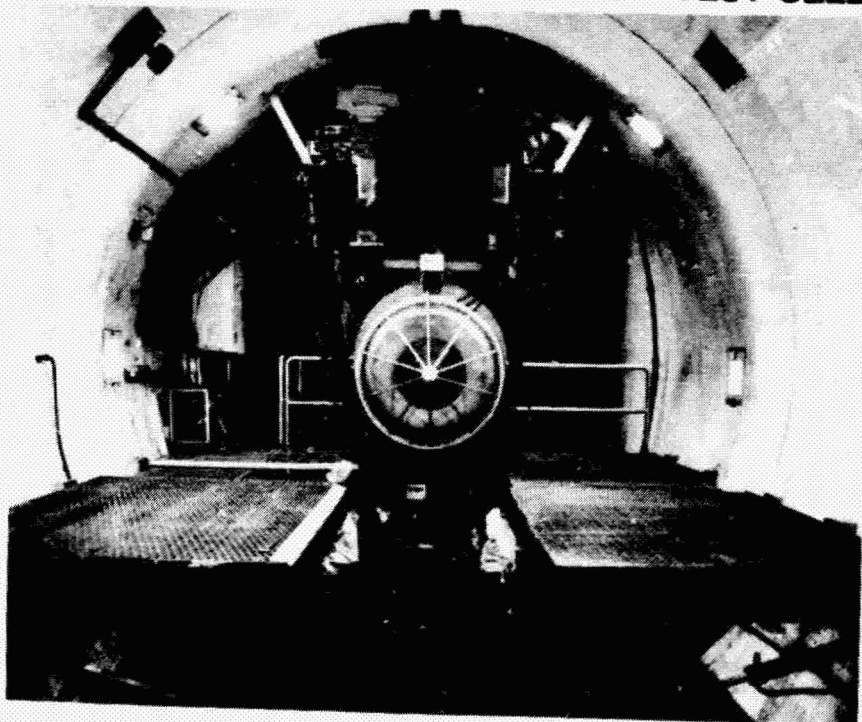


Figure 23

## QCGAT ENGINE AT ACOUSTIC TEST SITE

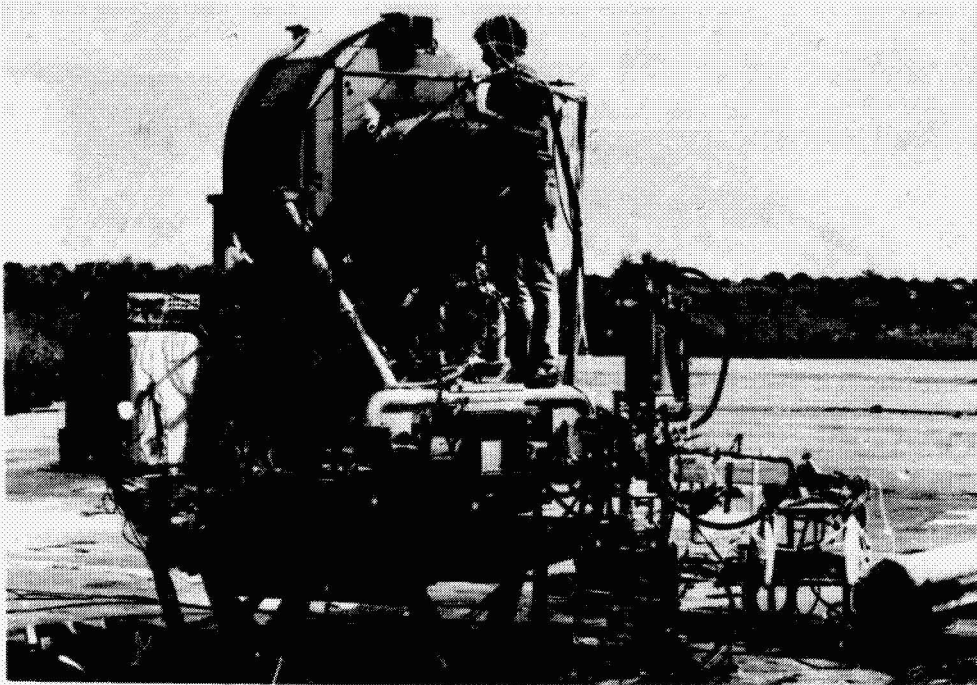


Figure 25

## QCGAT ENGINE IN DEVELOPMENT TEST CELL

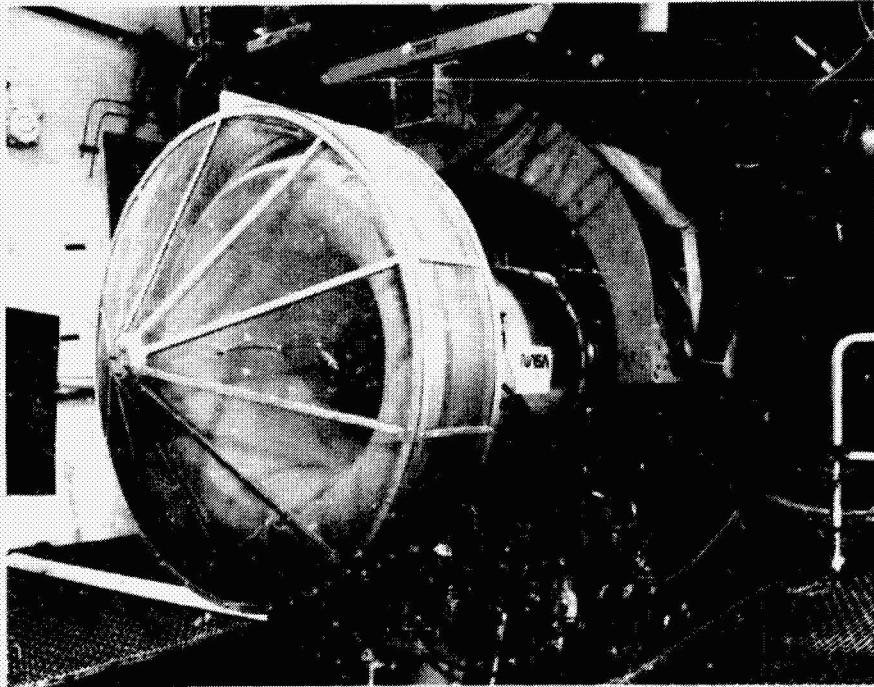


Figure 24

**NASA - AVCO LYCOMING**  
**Quiet Clean General Aviation Turbofan**

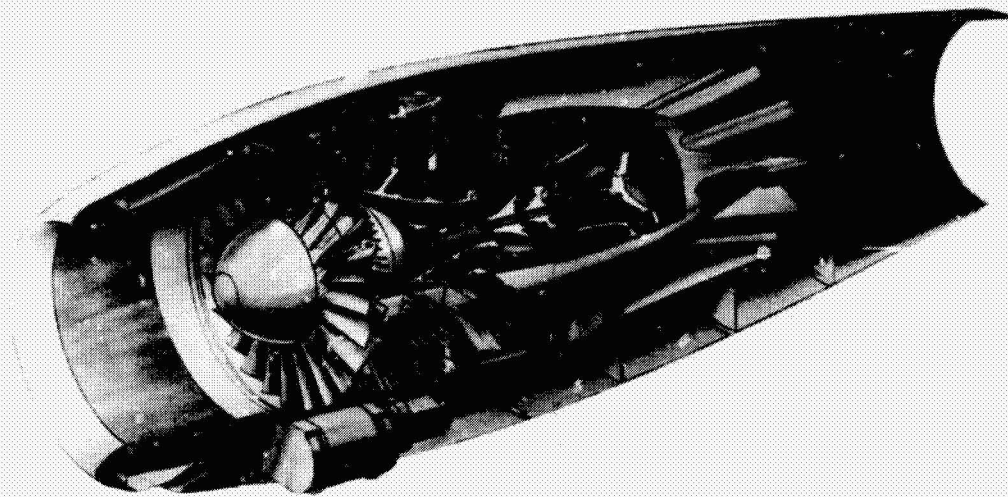


Figure 26

**QCGAT NACELLE ACCESS PANELS**

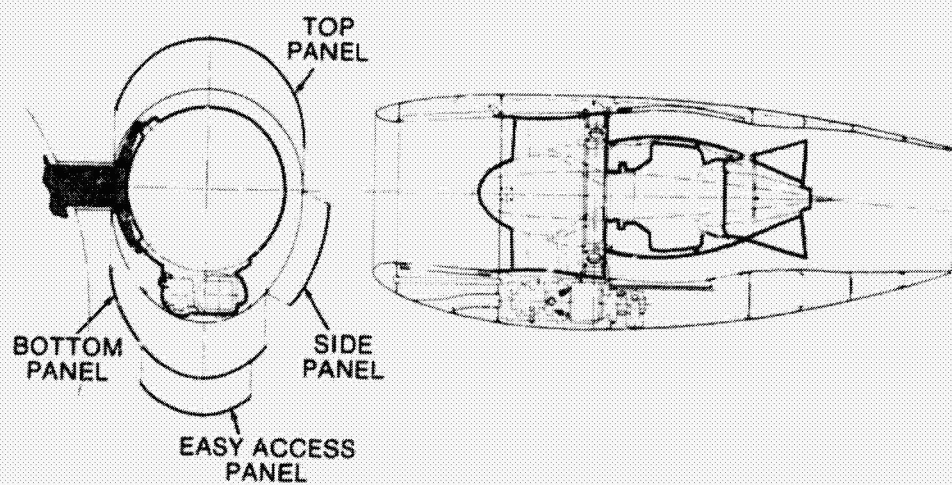


Figure 27



## QCGAT NACELLE EXTERNAL GEOMETRY

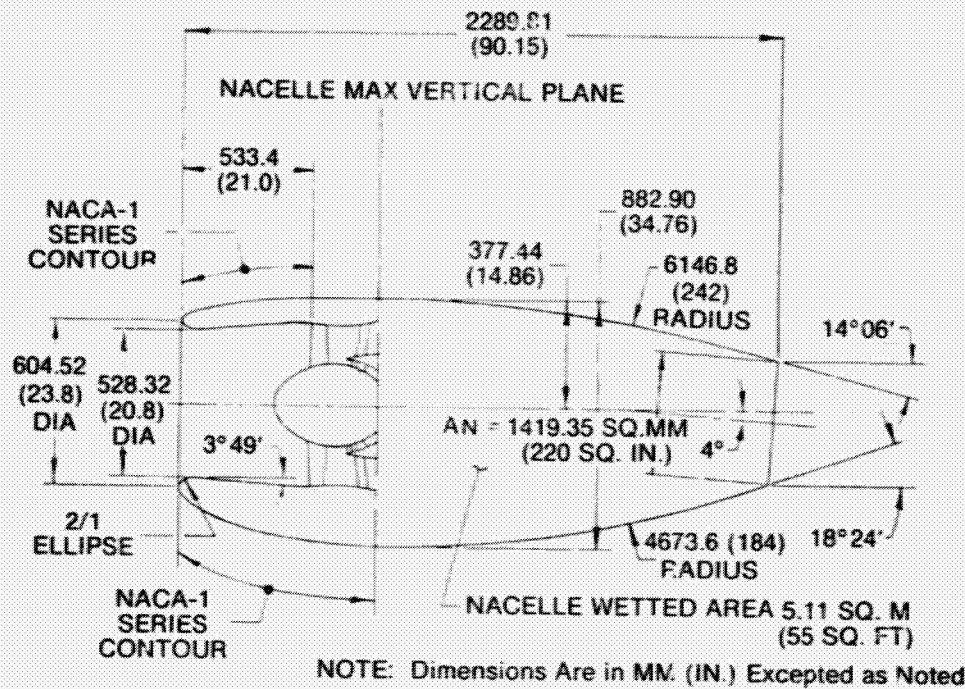


Figure 28

## QCGAT FLIGHT NACELLE SIMULATION

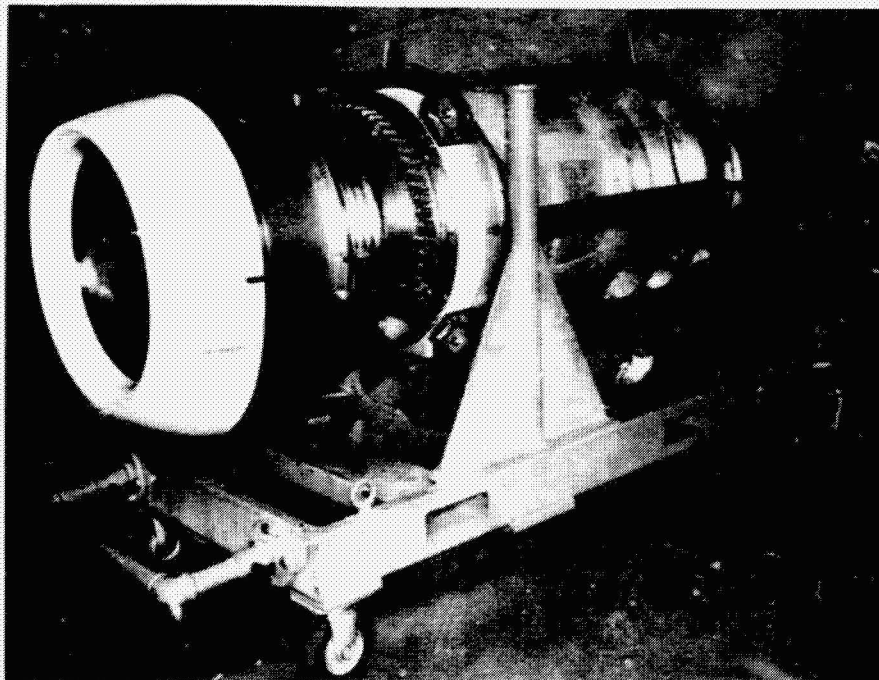


Figure 29

## REPLACEABLE INLET LIPS

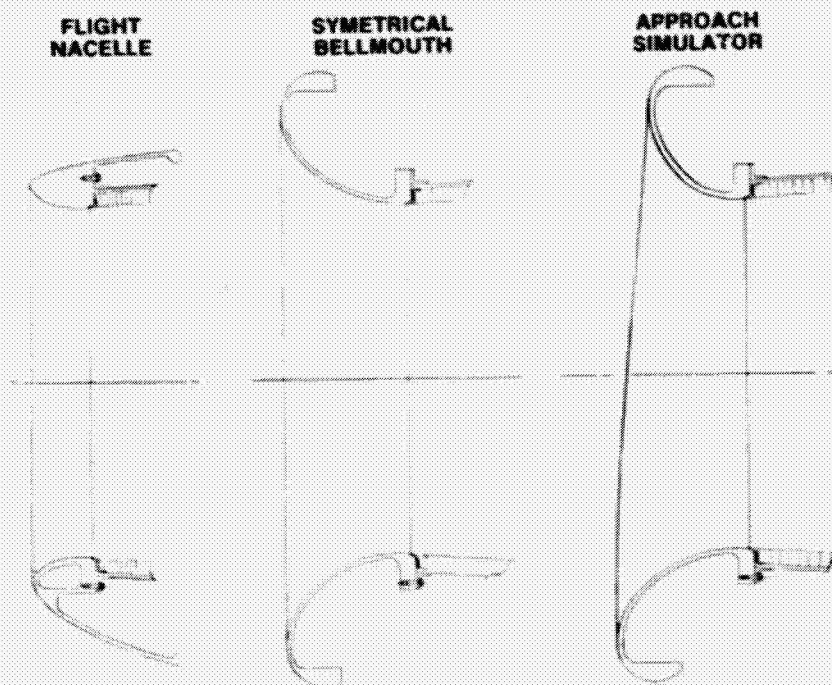
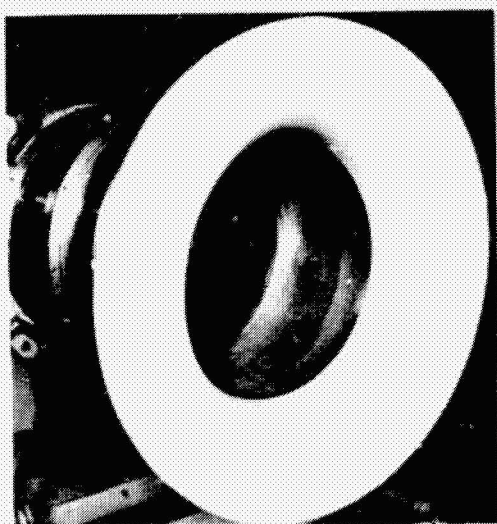


Figure 30

## BELLMOUTH INLET



## FLIGHT NACELLE INLET

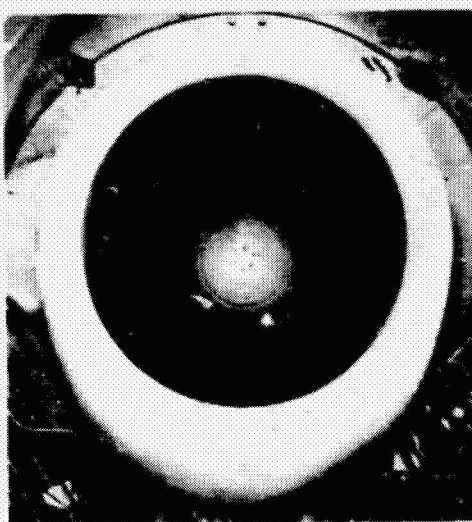


Figure 31



### QCGAT MIXER ASSEMBLY

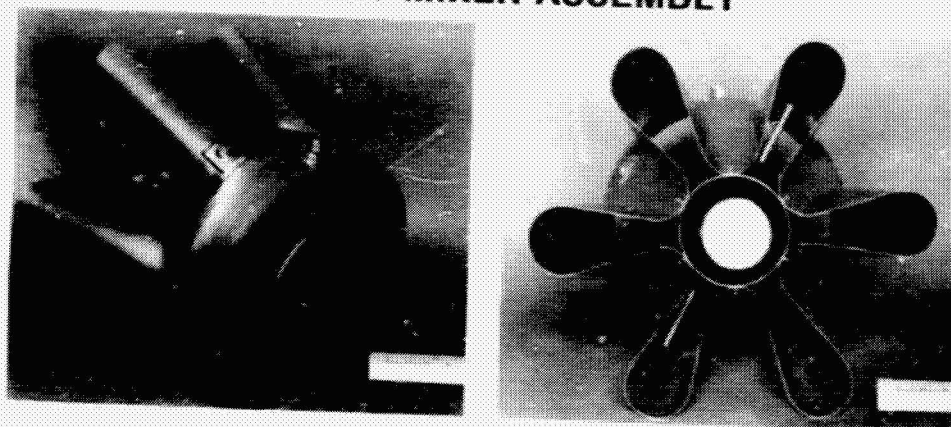


Figure 32

ORIGINAL PAGE IS  
OF POOR QUALITY

35  
N 80-22332

**AVCO LYCOMING QCGAT PROGRAM DESIGN CYCLE,  
DEMONSTRATED PERFORMANCE AND EMISSIONS**

**Phil Fogel and Angelo Koschier  
Avco Lycoming Division**

**SUMMARY**

Lycoming was awarded a NASA contract to design and build a quiet, clean, general aviation turboprop (QCGAT) using existing technology for noise and emissions reduction. In addition, to the noise and emissions considerations, the Lycoming QCGAT engine was designed to provide both minimum fuel consumption in cruise and maximum take-off capability. The engine, which was built and tested at Lycoming, has met and, in some cases, surpassed the design goals for emissions. The engine program has also demonstrated that emissions and noise reduction technology can be effectively applied to small turboprop engines without significant performance penalties.

**INTRODUCTION**

This paper describes the basis for the cycle and component selection, for the Avco Lycoming - NASA QCGAT engine, and the resulting demonstrated performance and emissions of the complete engine. An artist's conception of a cut-away view of the propulsion system is shown in figure 1.

The Avco Lycoming QCGAT engine is a high bypass ratio, twin spool turboprop engine of modular design. It incorporates a front fan module driven by the LTS101 core engine modified, as required, to achieve the QCGAT goals. The engine is housed in a nacelle incorporating full length fan ducting with sound treatment in both the inlet and fan discharge flow paths.

Design goals of components developed under this contract and results of component tests are presented, herein, together with full engine test results.

In the emissions portion of this paper, the rationale behind the combustor design selected for the Avco Lycoming QCGAT engine is presented as well as the test results. Total system (engine and nacelle) test results are also presented.

Lycoming's goal under this contract was not only to demonstrate the transfer of state-of-the-art acoustics and emissions technology currently used on large engines to small engines, but to build this around a high performance engine and airframe system attractive for the 1980's and beyond. It is clear that a high performance fan engine integrated with an advanced airframe design concept is advantageous primarily for high performance twin engine aircraft currently propelled by piston or small turboprop engines in the 373 (500) to 746 (1000) kilowatt (shaft horsepower) class. This segment of the market which has recently shown a strong growth, is expected to continue, especially with the introduction of a quiet, clean high performance aircraft which offers the highest benefit, in terms of noise and pollution reduction, for those communities living at airport boundaries.

The engine installed in the aircraft must offer modern high performance, economical cruise speeds beyond the reach of present turboprop applications and a range over 2224 kilometers (1200) (nautical miles). Prime cruise altitude was targeted for 7620 m (25,000 ft.) at Mach 0.6, with a potential to climb and cruise at 12,192 m (40,000 ft.). These targets were based on data received from aircraft operators.

#### PERFORMANCE CYCLE ANALYSIS

Design and trade-off studies were performed to define the optimum cycle in terms of noise, emissions and performance. The rationale used to select the overall engine characteristics and the fan configuration is exemplified in figures 2 and 3. The optimization study assumed component efficiencies expected at the critical operating conditions:

sea level, static take-off  
7620 m (25,000 ft.) Mach 0.6 cruise  
1524 m (5,000 ft.), hot day single engine climbout

Figure 2 shows engine specific fuel consumption (SFC) versus fan pressure ratio for selected values of bypass ratio. As shown, there is a point of minimum specific fuel consumption for each fan bypass ratio. Higher bypass ratios coupled with lower fan pressure ratios results in lower specific fuel consumption. This, however, has to be moderated because of two factors: installation losses and mechanical complexity. An increase in engine bypass ratio results in increased engine-nacelle drag and weight, which in turn causes an increase in airframe weight or reduction in payload. Also, further increase of the bypass ratio would require a variable geometry exhaust nozzle to prevent excessive fan unloading with resulting loss in fan cruise efficiencies.

The effect of an increase in cycle pressure ratio on SFC is shown in figure 3. Although, increasing cycle pressure ratio decreases SFC, any increases in high compressor pressure ratio beyond approximately 10.2 would require the added complexity of an additional low pressure turbine stage.

As a result of the design study, an initial design bypass ratio of 9.6 and high compressor pressure ratio of 10.2 were selected. Installation weight and nacelle drag effects were considered.

The impact of the selected cruise design point on the maximum thrust, at the critical single engine climbout condition 308°K (555°R) ambient day at 1524 m (5,000 ft.), 69.5 m/sec (135 knots) was examined. This flight requirement was used to size the engine.

It was found that the 7620 m (25,000 ft.) Mach 0.6 design point, when lapsed to 1524 m (5,000 ft.), produces a maximum thrust for the selected bypass ratio.

The selected design cycle is presented in table 1. The changes in the engine parameters, shown in the table 1, from initial performance analysis were caused by detail component design and final cycle optimization for maximum thrust at the single engine climbout condition.

The QCGAT engine installed performance goals for the two prime flight conditions are shown in table 2. This installed performance is with the nacelle system including the flight lip, mixer nozzle and acoustic treatment. The sea level static take-off thrust is 7166 N (1611 lbf) and specific fuel consumption is 0.037 kg/hr/N (0.363 lbm/hr/lbf). For the 7620 m (25,000 ft.) Mach 0.6 cruise, the thrust is 2157 N (485 lbf) and specific fuel consumption is 0.064 kg/hr/N (0.628 lbm/hr/lbf).

A mixer nozzle, reference 1, was chosen for the engine configuration because of acoustic and performance reasons. Figure 4 presents the estimated variations of specific fuel consumption, along an engine operating line, with total net thrust at the selected cruise condition, for the split and forced mixer exhaust systems. As shown, a potential performance gain, at the cruise thrust, of approximately 3.0 percent could be realized with a mixer.

## **COMPONENT DEVELOPMENT AND TEST**

### **Core Engine Definition**

The Avco Lycoming LTS101 turboshaft engine was selected as the basic core for QCGAT engine. Core component modifications required, to meet QCGAT design goals, were Lycoming funded.

### **Component Development**

The major components developed, under the NASA contract, were the fan module, reduction gearing and the nacelle system which includes the forced mixer nozzle. The fan and nacelle were designed with low noise as a primary criteria.

In addition, combustor system modifications were made, as required, to meet the emissions goals.

### **Core Compressor**

The core compressor was tested to establish mechanical and aerodynamic performance with the turbofan inlet duct. The compressor performance and surge characteristics with pressure distortion as measured during the fan component testing were also established.

The rig test results showed that the compressor efficiency was within 1.0 percent of the design goal.

The compressor showed high tolerance to pressure distortion produced by the fan.

Also, the turbofan inlet duct caused a reduction in airflow to the compressor of 1.0 percent at the QCGAT operating conditions.

### **Gas Producer Turbine**

Rig tests on the initial gas producer turbine hardware confirmed that the design efficiency at this stage was met within 1.0 percent. However, the nozzles were substantially larger in flow area than design.

An attempt was made to correct for flow size, by reducing the annulus area formed by the inner and outer wall contour. This corrected the flow area problem but caused cascade losses which reduced stage performance by approximately 3 points.

In addition, the interturbine duct pressure losses increased because of a resulting change in the turbine exit swirl angle.

A redesign of the nozzle and rotor, to recover gas producer efficiency, was completed in July 1979 and the revised hardware is being procured.

#### Fan Component

An experimental evaluation of the QCGAT fan module has shown that the bypass performance has exceeded design goals. At the design pressure ratio (1.38) and speed (11,200 RPM), stage polytropic efficiency of 0.875 was demonstrated. This exceeded the design goal efficiency of 0.870. Bypass airflow at this point was 33.7 kg/sec (74.3 lbm/sec) compared with a goal of 33.6 kg/sec (74.0 lbm/sec).

Limited distortion testing was done to insure satisfactory engine operation. The response of a turbofan to inlet distortion is of prime importance from the viewpoint of aerodynamic performance and mechanical integrity of the blades. Significant distortions occur in aircraft installations as a result of intake flow separation induced either by crosswinds or high angles of attack.

The Lycoming QCGAT fan rotor demonstrated very good aerodynamic and mechanical performance under inlet distortion conditions which are representative, or in excess, of those found in typical turbofan installations.

#### Low Pressure Turbine

The low pressure turbine, which was not rig tested, appeared to perform as anticipated based on measured engine data.

#### COMPONENT STATUS SUMMARY

Engine performance estimates obtained from math model simulations, based upon component test results, showed that further component development of the core, which was initiated in the spring of 1979, was required to achieve performance goals.

However, as a result of the analysis, it was concluded that the Lycoming QCGAT engine was a viable vehicle for demonstrating noise, emissions and specific fuel consumption improvements which were the program's objectives.

## **FULL ENGINE TESTS**

### **Referee Configuration**

Following the component rig tests, the full engine and nacelle system tests were conducted. Two engine configurations have been tested. The referee configuration consists of a calibrated bellmouth followed by a straight inlet duct to the fan shroud as shown in figure 5.

In the exhaust system, the bypass and core flows are physically separated (see figure 6). Separate exhaust nozzles permit individual change of fan pressure ratio and variation of the power split between the fan and core.

### **Test Nacelle Configuration**

The QCGAT test nacelle configuration is shown, in figure 7, with the flight inlet lip and diffusing duct which is mounted to the fan shroud. The flight lip can be readily interchanged with the bellmouth or the approach simulator inlets.

Details of the test nacelle are shown in figure 8. The diffusing duct following the inlet contains interchangeable hardwall or acoustically treated softwall liners. The nacelle rear section consists of a core cowl covering the core engine while providing a smooth aerodynamic inner wall contour for the fan flow surrounding the core. The common mixed exhaust nozzle clamps to the rear face of the fan frame and contains the removable duct portion of either hardwall or softwall panels.

### **Engine Test Plan**

Various combinations of the two basic engine configurations, the referee and test nacelle, were tested during the performance calibration sequence.

Table 3 shows an overview of the 7 prime engine configurations which were tested in order to determine the performance characteristics of the engine and nacelle system components. Prior to these tests, a baseline engine configuration was tested with a calibrated bellmouth coupled to a constant area duct and split exhaust.

The first three configurations, listed in table 3, with the split, or referee exhaust system, were tested with the diffusing flight inlet duct and the various interchangeable inlet lips.

All tests with the split exhaust were performed without the acoustic panels. The referee configuration with a bellmouth inlet was also used for the emissions sampling.

The test nacelle configuration with the mixed exhaust was initially tested, for performance purposes, only with the bellmouth inlet. First, tests were conducted with hardwall panels in the inlet and fan bypass exhaust. Then acoustic panels were placed in the inlet only. Finally, the engine was tested with acoustic panels in both the inlet and fan bypass exhaust. The installed performance demonstration was with the flight nacelle inlet, mixer nozzle and full acoustic treatment.

### Referee Engine Tests

The purpose of the initial tests with the referee configuration was to evaluate mechanical engine operation and stress levels on fan and gear components.

Subsequent tests using the referee system, were conducted to evaluate overall engine and component performance prior to evaluating losses associated with acoustically treated nacelle system. Variations in performance attributed to the mixer system was also to be determined.

The purpose of these tests were twofold: first, to establish a base calibration for determining component performance. Secondly, to evaluate inlet pressure losses associated with the diffusing duct coupled to the various inlet lips. As previously stated, emissions sampling was also conducted using the split exhaust configuration.

Detailed analysis of test data has indicated that the diffusing duct and various inlets had a negligible impact on the overall engine performance. The engine test results with the referee configuration confirmed the predicted engine performance.

### Nacelle Engine Tests

Following the referee system performance and emissions tests, the installed nacelle test sequence was conducted. The purpose of these tests was twofold: first, to establish engine performance with a mixer nozzle; second, to evaluate the impact of the inlet and fan bypass exhaust acoustical panels on engine performance. After the performance evaluation tests, the engine was transferred to the acoustic test site for noise evaluation.



Table 4 shows a comparison between the demonstrated installed engine thrust and specific fuel consumption with the design goals. The measured static thrust and specific fuel consumption are 6485 N (1458 lbf) and 0.0400 kg/hr/N (0.392 lbm/hr/lbf). The cruise performance was estimated based upon engine static test data and component rig test results.

## PERFORMANCE SUMMARY

Engine test results indicated that the acoustic panels, used for noise reduction, had a negligible influence on the overall engine performance. The estimated cruise performance of the Avco Lycoming QCGAT engine, in terms of specific fuel consumption, is approximately a 10.0 percent improvement over currently available small turbofan engines in the 13,344 N (3000 lbf) or less thrust class.

Also, although the program performance goals were not achieved, the loss in engine performance has been identified as deficiencies in the turbine section of the core engine. The performance of the fan, which was developed under the NASA contract, exceeded the design goals. A redesign of the affected hardware has been completed under a separate Lycoming funded program. Rig tests are scheduled to be conducted to evaluate the redesign as soon as the hardware is available.

## EMISSIONS

### Emission Standards

In 1970, Congress passed the Clean Air Act. This Act, which was to be effective in 1971, directed the Environmental Protection Agency to establish emissions standards applicable to aircraft. These standards, reference 2, for small turbofan aircraft, which have now been abandoned by the EPA, were kept as NASA goals for the QCGAT engine program. To achieve these emissions limits, the basic combustor design used in the LTS101 engine, references 3 and 4, was selected.

### Combustor Design

This design, which is a circumferentially stirred combustor, is shown in figure 9. In principle, the primary air is admitted through slots in the liner header producing flow circulation about a circumferential mean line. Air jets, called "folding jets" entering through the inner wall reinforce the primary zone recirculation, and the vortex fills the

full annular height of the liner.

The vortex spreads circumferentially in both directions and is forced to turn in the axial direction on either side of the folding jets and the mean path of the combustion zone flow vortex takes the shape of a horseshoe. The number of fuel injectors is thereby reduced by one half, compared with normal practice, because of this unique combustor primary zone aerodynamic concept.

#### Emissions Projections

Emission measurements, for this type of combustor, attained from the LTS101 engine were available for use in predicting emissions for the QCGAT performance cycle. Table 5 shows the estimated emissions values, for the QCGAT cycle, with the production LTS101 combustor. These EPA parameters were generated for a take-off and landing cycle for class T1 aircraft (reference 2).

These emissions projections indicated that further development of the LTS101 combustor was required to reduce smoke. The hot end durability was in question because of the more severe operating conditions of the QCGAT engine.

#### Combustor Modifications

Airblast injectors, which replaced the dual orifice injectors, were selected to reduce smoke. The introduction of the airblast injectors also increased combustor efficiency and oxides of nitrogen (NOx) at idle.

Increasing the combustor pressure drop for temperature distribution control, also increased NOx and combustor efficiency while appreciably decreasing carbon monoxide and unburned hydrocarbons. This is typical of the improved primary zone mixing, which results from the higher pressure drop.

Air partition modifications were then made, as required, to meet the design goals for NOx.

Figure 10 presents the effect of air partition modifications on NOx. Unburned hydrocarbons and carbon monoxide were within the goals in all tests. Initially, the NOx slope for the LTS101 combustor was as predicted, and met the goal. However, as the combustor pressure drop was increased to reduce smoke, NOx increased.

Air partition modifications, as previously stated, were then made to meet the NOx emissions goal.

The final selected QCGAT liner, which met the goal, has a slightly steeper slope than the initial configuration.

The Lipfert correlation, reference 5, for conventional combustors is shown for comparison.

### Emissions Sampling

Development and initial emissions testing of the combustor was conducted in the laboratory. After the laboratory tests, the QCGAT liner was transferred to the engine for demonstrated emissions sampling.

The emissions test probes were installed as shown in figure 11. The probes, which are cruciform-shaped, were set at two angular positions. One probe measured along the horizontal and vertical axes. The other probe was rotated 45 degrees.

Table 6 is a comparison of the emissions test results with the NASA goals. Measurements from the engine test showed that the unburned hydrocarbons were 60 percent lower than required. The carbon monoxide was 30 percent lower, oxides of nitrogen 1.0 percent higher and the smoke number 50 percent lower than the goal.

### EMISSIONS SUMMARY

The emissions requirements of the QCGAT engine have been met and, in most cases, surpassed. The QCGAT combustor provides substantial margin for carbon monoxide and unburned hydrocarbons emissions while meeting the goal for NOx within the scope of the program.

The combustor system modifications required to meet the emissions goals had a negligible effect on engine performance.

### CONCLUSION

The QCGAT development program was designed to demonstrate, as well as advance, state-of-the-art technology with regard to noise, emissions and fuel economy of small turbofan engines used in general aviation-type aircraft. The program objectives, in terms of emissions and fuel consumption, were met.

With the knowledge and experience gained through the NASA-Avco Lycoming engine program, the thrust and SFC goals, although not demonstrated within the time period of the program, are achievable with additional component development.

#### REFERENCES

1. J. F. Hurley, L. F'Anson, and C. Wilson, "Design of an Exhaust Mixer Nozzle for the Avco-Lycoming Quiet, Clean General Aviation Turbofan (QCGAT)." Avco-Lycoming Div., Avco Corp., Proj. FEDD, NASA CR-159426, 1978.
2. Emissions Standards and Test Procedures, Title 40, CFR Part 87, published in the Federal Register, July 17, 1973.
3. U.S. Patent 3,671,171, "Annular Combustors", Brian W. Doyle.
4. U.S. Patent 3,645,095, "Annular Combustor", Jerry O. Melconian.
5. Lipert, F.W., "Correlation of Gas Turbine Emissions Data", ASME Paper 72-GT-60.

## RESULTS OF DESIGN STUDY

ALTITUDE = 7620m(25,000 FT), MACH = 0.6

	<u>SELECTED DESIGN</u>
Fan Pressure Ratio	1.36
Cycle Pressure Ratio	13.7
Core Compressor Pressure Ratio	10.3
Thrust/Total Airflow, N/kg/sec(lbf/lbm/sec)	113.7(11.6)
Bypass Ratio	9.4

Table 1.

## AVCO QCGAT PERFORMANCE GOALS

(STANDARD DAY, INSTALLED)

	<u>SEA LEVEL STATIC</u>	<u>7620m(25,000 ft) MACH = 0.6</u>
Rating	Takeoff	Cruise
Thrust, N(lbf)	7166(1611)	2157(485)
SFC, kg/hr/N(lbm/hr/lbf)	0.0370(0.363)	0.0640(0.628)

Table 2.

### ENGINE CONFIGURATIONS TESTED (PERFORMANCE TESTS)

<u>ENGINE CONFIGURATION</u>		<u>ACOUSTIC TREATMENT</u>	
<u>INLET</u>	<u>EXHAUST</u>	<u>INLET</u>	<u>BYPASS</u>
<b>REFEREE CONFIGURATION</b>			
*Bellmouth	Split	Hardwall	Hardwall
Flight	Split	Hardwall	Hardwall
Approach Simulator	Split	Hardwall	Hardwall
<b>TEST NACELLE</b>			
Bellmouth	Mixer	Hardwall	Hardwall
Bellmouth	Mixer	Softwall	Hardwall
Bellmouth	Mixer	Softwall	Softwall
Flight	Mixer	Softwall	Softwall

\*Emission Test Configuration

Table 3.

### AVCO QCGAT PERFORMANCE (STANDARD DAY, INSTALLED)

	<u>GOAL</u>	<u>DEMONSTRATED</u>
<b>SEA LEVEL, TAKEOFF</b>		
Thrust, N(lbf)	7166(1611)	6485(1458)
SFC, kg/hr/N(lbm/hr/lbf)	0.0370(0.363)	0.0400(0.392)
<b>DESIGN CRUISE, 7620m(25,000 ft) MACH = 0.6</b>		
Thrust, N(lbf)	2157(485)	1850(416)*
SFC, kg/hr/N(lbm/hr/lbf)	0.064(0.628)	0.074(0.723)*

\*Estimated from Static Data

Table 4.

**INITIAL ESTIMATED QCGAT EMISSIONS**  
**LTS 101 COMBUSTOR**

	<u>UNC</u>	<u>CO</u>	<u>NOx</u>	<u>SMOKE NUMBER</u>
Estimated Values*	0.034 (1.2)	0.238 (8.4)	0.096 (3.4)	70.0
NASA Goals*	0.045 (1.6)	0.266 (9.4)	0.105 (3.7)	45.0

\*g/kNs (lbm/1000 lbf thrust hr-cycle)

Table 5.

**QCGAT EMISSIONS RESULTS**

	<u>UNC</u>	<u>CO</u>	<u>NOx</u>	<u>SMOKE NUMBER</u>
Goal*	0.045 (1.6)	0.266 (9.4)	0.105 (3.7)	45
Engine Test*	0.017 (0.6)	0.193 (6.8)	0.106 (3.75)	24
Engine Test/Goal	0.4	0.7	1.01	0.5

\*g/kNs (lbm/1000 lbf thrust hr-cycle)

Table 6.

# AVCO LYCOMING QCGAT ENGINE

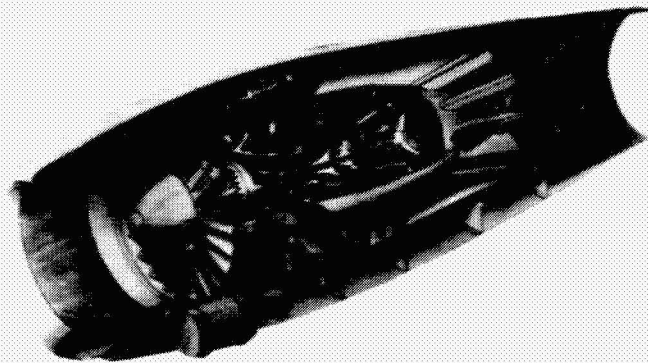


Figure 1

## FAN PRESSURE RATIO SELECTION (UNINSTALLED)

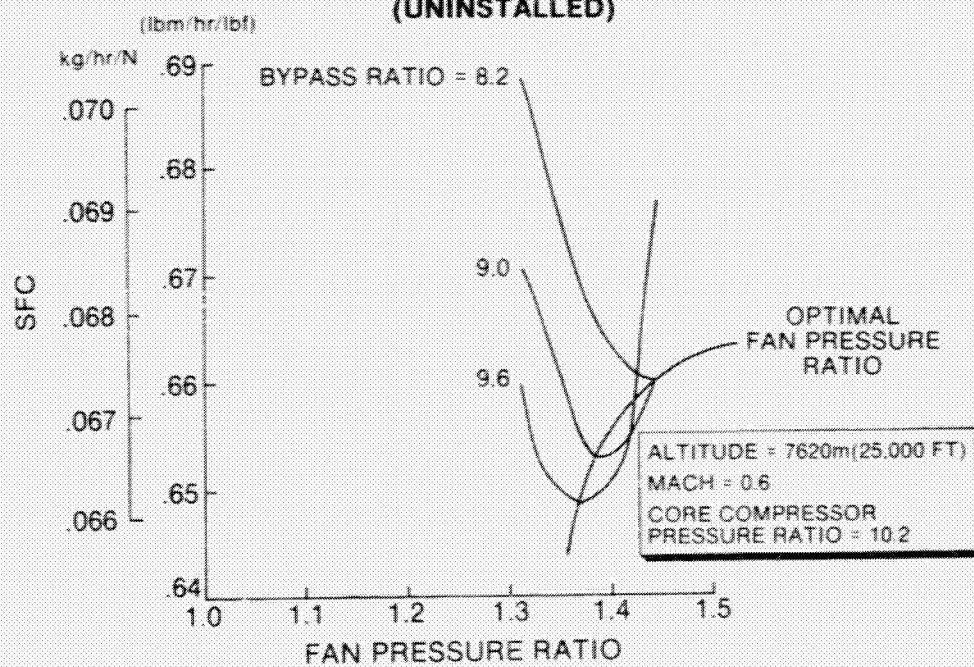


Figure 2

ORIGINAL PAGE IS  
OF POOR QUALITY



## SELECTED DESIGN (UNINSTALLED)

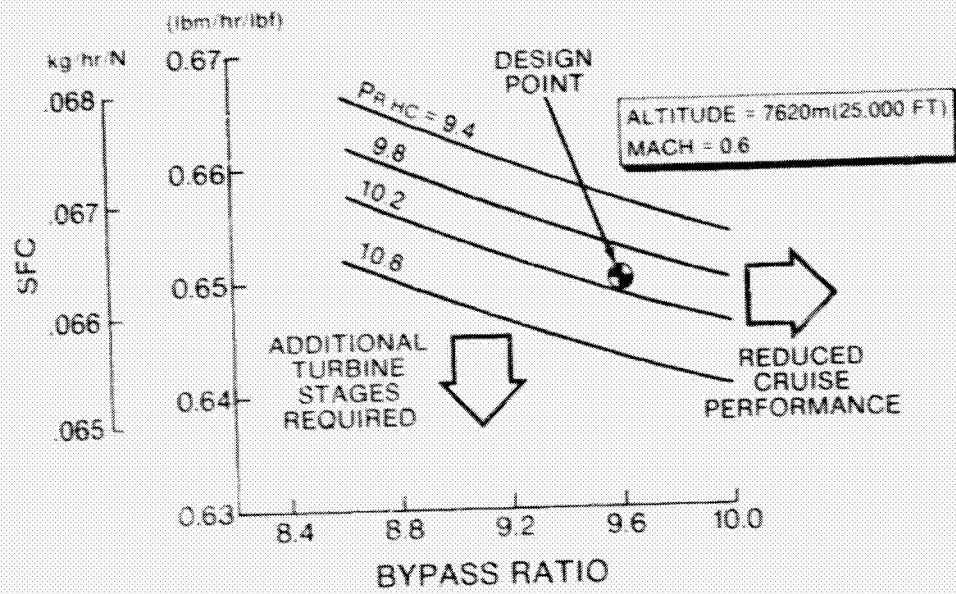


Figure 3

## PREDICTED INFLUENCE OF MIXER Fn vs SFC

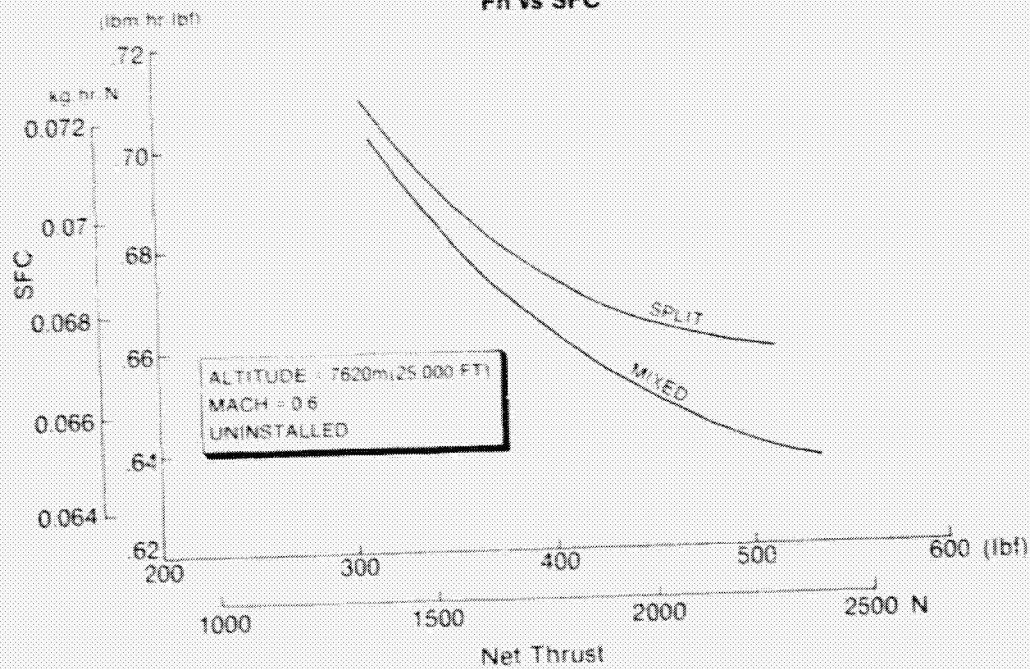


Figure 4

## QCGAT REFEREE CONFIGURATION

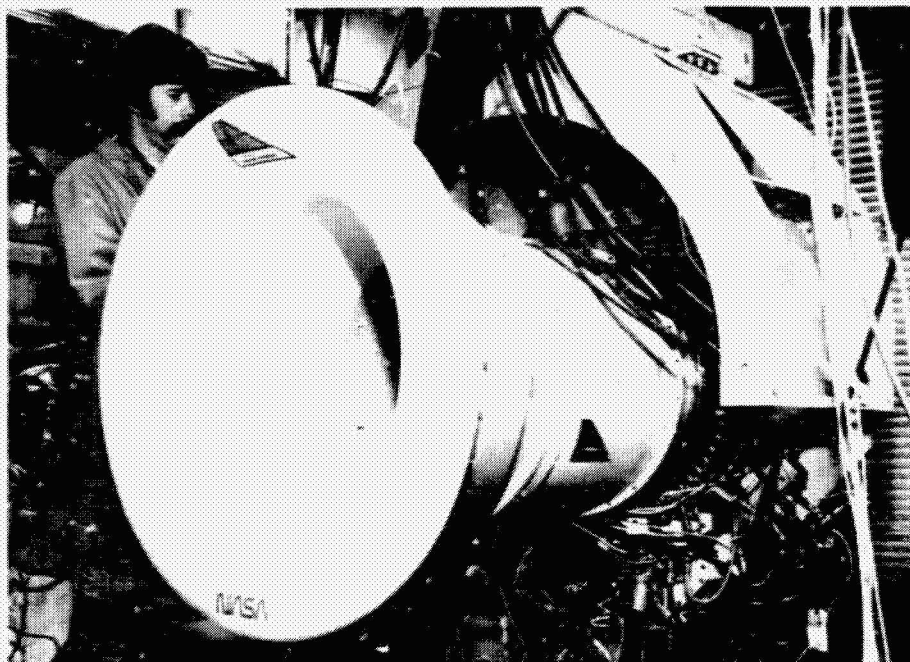


Figure 5

## QCGAT REFEREE CONFIGURATION

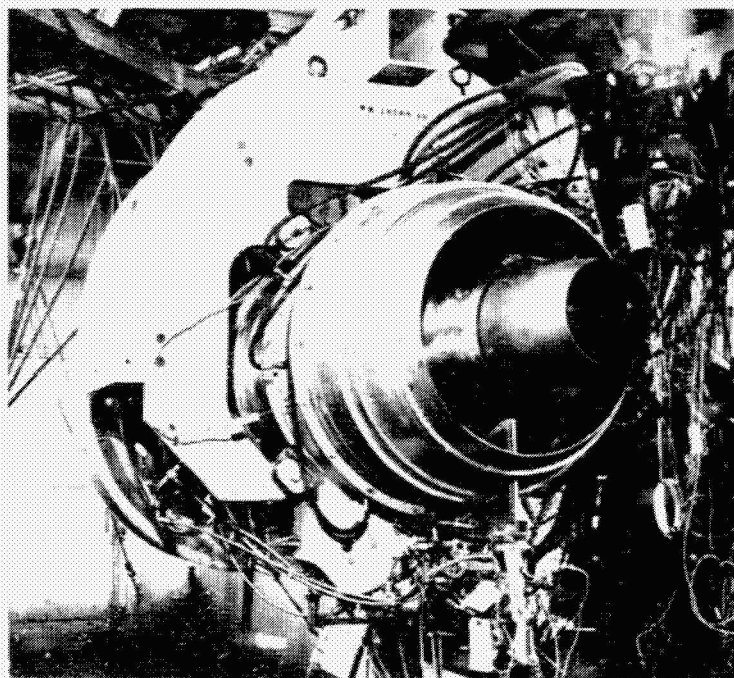


Figure 6

## QCGAT TEST NACELLE

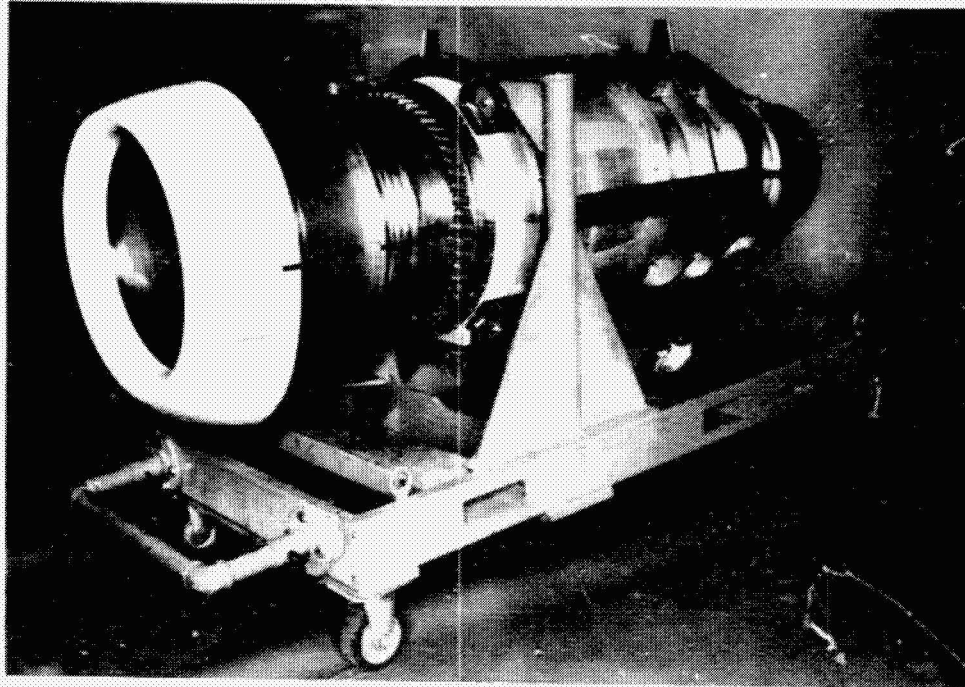


Figure 7

## QCGAT TEST NACELLE

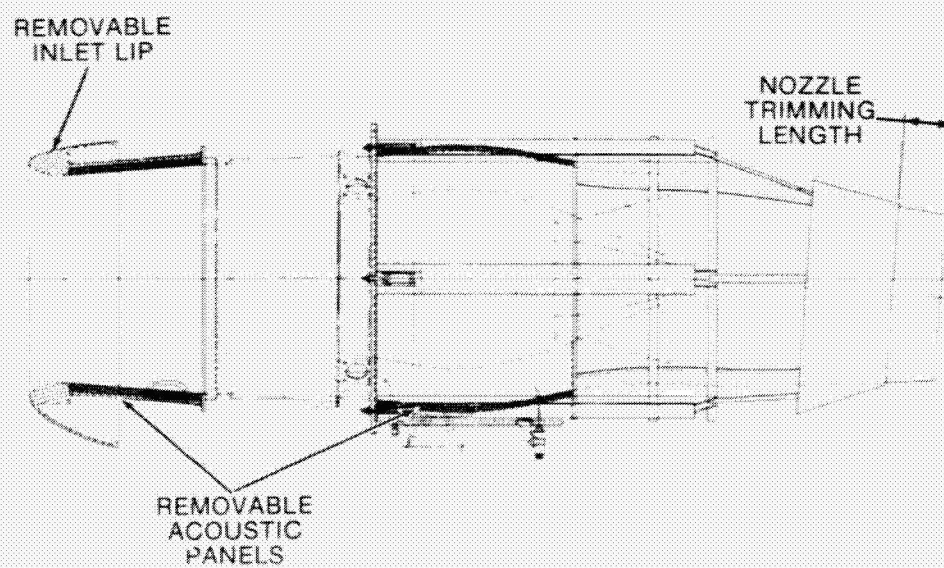


Figure 8

## QCGAT COMBUSTOR

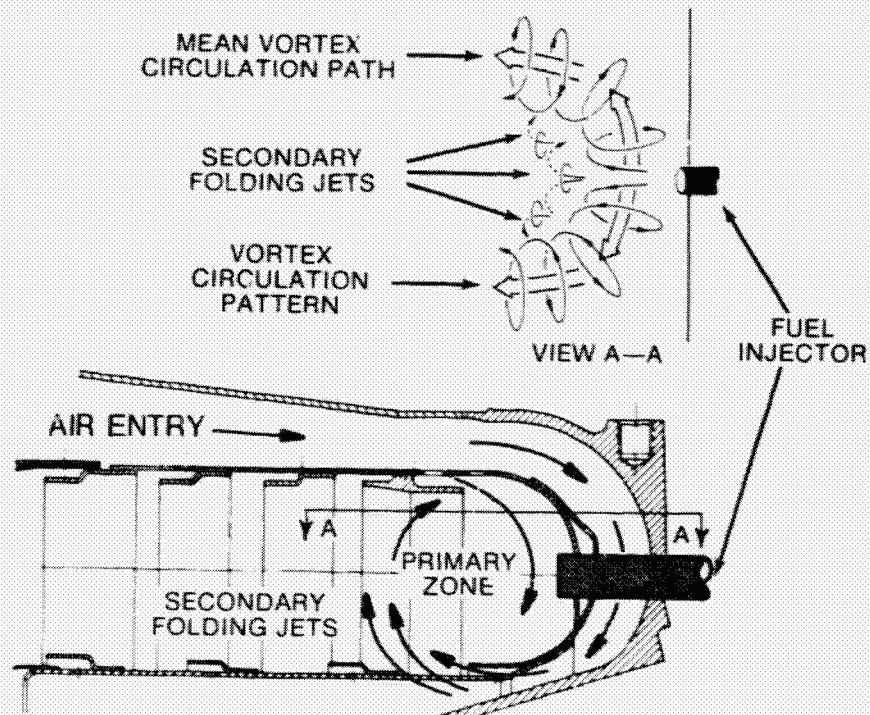


Figure 9

## NO<sub>x</sub> vs COMBUSTOR INLET TEMPERATURE

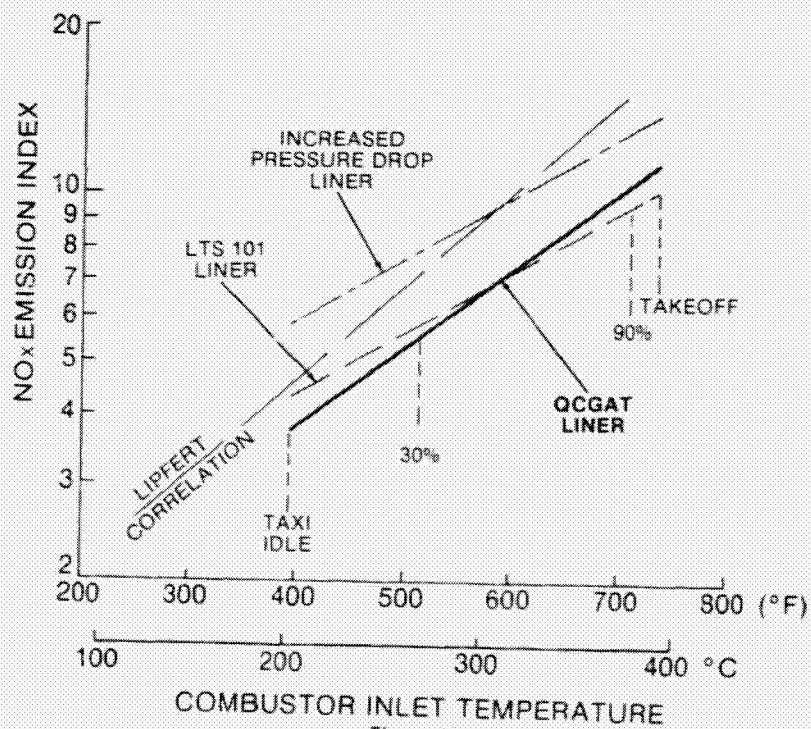


Figure 10

## ENGINE EMISSIONS SAMPLING TEST

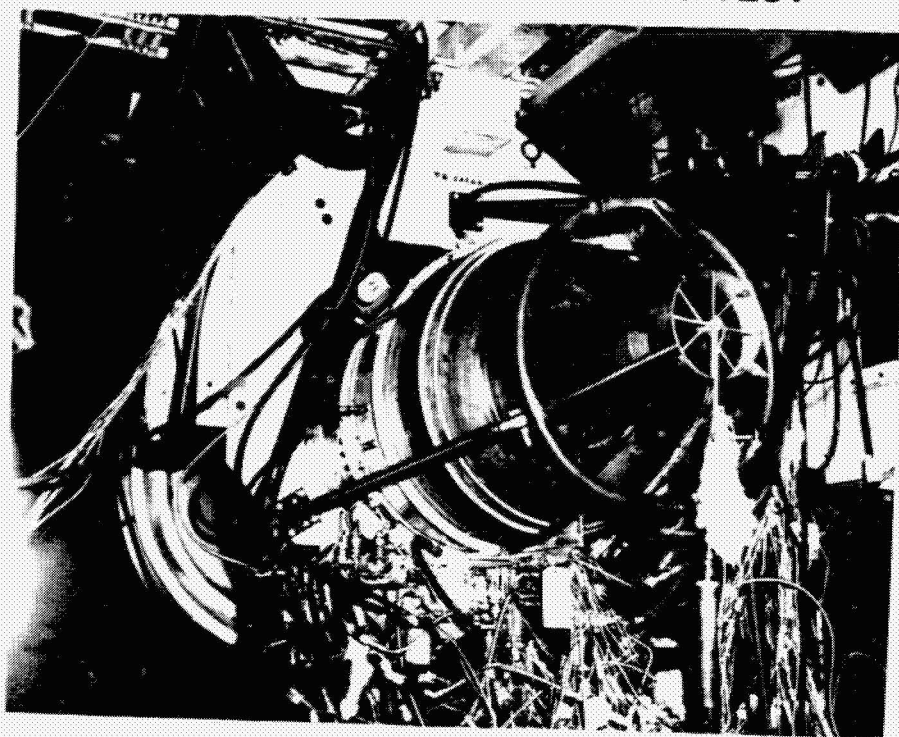


Figure 11

26  
N 80-22333

**AVCO LYCOMING QUIET CLEAN GENERAL  
AVIATION TURBOFAN ENGINE**

**Craig A. Wilson  
Avco Lycoming Division**

**SUMMARY**

Avco Lycoming participated in the NASA QCGAT program by developing a fan module using an existing turboshaft engine. The fan was designed using the latest in large engine noise control technology. A mixer was added to reduce the already low exhaust gas velocity. A nacelle incorporating sound treatment was provided for the test engine. The noise prediction model was used through the design process to evaluate the various design alternatives. Acoustic tests were then made to verify the prediction and identify the noise characteristics of the fan, core, jet, and sound treatment. Analysis of the recorded data yielded close agreement with the expected results. Core noise, as was expected, was the predominant source of noise for the QCGAT engine. Flyover noise predictions were made which indicated that the Avco Lycoming QCGAT engine would meet the goals set for the QCGAT program.

**INTRODUCTION**

The Avco Lycoming Quiet Clean General Aviation Turbofan engine program was designed to demonstrate the latest gas turbine engine noise control technology in a general aviation size engine. A considerable amount of work has been done to identify the design features that offset the generation of noise. And this work is still in progress as can be witnessed by the complexity of the facilities at the Lewis Research Center and elsewhere. The majority of this work, however, has been directed toward the commercial transport class of engines. The QCGAT program was designed to broaden the scope of this effort to include the general aviation size engine. The significant features of the QCGAT design are the low exhaust velocity achieved by a high bypass fan design, the use of a mixer, no inlet guide vanes, subsonic fan blade design, large blade to vane spacing, a high vane to blade ratio, the acoustical lining of the inlet and discharge fan ducts and the use of a long inlet duct. The nacelle and aircraft play an important roll in incorporating these features in the overall acoustic design. For example, the mixer is enclosed in a shroud formed by the nacelle. The fact that forward airspeed mitigates the amount of jet noise

generated has also been factored into the design. These features were optimized for the QCGAT aircraft based upon the results of our prediction of the acoustical performance of the engine aircraft system and the impact of each component on the overall design. The QCGAT noise goals were selected by NASA to force a design that included the latest noise control technology. We responded with an engine design that consisted of adding a new fan design module that incorporated the latest noise techniques of one of our turboshaft engines. Our original estimates of the engine noise emissions, based upon that design, are shown in figure 1. Our analysis indicated that the takeoff noise levels would be 4 EPNdB below the goal, the sideline 6 EPNdB below, and the approach 9 EPNdB. This analysis indicated that the core would be the dominant noise source at each measurement position, with the fan contributing to the approach noise and the jet contributing to the takeoff noise levels. Note that the goals are given in terms of aircraft flyover noise. The takeoff measurement point lies 3.5 nautical miles down range from brake release with the aircraft flying directly overhead. The sideline measurement point also lies down range on a takeoff but is displaced 1/4 of a nautical mile to the side and consists of a series of points in order to determine maximum noise level. The approach measurement point is located under the landing flight path at a point 1 nautical mile from the runway threshold. As the approach glide slope is defined as  $3^\circ$  the altitude of the aircraft over the measurement point is 370 feet. Thus we had to consider aircraft performance in the engine design. For this we worked with the Beech Aircraft Co. to define the characteristics of a twin engine QCGAT powered aircraft. With respect to noise, the rate of climb at takeoff, the power required at approach and the geometry of the wing were determined. Airframe noise, however, was not included in our noise estimates.

The design and performance of this aircraft plays an important part in the noise emissions of the QCGAT engines. As has already been discussed, the approach speed and takeoff performance can vary to meet the market requirements of the aircraft. For example, a lower approach power could have been used that would have resulted in lower approach noise levels. As the approach noise levels were predicted to be low, we felt that a small penalty was acceptable to reduce field length requirements. This will allow the aircraft to be certified for use at a large majority of the existing air fields in the United States.

Gas turbine engine noise source identification and control, figure 2, starts with the engine and its geometric and performance characteristics from which prediction of its noise emissions can be made. The engine noise is subdivided into five distinct noise generating mechanisms. They are the fan, compressor, combustion process, power turbines, and the turbulent mixing of the exhaust jet with the ambient air. The majority of

the work done to advance the state-of-the-art gas turbine and aircraft noise identification and prediction was, and is, being carried out by NASA as part of their Aircraft Noise Prediction Procedures (ANOPP), References 1 thru 5. This work has formed the basis of our noise prediction efforts. Of course, we have made certain modifications in order to more accurately reflect our experiences.

These prediction procedures are continuously updated to more accurately predict the engine noise levels. Given the aircraft performance and applying flight effects aircraft flyover noise can be calculated.

### ENGINE DESIGN AND NOISE PREDICTION

The first task was to design a fan module for the engine. This involved several iterations to access the design alternatives. Fan noise reduction was achieved through the use of a low pressure ratio fan to reduce blade loading and noise generation. This has to be part of the fan design from its conception. Other fan design features as shown on figure 3, have been shown to result in quieter fan designs for the large turbofan engines. Specifically, the fan blade tip speed should be designed to be subsonic. Thus multiple pure tones, or "Buzz Saw Noise" are eliminated altogether. The design relative tip mach number for the QCGAT engine is 1.13 which yields a subsonic value at all sea level operating points. The distance separating the blades from the exit guide vanes should be large when compared to the blade width to reduce rotor stator interaction noise that is expressed in fan broadband noise. We used a value of 2.3 for this ratio. The ratio of fan vanes to blades was optimized at a value of 2.5. This was to eliminate what are known as spinning modes that propagate at the blade passing frequency fundamental. In addition, inlet guide vanes were not used in our fan design. To further insure that inlet turbulence was reduced, a long inlet duct was included in the nacelle design. These features were accounted for in our prediction of the fan noise levels. Our prediction indicated that the fan would be a contributor along with the core only to the approach power levels. By identifying the effect of the various alternatives with the aid of our prediction procedures we were able to maintain this balance to achieve a low noise signature at approach.

An aircraft engine operates differently in flight than it does tied down to a test stand. Its noise characteristics also change. In flight, the air inflow is streamlined due to both flight cleanup affects of the forward air speed and the absence of ground turbulence that influence the generation of fan noise, particularly the tone at the blade passing frequency. Forward flight however, has its greatest impact on the generation of jet noise (see figure 4). It acts to reduce the relative velocity between the exhaust



and the ambient air. This can play an important part in the overall design of the engine aircraft system. For example, the airspeed at takeoff is in part determined by the length of runway availability. A longer takeoff roll would permit a higher takeoff speed. Consequently, the same jet noise level and relative velocity could have been achieved using a higher exhaust velocity.

As the aircraft flies past the observer, the sound varies in both time and spectral content. Dynamic amplification acts to increase the noise level as the aircraft approaches, and reduce the noise levels as it recedes. Then there is the doppler effect that imparts a frequency shift to the noise spectrum as the aircraft flies past. These phenomena must be accounted for to accurately predict the perceived noise of the aircraft.

It is the reduction in jet noise that has the greatest potential for noise reduction.

Jet noise is thus the second major element in the QCGAT engine design. A high bypass fan design is used to reduce the exhaust velocity and therefore reduce the noise generated by the turbulent mixing of a high velocity jet. The jet noise predictions indicated the jet would contribute to the takeoff noise and possibly cause the aircraft engine combination to exceed the limits set by the QCGAT goals at the reduced thrust and altitude condition. The calculations showed that the differences between the core engine and the fan exhaust gas velocities would contribute to this turbulent mixing noise (see figure 5).

A six element mixer was then designed to mix the core engine and fan exhaust gas to yield a single low velocity exhaust jet. The mixer, however, is not entirely free of side effects. Pre and post mixing turbulence can be an additional source of noise that has to be dealt with. These noise sources can be reduced by the addition of a shroud. In our design we provided that shroud by extending the nacelle considerably past the mixer to affect a better mix.

The high bypass fan and mixer were designed to reduce the jet noise component to a noise level below that of the core when forward flight effects cause reduction to occur in the jet noise. That leaves the core noise component. Core noise means the noise generated by the combustion process. The engine compressor and turbine noise were predicted to be above the audible range. Their noise sources do not contribute to the perceived noise of the QCGAT engine and were not considered in the design.

Core noise models have, for the most part, been empirically derived. The ANOPP routine was found to be adequate for our turboshaft engines. This prediction model uses combustor mass flow, temperature rise, and pressure drop as the basis for predicting core noise (see figure 6). Empirical data also suggest a 7 to 10 dB reduction for the turbofan version of this model. Core noise is now recognized as a major source in turbofan engine noise and is the focus of much research. We are working on this both in-house and with NASA. However, we have not included any new core noise control features. Some of the design modifications for emissions may have contributed to higher core noise levels. As our prediction showed from the beginning, the core was going to be a significant contributor to the noise characteristics of the aircraft. Consequently, we felt that further fan and jet noise reduction would have been unwarranted.

It has been long recognized that the fan inlet and discharge ducts of the engine nacelle (see figure 7) offer ideal locations for the installation of sound treatment to absorb the noise generated by the fan. Absorptive material are particularly efficient in absorbing sound energy in the high frequency region where much of the acoustical power radiated by the fan is concentrated. In addition, the sound treatment can be constructed of flight worthy materials that add little weight to the aircraft. Finally, the theory and experience of designing sound treatment panels are sufficiently sophisticated to accurately predict the results that will be achieved by a particular design. Consequently, sound treatment panels were employed for the QCGAT engine nacelle to determine the benefits that would be derived from their incorporation in an aircraft design.

The sound attenuation requirements were determined by comparing the predicted noise levels with the QCGAT program goals. The approach position represented the only point where the fan noise was predicted to contribute to the aircraft noise levels. In addition, the frequency of the blade passing tone at approach is located in the more heavily weighted part of the audible spectrum. Consequently, the approach power point was selected for the design of the sound treatment. At the other positions the fan does not contribute to the aircraft noise levels. The Lockheed California Company was contracted to design the sound treatment for the nacelle. Given the dimensional limitations the nacelle imposed upon the placement of the sound treatment and the engine operating parameters at approach, Lockheed generated a set of design curves from which the sound treatment was designed. These curves were based upon an analytical and empirically derived solution to what are known as the convected wave equations. These equations describe the sound generated by the fan as modes of acoustic energy rotating with and against the fan. This acoustic energy can only propagate under certain boundary conditions. The physical characteristics and operating parameters form these boundary conditions

and determine which modes will propagate. Lockheed performed this analysis and recommended a design. We then took this design to our Nacelle contractor, Avco Aerostructures, for fabrication.

The Lockheed design recommendations are shown in figure 3. Their design was for a single degree of freedom panel for both the inlet and discharge ducts. This design consists of a solid backing plate held 16 mm (5/8 in) off an inner plate perforated to a 5% open area. A honeycomb cell structure material separates the inner and outer plates. The inlet panel is 330 mm (13 in.) long to fill the available space in the inlet duct. The discharge sound treatment consists of a 45.7 mm (18 in.) long panel on the outer duct wall. The inner duct wall formed by the core cowl was not treated. The discharge panel was terminated before the start of the mixer to simplify the design. Otherwise the radiant heat from the mixer would have necessitated the selection of more expensive materials.

The predicted insertion loss for the fan inlet sound treatment panel at the approach and takeoff points are shown in figure 9. The sound treatment as mentioned earlier was designed for the approach condition. At this power setting the peak attenuation is made to coincide with the blade passing frequency. The insertion loss is higher at the takeoff condition due to the increase in air flow through the engine. The blade passing frequency at takeoff is also higher. The result is an attenuation approximately the same as that for the approach condition.

The predicted attenuation for the fan discharge treatment are in figure 10. The duct width between the inner and outer wall makes the treatment more effective even though the inner wall is not treated.

The test nacelle and sound treatment panels were fabricated by Avco Aerostructures in Nashville, Tenn. The test nacelle was designed without the outer skin and to take insert panels in the fan inlet and discharge ducts where ordinarily the sound treatment would have been placed. Two sets of inserts were fabricated. Each was designed to be of one piece to ease removal and installation during testing and to be rigid enough to maintain the desired wall contours. The panels were of sandwich construction with a honeycomb structure separating the inner and outer plates. The thickness of the honeycomb was determined by the Lockheed sound attenuation requirements. One set was fabricated with a solid inner plate, and one set (see figure 11) was fabricated with an inner plate perforated to achieve a 5% open area. This way we could test the engine with and without sound treatment in the nacelle.

The small radius of the inlet and discharge ducts limited to the depth of honeycomb that could be used without warping the cell structure walls.

Plugging the holes was also considered during design. The honeycomb material selected used a small cell pattern in order to be flexible enough to take the curvature. This meant that there would be fewer holes per cell and more holes blocked by the cell walls as the honeycomb was laid over the perforated plate. Fortunately, we were able to use an adhesive that migrated up the cell walls and did not plug holes. The perforated plate was punched to a 6% open area. When the honeycomb was then bonded to it, the open area was reduced to 5%.

The program goals are given in terms of aircraft flyover noise parameters. Experience has shown that when the engine is placed above the wing, the wing serves as a barrier. A barrier attenuation routine was included in the aircraft model to account for this effect. As shown in figure 12, the wing creates a shadow zone that moves along with the aircraft. As only a small fraction of the noise is refracted around the leading and trailing edges of the wing, the forward radiated fan noise will not reach the ground as the shadow zone passes by.

#### ACOUSTIC TEST PHASE

The test phase took most of the month of August to complete. The goals of the test program are shown in figure 13. They were to verify the noise predictions through comparison with measured data, determine the noise reduction of the mixer, and determine the effectiveness of the sound treatment panels.

A test plan was prepared to accomplish these goals. The normal method of recording the noise emitted by the engine is to record the sound pressure levels at nineteen locations on an arc 100 feet from the engine. With the microphones located every 10 degrees, a full set of data over an arc of 180 degrees can be obtained. Four power settings corresponding to the operating envelope of the engine were used. In addition to the far field microphones, acoustic probes were placed on the engine to aid in identifying core and mixer components and the noise reduction of the sound treatment. A barrier was also used during part of the testing to aid in isolating the fan inlet and discharge component sound levels.

Three separate engine configurations were used during the acoustic testing of the QCGAT engine. They are a split flow exhaust nozzle configuration called the referee system, the hardwall nacelle in which the test nacelle, mixer, and hardwall fan inlet and discharge panels were used and the soft-wall nacelle in which the hardwall panels were replaced with the sound treatment panels. Each configuration was tested to record the effect on engine noise at four power settings. The QCGAT engine was mounted in a test frame and after a series of tests in our test cells, it was moved to our

free field test site. This site is located close to the plant in an area free of most noise intrusions and where testing will not intrude into the local community.

The engine in the nacelle and test frame were installed on a rotating test stand. This stand is capable of rotating a full 360 degrees. The normal method of testing is to record the noise of the engine on an arc 100 feet from the engine by five microphones placed 10 degrees apart as shown on figure 14. By rotating the engine and repeating the test points, a full 180 degrees of noise can be obtained with some overlapping points. The microphones at the 170 and 180 degree points were in exhaust stream and were not used.

Positions 5 and 6 indicate the orientation of the engine inlet during the barrier test.

One-half inch condenser microphones fitted with wind screens were placed on the ground as used and recommended by NASA. This allows for a simple 6 dB correction to be used when correcting the measured data to free field conditions for comparison with the predicted noise levels. The microphone array is shown in figure 15. The signal conditioning instrumentation are located in the acoustic data acquisition trailer where the data is recorded on magnetic tape for later analysis.

A sample of the engine performance data is given in Table I. At each test point, a complete set of engine performance data was recorded for use in predicting the engine static noise levels for comparison with the measured sound levels.

The ambient pressure, temperature, and relative humidity were also recorded.

Fan noise is composed of tones that are easy to identify near the axes of the engine, but they blend together at the 90 degree locations. The purpose of the barrier then was to isolate the fan inlet noise from the fan discharge noise by physically placing a barrier between them. This was accomplished at the free field test site with the barrier shown on figure 16. The barrier was constructed of a fixed partition 14 feet high by 20 feet long and a movable partition through which the engine inlet protruded. This effectively removed the fan discharge noise from the measurements of the fan inlet noise. By rotating the engine 40 degrees between measurements, data was recorded over an arc of 80 degrees. The movable partition was then pulled out and the engine rotated 180 degrees so that the exhaust protruded through the barrier when it was moved back into position. The fan discharge noise was then recorded without fan inlet noise contributions. Both of these tests were

run at the same four power setting with the hardwall and the softwall nacelles installed on the engine.

The locations of the engine mounted probes are shown on figure 17. Half-inch condenser microphones were located upstream and downstream of the sound treatment to measure the noise reduction across the inlet sound treatment panels. Semi-infinite wave guide probes supplied by NASA were used to sample the acoustic pressure levels in the primary engine exhaust and at the mixer exhaust plane. These probes consisted of 1/4 inch condenser microphones in a sealed tube. A low volume flow of nitrogen at a pressure just above that in the duct provided a gas seal to prevent hot exhaust gas from entering the tube where it could damage the microphone.

These probes were designed to record the acoustic pressure levels at the indicated probe locations. The recorded data will also be used in coherence analysis to determine what part of the noise in the engine is in fact radiated out to the different far field measurement locations.

The split flow nozzle configuration with the semi-infinite wave guide probes installed in the primary exhaust nozzle are shown on figure 18. This configuration was used to obtain baseline data for comparison with mixer noise levels.

#### DATA ANALYSIS

The data recorded on magnetic tape was then analyzed. Reducing, organizing, and cataloging all this data was a time consuming task. The analysis was straight forward. During the individual test runs, the engine performance was monitored and the relevant ambient and operating parameters recorded. Using these data and the appropriate cycle sheet data, we could predict the expected sound pressure levels. These were then compared point by point, frequency by frequency, and angle by angle with the measured sound pressure levels. In this manner, we estimated the contribution of each component to the overall noise levels at each power setting. The predictions were then adjusted to reflect this comparison, and the correlation was run again. We also evaluated the insertion loss due to the sound treatment and determined the mixer noise reduction.

With the appropriate flight corrections and aircraft performance estimates, we were ready to estimate the flyover noise levels. The individual component contribution to the overall noise levels were determined on a spectrum basis as shown on figure 19. This plot consists of the one-third octave band sound pressure levels over a frequency range from 25 Hz to 20,000 Hz. The procedure for deriving the flyover noise levels only considers the sound pressure levels from 50 Hz to 10,000 Hz. The pre-

dicted fan noise contribution was overlaid. The calculations correctly located the blade passing tone, its harmonics and the broadband component. The magnitude of the blade passing tone fundamental however was under-predicted. Next, the predicted jet noise component was added as shown on figure 20. As was expected, the jet component does not contribute directly to the noise levels at the low power setting when the predicted core noise component is added to the noise spectrum as shown on figure 21. The predicted spectra matches the measured spectral shape. The agreement however is only fair in the mid-frequency region at the blade passing tone fundamental. This same analysis was carried out for the softwall and split flow configuration. The analysis was also carried out at each power setting. The high power setting is shown on figure 22. Note that the agreement is only fair across the mid and high frequency regions of the spectrum. The low frequency part of the spectra appear to be in close agreement. Here the jet noise component is predicted to be the predominant source. Based upon this comparison and similar ones at other power settings and configurations, we concluded that the jet noise prediction routine is adequate for the QCGAT program. Consequently, the predicted jet noise levels could be analytically removed from the measured data. The remaining noise levels would then be that composed of the core and fan components. Once the jet component had been removed the sound power levels attributed to the core were then compared with the predicted core sound power levels as shown in figure 23. Also plotted are the sound power levels derived from the acoustic probes located in the primary exhaust. The probe data are shown more as a confirmation of the slope rather than the sound power levels correctly calculated. These data indicate that the core noise model underpredicts the core noise level by roughly 3 dB. This underprediction appears to be independent of the power setting of the engine. A simple 3 dB correction factor was therefore applied to the core noise prediction procedures. After making this refinement to the core noise model, the predicted-to-measured correlation was then rerun. Figure 24 shows that comparison. The spectral agreement between the measured and predicted data is good over the frequency range of interest. Note that the sound levels in the band containing the tone at blade passing are also in good agreement. This indicates that the core noise contributes across the spectrum. The dominance of the core noise can be seen in figure 25. The noise levels in the discharge quadrant are dominated by the core component to the extent that the fan component is almost entirely masked. The core noise component is present in the forward quadrant. The reduction in the fan noise levels by the sound treatment was hard to discern for this reason. When the core noise component is removed from the one-third octave band containing the blade passing tone, and the resulting blade passing tone is plotted against the angle from the inlet, as shown on figure 26, a fan tone directivity plot is formed. The predicted sound pressure levels at the peak angles are also shown for the inlet and discharge quadrants. The expected

results with the barrier in place come from the prediction procedures. Only when the barrier is in place will the measured data approach these lines which it does as can be seen by the dotted lines. This plot shows how the fan noise contributes to the forward and aft radiated engine noise levels. If an observer were to move past this plot as indicated, the noise levels experienced would first rise and then fall off as the observer moved past. Once past the engine, the noise levels would then rise again as the discharge fan noise reached the observer. This is roughly how the static data was converted to observed flight sound levels. At the high power setting (figure 27) the core noise obscures the aft fan tone from the analysis. A small adjustment was made to the fan noise model from which these data were derived. This adjustment had to do with the effect of relative tip design mach number. With this adjustment, we concluded from the agreement shown here and on the previous figure that the fan noise model is accurately computing the fan noise levels. The sharp dip at the 60 degree point is due to the fact that the data from 0 to 40 degrees were recorded at slightly different power settings than the data from 50 to 90 degrees. The predicted data shows this same dip. We feel this is an artifact of the data acquisition process and is not a characteristic of the fan noise. The individual component contributions appear to be adequately predicted once the noted corrections have been made. Figure 28 shows a final comparison of the measured and predicted overall sound power levels. This plot was generated to verify the accuracy of the prediction techniques for the static case before proceeding to the flyover analysis. The agreement shown here indicates to us that the updated noise prediction model accurately reflects the static noise emissions of the QCGAT engine.

As noted earlier, it was difficult to discern the noise reduction of the sound treatment panels from the far field data. Figure 29 shows the one-third octave band sound pressure levels at the upstream and downstream microphone locations in the inlet. Here the acoustic energy is propagating against the air flow in the inlet duct. The upstream microphone then recorded the inlet noise after it had passed through the treated part of the inlet duct. Figure 30 shows that the expected insertion loss and the insertion loss derived from the test data. These are the values that will be used in the flyover noise estimates. Figure 31 shows that the expected and estimated insertion loss for the fan discharge duct sound treatment panels. The discharge panels had no provision for microphones and were unable to discern a noise reduction from the far field data due to the presence of the core noise. We have assumed that the treatment is functioning properly. The estimated values for the discharge sound treatment panels are shown here.

The jet noise levels were predicted to be low due to the use of a high bypass ratio fan. Figure 32 shows the difference between the noise spectra



of such an engine fitted with the split flow nozzle configuration and with the mixer nacelle configuration. The shaded area represents the static noise reduction of the mixer. Above 250 hertz, the core noise source starts to mask the jet noise and above 1000 hertz, the fan is dominant. When flight effects are added, both the mixed and split flow jet components will drop leaving the mixed flow jet noise levels below the core noise levels. The split flow noise levels would drop and be roughly equal in magnitude to static jet noise levels.

The procedures employed (figure 33) in the QCGAT program to assess the noise emissions of a QCGAT powered aircraft are the Federal Aviation Administration's certification procedures for turbojet powered aircraft (Reference 6). This is a very rigorous method. Basically, the FAA requirements call for measuring the aircraft noise every half second as the aircraft flies over the measurement point. For this analysis, predicted data was substituted for the actual measurements. The demonstration engine performance and the Beech aircraft design were used to compute the individual test point performances. These data were entered into the prediction procedures. The appropriate flight and wing shielding effects were then applied to the individual component noise predictions. The aircraft noise signature was then derived by combining these into a table of aircraft noise. Then by analytically moving the aircraft noise table past the measurement point, the time history of the flyover could be constructed for each half-second interval. These sound levels were then used to compute the tone corrected perceived noise levels for the flyover event. The maximum tone-corrected perceived noise levels was then found along with the time the aircraft noise is within 10 PNdB of the maximum. From these data, the effective perceived noise level is calculated.

Figure 34 shows the tone corrected perceived noise levels versus time for the approach flyover. The maximum tone-corrected perceived noise level, labeled PNLTM occurs after the aircraft has passed directly overhead. The time the PNLTM was within 10 PNdB of the value is 8.5 seconds. This plot also shows that the fan inlet and discharge noise are heard at separate times. The valley between the peaks is caused by the lower sound levels generated at the sideline positions. Wing shielding, the shaded portion, acts to cut the inlet peak off early and makes this valley deeper. The core noise component is heard after the aircraft is past as most of the core noise is in the aft quadrant of the engine. Because of the duration correction, the fan component noise levels are higher and contribute more to the effective perceived noise levels. Figure 35 is the same type of plot showing the takeoff flyover tone-corrected perceived noise level time history. Here the time the noise is within 10 PNdB of the max is much longer. At

the approach condition, the altitude at flyover is 370 feet. For the take-off condition, it is 2600 feet. Consequently, the time will be considerably longer. The maximum tone-corrected perceived noise level also occurs much later as the sound requires longer to reach the observer and because the dominant noise sources are the core and jet. These components radiate most of their acoustic energy in the rear quadrants and, as such, are not heard until the aircraft is past the observer. Also shown here are the higher noise levels of a split flow nozzle configured aircraft. Here the jet component contributes more to the aircraft noise levels both in magnitude and duration. The duration is increased because the jet noise peaks farther aft than does the core noise. This means that the peak noise occurs later in the flyover. Thus, the addition of the mixer not only reduces the aircraft flyover noise levels, the aircraft noise does not linger as long.

### CONCLUSION

For an aircraft powered by two Avco Lycoming QCGAT engines installed in a nacelle that includes a mixer and fan inlet and discharge sound treatment panels and mounted over the wings, the effective perceived noise levels for the takeoff, sideline, and approach conditions will be 68.4, 7.06, and 77.3 EPNdB, respectively. These noise levels shown in figure 36, are below the limits set by the QCGAT program goals. In the analysis, the effect of several alternative engine configurations on the aircraft noise was assessed. For example, removal of the sound treatment panels would add 2 EPNdB to the approach noise levels and still be below the QCGAT goals. The other positions would not be affected. The noise levels shown here are for the engine that was tested and delivered to NASA. When the iterations are completed for this engine design, the increased thrust of the engine will mean that the aircraft will achieve an altitude of 3600 feet over the takeoff point versus the present 2600 feet. This will result in a 3 EPNdB reduction in the takeoff noise levels and a 1 EPNdB reduction in the sideline noise levels. In this case, the split flow exhaust nozzle configuration would be within 1 EPNdB of the QCGAT goals. Figure 37 shows the Avco Lycoming QCGAT engine effective perceived noise levels plotted against the Federal Aviation Administration's Stage III noise standards and the high technology that used by NASA for the QCGAT program goals. This demonstrates that the technology that has worked for the large engine can be transferred to the general aviation size engine. Consequently, turbofan engine noise emissions should not be a constraint to the growth of the general aviation market.

In summary, (see figure 38) large turbofan noise control technology was successfully applied to a general aviation size engine. The stringent program goals set by NASA forced a design that required the use of a

design that required the use of a quiet fan and integration of the nacelle and aircraft in the engine design. This demonstrates that the QCGAT program goals can be met with the latest noise control techniques without incurring a performance penalty.

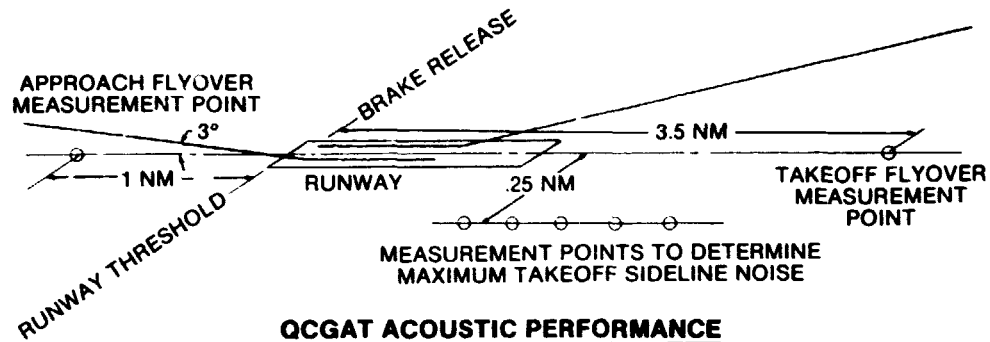
## REFERENCES

1. Stone, J. R. : Interim Prediction Method for Jet Noise. NASA TM X-71618, 1974.
2. Huff, R. G. ; Clark, B. J. ; and Dorsch, R. G. : Interim Prediction Method for Low Frequency Core Engine Noise. NASA TM X-71627, 1974.
3. Heidman, M. F. : Interim Prediction Method for Fan and Compressor Source Noise. NASA TM X-71763, 1975.
4. Dunn, D. G. : Aircraft Noise Source and Contour Estimation. NASA CR-114649, 1973.
5. Gillian, R. E. ; et al. : ANOPP Users Manual. July 1978.
6. Federal Aviation Administration Noise Standards, Title 14, Code of Federal Regulation, Chapter I, Part 36.

Table I  
**TYPICAL ENGINE PARAMETERS**  
RECORDED DURING NOISE TESTS

ENGINE PARAMETER	TEST CONDITIONS	
	LOW POWER SETTING	HIGH POWER SETTING
Fan Rotor Speed, rpm	5376	9184
Fan Blade Passing Frequency, Hz	2150	3673
Fan Relative Tip Mach Number	.509	.89
Fan Airflow, kg/sec(lb/sec)	14.8(32.6)	26.3(57.9)
Fan Temperature Rise, °C(°F)	6.7(12)	15(27)
Combustor Airflow, kg/sec(lb/sec)	1.33(2.95)	2.37(5.22)
Combustor Temperature Rise, °C(°F)	630(1135)	878(1580)
Jet Exit Velocity, kg/sec(ft/sec)	106(350)	194(636)
Jet Exit Temperature, °K(°R)	358(645)	389(697)

## QCGAT POWERED AIRCRAFT NOISE GOALS



CONDITION	EPNL GOAL EPNdB	PREDICTED ENGINE EPNL, EPNdB
Takeoff Flyover	69.4	64.8
Takeoff Sideline	78.4	71.7
Approach Flyover	83.4	73.8

Figure 1

## AVCO LYCOMING AIRCRAFT ENGINE NOISE PREDICTION PROCEDURES

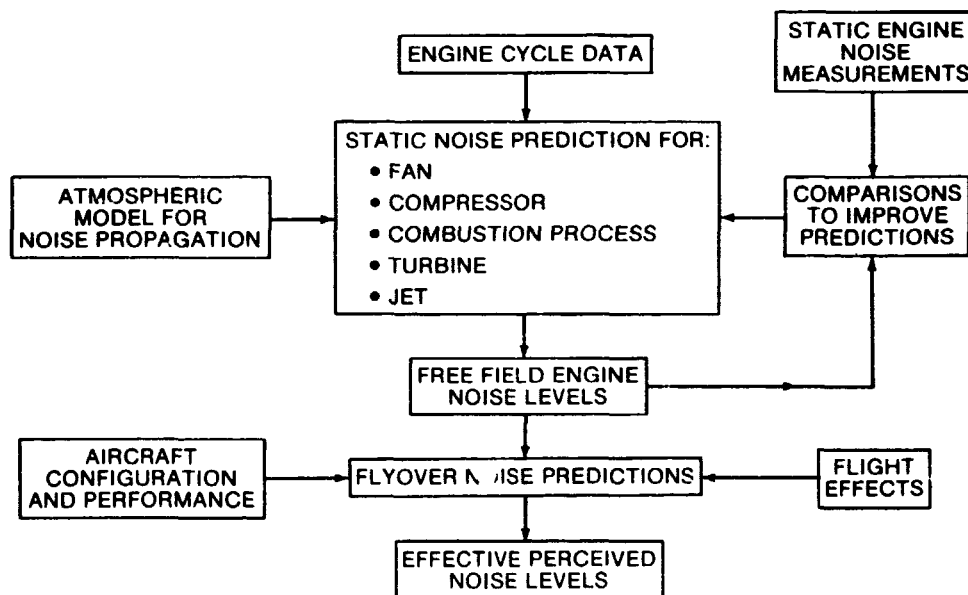


Figure 2

## FAN NOISE REDUCTION TECHNIQUES

<u>PARAMETER</u>	<u>TECHNIQUE</u>
Blade Loading	Low Pressure Ratio
Blade Tip Speed	Subsonic
Blade to Vane Spacing	Greater Than 2 Blade Widths
Vane to Blade Ratio	Greater Than 2
Inlet	No Inlet Guide Vane Low Inlet Turbulence

Figure 3

## FORWARD FLIGHT EFFECTS

- Reduce Inlet Turbulence
- Reduce Jet Noise
- Dynamic Amplification
- Doppler Shift

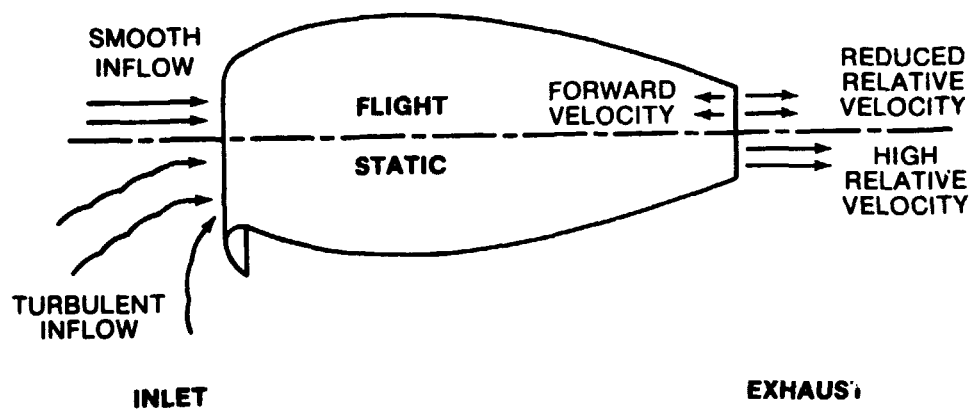


Figure 4

## EFFECT OF NOZZLE CONFIGURATION ON JET NOISE

WITH HIGH BYPASS FAN

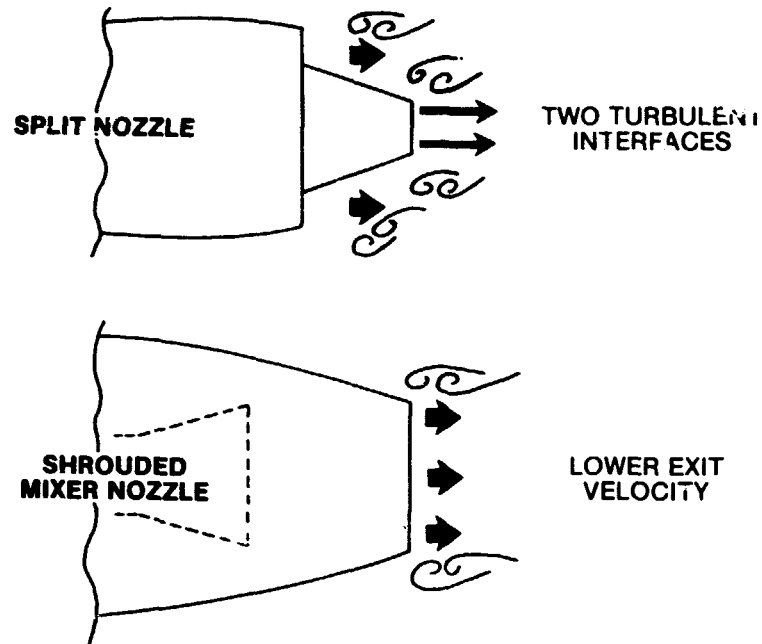
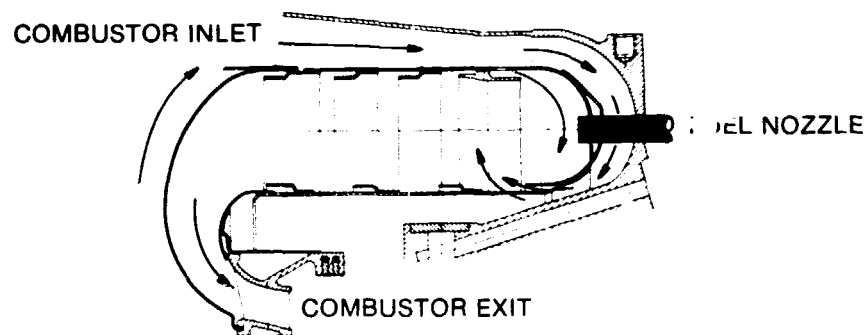


Figure 5

## CORE NOISE MODEL

(GOOD AGREEMENT FOR TURBOSHAFT ENGINES)



Noise a Function of:

- Mass Flow
- Temperature Rise
- Pressure Drop

Figure 6

# **QCGAT FLIGHT NACELLE** **with** **SOUND TREATED PANELS INSTALLED**

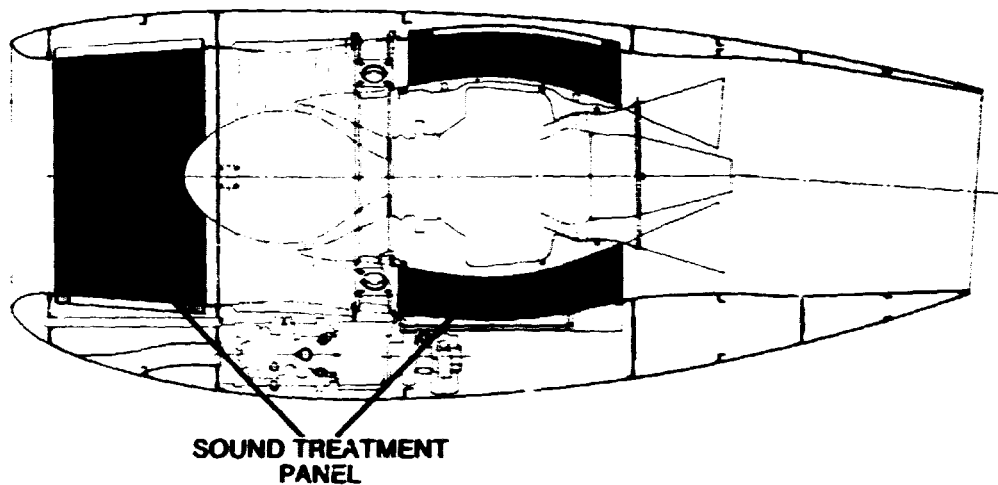


Figure 7

## **LOCKHEED DESIGN RECOMMENDATIONS** **FOR SOUND TREATMENT PANELS**

	<u>THICKNESS</u>	<u>LENGTH</u>	<u>OPEN AREA</u>
Fan Inlet	16mm(0.63 in.)	330mm(13 in.)	5%
Fan Discharge	16mm(0.63 in.)	460mm(18 in.)	5%

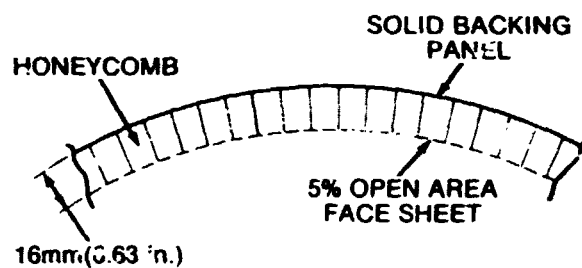


Figure 8

## PREDICTED FAN INLET ATTENUATION

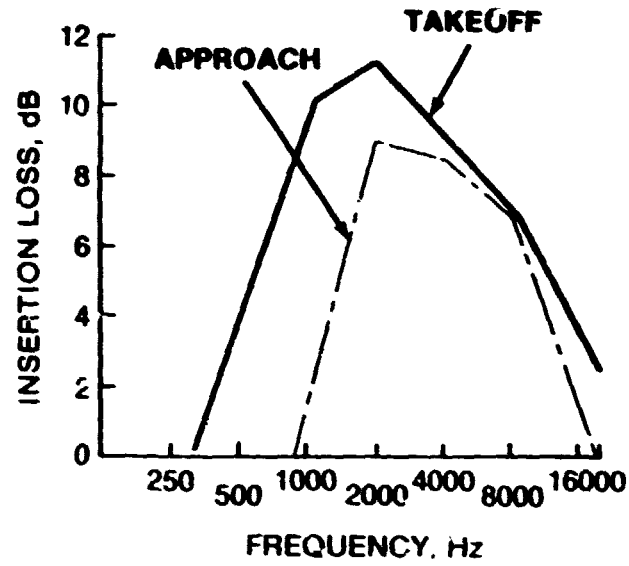


Figure 9

## PREDICTED FAN DISCHARGE ATTENUATION

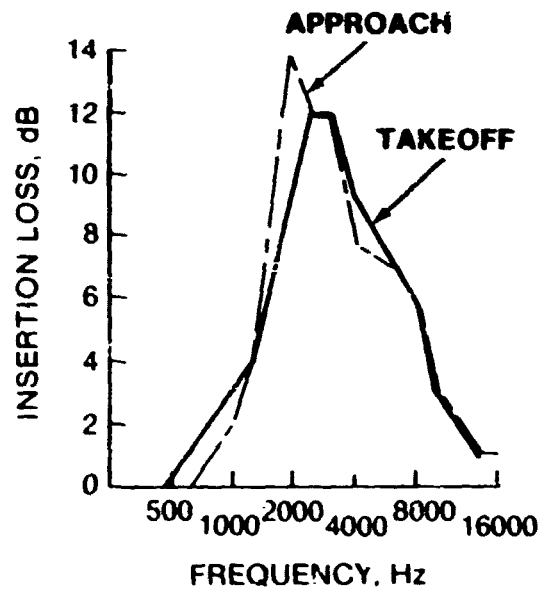


Figure 10



## QCGAT TEST NACELLE SOUND TREATMENT PANELS

INLET PANEL

DISCHARGE PANEL

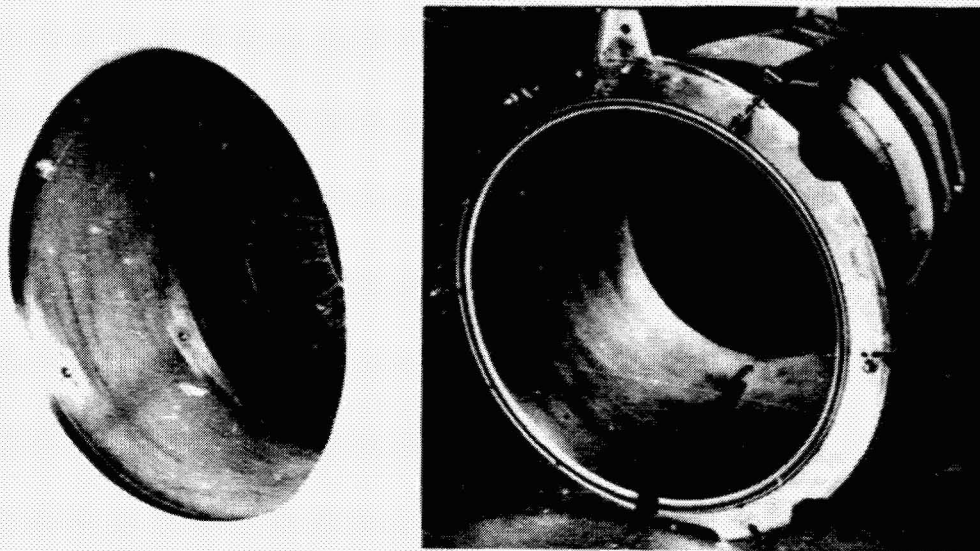


Figure 11

## WING SHIELDING MODEL

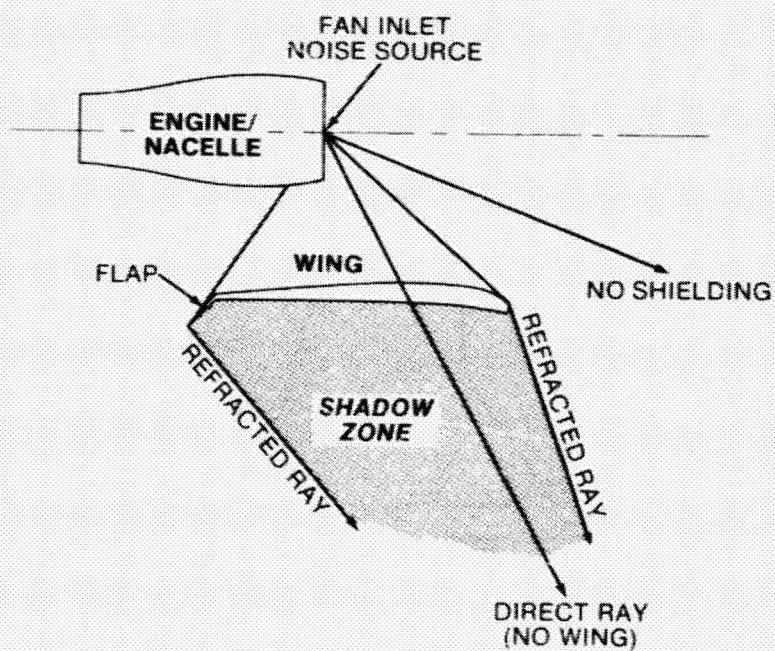


Figure 12

ORIGINAL PAGE IS  
OF POOR QUALITY

## NOISE TEST PROGRAM

### OBJECTIVES

- Verify Prediction Procedures
- Evaluate Influence of Mixer
- Determine Effectiveness of Sound Treatment Panels

### NOISE MEASUREMENT (4 Thrust Levels - 180° Arc)

- Fan Noise - Use Barrier to Isolate Inlet - Discharge Components
- Core and Mixer Noise - Acoustic Probe
- Sound Treatment Panel Effectiveness - Flush Mounted Microphones

Figure 13

## SOUND SITE TEST ARRANGEMENT

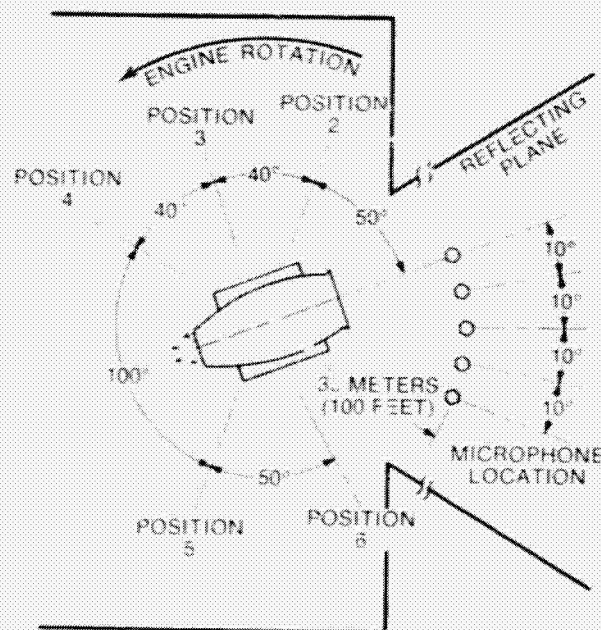


Figure 14

## LYCOMING FREE FIELD TEST SITE

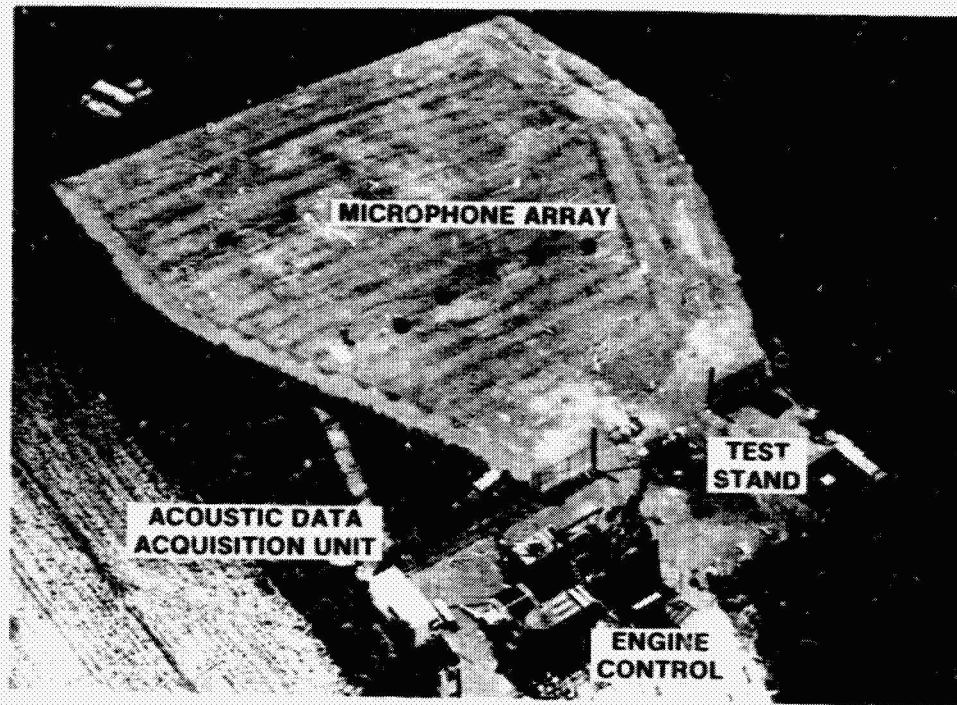


Figure 15

## SOUND ISOLATION BARRIER (ISOLATE FORWARD AND AFT RADIATED FAN TONES)



Figure 16

## NEAR FIELD ACOUSTIC PROBE LOCATION

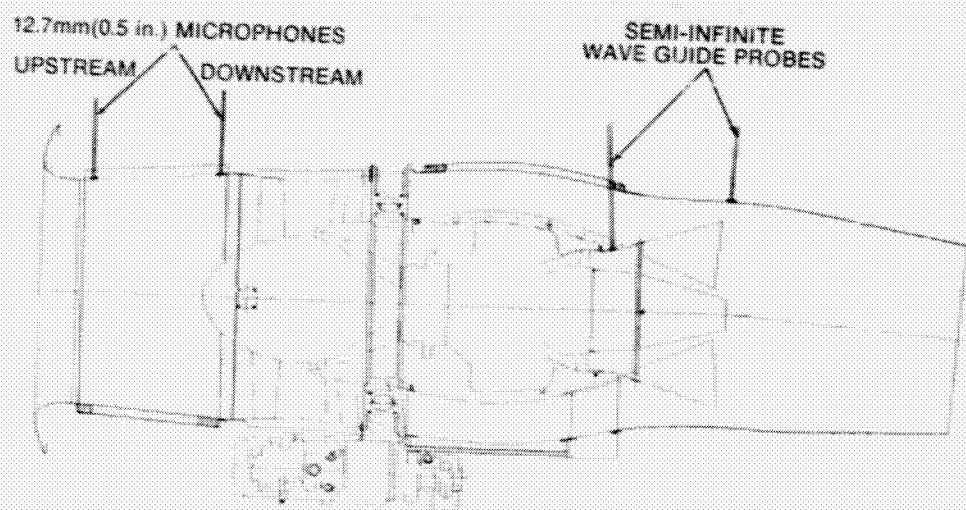


Figure 17

## WAVE GUIDE PROBES INSTALLED DURING REFEREE TEST

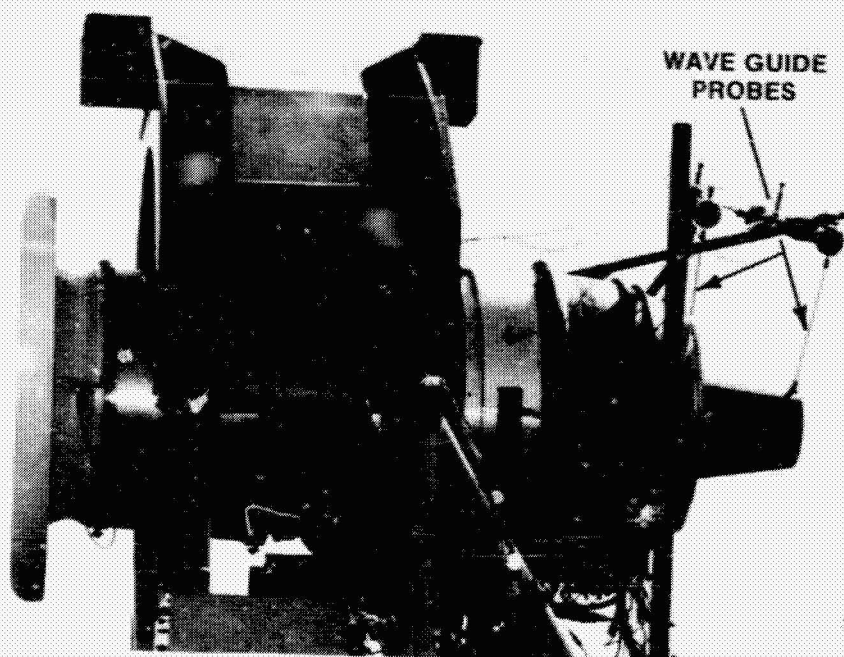


Figure 18

## VERIFICATION OF PREDICTION TECHNIQUES

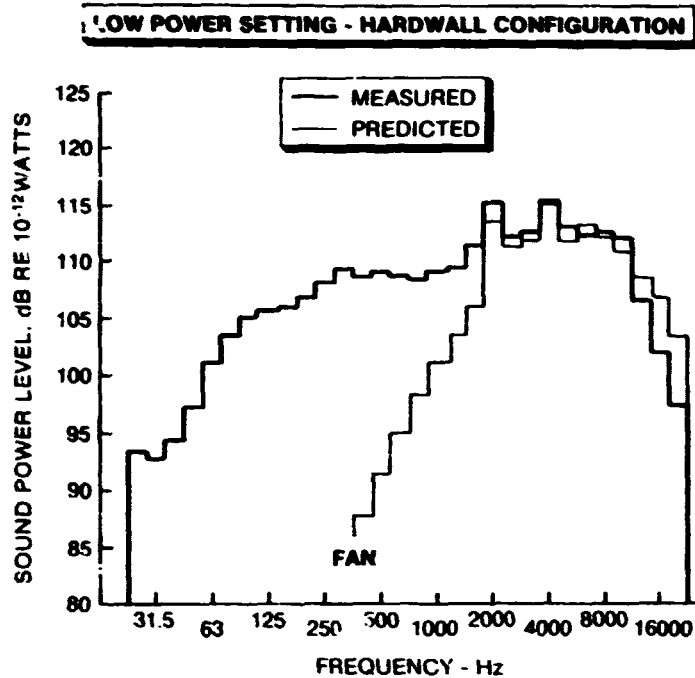


Figure 19

## METHOD OF ANALYSIS

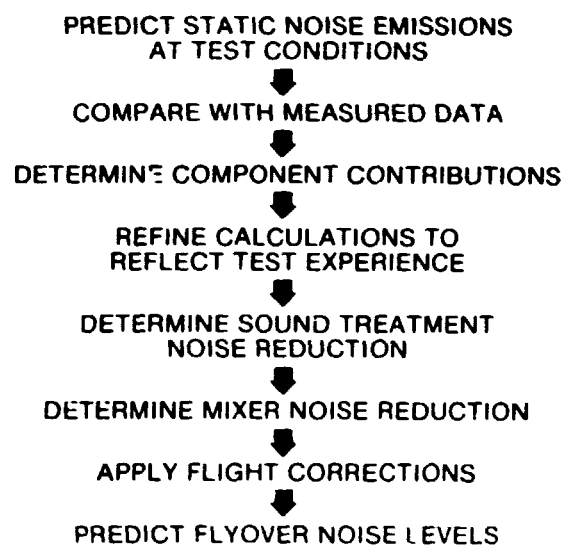


Figure 20

## VERIFICATION OF PREDICTION TECHNIQUES

### LOW POWER SETTING - HARDWALL CONFIGURATION

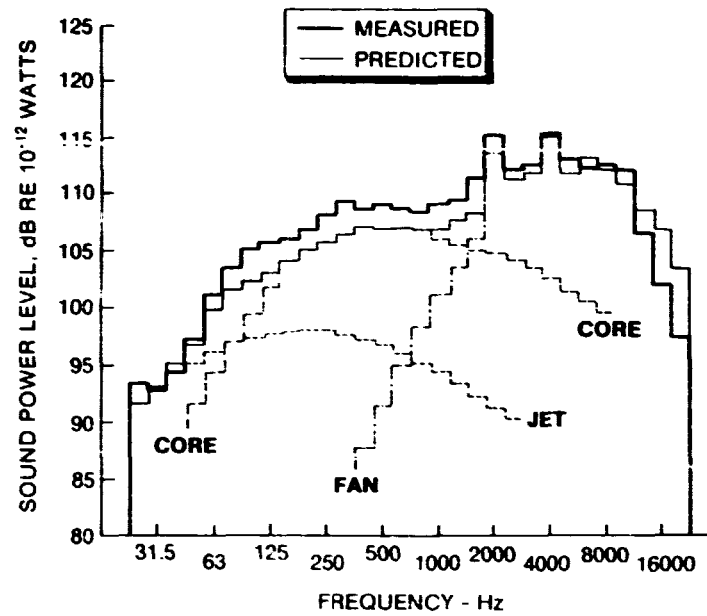


Figure 21

## VERIFICATION OF PREDICTION TECHNIQUES

### LOW POWER SETTING - HARDWALL CONFIGURATION

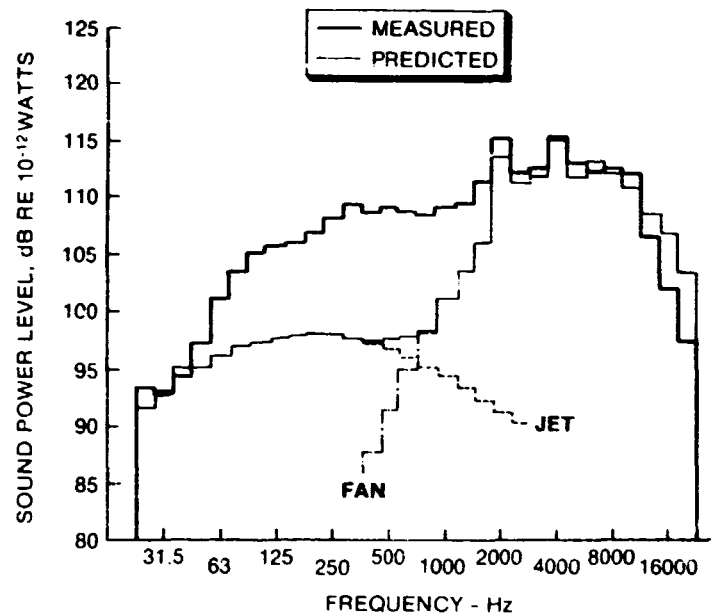


Figure 22

## CORE NOISE PREDICTION

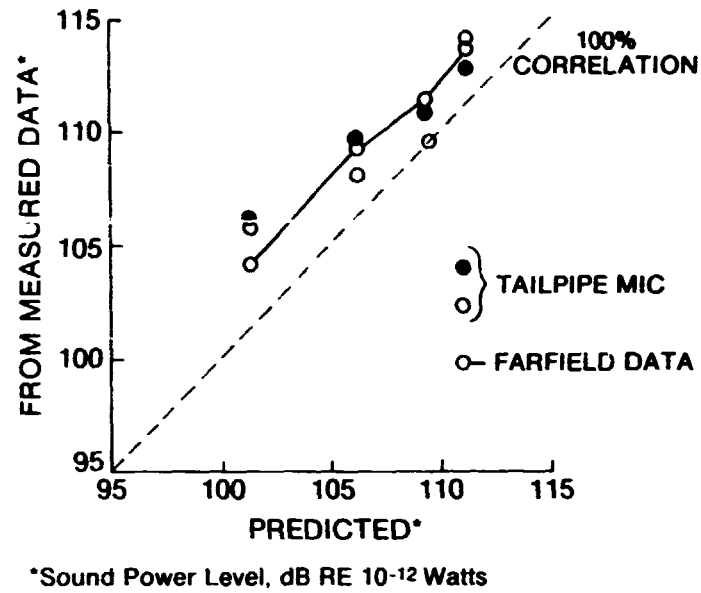


Figure 23

## RESULTS WITH UPDATED CORE NOISE MODEL

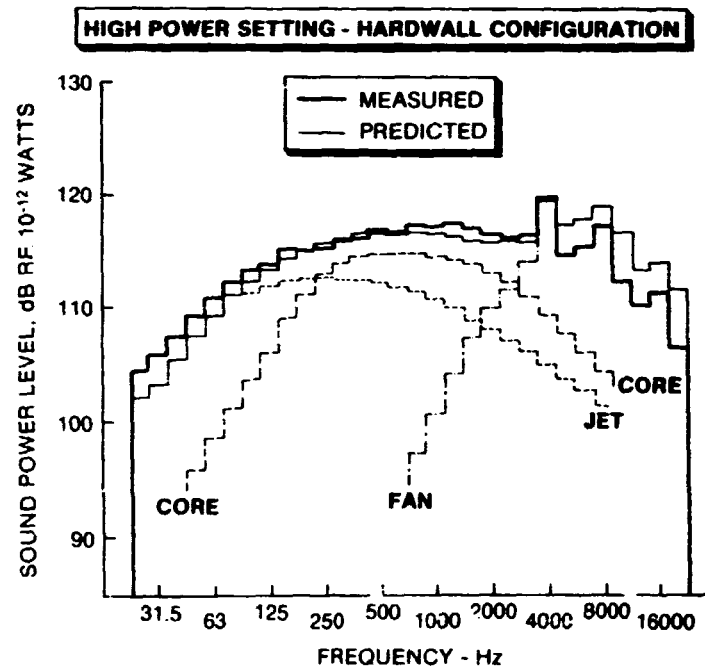


Figure 24

## TYPICAL INLET AND EXHAUST NOISE SPECTRA

- Fan Tone Masked By Core Noise

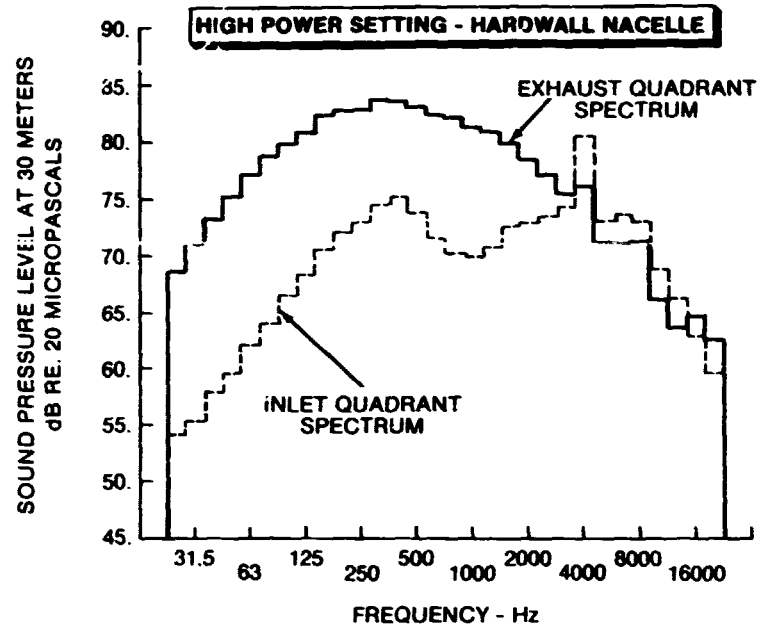


Figure 25

## FAN TONE DIRECTIVITIES

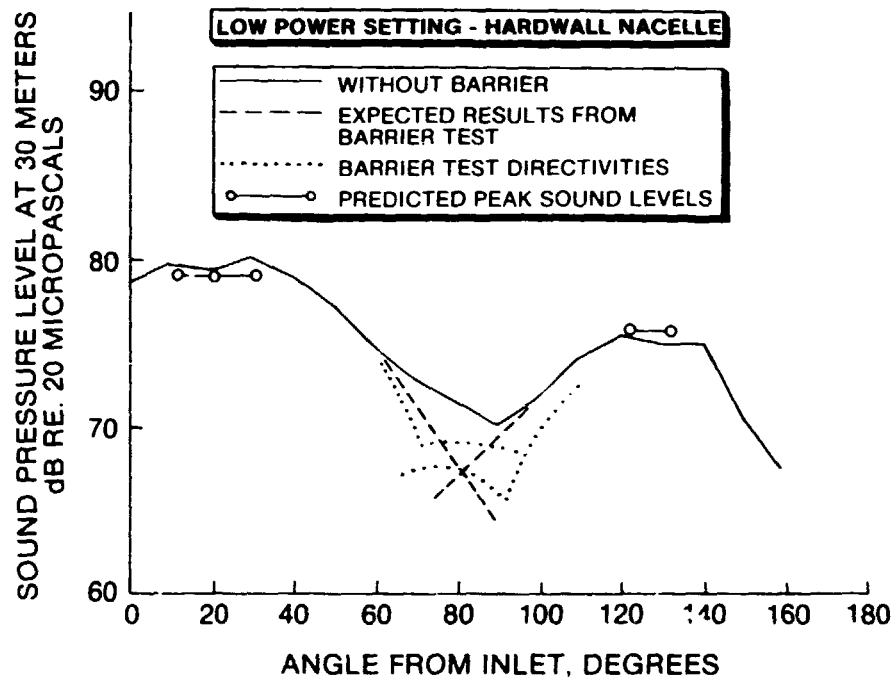


Figure 26



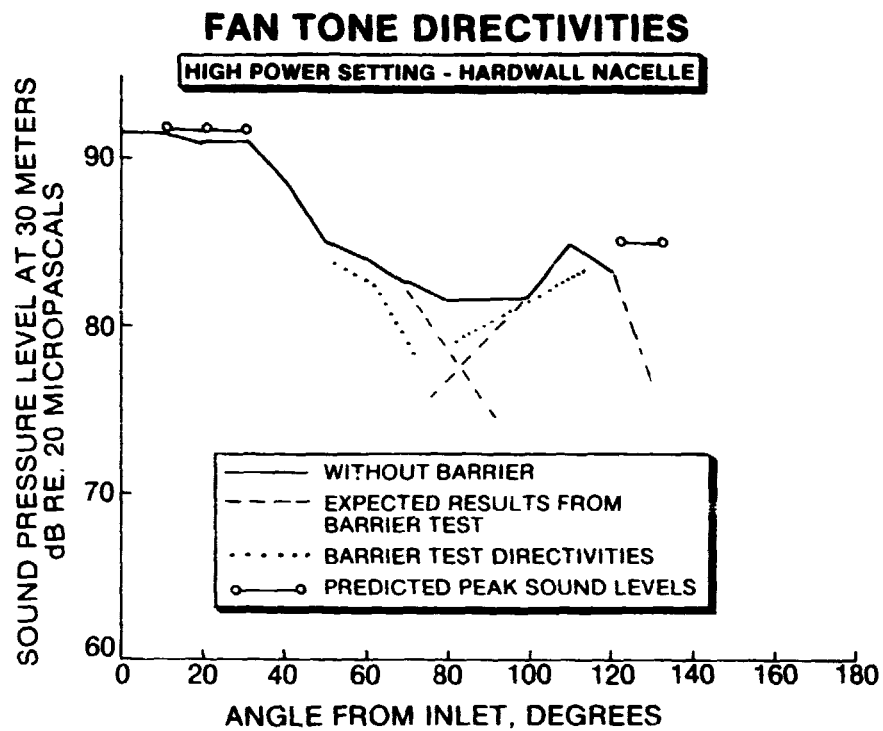


Figure 27

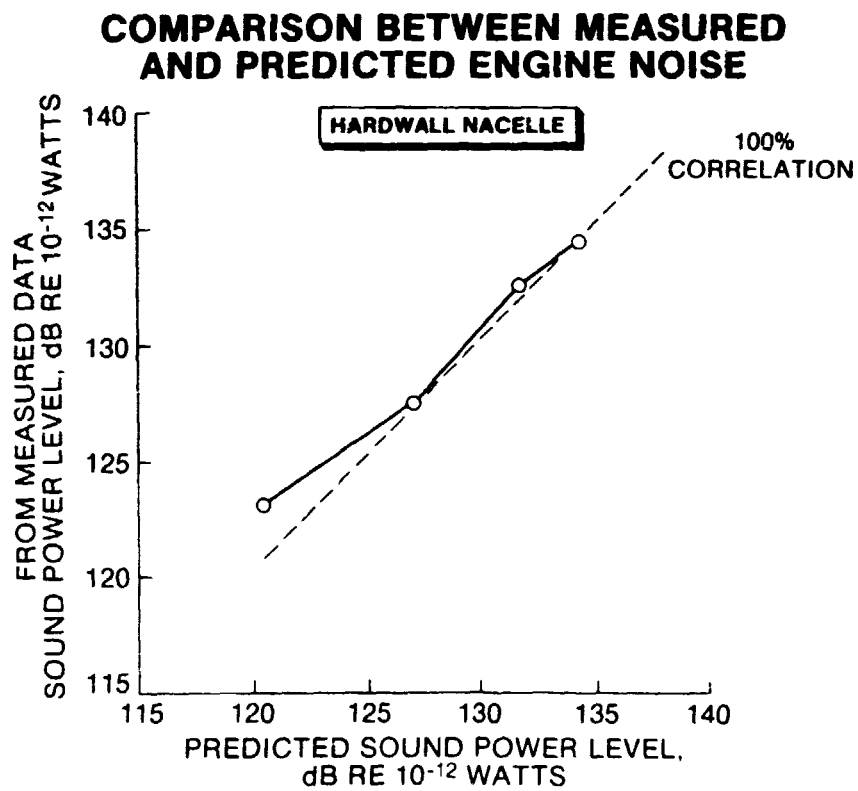


Figure 28

## INLET TREATMENT NOISE REDUCTION

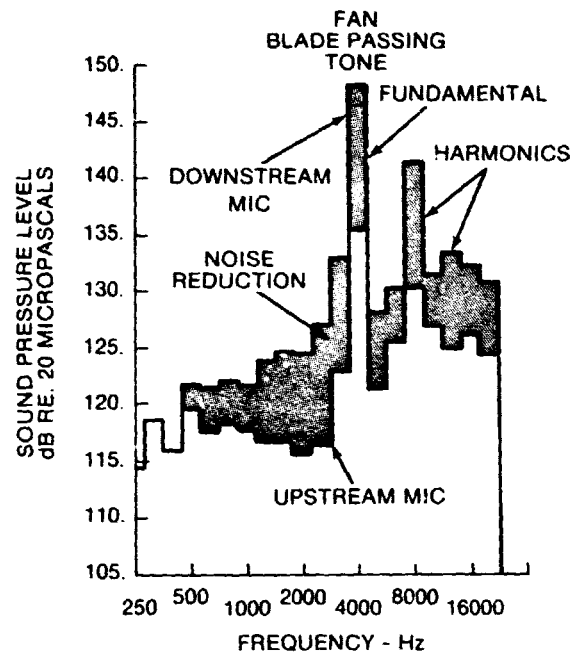


Figure 29

## FAN INLET SOUND TREATMENT

- Treatment Estimated to Meet Design Specifications
- Analysis Limited By Low Fan Sound Levels

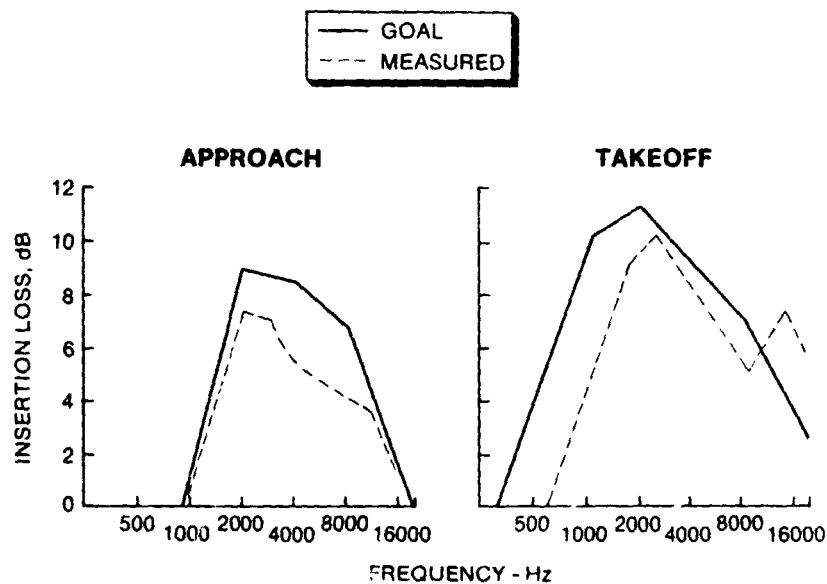


Figure 30

## FAN DISCHARGE SOUND TREATMENT

- Treatment Estimated to Meet Design Specification
- Analysis Limited By Low Fan Sound Levels

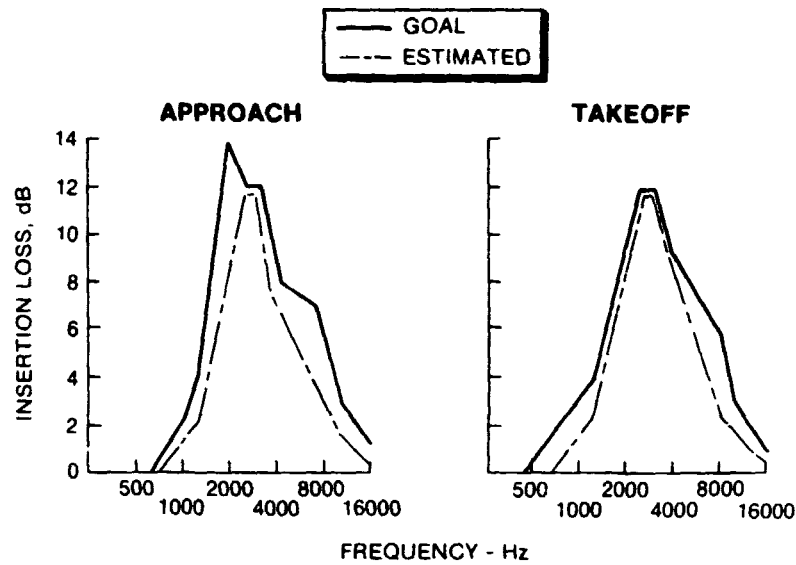


Figure 31

## NOISE REDUCTION DUE TO MIXER

- Greater Than 5 dB
- Coincides with Predicted Results

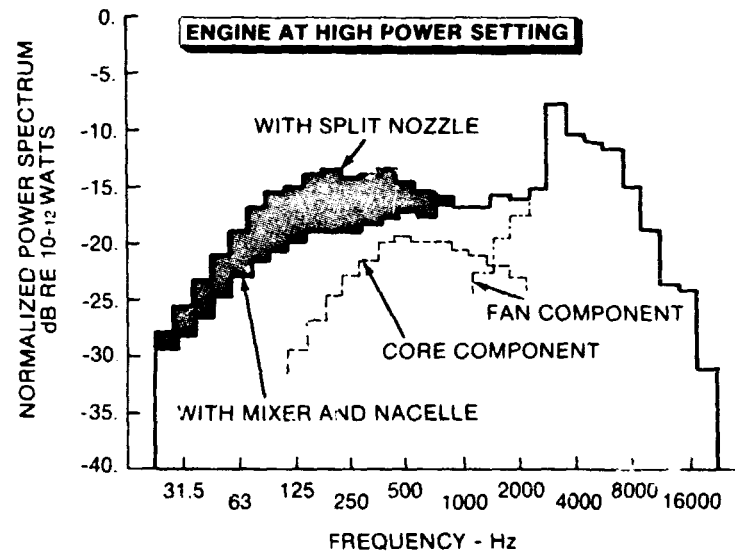


Figure 32

## QCGAT FLYOVER NOISE CALCULATION PROCEDURE

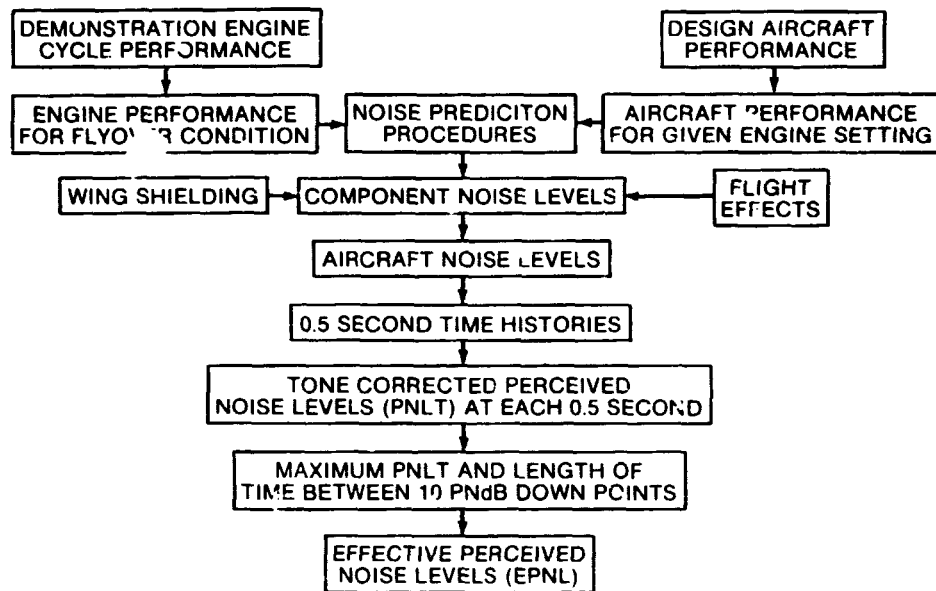


Figure 33

## COMPONENT CONTRIBUTION TO APPROACH NOISE

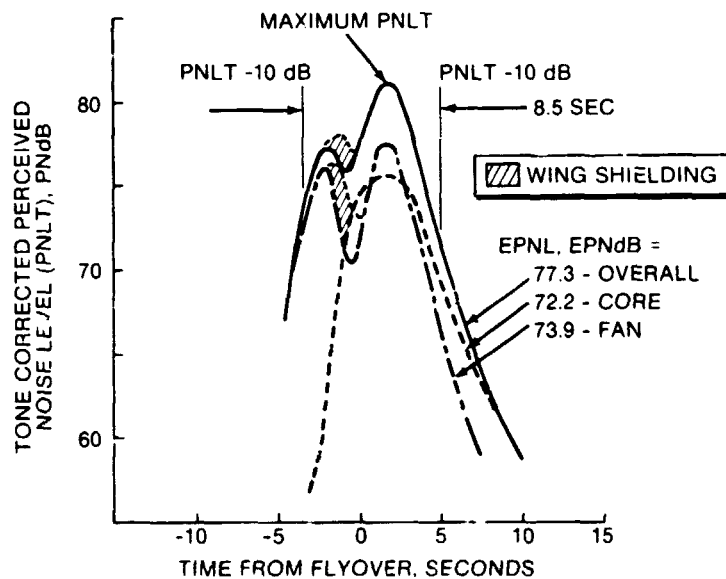
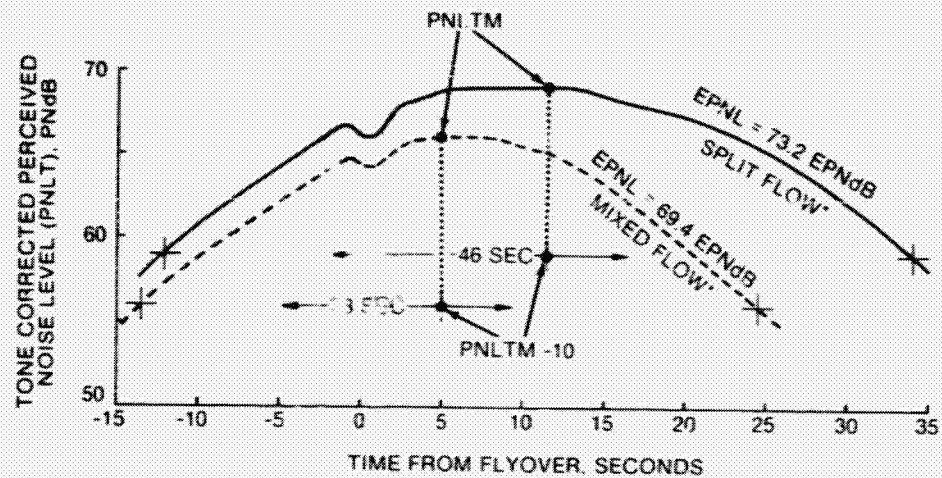


Figure 34

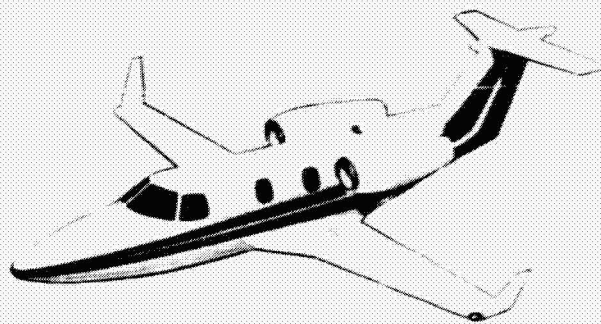
## TAKEOFF FLYOVER NOISE



\*No Sound Treatment

Figure 35

## QCGAT PREDICTED NOISE PERFORMANCE



### QCGAT ACOUSTIC PERFORMANCE

CONDITION	EPNL GOAL EPNdB	DELIVERED ENGINE EPNL, EPNdB
Takeoff Flyover	69.4	68.4
Takeoff Sideline	78.4	70.6
Approach Flyover	83.4	77.3

Figure 36

## QCGAT vs FAR PART 36 LIMITS

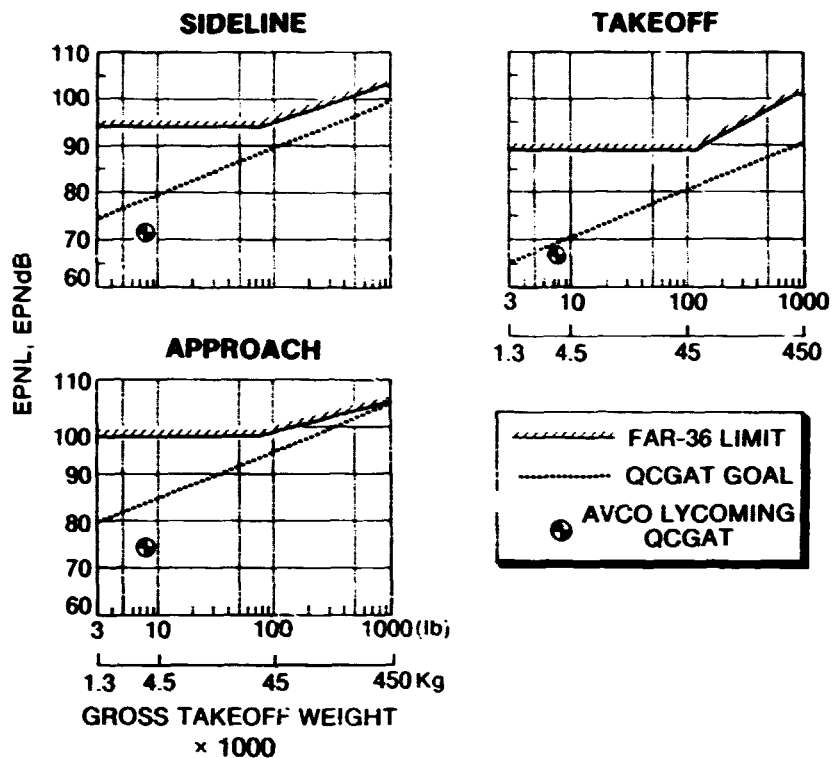


Figure 37

## SUMMARY

- Successful Application of Large Turbofan Noise Control Technology in a General Aviation Size Turbofan Engine
- All QCGAT Noise Goals Demonstrated (Takeoff, Sideline and Approach)
- Used Available Noise Control Techniques to Meet Stringent Noise Goals Without a Performance Penalty
- Noise Need Not Be a Constraint to General Aviation Growth

Figure 38



25 27  
N80-22334

## SUMMARY OF NASA QCGAT PROGRAM

Gilbert K. Sievers  
National Aeronautics and Space Administration  
Lewis Research Center

As was stated in the program overview, the QCGAT program objectives were to demonstrate that the application of large turbofan engine technology to small general aviation turbofan engines can achieve low noise, low emissions, and acceptable fuel consumption.

### NOISE GOALS

Figure 1 shows the takeoff noise goal. This is the same figure that was shown in the overview, except that the results predicted from ground static testing are shown. Avco is quieter than the goal while AiResearch is meeting the goal. For the sideline and approach conditions (figs. 2 and 3), both engines are quieter than the goals. By meeting or bettering these stringent NASA noise goals, we believe that QCGAT has demonstrated that noise need not be a major constraint on the future growth of the general aviation turbofan fleet.

### EMISSION GOALS

The measured emission results for the AiResearch QCGAT engine are shown in figure 4. For each pollutant, the bar at the left shows the published level of the production TFE-731-2 engine. The bar in the center shows the QCGAT goal and the bar at the right, the measured QCGAT results. As can be seen, the carbon monoxide emissions were lower than the goal; the goal for the unburned hydrocarbons was met; and, while the  $\text{NO}_x$  goal was not met, QCGAT  $\text{NO}_x$  emissions are lower than those of the production TFE-731-2. Also, engine smoke was not visible.

The measured emission results for the AVCO QCGAT engine are shown in figure 5. No comparisons with production engines are made because there are no comparable production engines. However, it can be seen that measured emissions for carbon monoxide and unburned hydrocarbons are lower than the stringent goals and that  $\text{NO}_x$  is right at the goal. Again, this engine does not produce visible smoke.

### PERFORMANCE GOALS

A comparison of the AiResearch QCGAT engine measured performance with the performance goals is given in table I. The AiResearch QCGAT engine met its



thrust goals both at sea level takeoff and at design cruise. The sea level takeoff SFC is about 2 percent higher than the goal, but at design cruise, where it really counts, the SFC is lower than the goal and is approximately 9 or 10 percent lower than the current production TFE-731-3.

A comparison of the AVCO QCGAT engine measured performance with the goals is given in table II. The AVCO QCGAT engine did not meet the sea level takeoff or design cruise goals for either thrust or SFC. However, the measured numbers are quite respectable. It must be remembered that this engine did not evolve from a mature production engine as did the AiResearch QCGAT engine. It is believed that the AVCO QCGAT engine is one iteration away from meeting the goals.

### CONCLUSIONS

The major goals for the QCGAT project were met and the project was completed on schedule and within the NASA budget. We consider this to have been a very successful NASA joint effort with industry.

TABLE I. - AIRESEARCH QCGAT PERFORMANCE

[Standard day; installed]

		Goal	Measured
Sea level takeoff	Thrust, N(lb)	17312 (3892)	17312 (3892)
	SFC, kg/hr-N (lb/hr-lb)	0.0431 (0.423)	0.0440 (0.431)
Design cruise M = 0.8 12 200 km (40 000 ft)	Thrust, N(lb)	4017 (903)	4017 (903)
	SFC, kg/hr-N (lb/hr-lb)	0.0759 (0.744)	0.0756 (0.741)

TABLE II. - AVCO QCGAT PERFORMANCE

[Standard day; installed]

		Goal	Measured
Sea level takeoff	Thrust, N(lb)	7166 (1611)	6485 (1458)
	SFC, kg/hr-N (lb/hr-lb)	0.0370 (0.363)	0.040 (0.392)
Design cruise M = 0.6 7600 km (25 000 ft)	Thrust, N(lb)	2157 (485)	1850 (416)
	SFC, kg/hr-N (lb/hr-lb)	0.0640 (0.628)	0.0737 (0.723)

## TAKEOFF NOISE LEVELS

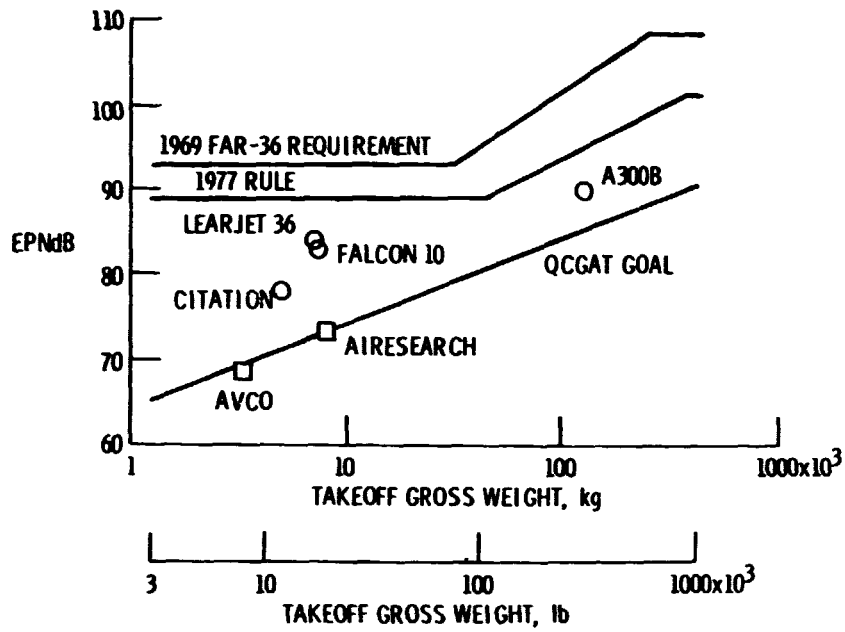


Figure 1

## SIDELINE NOISE LEVELS

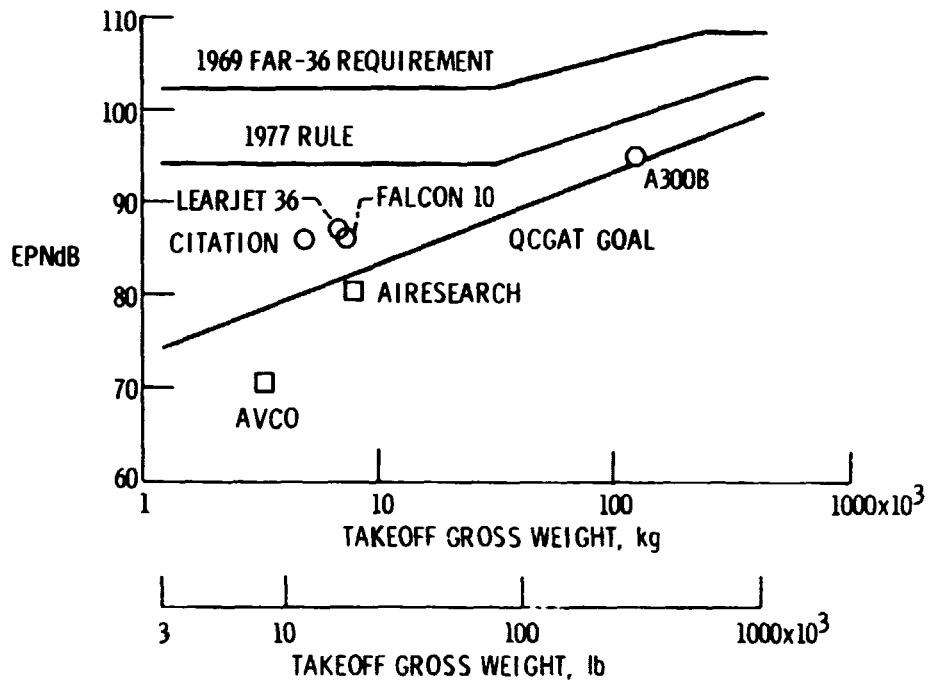


Figure 2

## APPROACH NOISE LEVELS

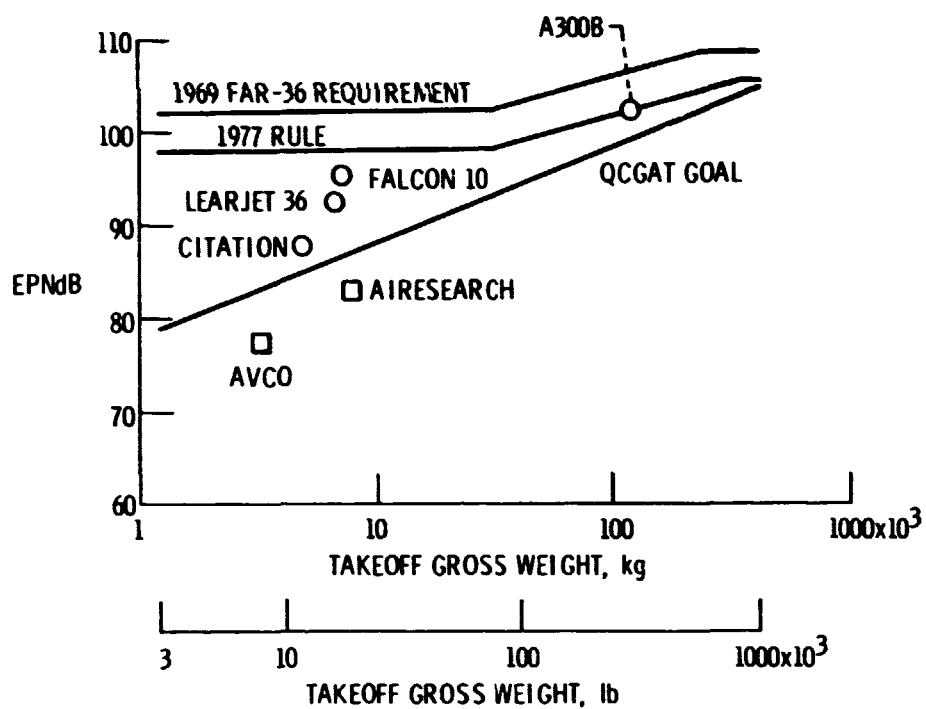
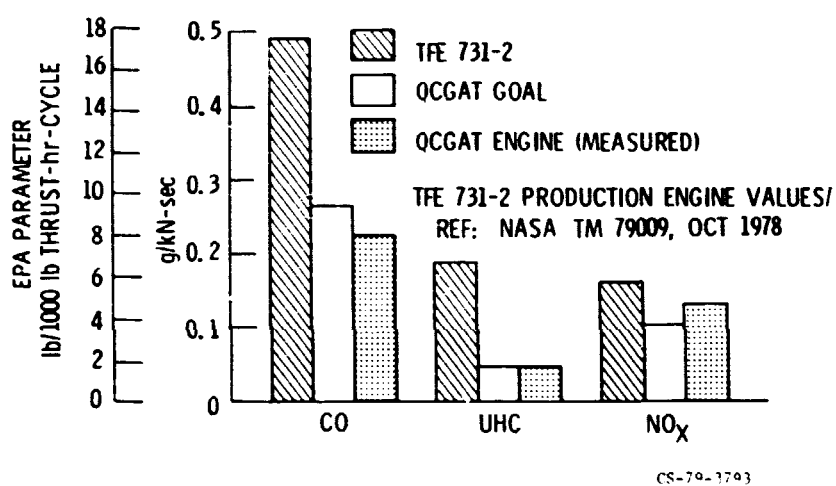


Figure 3

## AIRESEARCH QCGAT EMISSIONS



CS-70-1703

Figure 4

### AVCO QCGAT EMISSIONS

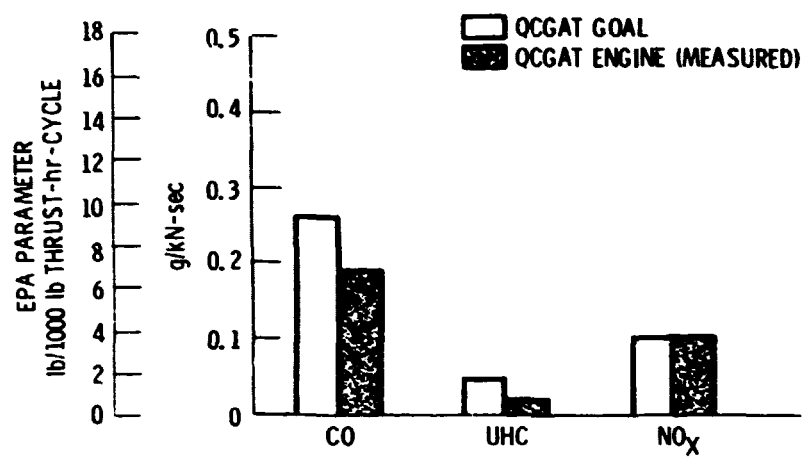


Figure 5

28  
N 80-22335

## NEW OPPORTUNITIES FOR FUTURE, SMALL, GENERAL- AVIATION TURBINE ENGINES (GATE)

William C. Strack  
National Aeronautics and Space Administration  
Lewis Research Center

### SUMMARY

The results of four independent contracted studies to explore the opportunities for future small turbine engines are summarized in a composite overview. Candidate advanced technologies are screened, various cycles and staging arrangements are parametrically evaluated, and optimum conceptual engines are identified for a range of 300 to 600 hp applications. Engine improvements of 20 percent in SFC and 40 percent in engine cost were forecast using high-risk technologies that could be technically demonstrated by 1988. The ensuing economic benefits are in the neighborhood of 20 to 30 percent for twin-engine aircraft currently powered by piston engines.

### INTRODUCTION

The preceding portion of this conference was devoted entirely to business jet external noise and pollution, primarily, and fuel economy, secondarily. This turbofan-powered segment of general aviation represents about one-fourth of U.S. engine net factory billings even though only 2 percent of the general-aviation aircraft engines sold are of this type (fig. 1). The remainder of the conference will address the concerns of the other 98 percent. At the lower cost end are the single-engine airplanes powered by 100- to 300-hp piston engines. About 23 000 of these were produced last year. The twin-piston powered airplanes utilize 200- to 400-hp engines of which about 8000 are produced annually. The turboprop aircraft are mostly twins that require 500- to 1000-hp engines. The U.S. produced about 750 of these last year, and Canada produced approximately the same number. Collectively, these three categories represent 3/4 of the general-aviation engine net billings. Last year the total general-aviation engine billings were about 70 percent as large as those for the large commercial transport turbofans.

The principal problems facing these three categories are not so much environmental as they are economic, fuel, and safety related (fig. 2). Perhaps of greatest concern is the cost and availability of aviation fuels. Continued steep price hikes and the vulnerability of aviation gas to severe production cutbacks, or outright elimination, propels our quest for true multifuel powerplants. The safety of this class of aircraft continues to be questioned - with the spotlight alternating between airplane and automotive safety record comparisons and the controversial one-engine-out twin problem. Engine dependability

is especially important in these smaller aircraft. Passenger comfort levels are far less than those of larger turbofan aircraft, and the powerplant is a major cause of the discomfort. Other concerns involve propulsion-related acquisition and maintenance costs - especially for turboprop engines (fig. 3). NASA's involvement in addressing these concerns for the smaller general-aviation powerplants is recent. Two years ago we recognized that the tiny amount of R&T effort devoted to small general-aviation turbines was not in proportion to their actual importance. As the first step in rectifying that situation, we initiated a series of analytic studies - known as the GATE studies - to explore small turbine technology opportunities. The question was: If we hypothesize a brand new, small turbine engine that incorporates, say, 1988 level technology, what size should it be; how should it be configured; and what benefits would it bestow upon us? The purpose, then, became one of providing information to assist us in planning future research. We wanted to emphasize technologies that had high payoff and high risk, but which could be ready for production development by 1988 (given sufficient funding) and for mass production by the early 1990's. These engines could be as much as 1000 hp, but no more, but we emphasized sizes below 600 hp since we perceived this size class to be potentially the most rewarding - and challenging. We also emphasized aircraft cost of ownership as a criterion of merit during the conceptual design process.

The first task of these studies was a 1988 market forecast that considered all types of small airplanes and helicopters. This forecast determined engine power sizes and other requirements of interest. Most of the study effort, however, was devoted to broad-scope parametric analyses wherein various cycles, staging arrangements, and technologies were subjected to trade-off and screening evaluations to determine optimum engine configurations for each important mission identified in the market forecast. Then, anticipating that the marketplace could not afford different optimum engines for each application, an evaluation was made of a single common core to be used in a family of engines. And finally, the required R&T program was defined.

We at NASA did some of these assessments ourselves, but most were done under contract to these four companies working independently: Garrett/AiResearch, Detroit Diesel Allison, Teledyne CAE, and Williams Research. Within a general framework, we permitted the company teams the freedom to pursue directions and opportunities that they (rather than we) perceived as most attractive. This freedom sometimes led to uniformity, for example, all companies expressed a strong preference for turboprops instead of turbofans or turboshafts, and sometimes to interesting diversity, for example, the engine configurations and technologies varied considerably as did engine cost estimates.

The engine cost estimates were especially intriguing in the GATE studies because of the obvious opportunity to turbinize a portion of the piston-powered market. The turbine engine is pretty much accepted as the most desirable type of powerplant because of its many virtues - it has very low vibration levels, high reliability, multifuel capability, a better safety record, low weight, fewer emissions, less maintenance, and smaller installation losses. Despite these advantages, the use of turbine engines has been blocked at about the 500 hp level because of its higher fuel consumption and, especially, its 3:1 price premium (fig. 4). The challenge, of course, is to overcome the cost and fuel bar-

riers without sacrificing all the superior qualities. The trouble is that current technology does not allow this.

If we attempt to lower cost significantly, the efficiency suffers too much (fig. 5). But, if advanced technology could move the cost-efficiency band down far enough, we could certainly design a cost-effective small turbine or, if we choose, a better performer without cost reduction. On the other hand, if advanced technology could not lower the band sufficiently, then only the high performance option is open. In the end, three GATE study team pursued the low-cost turbine versus piston theme, and the fourth pursued a high-performance, advanced turbine versus current turbine theme.

The results of the four contracted studies are presented herein by selective examples that illustrate the main points in a representative fashion. The detailed results are documented in references 1 to 4.

#### CYCLES AND CONFIGURATIONS

In figure 6, design turbine-inlet temperatures of 1800°<sup>o</sup>, 1900°<sup>o</sup>, and 2200°<sup>o</sup> F are compared in terms of airplane total cost of ownership, fuel consumption, operating cost, acquisition costs, and engine cost. For all of these criteria, the optimum temperature level is 2200°<sup>o</sup> F, or about 400°<sup>o</sup> F above current small-engine levels. Although it appears that temperatures in excess of 2200°<sup>o</sup> F would be even better, 2200°<sup>o</sup> F was judged to be the highest temperature compatible with the materials available in the 1900's. The engine cost of the 2200°<sup>o</sup> F engine is 40 percent less than that of the 1800°<sup>o</sup> F engine because of a combination of factors. First, the physical size is about 40 percent smaller because the specific power improves substantially and because a smaller aircraft is required to do a given mission. In addition, the 2200°<sup>o</sup> F engine incorporates more cost-reducing technology, which retards the normal growth of cost with temperature and which keeps the cost per unit airflow nearly constant. Likewise, the 2200°<sup>o</sup> F engine weighs about 40 percent less than the 1800°<sup>o</sup> F engine. In fact, the airplane fuel consumption is improved 15 percent, not because the cycle efficiency improves (in fact, it is only 1 percent better), but because the engine weight is reduced. The engine weight and cost savings also produce 15 to 20 percent improvements in airplane acquisition cost, operating cost, and total cost of ownership.

In a similar vein figure 7 displays cycle pressure ratio effects. In the lower plot, engine cost is displayed as a band that was drawn from four compressor point designs: a single-stage centrifugal at 9:1 pressure ratio and a relative cost of 1.0, a two-stage centrifugal at 20:1, an axicentrifugal at 11.3:1, and a three-stage axicentrifugal at 15:1. The band width indicates the increasing cost associated with more compressor stages at a fixed pressure ratio. Cost increases rapidly with pressure ratio as more compressor and turbine stages are required. Likewise, at any given horsepower level, weight increases too, so the power-to-weight ratio, shown in the upper part, becomes worse. Unfortunately, at the small airflows required in these applications (2 or 3 lb/sec), the cycle efficiency is not increasing rapidly enough to offset these adverse trends. In fact, as the SFC band shows, things are even worse

than that. While the 11.3:1 engine is 6 percent more efficient than the 9:1 engine, the 15:1 and 20:1 engines are actually slightly worse than the 11:1 engine because the component efficiencies are suffering too much at the very small corrected airflows in the final stages. Hence, the minimum fuel solution is about a 12 or 14:1 compressor pressure ratio, but the lowest aircraft cost of ownership solution is about 9:1.

As a third example of these trade-offs, figure 8 presents a summary of one team's efforts to determine the best overall engine configuration for a medium pressurized twin. They considered a turbofan with a gas-generator consisting of a single centrifugal compressor hooked to a one-stage radial turbine. They also considered a free-turbine turboprop in three different versions: The first has the same simple arrangement as the turbofan; the second has a two-stage centrifugal compressor; and the third has an axial turbine replacing the radial turbine. Actually, the little diagrams only show the gas-generator portions, but all four of these configurations also have a two-stage axial-power turbine. And finally, they considered two arrangements of a single-shaft turboprop: both use a single centrifugal compressor, but the first has one axial turbine following a radial turbine, and the second has three axial stages. The evaluation criteria are airplane total cost of ownership, fuel consumption, operating cost, acquisition cost, and engine cost, and the values quoted are all relative to the second option - the simplest free-turbine turboprop. The bars are ordered from left to right in the same sequence as the top little diagrams. The most obvious result is that the turbofan is simply not in the running at all. Its penalties, which are caused by its low efficiency at low flight speeds, run from 25 to 65 percent. Actually, the optimum choice is not the simple free-turbine baseline but rather the even simpler single-shaft configuration with one less turbine stage. However, in consideration of other factors, especially commonality with helicopter turboshaft requirements, this team marginally preferred the free-turbine baseline.

After many trade-offs such as these and iterations with the marketing analyses, the four teams settled on the cycles and configurations shown on the right-hand side of figure 9. These engines are all turboprops ranging from 335 to 565 hp and are aimed primarily at the high-performance single-engine and twin-engine airplane applications. For comparison, both a representative current production turboprop (uncooled, old technology) and a hypothetical turboprop incorporating currently available modern technology are illustrated on the left-hand side of this figure. Allison's choice is a cooled, 2200° F maximum turbine-inlet temperature, 14:1 pressure ratio, free turbine design. Two centrifugal compressors are driven by two axial turbine stages, and another two-stage turbine drives the propeller load on a second spool. This design differs from both the current production engines and the hypothetical modern engines mainly in having a better cycle and higher component efficiencies. Its performance is much better, although its estimated cost differs little. Garrett also chose a two-stage free power turbine, but selected a single 9:1 centrifugal compressor driven by a one-stage radial turbine in their pursuit of lowering cost. Teledyne's low-cost engine quest led to an engine family that is described later. But its basic element is a very simple core engine which consists of a single centrifugal compressor connected to a single radial turbine. This turbine also drives the propeller load on a common shaft. Their turbine rotor is



uncooled and requires a very sporty, very advanced design, which is discussed later. Finally, Williams Research sought low cost through a very unconventional approach. Rather than the conventional idea of eliminating cost by eliminating parts, they propose utilizing known ways of producing very inexpensive parts at lower cost. The result was an uncooled, single-shaft, axicentrifugal arrangement with six axial compressor stages and four axial turbine stages at modest temperature but relatively high pressure ratio. This concept is described in more detail later also.

#### ENGINE PERFORMANCE AND COST

The performance estimates for these engines are summarized in figure 10. Usually we think of SFC rising smoothly as we decrease engine size because of adverse scaling effects. However, whenever a new engine is introduced, it may distort our expected curve simply because of its advanced technology relative to older, well-established engines. This happened a few years ago when the T700 was introduced. It yanked the curve down to form a "knee" in the trend curves at 1500 hp. Exactly the same thing would happen again if GATE technology engines were introduced at 400 to 600 hp, since they would be 20 percent more efficient than current production engines of the same size. The technologies that lead to this are described later.

The three low-cost-theme study teams projected engine costs in two ways. The first presumes no increase in production rates and simply reflects the intrinsic cost-reduction potential of using advanced technology (fig. 11). The magnitude of this saving is about 40 percent. In other words, GATE engines would be 40 percent cheaper to produce than today's engines. But, once a saving of this size materializes, it would trigger increased sales, and this opens up the possibility of a new manufacturing facility dedicated specifically to GATE engines, which, in turn, would cause even further savings - for a total reduction of as much as 60 percent. At the same time, market demand would increase to the neighborhood of 10 000 engines/year/company (assuming that two companies split the market equally). Hence, without sacrificing too much performance, the pursuers of the low-cost theme are predicting that GATE technology could provide the key that unlocks this potential. To put the cost estimates in better perspective, figure 12 shows engine specific cost estimates for all four companies against a backdrop of the current cost situation. Current turboprops cost about three times as much as piston engines. But remember, turboprop production rates are two orders of magnitude less than piston engine rates. Allison's rather sophisticated machine is estimated to cost about the same as current turboprops, and it triggers modest increases in sales. The low-cost theme estimates of Williams, Garrett, and Teledyne at 10 000 units per year closely approach the piston engine cost band, and this obviously represents a major departure from today's scenario. Of course dollars per horsepower alone is not sufficient since differing lapse rates, installation factors, fuel consumption, etc., are equally important considerations. The net effect of all these factors is shown later in the mission analysis results.

## TECHNOLOGIES

But what are the technologies behind these improvements? Certainly nobody could go out today and start building engines like these. Actually, it is somewhat difficult to succinctly summarize the advanced technologies identified in these studies because each study team incorporated different ones - at least in detail they are different. Nevertheless, figure 13 lists some of them in a composite fashion, although not all of these would be present in a single design. In the gearbox area the use of powdered-metal gears and laser hardening was recommended by several teams to reduce cost and improve properties. Composite material gear cases were recommended by Allison for stiffness and weight savings, while Teledyne suggested die-cast aluminum for a cost saving. Teledyne also recommended a composite drive shaft, and nearly all teams recommended full authority digital controls. However, the key elements in all of the concepts involved the rotating machinery. Except for Williams, each team sought high-performance centrifugal compressors using advanced analysis techniques, some form of passive clearance control, and backward curvature. High stage loadings without severe performance penalties were prevalent. And new manufacturing processes, such as using powdered-metal titanium for the rotors, appeared.

Technologies for the core turbine were especially diverse. Two companies selected high-temperature radial design: Teledyne, with an uncooled, powered-metal concept and Garrett with a cooled, laminated construction process. Allison selected a high-temperature axial arrangement with a cooled, dual-property rotor and possibly ceramic stators. Again, passive clearance control was cost effective, and improvement of efficiency through better three-dimensional flow analysis is required. Similar improvements were identified for combustors and power turbines.

The first of several example key technology elements is illustrated in figure 14. This one represents the attainment of a 9:1 pressure ratio compressor, at high efficiency, in a single stage. It requires advanced three-dimensional blading with high tip speeds and high inducer Mach numbers, an improved three-dimensional diffuser, better flow analysis and better experimental measurements, improved surge margin, and a low-cost fabrication technique that yields essentially a net shape part from powdered-metal titanium. The benefit is to improve compressor efficiency by 3-1/2 points relative to a current technology 9:1 single-stage machined compressor, while reducing cost to be competitive with cast designs. While the 4 percent engine cost saving is not as large as for some other components, it also saves 6 percent in engine weight, compared with a two-stage compressor that would otherwise be required with current technology.

The second example is Teledyne's proposed uncooled, but high-temperature, radial-inflow turbine. Its concept is based on their recent development experience with a 120-hp turbogenerator set for the Army plus some encouraging analytical work. Figure 15 shows the results of a preliminary analysis to verify the concept's life potential. The stress-rupture life was evaluated for two different blade geometries. One is relatively thin in the root region and has a cross-sectional area that tapers down at the tip to 1/16 that at the root (i.e., it has an area taper ratio ATR of 16). The other is thicker at the root and has

a taper ratio of 3:1. The evaluation assumed the use of equiaxed IN-100, a current material, to give a high confidence level. Actually through, advanced materials and directional solidification would probably be used to increase the design's integrity. This design is very highly loaded, with tip speeds approaching 2500 ft/sec and transonic exit velocities at a maximum turbine gas temperature of 2250° F. Under these conditions, the blade metal temperature is 1800° F at the tips, and the lifetime is only 200 to 100 hr. However, their engine is flat rated and will not require such high temperatures at take-off or at any other normal condition. At cruise, the gas temperature is down to 1950° F, which yields 1552° F maximum metal temperatures. This yields a 3000-hr life for the 16:1 ATR design or a 10 000-hr life for the 31:1 ATR design. However, it is not certain that the 31:1 ATR is practical because of increasing flow-path restrictions in the root regions (more detailed analyses are required to determine an optimum ATR).

The third example is Garrett's cooled, radial turbine concept (fig. 16). It consists of a set of photoetched laminates diffusion-bonded to form integral cooling passages. After bonding, the part is electrochemically milled to the full three-dimensional desired aerodynamic shape. Advanced powdered-metal sheet stock fabrication methods must be used to lower cost and thereby permit the use of high-strength materials such as Astroloy. The net benefit would be a 9.8 percent efficiency improvement relative to current, cooled axial turbines while reducing cooling bleed 20 percent and engine cost 21 percent.

The final example is that of an approach that does not apply specifically to a single component but rather influences the entire engine. It is Williams' unconventional approach to lowering cost through the use of restricted-geometry blade and vane aerodynamic shapes. The concept is to design for very low, rather than high, stress levels as depicted in figure 17. This allows perhaps a 150° to 200° F increase in turbine metal temperature without cooling, or, with an advanced material, much higher temperatures to exploit their specially shaped temperature-stress curves. With MA 6000E, for example, an extra 300° is possible. Either way, the lower stresses (perhaps 1/2 of conventional) imply lower design speeds, and this, in turn, means lower blade loadings, which permit the use of low-cost, simplified blade manufacturing techniques. Specifically, all compressor blades could have the same airfoil section, be of constant chord and camber, and be uniformly twisted; in fact, because only the lengths would differ, the parts cost would be dramatically lowered. The corollary is that higher pressure ratios are obtainable without much cost penalty. Then all the blades are held in place as the hub is formed around them in a single operation. The compressor vanes and all of the turbine airfoils are formed in the same way. The total result is a very different looking small engine concept which attempts to achieve low cost without performance sacrifice by incorporating a large number of very low-cost parts instead of a very small number of relatively expensive parts.

#### COMMON CORE

Another concept for reducing engine cost involves using a common core for a family of engines. Retaining parts commonality without sacrificing too much performance is the key here because each of the diverse mission applications

prefers a different optimum engine. One approach to this dilemma is illustrated in figure 18 which shows Teledyne's C9 core engine slightly modified to accommodate some additional parts that are required to reconfigure the engine for more power. This is done by adding a supercharging axial compressor stage, an axial turbine stage to provide the extra power, and a set of extra gears, which are duplicates of the first set to handle the increased power. This allows a 335-hp engine to grow 70 percent to a 565-hp derivative with on a 4-inch extension (from 34 to 38 in.), a 31-lb weight increase (from 172 to 203 lb), and a 54 percent increase in cost (fig. 19). At the same time, the SFC is 10 percent lower due to the increased cycle temperature and pressure and component rematching. The price of commonality in this case is a 2 percent SFC penalty for the basic core engine. This results from the lower turbine temperature required to accommodate a common fixed-area nozzle. The benefits of this approach to commonality are a 7 percent lower cost and a 16 percent weight reduction for the C9 335-hp version relative to the next best approach, which is using a single, large configuration and then shaving the flowpath area to reduce power.

#### AIRCRAFT BENEFITS

The effect that these technologies, both individually and collectively, would have if GATE engines were installed in conventional but slightly improved airframes flying missions moderately more difficult than today's will be illustrated with several examples. In each case the hypothetical aircraft is resized to accommodate the new engines. First, the Allison GATE engine was compared with a scaled turboprop version of their most recently improved 250 series turboshaft engine. Their GATE engine incorporates considerable materials and aerothermodynamic improvement which accounts for higher cycle efficiency and smaller size. Specifically, a dual-property, axial, high-pressure turbine, while slightly more expensive initially, yields long life and much less engine maintenance cost. Similarly, a transpiration cooled, Lamilloy combustor, while not inexpensive itself, allows the use of a short, compact, and long-TBO (time between overhauls) combustion system. Ceramic rotors were not judged appropriate for manned aircraft application in this time frame, but Allison suggested that ceramic stators may be, although even they are only marginal. Lastly, a fiberglass/polyimide composite gearbox showed a slight cost advantage. Allison's advanced technology engine yielded 20 percent better SFC and 23 percent less weight. It costs 3 percent more to buy, but 35 percent less to maintain than a comparable current turboprop. A range of aircraft benefits are shown in the following list corresponding to the three aircraft types that they investigated (an unpressurized twin, a heavy twin, and a twin-engine helicopter):

##### Technologies:

1. Advanced materials and aerothermodynamics - higher cycle efficiency and smaller size
2. Dual property axial high-pressure turbine - much lower maintenance cost (5000 hr TBO)
3. Ceramic turbine stator - slight cost reduction
4. Lamilloy combustor - permits 5000 hr TBO at high temperature
5. Composite gearbox case - slight cost reduction

Engine improvements:

1. SFC - 20 percent
2. Weight - 23 percent
3. Cost -3 percent
4. Maintenance cost - 35 percent

Aircraft benefits:

1. Fuel burned - 23 to 32 percent less
2. Gross weight - 11 to 21 percent less
3. Purchase price - +7 percent
4. Ownership cost - 8 to 20 percent less

Although the purchase prices do not change much, 23 to 32 percent less fuel is burned, and ownership costs drop 8 to 20 percent.

In a similar way, the other companies listed the technology elements that survived their screening processes and ordered them as shown in table I, a Garrett example. The benefits of each of the advanced technologies are given relative to a hypothetical, all-new engine using currently available technology. For example, the high-pressure laminated turbine technology raises the core turbine efficiency by 9.8 percent, reduces engine cost 21 percent, weight 7 percent, and SFC 7.4 percent and yields a benefit cost ratio of 56:1. The benefit is defined as the ownership saving over 20 years for a fleet of 15 000 medium-sized, twin-engined airplanes. The cost is the research investment required to demonstrate technology readiness. The single-stage powdered metal titanium advanced compressor is 1 percent less efficient than a machined two-stage current technology compressor; yet it costs and weighs enough less to offset this penalty. Another technology with large benefits is a low-pressure turbine that operates at a high work factor but low speed. Collectively, these technologies provide a 36 percent lower cost reduction, 20 percent lighter weight, and 13 percent better SFC relative to the best that we could do with today's available technology. One of the key elements is clearly the laminated turbine technology, which provides roughly one-half of the benefits.

#### Aircraft Fuel

Now we can return to the most challenging issue, identified at the outset: comparing advanced GATE type engines with piston engines. One of the disadvantages of current turboprops is that they consume too much fuel: about 10 percent more than current piston engines for a typical twin-engine aircraft mission. This is because their installed cruise thrust-SFC is inferior. GATE engines would eliminate most of this SFC difference as shown in figure 20. Since their installed engine weight is only 1/3 or 1/4 as much as a reciprocating engine, the resulting GATE-powered airplane would actually save 5 to 15 percent fuel. Since avgas costs as much as 20 percent more per BTU, the real fuel cost savings are substantially greater than that.

#### Aircraft Economics

A representative illustration of how a GATE-powered airplane compares with a reciprocating-powered airplane in economic terms is shown in table II for a

light-twin airplane that cruises at 10 000 feet at 225 knots for 1100 nmi, is flown 500 hr/yr, and is sold after 3 years. The baseline is a current-technology, reciprocating-powered airplane that requires two 380-hp piston engines weighing 550 lb, each, that together burn 172 gallons of fuel. The airplane takeoff weight is 6200 lb; the engines cost \$11 000 each; the airplane costs \$207 000 total; it costs \$51/hr to operate and, for the three-year ownership period, costs a total of \$170 000. The percent changes for three different advanced engine options are shown in the right-hand columns. The first is an improved reciprocating engine presuming simply 10 percent lower SFC. It produces rather modest aircraft economic improvements: 5 percent in total cost of ownership. Option 2 is a current technology turboprop, but produced at a rate of 10 000 units per year. It too is not very attractive - only a 3 percent net savings. Option 3, one of the low-cost GATE turboprops, is much more attractive. This airplane would be 20 percent smaller and burn 8 percent less fuel, and, although the engine cost is up 23 percent, the complete aircraft cost is down 14 percent, and the operating cost is down 28 percent, for a total ownership saving of 20 percent.

If we expand our scope to include the other low-cost GATE versions and other applications (fig. 21), we see that, as a class, the twin-turboprop airplanes would cost 15 to 25 percent less to buy and 30 to 40 percent less to operate than their piston-powered counterparts. However, the benefits for high-performance, single-engine airplanes are only one-third to one-half as much. Nevertheless, any economic benefits at all must be considered a bonus, inasmuch as the argument for turbinization could be predicated on noneconomic virtues alone. The obvious question is: When do these economic benefits disappear? A rough estimate of this is shown in figure 22 where a few data points from each study are plotted in terms of the reduction in ownership cost of GATE-powered airplanes relative to current reciprocating-powered airplanes as a function of the required shaft horsepower for the reciprocating aircraft version. The twin-engine airplane data looks impressive, showing 20 to 30 percent benefits. The single-engine data are too sparse to be certain, but it appears as though the economic incentive goes to zero somewhere in the 200-hp region. Of course, even at zero or slightly negative economic change turbinization is still attractive.

#### MARKET IMPACT

Obviously, major benefits of this magnitude cause a large impact in the marketplace. The marketing forecasts that go along with the preceding are summarized in figure 23 for each study team in terms of the total number of turbine engines produced, both with and without an instantaneously mature GATE engine in 1988. Since GATE technology engines could not actually even enter service until the early 1990's, this is merely an indication of impact rather than an actual forecast. The picture is certainly striking because of the quite different estimates. Allison's modest forecast is in agreement with their more conservative cost estimates, while Teledyne predicts a huge gain due to their lower cost estimates and broad engine-size family. All of the estimates are much greater than the 1500 engines produced in 1976. Half of these were turboshaft engines for helicopters. However, the future GATE scenario forecasts that the turboprop would strongly dominate. A composite average of these four forecasts is shown

in figure 24. A total of 20 000 GATE technology turbine engines would be manufactured annually, mostly turboprops, compared with one-fourth as many without GATE technology. The aircraft market results are shown with the pie charts, both with and without GATE technology engines. Without GATE, the turboprop share is forecast to grow from its current level of 2 percent to a level of 5 percent. With GATE, it would grow to about 35 percent, or a sevenfold increase. The twin-piston market would practically disappear, from 12 to 2 percent, while the single-engine piston portion would shrink from 68 to 47 percent, but it still would remain very large.

### CONCLUSIONS

A summary of what we perceive the major study result to be is displayed in figure 25. The most challenging, but rewarding, opportunity for small general-aviation turbine engines lies in the 300 to 600 hp region. Here, the proper combination of simpler design, improved materials, higher component efficiencies, cheaper manufacturing technologies, and core commonality could result in sufficiently lower engine cost, SFC, and weight to overcome the traditional turbine engine cost barrier at the 500 hp size. Plotted here are the trends of aircraft cost versus engine size, and the large gap between reciprocating-powered and turboprop-powered aircraft is apparent. GATE technology permits large improvements in aircraft economies at the upper end of the reciprocating-powered class and fills in the gap between the relatively inexpensive reciprocating aircraft and the expensive turboprop aircraft. In turn, this brings the many other virtues of turbine engines to a much broader spectrum of users and applications.

### REFERENCES

1. Baerst, C. F.; and Furst, D. G.: General Aviation Turbine Engine (GATE) Study Final Report. NASA CR-159482. (AiResearch-21-2997, AiResearch Manufacturing Co. of Arizona; NASA Contract NAS3-20755.) NASA CR-159482, 1979.
2. Gill, J. C., et al.: Study of an Advanced General Aviation Turbine Engine (GATE). (EDR 9528, Detroit Diesel Allison; NASA Contract NAS3-20756.) NASA CR-159558, 1979.
3. Smith, R.; and Benstein, E. H.: Advanced General Aviation Turbine Engine (GaTE) Study. (CAE-1600, Teledyne CAE; NASA Contract NAS3-20757.) NASA CR-159624, 1979.
4. Lays, E. J.; and Murray, G. L.: Advanced General Aviation Turbine Engine (GATE) Concepts. (WCR-78-113-15, Williams Research Corp., NASA Contract NAS3-20758.) NASA CR-159603, 1979.

Table I  
ADVANCED TECHNOLOGY BENEFITS

TECHNOLOGY	$\Delta \eta$ , PTS	$\Delta$ COST, %	$\Delta$ WT, %	$\Delta$ SFC, %	BENEFIT/ COST RATIO
HP LAMINATED TURBINE	+9.8	-21	-7	-7.4	561
PM TI SINGLE STAGE COMPRESSOR	-1.0	-4	-6	+1.4	232
LOW COST FUEL NOZZLES	----	-1	0	0	144
ELECTRONIC CONTROL	----	-2	0	0	132
HIGH WORK/LOW SPEED LP TURBINE	+6.0	-5	-7.0	-7.0	498
LASER HARDENED GEARS	----	-3	0	0	226
TOTAL	----	-36	-20	-13.0	402 (AVG)

NOTES

1. CHANGES ARE RELATIVE TO HYPOTHETICAL CURRENT TECHNOLOGY TURBINE ENGINE
2. CLEARANCE CONTROL BENEFITS ARE INCLUDED IN ABOVE
3. BENEFIT DEFINED AS OWNERSHIP COST SAVINGS OVER 20 yr FOR 15 000 MEDIUM TWIN A/C
4. COST IS NASA R & T COST

SOURCE: GARRETT

CS-79-4210

Table II  
GATE TURBOPROP AIRPLANES WOULD BE CHEAPER

LIGHT TWIN AIRPLANE <sup>1</sup>	CURRENT TECHNOLOGY RECIP	% CHANGES		
		ADV TECH RECIP (-10% SFC)	CURRENT TECH TURBOPROP <sup>2</sup>	GATE TURBOPROP <sup>2</sup>
SHP, SLS TO	380	-2	-11	-14
ENGINE WEIGHT	550 lb	-3	-68	-75
MISSION FUEL	172 gal	-10	10	-8
GROSS WEIGHT	6 200 lb	-4	-15	-20
ENGINE COST	\$11 020	-2	113	23
ACQUISITION COST	\$ 207 K	-3	6	-14
OPERATING COST	\$ 51/hr	-6	-14	-28
TOTAL COST OF OWNERSHIP	\$ 170 K	-5	-3	-20

<sup>1</sup>CRUISES AT 10 000 ft, 225 KNOTS FOR 1100 n. m., 500 hr/yr FOR 3 yr

<sup>2</sup>ASSUMING 10 000 ENGINES/yr PRODUCTION

SOURCE: GARRETT

CS-79-4190



# U.S. CIVIL AIRPLANE ENGINE PRODUCTION

1978, ESTIMATED

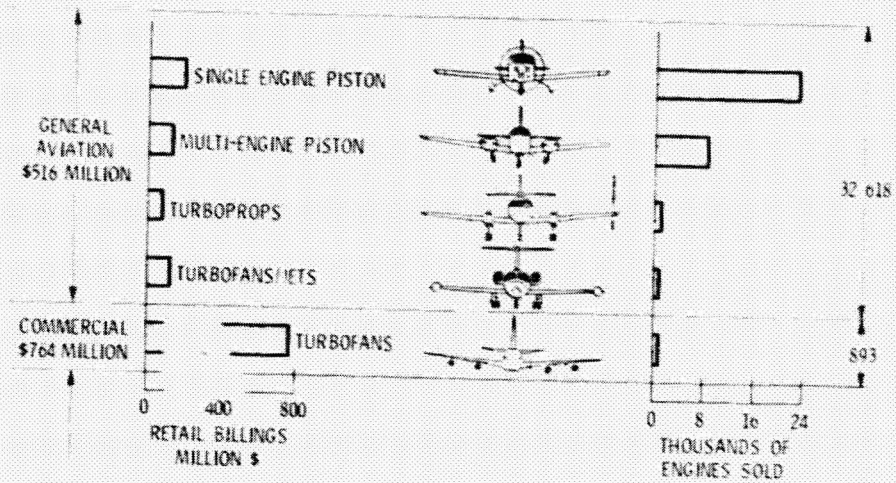


Figure 1

## GA PROPULSION CONCERNS

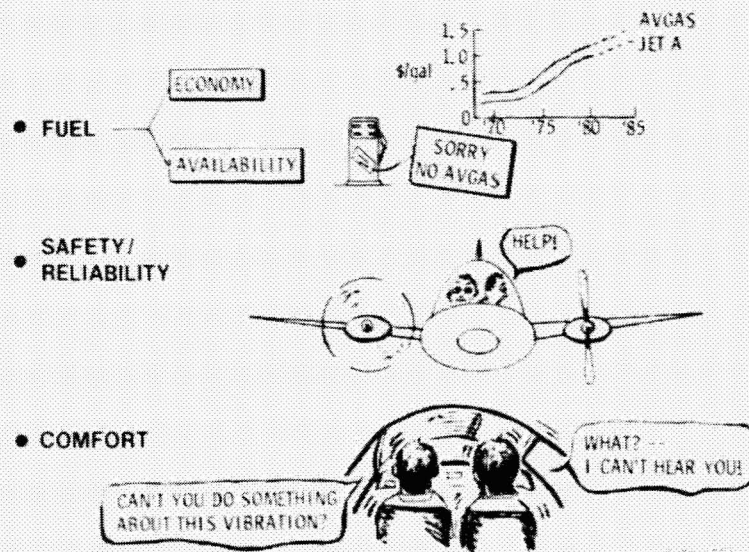
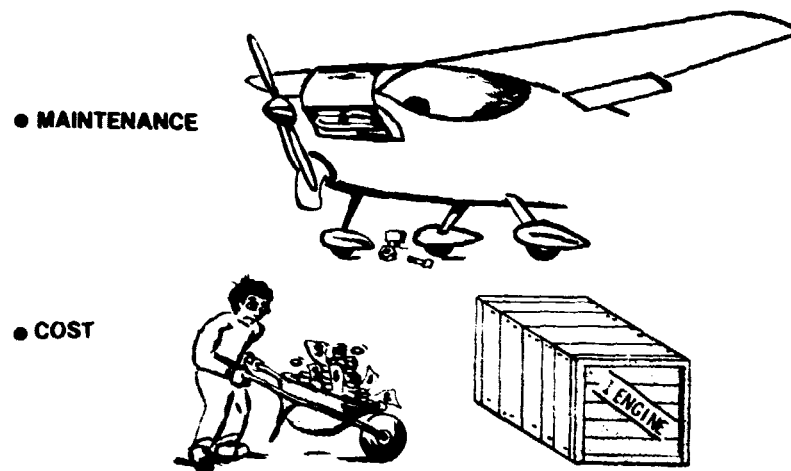


Figure 2



CS-79-1712

Figure 3

### CURRENT ENGINE SELECTION FOR LIGHT AIRPLANES

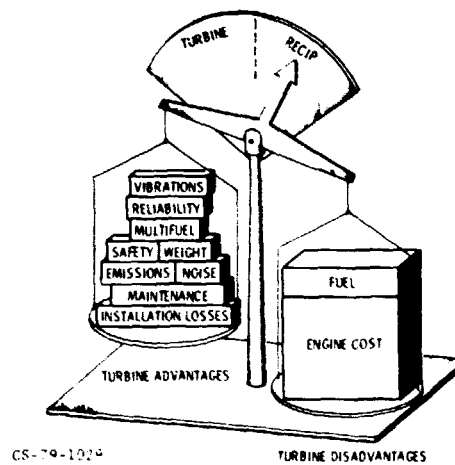


Figure 4

## EXPLOITING ENGINE TECHNOLOGY DIFFERENTLY

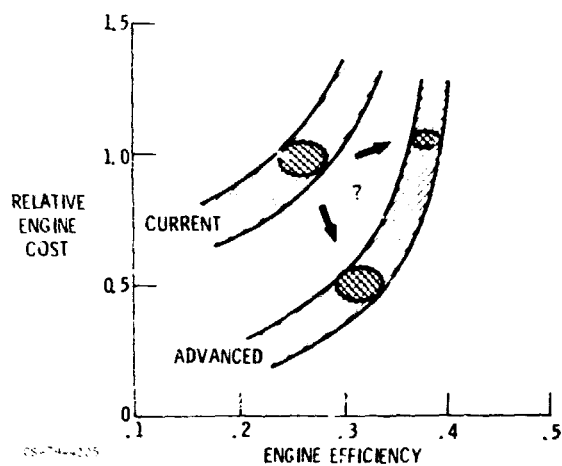


Figure 5

## TURBOPROP MEDIUM PRESSURIZED TWIN

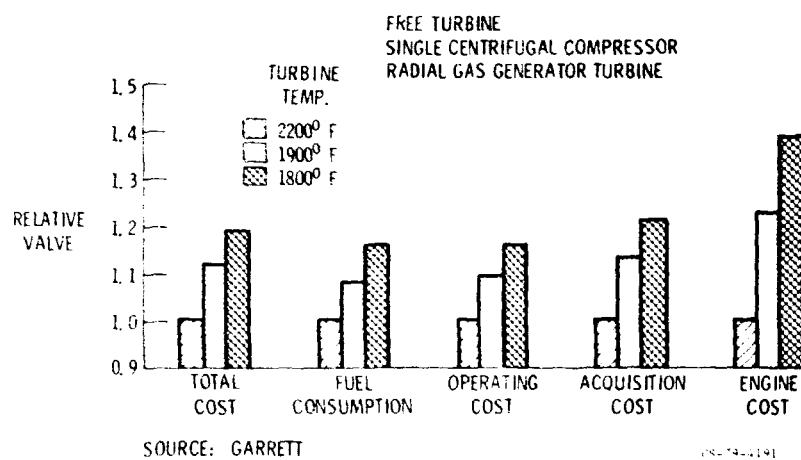


Figure 6

## EFFECTS OF INCREASING CYCLE PRESSURE RATIO

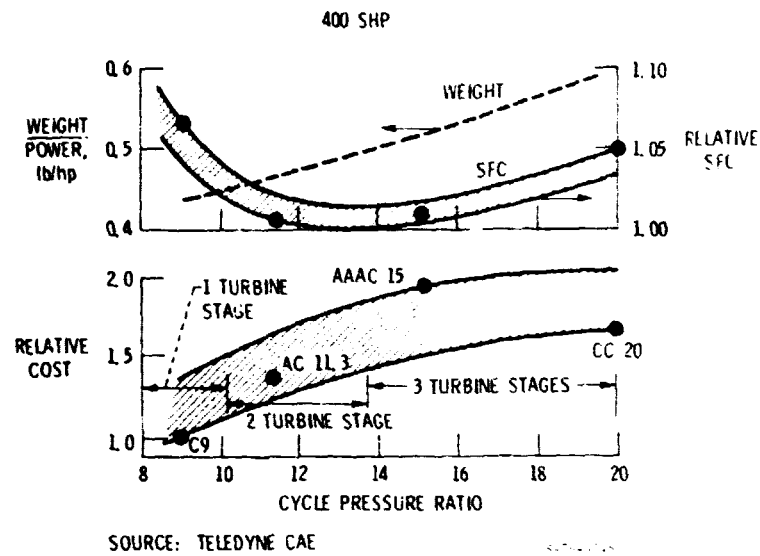


Figure 7

## GAS GENERATOR CONFIGURATIONS

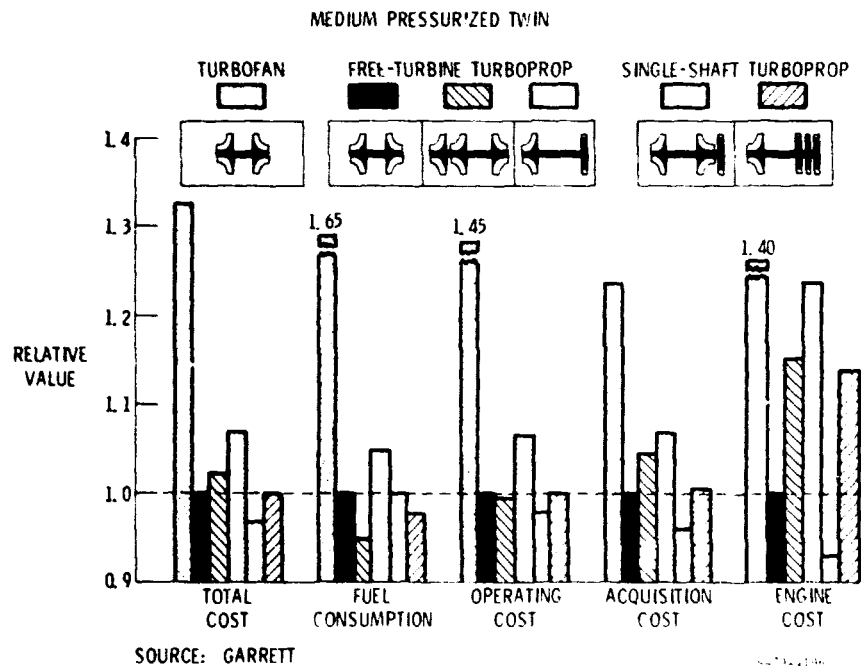


Figure 8

## FUTURE TURBINE ENGINE ALTERNATIVES FOR SMALL GENERAL AVIATION AIRCRAFT

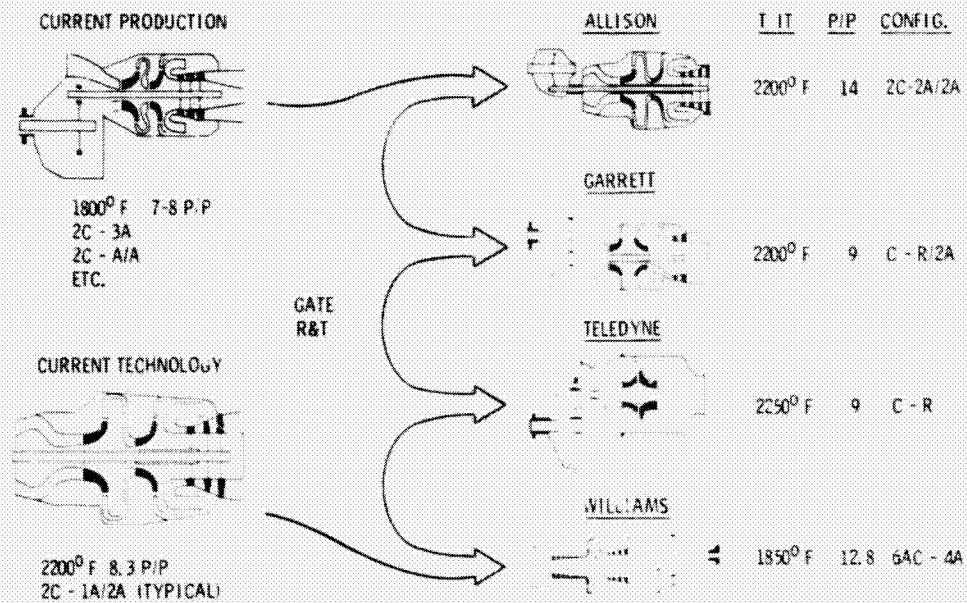


Figure 9

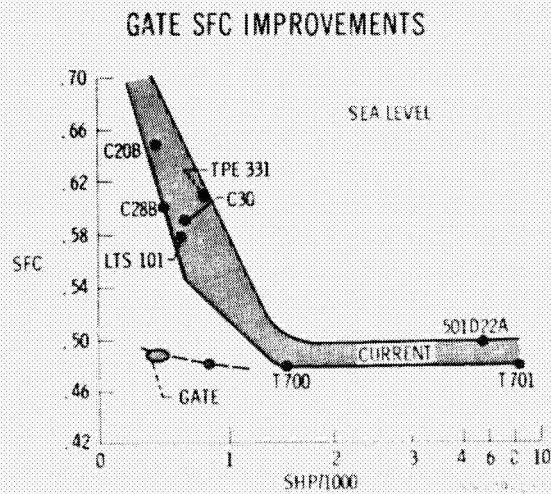


Figure 10

## BARRIER TECHNOLOGY

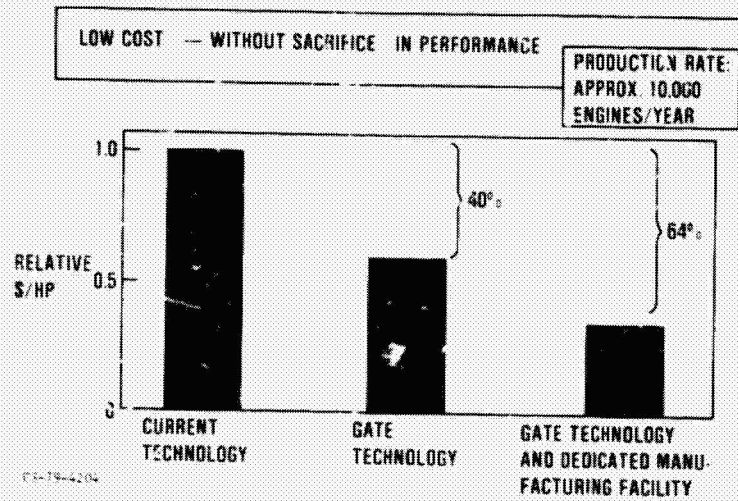


Figure 11

## COST REDUCTION FORECAST FOR GATE TECHNOLOGY ENGINES

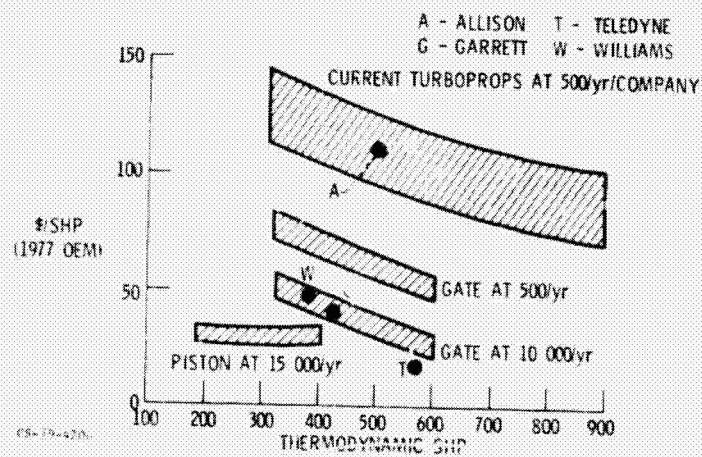


Figure 12



## GATE TECHNOLOGIES

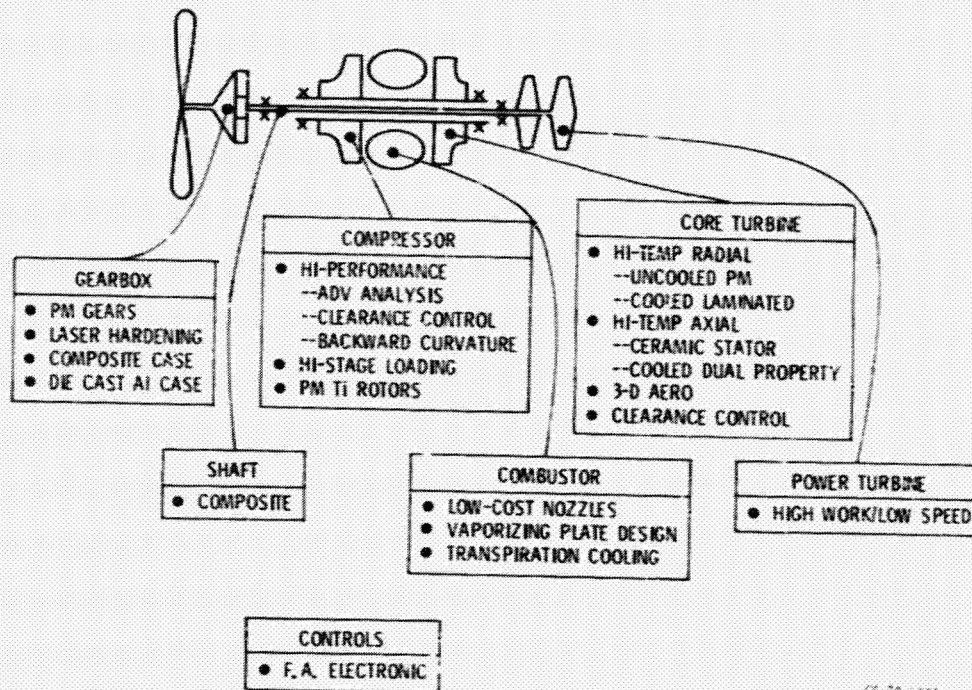
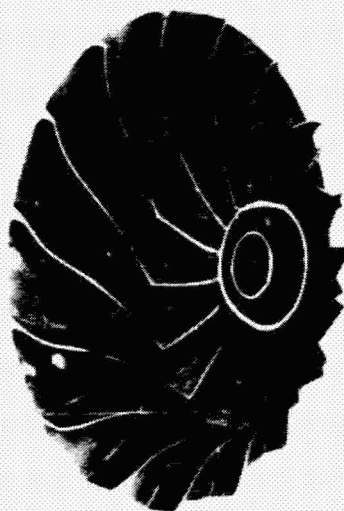


Figure 13

## SINGLE STAGE CENTRIFUGAL COMPRESSOR



### TECHNOLOGY

- HIGH STAGE LOADING
- ADVANCED ANALYSIS
- LDV MEASUREMENTS
- OPTIMIZED DIFFUSION RATIO
- 3D DIFFUSER
- BOUNDARY LAYER BLEED
- CLEARANCE CONTROL
- GOOD SURGE MARGIN W/O VAR GEO
- HIP PM Ti NET SHAPE

### BENEFITS

- +3.5 POINTS IN EFFICIENCY
- 4% ENGINE COST REDUCTION
- 6% ENGINE WEIGHT REDUCTION

Figure 14

## RADIAL TURBINE LIFE

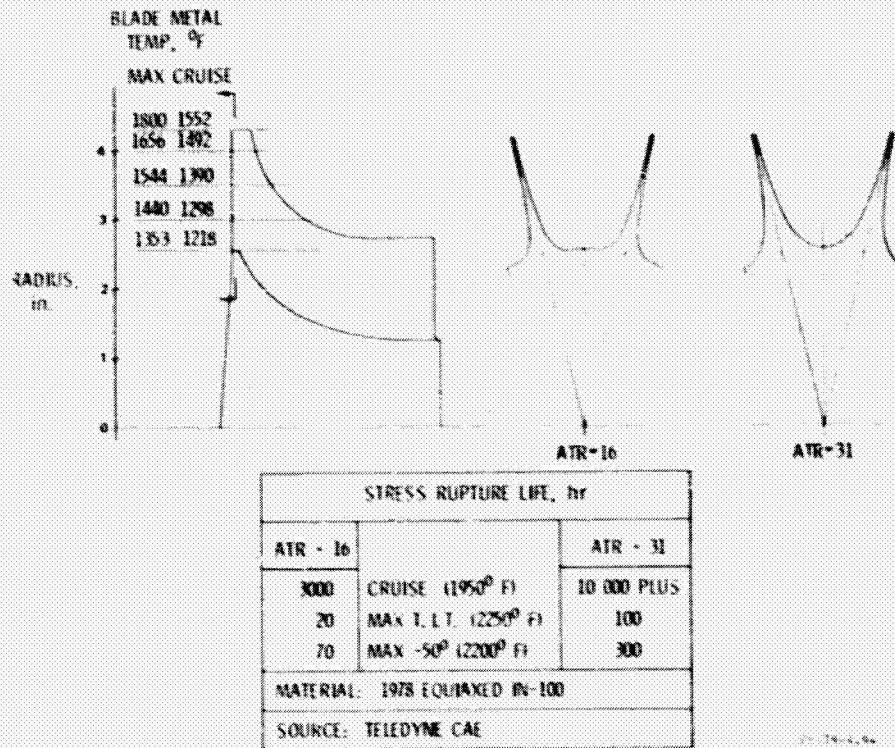


Figure 15

## INTEGRAL COOLED RADIAL HP TURBINE

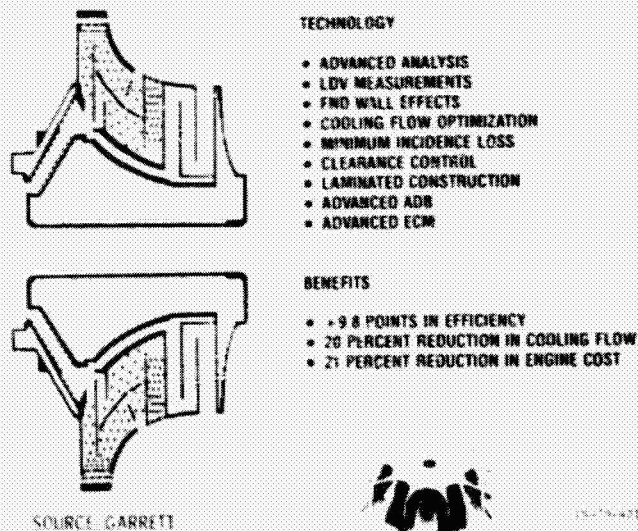
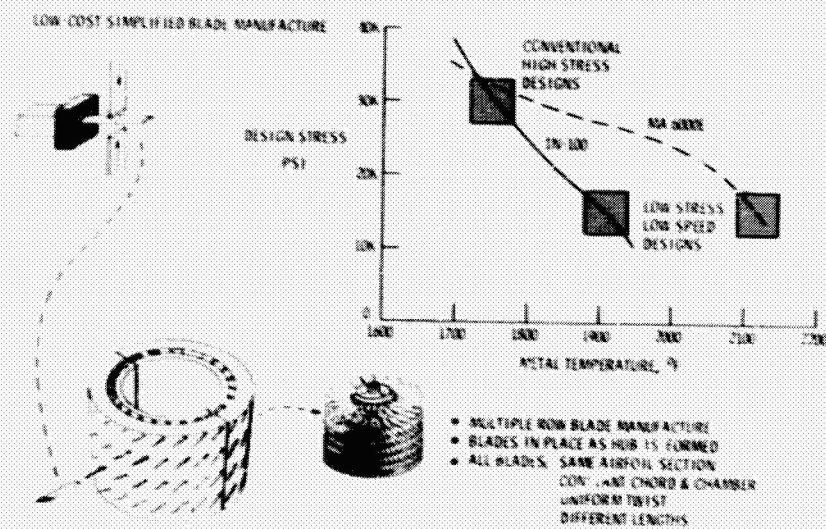


Figure 16



# MANUFACTURING TECHNOLOGY AREAS COMPATIBLE WITH RESTRICTED AERODYNAMIC SHAPES

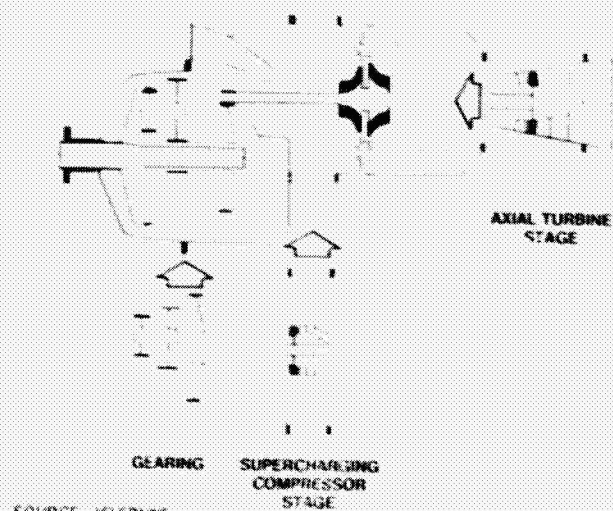


SOURCE: WILLIAMS RESEARCH

CP-104-2015

Figure 17

## ADD COMPONENTS TO C9 CORE



SOURCE: JELEDYNE

CP-104-2015

Figure 18

## COMMON CORE APPROACH

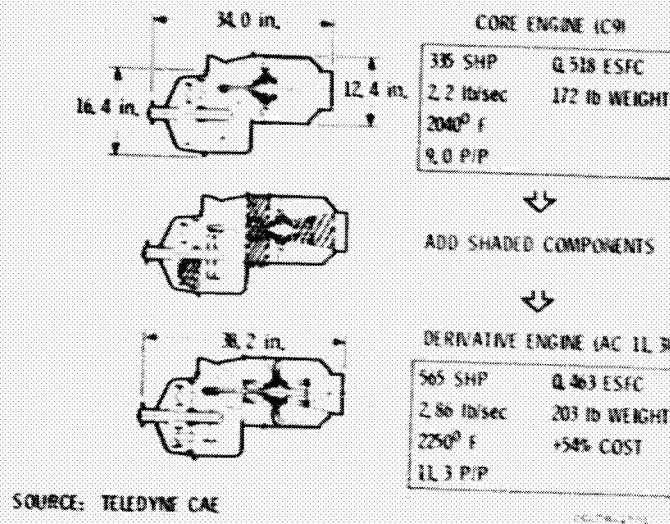


Figure 19

## EFFICIENCY IMPROVEMENT PLUS WEIGHT ADVANTAGE SAVES FUEL

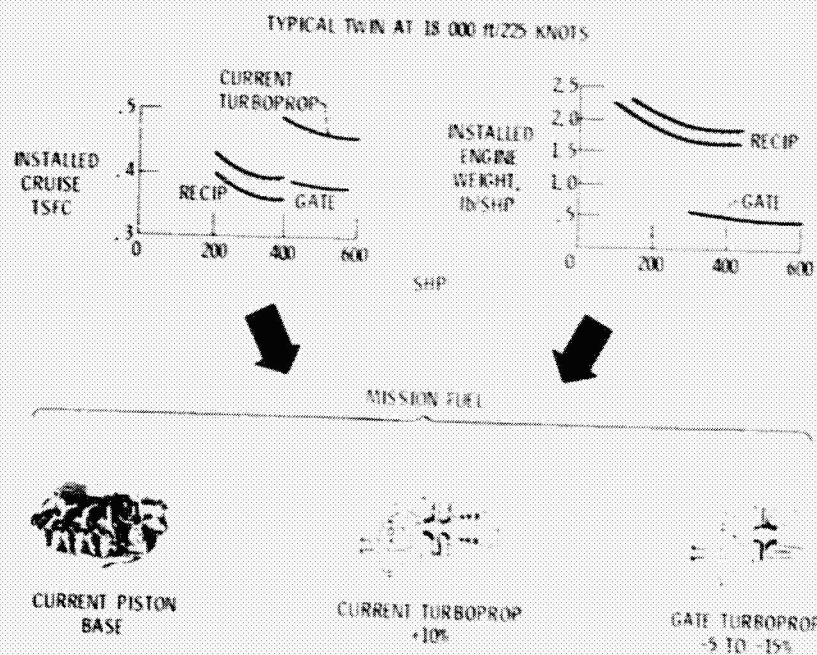


Figure 20

## BENEFITS RELATIVE TO CURRENT RECIPROCATING ENGINE

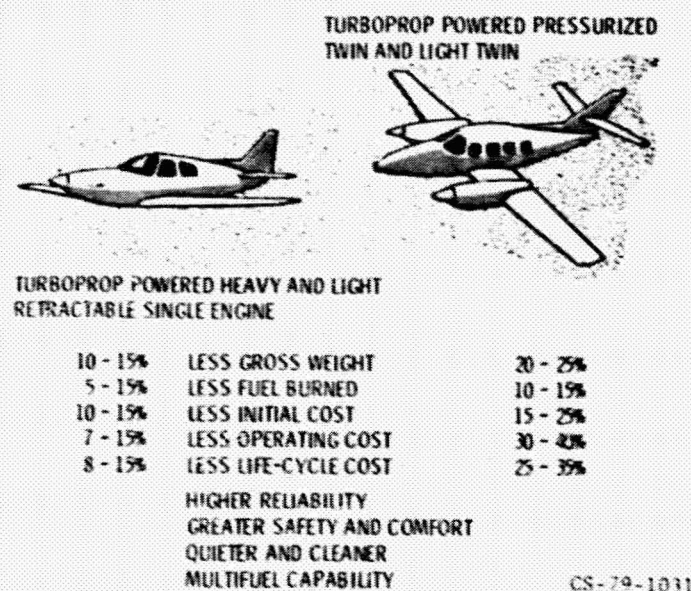


Figure 21

## GATE POWERED AIRCRAFT HAVE LOWER COST OF OWNERSHIP THAN EQUIVALENT RECIP POWERED AIRCRAFT

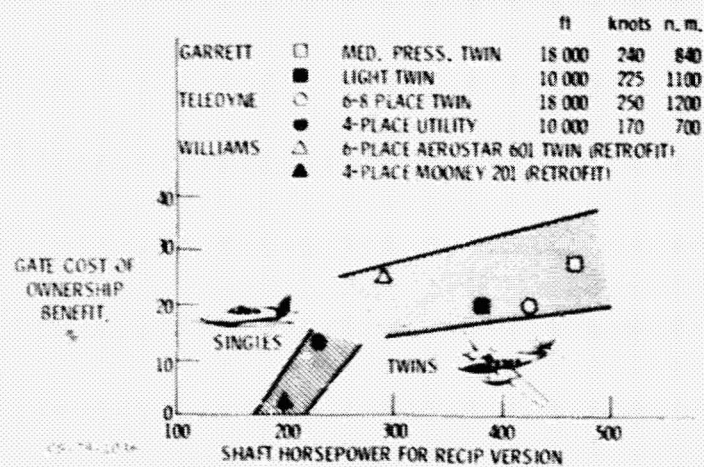


Figure 22

# 1988 CIVIL TURBINE ENGINE MARKET UNDER 1000 SHP

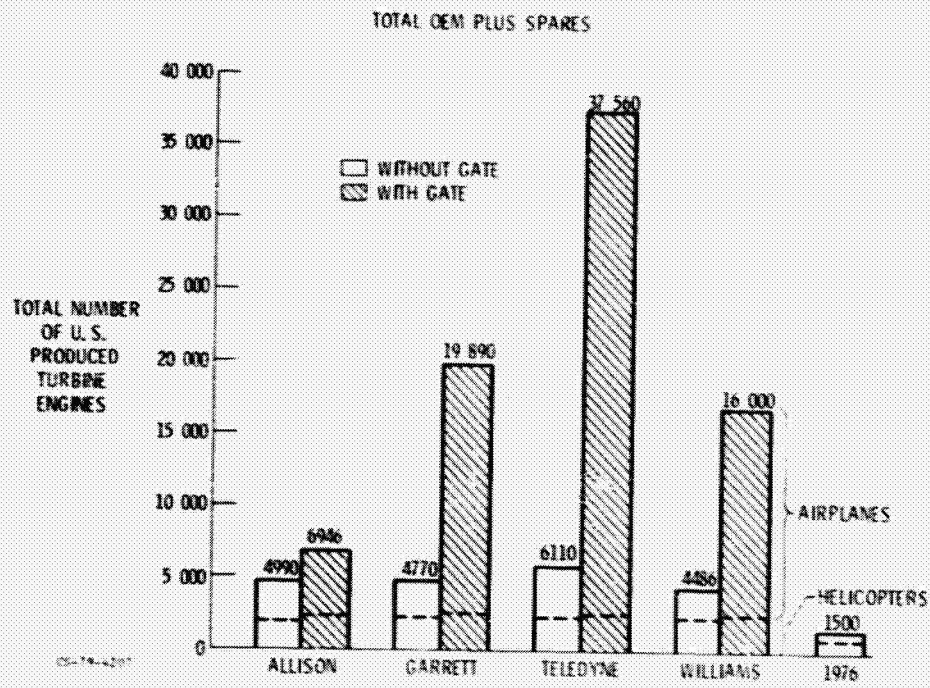


Figure 23

## 1988 PRODUCTION FORECASTS

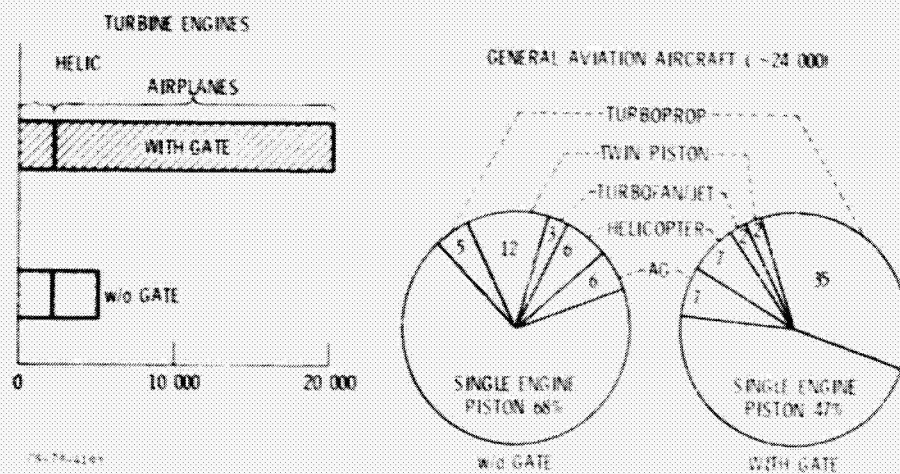


Figure 24

## GATE TECHNOLOGY COULD EXPAND DOMAIN OF SMALL TURBINE ENGINES

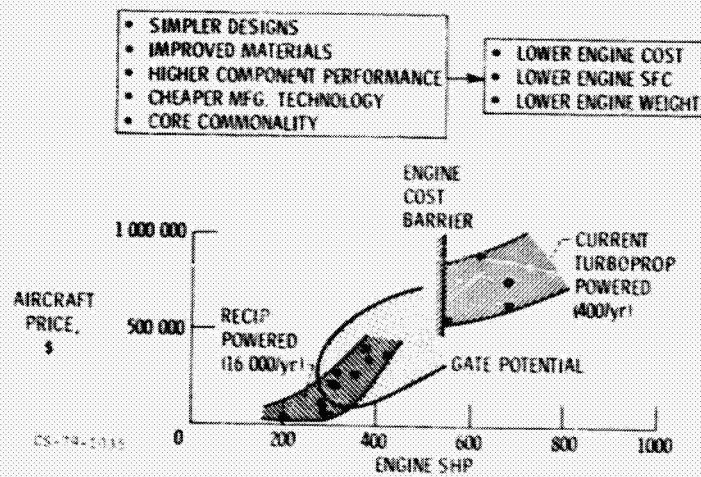


Figure 25



29  
N 80-22336

## AN OVERVIEW OF NASA RESEARCH ON POSITIVE DISPLACEMENT GENERAL-AVIATION ENGINES

Erwin E. Kempke, Jr.  
National Aeronautics and Space Administration  
Lewis Research Center

NASA is involved in a research and technology program related to improved and advanced general aviation engines. The overall goals of the program are to develop the technology to improve fuel economy, reduce engine weights and installation drag, and provide for broad-specification fuel or multifuel usage. Its two major technical thrust are directed at the near-term improvement of conventional air-cooled spark-ignition piston engines and at future alternative engine systems based on all-new spark-ignition piston engines, lightweight diesels, and rotary combustion engines that show potential for meeting program goals in the midterm and long-term future.

The conventional piston engine activities involve efforts on applying existing technology to improve fuel economy, investigation of key processes to permit leaner operation and reduce drag, and the development of cost effective technology to permit flight at high-altitudes where fuel economy and safety are improved.

The advanced engine concepts activities include engine conceptual design studies and enabling technology efforts on the critical or key technology items.

### NEAR-TERM IMPROVEMENT OF CONVENTIONAL ENGINES

The objective of the ongoing near-term improvement of conventional engine effort is to identify and foster the near-term technology base to reduce fuel consumption by 20 percent, extend the cruise altitude capability and decrease emissions.

The program addresses several specific technology elements through a combination of contract and in-house projects. The most significant are

- (1) An investigation of using existing technology to modify a piston engine for the purpose of improving fuel economy and reducing exhaust emissions.
- (2) An effort to improve cooling and reduce installation drag.
- (3) An effort to improve understanding of the combustion process to allow leaner burn operation.
- (4) Research to determine improved fuel-injection system characteristics.
- (5) A contractual effort to define the benefits and optimum design requirements of an advanced, cost-effective general-aviation high-altitude turbocharger.

Each of these elements will now be discussed in more detail.

#### Near-Term Modifications

Teledyne Continental Motors Aircraft Product Division, under a NASA cost sharing contract, is researching and developing methods to improve the fuel economy and reduce the exhaust emissions of its aircraft piston engines. Their research has resulted in the development of four concepts which, when applied to such an engine, permit leaner operation and thus improved fuel economy and simultaneously reduced exhaust emissions of hydrocarbons and carbon monoxide. The four chosen concepts as shown in figure 1 are

- (1) A timed, air-density-compensated fuel-injection system, which replaces the familiar low-pressure continuous-flow system.
- (2) A thermal barrier exhaust port liner for improved cylinder head cooling.
- (3) Air injection which in combination with the exhaust port liners reduces the exhaust valve stem temperatures to levels below the baseline engine while increasing CO and HC oxidation in the exhaust.
- (4) Variable spark timing to maintain best power spark timing over a broader operating range.

A comparison of the emissions and fuel economy for the standard IO-520 engine configuration and the engine with these four concepts integrated is presented in table I. Emissions are shown as percentages of the proposed 1980 standards. EPA has announced its intention to withdraw these but have not yet done so. Note that the modified engine meets all of the standards and in addition demonstrates a 10 percent improvement in the high performance cruise fuel economy. It also exhibited a 22 to 30 percent improvement in the LTO fuel economy.

The final round of tests are presently being conducted with a flightworthy engine, and the contract is being extended to include an flight test phase in early 1980.

#### Cooling Drag Reduction

The objective of the cooling drag reduction program, a joint effort of the Lewis and Langley, is to develop and demonstrate the technology to improve the performance and economy of piston engine aircraft via reduced cooling and installation drag. Contemporary engine cooling and installation designs are based in part on technology and data developed for radial engines. These data and technology are not adequate for precise design of an engine installation using a horizontally opposed engine for which few data on the heat-rejection patterns are known. It has been estimated that the cooling drag for current designs ranges from 5 to 27 percent of the total airplane cruise drag. Recently completed tests in the Ames Research Center 40 by 80 ft wind tunnel have shown a cooling drag of 14 percent of total airplane cruise drag for one configuration. An integrated approach to engine cooling that includes reduced cylinder cooling



requirements and improved internal and external aerodynamics can reduce this drag by at least 50 percent.

This cooling study is strongly encouraged by the industry because many turbocharged installations now operate near detonation or cooling limits. This problem, which affects both safety and economy, will be greatly aggravated by efforts to fly higher through use of improved turbochargers.

NASA Lewis will award a contract by the end of 1979 for the first portion of the cooling program. This part of the program will determine the current practice and actual minimum cooling requirements for representative, present-day cylinder-head and barrel assemblies. Using these baseline results, various cooling concepts will be evaluated on their ability to reduce the cooling requirements. At least two of the most promising concepts will be selected, designed, integrated, and tested on the cylinder-head and barrel assemblies. To extend these experimental results to other cases, an analytical computer simulation model on the cylinder head/barrel assemblies will be developed in a joint effort of Lewis and the contractor.

A planned but as-yet unfunded follow-on contracted effort will use the above improved technology base and design information to design an optimized cylinder-head and barrel assembly and to conduct experimental verification tests on a single-cylinder engine. Parallel efforts in aerodynamics methodology will improve nacelle internal flow paths, inlets, and exits. Following the verification testing, a full-scale engine and nacelle will be built for wind tunnel and flight tests.

#### Combustion Process Studies

Spark-ignition combustion process studies are being conducted to provide the data base from which predictions of flow process and chemical reactions in homogeneous and stratified charge engines can be made. Included in this activity are efforts in developing diagnostic instrumentation, conducting experimental studies, and developing sophisticated computer models.

#### Combustion-Diagnostic Instrumentation

Instrumentation has been designed at Lewis that will determine on a per cycle, per cylinder basis, real-time measurements of the indicated mean effective pressure and percent mass of charge burned as a function of crank angle. Today, our systems are being used by both the aircraft and automotive industry.

We also have a good design for ionization probes, which are placed in the cylinder head to measure flame position and thickness as a function of crank angle.

Laser Doppler velocimetry (LDV) measurements of the velocities and turbulence levels for cold flow within the combustion chamber have been undertaken through a grant to Carnegie-Mellon University.

A contractual study with Barnes Engineering Co. has indicated that a laser can extend the usefulness of an infrared spectral radiometer. The study concluded that spacial resolution could be improved by using a high-energy laser to change the energy state of the specie of interest at the measurement point within the chamber. It can then be detected by the infrared device at a different wavelength than the surrounding carbon monoxide in the chamber.

A unique charge sampling system has been developed at Lewis which measures the local fuel-air ratio. The information provided by the system is used to establish the cyclic and spacial variation of fuel-air ratio within the combustion chamber at selected times in the cycle of an operating engine. Briefly, the sampling system works as follows: A very small volume of gas is sampled by a fast acting valve at any selected crank angle up to the start of combustion. The sample valve (fig. 2), which was developed from a General Motor's design, is shown installed in the cylinder head of a V-8 engine used for some of our combustion studies. The sample enters a high vacuum chamber and is analyzed by a mass spectrometer for fuel and air concentration. A digital electronic instrument was designed by NASA to control the sample valve, measure the output from the mass spectrometer, and perform the calculation to determine the fuel-air ratio.

All of the above instrumentation has proven to be extremely valuable in studying the role of turbulence and gas motions in combustion chambers. A principal goal is to formulate a general mass of charge burned equation which includes engine air-fuel ratio, speed, and torque. This result is important in Otto cycle modeling where until now the mass fraction burned curve was assumed to have a simple cosine relation.

#### Otto Cycle Computer Model

For the past 5 years Lewis has had a zero-dimension Otto cycle code effort. And since 1977 we have supported a program on internal combustion engine flame propagation and emissions at Princeton University (and now Carnegie-Mellon) with Dr. William A. Sirignano as the Principal Investigator. The major goal of the grant program remains the development of a theory and multidimension computer code for flows and combustion in a reciprocating engine. The variables to be considered are details of engine geometry and operating conditions and fuel chemistry. Predictions will include engine performance, fuel consumption, heat transfer, exhaust composition, and local flow velocities. The code will also predict the effect of turbulence intensity and scale effects, the effects of manifold and valve flow, and the chemical composition of the flow close to the walls. The basic approach includes not only developing the computer program, but also the experimental validation of key hydrodynamical features of the flow model. The status of this effort is as follows:

- (1) The code predicts the flow field for axisymmetric, unsteady, moving boundary, compressible, turbulent (scale and intensity) piston-cylinder flows.
- (2) The code extends beyond the valve into the manifold and consequently the initial conditions do not use assumed velocity and turbulence profiles but real engine variables such as valve diameter to cylinder bore ratios, valve lift curves, and entrance and exhaust flow angles and swirl.
- (3) The predicted flow field includes the boundary layers and hence surface effects.
- (4) The predicted flow field is sensitive to both large and small scale turbulence conditions.
- (5) Measurements of the axial and tangential components of mean flow and the rms of velocity fluctuations for two different operating conditions have been made.
- (6) Comparisons with the theoretical predictions are being made. The first examples are the low speed, open orifice, and turbulent nonreacting flows. The velocity profiles agree in shape, and good matching occurs in the vicinity of the orifice jet or in the region near the jet. Comparisons near the wall agree in shape, but the predicted velocity profile gradients are larger than the measured gradients. Good agreement occurs with the location and magnitude of the flow reversal region.

### Fuel Injection

Research is being conducted to improve the inlet-port fuel-injection system by extending the lean limit. To accomplish this requires a more complete understanding of the relationship of the fuel-air mixture preparation before induction into the combustion chamber and overall engine performance. The extent to which the microscopic and macroscopic degree of homogeneity of the mixture entering the combustion chamber affects performance is not well known. The classical theory concerning mixture preparation has been that a well mixed, homogeneous charge was necessary for lean operation. Various investigations have been conducted which tend to support this theory. However, these results are in conflict with the recent work of General Motors researchers who concluded that some form of heterogeneous intake charge "wetted" with fuel droplets and possibly with bulk stratification may be optimum for lean combustion. Accordingly, the NASA investigation is designed to provide additional information on this important aspect without assuming that complete vaporization yields optimum heat engine performance.

A logical first step in this investigation is the careful characterization of fuel injection spray nozzles. The physical state of the fuel-air mixture inducted into the cylinder is influenced by the properties of the spray emitted from the injector. Hence, key variables such as droplet size, velocity, and spatial distributions must be known as a function of nozzle design and operating parameters.

Spectron Development Laboratories, Inc., under a NASA contract is using a laser visibility method to obtain particle field measurements of different injectors under simulated engine manifold conditions.

Concurrently, manifold flow-visualization tests to establish the disposition of fuel-air mixture are being conducted at Lewis. One cylinder head of the TS10-360 engine has been modified to include a transparent acrylic intake section (fig. 3). Under a wide range of motored engine conditions, high-speed photographs are taken through fiber optics located at the right side of the intake section. The previously discussed sampling valve will be installed to measure the fuel-air ratio within the cylinder. From this information a correlation of the injector spray and position with the fuel-air mixture in the intake port and cylinder can be established.

After these flow visualization tests, single cylinder hot performance and emission tests will be conducted.

#### High Altitude Turbocharger Technology Program

Turbochargers have served General Aviation well, improving comfort, economy, safety, and performance by providing higher takeoff power and high-altitude capability at reasonable cost. The trend is toward even higher altitude capability for all size aircraft engines. Thus, an aircraft could safely fly over the weather and at the same time improve its flight efficiency. In response to a suggestion by its advisory committee, NASA has initiated an effort to identify, develop, and demonstrate the technology for a family of advanced but cost-effective turbochargers applicable to a spectrum of conventional and alternative engines. The projected program, which will emphasize near-term improved spark-ignition engines as the baseline, has three phases: system performance analysis and conceptual design study (phase I); reference configuration design and component verification testing (phase II); and final design and verification testing (phase III). Phase I has been funded and, depending on the results, funds for the remainder of the program will be considered.

#### ALTERNATIVE PROPULSION SYSTEMS

Although current aircraft engines operate at high levels of efficiency and reliability, changing requirements in terms of fuel economy, fuel availability, and environmental concerns have brought about the consideration of significantly improved or completely new types of engines for future aircraft. NASA has addressed this issue through a series of conceptual design study contracts with engine manufacturers.

The conceptual engine candidates under study are (1) improved/advanced spark-ignition piston engines, (2) lightweight diesel engines, (3) stratified-charge rotary engines, and (4) advanced turboprop engines which were in the preceding presentation.

The above-mentioned activities typically include several technical tasks, such as (1) technology evaluation and configuration selection, (2) conceptual design, (3) a preliminary airframe integration study, and (4) program recommendations to address each candidate's key technology requirements. The

status and results of the three internal combustion engine candidates will be presented following this overview.

The preliminary airframe integration study portions of this work will assess the apparent advantages of that particular concept compared with current engines.

Contractual studies will also be conducted to obtain from two general-aviation airplane manufacturers (Cessna Aircraft Co. and Beech Aircraft Corp.) a comparative evaluation of the four candidates in airplanes and on missions that are representative of the manufacturer's expected market share. The evaluations will be conducted on a consistent basis; that is, to the greatest extent practicable, the same or equivalent airplane and engine technology will be used for all direct comparisons.

In all cases, the airframe will be tailored to take maximum advantage of the candidate engine's unique features, or to minimize the adverse effect of its less-desirable features. The criteria of comparison will include airplane size, economics, and flight performance; fuel consumption and fuel tolerance; business factors; and an assessment of relative technological risks.

In the above comparative studies two types of aircraft will be used - a high-performance, pressurized single and a pressurized twin. The nominal engine size is 250 bhp (net, installed cruise power at 25 000 ft altitude). It is expected that results of these two contracts will allow a rational selection of one or more candidates for a contemplated NASA engine technology development and demonstration program.

Broader in-house studies are being conducted to evaluate additional types of aircraft and missions. Longer term supporting research and technology efforts are being conducted at Lewis. These efforts are aimed at evaluating selected key technology areas in order to verify concept potential and to enlarge the overall technology base. The diesel and rotary engine test cells are now operational, with baseline mapping complete. The buildup of the stratified-charge, single-cylinder facility is under way.

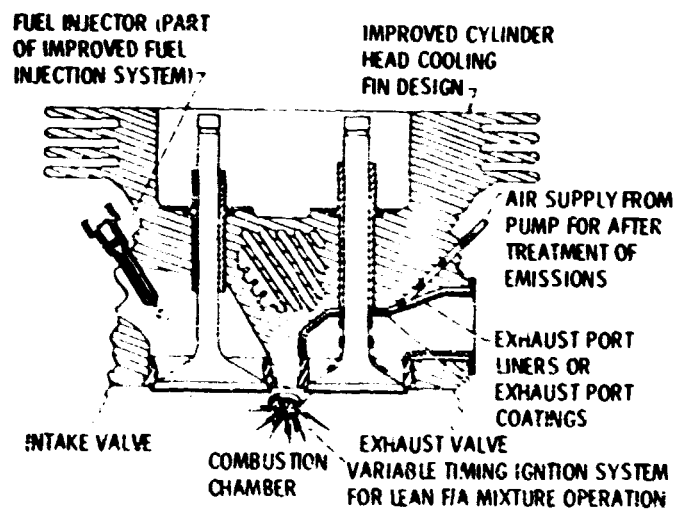
Table 1

## EMISSIONS AND FUEL ECONOMY COMPARISON

	BASLINE	COMBINED MODS
EMISSIONS, % EPA 1980 LEVELS		
CO	185	28
HC	122	11
NO <sub>x</sub>	10	86
BSFC, % CHANGE		
LTO	0	-30%
CRUISE	0	-10%

CS-79-4346

## INTEGRATED NEAR TERM MODS



CS-79-4347

Figure 1

GAS SAMPLING VALVE  
INSTALLED IN CYLINDER HEAD

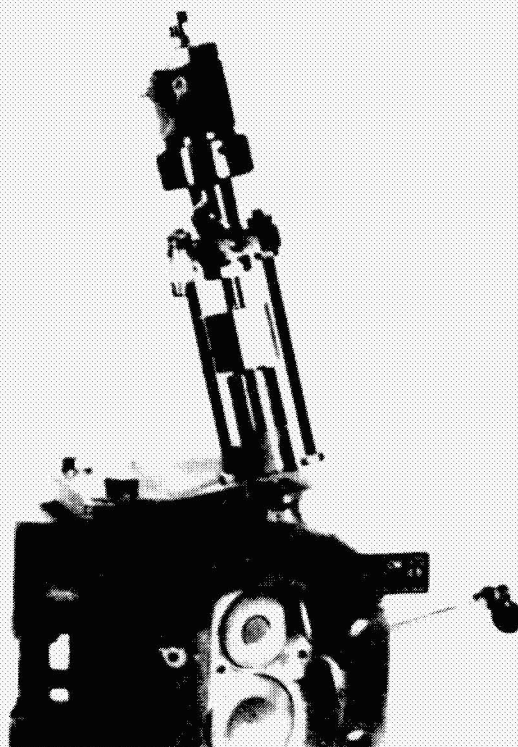


Figure 2

CYLINDER HEAD WITH TRANSPARENT INTAKE SECTION

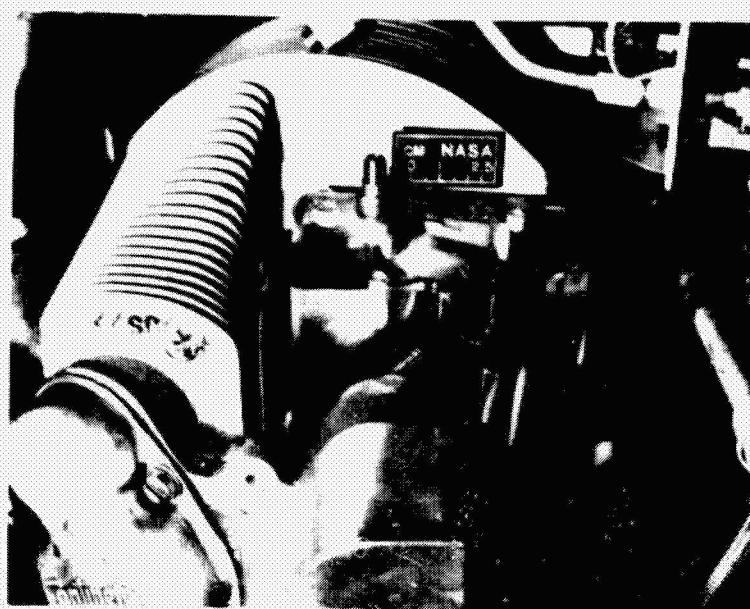


Figure 3

ORIGINAL PAGE IS  
OF POOR QUALITY





2/6  
N 80-22337

## THE SPARK-IGNITION AIRCRAFT PISTON ENGINE OF THE FUTURE\*

Kenneth J. Stuckas  
Aircraft Products Division  
Teledyne Continental Motors

### SUMMARY

A study is underway to define and apply those areas of advanced technology appropriate to the design of a spark-ignition aircraft piston engine for the late 1980 time period. Results of the study, so far, show that significant improvements in fuel economy, weight and size, safety, reliability, durability and performance may be achieved with high degree of success, predicated on the continued development of advances in combustion systems, electronics, materials and control systems.

### INTRODUCTION

The modern aircraft piston engine has represented the best compromise among fuel economy, weight, size, cost, ease of maintenance, durability and versatility. The evolution of the aircraft piston engine over the past 50 years has included the incorporation of appropriate new technology on a systematic basis, minimizing exposure to risk as this technology became well established and proven in lower risk military and automotive applications. As a result, the product which has evolved from this process has a demonstrated reputation of safety and reliability. Today, the spark-ignition aircraft piston engine serves as a prime mover for 93% of the nearly 200,000 active aircraft in the general aviation fleet.

In recent years, the reality of rising fuel prices coupled with the possibility of reduced fuel availability has added impetus to the search for items of advanced technology which, when incorporated in a newly designed aircraft piston engine, will continue to preserve the increasing utility of this segment of our U. S. transportation system.

### ADVANCED ENGINE CHRONOLOGY

Table 1, shows a chronology of events which we know from experience must be accomplished before an aircraft piston engine of a totally new design

\*NASA Contract NAS3-21272, Advanced Spark-Ignition Aircraft Piston Engine Design Study

can enter the marketplace.

In generating this schedule, we started at December 31, 1989 and worked backwards allowing time for Marketing and Customer Acceptance Testing, Engine and Airframe Certification Testing, Prototype Engine Build-up and Testing and Parts and Materials Procurement for the Prototype. At this point, we arrive at the time when the level of technology to be included in the engine must be frozen. This leads to a somewhat discouraging revelation. Our advanced technology engine of the late 1980's will reflect a level of technology that is five and a half years old! If we begin to develop the technology that we see emerging as of January 1, 1980, then we have about four and a half years to develop it to the point where it can be realistically included in our advanced technology engine.

#### TECHNOLOGY CATEGORIZATION

As part of our study we took all those areas of advanced technology we deemed appropriate to an advanced spark-ignition aircraft piston engine, and put them into categories which we ranked, from top to bottom, in order of importance or dependence, as shown in Figure 1.

Our study covered the topics of fuels; combustion systems; various means for extracting additional power from waste exhaust gases - supercharging, turbocompounding and bottoming cycles; engine operational systems such as fuel injection ignition and engine governing systems; configuration and cooling - shown here on the same level because of their intertwining relationship (some engines because of their configuration require liquid cooling); materials, from the standpoint of weight reduction and increased durability; manufacturing; engine auxiliary systems - such as air conditioning and electrical power generation and, finally, lubricants.

#### FUELS

The most important decision we had to make, and in many ways the most difficult, was the determination of fuel availability. We did a very thorough literature survey covering the past, present and future of the energy industry. We looked at not only the technical aspects of development of primary energy resources, but also the economic, social and political trends which might affect our choice of a future fuel.

Considering the fact that the U.S. has the energy equivalent of 33 times as much oil shale, coal and uranium as there is crude oil in the entire world, we came to the conclusion that petroleum-based fuels would be around for a long time to come to meet the needs of transportation. The assumption being, of course, that these needs will be met by the satisfactory development of the technology necessary to efficiently produce synthetic crude oil from our oil shale and coal resources within economic and environmental

constraints, and that non-transportation needs will be met by continued conservation measures and development of alternative non-petroleum fuels.

This study showed that there were two identifiable prospects for fuel for our advanced engine. First, for the near term, the continued use of 100LL avgas is indicated, which dictates the use of a homogeneous charge combustion system similar to that which is used today, and second, for the far term, we see the desirability of moving away from this highly specialized aviation gasoline, which comprises less than one percent of all the gasoline produced in the country today. For the far term, our choice of fuel is kerosene-based commercial jet fuel, which suggests the use of a stratified charge combustion system (Table 2).

A parallel can be drawn between the use of jet fuel in an advanced, spark-ignition aircraft piston engine and the increased production of diesel engine powered cars. One of the biggest problems associated with the introduction of a powerplant designed to operate on an alternate fuel is the availability of that fuel to the consumer. As in the case of the diesel-powered car where diesel fuel is widely available because of the existing distribution system for long haul trucking, jet fuel is becoming more widely available due to the increased use of jet-powered business and commuter airplanes.

The availability of two fuels suggested that our study should address the possibility of two advanced engines rather than one. The two engines we have chosen we will call moderate risk technology and high risk technology engines. Both engines are similar, except the moderate risk technology engine is designed to use 100LL avgas in a homogeneous charge combustion system and the high risk technology engine with a stratified charge combustion system will use jet fuel.

#### COMBUSTION SYSTEM

Once the matter of fuel availability was decided, then the choice of combustion systems could be determined. Shown in Figure 2, on the left, is a standard combustion chamber used on nearly all aircraft piston engines. The combustion chamber volume is hemispherical in shape, with one intake valve, one exhaust valve and two spark plugs per cylinder. On the right is the combustion chamber we are proposing for both the moderate risk and high risk technology engines. In the case of the moderate risk technology engine, the combustion system will use a low pressure fuel injection system where gasoline is injected in the intake manifold just upstream of the intake valve. The high risk technology stratified charge system will inject jet fuel at high pressure directly into the combustion chamber just before the piston reaches top dead center.

This combustion chamber we have called the HTCC, or high turbulence combustion chamber. Through the use of swirl and high turbulence, it permits the combustion of lean mixtures of fuel and air at high compression ratios

without the detonation which limits the compression ratio of the standard engine. With the HTCC combustion chamber, we have recently demonstrated the detonation-free operation of a homogeneous charge, 6-cylinder engine at a compression ratio of 12:1 compared to a compression ratio of 8.5:1 for a standard engine. This increase in compression ratio had the effect of improving fuel economy at cruise powers by 7 percent.

## TURBOCOMPOUNDING

Among the various means of extracting power from the waste exhaust gases of an internal combustion engine are turbocharging and turbocompounding. In an aircraft piston engine, turbocharging serves two purposes. First, it is a means of extracting greater power from a given engine displacement, and second it is possible to maintain that power from sea level to high altitudes. Turbocharging is a common practice in the aircraft piston engine industry. In 1979, about 65% of all aircraft engines manufactured by Teledyne Continental Motors will be turbocharged.

For our advanced engines we are proposing the use of turbocompounding in addition to turbocharging. The schematic in Figure 3, shows one method of employing turbocompounding. The exhaust gases leave the engine, "E", and pass first through a power turbine  $T_1$ , which transmits power back into the engine crankshaft through a speed reduction unit. The exhaust gases then carry their remaining energy to a turbocharger. The advantages of turbocompounding are that it is possible to extract one horsepower for every pound of weight added, and the combination of turbocharging plus turbocompounding is more efficient than turbocharging alone.

Although turbocompounding is not a novel idea in its application to aircraft piston engines, turbocompounding does constitute advanced technology of the basis that we will be attempting to apply it to an engine of only 350 horsepower, compared to the 3000 horsepower of the Wright engine and the Napier Nomad of the post- World War II era.

## ENGINE OPERATIONAL SYSTEMS

We see for the future a significant impact on our industry by the work that is now going on in the field of automotive electronics. There is no doubt that the auto industry represents the greatest potential for far term growth for the electronics industry. Partly responsible for this growth is the development of inexpensive and reliable signal transducers and the development of sophisticated electronic control system strategies.

For both the moderate risk and high risk technology engines we see the adaptation of all engine operational systems to electronic control. This means that the present three levers now in use to control engine speed, manifold pressure and fuel flow will be combined into a single lever by which

the pilot controls power. The trick is to be able to accomplish this task so that the systems exhibit fail-soft behavior. This means that a mechanical backup system will be required.

In view of the increasing complexity of our air traffic control system and the increasing amount of single-pilot IFR flying, the extent to which we can reduce pilot workload impinges directly on safety of flight. Table 3 lists those operational systems which will be converted to electronic control and the benefits derived from each.

### CONFIGURATION AND COOLING

We examined many different engine configurations and reduced our choices to the three shown in Figure 4. As far as cooling is concerned, our conclusions for these three configurations and an engine of 350 horsepower, was that liquid cooling provides no distinct advantage in either weight or cost over air cooling. In fact, when considering the added systems required for liquid cooling, a certain additional risk is involved. Since all engines are ultimately air-cooled, and because of the low temperature differentials present with liquid cooling, the placement of a radiator large enough to remove the rejected heat would pose a problem in the already compact design of an airplane for which this size engine is intended.

Only one of these configurations looked promising compared to the horizontally-opposed, six-cylinder design we ultimately chose, and that was the inverted V-8. The V-8 engine would be more vibration-free than the horizontally-opposed six, but from a cost and maintainability standpoint, six-cylinders are preferable. The radial design was rejected because of its large frontal area.

### ADVANCED MATERIALS

The use of advanced materials was considered from the standpoint of weight reduction and increased durability. Table 4 compares three engines where the weight of each is divided up among the materials it contains. The first engine is a TSIO-550 engine representing the present level of technology. It contains 8 lbs. of miscellaneous materials such as plastic, rubber and copper, 332 lbs. of steel, and 245 lbs. of aluminum, for a total weight of 585 lbs. Our moderate risk technology engine contains only 253 lbs. of steel and 215 lbs. of aluminum while we have added 10 lbs. of advanced materials for a total weight of 485 lbs., which is a weight reduction of 17% over the present engine. The reduction in use of steel and aluminum in this engine is brought about primarily by the more judicious use of these materials.

In the high risk technology engine we are using only 80 lbs. of steel, primarily in the crankshaft, reduction gears, cylinders and exhaust valves. The use of aluminum has been reduced somewhat and a total of 119 lbs. of advanced materials are used for an engine weight of 405 lbs., a 31% improve-

ment over the present day engine. In this engine the greatest part of the advanced material weight is titanium, with a small amount of reinforced plastic and ceramics.

Titanium is one of the most abundant metals to be found on earth. While titanium is not a rare metal, it is very costly to produce. The problem being that it is not usually found in great quantity in any one spot, but it's pretty much evenly distributed over the earth. Another problem is that it takes 13 times as much energy to produce a pound of titanium from ore as it does to make a pound of steel. What we are counting on here is an advancement in titanium production and metallurgy which would permit an overall savings in energy consumption to be realized. The question is whether the fuel saved by reducing the weight of the engine by 31% will be overcome by the energy used to produce the titanium in the first place.

#### ENGINE SPECIFICATION

Many of the details of the design study have been omitted for the sake of brevity, but Table 5 shows comparison of some of the specifications of the three engines we have discussed. All three are six-cylinder, horizontally-opposed. The current technology engine has a displacement of 550 cubic inches, with 420 cubic inches for the moderate and high risk technology designs. All three are rated at 350 BHP and can cruise at 25,000 feet at 250 BHP. At this cruise power the brake specific fuel consumptions are .446, .358 and .331, respectively. The service ceilings of our advanced engines are increased to 30,000 feet compared to 25,000 feet for the present engine.

We've already discussed the installed weight and type of fuel.

The TBO, or time between overhaul, for our current technology engine is 1400 hours, which we have increased to 2000 hours for the advanced engine.

To get an idea of the fuel economy improvements which were made, compare the power wasted in the exhaust of the three engines. The current technology engine dumps the equivalent of 319 HP out the exhaust at maximum cruise power. For the moderate risk technology engine this loss has been reduced by 33% to 214 HP, and by 51% to only 156 HP for the high risk technology engine.

#### IMPROVED AIRPLANE PERFORMANCE

Well, what does all this buy us? It's not enough to consider only the improvements in the engine. We must look at the bottom line. That is, what benefits do we see when the engine is installed in an airplane?

We are not quite finished with this part of our study. But here are some preliminary results based on the installation of the three engines in a current technology single-engine airframe.

What we've done here in Figure 5 is to simulate the installation of all three engines in an identical airframe designed for a chosen arbitrary mission profile for the high risk technology engine. We chose a range of 1000 nautical miles with 45 minutes fuel in reserve, a cruise altitude of 25,000 feet at 250 horsepower which corresponds to maximum cruise power for all three engines. The resulting calculations show that the present technology engine would have a range of only 518 nautical miles and the moderate risk technology engine, 814 nautical miles.

A relative efficiency was calculated for all three cases based on the payload each airplane could carry, multiplied by its speed and divided by its fuel consumption. The efficiency factor was then normalized to the value of 1.00 for the present technology engine. Based on this factor, the relative efficiency of the moderate risk technology engine was increased by 32% and that of the high risk technology engine by 49%. Of course, these factors will change depending upon the mission profile selected.

A similar analysis was done for the case of a twin-engine airplane (Figure 6), with similar results. In this case the mission profile was set at 1300 nautical miles for the high risk technology twin. The results show normalized relative efficiencies of 1.00, 1.37 and 1.57, respectively.

#### ENGINE DESIGN FEATURES

Figure 7 shows the top, side and rear external views of an advanced engine, pointing out some of the important features. Both the moderate risk and high risk technology engines will appear substantially the same, externally.

Compared to present engines, the gear-driven propeller shaft has been extended somewhat to accommodate a more streamlined cowling. The exhaust system is designed for good pulse recovery to enhance the power recovery of the turbocompounding power turbine. The speed reduction system from the power turbine to the crankshaft is a Nasvytis traction drive which was chosen over a gear reduction drive because of its potential for damping torsional vibrations and its lighter weight. The engine also includes an integral oil sump/oil cooler to save weight and volume.

In order to achieve a compact design, the exhaust system is on top of the engine rather than on the bottom. Because of this, the engine is designed for updraft cooling, instead of the usual downdraft method. This, in conjunction with an advanced airframe design and well-designed baffling will permit the design of a more efficient ram air pressure rise recovery plenum.

## CONCLUSIONS

While this study has not been completed, we have identified several items which require development in the next four and a half years in order for the proposed engines to become a reality by the end of the next decade, as outlined in Table 6.

The critical development items we have identified include; stratified charge HTCC combustion system and a compatible advanced ignition system; an improved efficiency, high pressure ratio, lightweight turbocharger; a reduction drive system for the turbocompounding power turbine; electronic control strategies appropriate to a turbocompounded aircraft piston engine, and a method to improve engine cooling and reduce cooling drag.

Other items of a non-critical nature which have been identified include the reduction of engine friction, the low cost production of titanium, the development of lightweight accessories and improved heat exchangers for oil cooling and induction air intercooling.



### ADVANCED SPARK-IGNITION AIRCRAFT PISTON ENGINE TECHNOLOGY BASE CHRONOLOGY (OPTIMISTIC)

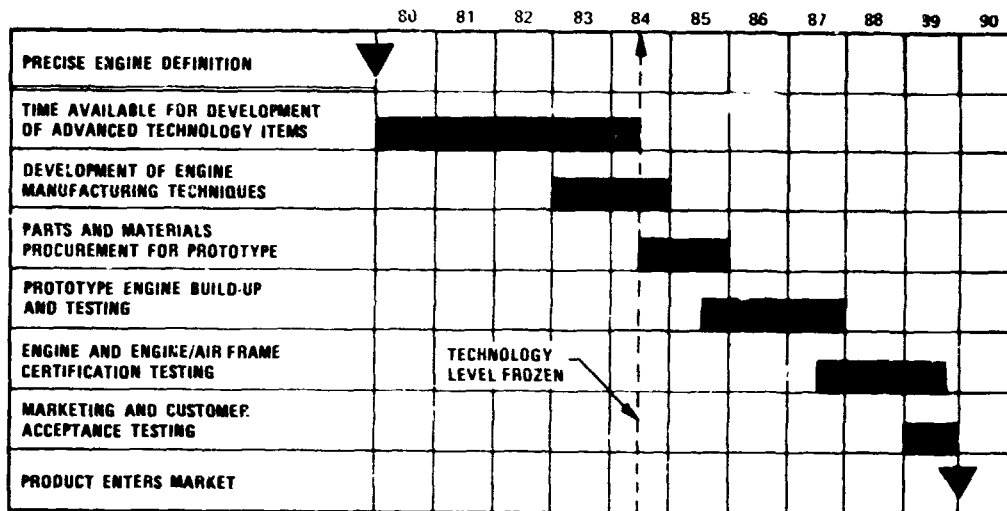


TABLE 1

### FUELS FOR ADVANCED SPARK-IGNITION AIRCRAFT PISTON ENGINE

#### NEAR TERM

- 100 LL AVGAS OR WIDE-CUT VERSION  
(HOMOGENEOUS CHARGE COMBUSTION)

#### FAR TERM

- KEROSENE BASE COMMERCIAL JET FUEL (JET A)  
(STRATIFIED CHARGE COMBUSTION)

TABLE 2

## ENGINE OPERATIONAL SYSTEMS

MODERATE RISK (HOMOGENEOUS CHARGE)	HIGH RISK (STRATIFIED CHARGE)
<ul style="list-style-type: none"> <li>● ELECTRONIC FUEL CONTROL                             <ul style="list-style-type: none"> <li>▲ ELIMINATES MANUAL MIXTURE CONTROL</li> <li>▲ REDUCES PILOT WORKLOAD</li> <li>▲ PROVIDES OPTIMUM FUEL ECONOMY</li> <li>▲ PREVENTS ENGINE DAMAGE DUE TO IMPROPER MIXTURE CONTROL TECHNIQUES</li> </ul> </li> <li>● ELECTRONIC SINGLE-LEVER POWER CONTROL                             <ul style="list-style-type: none"> <li>▲ ELIMINATES SEPARATE THROTTLE (RACK) AND PROP CONTROLS</li> <li>▲ REDUCES PILOT WORKLOAD</li> <li>▲ PROVIDES OPTIMUM ENGINE SPEEDS AND THROTTLE (RACK) SETTINGS</li> </ul> </li> </ul>	<ul style="list-style-type: none"> <li>● ELECTRONIC AIR CONTROL                             <ul style="list-style-type: none"> <li>▲ PROVIDES AIR THROTTLING FOR OPTIMUM FUEL ECONOMY</li> </ul> </li> <li>● ELECTRONIC IGNITION                             <ul style="list-style-type: none"> <li>▲ COUPLES IGNITION TIMING WITH FUEL INJECTION FOR OPTIMUM COMBUSTION</li> </ul> </li> <li>● ELECTRONIC SINGLE-LEVER POWER CONTROL (SAME AS MODERATE RISK)</li> </ul>

TABLE 3

## ADVANCED MATERIALS FOR ENGINE WEIGHT REDUCTION

	MISCELLANEOUS MATERIALS (lb)	STEEL (lb)	ALUMINUM (lb)	ADVANCED MATERIALS* (lb)	TOTAL ENGINE WEIGHT (lb)	PERCENT (%) WEIGHT REDUCTION
PRESENT 350 hp TSIO-550 ENGINE	8	332	245	—	585	0
MODERATE RISK TECHNOLOGY ENGINE	7	263	215	10	495	17
HIGH RISK TECHNOLOGY ENGINE	6	80	200	110	406	31

\*TITANIUM, CARBON/GRAPHITE/BORON REINFORCED PLASTICS, CERAMICS

TABLE 4

## ENGINE SPECIFICATION COMPARISON

	CURRENT TECHNOLOGY TSIO-650	PERCENT IMPROVEMENT	MODERATE-RISK TECHNOLOGY GTSIO-420	PERCENT IMPROVEMENT	HIGH-RISK TECHNOLOGY GTSIO-420/3C
CONFIGURATION ENGINE DISPLACEMENT	6-Cylinder/Horiz. Opposed 550 Cubic Inches	—	6-Cylinder/Horiz. Opposed 420 Cubic Inches	—	6-Cylinder/Horiz. Opposed 420 Cubic Inches
MAXIMUM RATED POWER/SPEED	350 Bhp/2,800 rpm	—	350 Bhp/3,200 rpm	—	350 Bhp/3,200 rpm
BRAKE SPECIFIC FUEL CONSUMPTION AT MAXIMUM CRUISE POWER (250 Bhp)	0.446 lb/Bhp-hr	28%	0.358 lb/Bhp-hr	28%	0.331 lb/Bhp-hr
SERVICE CEILING	25,000 ft	48%	35,000 ft	48%	35,000 ft
INSTALLED ENGINE WEIGHT	505 lb	17%	405 lb	31%	405 lb
TYPE OF FUEL	100 Octane	—	100 Octane	—	Jet A
TIME BETWEEN OVERHAUL	1,400 hr	43%	2,300 hr	43%	2,000 hr
EXHAUST ENERGY RECOVERY SYSTEM	Turbocharging	—	Turbocharging Turbocompounding	—	Turbocharging Turbocompounding
EXHAUST POWER UNRECOVERED AT MAXIMUM CRUISE POWER	95 hp	41%	58 hp	67%	12 hp

TABLE 5

## ADVANCED SPARK-IGNITION AIRCRAFT PISTON DESIGN STUDY TECHNOLOGY PROGRAM RECOMMENDATIONS

Critical Development Items	Non-Critical Development Items
<ul style="list-style-type: none"> <li>• STRATIFIED CHARGE HTCC COMBUSTION SYSTEM</li> <li>• ADVANCED IGNITION SYSTEM</li> <li>• IMPROVED EFFICIENCY, HIGH PRESSURE RATIO LIGHT WEIGHT TURBOCHARGER</li> <li>• REDUCTION DRIVE SYSTEM AND CLUTCH FOR TURBO COMPOUNDING TURBINE</li> <li>• ELECTRONIC CONTROL STRATEGIES APPROPRIATE TO TURBOCOMPOUNDED AIRCRAFT PISTON ENGINES</li> <li>• IMPROVED ENGINE COOLING AND COOLING DRAG REDUCTION</li> </ul>	<ul style="list-style-type: none"> <li>• REDUCED ENGINE FRICTION</li> <li>• LOW COST PRODUCTION OF TITANIUM</li> <li>• LIGHTWEIGHT ACCESSORIES</li> <li>• IMPROVED HEAT EXCHANGERS</li> </ul>

TABLE 6

## ADVANCED TECHNOLOGY CATEGORIES HIERARCHICAL STRUCTURE

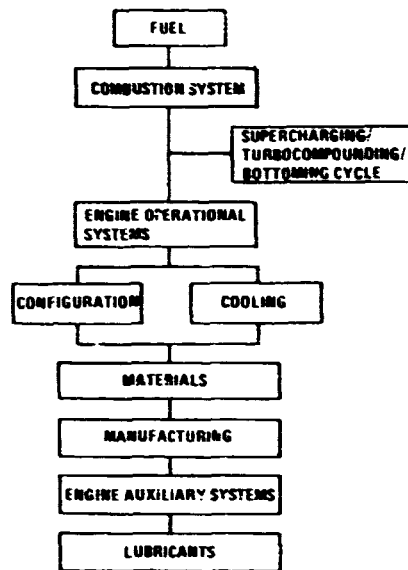


FIGURE 1

## HIGH COMPRESSION RATIO/LEAN BURN COMBUSTION CHAMBER

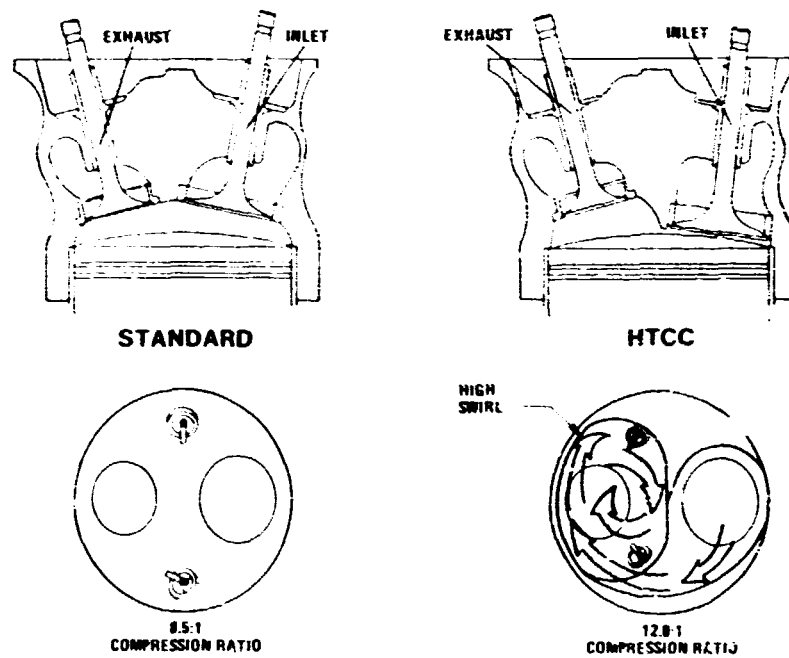


FIGURE 2

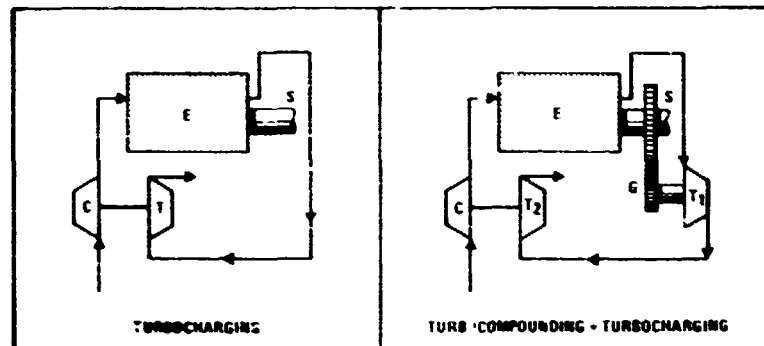


FIGURE 3

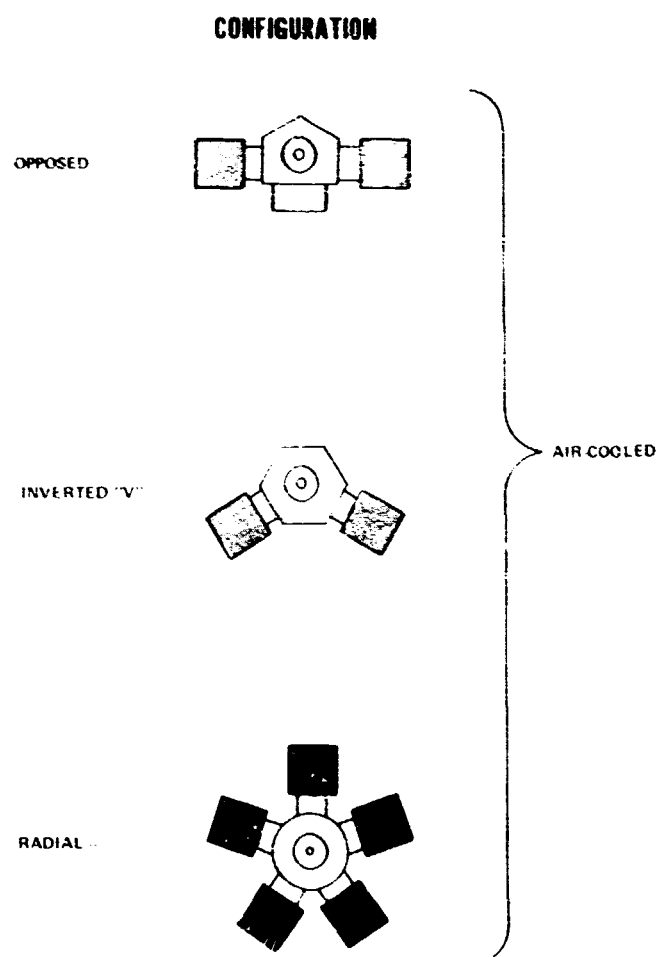


FIGURE 4

## ADVANCED TECHNOLOGY SINGLE-ENGINE AIRPLANE

RELATIVE EFFICIENCY	1.00	1.32	1.49
PAYLOAD WITH MAX. FUEL, LBS	1110	1160	1200
MAX. CRUISE SPEED, KTS	206	210	211

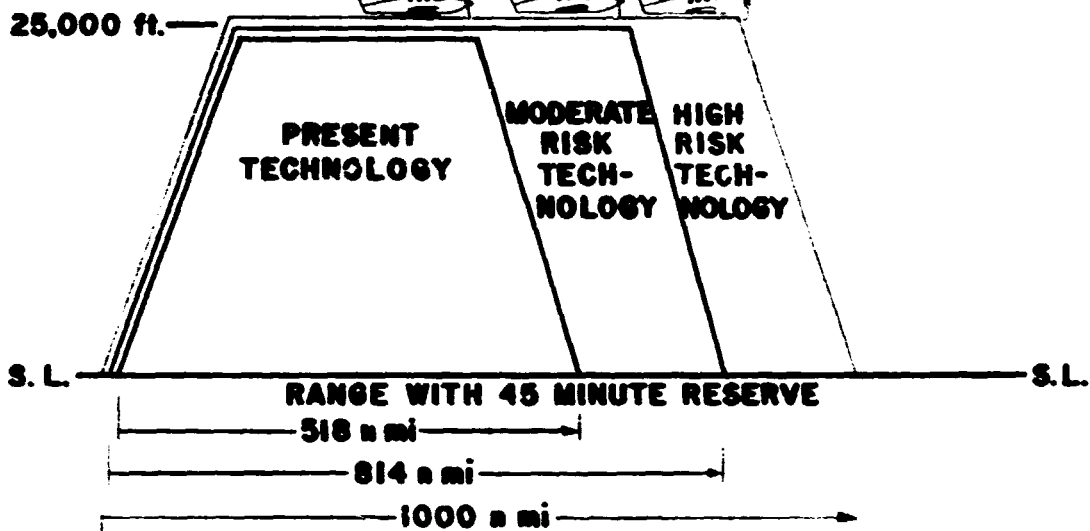


FIGURE 5

## ADVANCED TECHNOLOGY TWIN-ENGINE AIRPLANE

RELATIVE EFFICIENCY	1.00	1.37	1.57
PAYLOAD WITH MAX. FUEL, LBS	1220	1320	1400
MAX. CRUISE SPEED, KTS	233	237	237

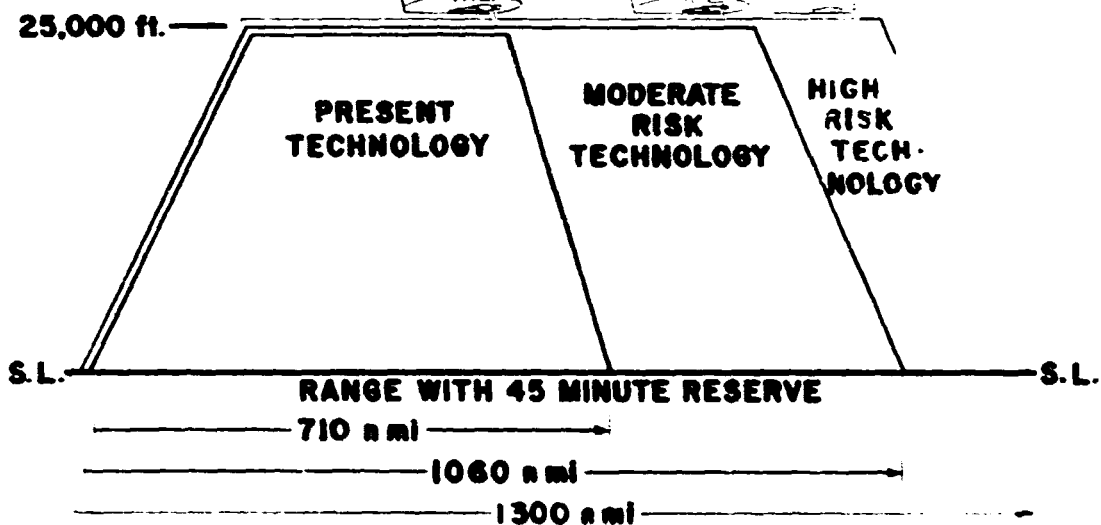


FIGURE 6

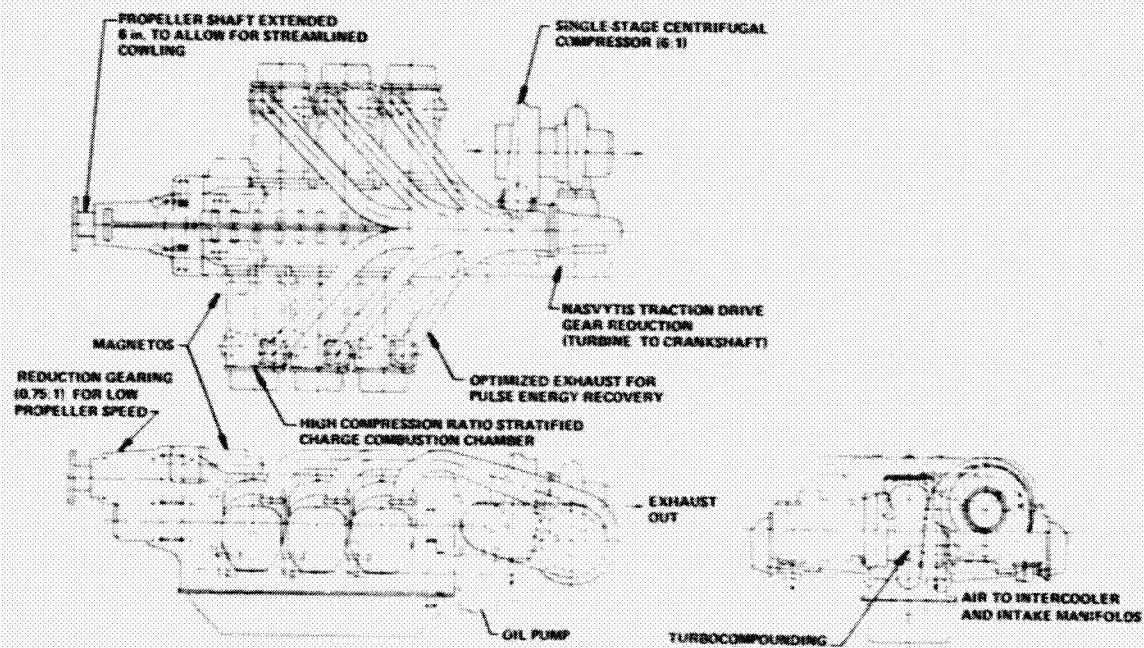


FIGURE 7





211  
N80-22338

## LIGHTWEIGHT DIESEL AIRCRAFT ENGINES FOR GENERAL AVIATION

Steven G. Berenyi and Alex P. Brouwers  
General Products Division  
Teledyne Continental Motors

### SUMMARY

This design study reintroduces the diesel engine as an aircraft powerplant. A methodical design study was conducted to arrive at new diesel engine configurations and applicable advanced technologies. Two engines are discussed and the description of each engine includes concept drawings. A performance analysis, stress and weight prediction, and a cost study were also conducted. This information was then applied to two airplane concepts, a six-place twin and a four-place single engine aircraft. The aircraft study consisted of installation drawings, computer generated performance data, aircraft operating costs and drawings of the resulting airplanes. The performance data shows a vast improvement over current gasoline-powered aircraft. At the completion of this basic study, the program was expanded to evaluate a third engine configuration. This third engine incorporates the best features of the original two, and its design is currently in progress. Preliminary information on this engine is presented.

### INTRODUCTION

Energy conservation, uncertainties of fuel supply and limited availability of high octane gasoline, have renewed the interest in the diesel aircraft engine, since its fuel economy is better than any type of aircraft engine currently in production.

Aircraft diesel engines have been developed before, notably the Junkers "JUMO", the Napier "NOMAD" and the McCulloch TRAD 4180. Of these, only the Junkers opposed piston, 2-stroke cycle engine ever reached the production stage. The Napier Nomad was a 2-stroke cycle, turbocompounded design. Its complexity and the fact that it invaded the territory of turbine engines probably accounted for its demise. The McCulloch engine came close to flying when the program was terminated for non-technical reasons.

New technologies, now under active development, will result in even better fuel economies than can be obtained with current state-of-the-art diesel engines. These technologies also make it possible to develop a powerplant which is more compact and lighter than current gasoline aircraft engines.

Two engines were investigated in the study, a 298 kW (400 HP) diesel for a twin engined airplane and a 149 kW (200 HP) diesel for a single engined aircraft.

The study consisted of three major phases:

1. Technology Analysis.

A survey of available aviation and automotive sources was conducted to identify new developments which offer potential benefits to an aircraft engine. These technologies were ranked and then evaluated on the basis of performance and adaptability.

2. Engine Concept Design.

The technologies which were chosen as a result of the evaluation and ranking process were applied to the design of the 149 and 298 kW engines. Performance, stress, weight, and cost calculations were made concurrently.

3. Engine/Aircraft Integration Study.

The results of Step 2 were then used in an engine-aircraft integration study to determine the performance improvement of an airplane equipped with these diesel engines.

Some of the technologies which were applied in these engine designs are anticipated to be available in the late 1980's. These technologies result in high level of performance and, although advanced, are not untried. The adiabatic engine, the catalytic combustor, and the high speed alternator envisioned are currently under development under various contracts. It should be noted here that, although the concept engine proposes the use of ceramic combustion system components, the use of such materials for "man-rated" aircraft may be 20 years away. These concepts were included primarily to show what may be ultimately possible. However, alternate less advanced solutions are also given which will result in a small reduction of performance when compared to the ultimate; but nevertheless will result in a powerplant which far outperforms the current gasoline aircraft.

## RESULTS AND DISCUSSION

### Advantages of the Diesel Engine

The diesel engine has always been burdened with the stigma of being heavy, thus offsetting its advantage of low fuel consumption for aircraft applications. If it is possible to build an engine that combines low fuel consumption and low weight, then that engine becomes a very attractive aircraft powerplant. Old and once discarded concepts can become attractive by applying new technologies.

A conventional diesel engine requires high compression ratios for starting and low load operation. This results in high firing pressures at full load when in fact the engine could run adequately at a much lower compression ratios. New

technologies make it possible to combine good startability with low firing pressures at full load. This study shows that the weight of the diesel can be reduced below that of current gasoline aircraft engines.

The diesel engine offers other advantages in addition to low fuel consumption, i.e.:

1. Lower operating cost.
  - Lower cost of fuel
  - Reduced maintenance
  - Extended TBO
2. Greatly reduced fire and explosion hazard.
3. Better in-flight reliability. No ignition and mixture control problems.
4. Multi-fuel capability.
5. No carburetor icing problems.
6. Improved altitude performance.
7. Safe cabin heating from exhaust stacks (less danger of carbon monoxide).
8. Exact fuel metering indicator. The rack position determines the fuel flow.
9. No electrical interference from ignition system

#### Previous Aircraft Diesel Engines

Table I shows a listing and design data of past aircraft diesel engines. No clear trends follow from this tabulation. Seven of the thirteen engines have a radial configuration, seven were aircooled, eight were 2-stroke cycle.

The tabulation becomes more meaningful if specific ratios are used. See Table II.

Some observations can be made from these tables. Average specific weight values are:

4-Stroke cycle engines	.710 kW/Kg
2-Stroke cycle engines	.926 kW/Kg
Aircooled engines	.783 kW/Kg
Liquid-cooled engines	.923 kW/Kg

The numbers indicate that a 2-stroke cycle engine can be expected to be lighter than a 4-stroke cycle engine. A comparison of aircooled and liquid cooled engines would seem to favor the liquid-cooled engine. However, the engine weights of liquid-cooled engines tabulated do not include the weight of the cooling package. With this modification, the corrected values then become:

Aircooled engines	.783 kW/Kg
Liquid-cooled engines	.805 kW/Kg

## New Engine Design Study

### - 298 kW Engine -

In addition to considering the historical background of aircraft diesel engines, a literature search was made and a technology base was established to evaluate any concepts that may be considered for an all new engine design.

The following criteria were observed in considering any new ideas:

1. The engine must be a piston/crankshaft type powerplant.
2. Be compatible with conventionally designed aircraft (size and drag).
3. Allow manufacture of an experimental model in five years.
4. Be ready for production in the late 1980's.
5. Meet 1979 EPA Emission Standards (guide-reference only).
6. Have multi-fuel capability.
7. Have engine performance comparable to current aircraft engine.
8. Have lower BSFC than present engines.
9. Maximum specific weights of .852 Kg/kW for the 298 kW and 1.095 Kg/kW for the 149 kW engine.
10. Life cycle costs equal or less than present aircraft engines.
11. Avoid problem areas encountered in current aircraft engine designs.

Design attributes that had to be considered included:

Performance, weight, size, C. G., fuel economy, reliability, multi-fuel capability, noise, life cycle cost, component costs, and technology required.

Figure 1 is a flow chart that shows the different possible combinations of design features that were considered and evaluated within the frame work outlined above.

A detailed description of each of these features is beyond the scope of this paper, but was included in the original basic study. The evaluation then resulted in the technologies that follow from Figure 1 by taking the high score items along the "common to all versions" and "radial 2-stroke cycle" lines.

#### Common to All Versions Line

Open Chamber  
Ceramic Pistons  
Insulated Exhaust Manifolds  
No Cylinder Cooling  
Tool Steel Piston Rings  
Composite Connecting Rods  
Synthetic Lube Oil  
High Pressure Fuel Injection  
Electronic Controls  
Conventional Oil Filter

#### Radial 2-Stroke Cycle Line

Individual Cylinders  
Low Compression Ratio  
Geared Prop Drive  
Loop Scavenge  
Independent Turbo Loop  
Catalytic Combustor

Conventional Fuel Filter  
Pendulum Damper

The engine concept was then laid out around these features.

Figure 2 shows an artist rendering of the proposed 298 kW 6-cylinder engine. Figure 3 shows the schematic of this engine. The design incorporates the technologies which were defined before.

The chosen system uses the Curtis loop scavenging. The intake ports and intake manifold are located at the propeller side of the engine, exhaust ports and exhaust manifold at the back end.

The cylinder liner and piston top are ceramics and, therefore, cylinder cooling will not be required. Tool steel piston rings will be required. Cooling air will be used only for the aftercooler, oil cooler, and the fuel injectors. The exhaust ports will be oil cooled.

Each cylinder receives fuel from a separate injection pump located in front of the cylinder (cool side of the engine). Failure of one pump still leaves 5/6 of engine power available. A high injection line pressure will be required to limit injection duration at high engine speeds.

The turbocharger can run independent of the engine. For that purpose a high speed starter/alternator and an oil pump are mounted on the turbocharger. A two-way valve is placed in the intake manifold. To start the engine, this valve is in the vertical position of the schematic, which results in a turbocharger loop independent of the engine. Combustor fuel is ignited by the heater. This heater can be turned off as soon as the catalyst becomes sufficiently hot. The cycle will become self-sustaining at approximately 1/3 of the maximum turbo speed, and the starter now runs as an alternator. Hot, high pressure air will flow to the engine when the two-way valve is partially opened. The cylinder intake ports are opened during approximately 120 crank-degrees, so hot air can flow through two cylinders for preheating on cold days. The high pressure air will next be admitted to the engine mounted bleed air starter to crank the engine. The whole sequence would be automatic.

This system offers many advantages:

1. The availability of hot induction air at start reduces the need for a high compression ratio. The engine will start and idle at a 10:1 compression ratio provided this hot, high pressure air is available to it during cranking. Thus, with this low compression ratio, the firing pressures are held down to 9650 kPa (1400 psig) at full load resulting in low engine weight.
2. The engine will start easily under cold conditions, a problem with current engines.
3. Hot start problems are eliminated.

4. The engine can be shut-off and the turbocharger kept running when the aircraft is on the ground for some period. Meanwhile, electric power, cabin heat or air conditioning remain available. This in effect converts the turbocharger into an APU.
5. The battery requirement is greatly reduced since engine cranking is accomplished by air pressure.

The use of synthetic oil is required in this engine design due to the hot cylinders. The synthetic oil can take higher temperatures and requires fewer changes than conventional petroleum based oils. Over the long term perhaps a method can be found to generate an airfilm between pistons and cylinder walls, in effect, using air bearing technology. This would also reduce the expected relatively high oil consumption which is inherent to 2-stroke cycle engines.

The engine design concept is shown in Figures 4 through 8. The cylinders are arranged in two offset banks of three cylinders each, acting on a single crankpin. The rotating and reciprocating inertias are 100% balanced by counterweights on the crank cheeks. The pendulum dampers are mounted to the counterweights and will be tuned for the 4-1/2 and 6th orders. The cylinders are uncooled and provided with ceramic liners. The intake ports and the intake manifold are located at the front side - the cool side of the engine. The exhaust ports and exhaust manifolds are located at the backside - the hot side of the engine. Two exhaust manifolds are required to prevent the exhaust pulse of one cylinder to interfere with the scavenging of the previous cylinder in the firing sequence. The piston tops are ceramic.

The small end of the connecting rods is designed to allow free rotation of the piston. This should reduce the wear rate of the piston rings. The big end of the connecting rods is designed as a slipper, i.e., each rod contacts only 1/3 of the circumference of the crankpin. This is possible for 2-stroke cycle engines because the combined load of gas pressure and inertias is always directed toward the crankpin. The bearing material will initially be conventional, but a study could be conducted later of self-lubricating and gas bearings to eliminate the need for oil in the crankcase.

Immediately in front of the first main bearing are 6 individual injection pumps, operated by a single lobed cam ring. Individual pumps were chosen to improve engine reliability - failure of one pump still leave 5 cylinders operable. Also, all fuel lines can have the same length resulting in the same injection timing for all cylinders.

A bevel gear in front of the cam ring drives the prop governor and the fuel priming pump.

A gear reduction reduces the crankshaft speed of 3500 rpm at take-off down to 2300 rpm propeller speed.

At the back of the crankcase is an accessory housing which contains the gearing for the engine oil pump, the vacuum pump, and the bleed air starter. The air starter drive is provided with a slip clutch to prevent engine damage in the case of a hydrostatic lock in one of the cylinders (accumulation of fuel

due to the leakage of a fuel injector). Four engine mounting points are provided on the accessory housing. Above the accessory case is the catalytic combustor assembly. Leading to it are the two exhaust manifolds and the air bypass for operation in the APU mode.

The turbocharger is located behind the accessory housing. Figure 8 shows the turbine to the left and the compressor in the center. To the right is a gear housing with the high speed alternator and turbo oil pump drives.

The aftercooler and oil cooler are located below the engine accessories.

The engine will operate with a dry sump.

The operating parameters for the 298 kW engine are shown in Table III and the sea level performance curve is included as Figure 9.

In addition to the performance projections, detailed calculations were made of weights, torsional vibrations, power component stresses, turbomachinery sizing, cooling requirements, and projected costs to manufacture.

Results of each of these studies are very favorable for the diesel engine, however, these details are beyond the scope of this presentation.

Emissions were not quantitatively addressed, however, the following qualitative statements are valid:

1. Hydrocarbons and carbon monoxide will be oxidized by the use of a catalytic converter.
2. NO<sub>x</sub> concentration will be minimized due to the relatively low peak pressures (9650 kPa) and lower peak temperatures.
3. Smoke levels should be relatively low since the minimum trapped A/F ratio will always be on the order of at least 24:1.

As with emissions, only qualitative evaluations were made of the anticipated engine noise as listed below:

1. The catalytic combustor and insulated exhaust stacks in series with the turbocharger should minimize direct combustion noise.
2. The absence of cylinder cooling fins should reduce externally generated vibratory noise.
3. The absence of valves, rocker arms, push rods, and camshaft should minimize internally generated mechanical noise.
4. The geared drive will allow a relatively low propeller speed, thereby, reducing prop generated noise.
5. Two-stroke cycle operation, however, tends to offset some of the gains noted above.

As was described earlier, this engine's feasibility relies heavily on new technology. Following are the areas where existing technologies need to be advanced to make such an engine feasible:

1. Piston rings - operating in uncooled cylinders.
2. Cylinders - ceramic components and their interface with metallic hardware.
3. Turbo starter/alternator operating at high speeds.
4. Catalytic combustor and its associated controls.
5. Cooling of the cylinder exhaust ports.
6. Piston lubrication.
7. Spherical connecting rod end.
8. Efficient fuel injection systems.

A comparison of the 298 kW engine was made with the 4-stroke cycle GTSIO-520-H gasoline engine.

Table IV shows this comparison in a tabular form.

Figure 10 is a size comparison. The frontal area of the diesel engine is 78% of that of a comparable gasoline engine.

#### - 149 kW Engine Design -

The technologies applied to the 149 kW engine are not as far advanced as in the case of the 298 kW engine. The 149 kW engine will primarily serve the private owner market where initial cost and ease of maintenance carry more weight than in the case of the corporate aircraft.

The engine will be easier to develop and manufacture.

Figure 11 shows an artist rendering of the proposed engine.

Figure 12 shows the schematic of the engine.

The following features are incorporated in the 149 kW design concept:

1. Radial configuration.
2. Two-stroke cycle Curtis loop scavenging.
3. Minimum cylinder cooling - reduced fin area.
4. Variable compression ratio pistons (VCR).
5. Mechanically driven centrifugal blower, declutched when not needed.
6. Glow plug starting aid in cylinders.
7. Conventional starter and alternator.
8. Conventional exhaust system (no combustor).
9. Direct propeller drive.

Calculations of the heat transfer through cylinder walls, as well as single cylinder engine tests have confirmed that the heat flux is highest through the cylinder walls surrounding the combustion chamber (when the piston is in top



dead center). The maximum gas temperature to which the cylinder wall is locally exposed drops off fast as the piston travels downward, resulting in a lower local average cycle gas temperature and, therefore, a reduced heat flux. It can be safely predicted that most cooling fins below the piston ring belt (piston in TDC) can be eliminated without an appreciable effect on cylinder wall, piston and piston ring temperatures. Using this approach results in an increase of cooling drag when compared to uncooled cylinders; but eliminates the need for ceramic components, thus making the engine a much more viable alternative for nearer term applications.

Since this smaller engine does not have the independent turbocharger loop, low compression ratio pistons cannot be utilized. Other means must be found to keep firing pressures down to 9,650 kPa. It becomes necessary to reduce the compression ratio under load to 10:1. However, the engine cannot be started or run idle at such a low compression ratio. In the case of the larger 298 kW engine, this was solved by means of the independent turbocharger loop which provides intake air of sufficient pressure and temperature to start the engine and the catalytic combustor which keeps the turbocharger at a high speed during engine idle operation. This is not the case here, therefore for this case a variable compression ratio piston is recommended.

The VCR piston, Figure 13 varies the compression ratio from 17:1 at start and low load to 10:1 at full load. This high C.R. is sufficient under normal ambient conditions to start the engine. Even the 17:1 compression ratio, however, does not provide a sufficiently high compression temperature to ignite the fuel at very low ambient temperatures. Operation of the glow plug may be required to assure good startability. It is also intended that glow plug operation would automatically be in effect at low throttle settings. This would be an added safety feature to assure absolutely no misfiring during descent mode operation.

Scavenging of a 2-stroke cycle cylinder requires that the intake manifold pressure exceeds the exhaust manifold pressure at any load and engine speed. The turbocharger, however, produces a negative  $\Delta P$  at low load. This is no problem for 4-stroke cycle engines where the piston does the scavenging. The 2-stroke cycle engine without a combustor requires an engine driven blower to produce a positive  $\Delta P$  across the cylinders at low loads. The blower will be disconnected at the load point where the turbocharger provides a positive  $\Delta P$ .

It also became obvious early in the design phase of the 149 kW engine that a direct drive would result in a smaller engine package and a weight reduction. The engine reliability is somewhat improved by this approach due to fewer parts required.

The chosen BMEP of approximately 1200 kPa is 100 kPa higher than the BMEP of the larger 298 kW engine. The much lower crankshaft speed dictated by the direct propeller drive will result in better scavenging and, hence, a larger amount of air trapped in the cylinder. It should, therefore, be possible to obtain this higher BMEP without an increase of cylinder temperatures. The detailed cycle calculations bear this out.

The 149 kW engine concept design then is shown in the Figures 14 through 18.

The cylinders are arranged in one bank of four cylinders. The rotating and reciprocating inertias are 100% balanced. The cylinders have a limited number of cooling fins to cool the combustion chamber. The necessity for a gear driven blower at the back side of the engine made it more practical to have the cylinder intake port at the back side and the exhaust manifolds at the front. The exhaust manifolds will be insulated to avoid radiation to the injection pumps. Two exhaust manifolds are required to avoid pulse interference between cylinders. The connecting rods are the slipper type. The big ends are wider than in the case of the 298 kW engine to compensate for the reduced circumferential contact length.

The use of synthetic oil is not essential in this engine because of lower cylinder temperatures (compared to the ceramic), but may be advantageous to extend the periods between oil changes.

Four individual injection pumps are provided driven off a single lobe cam ring. The centrifugal blower is driven off the propeller shaft through a lay shaft which is located above the crankcase between the cylinders #1 and #4. This arrangement was chosen rather than a drive from the rear end to avoid torsional problems. The nodal point lies close to the largest inertia member of the crankshaft system, that is the propeller. Putting the blower drive gear near this point reduces the input of torsional amplitudes into the blower drive. The lay shaft, which is a quill shaft, further isolates the blower from the crankshaft vibrations. However, this feature forced the use of a direct propeller drive. To put a propeller reduction gearing in front of the blower drive would have led to an unacceptable length of the engine. A weight analysis for this particular engine showed that the direct drive with the inherent larger piston displacement still results in a lighter engine than the geared drive.

The blower drive is provided with two clutches. One, the magnetic clutch, disengages the blower drive once the turbocharger has come up to speed. The location of the magnetic clutch is such that as much of blower drive as possible is disengaged to prevent unnecessary drag on the engine. A disc type slip clutch is provided to prevent large torsional amplitudes as they occur at low engine speeds due to cyclic irregularity from reaching the blower.

The turbocharger is mounted behind the engine, as are the oil cooler and the aftercooler. Two versions of the engine were drawn. One, as shown, for an aircraft with fixed landing gear. A second version of the engine was drawn which accommodates a retractable nose gear. The coolers are moved outboard and the turbocharger raised to provide space between cylinders #2 and #3 for the nose gear strut.

Table V presents the operating parameters of the 149 kW engine concept and Figure 19 shows the projected fuel consumption curve for this engine.

As with the 298 kW engine, calculations were made to define power component stresses, turbocharger and cooler sizing, torsional vibration definition, as well as cost and weight projections.

Table VI and Figure 20 are presented to show comparisons with today's state-of-the-art gasoline engines.

Again, as with the larger engine, all comparisons favor the diesel engine.

### Engine/Airframe Integration

This study was conducted as a subcontract by Beech Aircraft Corp. to evaluate the integration of the proposed diesel aircraft engines into future airframes and to determine the effect of the engine on aircraft performance and operating costs. The results were then compared with corresponding data for current production type gasoline engine powered aircraft.

### Engine Installation

Installation design layouts were made which show the 298 kW diesel mounted on a twin engine airplane and the 149 kW engine installed in a single engine aircraft with retractable landing gear. The Figures 21 through 23 show the twin engine installation; the Figures 24 through 26 show the single engine installation. Figure 27 and 28, the three view drawings, are based on the wing areas indicated by the performance synthesis program, the engine drawings and standard airplane proportions. Some pertinent features about the installation are as follows:

1. Engine mounts are of two basic types - cantilever and bed mount. A cantilever mount from the firewall was used in the twin and a bed mount incorporating the nose gear support structure was used in the single. "Dynafoal" type mounts would be used with the cantilever method to minimize vibration transmission to the airframe.
2. The induction system in both cases would be a NACA flush inlet, ducting and an air filter. Alternate air would be available to the engine through a door operated by differential pressure.
3. Both engines have a dry oil sump and require external oil tanks mounted in the engine compartments.
4. Both engines would have cooling air inlets providing air to a plenum chamber. Ducts from the plenum would direct air to individual cylinders, oil coolers, aftercoolers and fuel injectors as needed. On the single, cooling air exits are outboard of the nose gear on the lower side of the cowl. Exits from the twin nacelle would be at the lower aft end.
5. The installation drawings were done in enough detail to indicate the features noted above and to provide reasonable assurance that no major installation problems would be encountered with the proposed diesel engine concepts.

## Aircraft Configurations

Three view sketches of the airplane are shown in the Figures 27 and 28. Following are some characteristics of both planes:

### 1. Propeller Data.

Prop. diameter	2.057 m
Prop. speed at take-off	2,345 rpm
Tip speed at take-off	253 m/sec = .74a
a = Velocity of sound = $20.06 \sqrt{T}$ m/sec (T in °K)	
At standard ambient temp. 15.5°C	
a = $20.06 \sqrt{273 - 15.5}$ = 341 m/sec	
Prop. speed at economy cruise	1,790 rpm
Tip speed at economy cruise	193 m/sec
Prop. ground clearance	330 mm

### 2. Sight Angles.

The pilot's sight angles for the twin are indicated by A and B (Figure 27). The centerline angle over the nose, A, as indicated is about 12°. If the airplane were lofted, the angle from the pilot's actual eye position would be about 18° which is considered more than adequate. The smallest lateral angle B is 10°. This is also more than adequate especially compared to some current piston engine twins with larger nacelles.

### 3. Aircraft Data.

		Twin Engine Diesel	Twin Engine Gasoline
Airframe minus engine	(a) kg	1,860	1,860
Engines (2)	(b) kg	415	525
Empty weight (a) + (b)	(c) kg	2,275	2,385
Payload	(d) kg	726	671
Fuel load	(e) kg	653	598
Useful load (d) + (e)	(f) kg	1,379	1,269
Max. take-off weight (c) + (f)	kg	3,654	3,654
Wing span	m	13.05	13.05
Length	m	11.89	11.89
Tail height	m	3.87	3.87
Tail span	m	5.09	5.09
Wing area	m <sup>2</sup>	22.39	22.39

Figure 28 shows the single engine aircraft. Characteristics are:

### 1. Propeller Data.

Prop. diameter	2.134 m
Prop. speed at take-off	2,400 rpm
Tip speed at take-off	268 m/sec = .79a
Prop speed at economy cruise	1,800 rpm

Tip speed at economy cruise	201 m/sec
Prop ground clearance	356 mm

- The centerline angle over the nose for the single engine airplane C, is 9°. This should correspond to actual pilot's viewing angle of about 12°. This is probably adequate, especially when compared to some of today's long nose single engine aircraft.

### 3. Aircraft Data.

		Single Engine Diesel	Single Engine Gasoline
Airframe minus engine	(a) kg	667	667
Engine -	(b) kg	162	175
Empty weight (a) + (b)	(c) kg	829	842
Payload	(d) kg	340	333
Fuel load	(e) kg	180	174
Useful load (d) + (e)	(f) kg	520	507
Max. take-off weight (c) + (f)	kg	1,349	1,349
Wing span	m	11.16	11.16
Length	m	8.66	8.66
Tail height	m	3.14	3.14
Tail span	m	3.78	3.78
Wing area	m <sup>2</sup>	17.74	17.74

### Aircraft Performance Evaluation

The major tool used in the airplane design synthesis was a somewhat modified version of the synthesis method originally developed for the NASA GATE (General Aviation Turbine Engine) Study. The process was simplified for this purpose since take-off and cruise power could be specified as program inputs. The program is not accurate enough nor does it account for enough variables to actually design airplanes, but it is considered adequate to indicate trends in relative size and performance for airplanes theoretically equipped with sufficient engines. The main point to bear in mind when looking at the results of the program is that the objective is to provide an indication of the differences in performance and cost between diesel and gasoline powered airplanes. The methods used in estimating throughout are no better than 5 to 10% accurate, but the uniform assumptions and methods used in all cases would make the resulting differences good indications of the trends to be expected. This is the proper objective for a conceptual investigation.

Hypothetical gasoline and diesel powered airplanes were synthesized and compared in two ways. In one case, the airframe was held constant and the mission profile was allowed to change when the powerplant type changed. In the other case, the mission requirements were held constant and the airplane needed to perform that mission changed size as necessary to meet the mission requirements. These comparisons were made for both the single 149 kW and the twin 298 kW engine airplanes.

The results of the aircraft performance simulation program are shown in the Tables VII and VIII.

Table VII shows the differences in aircraft performance for a fixed airplane size.

The fixed parameters are:

- Max. take-off weight
- Max. landing weight
- Take-off distance
- Landing distance
- Stall speed
- Wing area

The advantages of the diesels with their high cruise power output and low fuel consumptions can be readily seen in the basic parameters of range, speed, and payload.

The advantages of the diesels with their high cruise power output and low fuel consumptions can be readily seen in the basic parameters of range, speed, and payload.

Table VIII shows the differences in airplane size for a fixed performance.

The fixed parameters are:

- Payload
- Max. cruise speed
- Range

The gasoline powered airplanes are bigger and considerably less efficient.

#### Operating Cost Estimates

Production costs were estimated by assuming that new airplanes would be designed and equipped with the diesel engines and, alternatively, compatible gasoline engines. Development, material, and labor costs were chosen to be of roughly the correct magnitude, but are intended primarily to illustrate cost differences due to using diesel instead of gasoline engines. Operating cost estimates were made using figures obtained from current estimates of average operating costs.

The acquisition cost estimates were based on information from the airplane synthesis process. The airplane empty weights were the main parameters used with FY79 rates for labor, material costs, and OEM engine costs. The estimating methods used are based on historical data and "learning curve" theory. An air-frame weight was estimated from the operating empty weight. This was used with estimating data to get material weights to which material cost could be applied. Manhour per pound data were used to get labor content to which labor rates were

applied. A production run of 600 units was used to amortize assumed development costs and to locate factors on the learning curves. When a basic factory cost was summed up, assumed manufacturer's and dealer's mark-ups were applied. Costs were included for currently typical optional equipment and avionics selections. The final total represented a dealer's price tag figure for a typically equipped airplane. Both the single and the twin were considered to be all new designs. The same sets of reasonably realistic assumptions were used throughout so the results are quite adequate for looking at differences between gasoline and diesel airplane prices within the overall accuracy of this study. Acquisition price percentage changes from the diesel to the gasoline engine powered airplanes is shown on the cost summaries. See Tables IX and X for the twin and single engine airplanes, respectively.

The columns headed "gasoline" refer to the airplanes for equivalent size to the diesels but with the mission capability as indicated in the performance estimates. The "equal plane performance gasoline" column refers to the airplanes that will do the same missions as the diesels but are bigger and less efficient.

The cost summary tables show the considerable overall cost advantages of the diesel powered airplanes. Gasoline airplanes of equivalent size cost less initially but this advantage is not sufficient in view of the reduced mission capability and higher overall costs. The biggest factors in raising the gasoline airplanes operating costs are fuel and overhaul expense, as indicated.

#### Propeller Noise Estimates

Propeller performance estimates were made to get some idea of the propeller sizes needed to realize a cruise propulsive efficiency of .85 for both the twin and single engine airplanes. These calculations indicated that a two-blade, 84 inch diameter, constant speed propeller will work for the single engine airplane. The propellers indicated for the twin are 81 inch three-blade. Estimates of 1000 ft. flyover noise predict values of 72 dB(A) for the single and 74 dB(A) for the twin. These compare favorably to the limits of 77.5 dB(A), respectively. Limits are based on airplane weight as set out in FAR 36, Appendix F. A favorable correction factor can reasonably be expected, creating a greater margin relative to the limits. The correction factor is based on detailed take-off performance estimates that are beyond the scope of this study. Even without correction factors, the noise regulations appear to present no problem for the conceptual diesel airplanes.

#### 186 kW (250 HP) Engine Configuration

A third engine configuration is currently under evaluation and design definition. This engine is rated at 186 kW (250 HP) net shaft power at 25,000 ft. cruise altitude. Table XI outlines the pertinent features of this engine configuration. Engine specifications are summarized in Table XII.

As shown in this table, a cruise fuel consumption value of .36 lb/hp-hr is projected for this engine. Some pertinent data comparing this projected fuel consumption with other engines is shown in Table XIII. Note that the projected value is relatively conservative compared to actual running engines, confirming the fact that an engine such as proposed is within reach.

### CONCLUSIONS

A study indicates that the diesel engine promises to be a superior powerplant for general aviation aircraft for the following reasons:

1. The diesel engine offers high cruise power at altitude and low fuel consumption. This will result in improved range, high cruising speed and more payload for a diesel engined aircraft.
2. The diesel powered airplane has a considerable overall cost advantage. Gasoline airplanes of equivalent size cost less initially, but this advantage is offset by reduced mission capability and higher operating costs.
3. The diesel engine presents no installation problems. Although the radial configuration is different than current gasoline engines, the mounting to the airframe is essentially the same and requires no major airframe modifications.
5. The independent turbo loop provides:
  - Easy cold and hot starts
  - Can crank engine indefinitely
  - Electric power available independent of engine operation (APU mode)
  - Reduced battery capacity
  - Cabin cooling or heating available while aircraft is on the ground
6. The radial cylinder configuration results in:
  - Low engine weight
  - Reduced engine friction
  - Absence of piston inertia forces
  - Compactness of the power package
7. The two-stroke cycle feature results in:
  - Weight reduction
  - Improved reliability due to fewer parts
  - Reduced frontal area



8. The following key technologies will be required to demonstrate the feasibility of the engines proposed in this study:

1985 (250 HP Engine)

- Combustion/scavenging in 2-cycle loop scavenged system
- High pressure ratio, high efficiency turbocharger
- High pressure fuel injection system
- High speed starter/alternator.

1985-2000 (400 HP Engine)

- All of the above
- Ceramic components
- Advanced lubricants (solids, air bearings, etc.)
- Catalytic combustor

**TABLE I**  
**Previous Aircraft Diesels**

Make	Model	Config.	Cycle	Cooling	No. Cyl.	Bore mm	Stroke mm	Displ. l	Compr. Ratio	Power kW	RPM	Wgt. kg	Year
1. Packard	DR980	Radial	4	air	9	122	152	16.1	16:1	174	2050	231	1930
2. Guiberson	A980	Radial	4	air	9	122	152	16.1	14.7:1	155	2050	231	1931
3. Deschamps		30° A	2	liquid	12	112	229	50.5	16:1	1000	1750	1089	1934
4. Bristol	Phoenix	Radial	4	air	9	116	190	28.75	14:1	318	2000	494	1934
5. Zbrojovka	ZOD	Radial	2	air	9	120	130	13.2	15:1	207	1600	297	1935
6. Hispano	Clerget 14F2	Radial	4	air	14	140	160	34.5	15:1	518	2200	600	1935
7. Salmson	SH18	Radial	2	air	18	118	150	29.5	16:1	481	1700	567	1935
8. Mercedes	OF2	60° V	4	liquid	12	135	210	53.9	15:1	592	1790	935	1935
9. Junkers	204	Opposed	2	liquid	6	120	2 x 210	28.75	17:1	570	1800	750	1935
10. Junkers	205	Opposed	2	liquid	6	105	2 x 160	16.6	16:1	444	2200	510	1936
11. Junkers (1)*	207 Turbo	Opposed	2	liquid	6	105	2 x 160	16.6	16:1	740	3000	649	1938
12. Napier (2)*	Nomad	Flat	2	liquid	12	152.4	187.33	41.0	16:1	1984	2050	1624	1953
13. McCulloch (3)*	TRAD-4180	Radial	2	air	4	98.43	98.43	3.0	15:1	150	2850	149	1970

\*Numbers in parentheses refer to list of references at the end of this report.

**TABLE II**  
**Specific Data of Previous Aircraft Diesels**

Make	Cycle	S/B	BMEP kPa	Piston Speed m/sec	Piston Heat Load kW/cm²	Spec. Power kW/l	Spec. Wgt. kW/kg
Packard	4	1.246	633	10.39	.165	10.81	.75
Guiberson	4	1.246	564	10.39	.147	9.63	.67
Deschamps	2	1.507	679	13.36	.459	19.80	.92
Bristol	4	1.301	664	12.67	.211	11.06	.64
Zbrojovka	2	1.083	588	6.93	.203	15.68	.70
Hispano	4	1.143	819	11.73	.240	15.01	.86
Salmson	2	1.271	575	8.50	.244	16.31	.85
Mercedes	4	1.273	736	12.53	.231	10.98	.63
Junkers 204	2	1.750	661	12.60	.420	19.83	.76
Junkers 205	2	1.524	729	11.73	.427	26.75	.87
Junkers 207	2	1.524	892	16.00	.712	44.58	1.14
Napier	2	1.229	1416	12.80	.906	48.39	1.22
McCulloch	2	1.000	1053	9.35	.493	50.00	1.01

**TABLE III**  
**Operating Parameters — 298 kW Engine**

	Take-off	100% Power Cruise	65% Power Cruise	
Altitude	0	6,096	6,096	meters
Power	298	298	194	kW
RPM	3,500	3,500	2,675	
Displacement	4.71	4.71	4.71	liters
Bore x Stroke	100 x 100	100 x 100	100 x 100	mm
BMEP	1,085	1,085	923	kPa
Compressor Pressure Ratio	4.06:1	8.30:1	6.25:1	
Nominal Compression Ratio	13.185:1	13.185:1	13.185:1	
Effective Compression Ratio	10.0:1	10.0:1	10.0:1	
Barometric Pressure	101.4	46.4	46.4	kPa
Ambient Temperature	15.5	- 25	- 25	°C
Intake Manifold Pressure	402.4	370.2	277.6	kPa
Intake Manifold temperature	116	116	116	°C
Exhaust Manifold Pressure	309.5	284.8	245.5	kPa
Scavenge System	Curtis Loop	Curtis Loop	Curtis Loop	
Scavenge Ratio	1.3	1.3	1.3	
Ratio Boost/Back Pressure	1.3	1.3	1.131	
Height Intake Ports	20.65	20.65	20.65	mm
Height Exhaust Ports	26.14	26.14	26.14	mm
Intake Ports Open/Close	61°47'	61°47'	61°47'	BBDC/ABDC
Exhaust Ports Open/Close	69°39'	69°39'	69°39'	BBDC/ABDC
BSFC-engine	206.8	212.9	194.6	g/kW-hr.
BSFC-combustor	18.2	6.1	0	g/kW-hr.
BSFC-powerpack	225.0	219.0	194.6	g/kW-hr.
Fuel Flow Powerpack	67.1	65.3	37.8	kg/hr
Air Density	.00279	.00256	.00205	kg/l
Air/Fuel Ratio	27.50	24.59	25.47	

**TABLE IV**  
**Comparison of GTSIO-520-H Gasoline and  
GTDR-290 Aircraft Diesel Engine**

	4-Stroke Cycle GTSIO-520-H Gasoline Engine	2-Stroke Cycle GTDR-290 Diesel Engine
Configuration	6 cyl. opposed	6 cyl. radial
Displacement l	8.52	4.71
Take-off RPM	3400	3500
Rated max. take-off power kW	280	298
Rated max. for cruising kW	210	298
Prop speed at take-off RPM	2278	2345
BSFC g/kW-hr:		
Take-off	425.8	225.1
100% power cruise	—	219.0
65% power cruise	273.7	194.6
Dimensions:		
Length mm	1429	1105
Width mm	865	632
Height mm	663	660
Engine weight dry, kg	262.4	207.5

**TABLE V**  
**Engine Operating Parameters**

	Take-off	100% Power Cruise	65% Power Cruise	
Altitude	0	3,048	3,048	meters
Power	149	149	97	kW
RPM	2400	2400	1800	
Displacement	3.14	3.14	3.14	liters
Bore x Stroke	100 x 100	100 x 100	100 x 100	mm
BMEP	1,187	1,187	1,029	kPa
Compressor Pressure Ratio	4.16:1	6.10:1	4.13:1	
Compression Ratio	Variable	Variable	Variable	
Max. C.R.	17:1 (effective)			
Min. C.R.	10:1 (effective)			
Barometric Pressure	101.4	69.6	69.6	kPa
Ambient Temperature	15.5	-5	-5	°C
Intake Manifold Pressure	411.8	411.8	280.9	kPa
Intake Manifold temperature	116	116	116	°C
Exhaust Manifold Pressure	316.8	316.8	255.4	kPa
Scavenge System	Curtis Loop	Curtis Loop	Curtis Loop	
Scavenge Ratio	1.3	1.3	1.3	
Ratio Boost/Backpressure	1.3	1.3	1.1	
Height Intake Ports	20.13	20.13	20.13	mm
Height Exhaust Ports	27.15	27.15	27.15	mm
Intake Ports Open/Close	± 61°	± 61°	± 61°	BBDC/ABDC
Exhaust Ports Open/Close	± 71°	± 71°	± 71°	BBDC/ABDC
BSFC	222.0	228.1	209.8	g/kW-hr.
Fuel Flow	33.1	34.0	20.3	kg/hr.
Air/Fuel Ratio	26.6	26.0	24.0	

**TABLE VI**  
**Comparison of TSIO-360-E Gasoline and TDR-192 Aircraft Diesel Engine**

	4-Stroke Cycle TSIO-360-E Gasoline Engine	2-Stroke Cycle TDR-192 Diesel Engine
Configuration	6 cyl. opposed	4 cyl. radial
Displacement l	5.91	3.14
Take-off RPM	2800	2400
Rated max. take-off power kW	149	149
Rated max. for cruising kW	112	149
Prop drive	direct	direct
BSFC g/kW-hr:		
Take-off	377.1	222.0
100% power cruise	—	228.1
65% power cruise	267.6	209.8
Dimensions:		
Length mm	1188	965
Width mm	795	800
Height mm	672	607
Engine weight dry, kg	174.6	163.2

**TABLE VII**  
**Comparison Gasoline and Diesel Aircraft Engines**  
**Airplane Size Fixed, Variable Performance**

		Single-Engine Diesel*	Single-Engine Gasoline*	Twin-Engine Diesel*	Twin-Engine Gasoline*
Rated power	kW/RPM	149/2400	149/2600	298/2300 (ea)	298/2267 (ea)
Max. take-off weight (gross)	kg	1349	1349	3654	3654
Max. landing weight	kg	1349	1349	3654	3654
Standard empty weight	kg	829	842	2275	2385
Useful load	kg	520	508	1378	1269
Usable fuel	l/kg	251/180	241/174	908/653	832/598
Payload (with full fuel)	kg	340	334	726	671
Altitude — m/% power		3048/100%	3048/75%	7620/81.5%	7620/75%
Max. cruise speed	km/hr	324	291	474	448
Range	km	1481	1468	2592	1726
Altitude — m/% power		3048/75%	3048/75%	7620/81.5%	7620/75%
Speed	km/hr	289	291	474	448
Range	km	1968	1468	2592	1726
Take-off distance (normal, OV. 15 m)	m	579	579	701	701
Landing distance (normal, OV. 15 m)	m	369	369	677	677
Stall speed (landing)	km/hr	85	85	135	135
Wing area	m <sup>2</sup>	17.7	17.7	22.4	22.4

\* All engines are turbocharged.

**TABLE VIII**  
**Comparison Gasoline and Diesel Aircraft Engines**  
**Performance Fixed, Variable Airplane Size**

		Single-Engine Diesel*	Single-Engine Gasoline*	Twin-Engine Diesel*	Twin-Engine Gasoline*
Rated power	kW	149	198	38 (ea)	414 (ea)
Max. take-off weight (gross)	kg	1349	1525	3654	4981
Max. landing weight	kg	1349	1525	3654	4981
Standard empty weight	kg	829	973	2275	3140
Useful load	kg	520	552	1378	1842
Usable fuel	l/kg	251/180	294/211	908/653	1552/1116
Payload (with full fuel)	kg	340	340	726	726
Altitude — m/% power		3048/100%	3048/75%	7620/81.5%	7620/75%
Max. cruise speed	km/hr	324	324	474	474
Range	km	1481	1481	2592	2592
Altitude — m/% power		3048/75%	3048/100%	7620/81.5%	7620/75%
Speed	km/hr	289	324	474	474
Range	km	1968	1481	2592	2592
Take-off distance (normal, OV. 15 m)	m	579	564	701	701
Landing distance (normal, OV. 15 m)	m	369	427	677	689
Stall speed (landing)	km/hr	85	93	135	135
Wing area	m <sup>2</sup>	17.7	17.0	22.4	29.9

\*All engines are turbocharged.

**TABLE IX**  
**Cost Summary**  
**Twin Engine**

Use 1000 Hours/Year

Airplane		Diesel	Gasoline	Equal Plane Performance Gasoline*
Acquisition cost		Base	- 3%	+ 7%
Fuel	\$/hr	26.79	42.30	58.69
Oil	\$/hr	6.98	1.53	2.13
Inspection & maintenance				
Airframe	\$/hr	9.20	9.20	9.20
Engine	\$/hr	13.80	13.80	13.80
Propellers	\$/hr	2.00	2.00	2.00
Engine exchange	\$/hr	19.82	34.84	48.34
Hangar rental	\$/hr	3.30	3.30	3.30
Insurance	\$/hr	6.18	5.99	6.59
Total DOC/Hr.	\$/hr	88.07	112.96	144.05
Total per year	\$	88070	112960	144050
Total for 5 years	\$	440350	564800	720250

\*Bigger airplane required to do the same job as the diesel.



**TABLE X**  
**Cost Summary**  
**Single Engine**

Use 500 Hours/Year

Airplane		Diesel	Gasoline	Equal Plane Performance Gasoline*
Acquisition cost		Base	- 4%	+ 11%
Fuel	\$/hr	8.54	9.90	13.20
Oil	\$/hr	.43	.38	.51
Inspection & maintenance				
Airframe	\$/hr	2.59	2.59	2.59
Engine	\$/hr	4.00	2.59	2.59
Propeller	\$/hr	.30	.30	.30
Engine exchange	\$/hr	4.28	7.57	10.09
Hangar rental	\$/hr	2.40	2.40	2.40
Insurance	\$/hr	5.90	5.90	6.54
Total DOC/Hr.	\$/hr	28.44	31.63	38.22
Total per year	\$	14220	15815	19110
Total for 5 years	\$	71100	79075	95550

\* Bigger airplane required to do the same job as the diesel.

**TABLE XI**

**250 Horsepower Engine Configuration Features**

Combined best features of 400 and 200 horsepower without high risk ceramic components.

Radial/geared

2-Stroke

4-Cylinder

Independent turbocharger loop

Conventional combustor

High pressure turbocharger (8:1)

TABLE XII

## 250 Horsepower Engine Configuration Specification

Displacement:	246 inches <sup>3</sup>
Rated Speed:	3500 RPM
Power:	250 Net Horsepower at 25,000 ft. 360 Net Horsepower at Sea Level
BSFC:	.371 lb/hp-hr at Cruise
Weight:	384 lb.

TABLE XIII

## Basis For Fuel Consumption Projections

1. Analytical fuel/air cycle calculations.
2. Verified by past published data on both 2 and 4 cycle diesel engines of similar features (low C.R. and high boost).
  - A. 4-Cycle-AVCR-1360
 

8:1 C.R.	250 BMEP	.395 BSFC
----------	----------	-----------
  - 4-Cycle-LCR-1790
 

11:1 C.R.	263 BMEP	.373 BSFC
-----------	----------	-----------
  - B. 2-Cycle-Napier Nomad
 

Base Engine	205 BMEP	.388 BSFC
With Turbocompounding		.345 BSFC
  - 2-Cycle-Junkers Lupo
 

		.345 BSFC
--	--	-----------
  - 2-Cycle-DDAD-8V92T
 

110 BMEP		.383 BSFC
----------	--	-----------
  - 2-Cycle-McCulloch
 

153 BMEP		.399 BSFC
----------	--	-----------
  - Average
 

		.375
--	--	------
3. Additional features of proposed engine favoring improved fuel consumption.
  - A. Reduced friction - only two-main bearings, no valve train, no mechanical blower.
  - B. Significantly improved injection systems and turbomachinery available with modern technology.



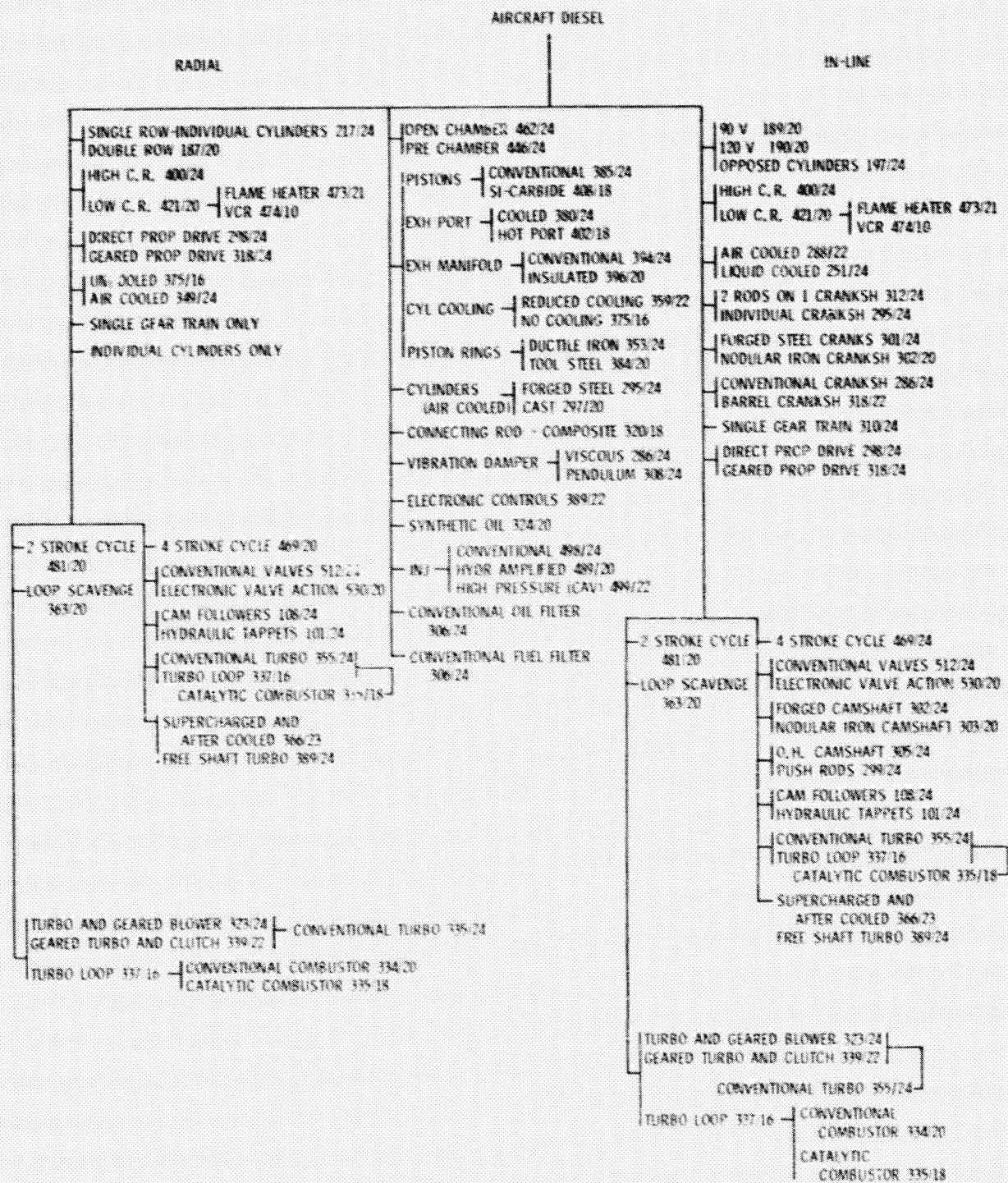


Figure 1

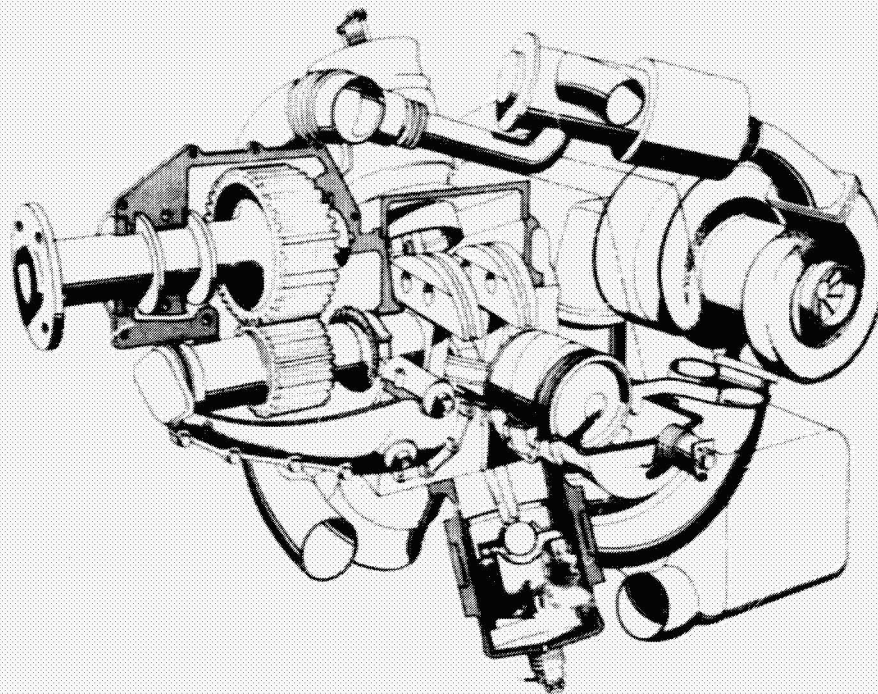


FIGURE 2 2000 kW DIESEL AIRCRAFT ENGINE

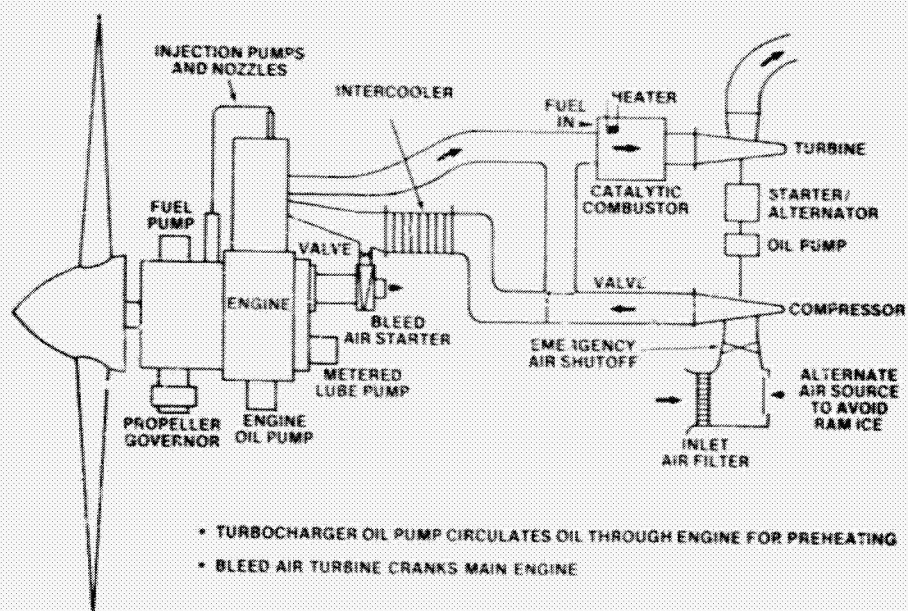


FIGURE 3 SCHEMATIC 2-STROKE ENGINE WITH INDEPENDENT TURBO LOOP/HOT ENGINE CONFIGURATION—NO COOLING/LOW COMPRESSION RATIO PISTONS

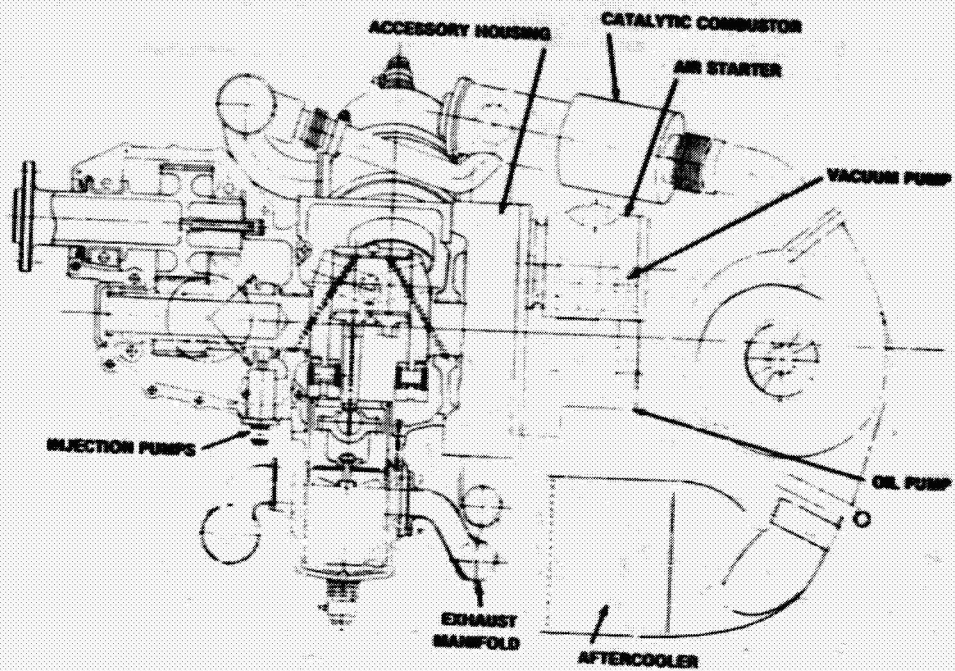


FIGURE 4 2000 kW AIRCRAFT DIESEL—LONGITUDINAL SECTION

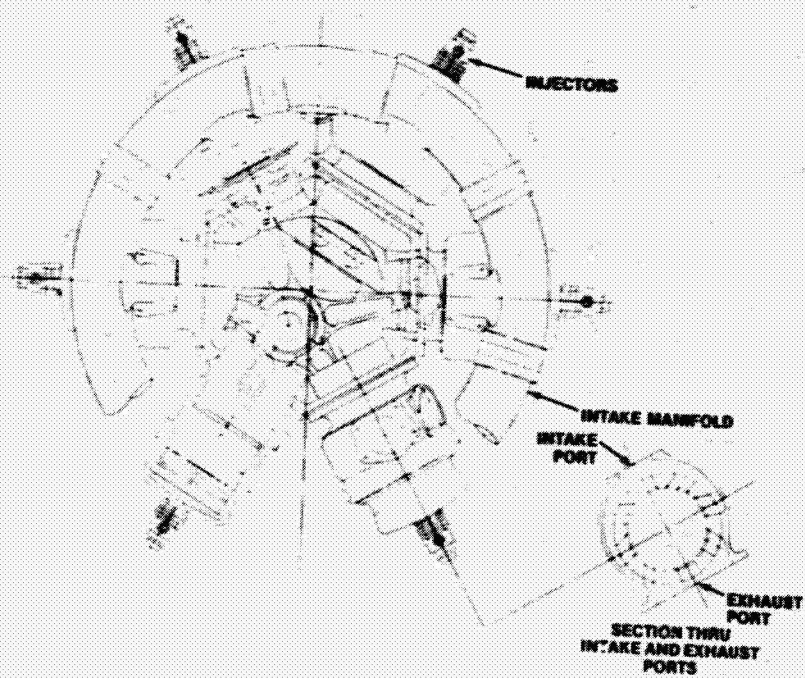


FIGURE 5 8 kW AIRCRAFT DIESEL—CROSS SECTION

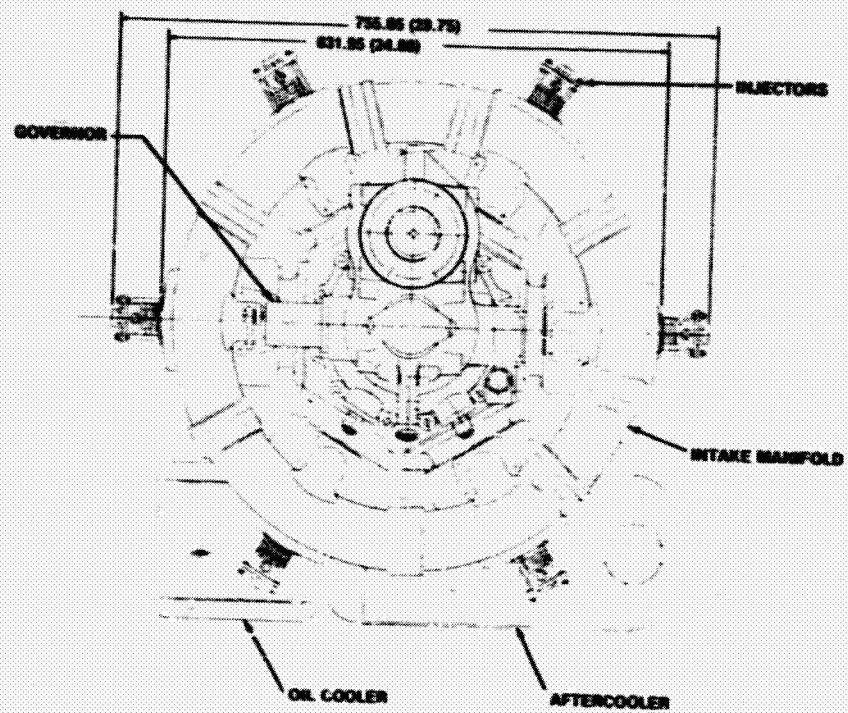


FIGURE 6 25 kW AIRCRAFT DIESEL—FRONT VIEW

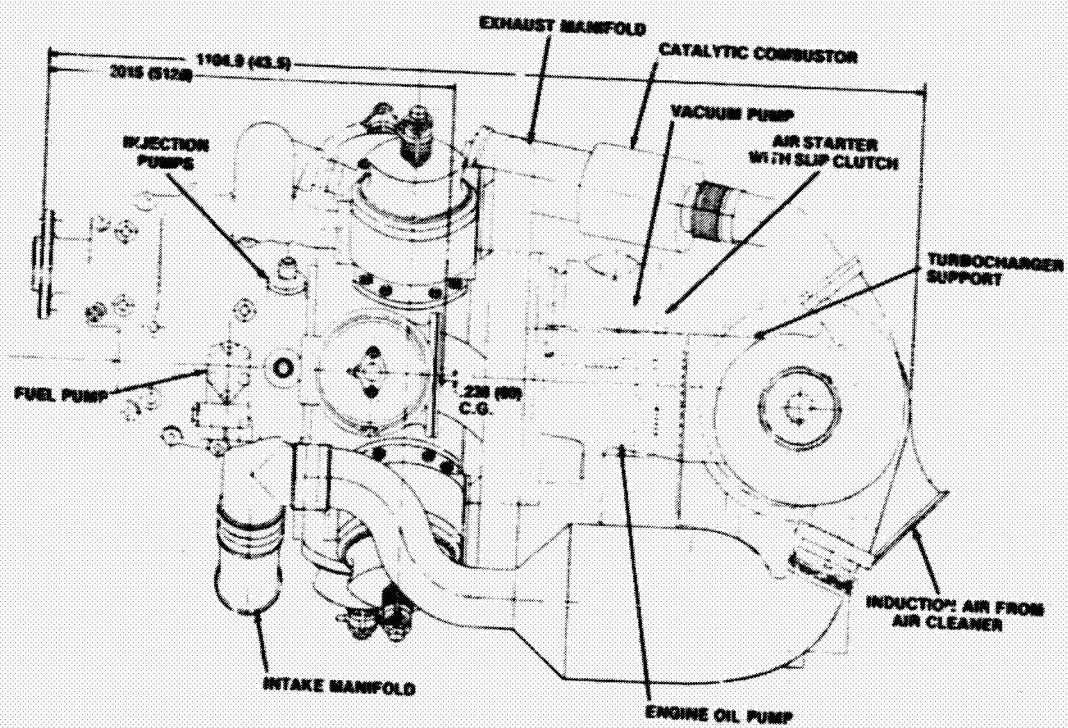


FIGURE 7 200 kW AIRCRAFT DIESEL—SIDE VIEW

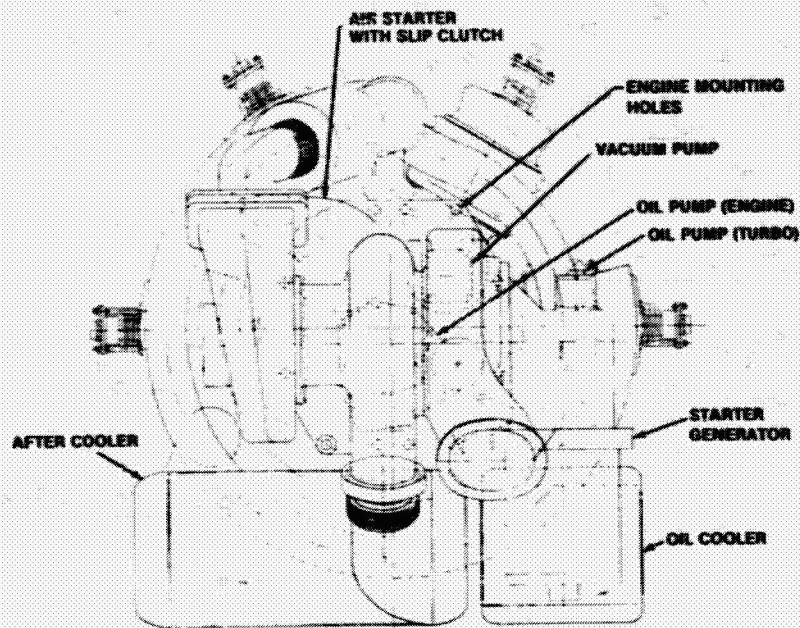


FIGURE 8 290 kW AIRCRAFT DIESEL—REAR VIEW

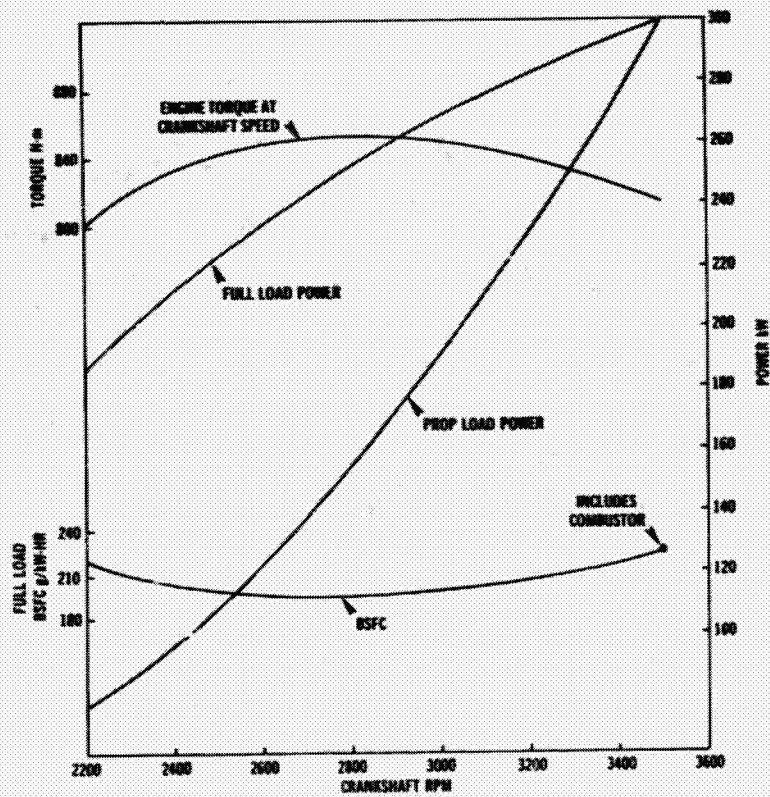


FIGURE 9 SEA LEVEL PERFORMANCE 6-CYLINDER RADIAL AIRCRAFT DIESEL ENGINE



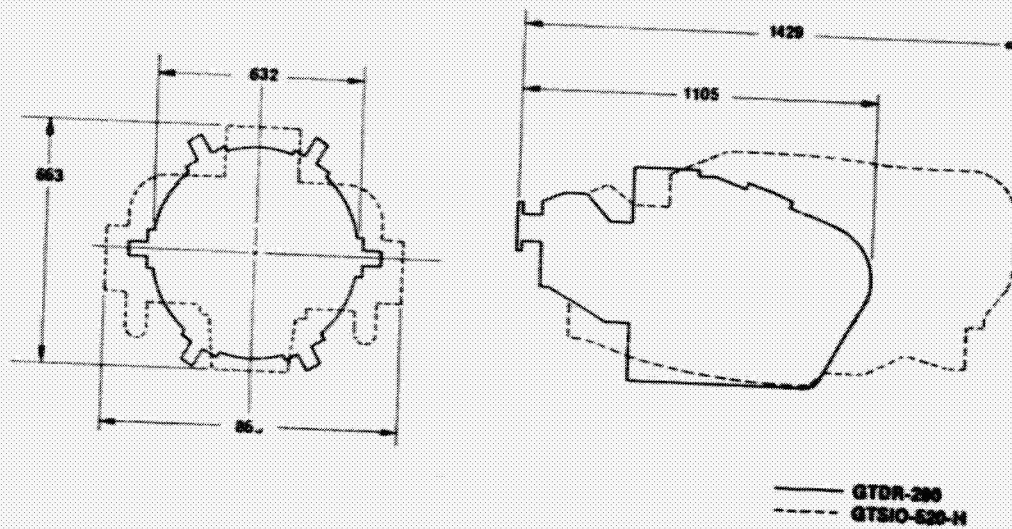


FIGURE 10 SIZE COMPARISON GTSIO-520-H AND GTDR-290 AIRCRAFT DIESEL ENGINE

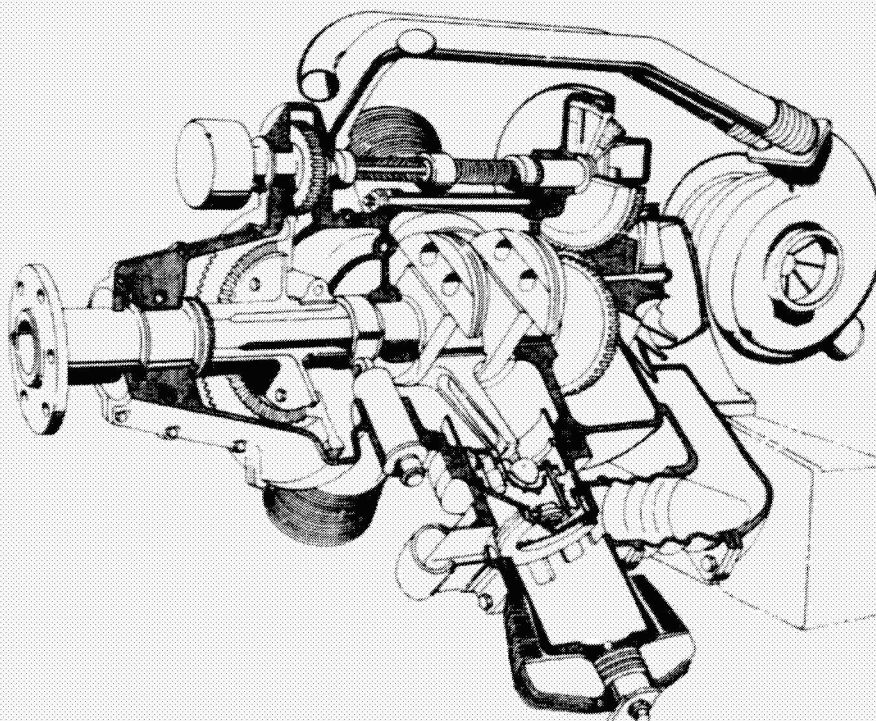


FIGURE 11 149AW, 4-CYLINDER DIESEL AIRCRAFT ENGINE

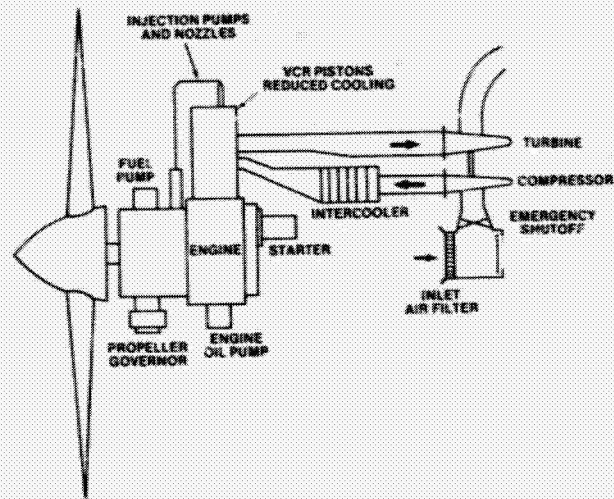


FIGURE 12 SCHEMATIC 2-STROKE TURBOCHARGED ENGINE REDUCED COOLED/VCR PISTONS

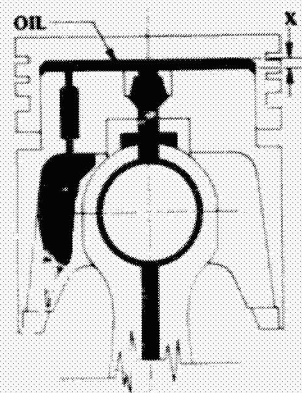


FIGURE 13 VARIABLE COMPRESSION RATIO PISTON

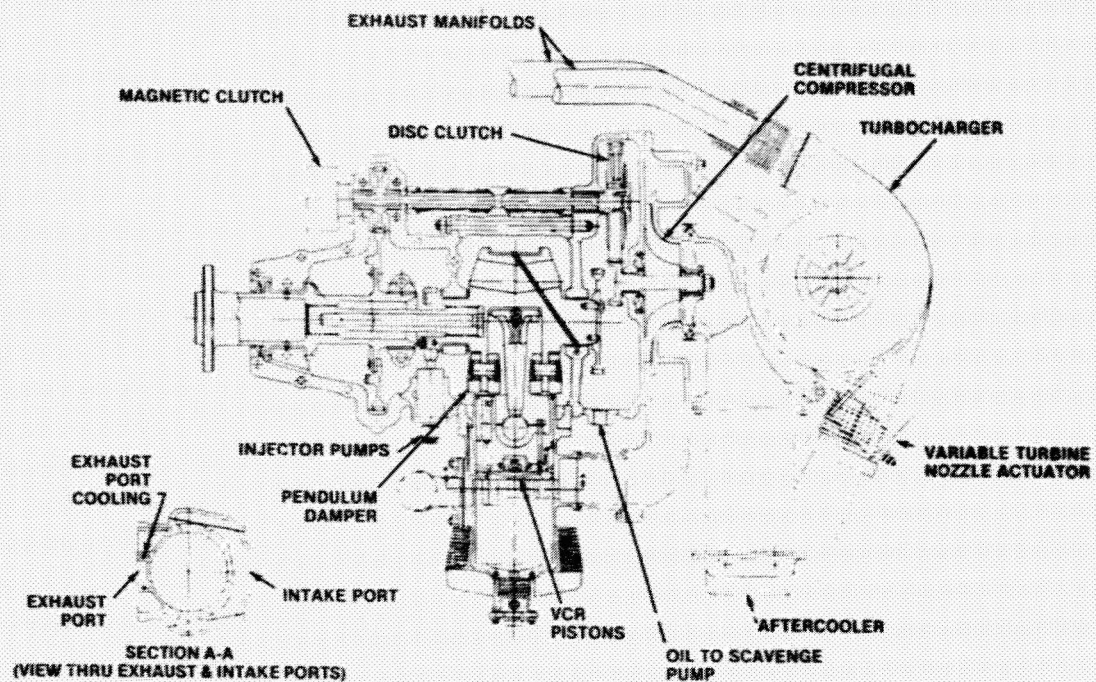


FIGURE 14 149 kW AIRCRAFT DIESEL—LONGITUDINAL SECTION

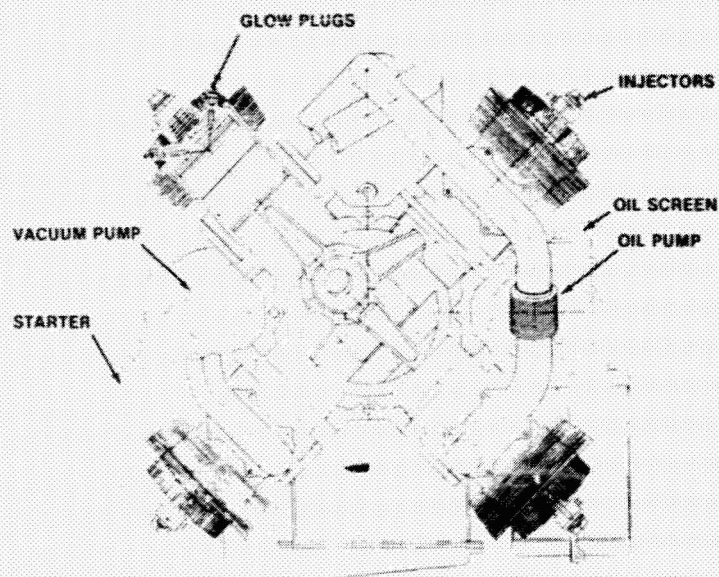


FIGURE 15 149 kW AIRCRAFT DIESEL—CROSS SECTION



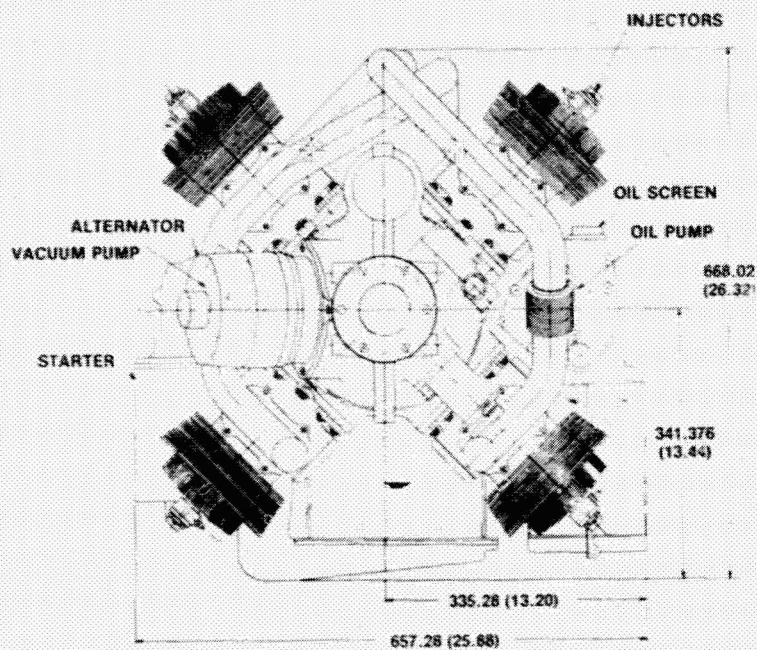


FIGURE 16 149 kW AIRCRAFT DIESEL — FRONT VIEW

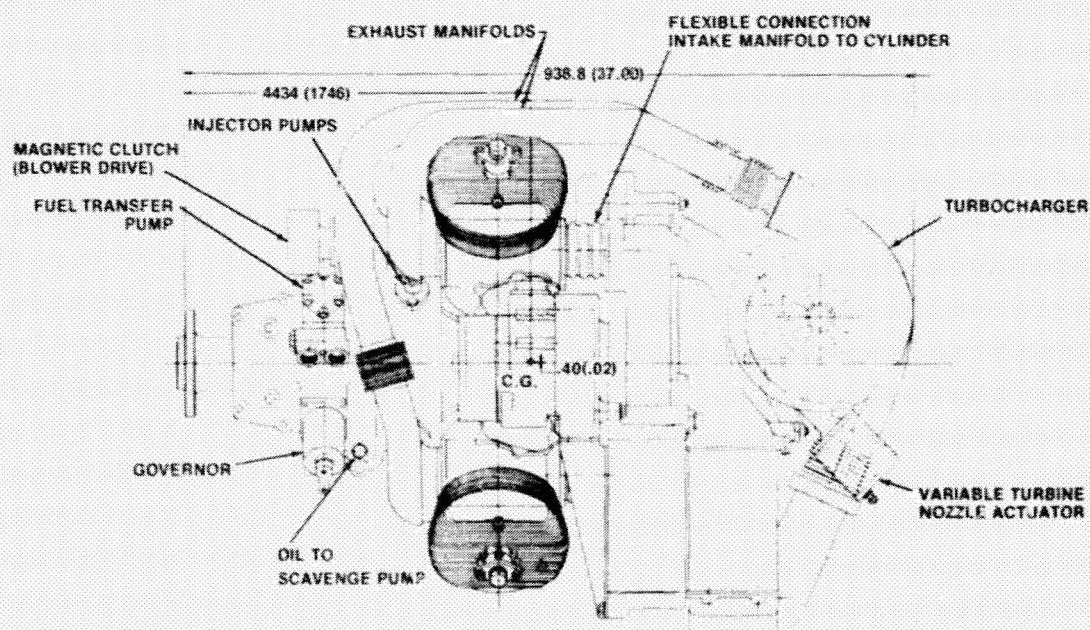


FIGURE 17 149 kW AIRCRAFT DIESEL — SIDE VIEW

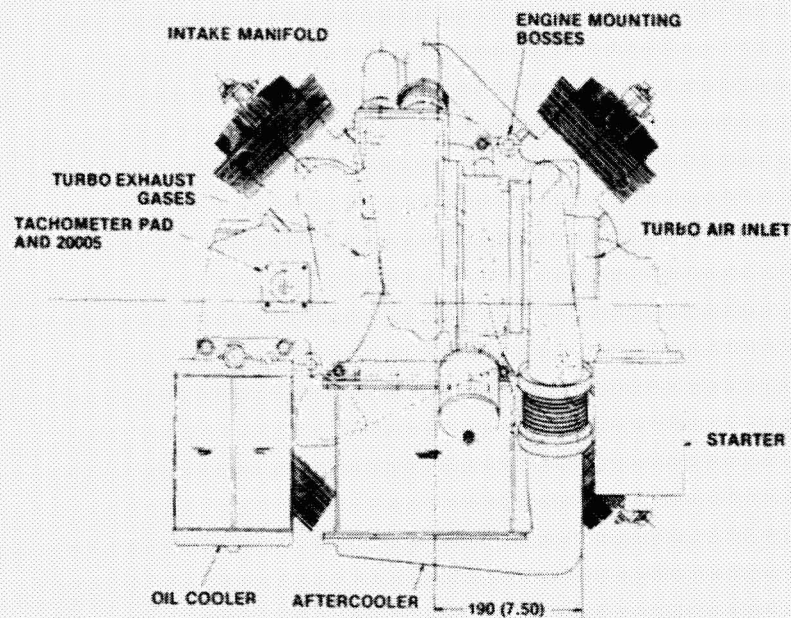


FIGURE 18 149 kW AIRCRAFT DIESEL—REAR VIEW

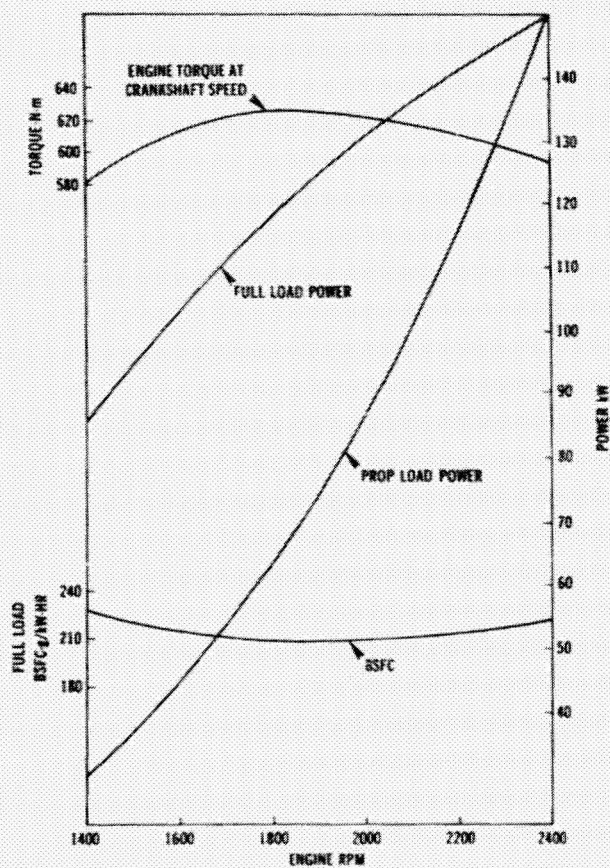


FIGURE 19 SEA LEVEL PERFORMANCE 4-CYLINDER RADIAL AIRCRAFT DIESEL ENGINE



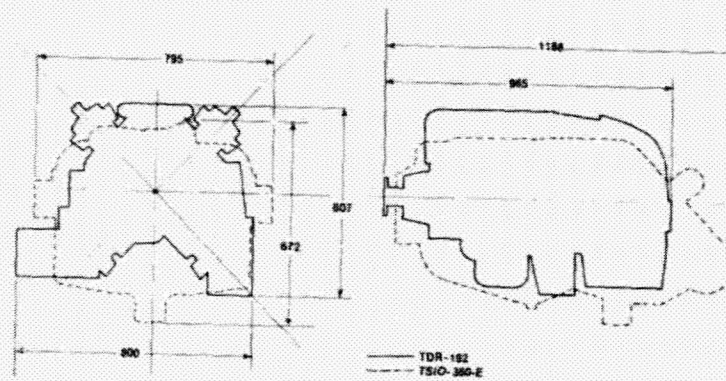


FIGURE 20 SIZE COMPARISON TSIO-360E AND TDR-192 AIRCRAFT DIESEL ENGINE

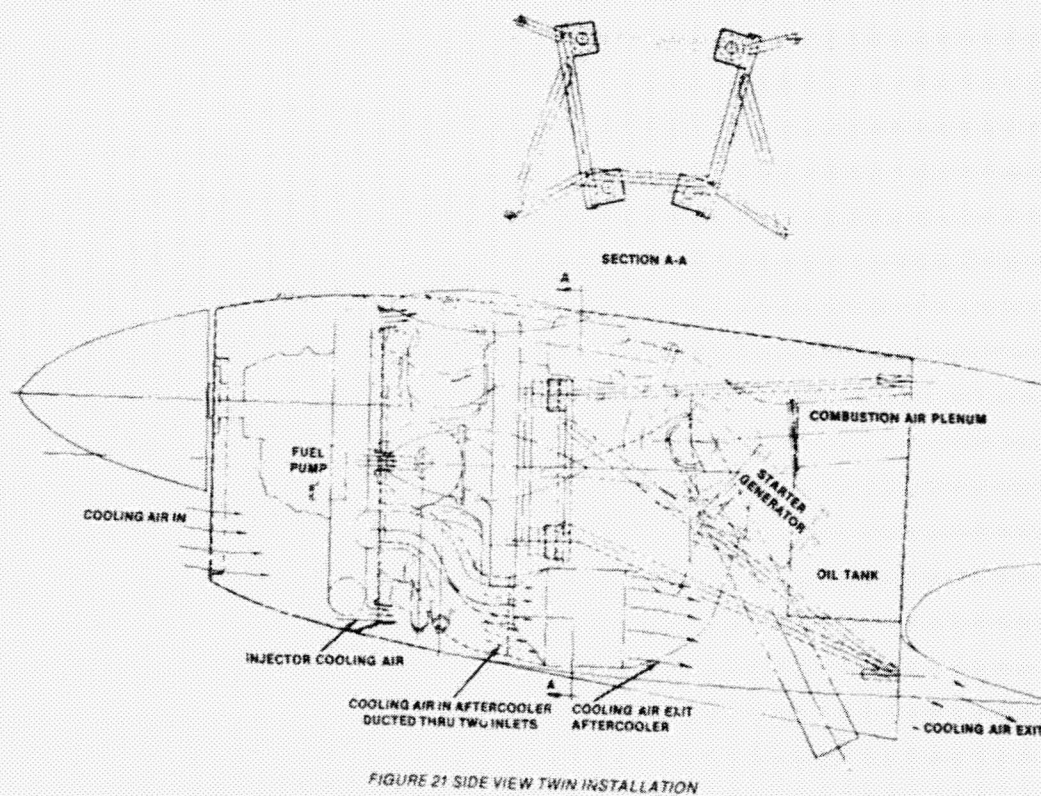


FIGURE 21 SIDE VIEW TWIN INSTALLATION

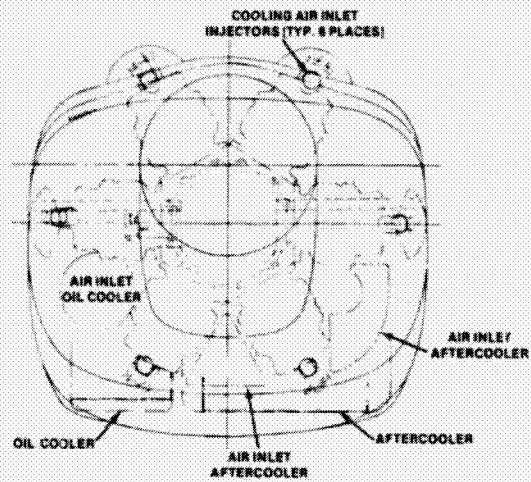


FIGURE 22 FRONT VIEW TWIN INSTALLATION

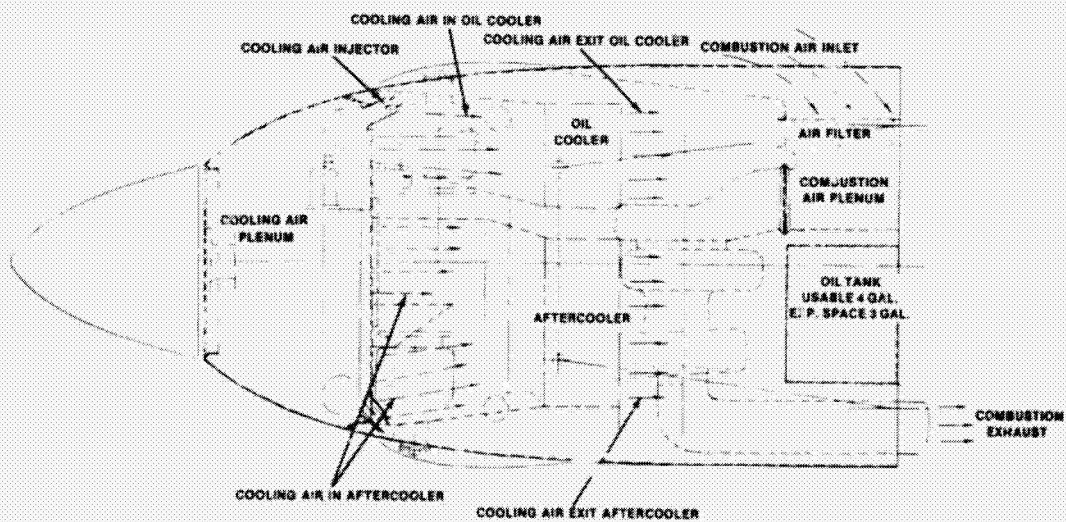


FIGURE 23 TOP VIEW TWIN INSTALLATION

ORIGINAL PAGE IS  
OF POOR QUALITY

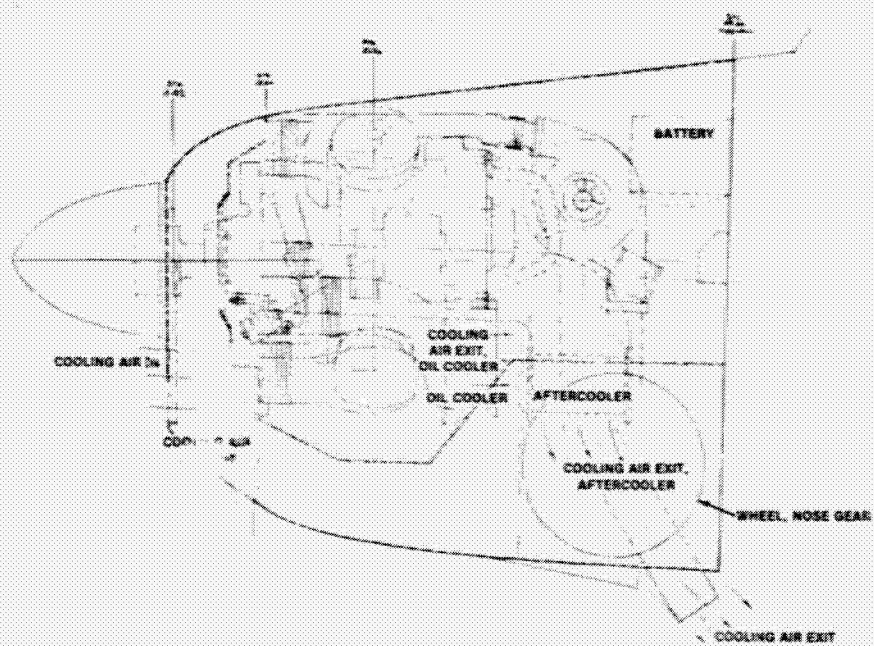
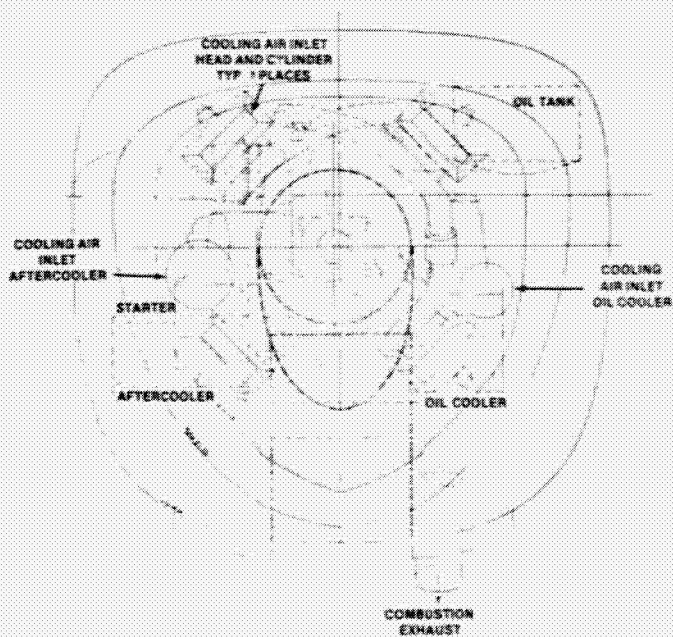


FIGURE 24 SIDE VIEW SINGLE INSTALLATION



FRONT 25 FRONT VIEW SINGLE INSTALLATION

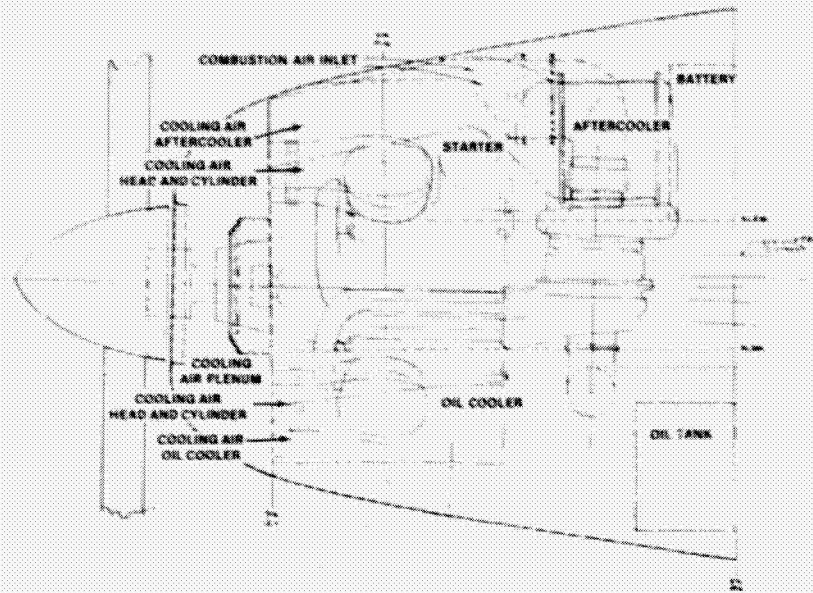


FIGURE 26 TOP VIEW SINGLE INSTALLATION

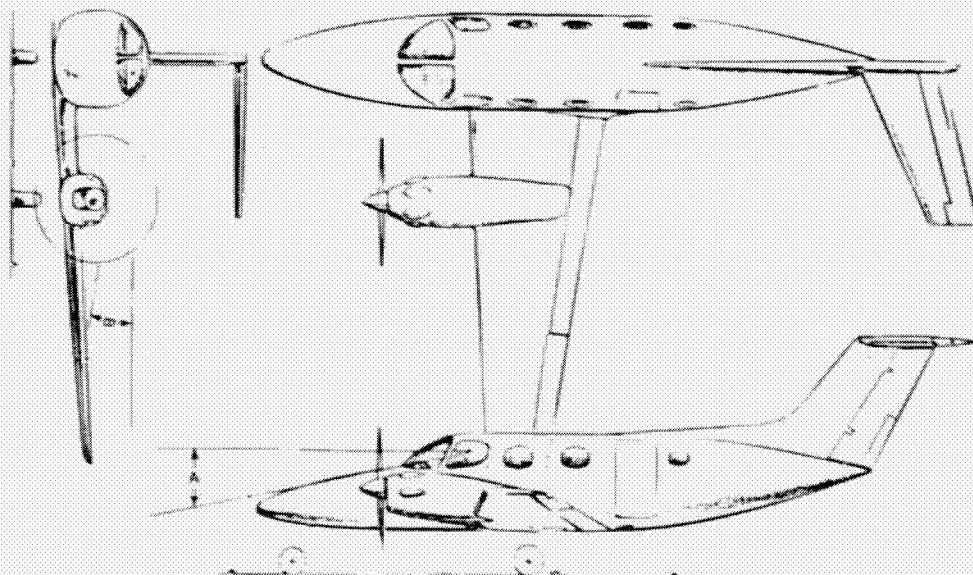


FIGURE 27 TWIN ENGINE AIRCRAFT CONFIGURATION

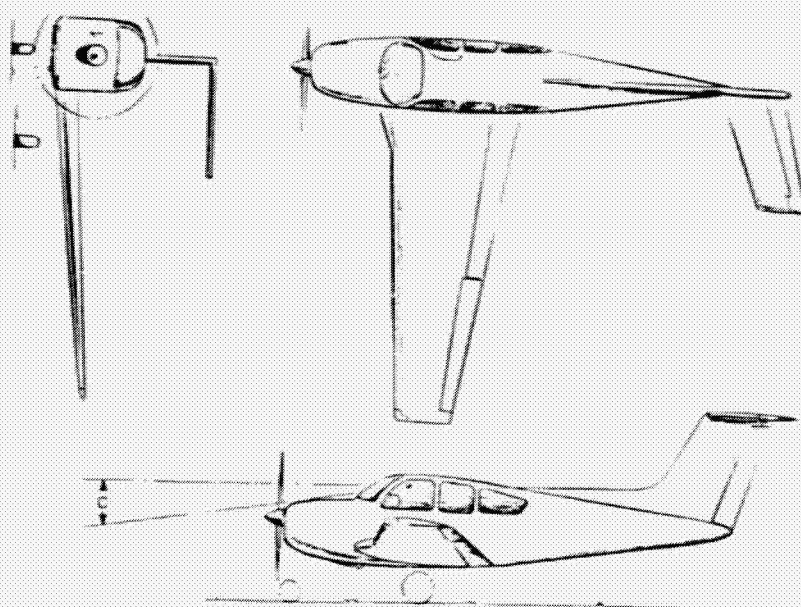


FIGURE 28 SINGLE ENGINE AIRCRAFT CONFIGURATION





D12

1 N 80 - 22339

## ADVANCED ROTARY ENGINE STUDIES

Charles Jones  
Curtiss-Wright Corporation

### INTRODUCTION

The intent of this paper is to review recent Rotary Engine Developments relevant to a Stratified Charge Rotary Aircraft Engine. In addition, present status of the NASA-funded Advanced Aircraft Engine Study, which is currently underway, will be briefly described.

### Background Work

Although Curtiss-Wright designed their first Wankel-type Rotary Engine in 1958 and ran this engine in early 1959, developments continued into 1962 before a reliable, durable and efficient baseline engine was demonstrated.

The first Stratified Charge trials were made that same year, directed towards a multi-fuel military engine. During the mid-60's period, two prototype Stratified Charge Rotary Engines were designed, built and developed through the early operational test stand stage (ref. 1). The RC2-60U10 (figure 1) was a liquid-cooled two rotor vehicular engine in the 160 - 200 HP class and the RC2-90 (figure 2) an air cooled 300 HP helicopter drone engine. The trochoid dimensions of these engines was the same as the 1958-designed 60 cubic inch single rotor engine (the RC1-60), but the rotor width was increased 50% for the RC2-90. Both engines proved their multi-fuel capabilities, but neither could match the fuel economy of our carbureted RC2-60U5 automotive prototype engine of the same era, which was comparable to existing automotive engines (ref. 2). Furthermore, the RC2-60U10 performed well at the lower powers and speeds, with shortcomings apparent at the other end of the operating regime, whereas the 90 cubic inch combustion configuration was subsequently developed to meet high power goals, only to show low end deficiencies. In both cases, however, the engines showed sufficient technical promise for their specific designed applications, but as a result of changes in military planning, the intended uses did not materialize and development was shelved.

Although thermal efficiency equal to our homogeneous charge Rotaries was never demonstrated with these engines, the inherent compatibility of the Rotary geometry with unthrottled and direct chamber injected Stratified Charge combustion led some to believe that the potential for superior performance had to be there. Figure 3 illustrates how the Rotary provides the required repetitive scheduled turbulence, without losses, while direct chamber injected reciprocating engines have to generate the required velocity gradients at a cost of

both volumetric and mechanical efficiency, further widening the specific power advantage of the Rotary.

Following the fuel crises of 1973, R&D efforts were reinitiated in an attempt to resolve whether or not this higher efficiency potential really existed. This time, our feasibility trials were directed towards automotive applications which meant not only wide power and speed range flexibility with fuel economy, but low or controllable emissions as well. Since hydrocarbon emissions at the very low speeds and powers typical of an automotive operating regime had proved the most difficult area for the homogeneous charge Rotary, new configurations were screened on the basis of road-load brake specific fuel consumption (BSFC) and brake specific hydrocarbons (BSHC). The 1973 attempt to combine the best features of RC2-60U10 and final RC2-90 injection/ignition designs into a single configuration which could run full range was successful and, for the first time, achieved better fuel consumption, on a variety of fuels, than the gasoline carbureted engine. This design improvement led to, in 1974, a more flexible arrangement whereby a separate pilot nozzle, with relatively small fuel flow, is used to trigger combustion. This design, shown in figure 4, uses a multi-hole main nozzle, located close to the trochoid surface to modulate fuel flow in response to power demand.

A number of variations of this basic approach were tested during the 1975 and 1976 periods of increased R&D activity and the results showed that the localized and controlled combustion could produce low "raw" hydrocarbons. The test findings did indicate, however, that increased rotor combustion pocket temperatures were required. In this case, these temperatures were achieved by use of an air-gap insulated surface plate attached to the rotor combustion face. The results, for two successive 8.5:1 compression ratio hot rotor designs (figure 5) show that the best of these was able to match the shaded area which represents modern automotive engine untreated HC levels. These data also illustrate that the results were similar for the different fuels tested. Although BSFC vs. BMEP also showed relatively small differences with these fuels there was no significant reduction of BSFC with the increased rotor temperatures used to reduce BSHC.

This early test work indicated that further HC reductions are possible with moderate intake throttling at the very low power/speed end of the regime and by an increase of compression ratio. Accordingly, the first test on the RC1-60 since interruption of the automotive-directed activity between early 1977 and the present, is now being run with a 10:1 compression ratio rotor. Since this compression ratio increase will also improve SFC, it is germane to look at the comparative trends. The test evaluation, which started in October, has not yet completely covered the nozzle-matching and injection dynamics sorting out process. Preliminary data, presented on an Indicated basis in figure 6, shows some promise; however, gain on a brake basis will be slightly less as a result of some friction increase.

The 1976 specific fuel consumption baseline curves (8.5:1 compression ratio) are shown in figures 7 and 8. Figure 7 compares results, for the same designs that demonstrated low hydrocarbons, to data which are representative for full-sized European automobiles powered by Diesel engines. Figure 8 adds other

speeds and compares VW sub-compact "Rabbit" Diesel 4 cylinder engine data developed for DOT (refs. 3-5). The relative sizes and weights of the comparable output Volkswagen Diesel 6 cylinder engine and a Stratified Charge Rotary engine are shown in figure 9.

The "cast iron rotor housing" curve illustrates the type of SFC improvement that was attained with a moderate increase of trochoid surface temperature. While a cast iron rotor housing was used for this test exploration, the temperatures tested do not preclude use of aluminum. Further work is required to define gain at higher levels.

It follows that if one can match the swirl or pre-chamber diesel on an engine-for-engine fuel consumption basis, then the smaller dimensions and reduced bulk has to mean better total vehicle system fuel efficiency. Furthermore, it is significant to note that Texaco has developed data (refs. 6, 7) to show that the United States would be able to obtain more usable Btu's per barrel of crude oil if the refineries were optimized to produce a broad base middle distillate fuel.

#### Testing of Other Sizes

The combustion efficiency shown for the automotive sized module is of interest for other applications only to the extent that the same technology can be scaled to the sizes required for the particular application. The scaling flexibility of the homogeneous charge engine has been demonstrated adequately over a per rotor displacement range of about 500:1 and 1 to 4 rotors but until 1978, Stratified Charge Rotaries with the current full-range design features had not been run in any other size. The earlier configurations (figure 2) had been run in the wider rotor 90"³ chamber and shown the same thermal efficiency (ISFC) as the RC1-60 (ref. 8).

In early 1977 the RC1-60 testing program was deferred for Engineering activity on a larger 350 cubic inch module. The 350 cubic inches per rotor was achieved by enlarging the trochoid by approximately two-thirds and widening rotor proportions by 25 percent.

The same technology and basic configurations developed in the RC1-60 were used for the 350 cubic inch engine, including a "reversed" configuration (ATC pilot) where the pilot and main nozzle relative position (BTC pilot) shown in figure 4 are interchanged. As of the end of 1976, this reversed design had showed promise but had not been evaluated to the point where it had surpassed the BTC pilot. The output targets for the larger engine were all established from the RC1-60 test results.

Although emissions will be measured subsequently in the program, none have been evaluated up to this point which has thus far concentrated on basic configuration and systems evaluations. The fuel economy and power milestones for this program to develop a military engine which, similar to an aircraft engine, emphasizes the higher output spectrum have all been met to date. Nonetheless, a comparison of excerpted basic performance results is of interest for those

phases of technology which are directly applicable and because of the illustration of scaling effects that it affords. Although the result comparisons will be from RC1-350 test results, the complete 4 rotor engine, the RC4-350, is shown in figure 10 for related interest in a multi-rotor engine.

The baseline performance work on the 1-350 engine has also been conducted with the same inserted rotor design and an 8.5:1 compression ratio, although higher compression ratio rotors will be evaluated in the near future.

The larger module size has the general advantage of more available space to accommodate nozzle variations within a given rotor housing and, operationally, is less constrained by spray impingement on the rotor and housing surfaces. There are other advantages to the larger combustion chamber size, which include reduced sealing line and leakage area ratio to charge volume, a similar favorable ratio for heat losses, and the same type of reduction in FMEP with scale that is generally observed with reciprocating engines.

To facilitate a direct comparison, the current available data for the two engine sizes, both having the design configuration shown in figure 4 (BTC pilot) are compared on an Indicated basis and equivalent (same apex seal velocity) RPM in figure 11. From figure 11 it can be seen that the RC1-350 and RC1-60 are very close at the lower IMEP's, whereas the 1-60 data shows lower ISFC (or better thermal efficiency) at the higher loads, indicating further probable improvements for the larger engine. The difference is believed to reflect the concentration of effort at this speed for the smaller engine, in view of its automotive significance, whereas the low speed range of the larger engine is of less interest for current applications. For the reasons just stated there is less available RC1-60 data at the higher speeds, but what is available suggests that the thermal efficiencies are reasonably close for both engines.

Figure 12 compares the RC1-350 data of figure 11 plus available RC1-350 data for the "reversed" configuration (ATC pilot) mentioned earlier, versus  $F_{1,2}$  ratio. The observed data shows that for a given mixture strength the RC1-60 develops higher IMEP's at equivalent speed, which would imply more effective air utilization. This IMEP trend may be misleading because the engines were not run with similar induction systems. If the IMEP data is "normalized" by correction to an equal volumetric efficiency basis (which has little effect on other plotted variables), the RC1-60 and RC1-350 with BTC pilot are very close and the RC1-350 with ATC pilot is slightly higher at the increased power end. The higher thermal efficiency of the RC1-350 ATC pilot does not say that the differences noted will necessarily hold for the RC1-60 size but it does imply that there is additional potential to be realized.

Figure 13 shows both curves on a BSFC basis, reflecting the differences in friction. Figure 13 shows that, despite the lower thermal efficiency at higher power with the BTC pilot design, the RC1-350 shows a brake basis advantage over the RC1-60 because of the lower specific friction. The ATC pilot configuration curve reflects both friction and combustion advantages. In addition to lower friction, the 350 cubic inch engine enjoys the advantage of better injection and ignition equipment. The influence of this last point will be clearer when the current RC1-60 testing, which also enjoys a similar equipment advantage over the earlier work, has progressed further.

The conclusion of this comparison is that the engine scales well, although demonstrated only in the larger sized direction. The baseline data of the RC1-350 at higher powers and speeds, with the scaling trends noted, will be used to estimate performance for the aircraft engine regime. This input will be important when weighing the system advantages of a lighter, smaller multi-rotor aircraft engine versus a somewhat heavier, but less expensive and slightly more efficient, larger module single rotor engine. The factors influencing this balance process for the current NASA contract are thus in clear focus and Cessna Aircraft Co., under sub-contract to Curtiss-Wright, will study the aircraft system trade-off sensitivity of various engine size choices.

### Current NASA Advanced Engine Study

#### Approach and Status

The objectives of the current NASA Advanced Rotary Combustion Aircraft Engine Design Study contract are to define advanced and highly advanced engines which will satisfy the following goals and criteria:

1. Engine performance and efficiency improved as compared to current engines: BSFC  $\leq 0.38$  lb/hp-hr @ 75% power cruise; specific weight  $\leq 1.0$  lb/hp @ takeoff power; cooling airflow x pressure drop product decreased by a factor of 2.
2. Efficient operation on 100/130 octane aviation fuel and one or more alternative fuels such as jet or diesel fuel, or low octane unleaded automotive fuel.
3. Emissions that meet the EPA 1979 piston aircraft standards. (If and when the revocation of these standards occurs, this goal will be reevaluated).
4. Engine direct manufacturing costs comparable to or less than present day spark-ignition piston aircraft engines.
5. Overall life cycle costs and maintenance lower than for current aircraft engines.
6. Altitude capability equal to present day spark ignition aircraft engines.

The approach that has been taken was to first survey all parallel and related technologies for application to an extension of the Stratified Charge developments summarized earlier. A total of 35 significant sources were identified and solicited for information. In addition many hundreds of abstracts located by source search were read and 220 papers obtained.

From a review of data from the above contacts, papers, and previous technology information developed by Curtiss-Wright, the candidate technologies shown in Table I were selected for more detailed evaluation. The evaluation form (figure 14) was developed as a means of carrying out the procedure for

ranking of the candidate technologies. The technology evaluation criteria were utilized in a system patterned after the one described in ref. 9.

A technology base was defined from which new approach selections were made for an "advanced" engine. They were the approaches estimated to be the most advanced technologies sufficiently proven and highly ranked to be available to an engine design initiated in 1985 or 1986. It is estimated commercial introduction would take place in the early 1990's.

In addition a selection of design approaches for a "highly advanced" engine were made. These were higher risk approaches likely to require a more extensive development program and/or a later introduction to the commercial market.

As a result of this ranking process, with the additional balancing overview reflecting concentrated rotary engine experience of those who did not participate in ranking, specific candidate technologies were selected (Table II). These inputs will be used to define a conceptual design for the advanced engine. The "highly advanced" engine will be described but not defined with installation, cross-sectional drawings, performance data, etc. which will be developed for the advanced engine. Comparative system analysis will be performed, however, by Cessna for both engine concepts in compatible general aviation aircraft.

Until the design study has been completed and we can assess the relative trade-offs of these candidate technologies against the contract objectives and goals, we cannot specifically weigh contribution significance. However, the promising choices have been sufficiently defined in the aforementioned screening process to single out selected items which can illustrate, in the following paragraphs, the nature of our choices.

#### 1. Turbocharging

The requirement of a near-future aircraft engine (250 HP cruise class) for increased altitude (25,000 feet plus) capability has focused more attention on the effects of turbocharging. Here, the Rotary Stratified Engine more closely resembles a Diesel than a conventional gasoline fueled engine, because of its ability to run well on extremely lean mixture ratios. Increasing the air charge rate to the engine not only improves the fuel economy by raising the mechanical efficiency (i.e., getting more output for essentially the same friction losses), but it permits operation at A/F ratios which give the best combustion and thermal efficiency. The characteristic curve shape for ISFC vs. mixture strength, shown in figure 12 for low speed, holds for cruise speeds as well although the absolute values change with speed. In essence, the BSFC curve can effectively be driven down to lower levels as shown qualitatively in figure 15 (ref. 10).

The quantitative degree that can be practically realized remains an unknown at this point, but from trends observed on the current naturally aspirated stratified engines, an SFC reduction of 17 percent can be predicted by high power cruise turbocharging to increase the airflow from an approximately 18 to 28 air-fuel ratio. The baseline absolute value of BSFC for the stratified

charge naturally aspirated engine is probably not the same as it would be for the corresponding cruise point of a gasoline engine at its approximately 15:1 air-fuel ratio, but the turbocharged stratified charge cruise BSFC would be lower than either type (stratified or homogeneous) naturally aspirated engine.

## 2. Increased IMEP and Speed/Improved Apex Seal Wear Materials/Retracting Apex Seals

The increase of mean effective pressure is accomplished by the turbocharging described above, trading-off the complexities of boost ratios higher than can be attained from commercial low-cost turbocharger units against engine size. However, wherever this best point resolution obtains as a result of our current analyses, the fact remains that higher effective pressures will be required. These higher operating levels of temperature and pressure have both stress and durability implications, which in turn will be reflected in the selection of specific operating limits and design configurations, some of which will be briefly reviewed in succeeding paragraphs.

The same type of trade-off has to be made with respect to maximum operating speed. Higher speeds obviously increase the engine output and thus improve specific power density. The Rotary engine has significant growth potential in the higher speed direction because it is not limited by valve dynamics and valve breathing restrictions, has complete dynamic balance, does not reverse direction of its sealing elements at top center, and has a relatively modest increase of friction with speed. Nonetheless, friction increases exponentially with speed and unless this high speed capability is reserved only for take-off power, the best specific fuel consumption will dictate rating at the lowest possible speed consistent with acceptable specific weight. Again, the Cessna sensitivity study will provide some insights into how this higher speed capability can be best utilized.

### a. Improved Apex Seal/Trochoid Material Combinations

The increase in engine output may require further development of superior apex seal and trochoid wear surfacing materials which have either been identified by our prior research efforts or have emerged as new technologies. The current tungsten carbide trochoid wear surfacing material has thus far shown relatively low apex seal velocity sensitivity and is adequate, with acceptable TBO and reliability standards, for any operating speed under consideration (ref. 11). It will probably also prove acceptable, possibly with lower wear apex seals, for any of the IMEP levels which can be obtained with single stage turbocharging. However, to illustrate potential, figure 16 shows that use of a Titanium carbide trochoid coating, in this case in a steel matrix, and with apex seals of the same material, shows substantially less wear than current materials. The particular material shown in this figure was plasma sprayed, which is a less expensive application technique than the current detonation gun process. At this stage of development, plasma-spraying cannot attain the same bond strengths, but plasma-spray technology is moving very fast and is expected to be a serious contender within a short time.

#### b. Retracting Apex Seals

For a more ambitious technology step, which we reserve for the "Highly Advanced Design", it is possible to have the high specific output of high speed without facing the more severe apex seal wear environment of higher seal pressures plus higher speed. Since apex seal leakage is a time-weighted factor, at high engine speeds a small leakage area can be tolerated without serious consequence. Seal designs which retract from trochoid contact at high rotational speeds are available, but not tested. One of several alternate approaches, in this case taking advantage of the centrifugal forces to pull the seal back at high speeds, is shown in figure 17.

#### 3. High Strength High Temperature Aluminum Casting Alloy

The increases in IMEP and speed, as stated earlier, will introduce higher operating temperatures. The anticipated degree of temperature increase, to be confirmed as the current study progresses, can be paced by the degree of strength improvement that new materials have introduced. The choice of liquid cooling for general aviation engines (ref. 10) on the basis of improved system efficiency and better metal temperature control is particularly significant at the higher outputs of the advanced engines.

Essentially all of our Rotary engine cast aluminum rotor housings have been AMS 4220, based on our reciprocating aircraft engine experience. It has proven to be a durable high temperature material with good fatigue life under cyclic loading. A new aluminum high temperature casting alloy, AMS 4229, has been on the scene for several years. It has not been tried here because our applications have not required the additional strength and, until recently, very few foundries were willing to cast the new alloy. Today, however, 15 foundries in the U.S. use this alloy, which has markedly higher strength and ductility than AMS 4220.

Figure 18 shows calculated predictions, based on ultimate tensile strength, ductility, and modulus of elasticity, of low cycle thermal fatigue life at 400°F, representative of high power cruise peak temperatures, for AMS 4220 and 4229. The same type of improvements can be demonstrated at higher temperature levels, should they prove desirable as the study progresses.

#### 4. Rotor Combustion Flank Insulation/Adiabatic Engine

The background discussion of Stratified Charge hydrocarbon testing made reference to rotor combustion surfaces which were raised in temperature, by use of insulated plates, to reduce HC formation. HC formation is not expected to be a consideration for an aircraft engine operating regime (ref. 10), but the insulated rotor surface will reduce oil heat rejection and thus reduce system weight and bulk.

Early testing with the RC engine had shown that Zirconium oxide, plasma sprayed on the rotor combustion face, was effective with gasoline homogeneous charge engines, but did not have adequate thermal shock strength in a stratified charge application where direct fuel impingement was possible. However,



considerable development of thermal barrier coatings of this type has taken place, largely at NASA-Lewis, since that time, particularly for gas turbine components.

The "Highly Advanced Engine" (Table II) reflects inclusion of a zirconium oxide rotor hot surface coating of .060" thickness. Figure 19 shows that, for an assumed 90"³ rotor this coating thickness is calculated to reduce the rotor heat rejection to the engine oil by approximately one third.

The same type of coating would also be applicable for an "Adiabatic" Rotary engine. However, despite the fact that we consider Rotary engines intrinsically more adaptable to the completely unlubricated "Adiabatic" engine approach than a reciprocating engine (largely because either retracting or the uni-directional ceramic apex seals with their advantage of gas hydrodynamic film lubrication, against a ceramic trochoid surface appear closer to realization than their reciprocating counterparts) we did not consider an engine of this type to be within contract objective guidelines of even the "highly advanced design technology" and did not consider it further.

#### Directions

Our present carbureted prototype aircraft engine, the liquid-cooled RC2-75 (ref. 10) shown in figures 20 and 21 was the obvious starting point. To illustrate what the presently planned trends of higher IMEP and RPM would mean in terms of this engine, mock-ups of both single and twin rotor 75 cubic inch Stratified Charge and turbocharged aircraft engines have been prepared to supplement this presentation. The RC1-75, which measures 34 1/2" x 21 1/2" x 20", without coolers, is predicted to develop 235 HP @ take-off under currently envisioned limits for IMEP and speed for the advanced engine and 300 HP for the "Highly Advanced" technology. The same numbers for the RC2-75 are 40 1/4" x 21 1/2" x 20" and 470 HP and 600 HP for respective technology levels. Taking the same values of IMEP and speed used to make the advanced engine estimates, and applying it to the contract goal engine of 250 HP cruise to 25,000 feet, results in a two rotor engine outline as shown in figure 22. The coolant and oil coolers, which presumably would be remotely located for system optimization, are not included.

This particular arrangement, with accessories held to a minimum overall diameter, would be biased towards a twin engine installation. However, it should be understood that this is a preliminary look since, as stated earlier, the economic advantages, as well as fuel injection technology limits, favor a larger single rotor engine and, secondarily, more precise definition of IMEP and speed, upon which these projections were based, is still being determined.

While the specifics may vary from those defined at the point when all work on this contract has been completed, the effort to date has clarified what we see as the advantages of this type of Rotary Stratified Charge engine. These are listed in Table III.

### Closure

The Rotary Engine, in its carbureted form, is uniquely suited to aircraft engine propulsion because of its advantages of size, weight, simplicity, smoothness, scaling flexibility and growth potential. Recent parallel hardware and test developments have shown that this engine type is particularly adaptable to unthrottled direct injected stratified charge, resulting in additional features of wide range fuel capability and superior fuel economy. As a result of the Stratified Charge Rotary Engine's ability to perform efficiently over a broader range of mixture strengths, without regard for fuel octane or cetane rating, turbocharging can extend the demonstrated potential to the complete aircraft engine operating regime. This combination of system efficiency plus fuel choice optimization possibilities is being carefully examined as we continue into an era of critical energy resource allocations.

## REFERENCES

1. Jones, Charles; Lamping, Harold D.; Myers, David M.; and Loyd, R.W.:  
An Update of the Direct Injected Stratified Charge Rotary Combustion  
Engine Developments at Curtiss-Wright. SAE Transactions 1978, Paper  
No. 770044.
2. Jones, Charles: A Survey of Curtiss-Wright's 1958-1971 Rotating Combustion  
Engine Technological Developments. Paper No. 720468, May 1979.
3. Hofbauer, P.; and Stator K.: Advanced Power Systems, Part 2 - A Diesel  
for a Sub-compact Car. SAE Paper No. 770113, February 1977.
4. Contract No. DOT-TSC-1193 Contractor's Presentation, September 1977:  
Data Base for Lightweight Automotive Diesel Power Plants - Volkswagenwerk  
AG.
5. Wiedemann, B.; and Hofbauer P.: Data Base for Light-Weight Automotive  
Diesel Power Plants. SAE Paper No. 780634, June 1978.
6. Tierney, W.T.; Johnson, E.M.; and Crawford, N.R.: Energy Conservation of  
the Vehicle-Fuel-Refinery System. SAE Paper No. 750673, June 1975.
7. Tierney, W.T.; and Wilson, R.F.: Adequate Future Transportation Demands  
Vehicle-Fuel-Refinery System Optimization Today. Presented at the API  
Michigan Meeting, January 1976.
8. Jones, Charles: A Progress Report on Curtiss-Wright's Rotary Stratified  
Charge Engine Development. SAE Paper No. 741206, October 1974.
9. Bergey, Karl H.: New Technologies for General Aviation Aircraft. SAE  
Paper No. 790613, April 1979.
10. Jones, Charles: A Review of Curtiss-Wright's Rotary Engine Developments  
with Respect to General Aviation Potential. SAE Paper No. 790621,  
April 1979.
11. Lamping, Harold D.; Galliers, M.W.; and Wolosin, S.M.: Rotary Combustion  
Engine Trochoid Coatings and Seals. SAE Paper No. 741043, October 1974.

TABLE I  
CANDIDATE TECHNOLOGIES CONSIDERED

SOLID-STATE IGNITION TRIGGER VS MECHANICAL TRIGGER	RETRACTING APEX SEALS
PIESMA JET IGNITION SYSTEM	THERMOSTATICALLY CONTROLLED MOTOR OIL COOLING
ELIMINATING PILOT INJECTOR	TURBOCHARGER WITH VARIABLE AREA TURBINE
HIGH TEMPERATURE ALUMINUM CASTINGS	SPARK IGNITION START/AUTO-IGNITION RUN
TURBOCHARGER	ALUMINUM ROTOR (REINFORCED LAMDS)
THIN WALL (IRON) ROTOR	INSULATED ROTOR - THERMAL BARRIER COATING
EXHAUST PORT THERMAL LINER (METALLIC)	INDEPENDENT DUAL IGNITION
IMPROVED LUBRICANTS	VARIABLE COMPRESSION RATIO
MULTIPLE POWER SOURCE FOR IGNITION	INSULATED ROTOR - INSERTS ON METALLIC PAG INSULATOR
INDUCTION AIR INTERCOOLER	ADIABATIC ENGINE CERAMIC END WALLS
VARIABLE DISPLACEMENT PRESSURE OIL PUMP	COMPOSITE ROTOR (REINFORCED APEX SEAL LAMDS)
PROVISION FOR COUNTER-ROTATING PROPELLERS	ELECTRONIC INJECTION (FUEL)
TOTAL DIAGNOSTICS	ADIABATIC ENGINE CERAMIC ROTOR INSERTS
ELECTRONIC IGNITION SCHEDULE	TURBOCOMPOUND
COMPUTER VS MECHANICAL TIMING	ADIABATIC ENGINE - CERAMIC ROTOR HOUSING LINER
FIBER OPTICS DATA BUS	PILOT NOZZLE TRIGGER FOR IGNITION SYSTEM
LOW PRESSURE DROP HEAT EXCHANGERS	HIGH SPEED PROPELLER (NO REDUCTION GEAR)
MAGNETIC TRACTION SPEED REDUCER (PROP)	MAGNETIC TRACTION SPEED REDUCER (TURBOCOMPOUND DRIVE - IF USED)
ALTERNATE COOLING FLUID	ADIABATIC ENGINE - CERAMIC ROLLING ELEMENT BEARINGS
COMPOSITE ROTOR HOUSING (WEAR RESISTANT LINER)	
WING LEADING EDGE WITH INTEGRAL COOLANT COOLER	
ALTERNATE MATERIALS SEALS	

TABLE II  
NEW TECHNOLOGY SURVEY: CANDIDATE TECHNOLOGIES SELECTED FOR DESIGN STUDY

ADVANCED DESIGN

TURBOCHARGING

HIGH STRENGTH HIGH TEMPERATURE ALUMINUM CASTING ALLOY

LIGHTWEIGHT ROTOR

EXHAUST PORT THERMAL LINER

INDUCTION AIR INTERCOOLER

COUNTER-ROTATING PROPELLERS

ON-BOARD DIAGNOSTICS

IMPROVED APEX SEAL/TROCHOID MATERIAL COMBINATIONS

INCREASED IMEP AND SPEED

HIGHLY ADVANCED DESIGN

VARIABLE AREA TURBINE TURBOCHARGER

RETRACTING APEX SEALS

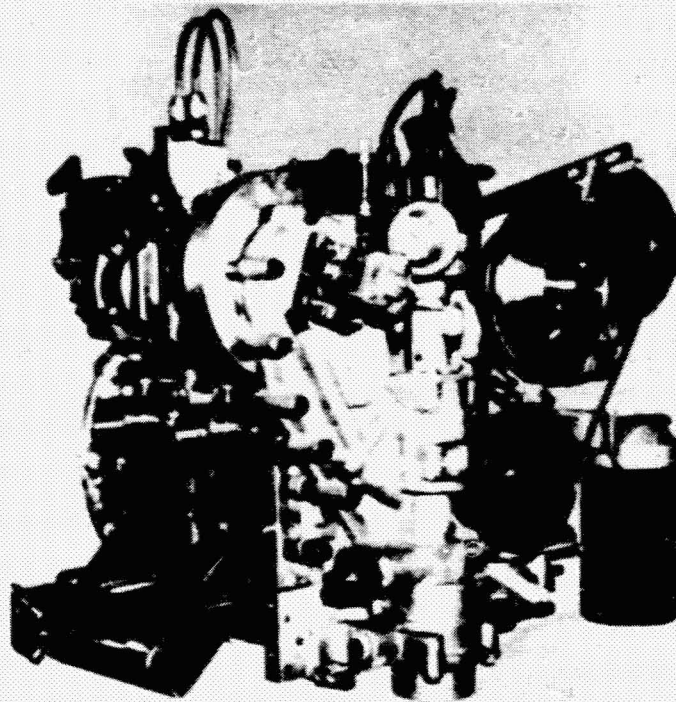
ROTOR COMBUSTION FLANK INSULATION

ADDITIONAL INCREASED IMEP AND RPM

**TABLE III**  
**ADVANTAGES OF THE ROTARY STRATIFIED CHARGE AIRCRAFT ENGINE**

MULTI-FUEL CAPABILITY  
SMALL FRONTAL AREA  
LOW ENGINE WEIGHT  
REDUCED ENGINE COOLING AIR DRAG  
IMPROVED RELIABILITY DUE TO FEWER PARTS  
LOWER EXHAUST GAS TEMPERATURES  
NO VALVES OR CAMS  
SAFER CABIN HEAT  
COOLANT COOLERS CAN BE WING DE-ICING  
MORE RAPID FLIGHT DESCENTS PERMISSIBLE  
LOW COST TURBOCHARGER FROM OTHER PRODUCTION RETAINED  
SMALL EXHAUST AND INTAKE MANIFOLD VOLUMES BENEFIT TURBOCHARGING  
LOW EXHAUST EMISSIONS  
LOW FUEL CONSUMPTION  
SMOOTH - BALANCED OPERATION  
GOOD LOW TEMPERATURE STARTING CAPABILITY  
LOW NOISE LEVEL  
PROVEN PRODUCTIBILITY OF ROTARY ENGINE

# RC2-60U10 LIQUID-COOLED STRATIFIED ENGINE (1965)



WEIGHT.....294 LB

WIDTH.....24 IN.

LENGTH.....24 IN.

HEIGHT.....24 IN.

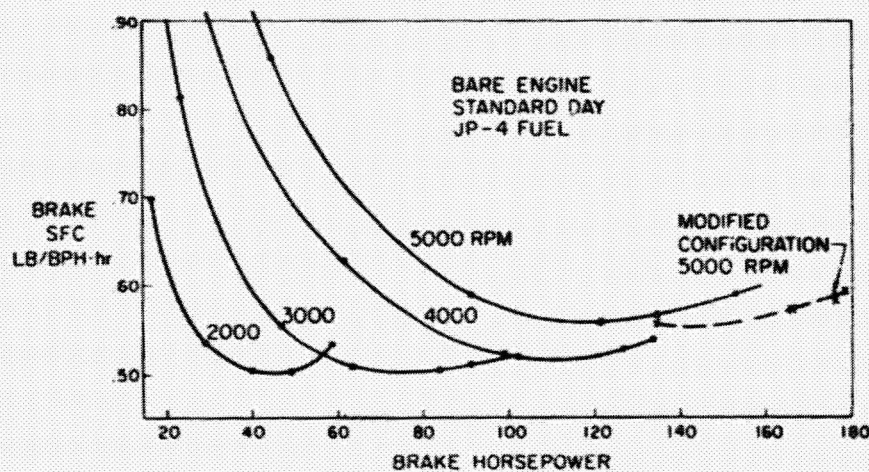
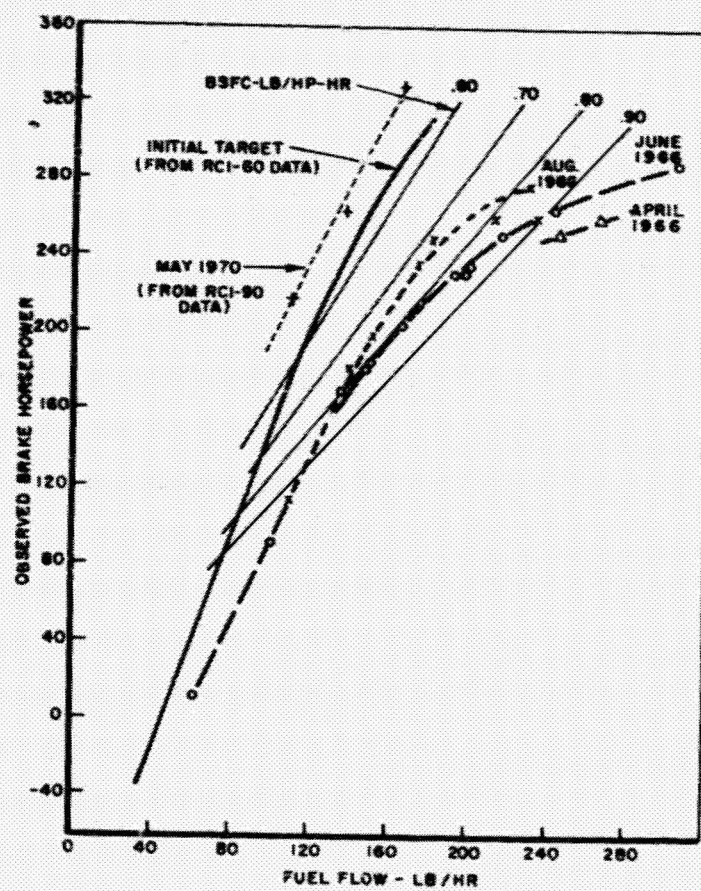
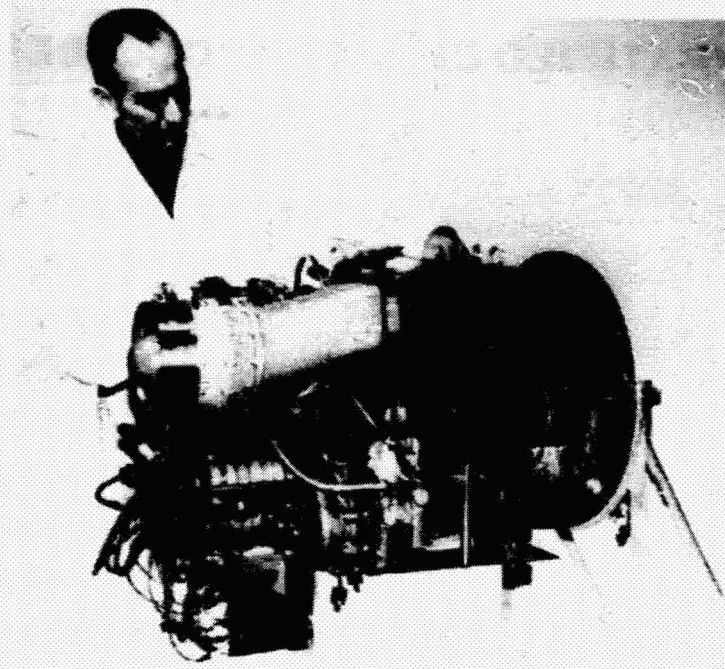


Figure 1





RC2-90 AIR-COOLED STRATIFIED CHARGE RC ENGINE (1966)

Figure 2

ORIGINAL PAGE IS  
OF POOR QUALITY

## STRATIFIED CHARGE PROCESSES

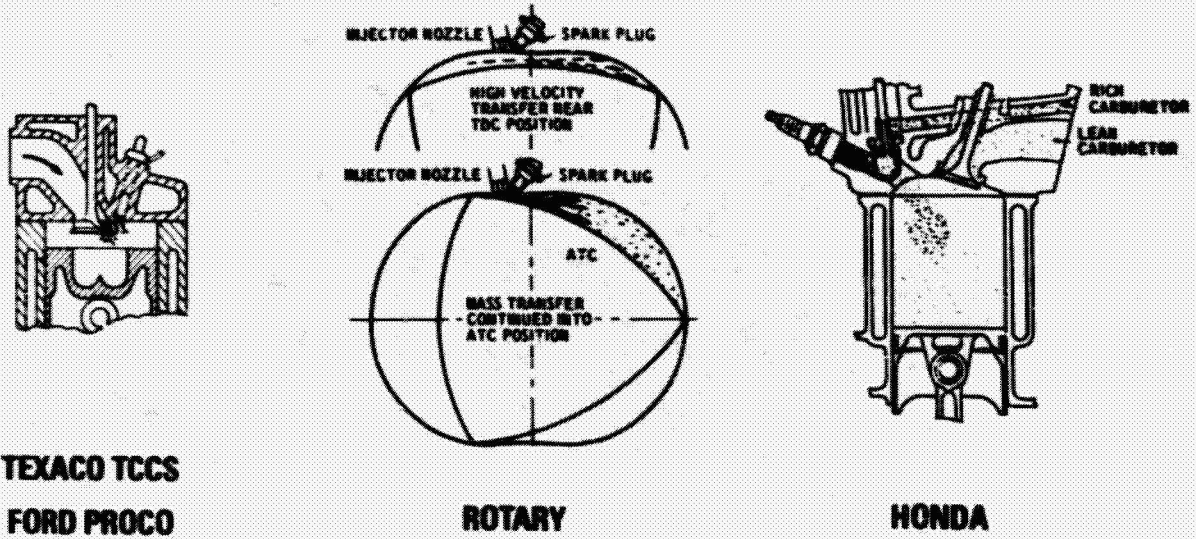


Figure 3

## BTC PILOT TANDEM DUAL

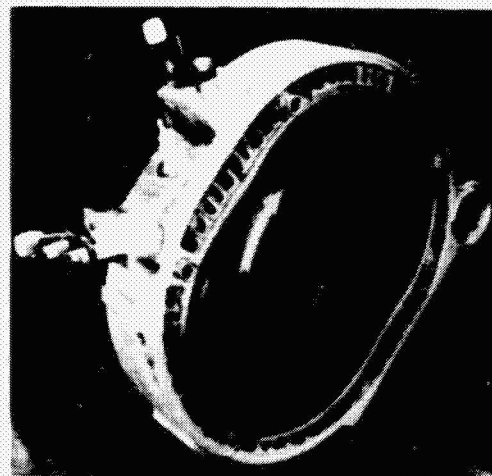
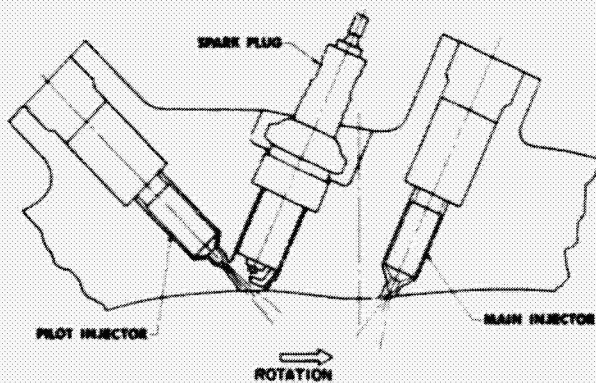


Figure 4



## SPECIFIC HYDROCARBON EMISSIONS

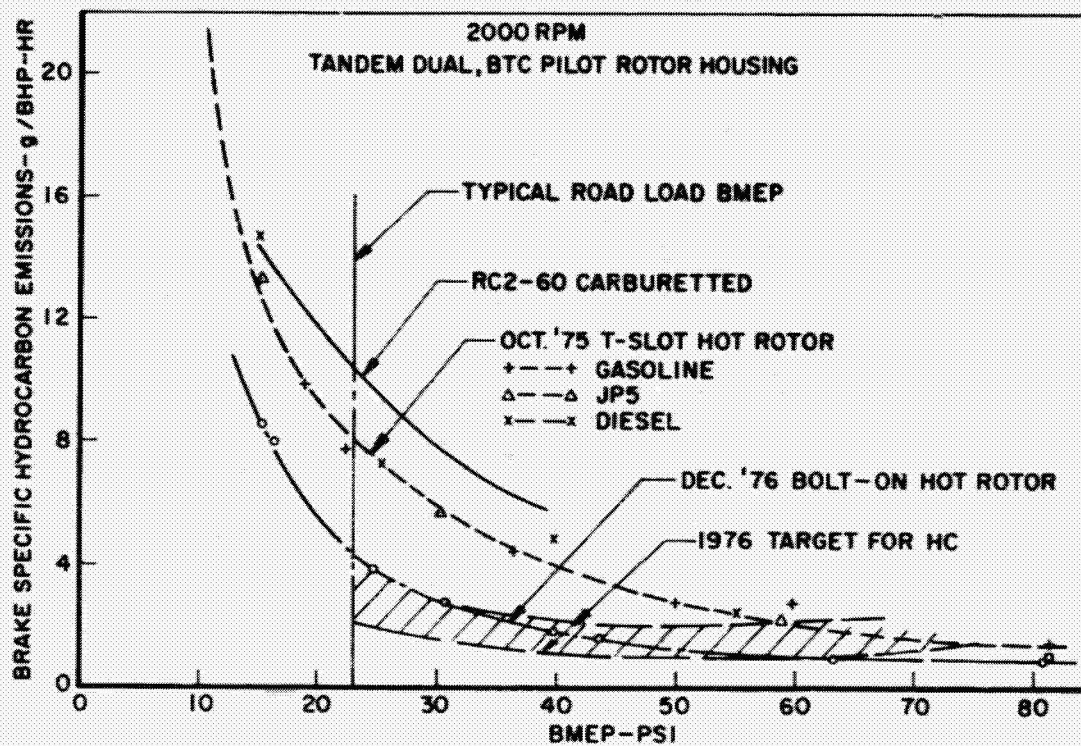


Figure 5

## ISFC vs MEP, RC1-60 BTC PILOT

Preliminary Data for 10:1 Compression Ratio vs 8.5:1

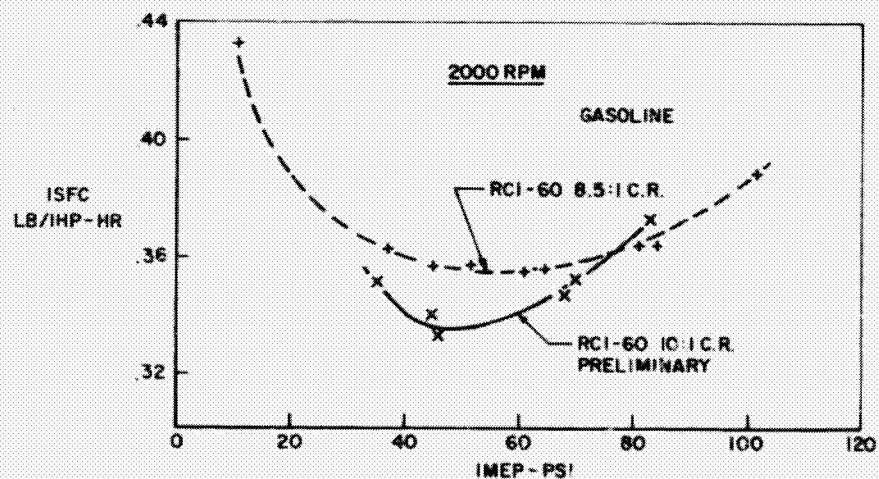


Figure 6

## PART LOAD FUEL CONSUMPTION COMPARISON SCRE VS AUTOMOTIVE PRE-CHAMBER DIESEL

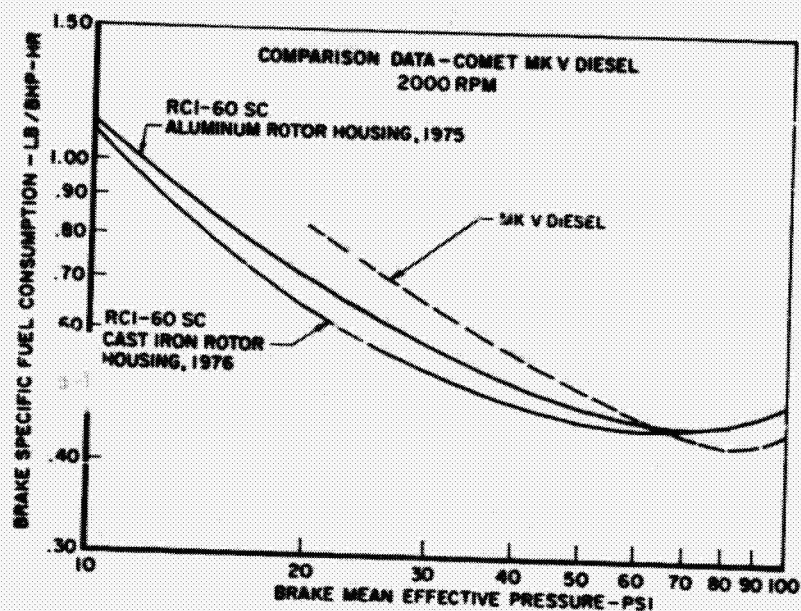


Figure 7

## COMPARISON DATA - BSFC vs BMEP

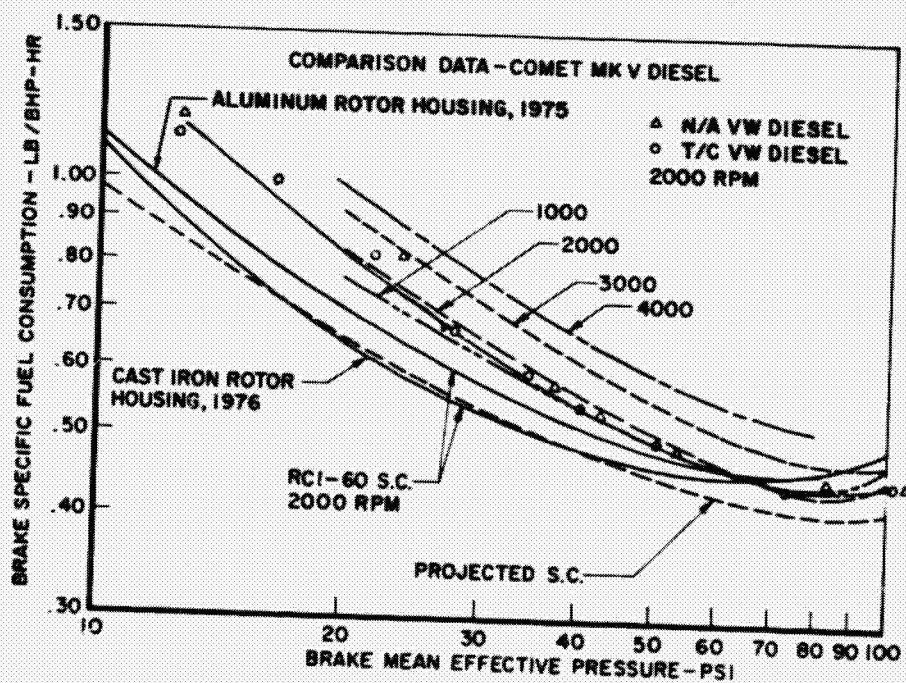
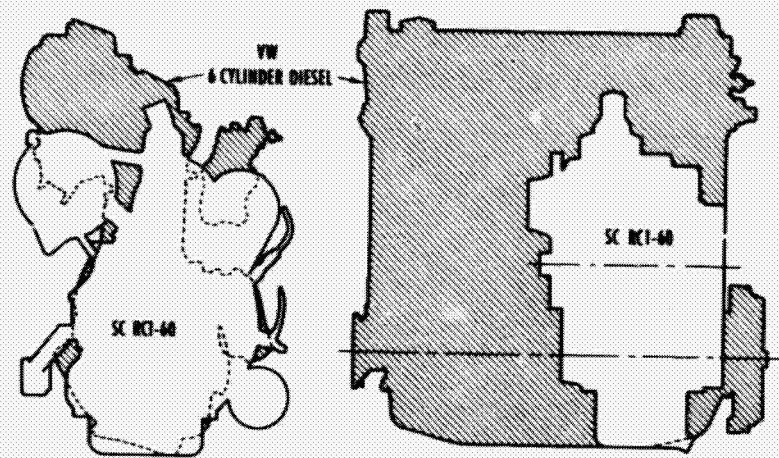


Figure 8

# COMPARISON OF SC RC1-60 WITH VOLKSWAGON 6 CYLINDER DIESEL



	SC RC1-60	VW 6 CYL. DIESEL
kW (BHP) RPM	60 (80) 5000	56 (75) 4500
kg (LB)	109 (240)	104 (405)
L x W x H	368 x 559 x 635	700 x 490 x 700
INCHES	14.5 x 22 x 25	30.7 x 19.3 x 30.7

Figure 9

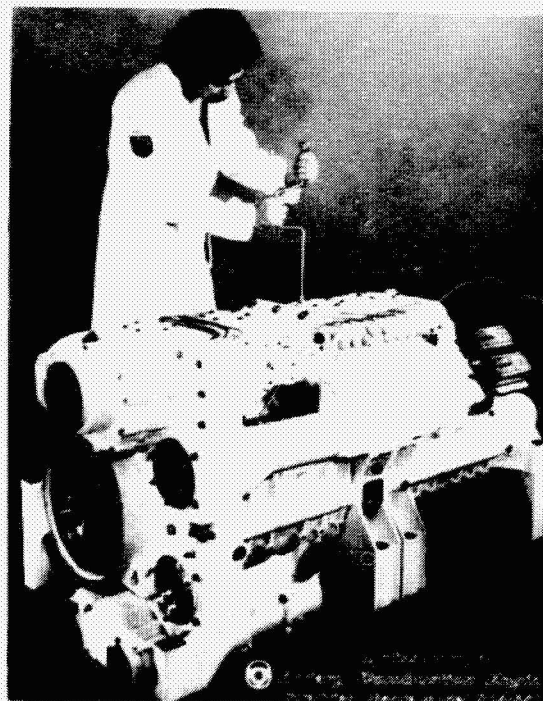


Figure 10

ORIGINAL PAGE IS  
OF POOR QUALITY

# **INDICATED SPECIFIC FUEL CONSUMPTION (ISFC) VS INDICATED MEAN EFFECTIVE PRESSURE (IMEP)** Comparison of RCI-60 and RCI-350 Data, BTC Pilot

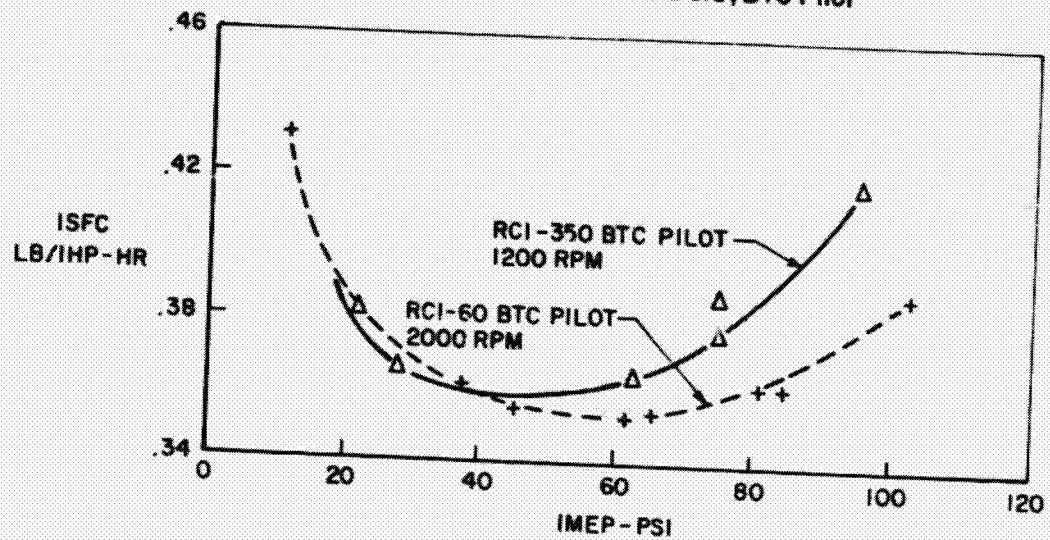


Figure 11

## **IMEP AND ISFC VS FUEL-AIR RATIO** RCI-60 and RCI-350

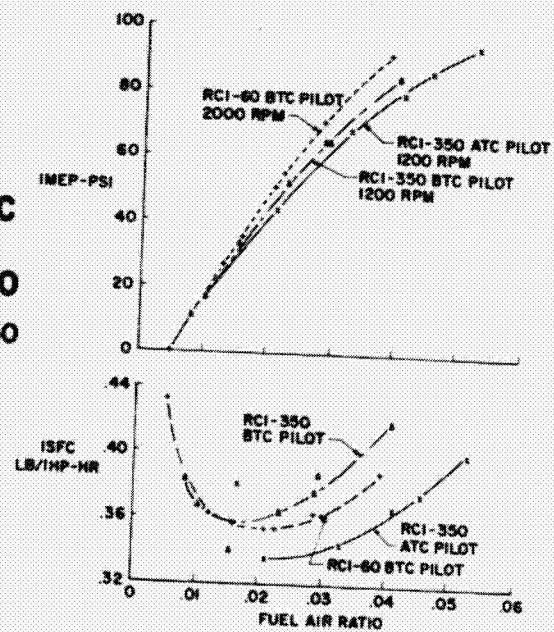


Figure 12

### BSFC vs BMEP, RCI-60 AND RCI-350

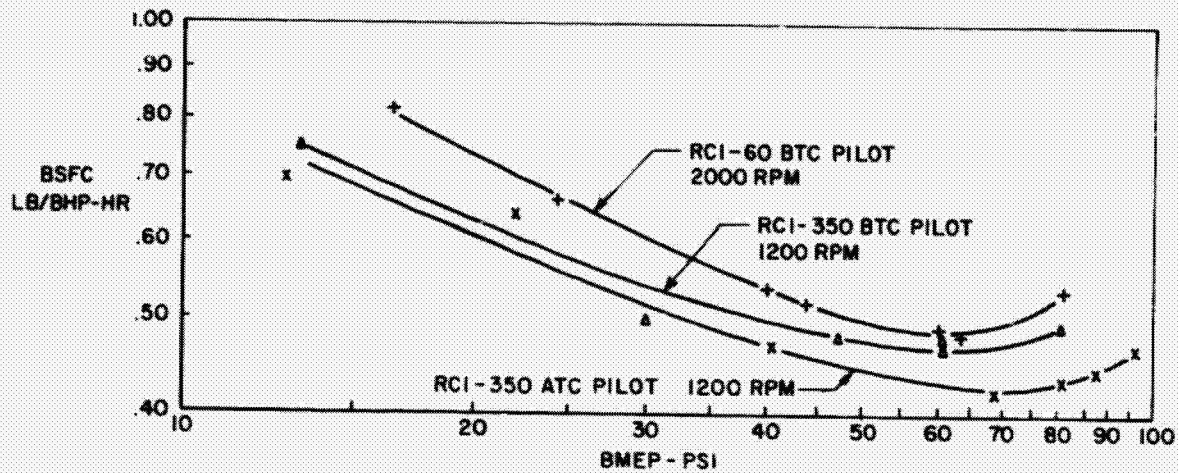


Figure 13

### ADVANCE ROTARY COMBUSTION AIRCRAFT ENGINE TECHNOLOGY/APPROACH EVALUATION

DESCRIPTION: \_\_\_\_\_ ITEM NO. \_\_\_\_\_

CRITERION	WEIGHTING	RATING (+3 to -3)		PRODUCT (WtR)	
Safety	8				
Reliability	8				
Fuel Consumption	7				
Weight	7				
Cooling	7				
Initial Cost	7				
Multi-fuel Capability	7				
Performance	7				
Technological Uncertainty	6				
Life Cycle Cost	6				
Size & Shape	6				
Operational Characteristics	6				
Durability	5				
Maintainability	5				
Materials	3				
Noise	3				
Emissions	2				
TOTAL FIGURE OF MERIT		A	B	A	B

NOTES  
A - ADVANCED  
B - HIGHLY ADVANCED

Figure 14

EFFECT OF DECREASING STRATIFIED CHARGE  
ROTARY ENGINE DISPLACEMENT  
WITH CORRESPONDING INCREASE IN  
DEGREE OF TURBO-CHARGING

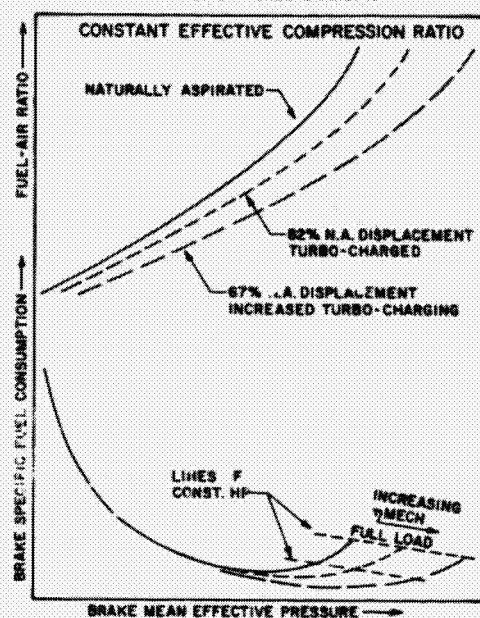


Figure 15

FERRO-TIC APEX SEAL HEIGHT WEAR AGAINST PLASMA SPRAYED  
FERRO-TIC TROCHOID COATING

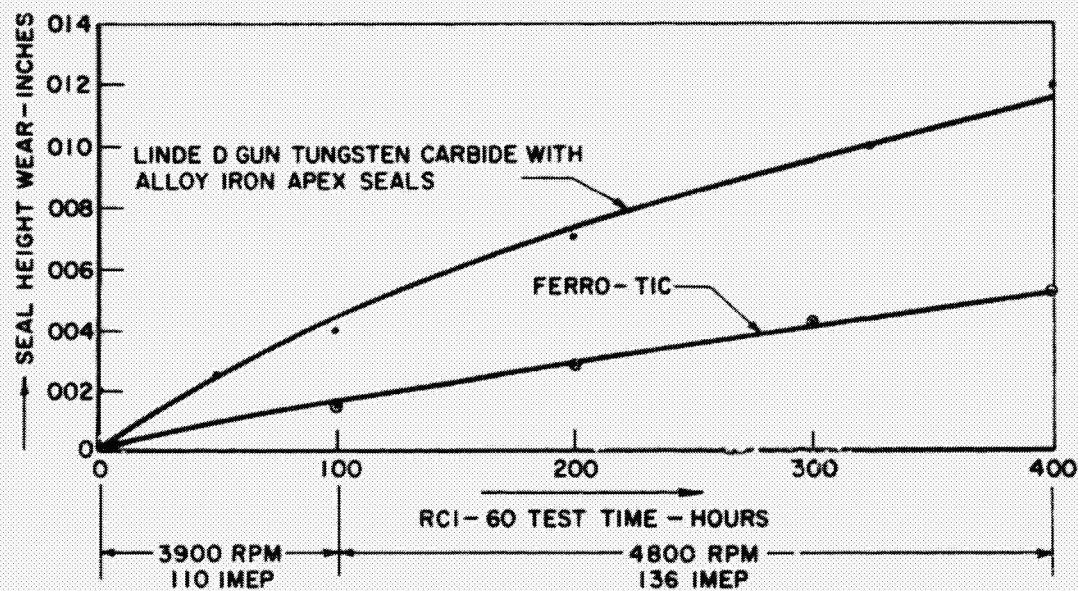


Figure 16

## COUNTERWEIGHT RETRACTED SEAL

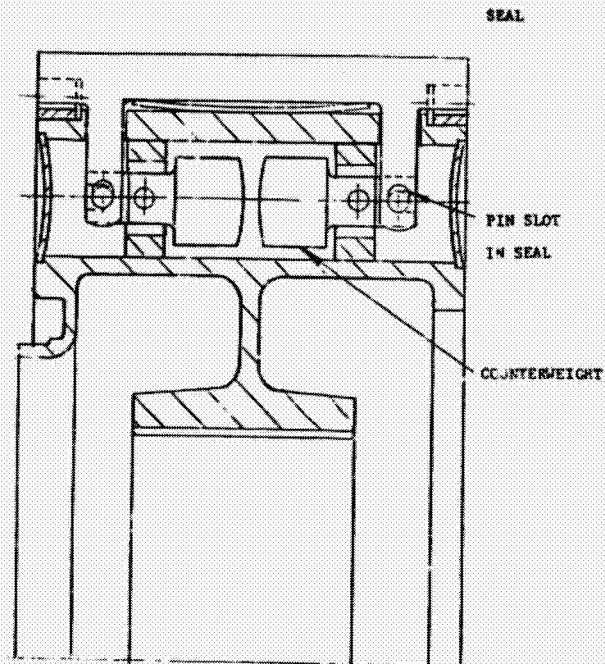


Figure 17

## LOW CYCLE THERMAL FATIGUE COMPARISON

STRESS LEVEL VS LIFE CYCLES  
AMS 4229 AND AMS 4220

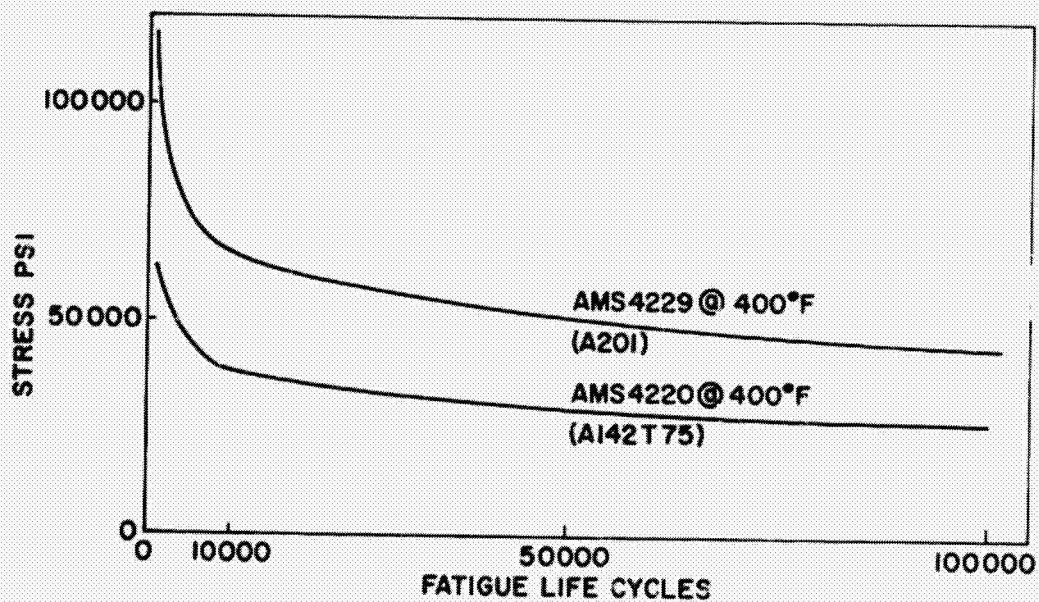


Figure 18

# RCI-90 ROTOR INSULATED WITH ZIRCONIUM OXIDE (ROKIDE Z)

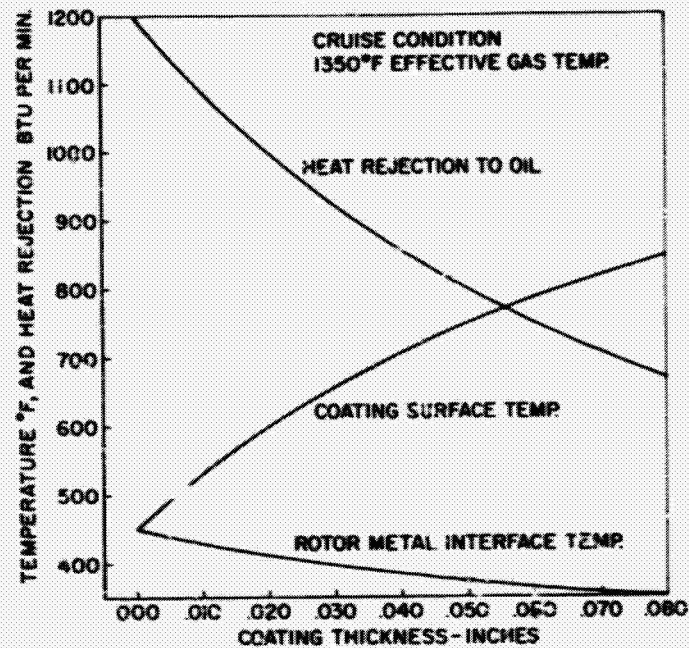


Figure 19

# RC2-75 AIRCRAFT ENGINE PROTOTYPE



Figure 20



## RC2-75 ON PROPELLER TEST STAND

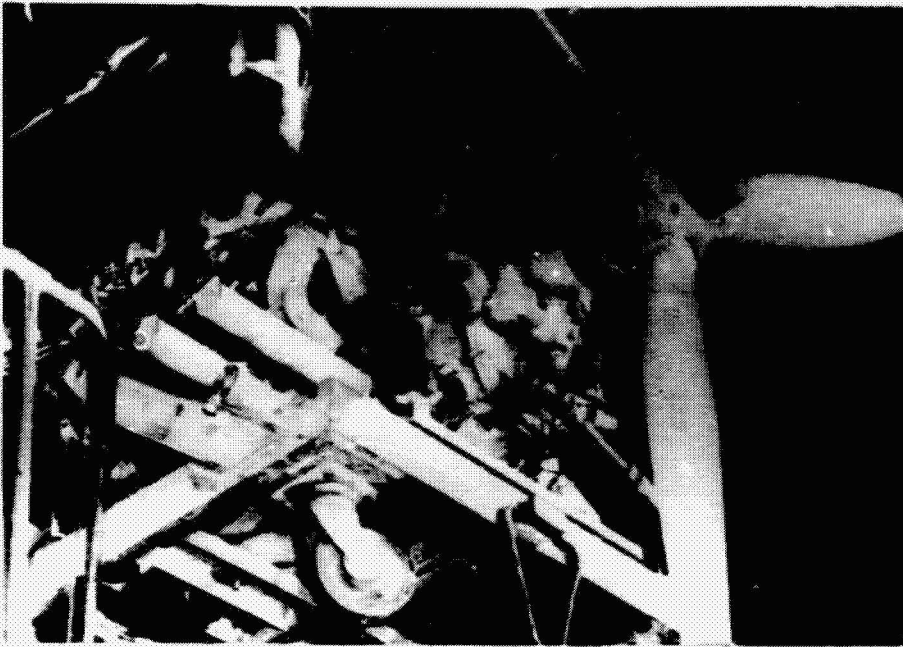


Figure 21

## ADVANCED ROTARY COMBUSTION AIRCRAFT ENGINE PRELIMINARY INSTALLATION STUDY (250 BHP MAXIMUM CRUISE TO 25000 FEET)

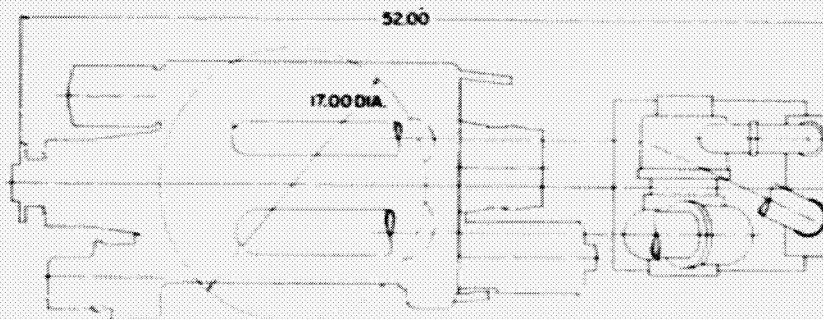


Figure 22

ORIGINAL PAGE 18  
OF POOR QUALITY

213  
N80-22340

**POSITIVE DISPLACEMENT TYPE GENERAL-AVIATION ENGINES:  
SUMMARY AND CONCLUDING REMARKS**

**Erwin E. Kempke, Jr.  
National Aeronautics and Space Administration  
Lewis Research Center**

During this session, the internal combustion engine program, its status and accomplishments have been presented. Both the near and longer term technical thrusts were discussed. Significant progress on both fronts has been made.

In the near term conventional engine area the integration of four modifications in a test engine provides for a 10 percent improvement in the high-performance-cruise fuel economy while meeting the emissions standards.

A new program aimed at improved cooling and drag reduction has been established. The Phase I effort on improved-cylinder head-and-barrel cooling will be underway at Teledyne Continental Motors, Aircraft Products Division, by the end of this year.

The grant program to develop and verify a realistic Otto cycle computer model shows significant progress at the two-thirds completion point. Today, calculations of two-dimensional unsteady, turbulent, compressible flow with moving boundaries are being made. The related ambitious experimental program to develop advanced combustion diagnostic techniques has been completed.

In the fuel-injection technology program the contract to Spectron is quantitatively characterizing the performance of various injector nozzles. The in-house flow visualization work is studying the same set of nozzles under motored engine conditions by means of high-speed photography.

The effort to define the benefits and requirements of advanced but cost effective turbocharger technology has been initiated. The RFP for Phase I is expected to be issued in early 1980.

For the longer term the results of the on-going studies involving alternative engine configurations were presented. The advanced spark-ignition piston engine study, which is 75 percent complete, shows 0.33 and 0.36 BSFC for the stratified charge and lean burn concepts, respectively. The two-stroke diesel shows 0.36 BSFC and 1.07 lb/hp for the 250-hp cruise version. The stratified-charge rotary engine study, which has been completed to the technology assessment task, continues to be a viable candidate.

The airplane and mission studies by Beech and Cessna will soon be underway. Results from these studies and the on-going Lewis effort will objectively evaluate, rank, and compare the three study engines with each other, with representative current-production engines, and with a highly advanced small

turboprop in terms relevant to the industry. The result of these activities in late FY 80 will be recommendations as to which concepts merit serious technology enablement programs.

The supporting research and technology included both contract and in-house elements. Diesel and rotary engine test cells at Lewis are now operational with baseline mapping complete. Active research programs are underway in such areas as supercharge versus compression ratio tradeoffs for optimum performance; fuel-injection rate, timing, and other parameters; and ceramic combustion-chamber insulation materials. A Curtiss-Wright program confirmed that efficiency improvements in the RC2-75 could be achieved by increasing compression ratio and relocating spark plugs: the BSFC at cruise was improved from 0.54 originally to 0.47.

The University of Michigan, working under a NASA grant, recently completed feasibility tests of a dieselized current-production spark ignition cylinder. These tests indicated that moderate firing pressures at low compression ratio resulted in improved cruise BSFC, thus indicating the possibility for considerably reducing the specific weight of a diesel.

In conclusion, the results of the near-term conventional engine activities have shown that it may soon be possible to improve both economy and cooling efficiency. Since the technology is being developed in terms of current production engines under the constraint of remaining compatible with existing facilities, processes, etc., it can be incorporated into OEM production with little adverse effect. By the same token this technology is potentially available for incorporation by retrofit.

Farther into the future it appears that the internal combustion engines discussed today are all viable candidates. They have the potential of improving significantly on the present situation in terms of fuel economy, weight, alternative fuels capability, and other characteristics. In addition to these readily quantifiable benefits, there are further benefits in the areas of safety and all-around utility. Over-the-weather cruise altitude capabilities could eliminate up to 25 percent of all weather-related accidents at the same time it is providing more efficient and comfortable flying conditions. Although the candidate engine selection process will be difficult, it is anticipated that a preliminary selection may be possible after comparative engine/airframe results are in hand. However, regardless of which candidate is selected, the potential powerplant advancements are synergistic with expected improvements in structures, aerodynamics, materials, and avionics which together will result in significantly improved airplanes for the 1990's and beyond.

314  
N 80-22341

## NASA PROPELLER TECHNOLOGY PROGRAM

Daniel C. Mikkelsen  
National Aeronautics and Space Administration  
Lewis Research Center

The vast majority of general-aviation aircraft manufactured in the United States are propeller powered (approximately 98 percent in 1978). Most of these aircraft use propeller designs based on technology that has not changed significantly since the 1940's and early 1950's. This older technology has been adequate; however, with the current world energy shortage and the possibility of more stringent noise regulations, improved technology is needed. Studies conducted by NASA and industry indicate that there are a number of improvements in the technology of general-aviation propellers that could lead to significant energy savings. New concepts like blade sweep, proplets, and composite materials, along with advanced analysis techniques have the potential for improving the performance and lowering the noise of future propeller-powered aircraft that cruise at low speeds. Current propeller-powered general-aviation aircraft are limited by propeller compressibility losses to maximum cruise speeds near Mach 0.5. The technology being developed as part of NASA's Advanced Turboprop Project offers the potential of extending this limit to at least Mach 0.8. At these higher cruise speeds, advanced turboprop propulsion has the potential of large energy savings compared with aircraft powered by advanced turbofan systems.

This paper summarizes NASA's program on propeller technology applicable to both low and high speed general-aviation aircraft, and outlines the overall program objectives and approach.

### EFFICIENCY TRENDS

The free-air propeller is the propulsive device that has the highest level of inherent efficiency for subsonic aircraft. A comparison of the installed cruise efficiency of propeller-powered and turbofan-powered propulsion systems is shown in figure 1 for a range of cruise speeds. The installation losses included with the propeller-powered systems are nacelle drag and internal cooling airflow losses. For the turbofan-powered systems the losses include fan cowl external drag and the internal fan airflow losses associated with inlet recovery and nozzle efficiency. The installed efficiency available with current technology propeller-powered general-aviation (GA) aircraft ranges from about 70 to 75 percent for reciprocating powered applications to slightly over 80 percent for turboprops. The reciprocating system performance is slightly lower due to higher nacelle drag and large internal cooling airflow losses (ref. 1). The installed performance of the current lower speed turboprop systems remains high to about Mach 0.5; about this speed, efficiency falls off significantly because of large propeller compressibility losses. These propellers are generally designed with blades of thickness to chord ratios (at 75 percent radius) that range from about 5 to 7 percent. These rather thick blades, when operated at relatively high tip helical Mach numbers, are the main cause of these losses.

The advanced, high-speed turboprop shown in figure 1 is a new propulsion concept that has the potential of eliminating or minimizing compressibility losses at flight speeds to Mach 0.8. The level of potential installed efficiency projected for the advanced turboprop is considerably higher than that available with comparable technology high-bypass turbofan systems. At Mach 0.8 the installed efficiency of turbofan systems would be approximately 65 percent compared with about 75 percent for the advanced turboprop. This large performance advantage for the advanced turboprop may offer the potential for some attractive energy savings for future high performance business aircraft.

#### ADVANCED, HIGH-SPEED TURBOPROP

To achieve the performance potential of the advanced, high-speed turboprop, several new concepts and advanced technologies are required. (See fig. 2.) These new concepts and advanced technologies are discussed in references 2 and 3. The advanced propeller would be powered by a large, modern turboshaft engine and gearbox to provide the maximum power to the propeller with a minimum engine fuel consumption. Propeller efficiency would be kept high by minimizing compressibility losses. In the outboard part of the propeller blading, these losses would be minimized by using sweep and thin blade sections (2.4 percent thickness to chord ratio at 75 percent radius). Blade sweep would also reduce propeller source noise both during takeoff and landing and during high-speed cruise. In the inboard region an area-ruled spinner, in combination with an integrated nacelle shape, would be used to reduce the local velocities through the propeller to minimize losses in this region. A power loading (shaft horsepower divided by propeller diameter squared) about five times higher than that in current GA turboprops would be used to minimize propeller diameter and weight. Eight or ten blades would be required to maximize ideal efficiency during high-altitude, high-speed cruise. In addition to these advanced concepts a modern blade fabrication technique would be used to construct the thin, highly swept and twisted blades.

The program that NASA has underway to address the technology requirements of the advanced turboprop is shown in figure 3. The advanced turboprop project, part of NASA's Aircraft Energy Efficiency (ACEE) program, has the goals of a 15 to 30 percent fuel saving relative to turbofan-powered aircraft, a significant reduction in turboprop propulsion-system-related operating costs, and a cabin ride quality equivalent to the best turbofan-powered aircraft. The four major elements of the advanced turboprop project are shown in figure 3.

In the first, propeller and nacelle, technology work is currently underway in propeller aerodynamics, acoustics, and blade structures. The use of advanced aerodynamics concepts in the design of high-speed propellers is discussed in reference 2, and some recent wind tunnel results are presented in reference 4. A photograph of an advanced high-speed propeller model is shown in figure 4. This model, along with three others, was tested in the Lewis 8- by 6-foot wind tunnel. High performance and some significant noise reductions were obtained during high-speed cruise testing of these models. Some design study results on advanced propeller acoustics and blade structures are contained in references 5 and 6.

The second major project element, cabin environment (fig. 3), concerns the aircraft fuselage, which may be in the direct noise path of the propeller. The fuselage will have to adequately attenuate this noise source if the cabin environmental goals are to be achieved. Some recent analytical studies on fuselage interior noise control for high-speed turboprops are presented in references 7 and 8. Fuselage vibration is also an important cabin environmental consideration, and future advanced turboprop aircraft will have to be designed to minimize or control any undesirable vibrations.

The third major element, installation aerodynamics, is concerned with the accelerating, swirling, propeller slipstream passing over a wing. The technology challenge here is to design the overall aircraft to achieve the best combination of propulsion system performance and airplane lift-to-drag ratio, while maintaining adequate aircraft stability and control. Results from a recent experimental investigation of propeller slipstream wing interactions at cruise speeds near Mach 0.8 are presented in reference 9.

The final major element is the key mechanical components. Advanced design and packaging technology for the core engine, gearbox, and propeller will be required if an advanced turboprop is to reduce maintenance costs and improve reliability. A study of current-generation turboprop reliability and maintenance costs is presented in reference 10 along with an estimate of the potential improvements available from advanced technology.

Because the four major elements of the advanced turboprop project are highly interrelated, aircraft trade-off studies are being made to insure that these technologies are properly integrated and that progress is being made toward achieving the overall project goals. A summary of the progress made under NASA's advanced turboprop project is contained in reference 3. Also, papers that were presented at this conference by Gatzen, Jeracki, and Bober show the potential and some of the recent aerodynamic advances made as part of this project.

#### LOW-SPEED PROPELLERS

Current-generation propeller-powered GA aircraft operate at cruise speeds of Mach 0.5 and below. The technology trends that are projected for the propellers of these lower speed aircraft are shown in figure 5. The sketch in the lower left of this figure depicts current-technology propellers. These propellers are designed based on a trade-off of the four factors enclosed in the center circle. For many applications performance is traded off to meet noise and cost goals. Solid aluminum blade construction is used in most designs, and this can result in a potential weight penalty when compared with some of the future advanced materials which are being studied. The design trade-off on future advanced technology low-speed propellers may be altered because of two key factors - outside drivers and technology opportunities. The outside drivers are the high cost and fuel availability problems due to the energy shortage, the possibility of more stringent government noise regulations, and the need to retain or improve aircraft safety. In the technology opportunity area several new concepts are currently under study that show considerable performance and noise

benefits. Advanced analysis techniques will make it possible to better understand propeller and nacelle aerodynamics and acoustics for additional benefits. Also, lightweight high-strength composites show considerable promise. When these outside drivers and technology opportunities are applied to future advanced technology propellers, the design may be altered to optimize performance to a lower noise goal using lightweight composite blades of advanced shape. This may result in a small propeller cost increase; however, this penalty should be more than overcome by the large potential performance and weight advantages. An advanced technology low-speed propeller may resemble the design depicted in the sketch on the upper right of figure 5. Some of the advanced features incorporated in this design are blade sweep, proplets (propeller tip device), advanced airfoils, composite blades, and improved integration of the propeller and nacelle.

The NASA research program that addresses the projected technology trends of low-speed GA propellers is summarized in figure 6. A cost-benefit study that evaluates the effect of advanced technologies on low-speed propellers is being conducted by the McCauley Accessory Division of the Cessna Aircraft Company. The NASA Langley Research Center is sponsoring two grant programs on reducing propeller source noise. MIT is evaluating several approaches for reducing noise while optimizing performance (refs. 11 and 12). In a complementary program Ohio State University is evaluating an alternative noise reduction approach in a flight test program. In the propeller performance area, Purdue University, under a NASA grant, is involved in a program to investigate several advanced concepts that show considerable potential for improving propeller performance. In addition, the current low-speed propeller aeroacoustic design methodology is being evaluated and enhanced through a cooperative program between Ohio State University and Lewis.

General-aviation propellers are usually designed as separate propulsion components without properly accounting for the aerodynamic interaction between the nacelle (or fuselage) and the propeller. A program is underway at Mississippi State University to develop technology that will allow the propeller and nacelle to be designed in a more unified approach. This program should lead to improved overall propulsion system performance for general-aviation aircraft.

Propeller dynamics and aeroelastics can be serious design limitations for both current and future advanced low-speed propellers. To better understand this important area, NASA is sponsoring a research program at Pennsylvania State University (ref. 13). More detailed information on NASA's low-speed propeller research is contained in individual papers given by Keiter, Green, Korkan, and McCormick at this conference. A summary of the Purdue University research program on advanced performance concepts is shown in figure 7. This program, under the direction of Dr. John Sullivan, includes analytical and experimental research on such new concepts as proplets (tip devices) and swept blades (ref. 14). A new swept lifting line analysis program is being developed at Purdue, and they are verifying this analysis and determining the performance potential of advanced concepts through subscale propeller wind-tunnel tests using some improved test techniques. These new techniques include the laser velocimeter system shown in figure 7.

The approach being used by Mississippi State University to develop improved propeller-nacelle integration technology is shown in figure 8. They have conducted an extensive search of the propeller literature to assist in evaluating potential loss mechanisms and to see which of the results apply to modern GA propeller-nacelle geometries. Mississippi State also plans to conduct full-scale propeller wind-tunnel tests (in the Langley full-scale tunnel) in combination with analytical studies to develop the improved propeller-nacelle integration technology. This research should lead to better overall propulsion system performance for general-aviation propeller-powered aircraft.

In addition, to the advanced, high-speed propeller wind-tunnel test program discussed earlier, NASA is also testing lower speed GA propellers. A 5-foot-diameter model of one of these low-speed propellers is shown in figure 9. This propeller, along with three other designs, was tested in the Lewis 10- by 10-foot wind tunnel to compare measured performance with analytical predictions. Results from this comparison will be used to develop enhanced analytical prediction procedures for this category of propeller.

#### CONCLUDING REMARKS

The world energy shortage has led to the need for more fuel efficient GA aircraft. Propeller-powered propulsion, with its inherent high level of efficiency, remains an attractive propulsion concept. Current GA aircraft are limited to maximum cruise speeds near Mach 0.5 because of propeller compressibility losses. The NASA research program on these lower speed propellers offers the potential of significant performance improvements and noise reductions through the development of advanced concepts and new analytical design procedures. Extending the current cruise speed limitation to at least Mach 0.8, with a large potential fuel saving compared with turbofan powered aircraft, may be possible with the technologies that are being developed under NASA's Advanced Turboprop Project.

#### REFERENCES

1. Corsiglia, V. C.; Katz, J.; and Kroeger, R. A.: Full Scale Wind Tunnel Study of Nacelle Shape on Cooling Drag. AIAA Paper 79-1820, Aug. 1979.
2. Mikkelsen, Daniel C.; et al.: Design and Performance of Energy Efficient Propellers for Mach 0.8 Cruise. NASA TM X-73612, 1977.
3. Dugan, James F., Jr.; Gatzen, Bernard S.; and Adamson, William M.: Prop-Fan Propulsion - Its Status and Potential. SAE Paper 780995, Nov. 1978.
4. Jeracki, R. J.; Mikkelsen, D. C.; and Blaha, B. J.: Wind Tunnel Performance of Four Energy Efficient Propellers Designed for Mach 0.8 Cruise. SAE Paper 790573, Apr. 1979.
5. Metzger, F. B.; and Rohrback, C.: Aeroacoustic Design of the Prop-Fan. AIAA Paper 79-0610, Mar. 1979.



6. Cornell, R. W.; and Rothman, E. A.: Structural Design and Analysis of Prop-Fan. AIAA Paper 79-1116, June 1979.
7. Revell, J. D.; Balena, F. J.; and Koval, L. R.: Analytical Study of Interior Noise Control by Fuselage Design Techniques on High Speed Propeller-Driven Aircraft. (Lockheed-California Company, NASA Contract NAS1-15427.) NASA CR-159222, 1980.
8. Rennison, D. C.; Wilby, J. F.; and Marsh, A. H.; Wilby, E.G.: Interior Noise Control Prediction Study for High-Speed Propeller-Driven Aircraft. (Bolt Beranek and Newman, Inc.; NASA Contract NAS1-15426.) NASA CR-159200, 1980.
9. Bencze, D. P.; et al.: Propeller Slipstream Wing Interactions at Mach No. 0.8. SAE Paper 780997, Nov. 1978.
10. Stolp, Philip C. and Baum, James A.: Advanced Turboprop Propulsion System Reliability and Maintenance Cost. SAE Paper 771009, Nov. 1977.
11. Succi, G. P.: Design of Quiet Efficient Propellers. SAE Paper 790584, Apr. 1979.
12. Larrabee, E. E.: Practical Design of Minimum Induced Loss Propellers. SAE Paper 790585, Apr. 1979.
13. McCormick, B. W.; et al.: The Analysis of Propellers Including Interaction Effects. SAE paper 790576, Apr. 1979.
14. Sullivan, J.: The Effect of Blade Sweep on Propeller Performance. AIAA paper 77-716, July 1978.

## INSTALLED CRUISE EFFICIENCY TRENDS

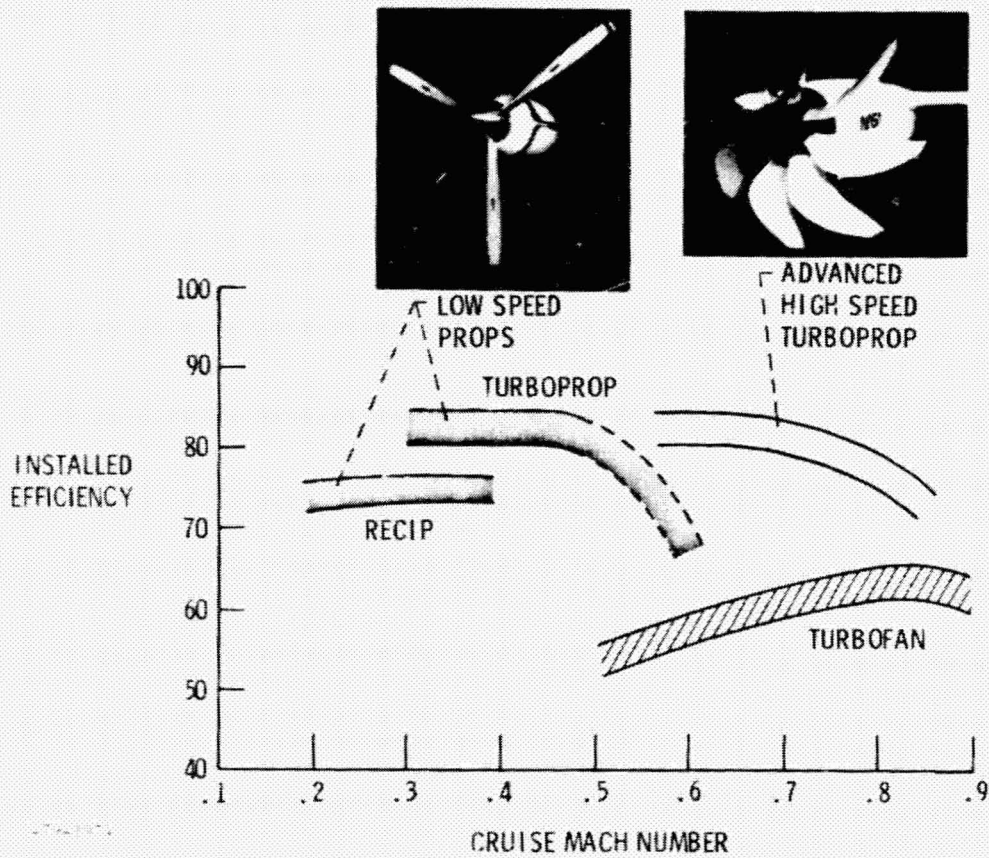


Figure 1

## ADVANCED TURBOPROP PROPULSION SYSTEM

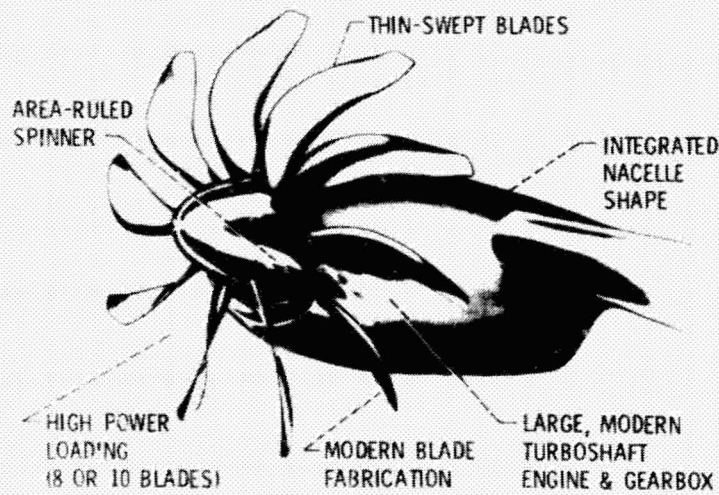
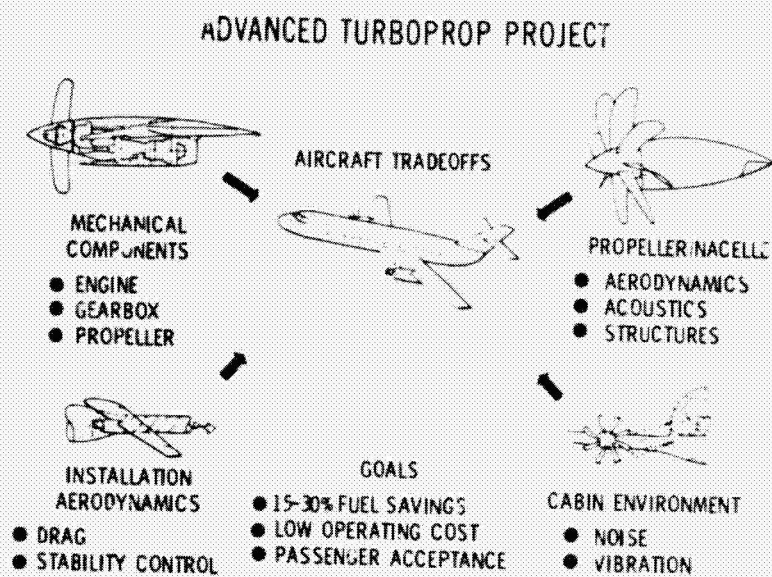


Figure 2

ORIGINAL PAGE IS  
OF POOR QUALITY



CS-79-4215

Figure 3

### HIGH SPEED PROPELLER WIND TUNNEL MODEL

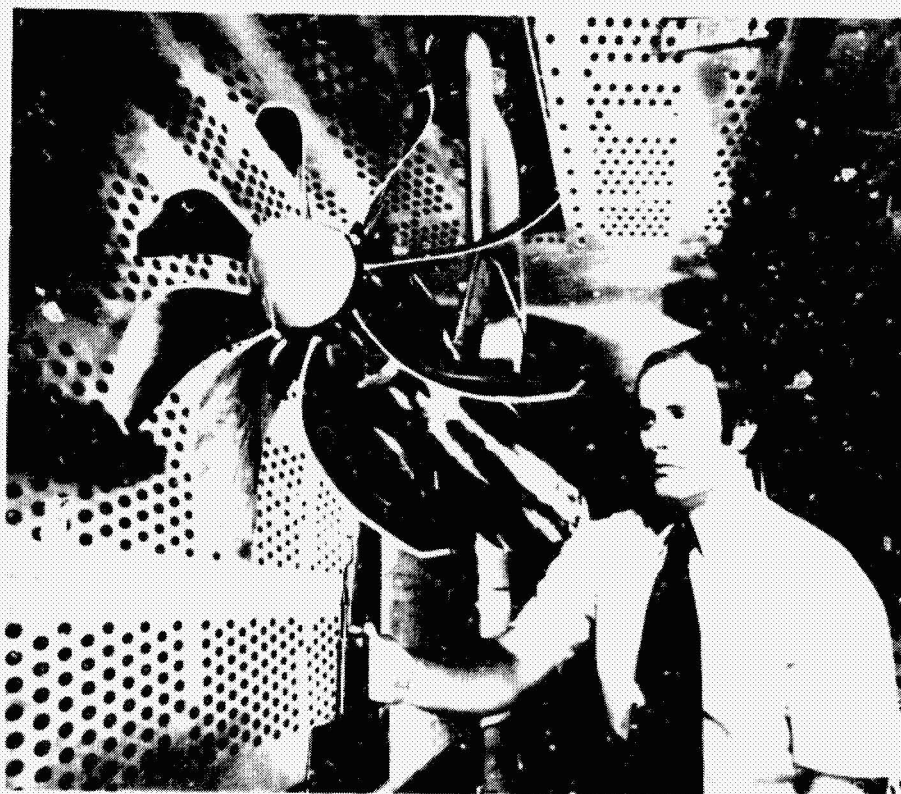
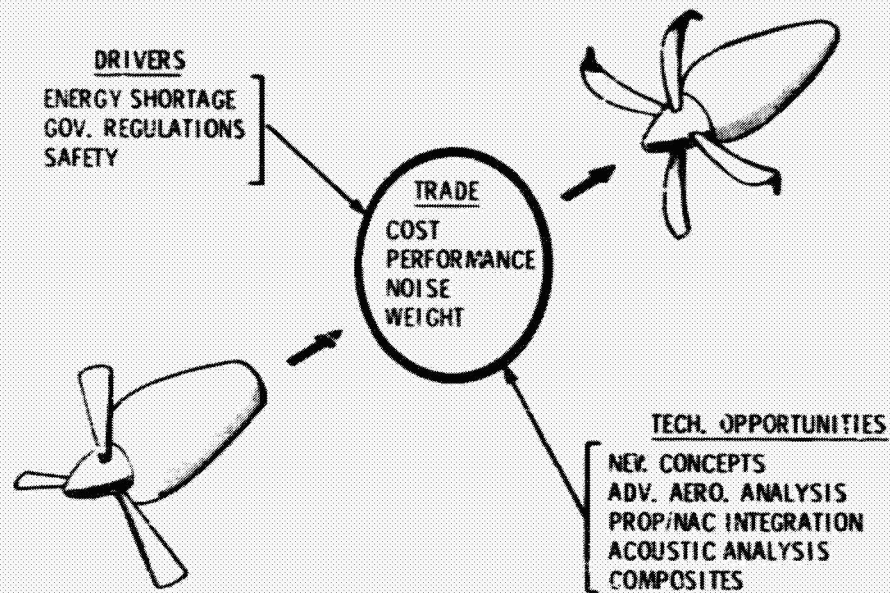


Figure 4

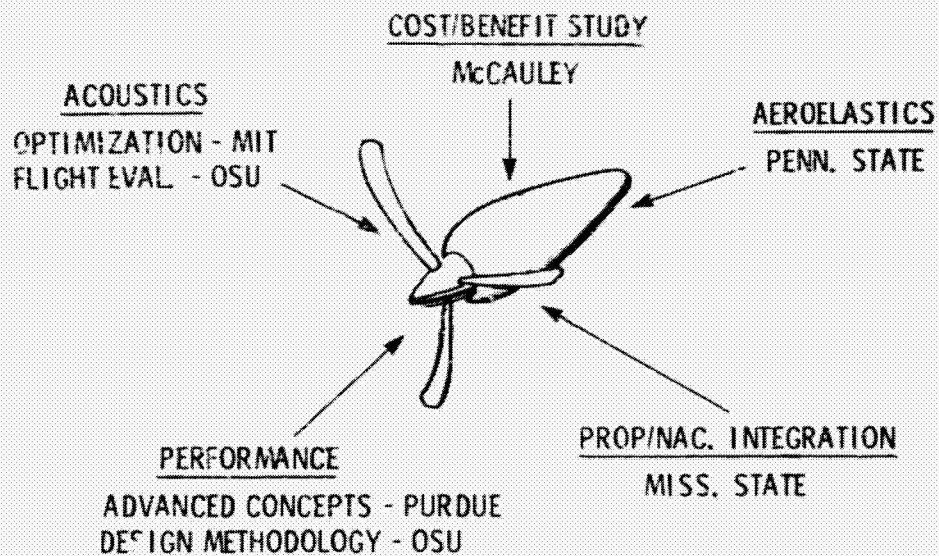
## LOW SPEED PROPELLER TECHNOLOGY TRENDS



CS-79-4091

Figure 5

## LOW SPEED PROPELLER RESEARCH PROGRAM

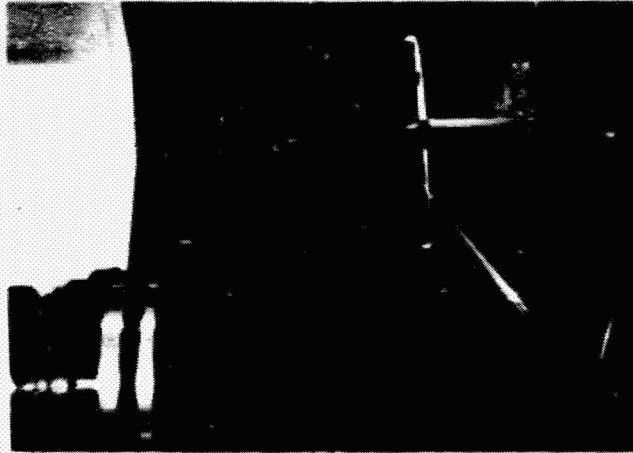


CS-79-4091

Figure 6



## ADVANCED PERFORMANCE CONCEPTS



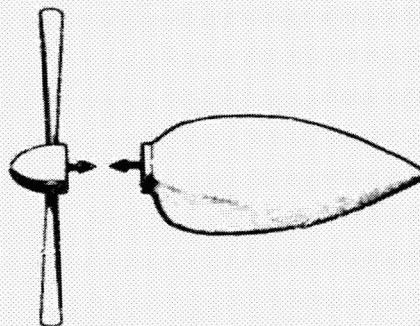
PURDUE UNIVERSITY

- NEW CONCEPTS
  - PROPLETS
  - SWEPT BLADES
- SWEPT LIFTING LINE ANALYSIS
- IMPROVED TEST TECHNIQUES

CS-79-4017

Figure 7

## PROPELLER NACELLE INTEGRATION



MISS. STATE

- EVALUATE LOSS MECHANISMS
  - LITERATURE SEARCH
  - WIND TUNNEL TESTS
- DEV. ADVANCED INTEGRATION TECH.

73-79-4091

Figure 8

# LOW SPEED PROPELLER WIND TUNNEL MODEL



Figure 9

RECEIVED  
JAN 10 1967  
NATIONAL BUREAU OF STANDARDS

215  
N 80-22342

## LOW SPEED PROPELLERS - IMPACT OF ADVANCED TECHNOLOGIES

Ira D. Keiter  
McCauley Accessory Division  
Cessna Aircraft Company

### ABSTRACT

Studies have indicated that the application of advanced technologies to General Aviation propellers can reduce fuel consumption in future aircraft an average of 10 percent, meeting current FAR Part 36 noise limits. Through the use of composite blade construction, up to 25 percent propeller weight reduction can be achieved. This weight reduction in addition to 7 percent propeller efficiency improvements through application of advanced technologies result in 4 percent reduction in direct operating costs, 10 percent reduction in aircraft acquisition cost, and 7 percent lower gross weight for General Aviation aircraft.

### INTRODUCTION

In order to insure that USA built General Aviation aircraft remain competitive and dominant in the world market place, support energy conservation needs, and meet the more stringent environmental controls, NASA sponsored programs are necessary to improve propeller technology based for the most part on that developed during the World War II era. Attention to the area of materials used and fabrication methods is the cornerstone leading to the pursuit of advanced technology concepts and sophisticated computer analysis tools to evaluate those concepts.

Preliminary indications are that proper techniques could be developed with the utilization of composite materials in the structure of propeller assemblies. A proper blend of design and fabrication techniques will result in significant weight and cost reductions, enhanced safety through improved fatigue life, greater adaptability to a variety of design concepts and less capital requirements to produce propellers suitable to the General Aviation market.

The use of lighter weight blades will permit both the increase in blade retention hardware safety margins and the reduction in weight and complexity of such hardware.

The combination of improvements in cost and weight reduction, fatigue life increases, more consistently produced airfoil sections, and more widely varied potential design selection has a significantly broadening effect on typical installation compromises which will be apparent as the potential impact of the various advanced technologies are enumerated in later sections of this paper.

It will be shown that significant propeller weight improvements are possible for current propeller/engine/aircraft installations while achieving improvements in performance and reduced noise, both within the aircraft and in the airport environment.

The potential propeller weight reductions and efficiency improvements can directly result in reductions in aircraft fuel consumption, direct operating costs, acquisition cost, and lower gross weight.

Improvements in propeller fatigue safety margins would permit corresponding increases in overhaul life, provide greater tolerance for field maintenance or lack of same and thus increase safety, productivity, and economy.

The current research program awarded to McCauley is needed to structure a realistic and effective technology plan for General Aviation propellers, to identify the advanced technologies and their potential costs and benefits, and to determine and identify areas of key technical risks and required research programs (Figure 1). It is hoped that once the areas of greatest potential are identified, NASA research funding can then be channeled into the most appropriate areas. The team comprising the current study effort (contract number NAS3-21719) is highlighted in Figure 2.

#### SENSITIVITY STUDIES

Sensitivity studies were performed to evaluate the potential of each technology element on propeller performance, noise, weight, and cost for the following two categories of General Aviation aircraft:

- I. Low speed (up to 250 knots)/low power (up to 350 HP), 2 - 8 place, single and twin engine, currently powered by reciprocating engines.
- II. High speed (up to 400 knots)/high power (up to 650 HP), 6 - 18 place, twin engine, turboprop.

In order to evaluate the improvement potential for the various technology elements, specific aircraft satisfying the characteristics outlined above for each category were chosen. The representative aircraft, illustrated in Figure 3, chosen for each aircraft category, are as follows:

Category I : Cessna 172N  
Cessna 210M  
Cessna 414A

Category II : Cessna 441



## TECHNOLOGY ELEMENTS INVESTIGATED

Technology elements were considered with the potential for improving airplane/mission characteristics such as fuel burned, direct operating cost, acquisition cost, and gross weight. The original scope of technology elements considered were screened to include any element felt to have any potential whatsoever based on McCauley experience, other's experience, and available literature. Each technology element was first evaluated in terms of its effect on propeller criteria of merit including performance, noise, weight, cost, and structural considerations. The total impact of the technology elements affecting performance and weight were then investigated to determine their impact on airplane/mission characteristics. The General Aviation propeller concept incorporating the appropriate advanced technologies is illustrated in Figure 4.

## PERFORMANCE CONSIDERATIONS

The following list of technology elements show potential for performance improvements. The element is specified along with the loss to be minimized, keeping in mind the practical limitations of each of the technology elements and their impact on other important propeller criteria of merit such as noise, weight, and structure.

Technology Element	Performance Loss To Be Minimized	Reference Utilized
Design optimization		
Decreased power loading	Axial momentum	1
Increased number of blades	Tip	1
Maintain tip speed	Axial momentum	1
Decreased activity factor	Profile	2
Use of proplets	Tip	Purdue Univ.
Use of sweep (helical tip mach number reduction)	Compressibility	2
Advanced technology airfoil type	Compressibility, profile	4
Decreased thickness ratio	Profile	2
Improved propeller/nacelle integration	Blade profile, nacelle drag	2,3
Improved surface finish	Profile	5,6,7
Maintainability of airfoil shape	Profile	7

The advanced technology concept of sweep is unique since it both improves performance and reduces noise. The predicted effect of sweep on performance and noise is shown in Figure 5. Sweep is structure limited with 25-30 degrees probably feasible for future General Aviation applications. The effect of sweep in addition to the effect of other significant advanced technology elements on cruise performance gains are shown in Figure 6. Power loading, number of blades, tip speed, activity factor, and proplets are grouped

together and classified as design optimization parameters. Maintainability of airfoil shape is not included since it is a parameter to prevent degradation through the use of composites and not to improve current technology.

## ACOUSTIC CONSIDERATIONS

The primary technology elements affecting acoustics are number of blades, tip speed, thickness ratio, activity factor, sweep, blade loading, advanced technology airfoils, and proplets.

The following is a list of these primary technology elements:

Technology Element	References Utilized
Design Optimization	
Increased number of blades	8
Decreased tip speed	
Decreased activity factor	
Use of proplets	Purdue University
Peak blade loading moved inboard	8
Use of sweep (helical tip mach number reduction)	8
Advanced technology airfoil types	
Decreased thickness ratio	

As with performance considerations, several elements are grouped together under design optimization. From the acoustic standpoint, all items other than advanced airfoils, sweep, and reduced thickness ratio are considered design optimization variables. The main technology elements affecting acoustics, including sweep whose effects were isolated earlier, are shown in Figure 7. These gains can be realized without any noticeable loss in performance. The delta dB(A) improvements possible are in many cases more than that required to meet noise regulations. During design tradeoff studies, the relative importance of each design parameter must be evaluated. Greater noise reductions could be obtained if one were willing to sacrifice performance.

## MATERIAL CONSIDERATIONS

In order to reliably meet the future performance and acoustic requirements of General Aviation propellers with weight reduction and approaching price competitiveness with aluminum, consideration of composite materials requires appropriate attention as a viable solution. Advanced filamentary composite materials combine low densities and low notch sensitivity with high strengths and stiffnesses. Adequate safety margins of current propellers can be further enhanced. Figure 8 outlines the advantages of composites and their associated propeller benefits. Because filamentary materials are only strong in the filament direction, careful consideration must be given to ply

orientation to match the design requirements.

Through variations in the composite matrix, blade sections can be tailored to meet the specific radial stiffness distribution required. The shape of primary bending and torsional modes can be altered effectively through the use of composites. Reductions in blade section size permissible with composites will result in higher blade deflections than are customary with aluminum. Blade aeroelastic instabilities can result from large out of plane deflections and must be given careful consideration.

Appropriate blade materials, type of hub retention system, methods of construction for composite materials, and material consideration for blade leading edge erosion resistant strips are all areas which must be addressed in detail.

### STRUCTURAL CONSIDERATIONS

In evaluating the structural integrity of advanced technology propellers, considerable attention must be given to the steady and alternating loadings experienced in service. The steady loads consist primarily of centrifugal, bending due to thrust loading, and torsion. The alternating vibratory loads are due to blade aerodynamic excitations and alternating torsional input due to reciprocating engine cylinder firing sequence and frequency. Aerodynamic inflow angles excite 1xP alternating loads which are primarily evident on turboprop installations being overshadowed by engine alternating torsionals in reciprocating installations. In all installations one should assure that 1xP resonance does not occur in the normal operating RPM range.

It is a relatively easy job to evaluate the steady loads on a propeller blade using conventional techniques. To determine the vibratory effects, however, with incorporation of advanced technologies such as sweep and proplets, may require the use of three dimensional finite element analysis rather than two dimensional beam analysis or lumped parameter matrix manipulation techniques currently utilized. With regard to vibratory analysis, available analytical techniques applicable to General Aviation propellers determine mode frequencies with good accuracy and vibratory loads and resultant stresses within 25-30 percent on turbine installations. The effect of alternating torsionals from reciprocating engines is currently not included in existing models. Experimental testing of strain gaged propellers is still relied upon heavily. Experience and experimental data will dictate allowable alternating stress levels with composites as is the case with aluminum alloys.

Using the torsional mode results from three dimensional finite element analysis (3-D FEA), the possibilities of stall flutter can be addressed. The stall flutter parameter is based on static torsional frequency, and semichord, velocity, and mach number at the 80 percent blade radius location. Through extensive experimental programs, a stall flutter boundary has been determined for conventional blade shapes. A similar boundary must be determined for blade shapes incorporating the advanced technology concepts outlined in Figure 4.

Stall flutter occurs under conditions of blade angle of attack and inflow velocity where a major portion of the blade is stalled. Stall flutter oscillations occur at the first torsional mode when the spanwise damping integration along a blade becomes zero or less. The conditions conducive to stall flutter are during static, takeoff, and reverse thrust operation.

By using the bending and torsional mode data from 3-D FEA and customarily presented in terms of a Campbell diagram, classical flutter can be addressed. Classical flutter can occur at high aircraft velocities where the mode spacing over the operating RPM range is insufficient and a coupling of torsional and bending modes occur (reference 9).

Because of the limited composite fatigue strength data available and the lack of analytical techniques to predict vibratory loads, the evaluation of fatigue life is highly qualitative. Only through extensive test programs and field experience, can the required data base of information be compiled from which the appropriate fatigue limits can be determined. This same process occurred many years ago to establish the current baselines utilized for aluminum.

#### BLADE WEIGHT, COST, AND AIRCRAFT MISSION CONSIDERATIONS

Preliminary screening of candidate materials indicates configurations of E-Glass, S-Glass, Kevlar, and Graphite with medium and high density epoxy cores to meet the mean load, alternating load, fatigue, and weight requirements of General Aviation propellers. Relative blade weight and cost comparison against aluminum are shown in Figure 9. In determining the impact of weight reductions through the use of composites it must be emphasized that the blade weight savings exist only with a direct replacement of aluminum blades. This does not take into account the blade retention area. Also, in order to achieve a desired compromise of advanced technologies between performance and noise, the potential weight savings may be reduced. In other words, the trends of decreased power loading through diameter increases, increased number of blades, sweep, and proplets will tend to increase weight while being offset through lower blade activity factors and lower thickness ratios (feasible because of composites).

The performance gains indicated earlier in addition to weight reductions possible through the use of composites have a direct effect on aircraft/mission characteristics such as fuel burned, operating cost, acquisition cost, and gross weight. In addressing mission analysis, payload, range, speed and aircraft lift to drag ratio are kept constant. Potential trip fuel savings versus aircraft cruise speed are shown in Figure 10. This assumes two hours at cruise, felt to be fairly representative. Studies indicate that average trip fuel reductions of about 10 percent result in 4 percent reductions in direct operating costs. Included in DOC determination are engine and airframe periodic maintenance, fuel and oil burned, reserves for engine and propeller overhaul, reserves for avionics, systems and miscellaneous. As fuel prices raise in the future, their effect on increases in DOC will be as indicated in Figure 11.

Aircraft acquisition cost reductions average about 10 percent. Reductions as affected by aircraft cruise speed are indicated in Figure 12. A twenty-five percent increase in propeller cost has been taken into account but does not alter the results since the propeller cost is so low in relation to aircraft cost. Studies also indicate average potential aircraft gross weight reductions of seven percent.

#### FUTURE RECOMMENDATIONS

It is apparent from the sensitivity studies performed on the various technology elements that NASA funding directed primarily into the areas of composite materials research, and the advanced technology concepts outlined in this paper can provide the data base required to achieve the stated airplane/mission improvements.

Since many technology elements improving performance have an adverse effect on acoustics and future government regulations controlling noise limits will probably be more stringent, it is imperative that research funding be expended in this area. This should include careful evaluation of current methodology of propeller noise prediction techniques and the unification into a common, recognized procedure for utilization by the General Aviation community. Experimental verification of resulting theories through wind tunnel testing and flight substantiation is necessary.

Through the use of composites, some of the more promising technology requirements will become possible such as thickness ratio reductions, sweep, lower activity factors, reduced power loading, more blades, advanced airfoils with complex curvature, smoother airfoil surface, and maintainability of airfoil shape in service. These factors lead to optimized designs meeting appropriate strength requirements. At a certain blade load level, the composite blade will deflect more. This can lead to aeroelastic instabilities which is an important area requiring NASA support. Although considerable research has taken place in the composite materials area, the product applications have not included propellers. The aircraft propeller is one of the most critically stressed aircraft components. It operates in a severe environment and is a major structural component with complex stress distribution. It is exposed to the wide range of variables created by power plants in a most intimate manner. The successful use of composite materials in General Aviation propellers will provide information on fatigue to establish limit lines of mean stress versus alternating stress for  $10^5$  and  $10^8$  cycles as typically represented on a Goodman diagram. Such information is not readily obtainable in any other application.

NASA sponsored research will help fill the gap in the application of composite technology (design and fabrication methods) between current applications and their potential use with propellers. Advanced composites technology has progressed to a point where reliable application as aircraft secondary structure is accepted and the application for primary structure is relatively close but the confidence level for commercial application has not been established. It is, therefore, highly desirable and appropriate to explore

this General Aviation application.

Specifically, the total cost of composite blades must be nearly competitive with aluminum blades in order to experience wide use in General Aviation. Research into low cost fabrication techniques is the key to achieving cost competitiveness. Wind tunnel testing with follow-on programs for flight test verification is necessary.

In the advanced airfoil design area, NASA has continually made efforts in improving communication with the General Aviation community over the past five years through workshops, symposiums, conferences, etc., and from these have come airfoil design implementation schedules satisfying the needs of wing designers. What is needed now is an airfoil technology plan to design airfoils specifically tailored for the widely varying fluid flow conditions which prevail along a propeller blade.

The area of propeller/nacelle integration is already receiving some attention by NASA with Grant NSG1402 to Mississippi State University. The first phase involving the collection of baseline data in the NASA-Langley full scale tunnel is just getting underway. Current program calls for investigation of nacelle shapes characteristic of those used in twin reciprocating engine installations. There should be future testing including a wide variety of propeller/nacelle configurations covering the broad range of aircraft/engine combinations typical of the General Aviation fleet.

NASA has supported analytical studies to provide special purpose user oriented programs to calculate propeller inflow velocity fields, steady and unsteady aerodynamic loads and mode shapes and frequencies. The next step should be to concentrate on analytical procedures to predict the vibrational loads and stresses the propeller is subjected to in service. The model must include the coupling effects of the propeller-engine system. Accuracy of existing prediction techniques is not acceptable except for 1xP analysis. Higher order stresses, prevalent with reciprocating engine installations are not predicted with adequate accuracy. A good, reliable prediction technique would eliminate much of the uncertainty which exists prior to vibration survey certification testing. Wasted time and cost associated with experimental testing of a configuration exceeding vibratory load limits could be nearly eliminated.

With the very competitive market in General Aviation which limits funds in research and development, it is very evident that NASA sponsored support is necessary to enhance the state of the art in the areas mentioned above. The key areas requiring future research enumerated above are highlighted in Figure 13.

#### CONCLUDING REMARKS

The study of a wide range of propeller design variables and advanced technologies has indicated that the potential exists for propeller performance improvements and weight reductions meeting consistently more stringent regulatory noise levels. Advanced technological development of propellers has

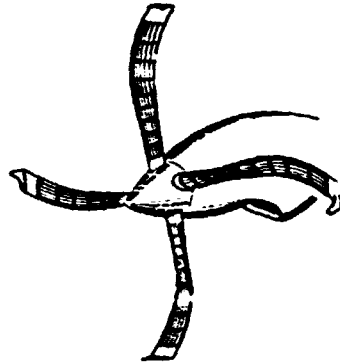
a direct impact on the fuel burned, direct operating costs, acquisition cost, and gross weight of General Aviation aircraft. NASA can assure that these goals are met by allocating appropriate funds in the areas where the greatest potential exists.

## REFERENCES

1. Anonymous: SBAC-Standard Method of Propeller Performance Estimation, Society of British Aircraft Constructors, Ltd. April 1950.
2. Goldstein, S.: On The Vortex Theory of Screw Propellers. Royal Society (London) Proc., 1929.
3. Hess, J.L.; and Smith, A.M.O.: Calculation of Potential Flow About Arbitrary Bodies. Progress in Aeronautical Sciences, vol. 8, 1967, pp.1-138.
4. Bocci, A.J.: A New Series of Aerofoil Sections Suitable For Aircraft Propellers. Aeronautical Quarterly, vol. 28, Part 1, Feb. 1977, pp. 59-73.
5. Hoerner, S.F.: Fluid-Dynamic Drag. 1965.
6. Hoerner, S.F.; and Borst, H.V.: Fluid-Dynamic Lift. 1975.
7. Stevens, W.A.; Goradia, S.H.; and Braden, J.A.: Mathematical Model For Two-Dimensional Multi-Component Airfoils In Viscous Flow. NASA CR-1843, July 1971.
8. Succi, George P.: Design of Quiet Efficient Propellers, SAE Paper 790584, SAE Business Aircraft Meeting, Wichita, April 1979.
9. Dugan, J.F. Jr.; Gatzen, B.S.; and Adamson, W.M.: Prop-Fan Propulsion-Its Status and Potential. SAE Paper 780995, SAE Aerospace Meeting, San Diego, November 1978.



## ADVANCED TECHNOLOGY PROPELLER STUDY



- IDENTIFY ADVANCED TECHNOLOGIES
- ASSESS BENEFITS . COSTS & RISKS
- DEFINE OPTIMUM CONFIG., MISSION ANALYSIS
- FORMULATE RESEARCH PROGRAM

FIG. 1

## TEAM COMPRISING STUDY EFFORT

- MCCAULEY  
PROGRAM MANAGEMENT, PERFORMANCE,  
COST, STRUCTURES
- CESSNA  
AIRPLANE MISSION ANALYSIS
- OHIO STATE  
ACOUSTICS
- MATERIALS SCIENCES & SAI  
COMPOSITES

FIG. 2

## BASELINE AIRCRAFT STUDIED



FIG. 3

## ADVANCED TECHNOLOGY CONCEPTS

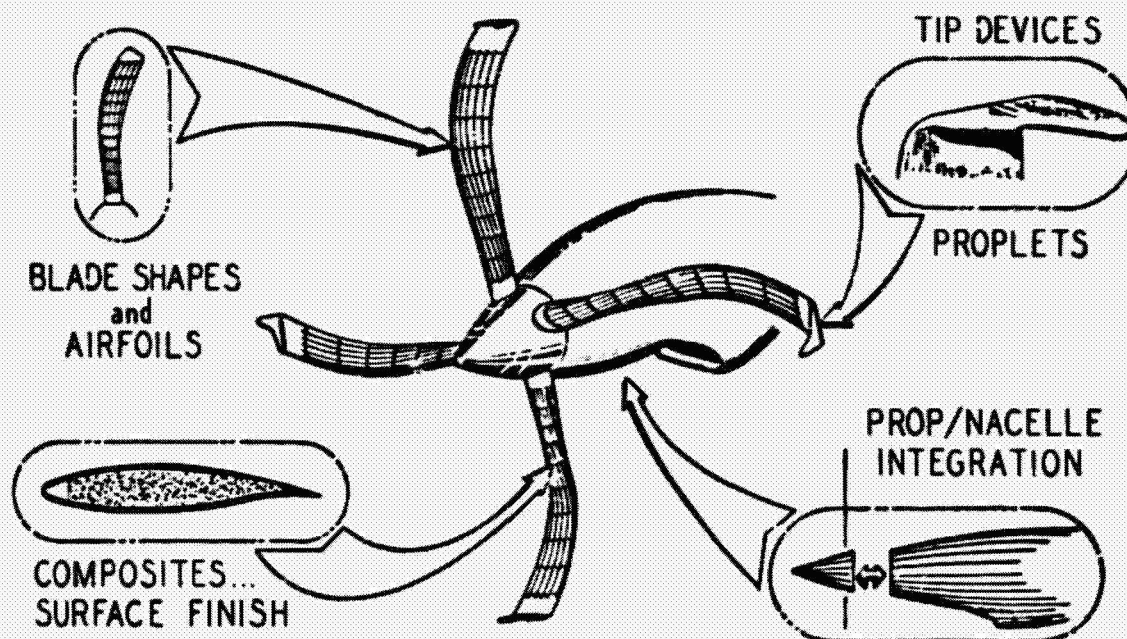


FIG. 4

# PREDICTED EFFECT OF SWEEP ON PERFORMANCE AND NOISE

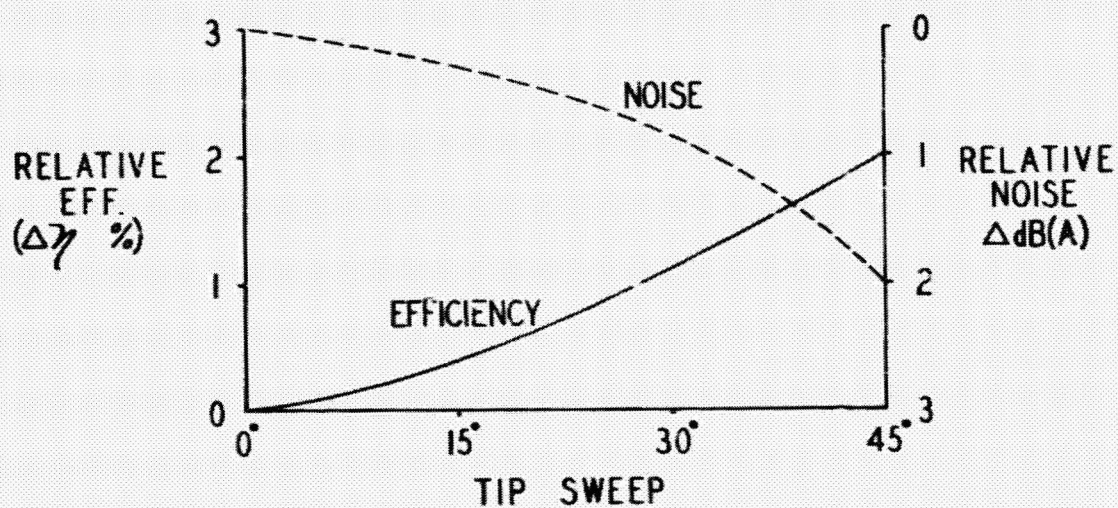


FIG. 5

# POTENTIAL CRUISE PERFORMANCE GAINS

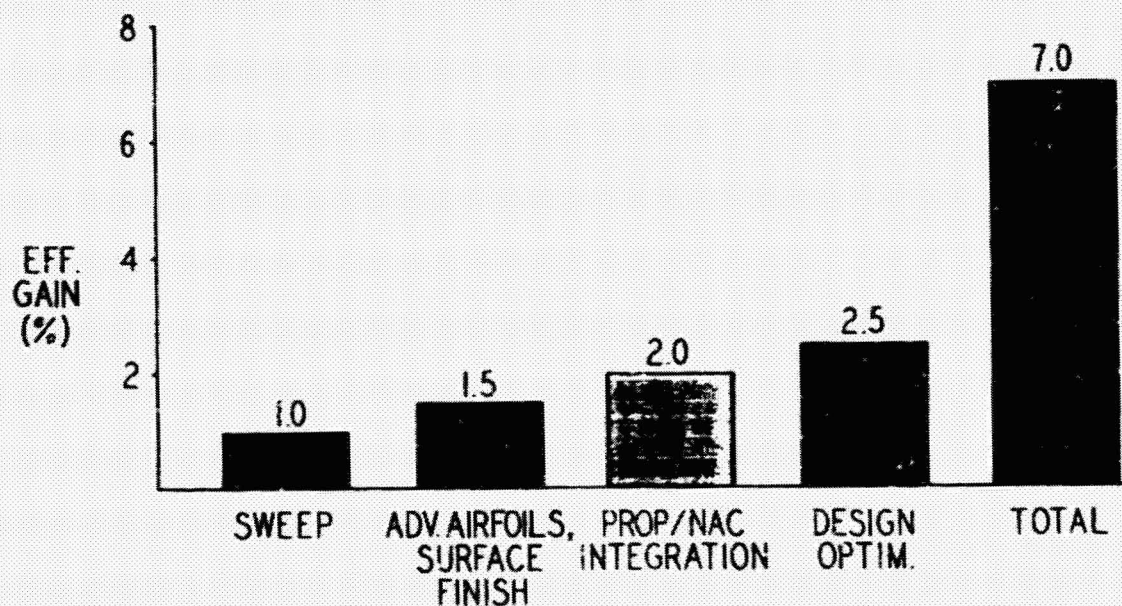


FIG. 6



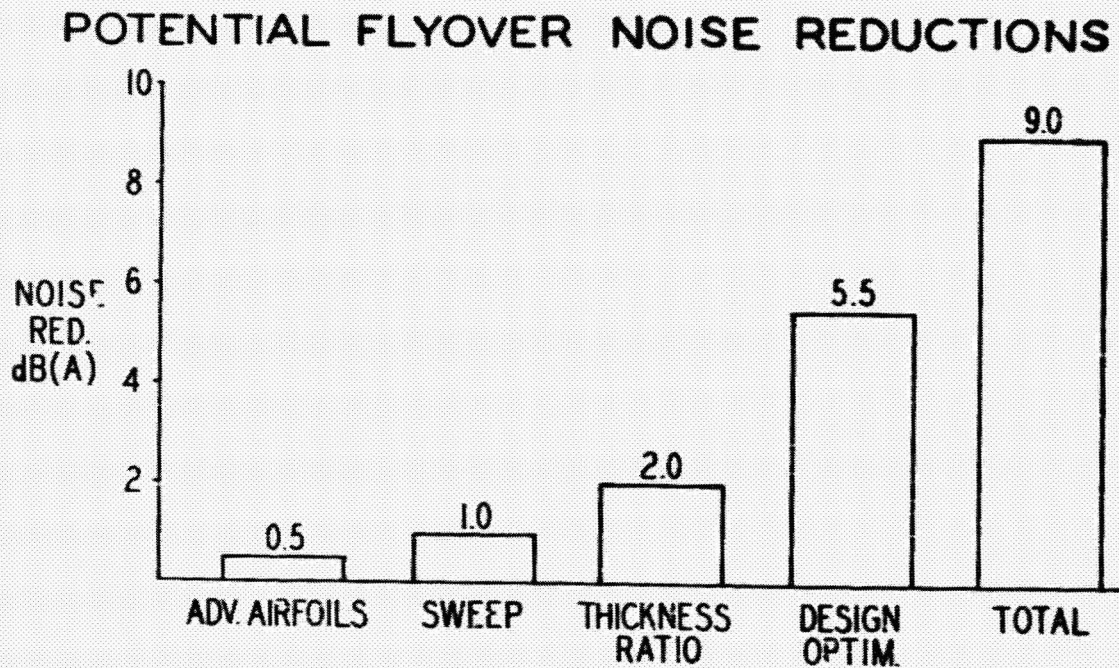


FIG. 7

### BENEFITS OF COMPOSITE MATERIALS

COMPOSITE ADVANTAGES	PROPELLER BENEFITS
GREATER STRENGTH LOWER DENSITY HIGHER MODULUS LOWER NOTCH SENSITIVITY	LOWER WEIGHT IMPROVED PERFORMANCE LOWER NOISE ENHANCED SAFETY MARGIN

FIG. 8

## BLADE WEIGHT AND COST COMPARISON

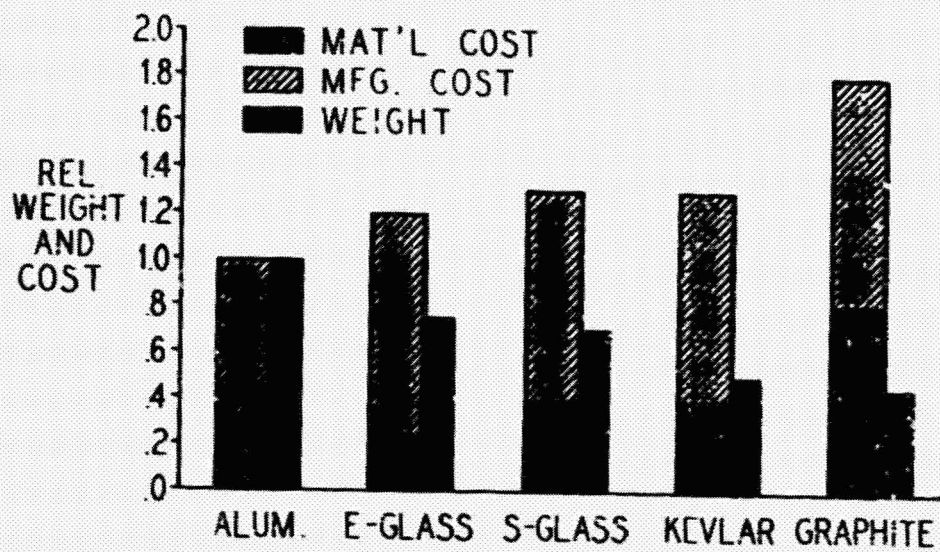


FIG. 9

## POTENTIAL TRIP FUEL SAVINGS

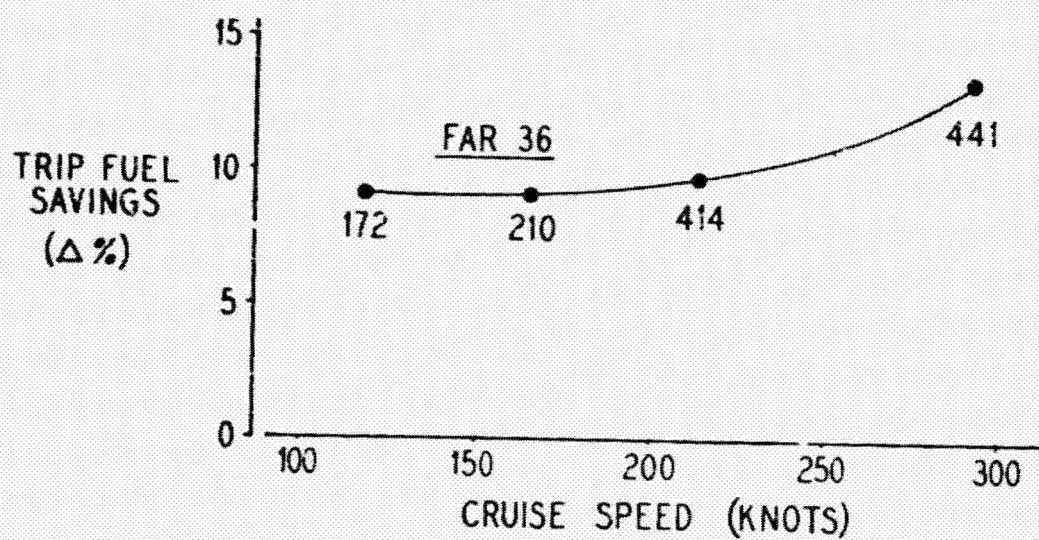


FIG. 10



## FUEL PRICE EFFECTS ON DIRECT OPERATING COSTS

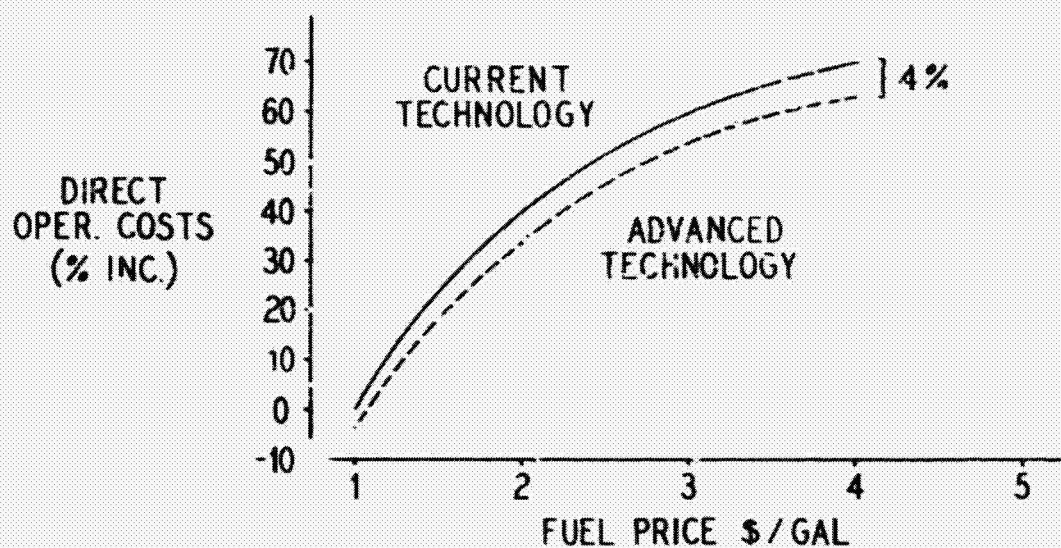


FIG. 11

## AIRCRAFT ACQUISITION COST REDUCTIONS

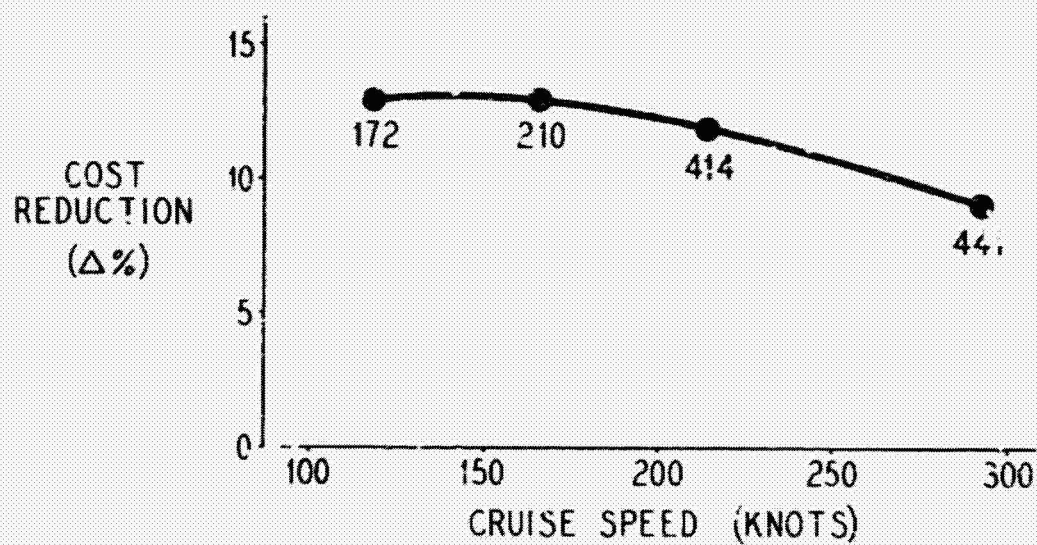


FIG. 12

## PROPOSED RESEARCH PROGRAM

- PERFORMANCE
- NOISE
- AEROELASTICS
- COMPOSITES
- OPTIMIZATION
- FULL SCALE VERIFICATION

FIG. 13

D/b

N 80-22343

## ADVANCED TURBOPROP POTENTIAL FOR HIGH SPEED

Bernard S. Gatzen  
Hamilton Standard Division, United Technologies Corporation

Over the last four years, there has been a significant amount of technical progress on an advanced propulsion concept called the Prop-Fan. I want to discuss this progress and what it might mean regarding high speed business aircraft. The Prop-Fan propulsion system is an advanced propeller driven by a turboshaft engine. The rotor technology is being pursued in NASA's ACEE program. Advancements in aerodynamics, acoustics, structures, and mechanical execution are involved and I'll touch on each of these subjects.

The major benefit attributed to the Prop-Fan is fuel savings resulting from improved performance. This propulsion device is aimed at airspeeds above 0.55 Mach where the turbofan is today's standard. Therefore, the key objective is high performance at high subsonic Mach number which results in fuel saved and reduced operating costs. However, in achieving this goal, certain other characteristics must not be sacrificed. It is necessary to remain a good neighbor around the airport, it is necessary to have a comfortable interior environment, and the aircraft safety must be uncompromised. All of these constitute the goals being worked towards in the Prop-Fan programs being conducted by NASA with Hamilton Standard participation.

Typically the turboprop on a business aircraft operates below 0.55 Mach, more in the area of 0.45 Mach, with very high efficiencies. The Electra turboprop had high efficiencies up to 0.6 Mach. Beyond these airspeeds, the efficiency drops off and the turbofan is king. The productivity of a 0.8 Mach turbofan versus a 0.5 Mach turboprop has clearly been demonstrated in the commercial passenger carrying market. With the Prop-Fan, the inherently high propeller type efficiencies are extended out to the turbofan operating regime of 0.8 Mach. With core engines of comparable technology, the Prop-Fan offers significant fuel savings over the entire Mach number range up to 0.85. I have generalized the projected fuel savings with Prop-Fans in place of turbofans based on a variety of aircraft studies conducted by Boeing, Douglas, both Lockheeds, Pratt & Whitney, General Electric, NASA and United Technologies. It shows maximum fuel savings at short and very long operating ranges. For short range aircraft, the mission is dominated by climb and descent, generally keeping airspeed below design capability. At very short range, it shows that a high design speed is not relevant to fuel usage. There is a bucket at 1500 to 2500 nautical miles with increasing fuel savings at longer ranges. Here, the fuel saving is reducing gross weight and a compounding effect takes place. Another attribute of the Prop-Fan is that further fuel savings are achieved by just reducing airspeed; this is not the case with the turbofan.



Let's compare the general characteristics of this advanced Prop-Fan with the typical business aircraft turboprop. I have already mentioned the significant difference with intended airspeed range. Coupled with this is operating altitude; the higher the Mach, the higher the altitude. Typically propellers are operated in cruise at maximum efficiency which translates into lower power loadings. This generally works out well for low speed aircraft which end up being sized for climb conditions. As design Mach is increased, the propeller becomes sized by cruise and selecting a power loading for peak efficiency would result in very large diameters. So, some efficiency is sacrificed for size and a higher power loading is selected. The blade count is increased to maintain high cruise efficiency levels and good low speed performance as well. The rpm's are similar but Prop-Fan favors the lower side to minimize the transonic effects as airspeed is increased.

In both aerodynamics and acoustics, it is necessary to design for operation of a large portion of the rotor area in the transonic regime. 800 fps at 0.3 Mach results in a tip helical Mach of 1.14. The key to maximizing aerodynamic efficiency is to eliminate compressibility losses and this is done by using the thinnest airfoils possible, consistent with structural integrity. Blade sweep is used in a manner similar to wing sweep to reduce the effective Mach number the airfoil section operates at. Nacelle shaping is accomplished to reduce the velocity through the disk with the primary emphasis to controlling inboard root choke. Area ruling is used in conjunction with nacelle shape to minimize drag losses in the root where the solidity is high. Lastly, an advanced airfoil shape may allow thicker airfoils or less sweep by raising the section critical Mach number above the point where compressibility losses rise rapidly. Three generations of model Prop-Fans have been designed, fabricated, and tested. Advanced aerodynamic analyses have been developed from existing propeller and fan expertise and applied to the design tasks. The aero analysis treats the inboard blade area as a cascade like a turbofan and the outboard area like a propeller. Only compressible 2D airfoil data are used. Both the effects of the nacelle and blade sweep are accounted for. With advanced design methods, achieving aerodynamic efficiency improvement at high Mach is accomplished with a methodical approach and a high confidence of success in place of the empirical, that is, cut and try approach.

The advanced aero design methods are allowing a fairly rapid focussing towards designs which improve upon Electra turboprop efficiencies. Of course, you can see that even the 1950's turboprop technology used in the Electra, which is the same as that used on the P3, is far superior to the typical general aviation turboprop. This is a direct result of the operating Mach number. The general aviation turboprops are designed to be highly efficient at 0.4 to 0.5 Mach cruise. The Electra technology offers no improvement there, but holds efficiency up high out to 0.6 Mach where it begins to drop off rapidly. Prop-Fan technology offers small gains at 0.6 Mach but holds efficiency up high out to 0.85 Mach. The Electra achieves efficiency improvement over general aviation turboprops through lower blade thickness ratios, both at the blade tips and roots. The Prop-Fan makes use of all the aerodynamic concepts discussed earlier: Thickness ratio, blade sweep and nacelle shaping. Wind tunnel test results on

two-foot model Prop-Fans have demonstrated 80% efficiency which is the program objective. Additional aero/acoustic designs are expected to improve upon these results by a few percent. Demonstration of this should occur next year. Further improvements in efficiency can be obtained by recovering swirl. As much as eight efficiency points are lost in the slipstream of a single rotation rotor. Portions of this are recoverable by having the wing act as stator vanes or by using a counter-rotating propeller.

As with aerodynamics, controlling the acoustic levels required advanced concepts and design methodologies. Both far field noise around the airport and interior noise in cruise must be controlled. Concepts which have been considered in acoustic analysis conducted to date include reduced thickness ratio, reduced tip speed with increased blade count, optimum blade planform including swept shapes, and advanced airfoils. Let's consider their impact on far field noise. Noise reductions in the far field have typically been achieved by reducing tip speed; this is a very powerful noise reducing means, but in the past has been accompanied by performance reductions as well. This traditional means of noise reduction can be accomplished without performance decrement by increasing rotor diameter, but this is usually an unattractive alternate. Studies with new acoustic design methodology indicates that significant noise reductions can be achieved with improved airfoils, higher blades count, and a more optimum blade shape. Both airfoil optimization and increasing the blade count have a compound impact on noise by reducing noise in themselves but also improving efficiency so that for constant thrust, a smaller diameter can do the same job. Improved blade shapes, including sweep, reduce noise significantly without diameter changes.

The advanced acoustic method mentioned above is a procedure developed specifically for Prop-Fan cruise near field noise control but is generally applicable for any turboprop noise analysis. The noise method recognizes the components of tone noise associated with thickness, loading, and quadrupole. Thickness and loading are linear components and are directly related to the blade surface pressure and geometric definition. Quadrupole is a non-linear component related to the velocity derivatives in air around the airfoil. Non-linear effects are important when the airfoils are operating near their section critical Mach number. This method which recognizes the details of the blade allows much more effective noise reduction designs.

As mentioned earlier, blade sweep can be a very effective means for performance improvement, that is, increasing efficiency and reducing noise. The advantages of sweep for Prop-Fan are quite significant for high subsonic airspeed where the blade tip helical Mach number is supersonic. The character of the aerodynamic and acoustic improvements differ in that efficiency peaks at about 40 degrees of tip sweep while noise continues to decrease as sweep increases. The reason is that noise reduction is attributed to eliminating compressibility effects as with aero and also to a cancellation phenomenon. In fact, the cancellation of source noise by sweep can be accomplished for subsonic tip helicals as well, once compressibility has been eliminated. For the latest Prop-Fan blade design

efficiency is up two percentage points and near field noise is down 18 dB compared to a straight blade. For the Prop-Fan, near field source noise at 0.8 Mach cruise is only one-third of the story associated with a comfortable interior of about 80 dB ). In order to achieve this very quiet aircraft interior noise level, source noise reductions are being pursued and the source noise objectives are considered achievable. Recent interior noise data indicates that further reductions are possible by correctly handling phasing and rotation effects. Synchrophasing can reduce the level in the peak noise area substantially. Finally, the fuselage is designed for attenuation and there is about 20 dB noise reduction for a standard turbo-fan type fuselage. Increased noise attenuation fuselage designs are under study and are considered practical. So, at 0.8 Mach it is possible to achieve a quiet interior. At lower Mach number it becomes easier.

The blade concept for improved efficiency and reduced noise must be structurally sound. Blade construction is key to a propeller/Prop-Fan design. It establishes the structural dynamics, is the major weight contributor, sizes the mechanical components, and establishes the maintenance and reliability philosophy. The spar-shell blade construction concept, where the spar is metal structure and the shell is lightweight fiberglass, offers a large weight reduction over the traditional solid aluminum blade and allows the shaping of the blade for enhanced performance with fewer constraints. This spar-shell concept is safer and offers improved reliability and enhanced maintenance. Reliability is improved in several ways such as an integral (buried) blade heater and individually replaceable blades. Failure probability is reduced by eliminating surface damage as a source of structural degradation. Hamilton Standard has accomplished blade designs for swept blades using traditional beam analysis and the more sophisticated finite element analysis technique. The accuracy and the level of information resulting from finite element analysis is quite superior to beam analysis. The stresses and deflections are defined everywhere on the spar, in the bond, and on the shell; and the mode shapes and natural frequencies are more precisely defined. The use of this advanced analysis technique will provide a blade design with high structural confidence and light weight. The Prop-Fan blade construction concept is an extension of the very successful current production fiberglass blade configuration. The highlights of the Hamilton Standard metal spar-composite shell experience are 5000 blades manufactured of 22 different designs. Thirteen achieved flight test status and four of these achieved production. The estimated blade flight time is 1.7 million hours.

I have reviewed the last 20 plus years of Hamilton Standard blade safety experience and the data shows about 35 million flight hours between in-flight blade fractures on reciprocating engines and no in-flight fractures on turbine engines in 60 million hours. This compares with general aviation data indicating about one million flight hours between fractures. A review of our blade fractures indicates that all were due to damaged exterior surfaces operating in the high engine vibratory environment of a recip. Elimination of the recip environment has eliminated blade fractures. It is projected that elimination of the environmental damage to the blade structure will reduce the probability of failure. Coupling this with

improved structural analysis techniques should virtually eliminate blade failures.

A study recently done for NASA determined the reliability and maintenance costs for a typical turboprop propulsion system such as the Electra. Specific problem areas were isolated and improved upon in a preliminary design of a new Prop-Fan propulsion system. It was found that significant reliability improvements and maintenance cost reductions could be achieved for both the propeller and the turboprop related portions of the gearbox. In both cases, adoption of a modern on-condition maintenance philosophy, thereby eliminating scheduled major maintenance and overhaul, reduced costs in half. It was found on the Electra gearbox that the non-turboprop functions of engine and airframe accessory drives accounted for about 25% of the gearbox unscheduled maintenance costs. Such drives are necessary for any propulsion system and should be accounted with the core engine for turboprops as they are for turbofans. Lastly, as mentioned earlier on advanced blades, improvements in cost can be made as a result of improved reliability and modularity. Simplified component hardware, individually removed with simple procedures finally results in dollars per flight hour which are very low. The propulsion system maintenance cost is dominated by the turbine core engine, not the propulsive device.

Advanced design techniques when applied to advanced turboprops or Prop-Fans operating at high subsonic Mach number have improved performance over both conventional turboprops and high bypass turbofans. They additionally offer uncompromised safety and high reliability/low maintenance characteristics. Application of this propulsion concept extends the traditional turboprop utilization in General Aviation to high Mach where significant gains can be achieved over turbofans.

## **ADVANCED TURBOPROP POTENTIAL FOR HIGH SPEED**

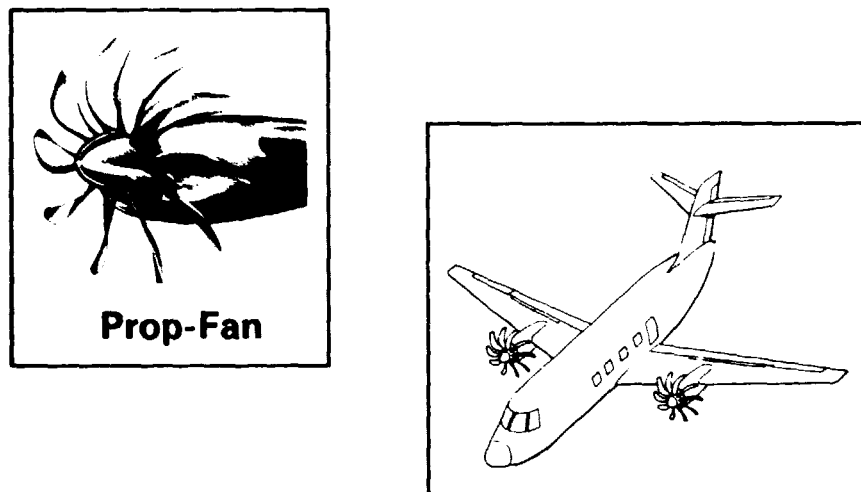


Figure 1

## **ADVANCED TURBOPROP OBJECTIVES**

- **Improved Performance Above  $M = 0.55$**
- **Low Airport Noise**
- **Turboprop Interior Comfort**
- **Enhanced Structural Integrity**
- **Reduced Operating Costs**

Figure 2

## VARIATION OF INSTALLED EFFICIENCY

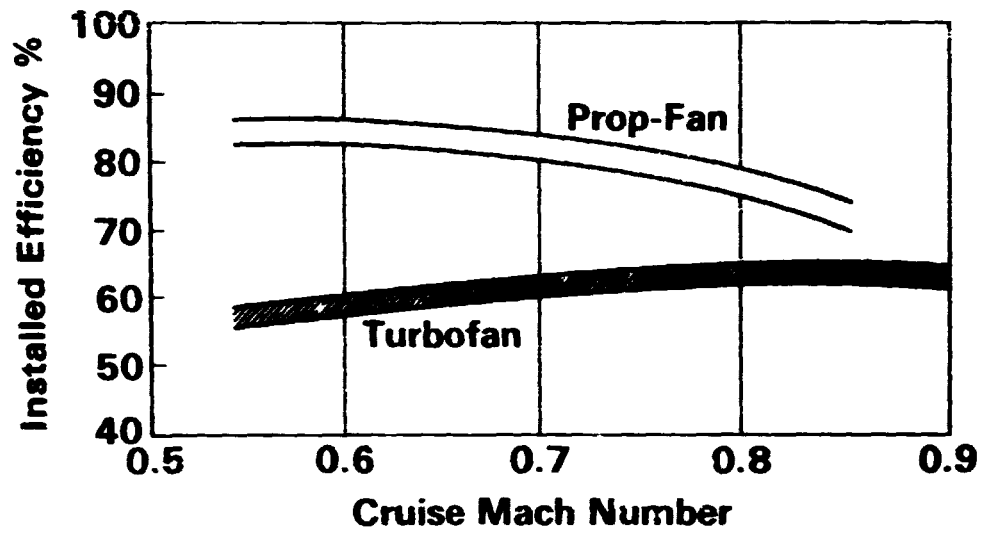


Figure 3

## FUEL SAVINGS Prop-Fan Vs. Turbofan

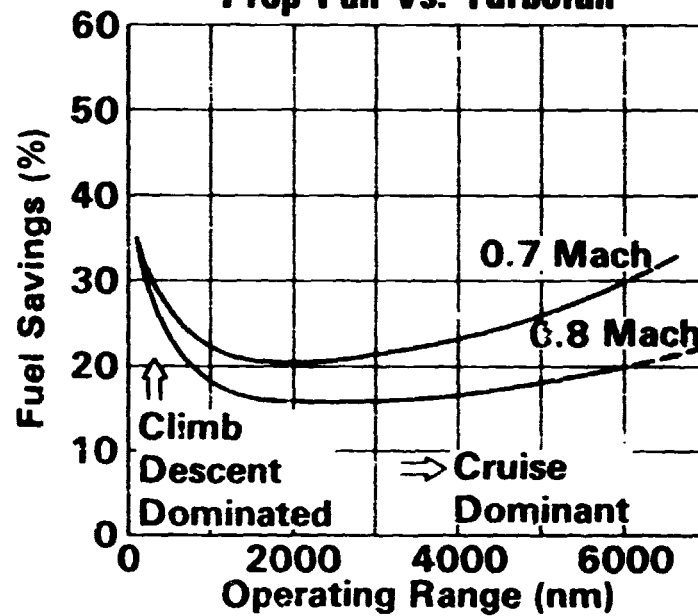
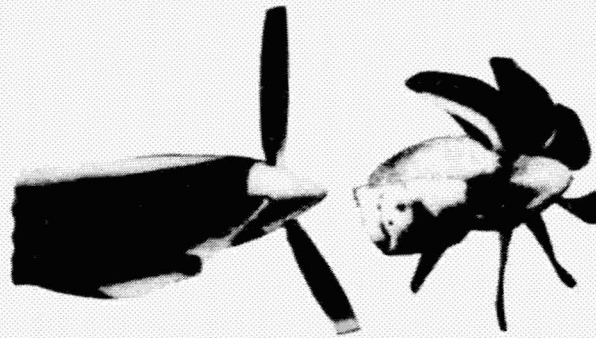


Figure 4

## TURBOPROP COMPARISON

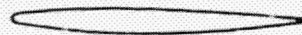


	<u>Conv. Turboprops</u>	<u>Prop-Fan</u>
<b>Mach</b>	0.3 to 0.5	0.6 to 0.8
<b>Altitude (Ft)</b>	15K to 30K	25K to 45K
<b>Power/Dia<sup>2</sup></b>	5-10	20-40
<b>Blades</b>	3 to 5	6 to 10
<b>Tip Speed (Fps)</b>	800 to 950	700 to 800

Figure 5

## ADVANCED AERODYNAMIC CONCEPTS

**Reduced Thickness**



**Blade Shape**



**Nacelle Shape**



**Area Ruling**



**Advanced Airfoils**



Figure 6

## ADVANCED AERO ANALYSIS

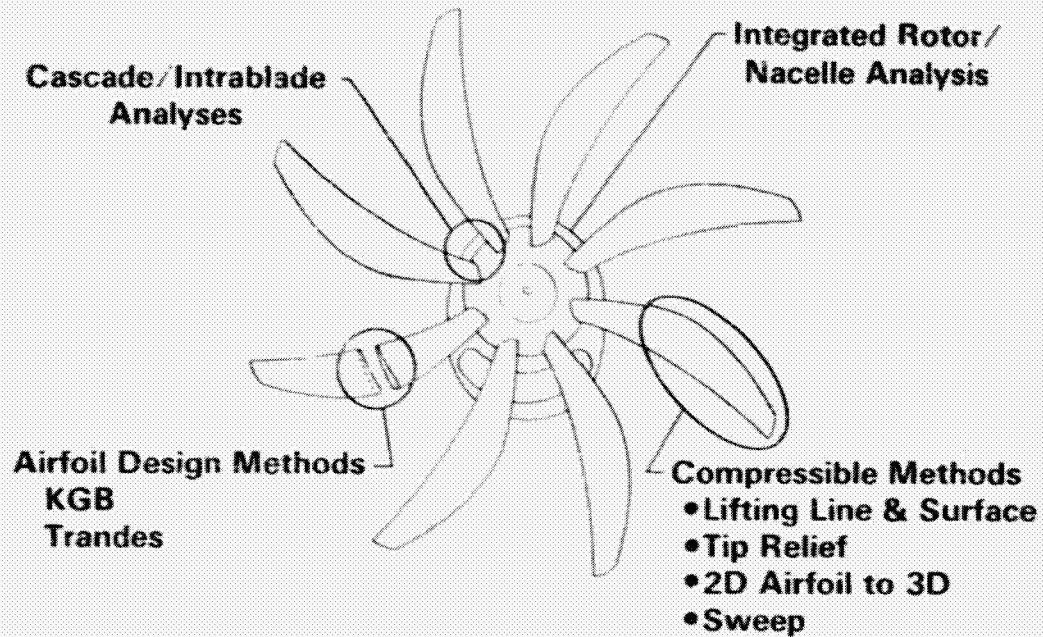


Figure 7

## TURBOPROP UNINSTALLED CRUISE EFFICIENCY TRENDS

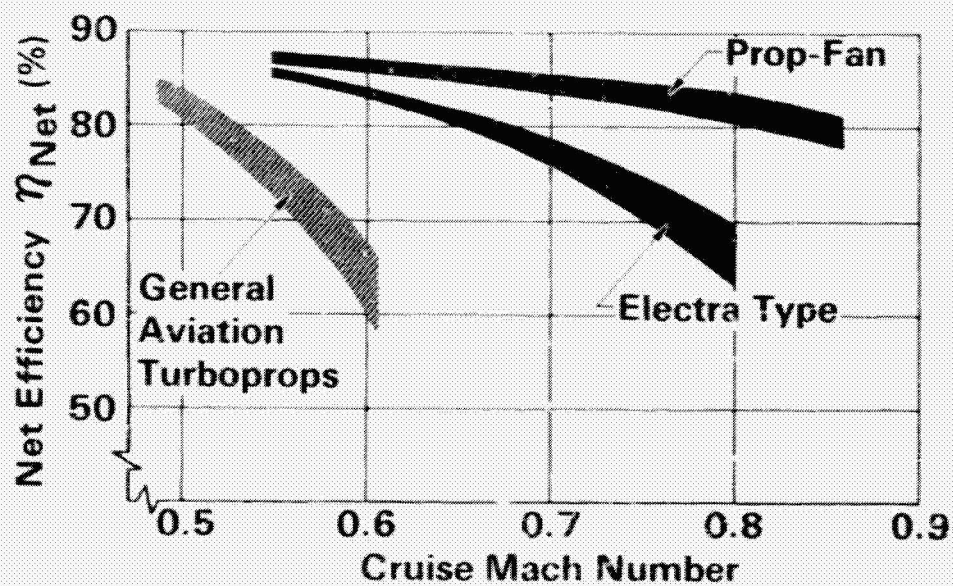


Figure 8



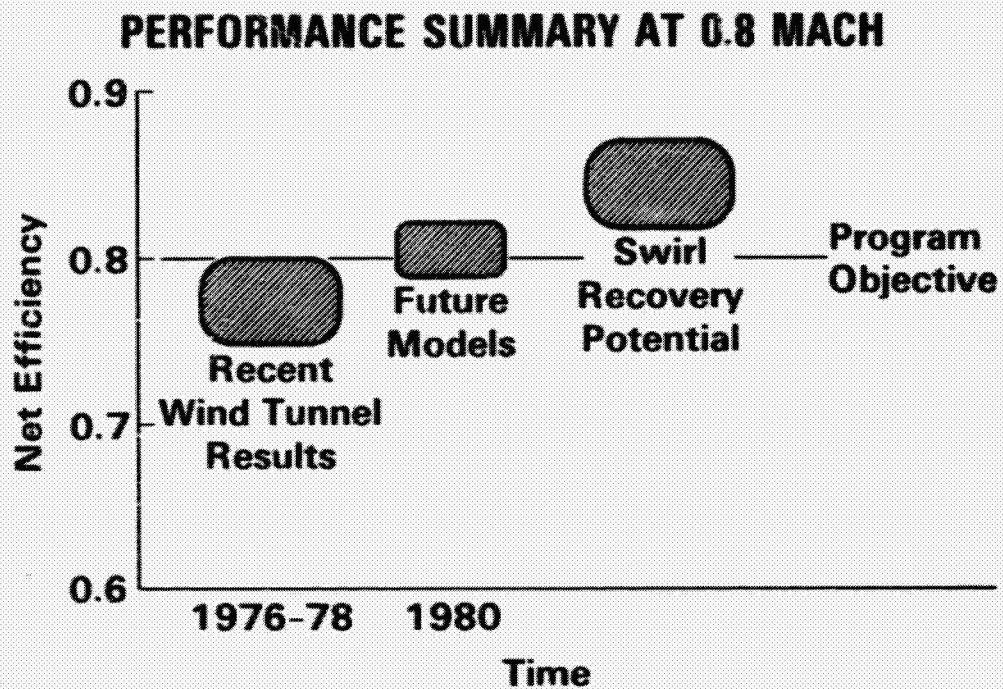


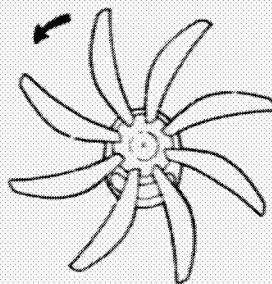
Figure 9

## ADVANCED NOISE REDUCTION CONCEPTS

Reduced Thickness



Lower Tip Speed and Increased Blade Number



Blade Shape and Sweep



Advanced Airfoils



Figure 10

## FAR-FIELD NOISE REDUCTION POTENTIAL (Constant Thrust)

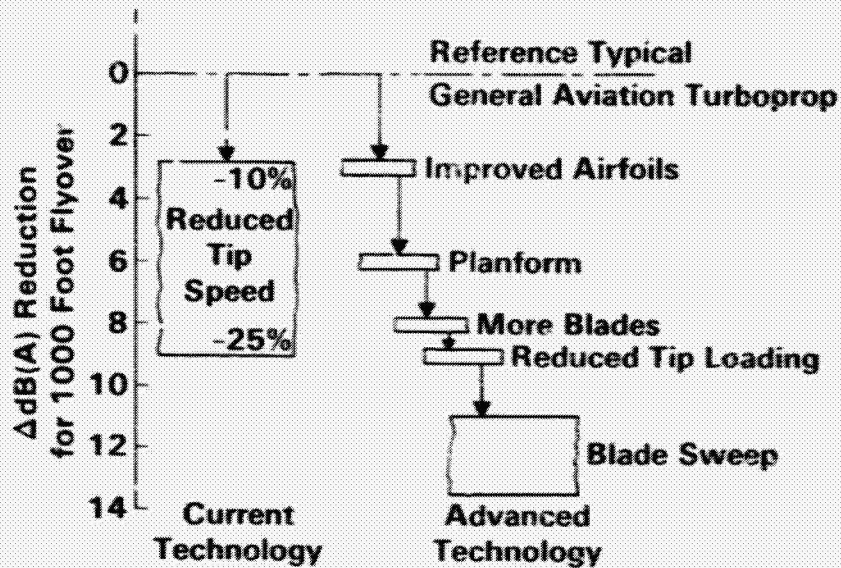


Figure 11

## ADVANCED ACOUSTIC ANALYSIS

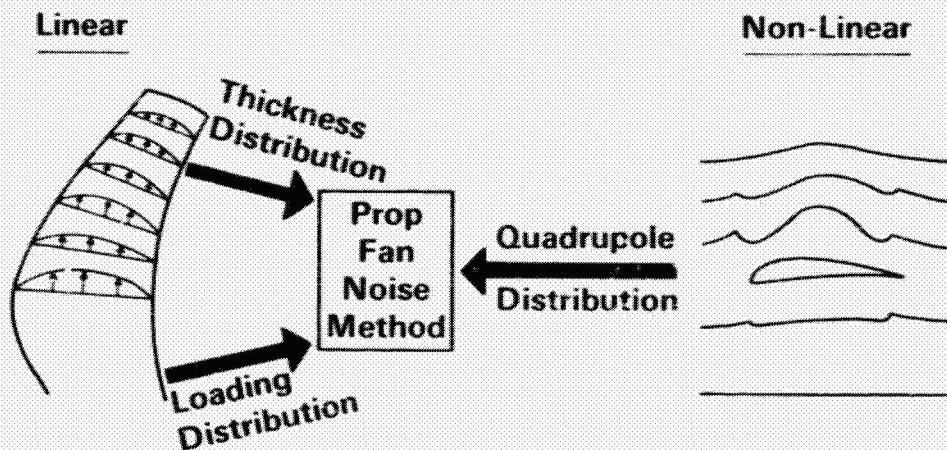


Figure 12

## EFFECTS OF BLADE SWEEP

0.8 Mach Cruise  
800 Ft/Sec Tip Speed

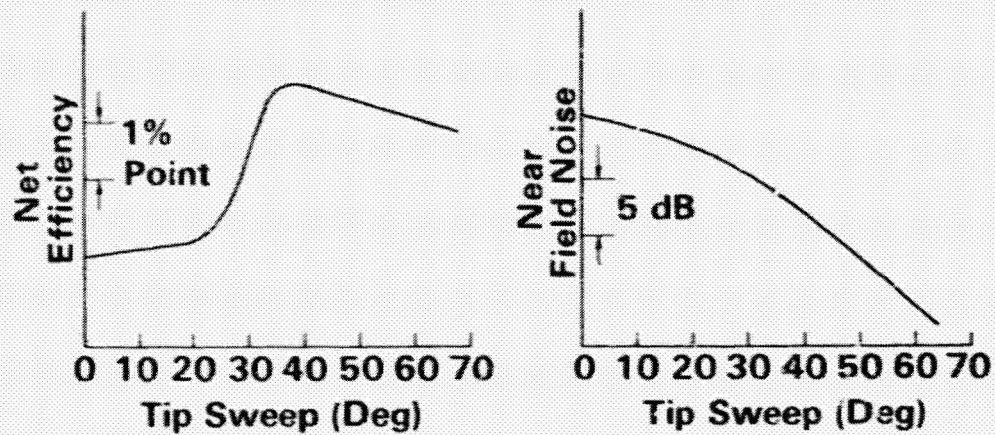


Figure 13

## ACHIEVING THE CABIN NOISE GOAL

0.8 Mach Cruise

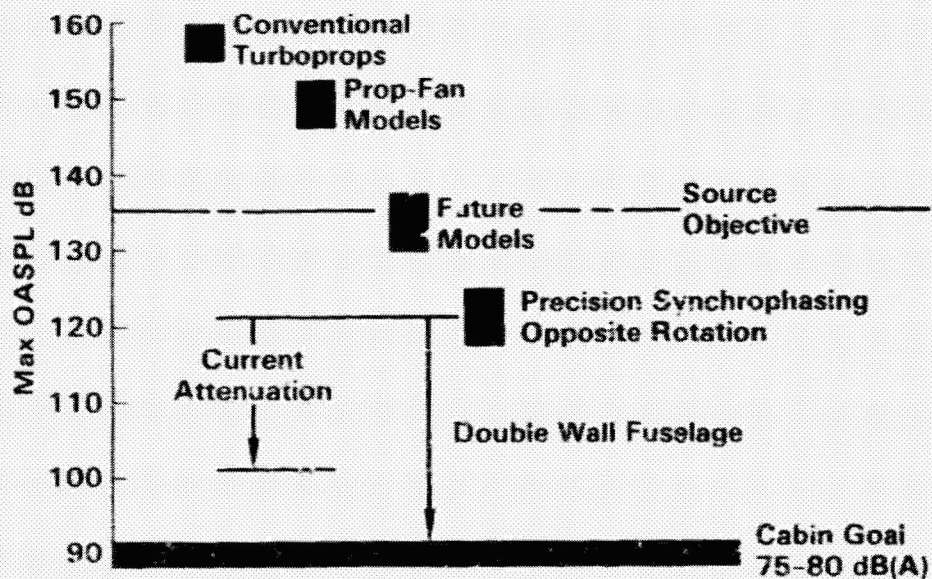
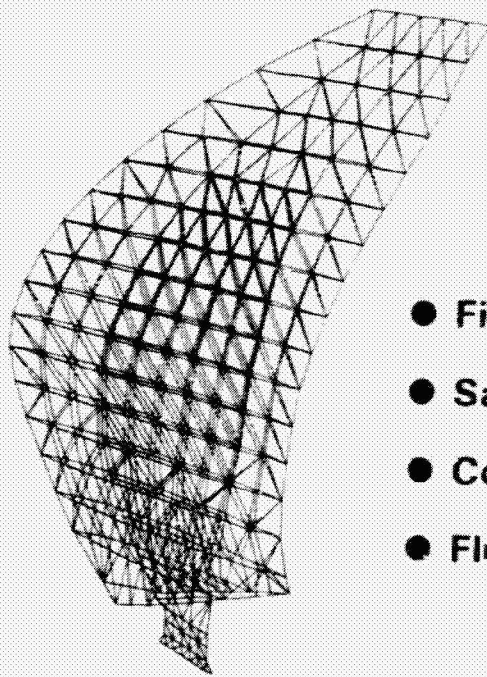


Figure 14

## **COMPARISON OF METAL SPAR-COMPOSITE SHELL AND SOLID ALUMINUM BLADES**

- **25-50% Weight Savings**
- **Enhanced Performance**
- **Greater Safety**
- **Reduced Maintenance**

Figure 15

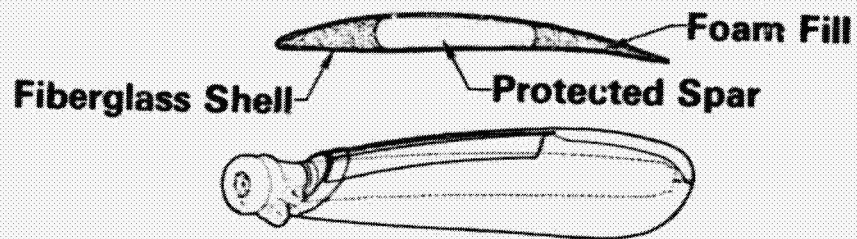


## **ADVANCED BLADE DESIGN TECHNIQUES**

- **Finite Element Analysis**
- **Safe Stresses and Deflections**
- **Controlled Natural Frequencies**
- **Flutter Free**

Figure 16

## CURRENT PRODUCTION FIBERGLASS BLADE



## PROP-FAN BLADE

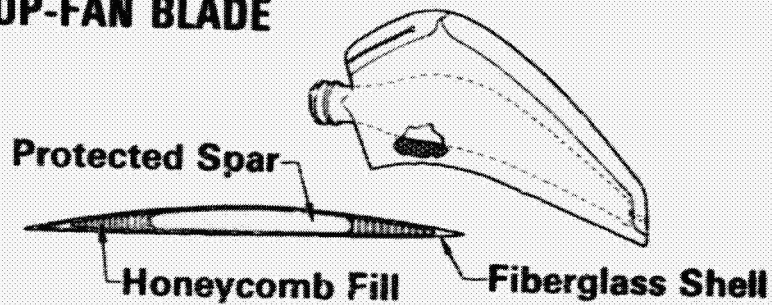


Figure 17

## BLADE SAFETY EXPERIENCE

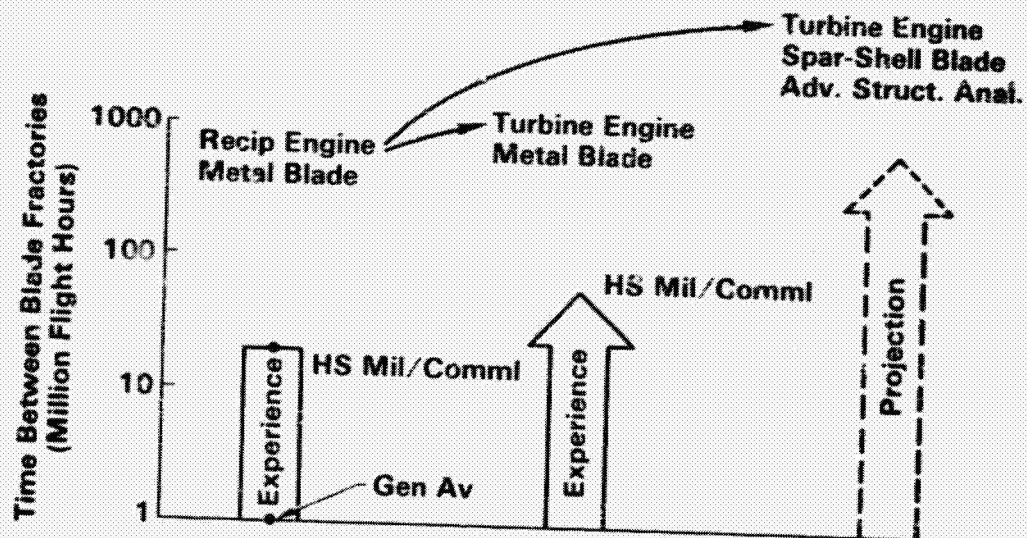


Figure 18

## REDUCED MAINTENANCE

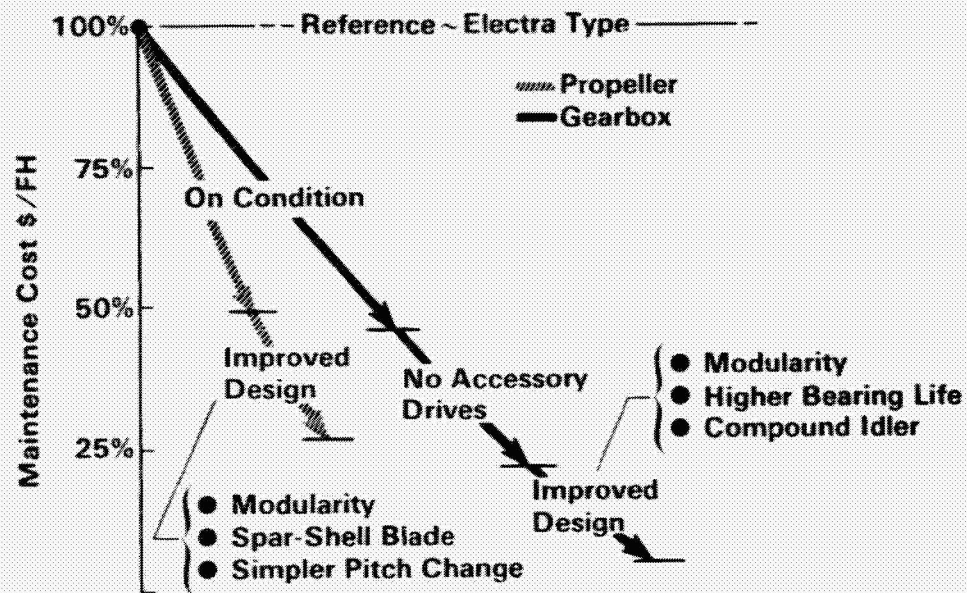


Figure 19

## SUMMARY

### Advanced Turboprops Can Meet Objectives

- Improved Efficiency
- Low Noise Profile
- High Safety & Reliability

And Offer New Potential for General Aviation

Figure 20



917  
N80-22344

## HIGH-SPEED-PROPELLER WIND-TUNNEL AEROACOUSTIC RESULTS

Robert J. Jeracki and James H. Dittmar  
National Aeronautics and Space Administration  
Lewis Research Center

The energy saving potential of the high-speed turboprop has been discussed with increased interest in recent years (refs. 1 to 9; with many additional references in ref. 1). Gatzen's paper at this conference indicated the benefits from and the approach to applying the high-speed propeller to business-jet type of aircraft. These aircraft fly in the Mach 0.5 to 0.8 range, above the speeds of present turboprop-powered executive aircraft, and at altitudes above 9.144 km (30 000 ft) where turbojet and turbofan engines are presently used. An advanced high-speed turboprop, however, has the potential for significant fuel saving compared with these two propulsion systems. The high flight speed and altitude and other design constraints make the high-speed turboprop a unique propulsion system.

This paper will present some aerodynamic concepts, explain how these are applied to advanced propeller design, and then show results from recent wind-tunnel tests at Lewis. This should give a feeling to why the concepts were used and their importance in obtaining good aerodynamic and acoustic performance. Figure 1 shows how unique this propulsion system really would be, based on the design concepts being considered for the high-speed turboprop. Most obvious are the blade sweep, long blade chords, and, of course, the large number of blades. Other details not easily seen in this photograph will be described later. These unique features come from the need to keep a reasonable propeller size and to fly efficiently and quietly at high speed and altitude. The large fuel saving potential and the lack of an adequate data base for this new propulsion concept prompted NASA to begin a test program to verify the high-speed turboprop potential for saving energy.

### AERODYNAMIC CONCEPTS

The high flight Mach number requires the designer to minimize compressibility losses. Some aerodynamic concepts that could be used are shown in figure 2. In the blade tip region compressibility loss is reduced by using thin airfoil sections and by sweeping the blade tip back, as illustrated by the two sketches at the top of the figure. In the hub region the blockage of the nacelle behind the propeller and area-ruffling, or sculpting-out of the spinner between blades, are used to reduce losses. These are illustrated by the next two sketches. Advanced airfoils designed for high performance and low noise signature were not part of these model designs, but these could be included

later as future improvements.

The effects of these concepts incorporated into a propeller design are shown in figure 3. This figure is based on the cruise condition at Mach 0.8 and presents the Mach number approaching the blade from the hub to the tip. The total Mach number, which includes both the free-stream component and the propeller rotational component, is the top curve. The Mach number starts just above the cruise Mach number at the hub, increases as the rotational velocity becomes larger, and reaches Mach 1.14 at the tip for the design conditions.

This local approach Mach number must be compared with the Mach number where each blade airfoil section enters into drag rise to evaluate how the propeller will perform. Therefore, for a thin blade with a thickness-to-blade-chord ratio of about 15 percent at the hub and down to 2 percent at the tip, isolated two-dimensional airfoil data were used to predict the Mach number at which each airfoil section would go into drag rise. That drag rise Mach number is the second curve in figure 3. Note that the local Mach number is above the drag rise Mach number from the hub to the tip and that across the entire blade is a large potential compressibility loss region. This loss region is depicted in figure 3 by the cross-hatched region.

The aerodynamic concepts shown in figure 2 were used to reduce these losses. In the tip region sweep reduces the component of velocity normal to the blade airfoil section, as is done for swept wings. So the Mach number is reduced from the local to the effective Mach number shown in figure 3. With the effective Mach number below the drag divergence Mach number in the tip region, the loss is significantly reduced. In the hub region nacelle blockage behind the propeller reduces the local Mach number through the propeller plane. That is plotted as the effective Mach number curve near the hub. Additional suppression is used here because, with the large number of blades, the hub blade sections operate as essentially a cascade or fan where blade-to-blade choking could be a problem. Area-ruling the spinner between blades gives further protection from choking by opening the flow area between the blades at the spinner. Further discussion of the application of these concepts to high-speed propeller design is given in references 1, 4, and 5, and blade structural design is covered in references 3 and 10.

#### PROPELLER MODEL DESIGNS

The concepts described above were used to design a series of propeller models for wind-tunnel testing in a cooperative program between Lewis and Hamilton Standard. The three basic blade planforms pictured in figure 4 represent the four propeller designs. In common are the blade tip speed of 244 m/sec (800 ft/sec), cruise power loading of 301 kW/m<sup>2</sup> (37.5 shp/ft<sup>2</sup>) (which is about four times that of a conventional propeller such as on the Electra), and eight blades. The planforms are identified by their sweeps of 0, 30°, and 45°. Here, the tip sweep is approximately the angle of the tip of the blade measured back from a radial line normal to the axis of rotation through the blade root.



The original 0 and 30° swept blades were designed using existing established analyses (ref. 11) that lacked a refined methodology to design the twist of a swept blade. Initial tests of the 30° swept design (SR-1) indicated a retwist was required (that is, redistribution of the blade load from hub to tip). The retwisted blade became the second 30° swept design (SR-1M). The 45° swept blade was swept, and the planform shaped for acoustic suppression as well as improved aerodynamic performance. More detailed discussions of the aeroacoustic design methodology are presented in references 3, 12, and 13.

Efficiency and noise level were predicted when these blades were designed. Those predicted efficiencies (listed in fig. 4) indicated improved performance with increased sweep. Those noise predictions indicated some reduction for 30° of sweep and significant reduction for the aeroacoustic 45° swept design.

The photographs in figure 5 show the 0, 30°, and 45° swept, 62.2-cm (24.5-in.) diameter propeller models installed on the Propeller Test Rig (PTR) in the Lewis 8- by 6-foot wind tunnel. The tunnel (ref. 13) has a porous wall test section to minimize any wall interactions. The PTR is powered by a 746-kW (1000-hp) air turbine using a continuous flow,  $3.1 \times 10^6$ -N/m<sup>2</sup> (450-psi) air system routed through the support strut. Force and torque on the propeller are measured on a rotating balance located inside of an axisymmetric nacelle behind the propeller.

#### PROPELLER AERODYNAMIC PERFORMANCE

Typical test results from the 45° swept design are shown in figure 6 to give an understanding of the way data were taken and used. This is the basic propeller data plot where net thrust efficiency and a dimensionless power coefficient are plotted as ordinates. The abscissa is the advance ratio, which is proportional to the ratio of flight or advance speed to blade tip speed. As tip speed increases from windmill (no power), the advance ratio decreases as shown by the two horizontal scales. Blade angle is set and data are taken from windmill to higher power as shown by the data symbols on the power coefficient plot. The blade angle ( $\beta_{3/4}$ ), measured at  $3/4$  of the propeller radius, becomes 90° when the chord of that airfoil section is aligned directly with the flight direction. As power is increased the thrust increases and, as seen in the upper data curves, the net thrust efficiency increases, reaches a peak, and then begins to drop off. Other blade angles yield similar power and efficiency curves.

At the design Mach number of 0.8, the design power loading and design tip speed give a power coefficient of 1.7 and advance ratio of 3.06. A solid line is drawn through this point on the power coefficient plot, intersecting the two lines of data shown. This solid line represents the design power at different propeller tip speeds. The efficiency at the design power can be found for each blade angle, indicated by each vertical line. Then the variation of net efficiency with advanced ratio (i.e., tip speed) at design power can be plotted as shown in figure 7. This plot is for models with area-ruled spinners at the design power loading at Mach 0.8. Curves of net efficiency versus advance ratio are compared for different sweep angles. Significant improvement can be seen in

going from 0 to 30° of sweep. The 45° swept blade shows still more improvement, especially at low advance ratios (corresponding to high tip speeds). The overall improvement at the design advance ratio of 3.06 is about 3 percent.

Other important design variations were investigated using the 30° swept designs. As noted in the description of the blade design, there were two different twist, or loading distributions, with the same 30° swept planform. The blade design with the revised (reduced) twist was tested with both a conic and an area-ruled spinner. The performance comparison is shown in figure 8. As in the previous figure, this one presents data for the design Mach number and power loading. The original design (baseline twist) was tested with a conic spinner and is the lowest of the three data curves. Retwisting to increase the load at the tip improved the performance near the design advance ratio, where the highest efficiency for that blade-spinner combination then occurred. That reduced-twist design was also tested with an area-ruled spinner. That change improved the performance about 1 percent over the full range of tip speeds tested. This figure indicates the benefit of area-ruling and that the proper twist or loading is required to obtain high performance.

Because figures 7 and 8 summarize data at the design power, the performance at the actual design point at Mach 0.8 can be obtained as the net efficiency at the advance ratio (3.06) corresponding to the design tip speed. Similarly, net efficiency at other free-stream Mach numbers can be obtained at the same power coefficient and advance ratio as the Mach 0.8 design point. The variation of performance with free-stream Mach number is shown in figure 9 at constant power coefficient and advance ratio, for the 0, 30°, and 45° swept blade designs with area-ruled spinners. This plot is interesting because the ideal efficiency, presented as the upper dashed line, is constant across the Mach number range for a given value of power coefficient and advance ratio. The ideal efficiency is the performance of an optimum propeller with no blade drag and, so, represents only axial momentum, swirl, and tip losses. Below that line is the real world where viscous and compressibility losses occur. As the data show, those losses increase as Mach number is increased.

Again, the benefit from sweep of about 3 percent is seen at Mach 0.8. The efficiency of the 45° swept model approached the value used in the studies which showed the large fuel saving potential for the high-speed turboprop. Actually, at power loadings lower than design, the efficiency slightly exceeded the study value. However, the lower power loading would require a larger and heavier propeller for the same aircraft installation. The 45° swept blade which achieved this high performance also retains fairly high efficiency out to Mach 0.85. More performance details are given in references 1, 4, 5, and 6.

#### PROPELLER ACOUSTIC PERFORMANCE

Acoustic data were also taken in the tunnel, since the cabin noise at cruise conditions is of concern. The transonic propeller relative tip speed of these blade designs has the potential for generating high noise levels. This noise needs to be minimized and fuselage attenuation needs some improvement. Wall-mounted pressure transducers were used to obtain near-field acoustic data

for the propeller models. (Further details are given in refs. 15 and 16.) Wave shapes of the near-field pressure signal during blade passages are shown in figure 10. These are enhanced pressure-time traces for both the straight blade and the aeroacoustically designed  $45^\circ$  swept blade. The transducer closest to the propeller was used (on the tunnel wall in the plane of the propeller). As can be seen, the trace for the straight blade shows a high amplitude, steep wave shape, which approaches the classic N wave shock pattern. However, in the plot for the quieter  $45^\circ$  swept blade, an almost sinusoidal wave was observed which is also of considerably less amplitude. These differences in the character of the traces indicated that the aeroacoustically designed planform of the  $45^\circ$  swept blade has been successful in reducing the sharp pressure rise that would normally be associated with transonic helical-tip-speed propellers.

Another comparison of the benefits of sweep makes the magnitude of the noise reduction more apparent. Figure 11 is a plot of the maximum blade passage tone on the tunnel ceiling versus the helical-tip (total, including flight and rotational) Mach number. The advance ratio and power coefficient for all of the data points are approximately the design values. Variation in helical-tip Mach number is obtained by taking data at different free-stream Mach numbers. The plots for both 0 and  $45^\circ$  swept blades exhibit a region of sharp noise increase with increasing helical-tip Mach number, which is then followed by a region where noise levels off. The tailored sweep of the  $45^\circ$  design provides noise reduction over the complete range of tip speeds. Near the cruise design tip Mach number of 1.14, the reduction is about 5 to 6 dB and appears to be even larger at the lower tip speeds tested. Data in reference 16 from a  $50^\circ$  swept blade, together with the data shown here, indicate that increasing tip sweep delays the sharp increase in noise to a higher tip Mach number. This delay in noise rise would be expected just as sweep delays the sharp drag rise of the blades by postponing the onset of shocks in the blade tip region. The overall noise reduction at high and low tip speeds indicates the benefit of the aerodynamic methodology of the  $45^\circ$  swept design.

Noise data were taken at positions in front of and behind the propeller plane on the tunnel ceiling. Figure 12 is a plot of the axial variation of the blade passage tone versus the axial position from the propeller plane plotted in propeller diameters. The ceiling itself is about 1.5 propeller diameters from the propeller tip. The same significant reduction in peak noise level for the  $45^\circ$  swept blade can be observed here as in figure 11. At Mach 0.8 cruise the noise from these propellers differs only slightly ahead of the propeller and tends to have the largest difference farther behind the propeller. Notice the directivity of the noise pattern. The peak noise level has dropped off significantly from the peak within a total distance of about 2 propeller diameters. This indicates that any required fuselage treatment would be limited in area. More details and data are given in references 15 and 16.

#### SUMMARY OF RESULTS

The noise reduction and the high measured performance show the aerodynamic and acoustic benefits of advanced propeller design concepts. High aerodynamic performance was obtained at Mach 0.8; within 1 percent of the study value used

to predict large potential fuel saving for the high-speed turboprop. Performance near 80 percent was obtained at lower than-design power loadings. Nacelle blockage was an important part of the designs, and area-ruling was shown to be important in improving measured performance. Blade tip sweep improved aerodynamic performance about 3 percent, while the aeroacoustic design of the 450 swept propeller reduced cruise near-field noise about 6 dB.

#### FUTURE IMPROVEMENTS

The performance results shown are attractive, and further refinements can be made. There is now a basis for improvements in design and analysis. Figure 13 indicates the future of high-speed turboprop improvements. The lower-left circle represents the current design procedures and model results described in this paper. The propellers were eight bladed, highly loaded, and designed using established analyses, although a number of advanced concepts were incorporated. Two new further advanced models are being designed and should be tested in 1980. These models are advanced, 10-bladed designs which have greater tip sweep and lower tip speed to improve the acoustic as well as the aerodynamic performance. Some refined analyses were available for the design of these blades (ref. 12).

The results of both the present tests and those planned in 1980 will be used to achieve an initial optimum design, called SR-7. When that propeller is being designed, additional advanced analyses (described in Bober's paper at this conference and ref. 11) will be available to further enhance the design process. Testing that design will conclude the present wind tunnel program on propeller performance and noise. Another approach which is under study by NASA as a future research area to further improve performance is to recover the thrust lost in the swirl of the propeller slipstream. The swirl loss for these highly loaded propellers can be as much as 6 to 8 percent in efficiency. Methods being considered for swirl recovery are coaxial counterrotation, wing contouring behind the propeller (to act like a stator), and the introduction of stators behind the propeller. This continued effort, shown in figure 13, is expected to allow future propellers to be designed for high-speed flight with both higher efficiency and significantly lower cruise noise.

#### REFERENCES

1. Jeracki, Robert J.; Mikkelsen, Daniel C.; and Blaha, Bernard J.: Wind Tunnel Performance of Four Energy Efficient Propellers Designed for Mach 0.8 Cruise. NASA TM-79124, 1979 or SAE Paper 790573, Apr. 1979.
2. Nored, Donald L.: Fuel Conservative Aircraft Engine Technology. NASA TM-78962, 1978.
3. Dugan, James F. Jr.; Gatzen, Bernard S.; and Adamson, William M.: Prop-Fan Propulsion - Its Status and Potential. SAE Paper 780995, Nov. 1978.

4. Mikkelsen, Daniel C.; et al.: Design and Performance of Energy Efficient Propellers for Mach 0.8 Cruise. NASA TM X-73612, 1977 or SAE Paper 770458, Mar. 1977.
5. Black, D. M.; Menthe, R. W.; and Wainauski, H. S.: Aerodynamic Design and Performance Testing of an Advanced 30° Swept, Eight Bladed Propeller at Mach Numbers from 0.2 to 0.85. NASA CR-3047, 1978.
6. Rohrbach, Carl: Prop Fan Offers Low Fuel Consumption at Today's Flight Speeds and Altitudes. AIAA Paper 76-667, July 1976.
7. Jackson, A. H., Jr.; and Gatzen, B. S.: Multi-Mission Uses for Prop-Fan Propulsion. Variable Geometry and Multicycle Engines, AGARD-CP-205, Advisory Group For Aerospace Research and Development, Paris, 1977, pp. 15-1 to 15-13.
8. Kraft, G. A.; and Strack, W. C.: Preliminary Study of Advanced Turboprops for Low Energy Consumption. NASA TM X-71740, 1975.
9. Rohrbach, C.; and Seery, M. E.: A New Look at the Turboprop. AIAA Paper 75-1208, Sept. 1975.
10. Cornell, R. W.; and Rothman, E. A.: Design and Analysis of Prop-Fan Blades. AIAA Paper 79-1116, June 1979.
11. Bober, L. A.; and Mitchell, G. A.: Summary of Advanced Methods for Predicting High Speed Propeller Performance. NASA TM-81409, 1980, or AIAA Paper 80-0225, Jan. 1980.
12. Metzger, F. B.; Rohrbach, C.: Aeroacoustic Design of the Prop-Fan. AIAA Paper 79-0610, Mar. 1979.
13. Hanson, D. B.: Near Field Noise of Supersonic Propellers in Forward Flight. AIAA Paper 76-565, July 1976.
14. Swallow, Robert J.; and Aiello, Robert A.: NASA Lewis 8- by 6-Foot Supersonic Wind Tunnel. NASA TM X-71542, 1974.
15. Dittmar, James H.; Blaha, Bernard J.; and Jeracki, Robert J.: Tone Noise of Three Supersonic Helical Tip Speed Propellers in a Wind Tunnel at 0.8 Mach Number. NASA TM-79046, 1978.
16. Dittmar, James H.; Jeracki, Robert J.; and Blaha, Bernard J.: Tone Noise of Three Supersonic Helical Tip Speed Propellers in a Wind Tunnel. NASA TM-79167, 1979.

ADVANCED LOW ENERGY TURBOPROP MODEL  
MACH 0.8 CRUISE

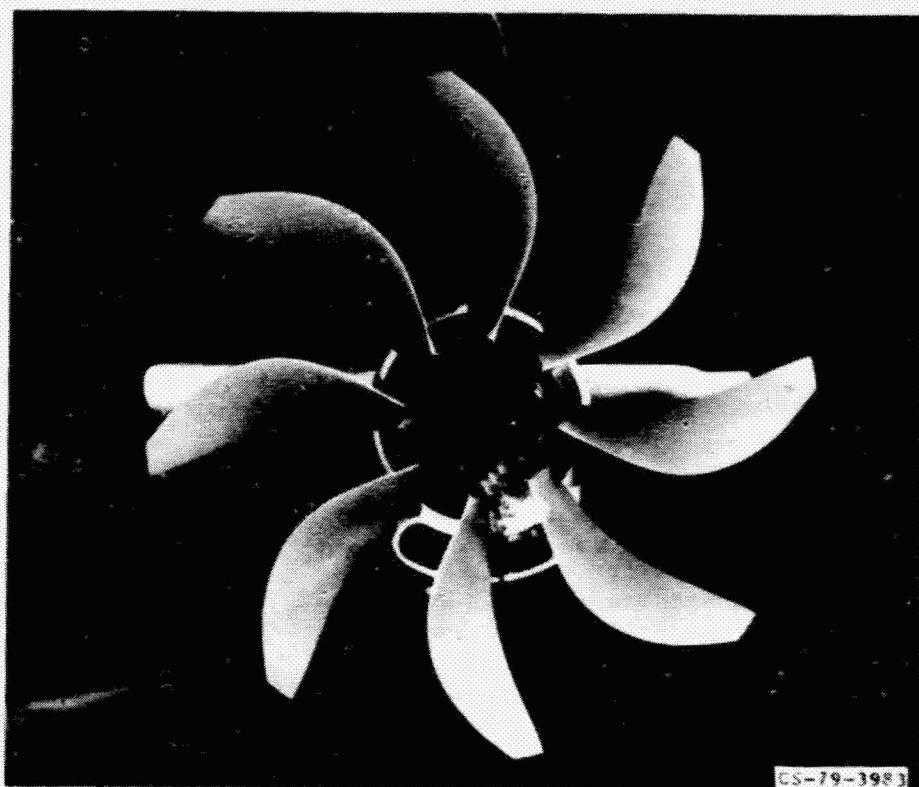


Figure 1

ADVANCED AERODYNAMIC CONCEPTS

REDUCED THICKNESS



BLADE SWEEP



NACELLE BLOCKAGE



SPINNER AREA RULING



ADVANCED AIRFOILS



CS-79-1472

Figure 2

## EFFECTS OF ADVANCED AERODYNAMIC CONCEPTS

$$M_0 = 0.8$$

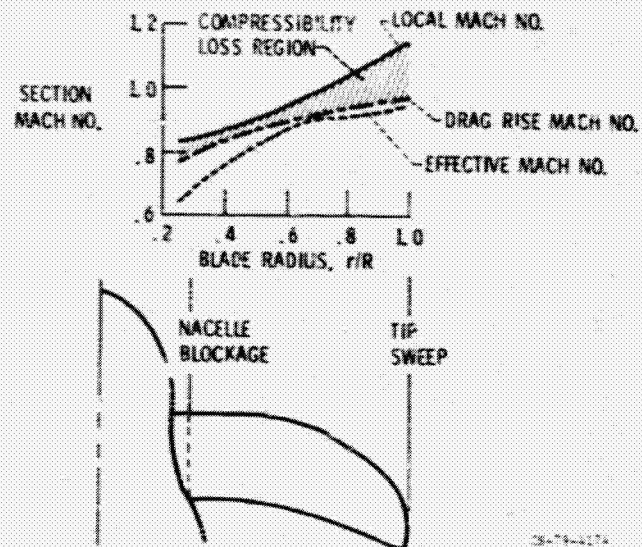
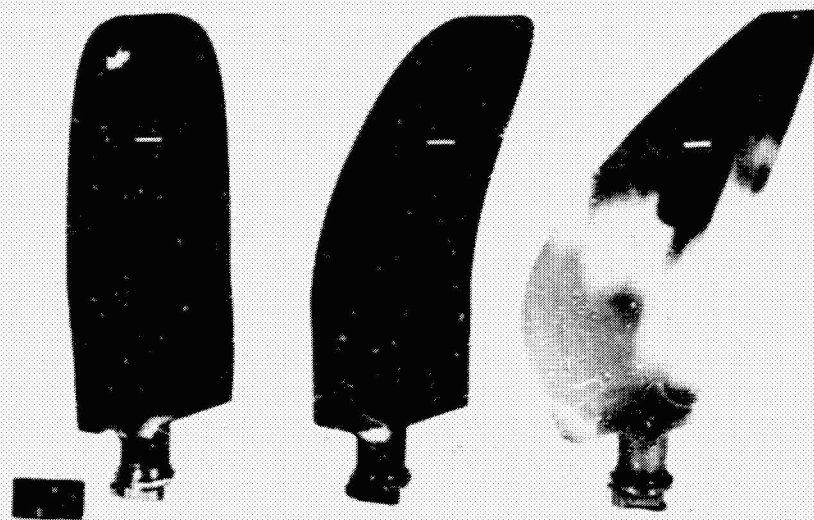


Figure 3

## PROPELLER MODEL COMPARISON

TIP SPEED, ft/sec 800  
POWER LOADING, hp/ft<sup>2</sup> 37.5  
NO. OF BLADES 8



	SR-2	SR-1, IM	SR-3
TIP SWEEP ANGLE, deg	0	30	45
PREDICTED DESIGN EFF, %	76.6	78.9, 79.3	81.1
PREDICTED DESIGN NOISE REDUCTION, ΔdB	REF.	-2	-6

Figure 4

# INSTALLATION OF PROPELLER MODELS IN THE 8X6 WIND TUNNEL

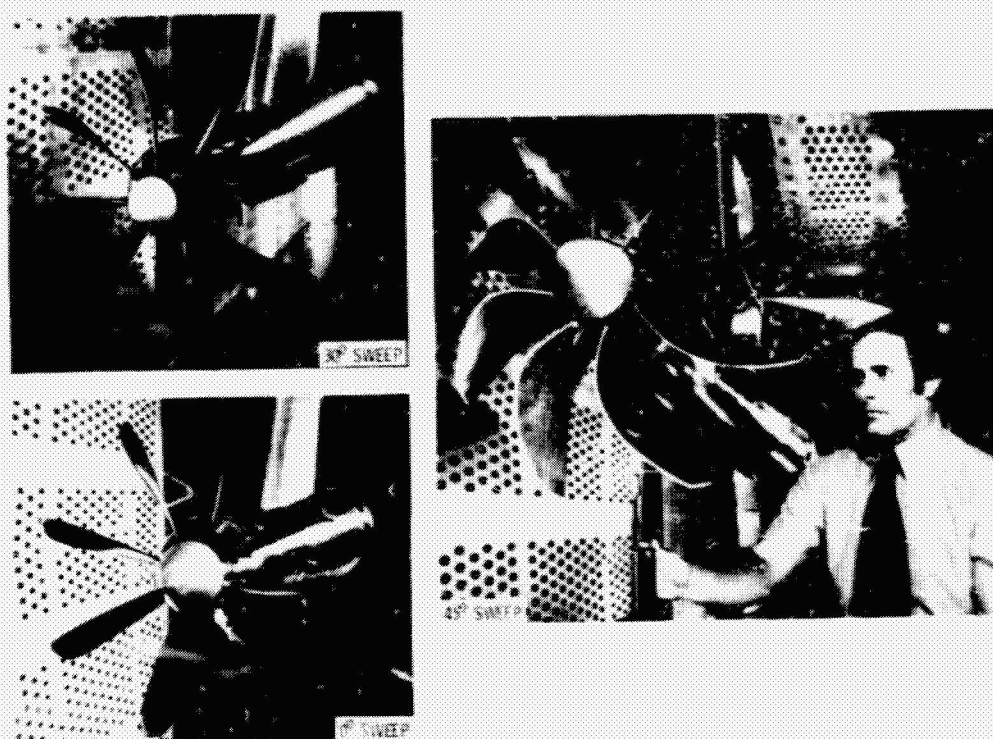


Figure 5

## EFFECT OF SWEEP ON NET EFFICIENCY

AREA RULED; MACH 0.8; 100% DESIGN POWER LOADING

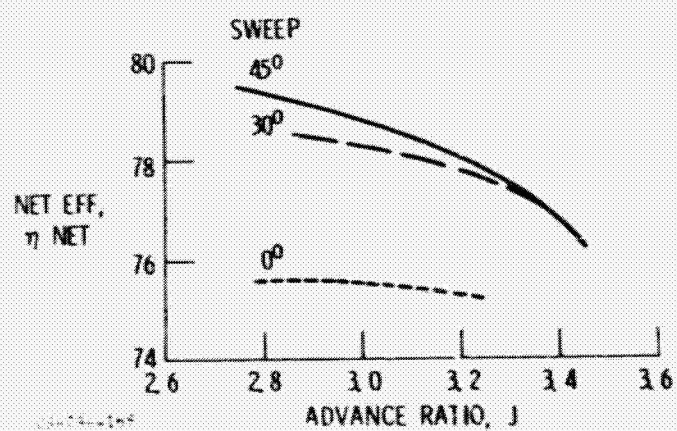


Figure 6



## BASIC MEASURED PERFORMANCE

45° SWEEP;  $M_0 = 0.8$

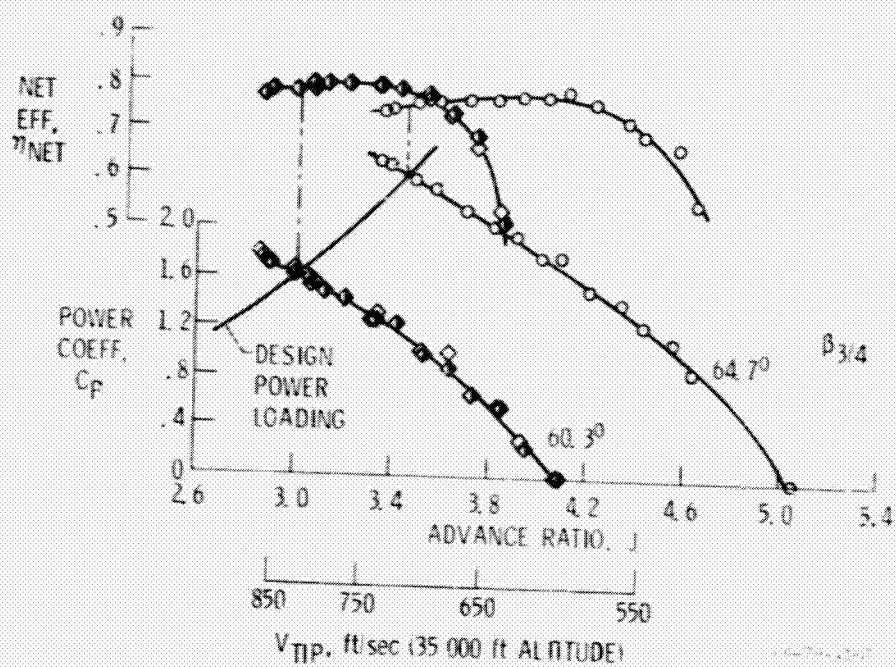


Figure 7

## EFFECT OF TWIST AND AREA RULING ON NET EFFICIENCY

30° SWEEP; MACH 0.8; 100% DESIGN POWER

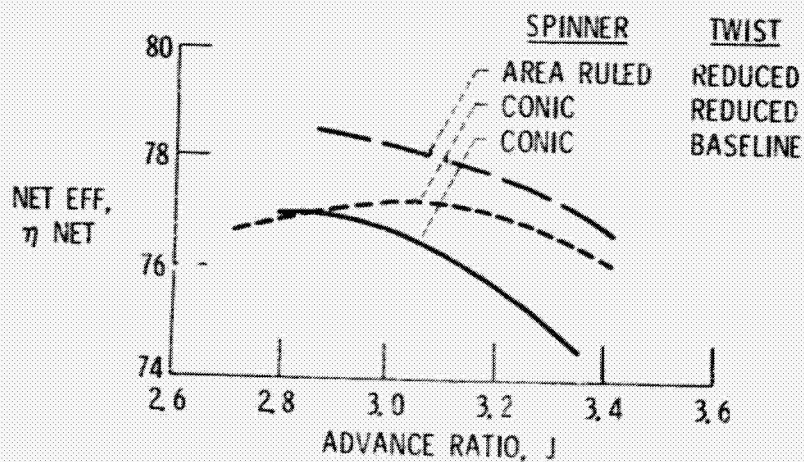


Figure 8

CS-79-4172

# HIGH SPEED PROPELLER PERFORMANCE SUMMARY

AREA RULED SPINNER

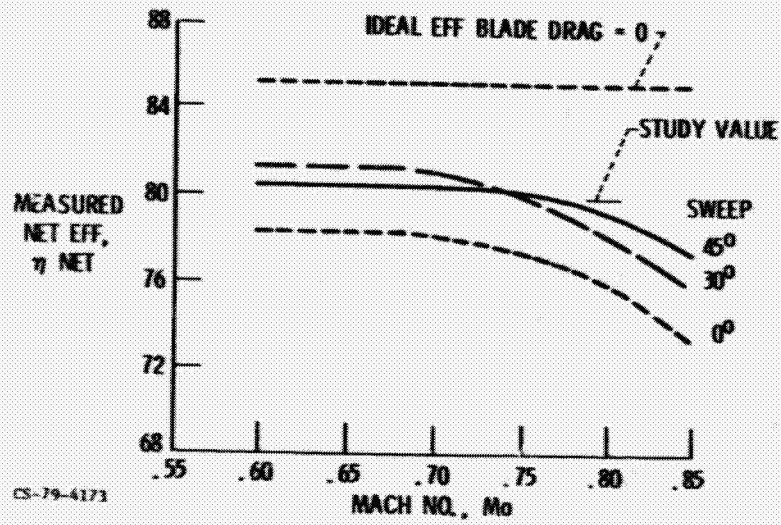


Figure 9

## EFFECT OF SWEEP ON ACOUSTIC PRESSURE SIGNAL

$M_0 = 0.8$ ; NEAR DESIGN CONDITIONS; NEAR FIELD

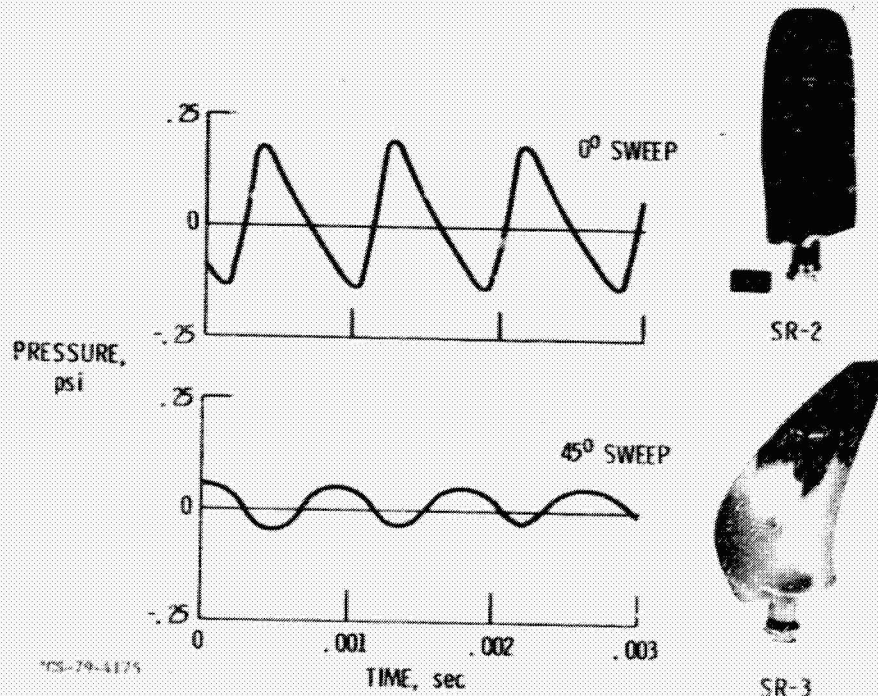


Figure 10

## EFFECT OF TIP MACH NUMBER ON MEASURED NOISE

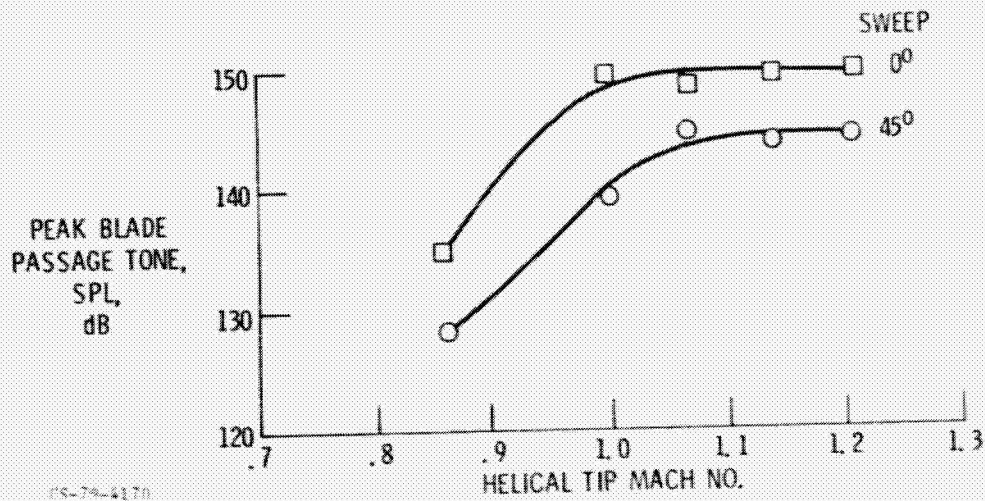


Figure 11

## DIRECTIVITY OF MEASURED NOISE

$M_0 = 0.8$ ; NEAR DESIGN CONDITIONS: NEAR FIELD

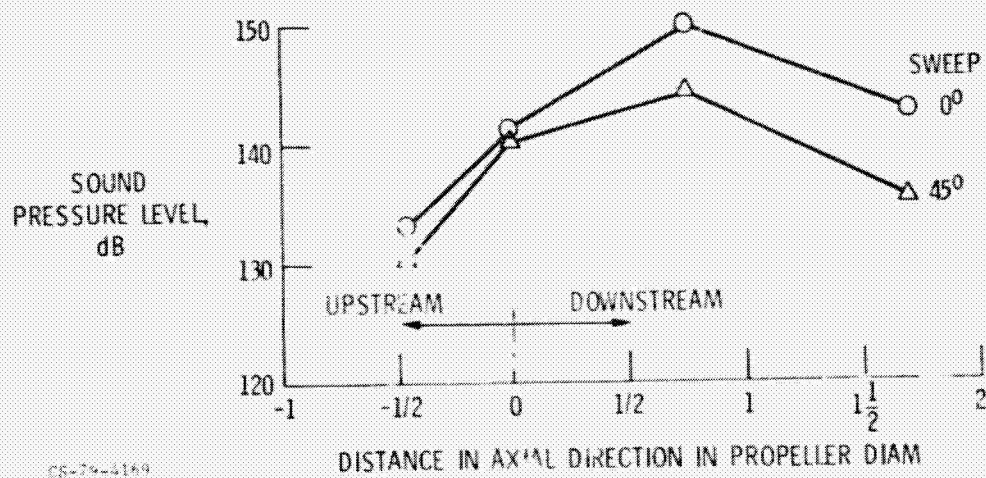
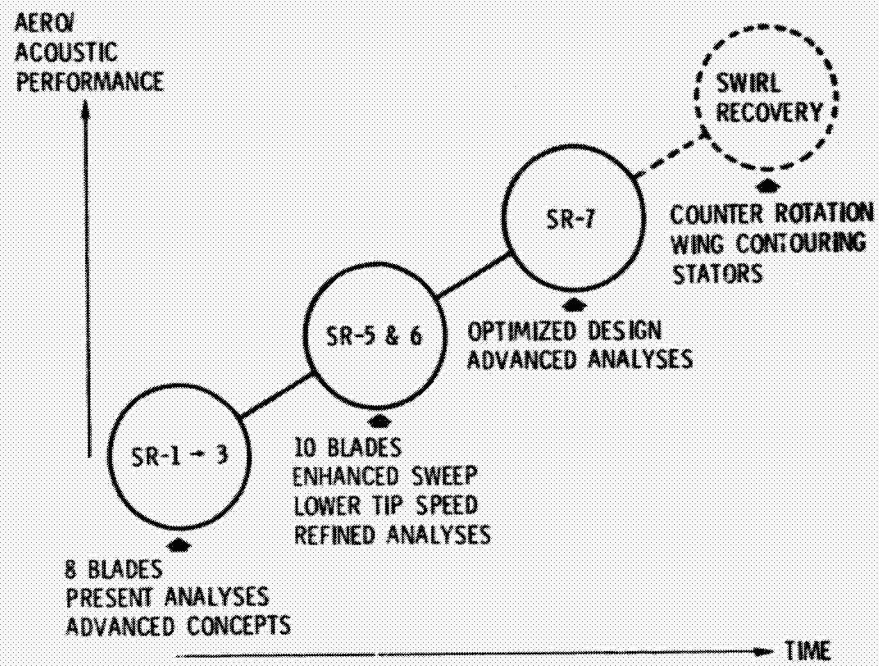


Figure 12

## HIGH SPEED PROPELLER RESEARCH PROGRAM



CS-79-4171

Figure 13

N 80-22345

## ADVANCED PROPELLER AERODYNAMIC ANALYSES

Lawrence J. Bober  
National Aeronautics and Space Administration  
Lewis Research Center

### SUMMARY

Three advanced analysis methods for predicting the aerodynamic performance of propellers are presented. Two of these analyses are lifting-line methods, and the third is a lifting-surface method. The approach used in each of the methods is described, and the capabilities are presented.

### INTRODUCTION

Increased concern over fuel cost and availability have fostered renewed interest in propellers for aircraft propulsion because of the propeller's inherent high efficiency compared with a turbofan. The quest for improved efficiency and lower noise at high subsonic flight speeds at 30 000 feet or more has forced propellers away from conventional designs toward the type shown in the previous paper. The combination of high flight speed and high rotational speed has resulted in propellers with a large number of highly swept blades having significant cascade effects in the inboard region of the blades. Carefully contoured nacelles contribute to the already complex flow field associated with the propeller. These radically different geometries and the complex flow fields they cause cannot be adequately analyzed using conventional aerodynamic performance analyses. To overcome the shortcomings of established approaches to propeller performance predictions, advanced propeller aerodynamic analyses are being developed as part of NASA's Advanced Turboprop Program.

This paper will discuss three advanced analyses currently under development. Two are lifting-line analyses in which each blade is represented by a single line of vorticity. The third is a lifting-surface analysis in which each blade is represented as a solid surface. Although these analyses were developed for the kinds of propellers described in the previous paper, they have features that are applicable to both low and high-speed general-aviation propellers. Before discussing the advanced analyses, an established approach to propeller performance prediction will be discussed.

### ESTABLISHED APPROACH

In a velocity potential solution for the flow around a propeller, the non-uniform spanwise loading on the blades causes a sheet of vorticity to extend

downstream to infinity as shown in figure 1. This vortex wake is shown as a finite number of filaments, but could more accurately be represented as an infinite number of vortex filaments. The vortex wake is important in propeller performance prediction since it causes an induced velocity at the propeller, thereby changing the local blade angle of attack.

The important features of this established approach are summarized in figure 1. Calculation of the induced flow in this approach is based on the work done by Goldstein (ref. 1) about 50 years ago. Because of the limited computing capability at that time, Goldstein used a very simplified model so that he could obtain an analytical solution for the induced velocity at the propeller due to the wake. He assumed that the shape of the wake was a rigid helix which was known to correspond to a lightly loaded propeller with optimum distribution of loading. To visualize a rigid helical wake, consider a plane normal to the axis of revolution of the propeller. The intersection of this plane with the rigid helical wake is a straight line. Another feature of this wake shape is that the pitch of the helix does not change with axial location. (This wake is shown in fig. 1.) Goldstein published results for single rotation propellers (ref. 1), and Theodorsen obtained results for coaxial counterrotating propellers using an electrical analogy (ref. 2). The induced velocities obtained from the Goldstein and Theodorsen results are strictly correct only for straight propeller blades. Also their original works contained no provisions for a nacelle since the vorticity extended to the axis of the propeller. These results form the basis of a procedure which has been refined over the years and has become an established approach to propeller performance analysis.

This procedure is implemented using a strip analysis in which the flow conditions are determined at one radial location at a time. For each strip the induced velocity is determined from Goldstein's or Theodorsen's results. The effect of the nacelle is taken into account in an approximate manner by assuming that at each strip the induced velocity is the same as for the entire propeller operating at the same velocity that exists at that strip. The total velocity is then the vector sum of the induced velocity, the local velocity for the isolated nacelle, and the rotational velocity. The flow velocity and the blade geometry determine the local blade angle of attack, which allows the determination of the lift and drag coefficients from isolated airfoil data. Sweep is taken into account through the cosine rule (ref. 3). These forces are resolved into thrust and torque components that can be integrated radially to get the propeller thrust, torque, power, and efficiency.

It is important to note that for any operating condition, the effect of the wake is assumed to be the same as for an optimally loaded propeller, even if there is a nacelle and spinner present.

## ADVANCED ANALYSES

### Curved Lifting-Line Analysis

The important features of this analysis are shown in figure 2. The wake is represented by a finite number of helical vortex filaments instead of the con-

tinuous sheet of vorticity used by Goldstein. Each filament has constant pitch, but its location relative to another is arbitrary as shown in figure 2. At any point on the blade, the induced flow due to each wake filament and the lifting line is calculated using the law of Biot-Savart (ref. 3). The total induced flow at any point is then the sum from all these vortices. This analysis is currently restricted to single-rotation propellers. The propeller blades are represented by curved lifting lines of arbitrary shape. The nacelle is restricted to being an infinite cylinder since the wakes cannot contract radially.

The strengths of the wake vortex filaments are related to the spanwise variation of lift on the blade. Thus it is necessary to solve for the blade and wake vortex strengths simultaneously. An important aspect of the solution procedure is the placement of the bound vortex at the quarter chord line and the requirement that the flow be tangent to the mean camber line at the three-quarter chord line. Thus no isolated airfoil data are needed since the lift at any radius can be determined from the vortex strength at the same radius. However, this approach cannot predict the blade drag. This analysis has been developed by Sullivan (ref. 4) at Purdue University under a grant from NASA Lewis Research Center.

An interesting application of this analysis is shown in figure 3, which shows the effect of proplets on propeller performance. A proplet is an aerodynamic device at the tip of the propeller blade similar to winglets, which have been shown to increase the lift-to-drag ratio of wings. If the proplet is properly integrated into the tip flow field, an improvement in performance as shown in figure 3 can be obtained. The plot shows the predicted efficiency as a function of power coefficient for a propeller with and without proplets. The results show an increase in efficiency due to the proplets of about 1 percent at low power and about 3 percent at high power.

The development of this analysis is continuing both at Purdue and at Lewis. Radially varying inflow velocities will be included to better account for the nacelle. A drag prediction procedure using isolated airfoil data will be implemented so that the effect of blade drag can be included.

#### Propeller Nacelle Interaction Analysis

The second advanced lifting-line analysis has more extensive capabilities, which are summarized in figure 4. This analysis was developed by United Technologies Research Center (ref. 5) under contract to Lewis. The wake is represented by a finite number of vortex filaments that are located on stream surfaces so that they conform to the shape of the nacelle. The pitch of these filaments is not constant, and they can contract in both the axial and radial directions. This capability is clearly shown in figure 4 just downstream of the propeller where the wake filaments are displaced radially because of the increasing nacelle diameter. This analysis is capable of analyzing both single and coaxial counterrotating propellers. The blades are represented by lifting lines and can have any arbitrary shape. The nacelle can be any axisymmetric shape.

The solution procedure in this analysis is as follows. First an inviscid solution for the nacelle alone is obtained. The results are used to locate the wake vortex filaments along stream surfaces and to determine the radially varying inflow for the propeller. The induced flow at the propeller due to each wake filament is calculated using the law of Biot-Savart (ref. 3). The total induced velocity at any radial location on a blade is obtained by summing the induced flow from the individual wake filaments and from the lifting lines. The blade lift and drag are determined from two-dimensional airfoil and cascade data. An iteration procedure is required to insure that the wake vortex strengths are consistent with the spanwise load distribution on the blade. A final optional step is to make the blade forces in a circumferentially averaged, viscous, compressible flow calculation.

For a propeller operating at high flight speed or high rotational speed, portions of the blades may be moving at supersonic speeds relative to the undisturbed flow. When this occurs some additional effects (shown in fig. 5) must be considered. In a supersonic flow a disturbance in the flow is felt only in a conical region downstream of the disturbance known as the region of influence. For the propeller shown in figure 5 only the shaded portion of the upper right hand blade is affected by what happens at the tip of the upper left hand blade. Thus, when the induced velocity due to the wake is calculated, it is necessary to limit the region over which each wake filament has an effect. A second consideration is that, when the tip is supersonic, the flow becomes highly three-dimensional near the tip due to the tip Mach cone. This effect is taken into account by applying a correction to the lift determined from isolated airfoil data.

The relative importance of some of these effects is shown in figure 6 where predicted power coefficient is shown as a function of advance ratio. The different curves were obtained using the same computer program but with different options for each curve to isolate certain effects. The configuration analyzed was an eight bladed propeller with  $30^\circ$  of tip sweep (denoted as SR1 in the previous paper). The curve labeled "rigid wake" was obtained using a rigid helical wake without the high-speed effects and is essentially the same as the results that would be obtained with the established approach. For the curve labeled "wake model," the wake filaments were distorted by the nacelle. (The high-speed effects again were not included.) The difference between the two curves is solely due to the different assumed wake shapes. The curve labeled "wake model and high-speed effects" includes the distorted wake and the high-speed effects described in figure 5. The difference between this curve and the "wake model" curve is solely due to the high-speed effects. As expected the largest difference between these two curves occurs at the lowest advance ratio, which corresponds to the highest tip speed. The high-speed effects cause the largest changes to the shape of the curves. From comparisons not shown here, it was found that the shape of the wake model and high speed effects curve agrees with the experimental results, indicating the treatment of these effects in the analysis is qualitatively correct.

Shown in figure 7 are results from the circumferentially averaged, viscous, compressible flow calculation for the configuration shown in figure 6. Each curve in figure 7 represents the radial distribution of circumferentially aver-



aged swirl velocity at that axial location. The uniform spacing of the curves ahead of the propeller indicates no swirl is present in the flow. The distorted curves in the vicinity of the blades indicate that swirl is being introduced into the flow. The uniform spacing of the curves downstream of the blades indicates that the swirl persists in the flow. These results from the viscous calculation are used to check fluid velocities between the blades and downstream of the propeller. If the velocities are too high, large losses due to shock waves can occur. These results also give the pressure and viscous drag on the nacelle in the presence of the propeller. United Technologies Research Center will be doing modifications and applications of this analysis under a follow-on contract.

### Lifting-Surface Analysis

The key features of the three-dimensional, compressible lifting-surface analysis are shown in figure 8. Also shown are partial front and side views of the grid on which the flow calculations are performed. The grid actually extends much further in the radial direction than is shown. The nacelle is required to be axisymmetric so that the flow between each two adjacent blades is the same. Thus it is only necessary to solve for the flow between two blades. The flow is required to be tangent to all solid surfaces and beyond the blade tips is assumed to be periodic. The equations of motion in finite-difference form, are solved at discrete points in the grid. The equations that are solved are the three-dimensional, unsteady, Euler equations, which govern the inviscid flow of a compressible fluid and can accurately represent the pressure variation caused by shock waves and the work done by the propeller on the fluid. The equations are solved by marching in time using an implicit finite-difference method until a steady state is reached. No wake modeling or two-dimensional airfoil data are required. Viscous effects, however, are not included. This analysis was developed by Kutler of NASA Ames Research Center and Chaussee of Nielsen Engineering and Research and is described in reference 6.

Results from this lifting surface analysis are shown in figure 9 for an eight bladed propeller having  $30^\circ$  of sweep at the blade tips. The plots show the distribution of static pressure coefficient on the suction and pressure surfaces of the blades at three spanwise locations from near the hub to near the tip. The most significant feature of these results is the predicted shock wave along the entire span of the blade. At the conditions for which these results were obtained, experimental data also indicate compressibility losses. The detailed spanwise and chordwise distribution of loading predicted by this code is important for improved propeller designs from acoustic and structural standpoints. Development of this code is continuing at Lewis.

### FUTURE PLANS

The development of these advanced analyses will continue. Initial comparisons of the analytical results from all these advanced methods with performance data have shown qualitative agreement (ref. 7). However, performance data cannot substantiate the details of the flow as predicted by the analyses. Thus an experimental program is planned for the Lewis 8x6 foot wind tunnel in 1980 to

provide detailed data for verifying these analyses. A laser velocimeter system (fig. 10) will be used to make these measurements since this type of system does not introduce hardware which might disturb the flow. This experimental program will define the details of the flow around the blades and upstream and downstream of the propeller. These results will pinpoint any deficiencies in the analyses so that quantitative, as well as qualitative, agreement can be obtained.

#### CONCLUDING REMARKS

Three advanced analyses for predicting propeller aerodynamic performance have been presented. The analytical approaches as well as the capabilities of these analyses have been described. Two of these analyses use a lifting-line representation for the propeller blades, and the third uses a lifting-surface representation. The detailed flow-field measurements to be made in the near future will provide data for validating the analyses, making them available as analytical tools for designing improved propellers.

#### REFERENCES

1. Goldstein, S.: On the Vortex Theory of Screw Propellers. Proc. Roy. Soc., (London), vol. 123, no. 792, Apr. 6, 1929, pp. 440-465.
2. Theodorsen, Theodore: Theory of Propellers. McGraw-Hill Book Co., Inc., 1948.
3. Kuethe, Arnold M and Schetzer, J. D.: Foundations of Aerodynamics. John Wiley & Sons, Inc., 1950.
4. Sullivan, J. P.: The Effect of Blade Sweep on Propeller Performance AIAA Paper 77-716, June 1977.
5. Egolf, T. A.; et al.: An Analysis for High Speed Propeller-Nacelle Aerodynamic Performance Prediction. Vol. 1 - Theory and Initial Application. Vol. 2 - User's Manual for the Computer Program. R79-912949-19, United Technologies Research Center.
6. Chaussee, D. S.: Computation of Three-Dimensional Flow Through Prop Fans. NEAR-TR-169, Nielsen Engineering and Research, Inc., 1979.
7. Bober, L. J. and Mitchell, G. A.: Summary of Advanced Methods for Predicting High Speed Propeller Performance. AIAA Paper 80-0225, Jan. 1980; also NASA TM 81409, 1980.

## ESTABLISHED APPROACH

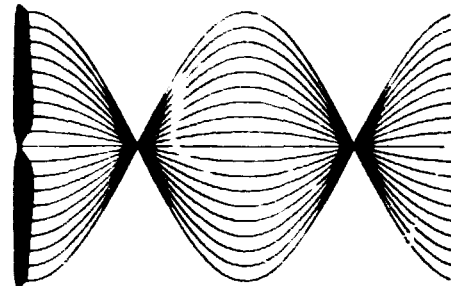
### MODEL

WAKE - RIGID HELICAL VORTEX SHEET

SINGLE OR COUNTER ROTATION

BLADES - STRAIGHT LIFTING LINE

NACELLE - NONE



### SOLUTION TECHNIQUE

STRIP ANALYSIS

CS-79-4089

Figure 1

## CURVED LIFTING LINE ANALYSIS

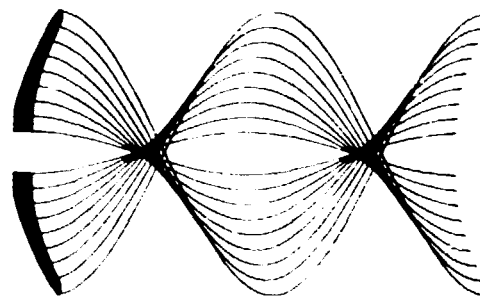
### MODEL

WAKE - RIGID HELICAL VORTEX FILAMENTS

SINGLE ROTATION

BLADES - CURVED LIFTING LINE

NACELLE - INFINITE CYLINDER



### SOLUTION TECHNIQUE

SIMULTANEOUS SOLUTION FOR BLADE

AND WAKE VORTEX STRENGTHS

CS-79-4088

Figure 2

## CURVED LIFTING LINE RESULTS

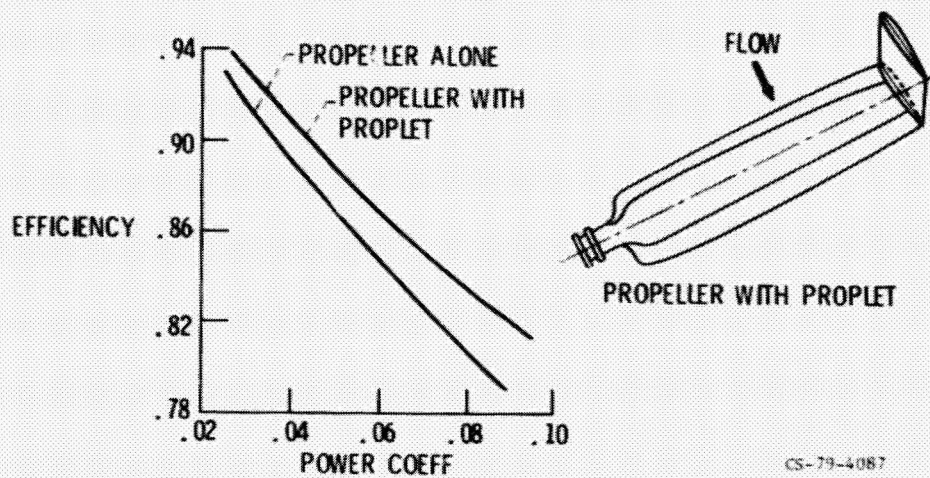
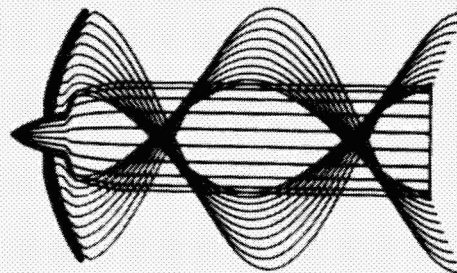


Figure 3

## PROPELLER NACELLE INTERACTION ANALYSIS

### MODEL

- WAKE - VORTEX FILAMENTS ALONG  
STREAM SURFACES
- SINGLE OR COUNTER  
ROTATION
- BLADES - CURVED LIFTING LINE
- NACELLE - ARBITRARY GEOMETRY



### SOLUTION TECHNIQUE

- INVISCID NACELLE SOLUTION TO  
LOCATE WAKE FILAMENTS
- INDUCED ANGLE OF ATTACK DUE  
TO WAKE
- BLADE FORCES USED IN  
CIRCUMFERENTIALLY AVERAGED  
VISCOUS FLOW

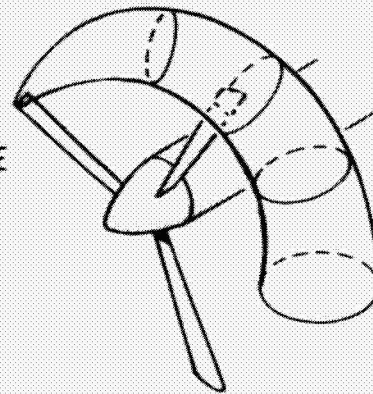
CS-79-4090

Figure 4

## HIGH SPEED EFFECTS PROPELLER NACELLE INTERACTION ANALYSIS

SUPERSONIC FLOW REGIONS OF INFLUENCE

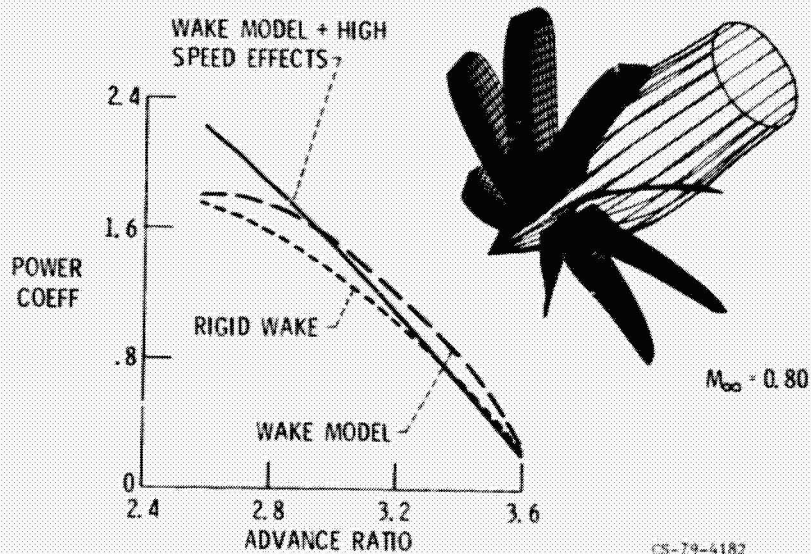
SUPERSONIC TIP CORRECTION



CS-79-3788

Figure 5

## EFFECT OF LIFTING LINE REFINEMENTS PROPELLER NACELLE INTERACTION ANALYSIS



CS-79-4182

Figure 6

# PROPELLER INDUCED SWIRL VELOCITIES PROPELLER NACELLE INTERACTION ANALYSIS

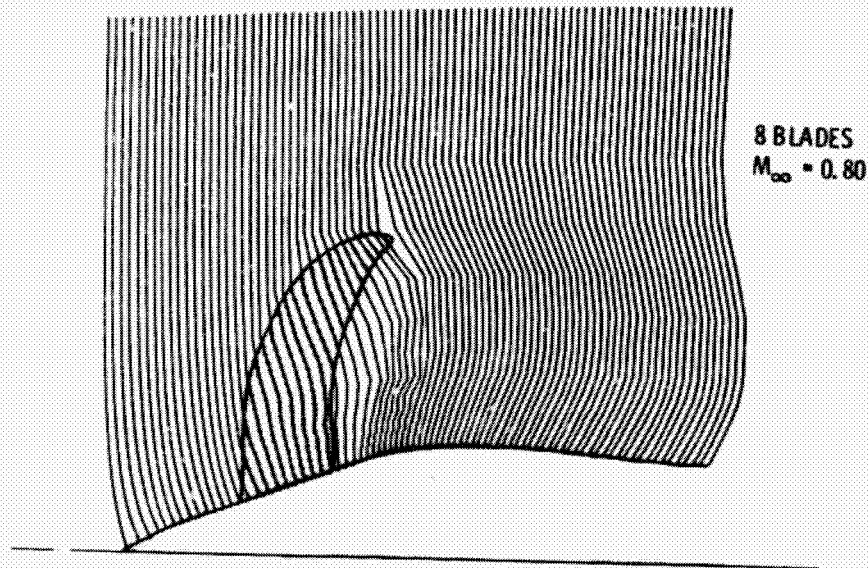


Figure 7

CS-79-3888

## 3-D COMPRESSIBLE LIFTING SURFACE ANALYSIS

ENTIRE FLOW FIELD SOLUTION  
3-D EULER EQUATIONS  
IMPLICIT FINITE DIFFERENCE METHOD

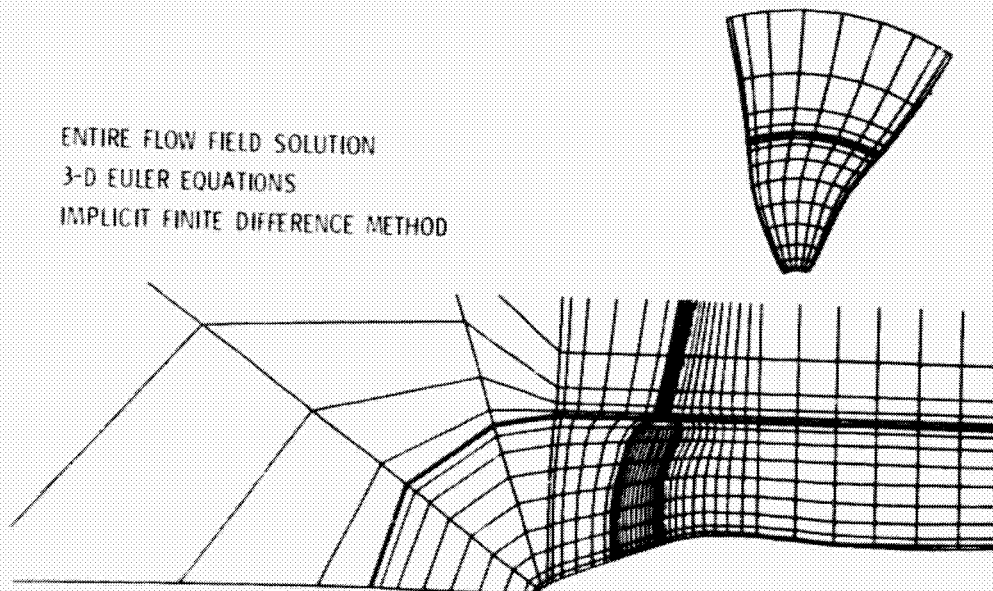


Figure 8

CS-79-4226

### 3-D COMPRESSIBLE LIFTING SURFACE RESULTS

$$M_{\infty} = 0.8, M_{TIP} = 1.15$$

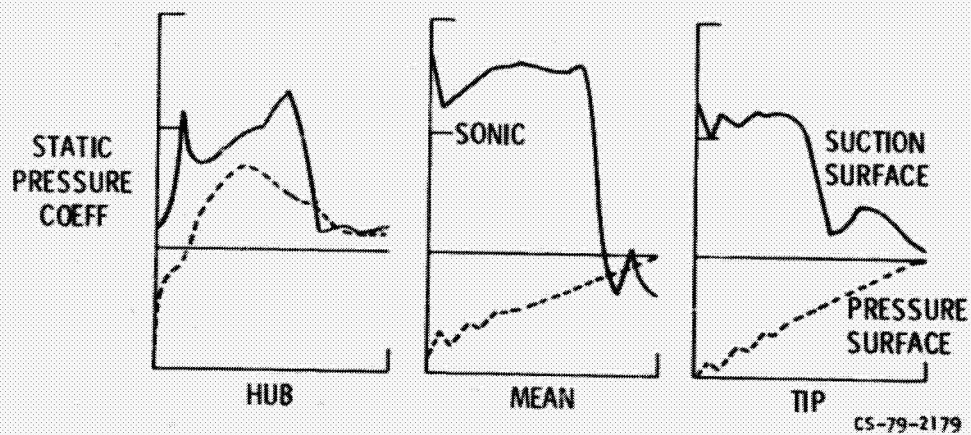


Figure 9

### LASER VELOCIMETER MEASUREMENTS

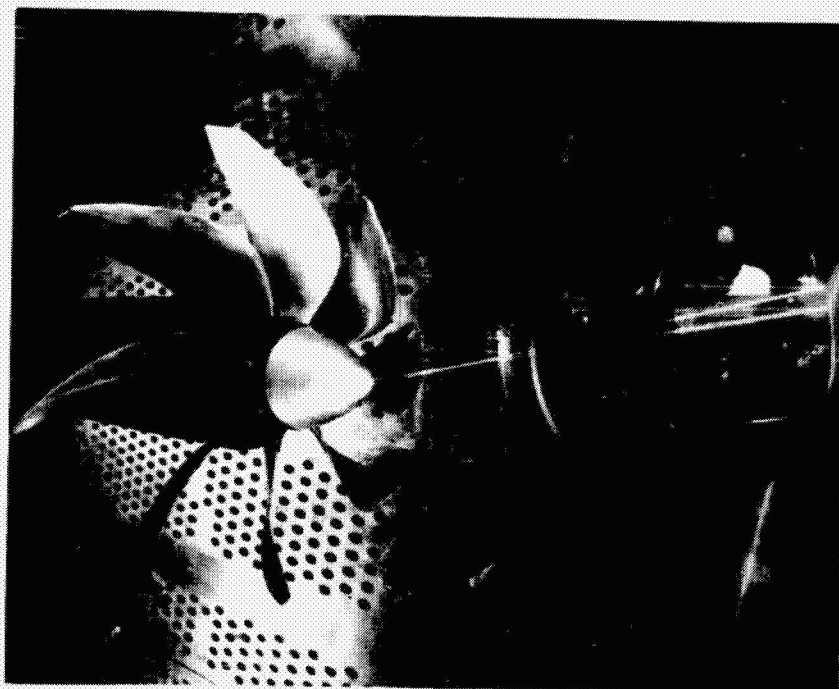


Figure 10

CS-79-1707

ORIGINAL PAGE IS  
OF POOR QUALITY



219  
N80-22346

## PROPELLER AEROACOUSTIC METHODOLOGIES\*

Kenneth D. Korkan and Gerald M. Gregorek  
The Aeronautical and Astronautical Research Laboratory  
Department of Aeronautical and Astronautical Engineering  
The Ohio State University

### SUMMARY

This paper briefly covers aspects related to propeller performance by means of a review of propeller methodologies; presentation of preliminary wind tunnel propeller performance data taken in the NASA Lewis Research Center 10 x 10 wind tunnel; discussion of the predominant limitations of existing propeller performance methodologies; and a brief review of airfoil developments appropriate for propeller applications. This paper is intended as a status report with the complete study to be documented at a later date.

### INTRODUCTION

Because of the increased emphasis on fuel efficiency for general aviation aircraft, there has been a renewed interest in the use of propellers. It has been estimated that in the use of the prop fan concept (Ref. 1), a fuel savings of approximately 36% can be realized over the turbofan through proper propeller design. Also, recent studies have shown a 5 to 7% savings in fuel efficiency can be obtained (Ref. 2) through proper propeller design and critical examinations of propeller-nacelle interactions. As a result, a study supported by the National Aeronautics and Space Administration Lewis Research Center was initiated involving the Ohio State University, Borst and Associates, Hartzell Propeller, Inc., and Rockwell Corporation of Bethany, Oklahoma to evaluate and enhance current analytical prediction methods for propellers designed specifically for the twin engine Rockwell Aerocommander 690B. This three year study has and will involve computer prediction studies in the theoretical evaluation of propeller performance; wind tunnel model tests conducted at the NASA Lewis Research Center; flight test comparisons; and enhancement of the theoretical methods by means of comparison with wind tunnel and flight tests. The intent of this paper is to briefly cover aspects related to propeller performance and to illustrate preliminary data resulting from the wind tunnel tests of two propellers in this study. It is intended that a report will be made available on the comparisons between the theoretical predictions and the complete experimental data set resulting from the wind tunnel tests.

\*This study was funded by NASA Lewis Research Center under NASA Grant NSG 3247.



## PROPELLER PERFORMANCE METHODS

A brief review of the methodologies (Ref. 3) used in predicting propeller performance (Fig. 1) has been included in this work for completeness. Propeller theories have proceeded from the simple Rankine-Froude momentum disc theory (Refs. 4,5) which assumes that the propeller disc is replaced by a disc with an infinite number of blades producing a uniform change in velocity of the stream passing through the disc. This theory is useful in calculating theoretical maximum efficiencies but does not deal in the details of the propeller configuration such as number of blades and blade thickness. These factors are considered in the blade element analysis (Refs. 6,7) the next degree of sophistication, which deals in the forward and rotational velocity components to determine the resultant velocity or the effective pitch angle and hence the angle-of-attack as seen by each airfoil section making up the propeller blade. Here the angle-of-attack is taken as the difference between the geometric pitch angle and the effective pitch angle (Fig. 2) and assumes that the induced flow past the blade element is the same as past a wing with an aspect ratio of six. The simple blade element theory has been used for preliminary calculations and in some cases gives accurate answers within 10% of the measured thrust and torque values.

More precise results may be obtained in the prediction of thrust and torque by calculating the local induced velocities at each radial station (Fig. 2) by means of vortex theory (Ref. 8). Here, the combination of simple momentum theory and blade element analysis results in a theory that also accounts for rotation of the slip stream. However this approach, although providing an accurate approximation, still does not account for tip losses, blade to blade interference, and nonuniform flow in the disc plane resulting from the presence of a nacelle.

The next order of development and accuracy came with the Goldstein lifting-line model (Ref. 9) where the blade is replaced by a series of horseshoe vortices as shown in Figure 1. The approximation of blade replacement by vortices is acceptable since most general aviation propellers have a relatively high aspect ratio. Also, the lifting line approach can utilize corrections for viscosity and compressibility but is accepted as an "approximate method" using the Goldstein factor. The Goldstein factor method is usually taken for lightly loaded propellers where the Betz condition holds, and does not apply to other than constant pitch propellers in uniform flow (Ref. 3). The lifting line problem can also be solved by the "rigorous method" using Lerb's induction factor method (Ref. 9) which is based on the velocity potential of helical vortex lines applied to any moderately loaded optimum or non-optimum propeller operating in a uniform or nonuniform free stream (Ref. 3). This is the method of analysis that has been used in the performance comparisons to be shown in a later section of this paper.

As the propeller configurations change to relatively small aspect ratio and/or large surface areas (Fig. 1) as in the prop-fan concept (Ref. 1), advanced analytical methods must be used such as the Ludwig-Ginzler lifting surface model (Ref. 10) to model the propeller flow field accurately. These advanced methods and the current state-of-the-art have been discussed by Bober

and Mitchell (Ref. 11) in addition to the importance of wake modeling.

It is the purpose of the present effort to compare directly with experimental data the theoretical prediction results of vortex theory and lifting line theory to determine the ranges of applicability and levels of accuracy. The current wind tunnel tests cover a broad range in advance ratios, blade angle settings, and flight conditions for four general aviation propellers, each having different activity factors and propeller blade sections. In so doing, the current methods may be enhanced to provide increased accuracy in the prediction of propeller performance.

### PROPELLER AIRFOIL DEVELOPMENT

Airfoil development for propeller applications has been limited with the continual use of the Clark Y and RAF 6 series airfoils. The last major development in this area occurred with the development of the NACA 16 series airfoils (Ref. 12) and as shown in Figure 3 does have relatively good performance in terms of the metric  $C_L/CD$  as a function of  $C_L$ . This airfoil has the characteristic "flat bottom", maximum thickness occurring at approximately the 50% point, and a small leading edge radius with many of the design characteristics dictated by manufacturing constraints. Therefore many propellers of today incorporate the Clark Y or RAF 6 airfoil series during the initial 50% of the blade transitioning to the NACA 16 series which has a high drag divergence Mach number in the outer segment of the propeller where the resultant Mach numbers can approach unity.

Bocci (Ref. 13) in a paper published in 1977 described a new series of propeller airfoil sections entitled the ARA-D series. Here, the manufacturing constraints have been relaxed as shown in Figure 3 resulting in a section incorporating increased camber on the underside of the airfoil; drooped leading edge to prevent leading edge stall at high angle-of-attack; and an increased leading edge radius. The results of this design approach can be seen in Figure 3 with an improvement over the performance of the NACA 16 series at the high lift coefficients. The importance of the airfoil section to propeller performance is indicated in Figure 4 where it can be seen that the airfoil pressure distributions which evolve into the aerodynamic coefficients determine the load distribution and also allows an acoustic evaluation by the strip method. In a later study, the authors (Ref. 14) have compared the aerodynamic performance and acoustic estimates of the ARA-D, Clark Y and NACA 16 series airfoils.

In the discussions of propeller airfoil development, the wind tunnel tests of the propellers in this study incorporate a variety of airfoil sections, i.e.,

- (a) Clark Y - NACA 16 airfoils
- (b) ARA-D airfoils
- (c) GA(W) airfoils
- (d) 6 series airfoils

Since all have been designed for the Aerocommander 690 B, a comparison of the

propeller performance can be interpreted as a comparison of these airfoils in terms of efficiency ( $\eta$ ), thrust coefficient ( $C_T$ ), and power coefficient ( $C_p$ ) which are discussed in the following sections.

#### EXPERIMENTAL PROPELLER PERFORMANCE MEASUREMENTS

Propeller performance experimental values were obtained in the present program through use of the Propeller Test Rig (PTR) (Ref. 15) installed in the subsonic leg of the 10 foot x 10 foot supersonic wind tunnel located at the NASA Lewis Research Center. The configuration tested also incorporated equivalent body of revolution representing the actual nacelle of the Rockwell Aerocommander 690 B including a scaled representation of the spinner (Fig. 5). Pressure orifices were located along the periphery of the nacelle at two azimuthal locations to aid in evaluating the drag of the nacelle and its effect on the performance of the propeller.

Three flight conditions were examined for the approximately 0.5 scale propellers, i.e., take-off ( $M = 0.11$ ), climb ( $M = 0.23$ ), and the cruise condition ( $M = 0.39$ ). The advance ratio ( $J$ ) was varied for a fixed blade angle setting by fixing the test section Mach number through manipulation of the wind tunnel second throat and changing RPM. Values of propeller thrust and torque were deduced from the experimental measurements and the thrust coefficient ( $C_T$ ), torque coefficient ( $C_Q$ ), power coefficient ( $C_p$ ), and efficiency ( $\eta$ ) were determined by this method. An appropriate range in  $J$  values was examined with respect to the actual operating conditions or until stall-flutter was encountered.

The first propeller tested on the PTR in the configuration shown in Figure 5 consisted of Clark Y-NACA 16 airfoils with an activity factor of 101. The preliminary results are shown in Figure 6 for the cruise condition ( $M = 0.39$ ,  $\beta = 48^\circ$ ) in terms of efficiency ( $\eta$ ) as a function of the advance ratio ( $J$ ). Also shown in this figure are the theoretical estimates using vortex theory\* and lifting line theory previously discussed. As can be seen, at the lower  $J$  values the lifting line prediction coincides with the experimental data with a resulting overprediction for  $J$  values in excess of 2.3. This may be compared directly with the vortex theory results which overpredicts the experimental data over the entire range of  $J$  values. A similar result is also found for an off-design condition as shown in Figure 7. Consideration of the climb condition ( $M = 0.23$ ,  $\beta = 32^\circ$ ) for this propeller, shown in Figure 8, indicates acceptable agreement between experiment and lifting line theory over the range in  $J$  values. Here vortex theory agrees well with the experimental data at the low  $J$  values with disagreement occurring at  $J$  values in excess of 1.2. As found previously, an investigation of the off-design condition as shown in Figure 9 also produces similar results.

---

\*The vortex theory is presently under examination to include the influence of the blade-spinner interference which could result in better correlation with experiment.

The second propeller tested having an activity factor of 83 utilized the ARA-D airfoil sections previously discussed. The initial comparisons are shown in Figure 10 and indicate that the lifting line prediction provides a reasonable correlation with experimental data for the cruise condition at a  $\beta$  of  $48^\circ$ . Here again, the vortex theory overpredicts that of the experimental data.

A complete set of data including comparisons with theory for  $C_T$ ,  $C_Q$ ,  $n$ , and  $C_p$  will be published for all four propellers tested. Determination of the range of validity of these theories in comparison with experimental data can then be investigated. Also, utilization of a wake rake probe (Fig. 11) is presently in use to obtain measurements of total pressure deficit, flow angularity, and static pressure measurements behind the disc plane of each propeller tested as a function of radial location. These data will result in independent thrust measurements as well as details of the propeller wake which can be compared directly to the current theoretical wake model being used. These results will be included in the reports previously mentioned at a later date.

#### LIMITATIONS OF CURRENT ANALYSES

The theoretical analyses that have been utilized in the comparisons with experimental data previously discussed are analytical models which contain limitations. For example, the importance of an accurate wake model and propeller/nacelle interactions has been emphasized by Bober (Ref. 11) in the prediction of high speed propeller performance predictions. Further, the result of a finite blade length, i.e., recognition of tip flow is necessary for an evaluation of three-dimensional effects. This effect has been treated by Cooper (Ref. 16) by obtaining a correction factor to the lift-curve slope as a function of the radial location but is valid for propellers using only NACA 16 and 6 series airfoils.

Also when considering limitations, the area of centrifugal viscous effects on the lift coefficient should be considered. In an experimental investigation by Himmelskamp (Ref. 17), he had found that there is a significant relationship between the magnitude of  $C_L$  and the radial location of the propeller blade. In a series of tests with a propeller made up of G0625 airfoils, Himmelskamp fixed the angle-of-attack at each radial location and measured the section lift coefficient. These values of  $C_L$  were then compared to the two-dimensional lift coefficient, as given in Figure 12, for the  $\alpha = 5^\circ$  case and found to be considerably higher with the greatest difference occurring at the root and decreasing as the propeller radius increased. These differences may be attributed to centrifugal viscous effects which obviously are not accounted for in two-dimensional theory. Since all propeller performance analyses utilize an airfoil data bank based upon two-dimensional experimental and analytical data, the differences indicated in Figure 12 if properly modeled could have a significant influence in the prediction accuracy of propeller performance theoretical values and resulting comparisons with experimental data.

As previously indicated, propeller performance analyses utilize airfoil data banks consisting of wind tunnel test and analytical computer codes.

Advancements made in the theoretical analysis of airfoils has been considerable with the availability of such subcritical computer codes as Smetana, et. al. (Ref. 18) and Eppler (Ref. 19). The more extreme case of both subcritical and supercritical flow over an airfoil can also be treated analytically as given by Garabedian, et. al. (Ref. 20) and Carlson (Ref. 21). Also the results of massive separation on an airfoil, i.e., theoretical investigations of the airfoil maximum lift coefficient has been under study by Barnwell (Ref. 22), Carlson (Ref. 23), and Dvorak (Ref. 24) and are being used on a limited basis.

To illustrate the applicability of these codes and resulting limitations, the LS(1)-0413 airfoil theoretical and experimental (Ref. 25) pressure distribution is shown in Figure 13 for  $M = 0.755$ ,  $\alpha = 0^\circ$ , and Reynolds number of  $5.11 \times 10^6$  condition. The comparison between experiment and theory is reasonable on both the upper and lower surface of the airfoil with respect to the maximum negative and positive  $C_p$  magnitude, location of the shock wave, and the base pressure value. However, if the Mach number is increased to  $M = 0.802$  for the same condition of  $\alpha$  and Reynolds number as shown in Figure 14, the mismatch between theory and experiment is evident indicating deficiencies in the theoretical analyses and/or experiment.

#### PROPELLER ACOUSTIC ANALYSIS MODEL

The emphasis has been on the propulsion performance of general aviation propellers, however recent effort has resulted in the design of efficient as well as quiet propellers. To this end an acoustic analysis (Ref. 26) has been derived that, provided the pressure distributions at several radial locations along the blade are specified, the resulting total noise due to loading and thickness can be predicted. The characteristic acoustic pressure signatures are shown in Figure 15 for the near field condition, from which the sound pressure level (dB) as a function of harmonic number or multiples of the fundamental can be calculated (Fig. 16). The accuracy of this theoretical approach is shown in Figure 16, which shows the comparison between measured and predicted noise for a series of static tests conducted by Hubbard (Ref. 27) for two near field locations. As can be seen, the comparison is reasonable as found in several other applications (Ref. 28) of this theoretical approach.

It was intended in the current study to obtain near field acoustic measurements of the propellers tested (Fig. 17). However, there are a series of problems associated with tunnel wall conditions that are currently under study before acoustic data can be taken with the desired accuracy.

#### SUMMARY

A preliminary summary of the study to date has indicated that:

- lifting line analysis gives overall better agreement with experimental results;

- at design climb, lifting line agrees well with measurements but overpredicts cruise performance;
- vortex theory overpredicts experimental results at both climb and cruise conditions;
- present prediction methods require improvement

It is intended that these wind tunnel data be compared to full scale flight test during 1980. Also, enhancement of the present theoretical models will be required as indicated in this phase of the study resulting in better comparison between experimental data and analytical predictions.

#### REFERENCES

1. Mikkelsen, D. C., Blaha, B. J., Mitchell, G. A., and Wikete, J. E., "Design and Performance of Energy Efficient Propellers for Mach 0.8 Cruise". SAE Paper 770458, March 1977 (Also NASA TM X-73612).
2. Keiter, I., "Low Speed Potential". Paper presented at the General Aviation Propulsion Conference, NASA Lewis Research Center, November 28-29, 1979.
3. Woan, C. J., and Gregorek, G. M., "Chebyshev Series Method in Computational Propellers". Aeronautical and Astronautical Research Laboratory, The Ohio State University, AARL TR 79-01, May 1979.
4. Rankine, W.J.M., "On the Mechanical Principles of the Action of Propeller", Trans. Inst. Nav. Arch., Vol. 6, 1865.
5. Froude, R. E., "On the Part Played in Propulsion by Difference of Fluid Pressure", Trans. Inst. Nav. Arch., Vol. 30, 1889.
6. Froude, W., "On the Elementary Relation Between Pitch Slip, and Propulsive Efficiency", Trans. Inst. Nav. Arch., Vol. 19, 1878.
7. Przewiecki, S., *Theorie Generale de l'Helice*, Paris, 1920.
8. Lanchester, F. W., Aerodynamics, Constable & Company, Ltd., London, 1907.
9. Goldstein, S., "On the Vortex Theory of Screw Propellers", Proceedings of the Royal Society (London), Series A, Vol. 63, 1929.
9. Lerbs, H. W., "Moderately Loaded Propellers With a Finite Number of Blades and an Arbitrary Distribution of Circulation", Trans. The Society of Naval Architects and Marine Engineers (SNAME), Vol. 60, 1952.
10. Ludwig, H., and Ginzel, I., "On the Theory of Screws With Wide Blades", Aerodynamische Versuchsanstalt, Goettingen, Report 44/A/08, 1944.
11. Bober, L. J., and Mitchell, G. A., "Summary of Advanced Methods for Predicting High Speed Propeller Performance", AIAA 80-0226, AIAA Eighteenth Aerospace Sciences Meeting, Pasadena, California, January 1980.

12. Lindsey, W. F., Stevenson, D. B., and Daley, B. N., "Aerodynamic Characteristics of 24 NACA 16-Series Airfoils at Mach Numbers Between 0.3 and 0.8", NACA TN 1546, December 1947.
13. Bocci, A. J., "A New Series of Airfoil Sections Suitable for Aircraft Propellers", *Aeronautical Quarterly*, February 1977, pp. 59-73.
14. Korkan, K. D., Woan, C. J., and Gregorek, G. M., "Effect of Airfoil Sections on Acoustic Performance of Propellers", Paper presented to the Advanced Technology Airfoil Research Conference, NASA Langley Research Center, March 1978.
15. Jeracki, R., "High Speed Results", Paper presented at the General Aviation Propulsion Conference, NASA Lewis Research Center, November 28-29, 1979.
16. Cooper, J. P., "The Linearized Inflow Propeller Strip Analysis", Wright Air Development Center, WADC TR 56-615, February 1957.
17. Himmelskamp, H., "Profiluntersuchungen an einem umlaufenden Propeller", Thesis Göttingen 1945. Report of the Max-Planck-Institut für Stromungsforschung, Göttingen, No. 2, 1950.
18. Smetana, F. O., Summey, D. C., Smith, N. S., and Carden, R. K., "Light Aircraft Lift, Drag, and Moment Prediction - A Review and Analysis", NASA CR-2523, 1975.
19. Eppler, R., "Private Communication", 1976.
20. Bauer, F., Garabedian, P., Korn, D., and Jameson, A., Supercritical Wing Sections II, A Handbook, Lecture Notes in Economics and Mathematical Systems, V. 108, Springer-Verlag, New York (1975).
21. Carlson, L. A., "Transonic Airfoil Analysis and Design Using Cartesian Coordinates", *J. of Aircraft*, Vol. 13, No. 5, May 1976.
22. Barnwell, R., "Private Communication", 1978.
23. Carlson, L. A., "TRANDES: A FORTRAN Program for Transonic Airfoil Analysis or Design", NASA CR-2821, June 1977.
24. Dvorak, F., "Private Communication", 1979.
25. Lee, J. D., Gregorek, G. M., and Korkan, K. D., "Testing Techniques and Interference Evaluation in the OSU Transonic Airfoil Facility", AIAA 78-118, AIAA 11th Fluid and Plasma Dynamics Conference, July 1978.
26. Woan, C. J., and Gregorek, G. M., "The Exact Numerical Calculation of Propeller Noise", AIAA Paper No. 78-1122, AIAA 11th Fluid and Plasma Dynamics Conference, Seattle, Washington (July 1978).

27. Hubbard, H. H., and Regier, A. A., "Free Space Oscillating Pressures Near the Tips of Rotating Propellers", NACA TN 1870, 1949.
28. Korkan, K. D., Gregorek, G. M., and Keiter, I., "General Aviation Propeller Study - Acoustic Analysis", Paper presented to the Sixth Annual General Aviation Technologyfest, Wichita, Kansas, November 1979.



# PROPELLER PERFORMANCE METHODS - REVIEW

- MOMENTUM DISC THEORY
- BLADE ELEMENT ANALYSIS
- VORTEX THEORY
- LIFTING LINE THEORY
- ADVANCED ANALYTICAL METHODS

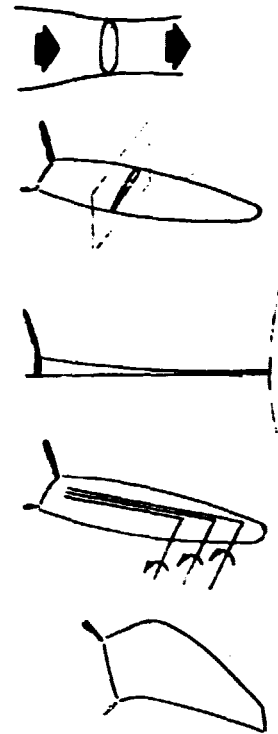


Figure 1

## CURRENT PERFORMANCE METHODS

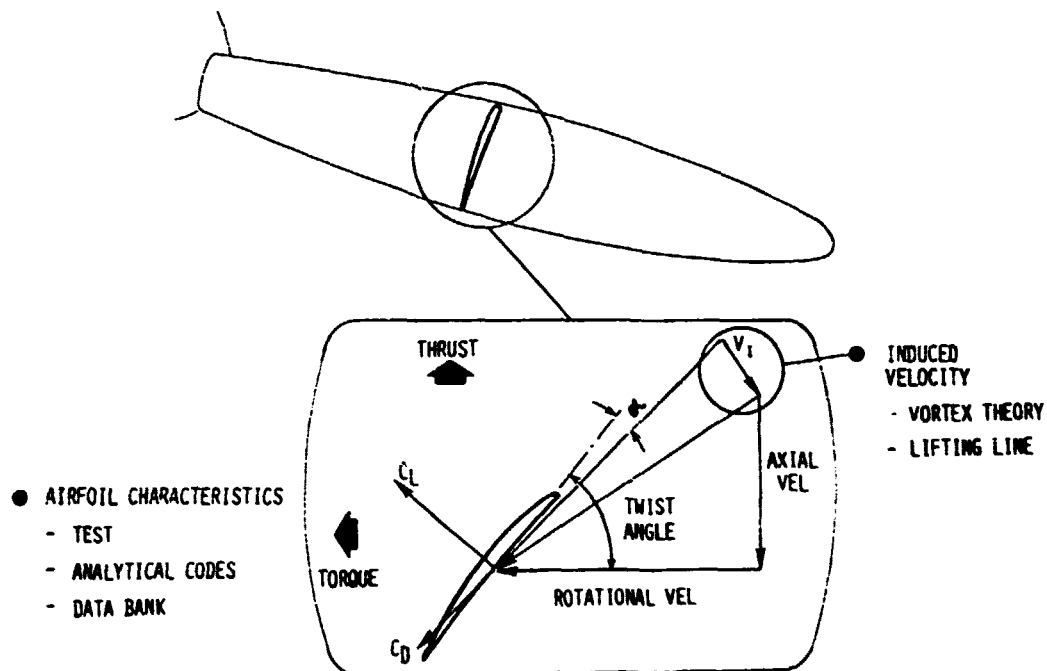
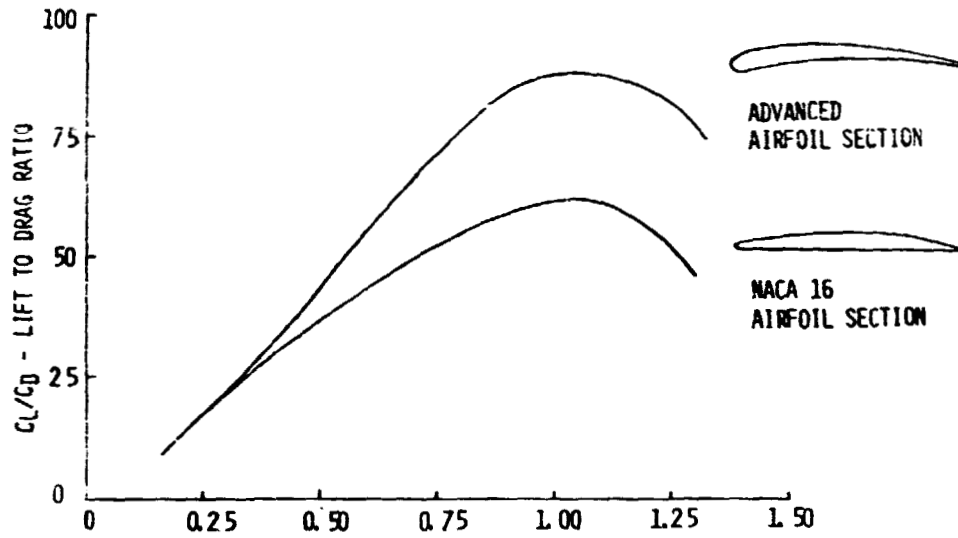


Figure 2

# AIRFOIL PERFORMANCE COMPARISON

(M = 0.4 T/C = 10%)



$C_L$  - LIFT COEFFICIENT

Figure 3

## BLADE AIRFOIL ANALYSIS

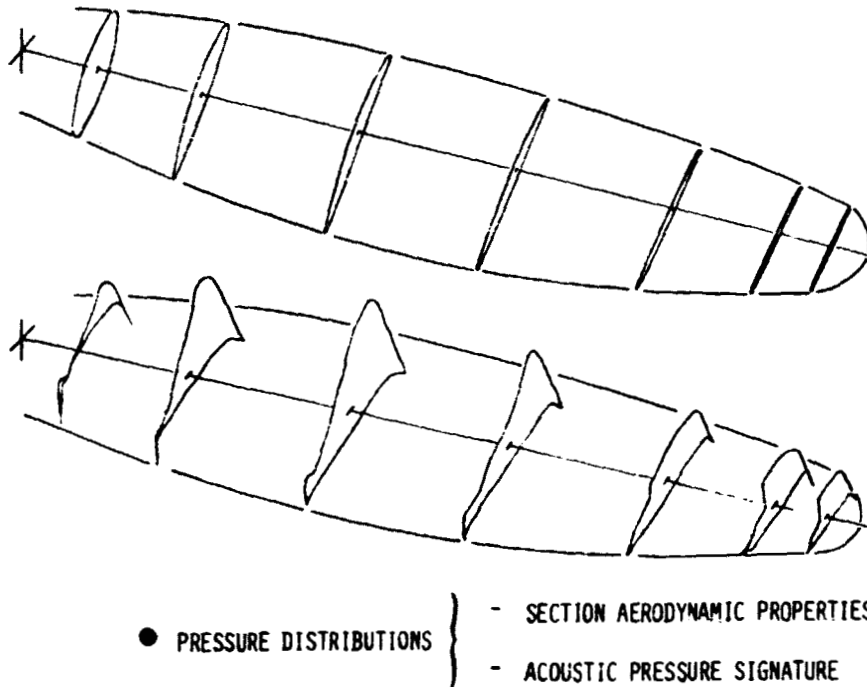


Figure 4

# GENERAL AVIATION WIND TUNNEL MODEL



Figure 5

## CRUISE PERFORMANCE COMPARISON M = 0.39/ AF = 101/ CLARK Y - NACA 16 AIRFOILS

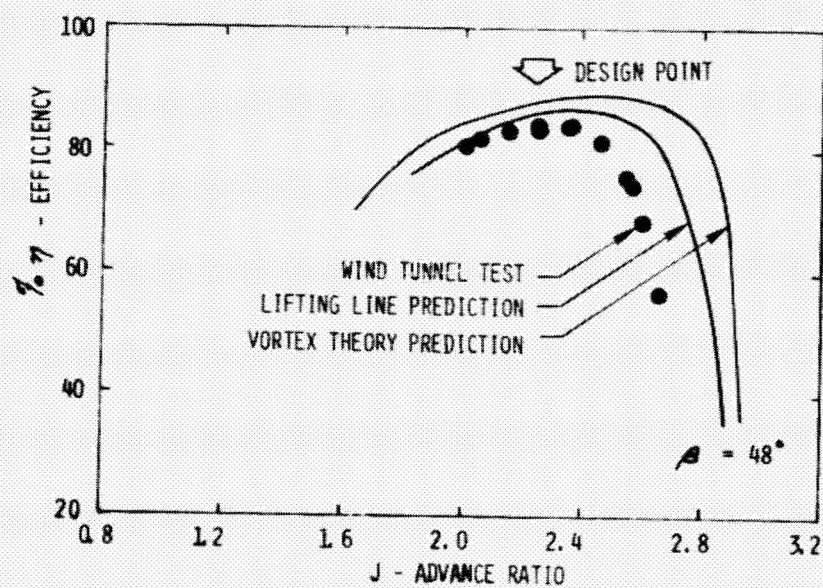


Figure 6

OFF-DESIGN CRUISE PERFORMANCE COMPARISON  
 $M = 0.39 / AF = 101 / \text{CLARK Y - NACA 16 AIRFOILS}$

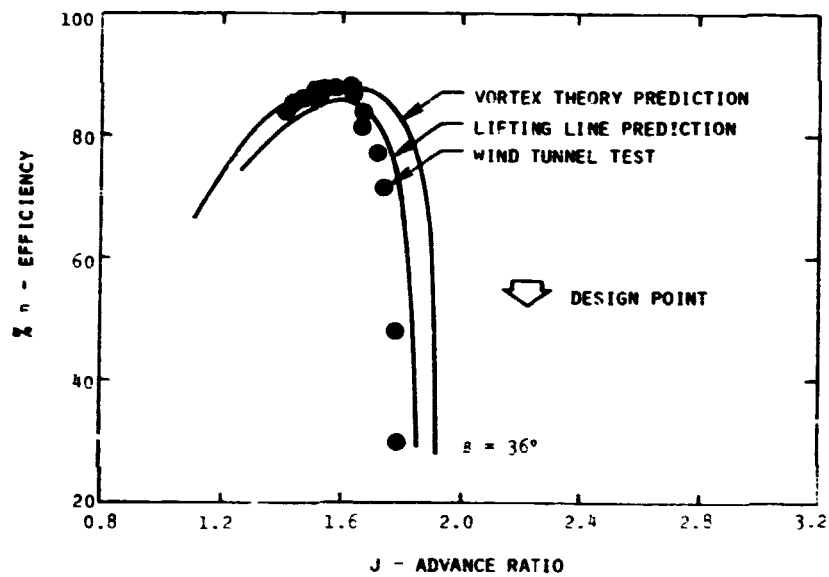


Figure 7

CLIMB PERFORMANCE COMPARISON  
 $M = 0.23 / AF = 101 / \text{CLARK Y - NACA 16 AIRFOILS}$

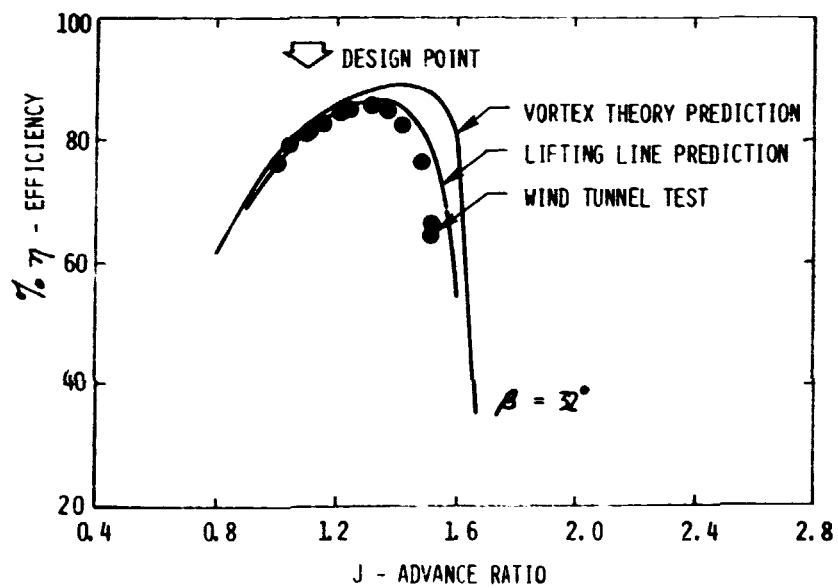


Figure 8

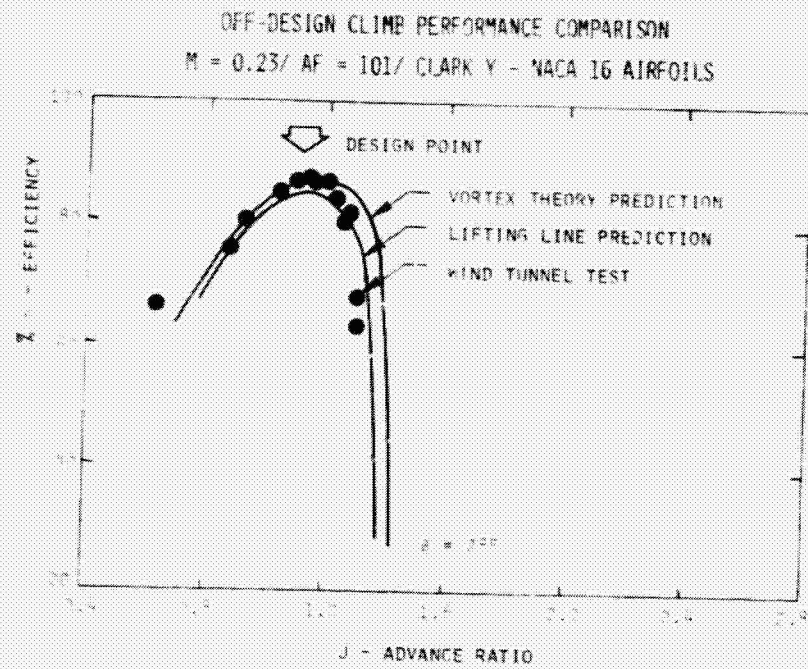


Figure 9

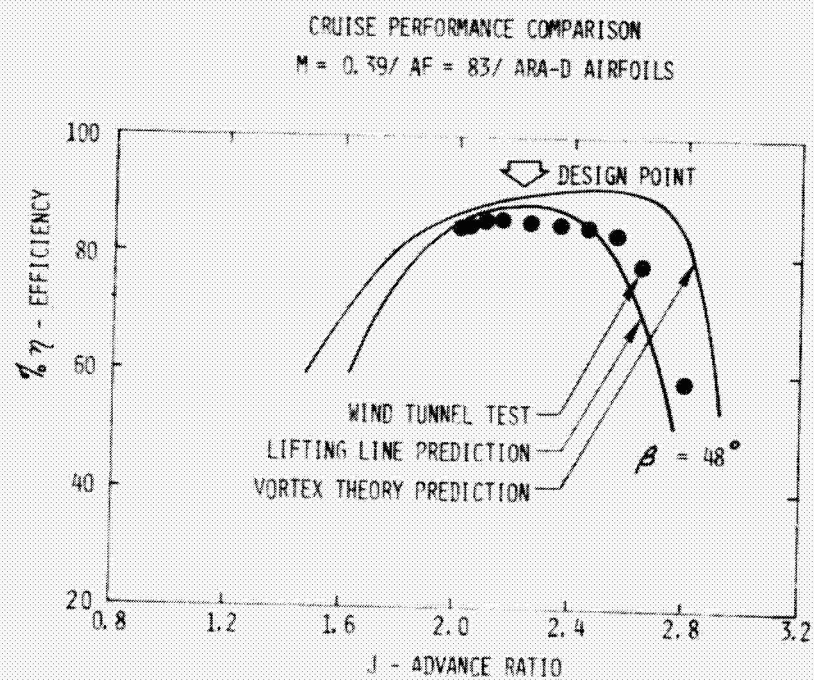


Figure 10

# WAKE RAKE SURVEY

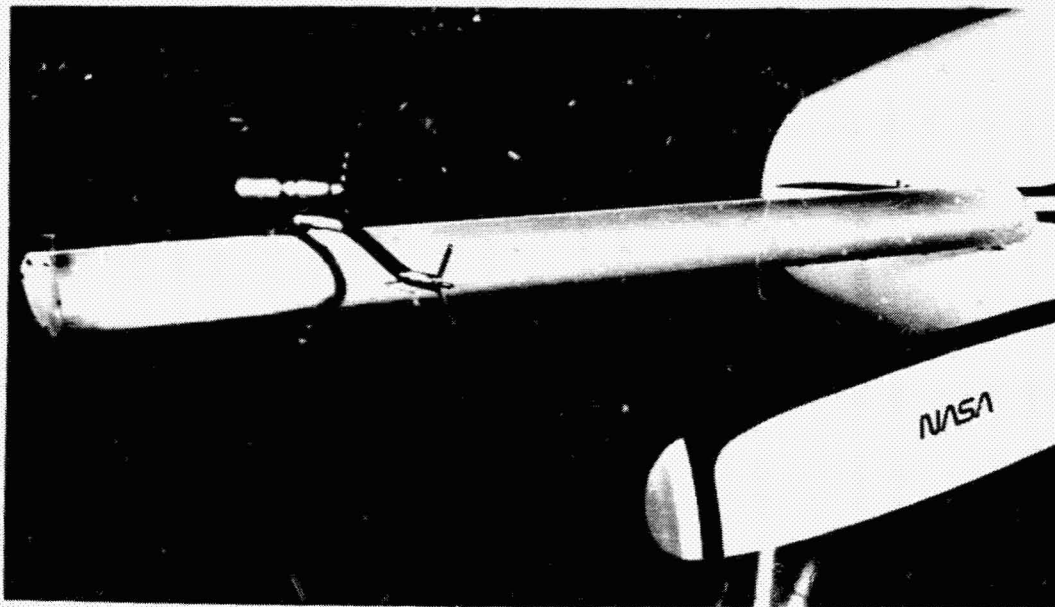


Figure 11

## CENTRIFUGAL VISCOUS EFFECTS ON LIFT

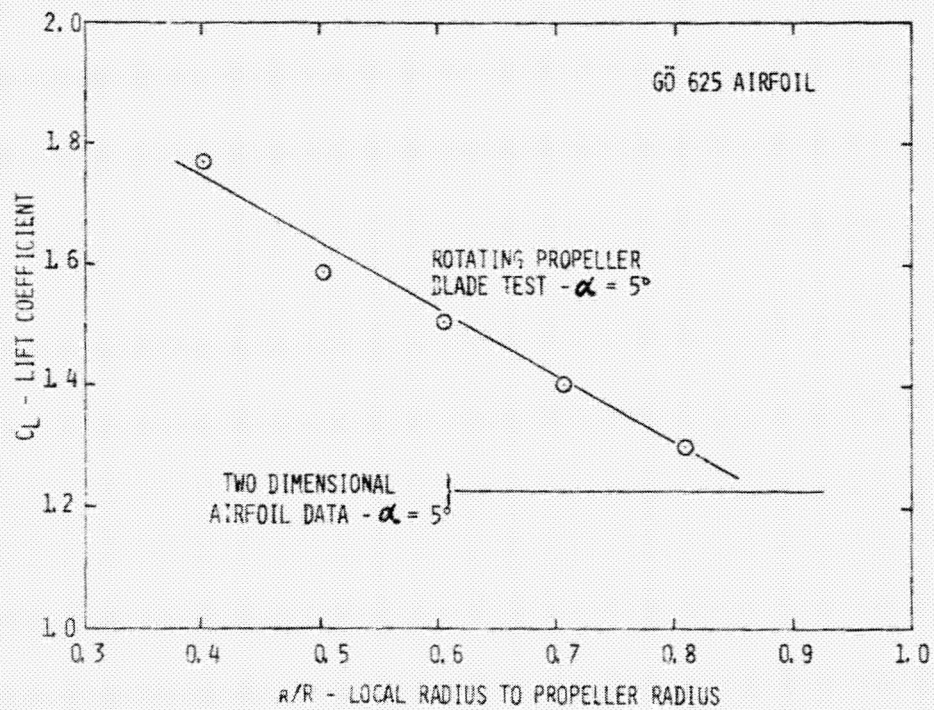


Figure 12



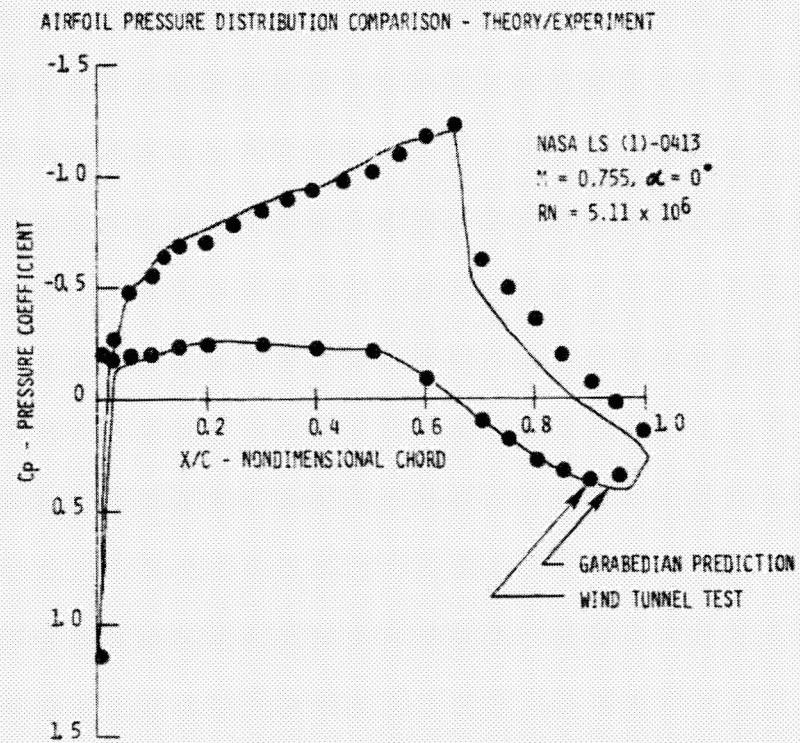


Figure 13

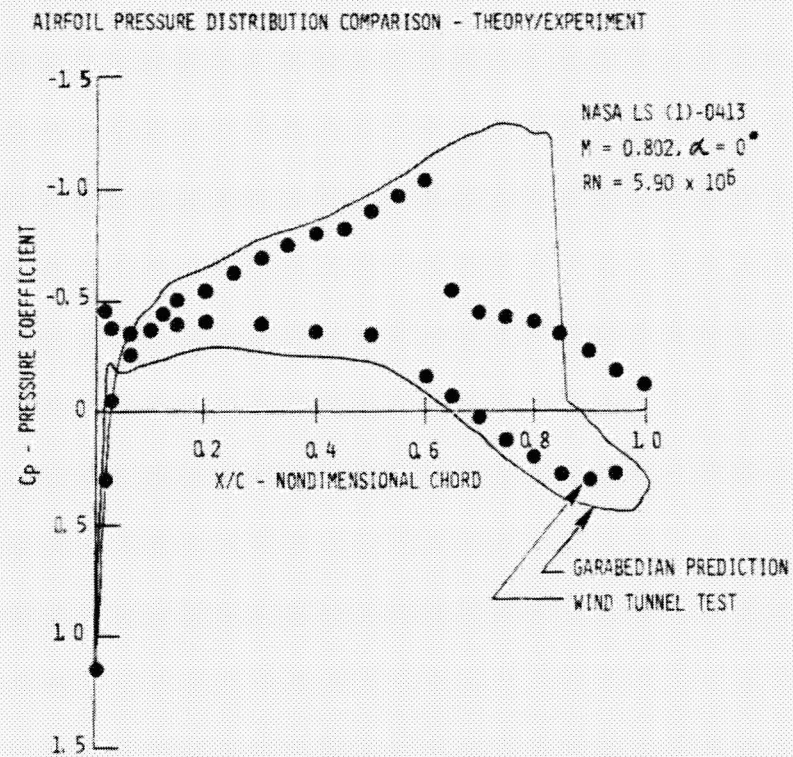
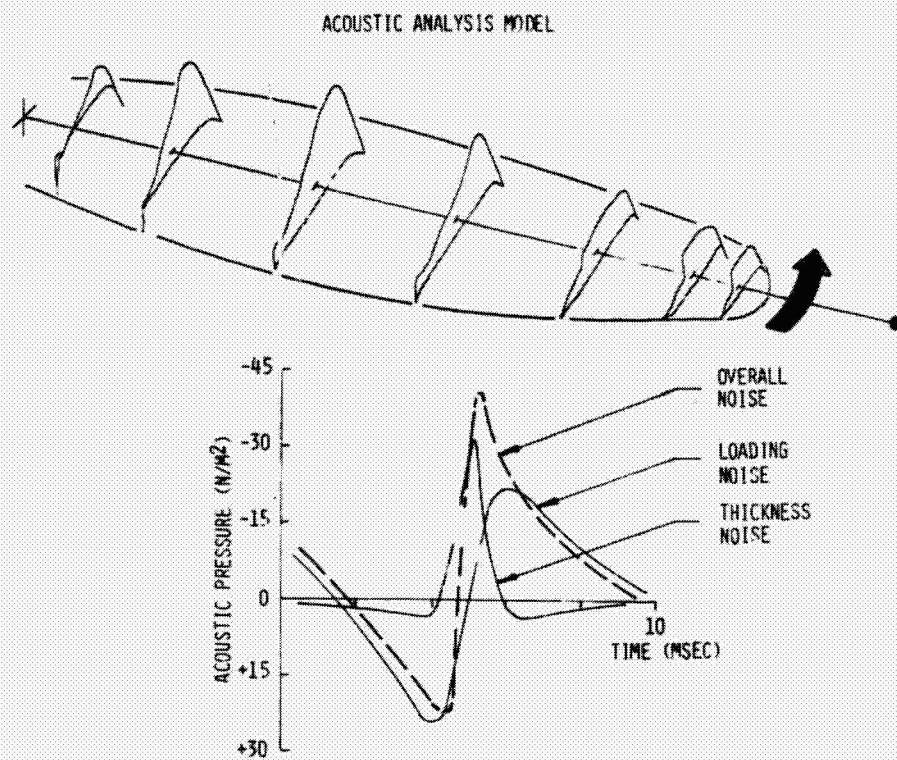
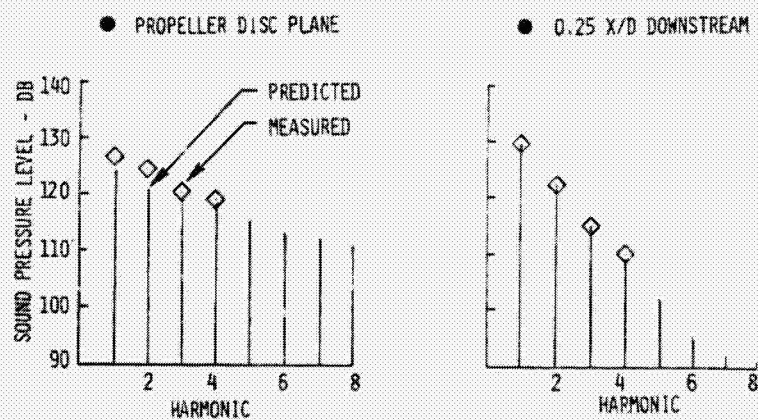


Figure 14



COMPARISON OF MEASURED AND PREDICTED NOISE





NEAR FIELD ACOUSTIC MEASUREMENTS



Figure 17

ORIGINAL PAGE IS  
OF POOR QUALITY

## NASA PROPELLER NOISE RESEARCH

George C. Greene  
National Aeronautics and Space Administration  
Langley Research Center

General Aviation Aircraft represent a cost effective solution to many of the public's transportation problems. Due to their fuel efficiency, propeller driven commuter aircraft are appearing in ever increasing numbers, replacing jet CTOL's on short block time, low passenger density routes. Business aircraft have experienced a steady growth in recent years. Add these aircraft to the large number of privately owned general aviation aircraft which are already in operation and the resulting propeller noise represents a growing national problem.

The purpose of NASA's propeller noise research program is to provide a technology base for reducing propeller noise with a minimum of performance, weight, and economic penalties. The thrusts of this program are shown schematically in Figure 1. Noise prediction technology represents the most basic part of the program. The emphasis of this activity is on the understanding of and prediction of propeller noise using basic principles of physics. Deficiencies in the prediction process identify areas where further research is needed. New research results are incorporated in the noise prediction process until predicted results are satisfactory. Engineering noise prediction methods can then be developed.

Propeller noise/performance optimization studies emphasize the development of practical propeller design technology. The current program in this area utilizes single-engine aircraft. Future efforts will include larger twin engine aircraft. New design technology will be demonstrated with flight programs as required.

The third program area is interior noise reduction. Research topics include definition of the source input to the fuselage sidewall, evaluation of sidewall transmission characteristics for different types of structures, and development and evaluation of advanced noise control treatments. This research is especially important in view of the high predicted noise levels for advanced high speed propellers.

This paper will describe the current research program in propeller noise prediction, noise/performance optimization, and interior noise reduction. Selected results will be presented to illustrate the status of current technology and the direction of future research.

### Propeller Noise Prediction Technology

Some characteristics of the propeller noise prediction effort are shown in Figure 2. The technology being developed is applicable to low and high speed propellers. It is based on the basic physics of the noise generation

process, rather than empirical methods. The technology is relatively sophisticated to permit analysis of complex configurations such as that proposed for a high speed turboprop. Noise prediction requires a knowledge of the propeller geometry and a description of the aerodynamic characteristics of the propeller. Examples of noise calculations using this technology are shown in Figures 3 and 4. Figure 3 shows a comparison of measured and calculated noise for a Twin Otter aircraft. Sound pressure level is shown as a function of frequency expressed in multiples of the blade passage frequency. The acoustic data were taken in the plane of the propeller with a microphone mounted on a boom on the aircraft wing. The measured data include noise from sources other than the propeller, but in general the agreement is very good.

Typical results for an advanced high speed propeller configuration are shown in Figure 4. Again sound pressure level is presented as a function of blade passage harmonic number. The measured data were taken in an acoustic wind tunnel using a four-bladed model of the propeller configuration shown in the photo insert. This propeller configuration is known as the SR-3. The agreement between theory and data for the overall level is very good with some errors occurring at the high frequencies. The causes of this error are under investigation and will probably result in refinements to the prediction technique.

#### Propeller Noise/Performance Optimization

Characteristics of the propeller noise/performance optimization program are shown in Figure 5. This is a joint NASA/EPA program to demonstrate that propeller noise can be reduced in an economically reasonable manner. The goal of this effort is to reduce light aircraft propeller noise by 5 dBA while maintaining or improving propeller performance. The effort consists of 1) optimization studies to assess the potential noise and performance benefits of various propeller parameters, 2) wind tunnel tests to verify design concepts, and 3) flight tests to demonstrate the noise reduction technology. Parallel efforts are being conducted at Massachusetts Institute of Technology and Ohio State University. Some results from this program are shown in Figures 6-13.

Figure 6 shows the effect of varying the propeller diameter. This assumes a constant shaft rpm so that this is essentially the effect of varying propeller tip speed. Noise in terms of dB<sub>A</sub> and efficiency are shown subject to the assumptions listed on the figure. For each calculated point, the propeller was optimized for that particular diameter. As can be seen both the noise and performance are quite sensitive to this parameter. A small percentage reduction in propeller diameter can result in a very substantial noise reduction. Efficiency is also compromised but not to the same extent that the noise is reduced. A reduction of propeller diameter must be accompanied by other parameter changes if the propeller efficiency is to remain constant.

The calculated effect of varying the number of propeller blades is shown in Figure 7. Subject to the listed assumption, this indicates that noise can be reduced by increasing the number of blades. Propeller efficiency is

not changed significantly by changing the number of blades. It should be remembered that these are calculated results and do not contain the effects of blade interference at the larger blade numbers. Figure 8 shows the calculated effect of varying radial load distribution on the blade. Subject to the assumptions listed, it is shown that noise can be substantially reduced by moving the peak of this load distribution inboard. There is an optimum location which results in maximum propeller efficiency, however the efficiency is not very sensitive to small changes in the position of this peak loading.

Figure 9 shows the calculated effect of blade sweep on propeller noise. The calculated points are for sweep angles from zero degrees, which represents a straight blade, to the extreme case of a propeller which is completely wrapped around itself. For practical sweep angles, which are relatively small, there is a slight noise reduction. The effect of sweep of this magnitude on performance has not been evaluated.

In order to test some of the concepts which were developed during the parametric studies, model propellers were constructed for testing in the MIT wind tunnel. Figure 10 shows two model propellers, a "quiet" propeller and a standard Cessna 172 propeller. Although not obvious due to the angle at which the photograph was taken, the modified propeller has the same diameter as the standard propeller. It has a wider cord which was designed to move the load distribution inboard on the propeller blade.

These propellers were tested over a wide range of conditions on a propeller spinning rig with and without an afterbody to simulate an aircraft fuselage. Figure 11 shows the test configuration in the MIT acoustic wind tunnel with a fuselage afterbody. Figure 12 shows a sample comparison of measured and predicted noise data. A schematic of the tunnel configuration is shown on the right part of the figure. The data are for the standard Cessna propeller model with no afterbody. Noise data were measured with a microphone mounted in the airstream 1 diameter from the center of propeller rotation. The data presented is a pressure time history for approximately 2 revolutions of the propeller. These data correspond to cruise conditions for an actual aircraft. As can be seen, the agreement between the predicted and measured noise is excellent. Similar results were obtained for other configurations.

After demonstrating the noise prediction techniques in the wind tunnel, full-scale propellers were designed for flight tests at both Massachusetts Institute of Technology and Ohio State University. Figure 13 shows the flight test aircraft which will be used by the OSU. It is a Beech Sundowner aircraft and is equipped with a microphone boom which can be extended to measure noise in and behind the plane of the propeller. Ground noise measurements will be made for 500-foot and 1000-foot flyovers. Noise measurements will be made with and without an engine exhaust muffler to determine the relative levels of propeller and exhaust noise. A similar flight demonstration will be conducted by MIT using a Cessna 172 aircraft; however, the MIT aircraft will not be equipped for near-field inflight noise measurements and will not have an engine exhaust muffler.

A final purpose of this program is to establish a center for effective distribution of propeller optimization technology. Because of its current involvement in the NASA program and its ready access to aircraft manufacturers, the Ohio State University Airfoil Design and Analysis Center has been chosen to serve this function.

### Interior Noise Reduction

Interior Noise Reduction involves altering the characteristics of the sound path from the source to the observer, as well as altering the characteristics of the noise source itself. The major elements of the interior noise reduction program are listed in Figure 14. The definition of the input or source for transmission studies is obviously important. The understanding of sidewall noise transmission mechanisms and the evaluation of potential noise control treatment are also key elements of the program. Structureborne noise is also of interest due to the problems encountered by small piston engine aircraft. One source of interior noise in light aircraft is vibration. This originates in the engine, is transmitted through the support structure, and is radiated into the cabin.

An example of structureborne noise research is shown in Figure 15. The research was directed toward determining the relative magnitudes of structureborne noise and noise from other sources such as the propeller which might be transmitted through the air and through the fuselage sidewall into the aircraft cabin. The principle feature of the setup shown is the use of stanchions located at the firewall on each side of the aircraft to support the engine weight and thrust loads so that the engine can be operated without any mechanical attachment to the fuselage. The fuselage is located in the correct geometry relative to the engine so that other noise sources are the same. The engine can also be attached to the fuselage in a normal configuration. The engine attached configuration provides the total interior noise from all sources and paths while the engine detached configuration provides all sources except the structureborne noise, so the difference provides the structureborne contribution.

The bar chart at the right of the figure indicates typical results. The total bar height indicates the total interior noise as measured in the engine attached condition. The shaded portion of the bar indicates the structureborne contribution. As indicated by the overall level bar at the right of the figure, detaching the engine reduced the level by 3 dB, indicating that the structureborne contribution is about equal to the contribution from all other source/path combinations. Examination of the spectrum indicates that the structureborne contribution is significant over a relatively wide frequency range, up to about 2000 Hertz. Current research efforts are directed toward prediction of the structurally transmitted noise and development of noise control methods involving control of both noise radiated from panels to the aircraft interior as well as noise transmitted through the engine mounting vibration isolators.

Fuselage sidewall transmission is very important for those aircraft which have wing-mounted propellers operating close to the fuselage sidewall.

Research is currently underway to evaluate possible structural treatments to improve the fuselage sidewall noise attenuation. An aircraft used in one such study is shown in the upper left photograph on Figure 16. This aircraft is an Aero Commander 680, modified for evaluating interior noise control treatments. To provide a baseline for structural modifications being investigated, the interior trim and insulation were removed in the area of interest and the windows were replaced with stiffened aluminum panels similar to the fuselage construction. These modifications are shown in the lower right photograph of the aircraft interior. The area investigated is shown as the shaded area in the sketch in the lower left of the figure.

Sidewall noise attenuation characteristics were measured for propeller noise inputs and for artificial noise inputs from the large horn shown in the photograph. Attenuation provided by the sidewall for the horn input is shown as noise reduction in the upper right of the figure. Noise reduction is the difference between the inside and outside sound levels as a function of the frequency. The two curves shown are for the bare sidewall and for the sidewall with 15 pounds of asphalt type, glue on mass added to the aircraft. These results indicate that even a modest amount of appropriately added mass may reduce interior noise by 4-15 dB depending on the frequency of noise.

Conventional treatment will not be sufficient for the new generation of high-speed propeller driven aircraft. Figure 17 shows the relationship between desired cabin noise levels and currently predicted propeller noise levels for current designs of high-speed propellers. The bar on the left indicates the range of noise levels experienced in testing of current propellers and the projected improvement due to advanced propeller design. These levels are on the order of 140 dB with possible improvements below that. Predicted interior noise levels and the interior noise goal are shown by the bars on the right. As can be seen, there is a gap of approximately 25 dB in the cabin attenuation which must be obtained from new technology. This problem is being addressed in two ways. First there are continuing efforts to reduce the noise of high-speed propellers through careful design of advanced configurations. In addition, improved estimates of propeller noise will be obtained in the summer of 1980 when a propfan model is flown on a Jet Star aircraft.

Analytical studies are also being pursued to define low weight, low-noise-transmitting sidewalls. Preliminary results from two studies are shown in Figure 18. The primary conclusion of this study is that acceptable cabin interior noise levels can be achieved using conventional technology. Both studies employed a double-wall design using an optimum combination of added mass, structural damping, and tuning of the structure. These studies estimated the acoustic weight penalties which would accrue for the types of aircraft listed in Figure 18. The weights listed are penalties in addition to the acoustic treatment weights currently carried. Although these weights are high, the potential of the propfan as a fuel efficient propulsion system is still viable.

### Future Research

Trends of future NASA research are shown in Figure 19. There will be a continued effort in the development and refinement of noise prediction methods. As these methods mature, simplified design techniques will be developed to permit their practical application. The emphasis of prediction and design technology will shift to twin and commuter size aircraft to reflect their growing importance. Interior noise research will continue for all classes of aircraft with a special emphasis on developing the technology necessary for the timely development of high-speed propeller-driven aircraft.



## GENERAL AVIATION NOISE RESEARCH

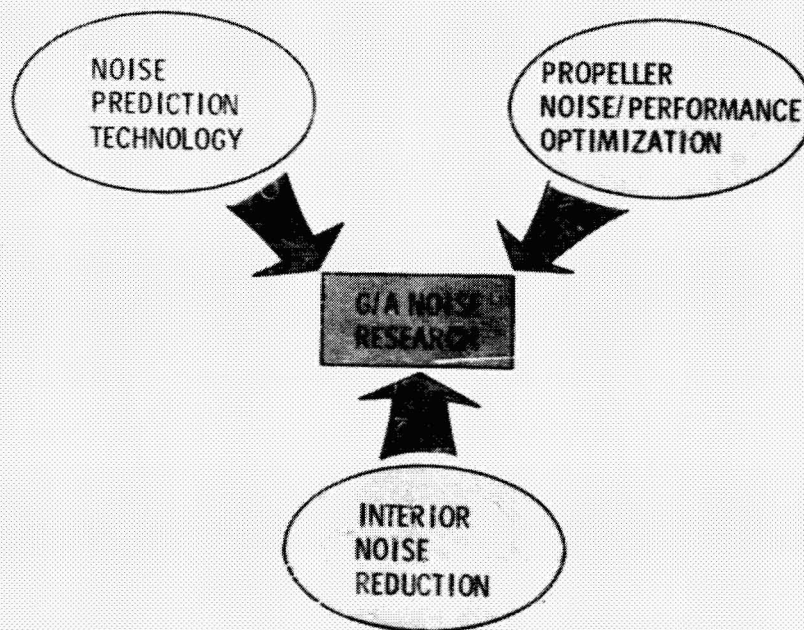


Figure 1

## PROPELLER NOISE PREDICTION TECHNOLOGY

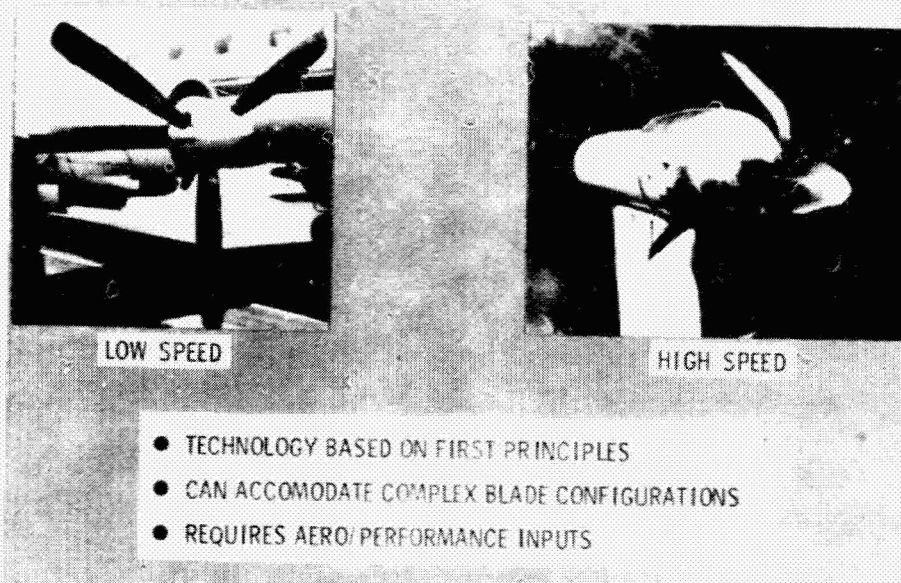


Figure 2



# COMPARISON OF MEASURED AND CALCULATED NOISE FOR TWIN OTTER AIRCRAFT

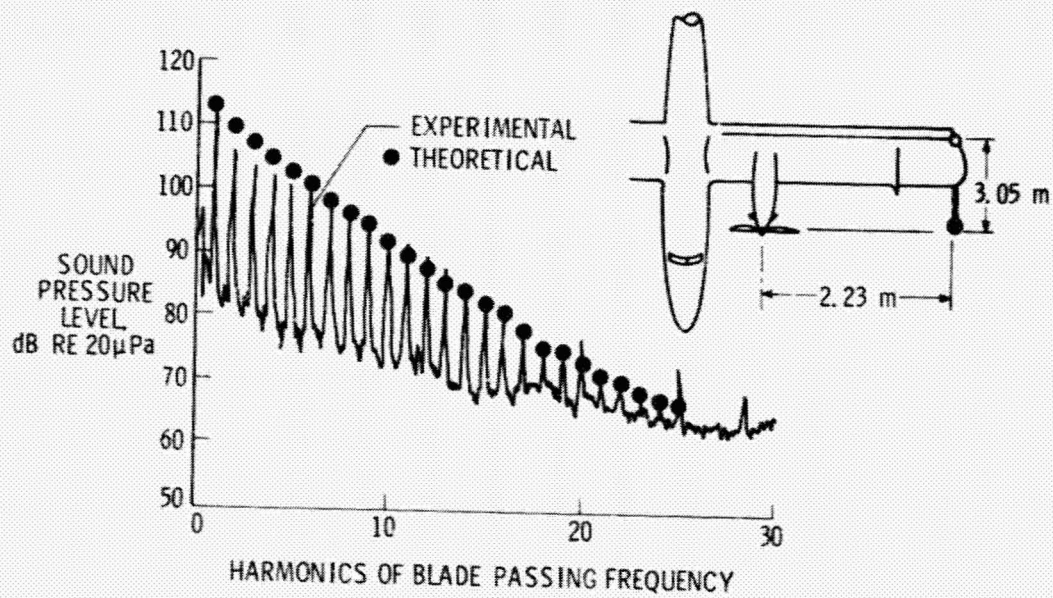


Figure 3

# COMPARISON OF MEASURED AND CALCULATED RESULTS FOR SR-3 PROPELLER

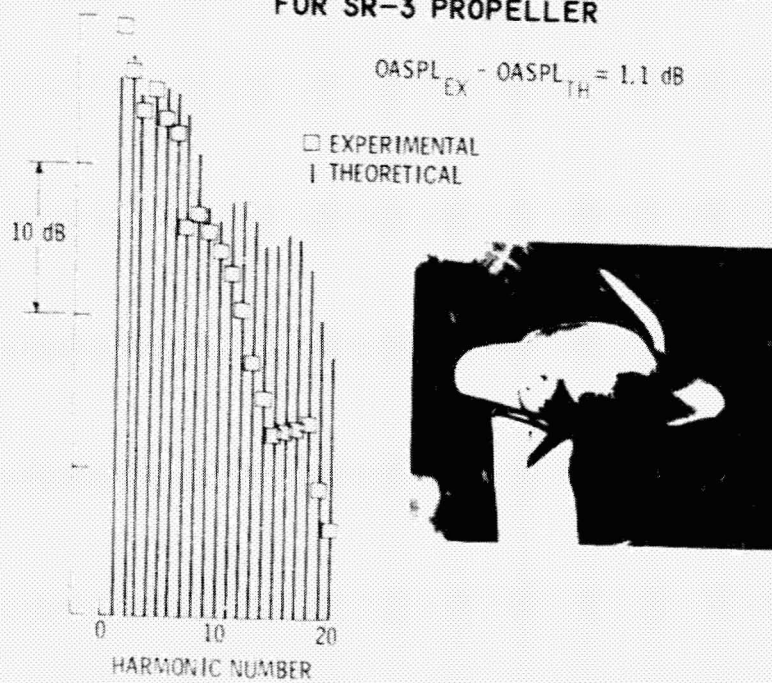


Figure 4

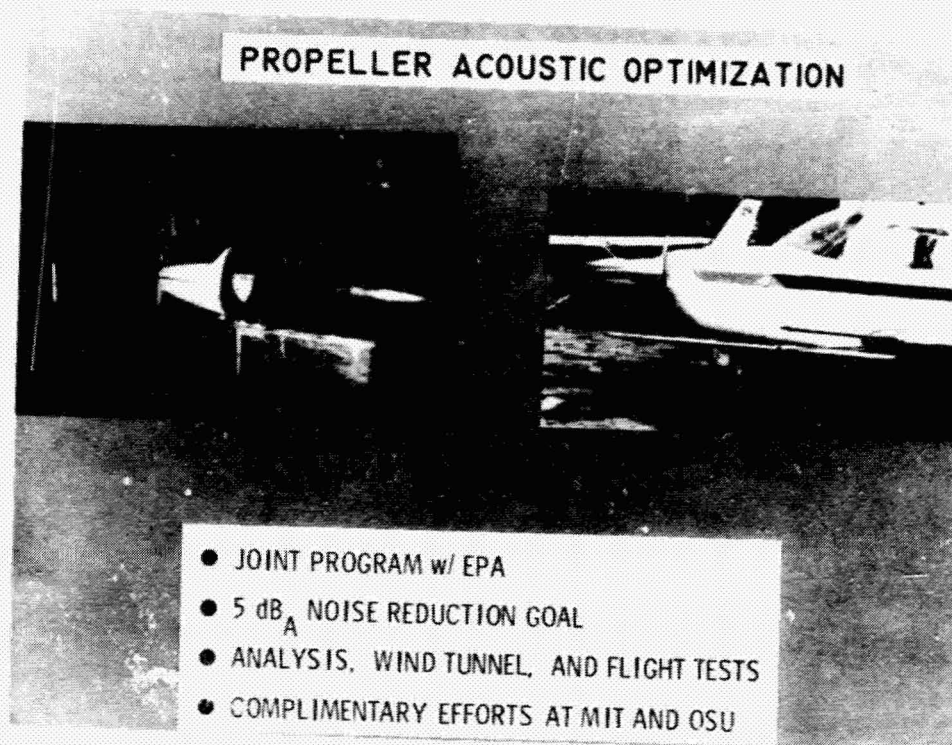


Figure 5

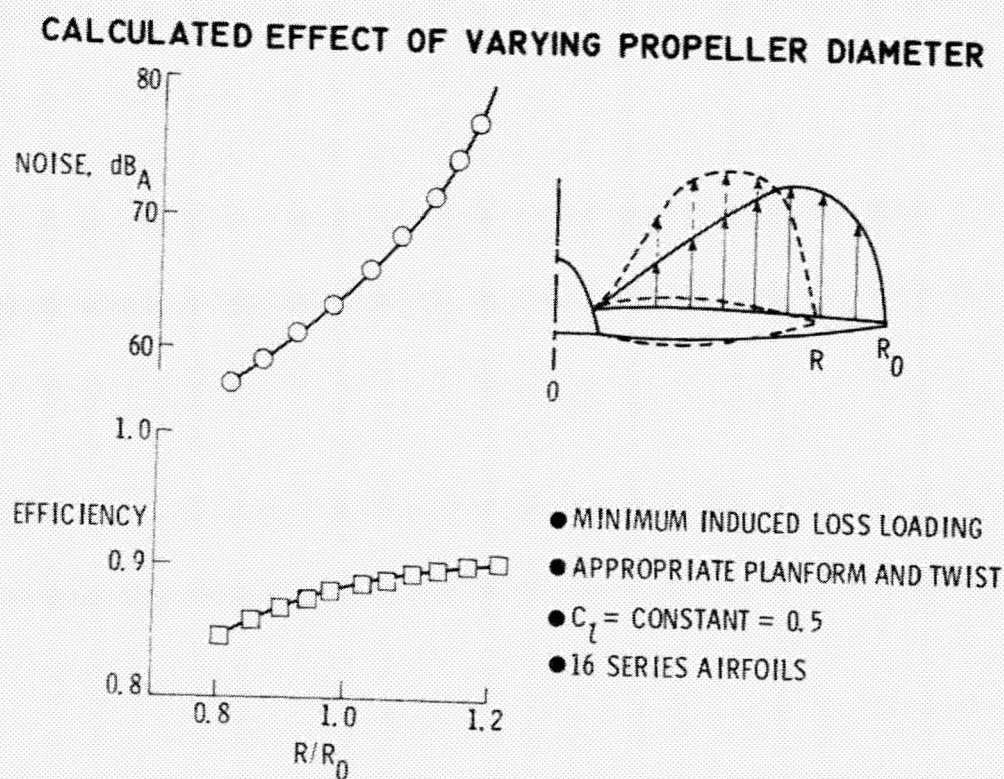


Figure 6



### CALCULATED EFFECT OF NUMBER OF BLADES

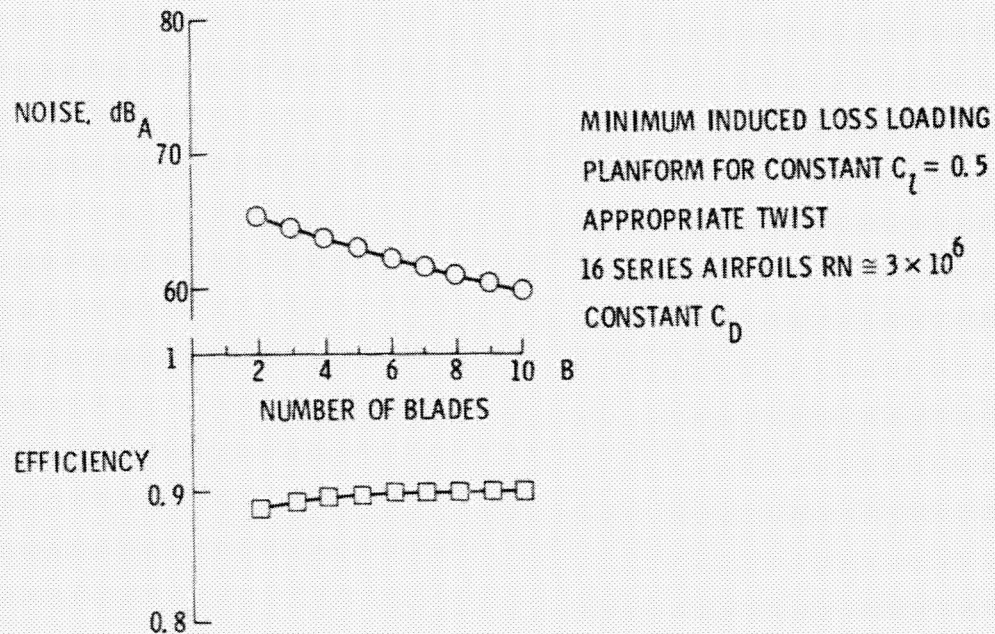


Figure 7

### CALCULATED EFFECT OF VARYING RADIAL LOAD DISTRIBUTION

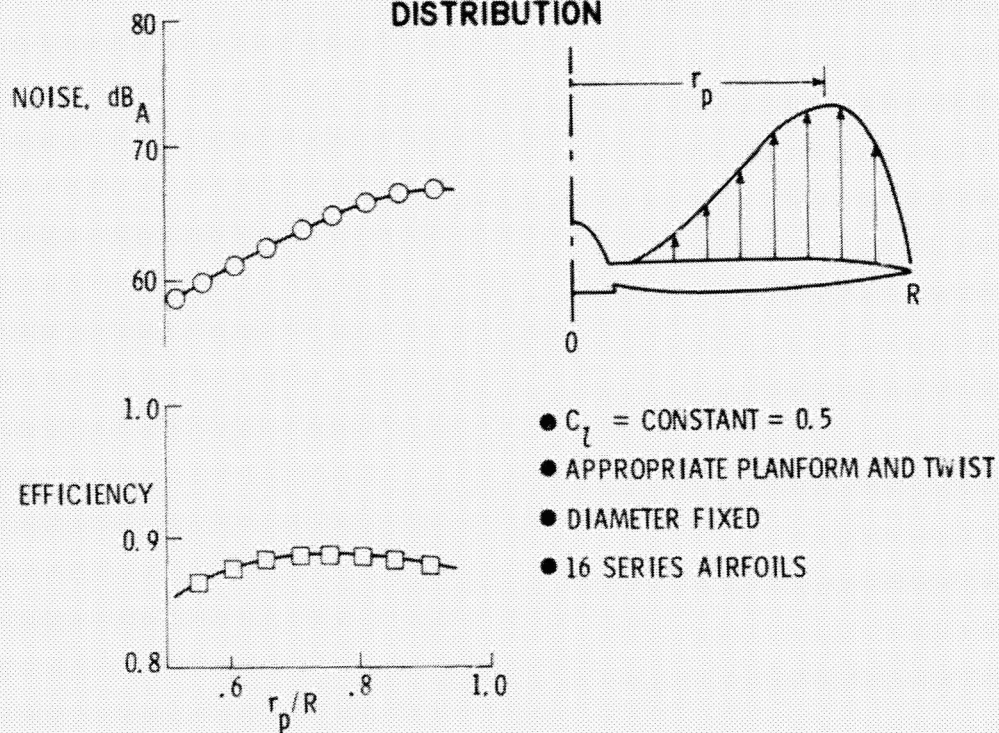


Figure 8

# CALCULATED EFFECT OF SWEEP ON TWO BLADED PROPELLER

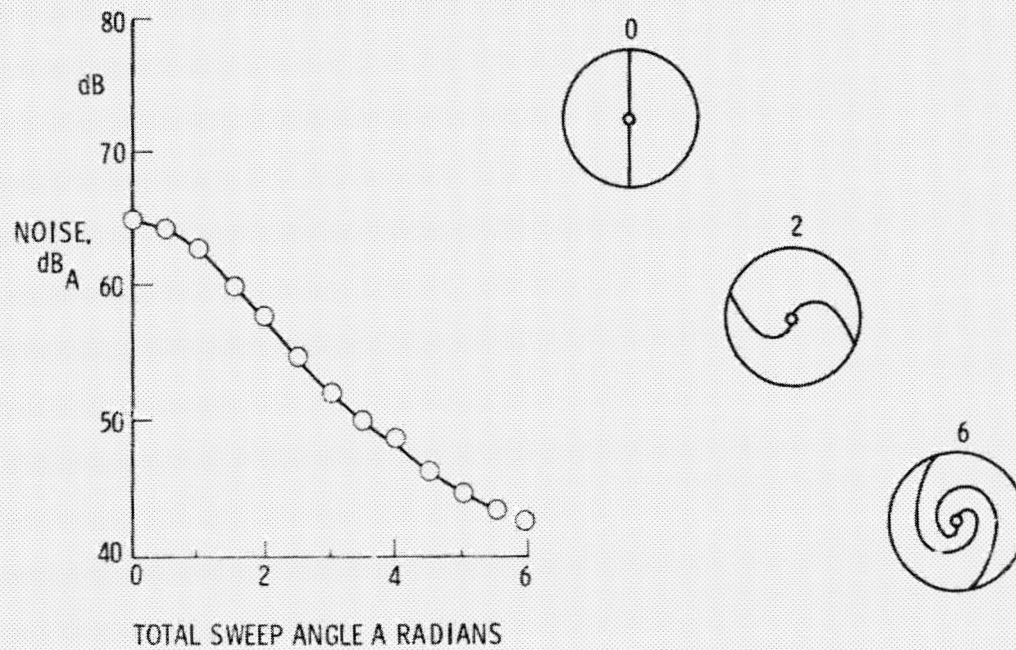


Figure 9

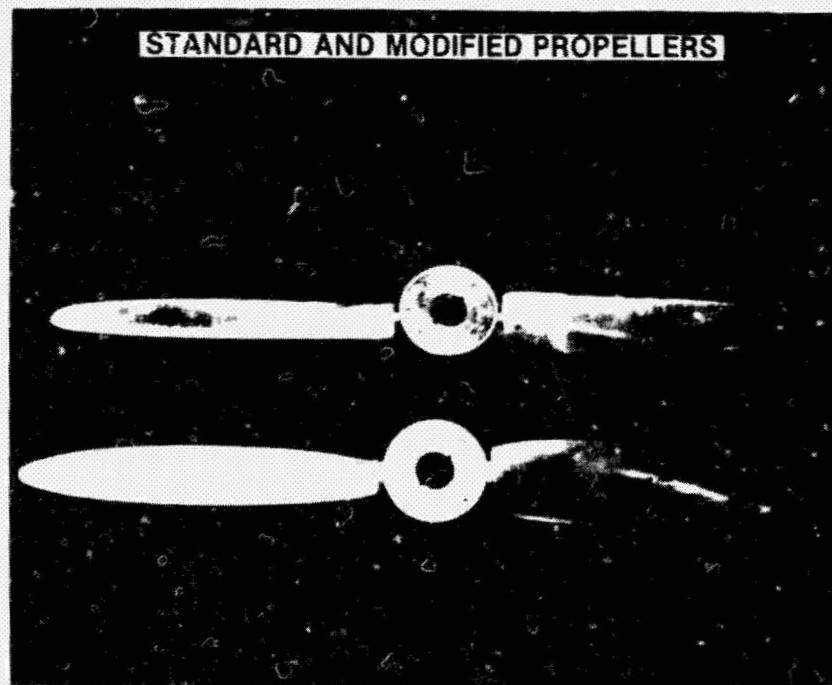


Figure 10



# PROPELLER TEST IN MIT WIND TUNNEL

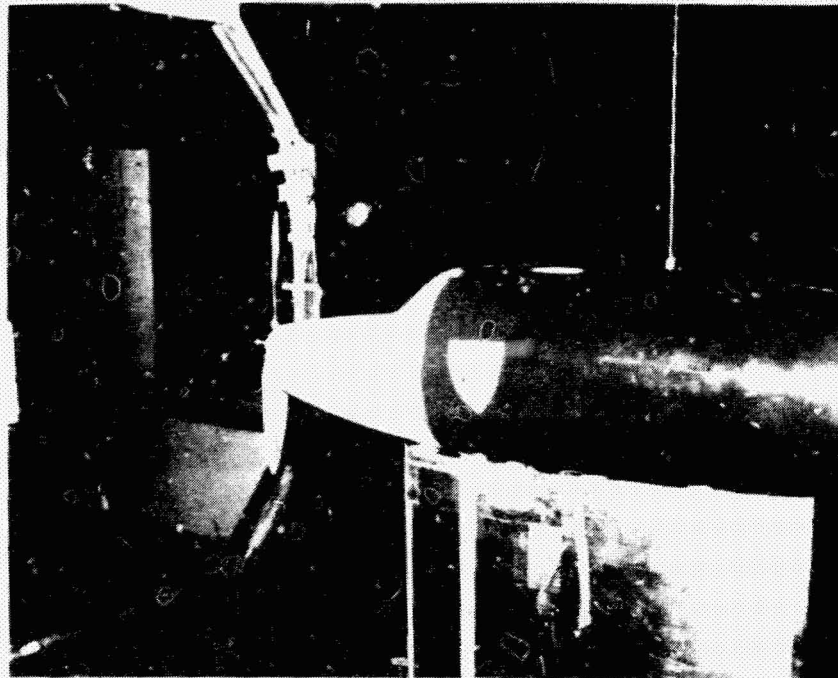


Figure 11

## COMPARISON OF MEASURED AND PREDICTED PROPELLER NOISE

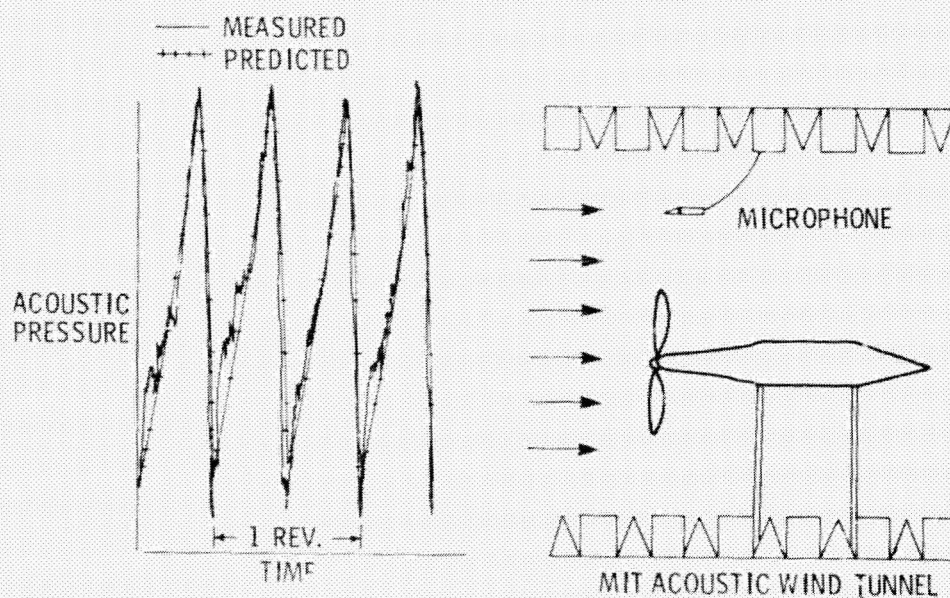


Figure 12

## OSU FLIGHT TEST AIRCRAFT

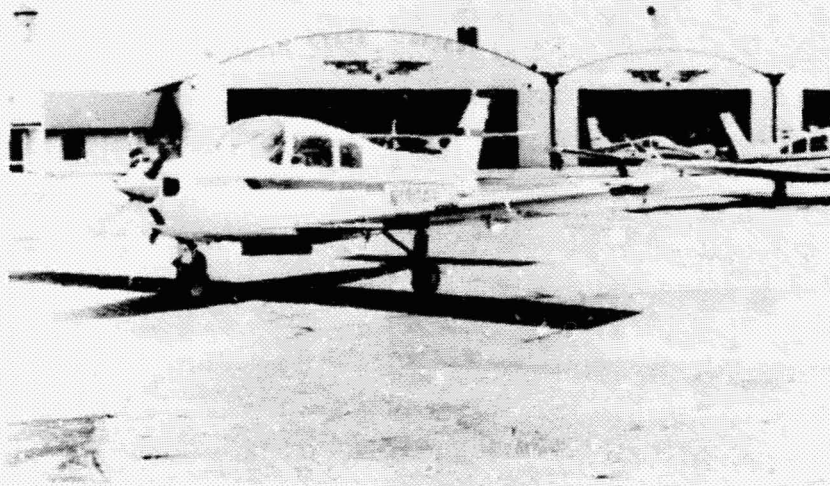


Figure 13

## INTERIOR NOISE REDUCTION

- SOURCE DEFINITION
- SIDEWALL NOISE TRANSMISSION
- NOISE CONTROL TREATMENT
- STRUCTURE BORNE NOISE TRANSMISSION

Figure 14



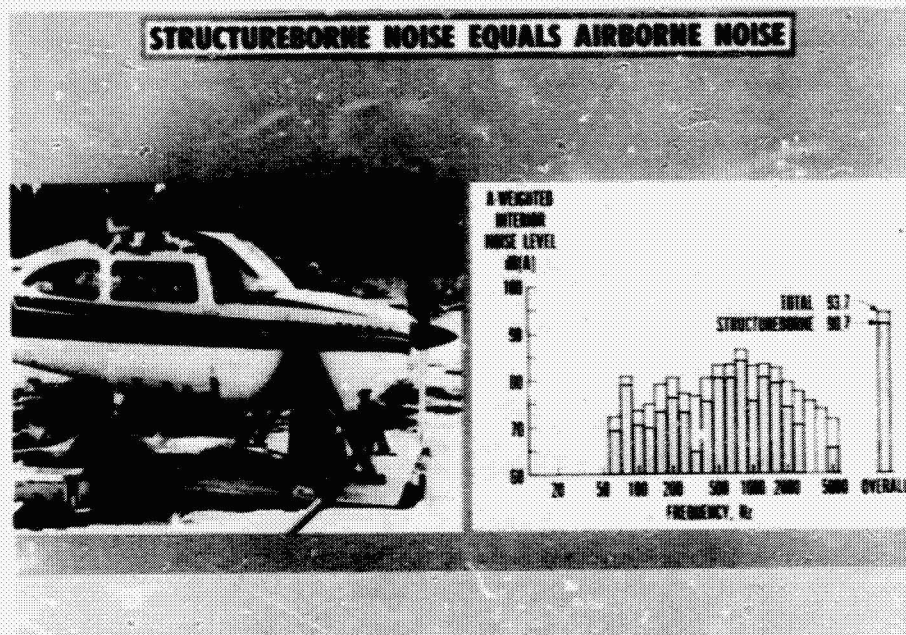


Figure 15

# EVALUATION OF INTERIOR NOISE CONTROL TREATMENTS



Figure 16

## HIGH SPEED TURBOPROP INTERIOR NOISE



PROPOSED QUIET PROP FAN

- SUPERSONIC SPEED AT PROPELLER TIP
- HIGH EXTERIOR NOISE LEVEL ON FUSELAGE
- ADVANCED FUSELAGE TREATMENT REQUIRED FOR PASSENGER ACCEPTANCE

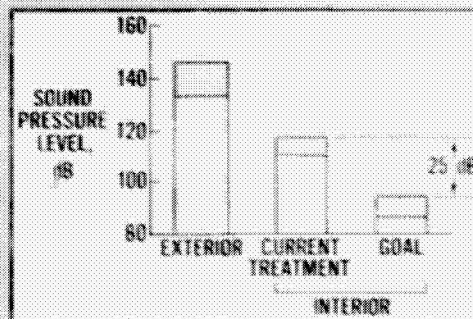
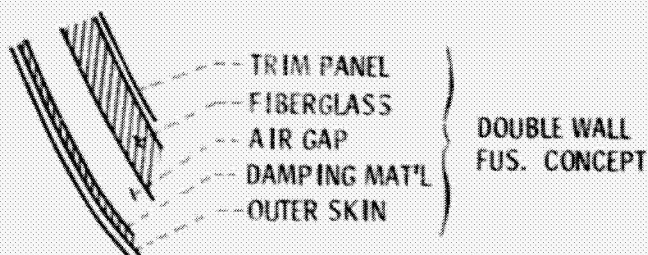


Figure 17

## FUSELAGE INTERIOR NOISE REDUCTION STUDY

$M = 0.8$ ,  $\Delta dB \approx 45$

INTERIOR = 80dBA



AIRCRAFT  
4 ENG. WIDE BODY  
2 ENG. SMALL A/C

GROSS WT.  
217 TO 252K  
30 TO 32K

$\frac{D_{PROP}}{D_{FUS.}}$   
0.6 TO 1.0  
1.0 TO 1.4

ACOUSTIC  
WEIGHT  
PENALTY  
% G.W.  
0.8 TO 2.3  
1.5 TO 1.7

Figure 18



## **FUTURE RESEARCH**

- CONTINUED DEVELOPMENT AND REFINEMENT OF PREDICTION METHODS
- EMPHASIS TO INCLUDE TWIN AND COMMUTER SIZE AIRCRAFT
- CONTINUING RESEARCH IN INTERIOR NOISE REDUCTION

Figure 19

## PROPELLER DYNAMIC AND AEROELASTIC EFFECTS\*

Barnes W. McCormick  
The Pennsylvania State University

### SUMMARY

Various aspects of propeller blade dynamics are considered including those factors which are exciting the blades and the dynamic response of the blades to the excitations. Methods for treating this dynamic system are described and problems discussed which may arise with advanced turboprop designs employing thin, swept blades.

### INTRODUCTION

A propeller on a shaft driven by an engine attached to an airframe represents a dynamic system. This system responds to excitations from the power plant as well as to unsteady aerodynamic forces on the blades. These unsteady forces result from the non-uniform inflow into the propeller as produced by an angle of attack or by interference from the fuselage, wing and nacelles. They can also be caused by aeroelastic phenomena such as classical or stall flutter.

The propeller-engine-airframe combination, as a continuous system, has an infinite number of degrees of freedom and hence, an infinite number of normal modes. Generally, a disturbance will excite all of the modes, but it is only a few of the lowest modes which are of importance.

For purposes of determining propeller blade vibrations one can treat the propeller as an isolated dynamic system excited by the unsteady torque at the hub from the engine and by the unsteady airloads distributed along the blade surfaces. The dynamic response of the propeller to these excitations determines the vibratory blade stress levels, a knowledge of which is essential to assuring an acceptable fatigue life of the blades. Noise and fuselage vibration levels are also dependent to some degree on the propeller dynamics.

This presentation will discuss briefly methods of calculating the dynamic behavior of a propeller and will present some results obtained to date on a NASA research grant to The Pennsylvania State University. This

\* supported under NASA Grants NSG-1308 and NSG-3304

grant involves not only the dynamics of the propeller but the unsteady aerodynamics as well; in particular, the interference with the fuselage, wing and nacelles.

The area of propeller blade dynamics promises to become even more important in the future with increasing application of fuel-efficient turbo-prop installations designed to cruise at high Mach numbers. These propellers, employing innovations such as composite materials, thin blades and sweep, will present challenges in their design and analysis which are not found with current all-metal blades. The environment for a propeller can be more severe than for the compressor of a turbofan engine. As shown in figure 1, at an angle of attack, the inlet duct serves to redirect the inflow into the compressor blades; whereas, the propeller blades experience an unsteady flow because of the angle of attack of the propeller's axis. More specifically, the section angle of attack at a given radius varies approximately sinusoidally with the azimuth angle with an amplitude proportional to the propeller angle of attack and the square of the advance ratio.

The brief discussion to follow of propeller dynamics is perhaps best summarized by reference to figure 2. In treating propeller dynamics, one is concerned with those factors which are exciting the system and with the response of the system to the excitation. These excitations may not depend on the dynamic response of the propeller or they may as in the case of stall flutter. An accurate calculation of the unsteady forces and propeller dynamic response is essential to assuring an adequate fatigue life for the propeller. Such calculations promise to become more challenging in the future as propellers are operated at high cruise Mach numbers. The introduction of new materials and the departure from today's conventional planform and airfoil shapes may also give rise to new problems associated with propeller dynamics.

#### UNSTEADY FORCES

In addition to the effect of angle of attack, non-uniformities in the inflow to a propeller result from velocities induced by the presence of the fuselage, wing and/or nacelles. These can cause both the magnitude and direction of the velocity vector in the plane of the propeller to vary with position (ref. 1). A computer code has been developed to predict this non-uniform velocity field. As shown in figure 3, the wing is replaced by a single horseshoe vortex having a span equal to that for a trailing rolled-up vortex sheet for an elliptic spanwise loading distribution. The fuselage and nacelles are panelled with sources being placed on each panel. The strengths of these sources are adjusted to assure that the velocity normal to the surface vanishes. This boundary condition can be relaxed to allow for cooling airflow through inlets.

Figure 4 presents the calculated variation of axial velocity for a typical single-engine light airplane as a function of azimuth position for 30% and 75% radial stations. The inboard section of the propeller is seen to experience a significant variation in the inflow equal to approximately 60% of the advance velocity as the propeller rotates. Also of interest is the

result shown on this figure that one need not model the complete fuselage in order to obtain an accurate description of the propeller inflow. In this case, the cowling, closed at the rear by a simple faired shape, results in a predicted inflow which is close to that obtained with the complete fuselage. These curves are not symmetrical about a value of  $180^\circ$  because the propeller is yawed relative to the fuselage.

As a result of non-uniform inflow, the aerodynamic loads on a propeller blade can vary significantly with azimuth position. However, the unsteady aerodynamic loads pale by comparison to the unsteady torque of a piston engine. Figure 5 presents some unpublished measurements obtained recently on a four-cylinder, horizontally-opposed engine operating at 1300 rpm. From the figure it is obvious why one should avoid operating an engine continuously at a speed corresponding to a normal propeller mode. The amplitude of the unsteady torque is of the order of 300% of the average value. For turboprop applications, the engine torque is essentially constant so, here, one is more concerned about the unsteady airloads.

#### BLADE DYNAMICS

The dynamic response of a continuous system to an excitation can be calculated by a solution of the differential equations governing the system or by a lumped-parameter method which approximates the continuous system by discrete masses and springs. Both of these approaches are being tried under the research grant previously mentioned.

Because of the complex propeller geometry and the nature of the exciting forces, a closed-form solution for the equations of propeller blade motion is highly unlikely, if not impossible. Instead, one resorts to classical energy methods to determine the normal modes of the propeller. These normal modes can then be applied to the method of generalized coordinates and forces to obtain the dynamic response. To accomplish the foregoing, one must resort to the use of large computer codes.

A typical propeller for a single, piston-engine, light airplane is shown in figure 6. In this laboratory study, the propeller is clamped in a universal testing machine. An electromagnetic shaker excites the blade at the tip, and a piezoelectric accelerometer measures the blade response at various points on the blade surface. Restrained at the hub by the large mass of the testing machine, the blade responds as if it is cantilevered from the hub with no elastic coupling to the other blade.

Figure 7 illustrates a different test set up for a shaker test. Here, supported on a soft rubber innertube, the propeller responds as a free beam. The electronic equipment is shown in this figure consisting of amplifiers, power supply, frequency generator, oscilloscope and a ubiquitous spectrum analyzer and averager. By sweeping the frequency and noting resonances, one can quickly determine the frequencies of the lower normal modes. A manufacturer will test each propeller model in the manner of this figure to assure that none of the lower modes correspond with exciting frequencies from the

engine. Since half of the cylinders of a four-cycle engine fire during each revolution, this impulse frequency in Hertz is given by the product of the rpm and the number of cylinders divided by 120.

Generally, the vibratory motion of a propeller blade will consist of a bending out of its plane of rotation coupled with a bending in the plane and a torsional displacement along the blade. Based on energy methods and the concept of a transmission matrix, a computer code has been developed (ref. 2) which predicts the normal modes for coupled bending-bending or coupled torsion with out-of-plane bending. The modelling of the complete coupling of all three motions has not been accomplished thus far. However, since present propeller blades are very stiff torsionally and in-plane, the lower modes of the coupled bending-bending and bending-torsion models have approximately the same frequencies which are determined principally by the relatively soft out-of-plane bending stiffness. Thus, the lack of a completely coupled numerical model is not too restrictive for the present. However, this may not be the case for future turboprop designs. For this reason a lumped-parameter model is being developed which will allow for complete coupling, sweep and, possibly, anisotropic materials. This model will be discussed briefly later.

The Campbell diagram for the propeller in the previous figures is presented in figure 8. Here, the fundamental exciting frequencies and harmonics for a four-cylinder, horizontally-opposed engine are superimposed on the natural frequencies of the first three normal modes. The predictions are based on the combined bending-bending model for the clamped hub. Observe that the natural frequencies increase with rpm due to centrifugal stiffening. Data points for zero rpm are included in the figure and agree fairly well with the predictions. In cruise, this particular propeller operates at around 2500 rpm. At this rotational speed, the fundamental exciting frequency of the engine and its harmonics do not coincide with any of the natural frequencies of the first three modes. It would not be well to operate this engine-propeller combination continuously at approximately 2200 rpm since the natural frequency of the first mode of the propeller, either clamped or free, coincides with the exciting frequency at this rotational speed.

#### STALL FLUTTER

In addition to responding to an unsteady inflow or engine torque, a propeller blade can experience the aeroelastic phenomena of stall flutter. This fact is not a new one, but is mentioned in the literature as early as 1941 (ref. 3). Unlike classical flutter which requires a combined bending and torsion motion together with a phase shift between the aerodynamic force and the angle of attack, stall flutter can occur as a pure bending or torsional oscillation. Because of negative damping provided by aerodynamic lift and moment beyond the stall, stall flutter can occur at much lower speeds than would be predicted for classical flutter. Figure 9 clearly illustrates the aerodynamic mechanism which can sustain stall flutter of a pure oscillatory nature (ref. 4). Three hysteresis loops for the moment coefficient are shown for a 0012 airfoil oscillating about mean angles of attack of 0, 12 and 24 degrees. For each loop the reduced frequency equals

.112 and the amplitude of  $\alpha$  equals 6 degrees. For  $\alpha = 0^\circ \pm 6^\circ$ , the airfoil is unstalled so that the closed integral of  $C_M$  over  $\alpha$  represents work which must be done by the system to sustain the oscillation. For  $\alpha = 24^\circ \pm 6^\circ$ , the airfoil is completely stalled so that, again, the area within the counter-clockwise closed hysteresis loop represents work which must be done by the system. For  $\alpha = 12^\circ \pm 6^\circ$  the situation is different. Here the area enclosed by the clockwise loop minus that enclosed by the counter-clockwise loop is positive as a result of the airfoil operating in and out of the stalled region. This net area represents work being done on the airfoil which represents negative damping; and hence, the possibility of a self-sustaining oscillation.

Some recent unpublished test data obtained at NASA LeRC with a model propeller are shown in figure 10. For a given blade angle, the section angles of attack increase as the advance ratio decreases. Thus, decreasing  $J$ , a value is reached below which a portion of the blade is stalled resulting in the inception of stall flutter as noted on the figure.

#### FUTURE STUDIES

A lumped parameter model of an elastic propeller blade is being developed as an alternate to the blade dynamics program described earlier. The lumped parameter model will allow one to calculate the dynamic response of the propeller to exciting forces and torques without determining the normal modes first. A simplified sketch to illustrate the model for the clamped hub case is shown in figure 11. Here the blade is divided into finite elements. The inboard end of each element is attached by three orthogonal equivalent springs to the adjacent element. The axes of two of these torsional springs lie along the principal axes of the blade sections. Their spring constants can be easily calculated knowing the section modulus of elasticity, moment of inertia and element length. Each element is also allowed to rotate along a locus through the shear centers of the sections. The third equivalent torsional spring in the radial direction at the shear center allows for this torsional motion.

If the mass center and elastic axis are not coincident, an acceleration transverse to the blade produces an inertial moment which tends to twist the blade. Also, the fact that the blade is twisted and tends to bend about the section major axis will produce a coupling between blade bending and torsion.

A program has been developed, based on modified vortex theory, which predicts the time-dependent blade loading given the velocity vector field in the propeller plane (ref. 5). In order to validate this program and to learn more about the details of the flow through a propeller, an experimental flight test program will be conducted to measure the unsteady velocities immediately behind a propeller for different flight conditions. Figure 12 illustrates a three-component, hot-film anemometer mounted on a transversing mechanism which is supported on a truss attached to the firewall. The probe is isolated from fuselage vibration by a soft mounting. The system is designed so that measurements can be taken around the azimuth at varying

radial locations and distances downstream of the propeller. The airplane to be used for this experiment is a Piper Cherokee 180 having a fixed-pitch propeller. For these tests the standard rear seat is replaced by a single seat on the left side with an instrument rack on the right side. The right front seat is removed and a battery pack put in its place.

In addition to the flow field measurements, it is planned to measure the unsteady bending moment distribution along the blade. Miniature strain gages will be bonded along the blade and the output transmitted across the hub by means of an FM multiplexing system.

#### CONCLUDING REMARKS

The subject of propeller blade dynamics promises to become more important in the future. Advanced turboprop designs incorporating thin, swept elastic blades, and operating in a non-uniform inflow environment, will require sophisticated analyses of their aeroelastic behavior. In addition to avoiding resonances at multiples of the propeller rotational speed, the designer may have to be concerned with the possibility of stall flutter.

#### REFERENCES

1. Jumper, S. J.: Computer Prediction of Three-Dimensional Potential Flowfields in which Aircraft Propellers Operate. M.S. Thesis, The Pennsylvania State University, February 1980.
2. Martinovic, Z. N.: A Study of the Dynamic Behavior of Propeller Blades. M.S. Thesis, The Pennsylvania State University, March 1979.
3. Bollay, William and Brown, C. D.: Some Experimental Results on Wing Flutter. Jour. Aero. Sci., vol. 8, no. 8, June 1941, pp. 313-318.
4. Carta, F. O. and Niebanck, C. F.: Prediction of Rotor Instability at High Forward Speeds, Volume III, Stall Flutter. USAAVLABS Tech. Report 68-18C, February 1969.
5. Aljabri, A. S.: Prediction of Propeller Performance and Loading in Uniform and Nonuniform Flowfields. M.S. Thesis, The Pennsylvania State University, November 1978.

# PROPELLER TURBOFAN COMPARISON

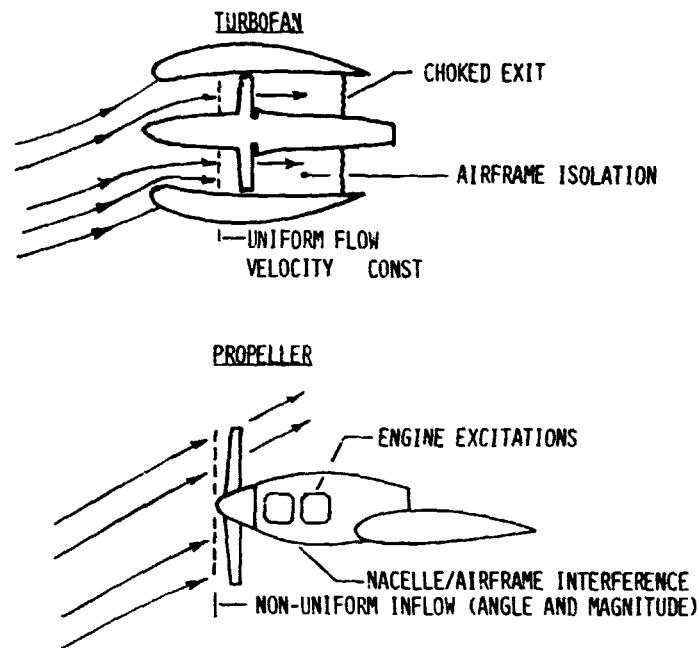


FIGURE 1

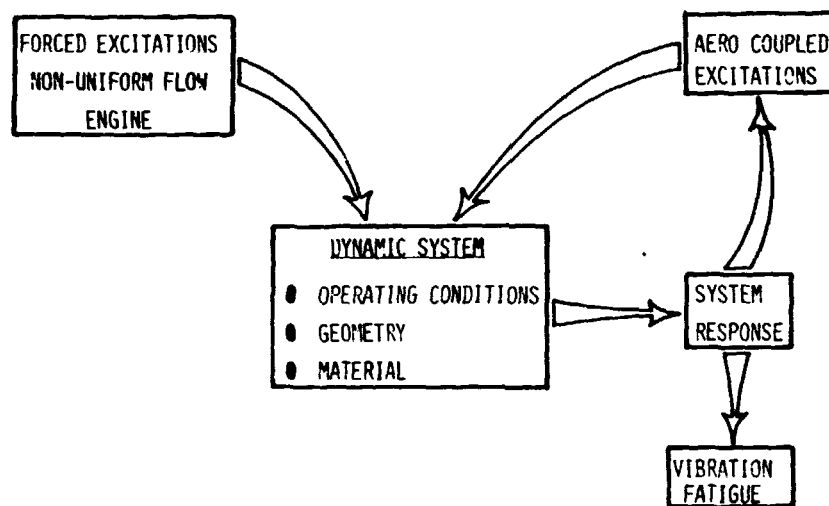
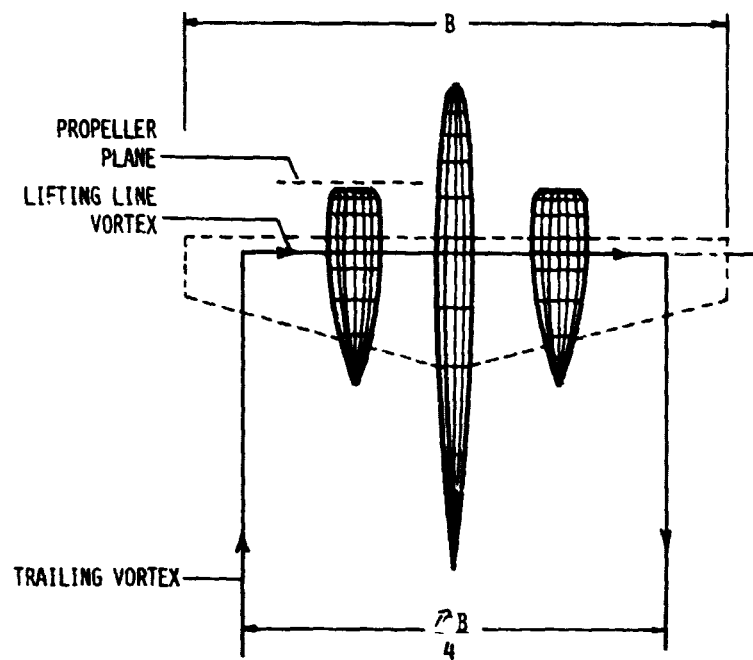


FIGURE 2





SIMPLIFIED WING-FUSELAGE-NACELLE NUMERICAL MODEL

FIGURE 3

PREDICTED AXIAL VELOCITY RATIO AT PROPELLER

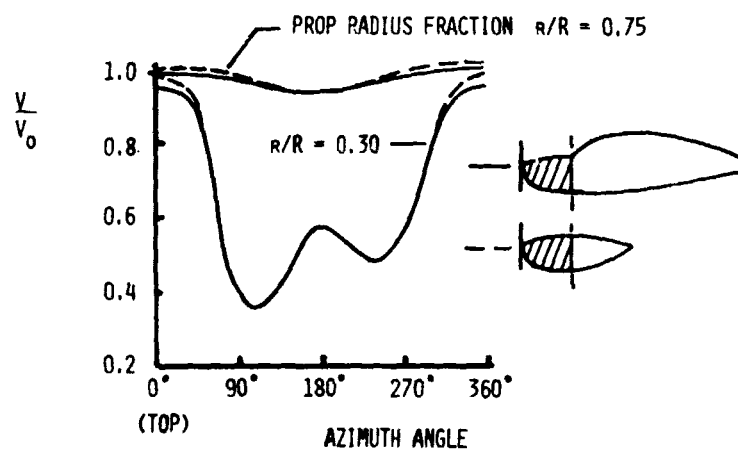


FIGURE 4

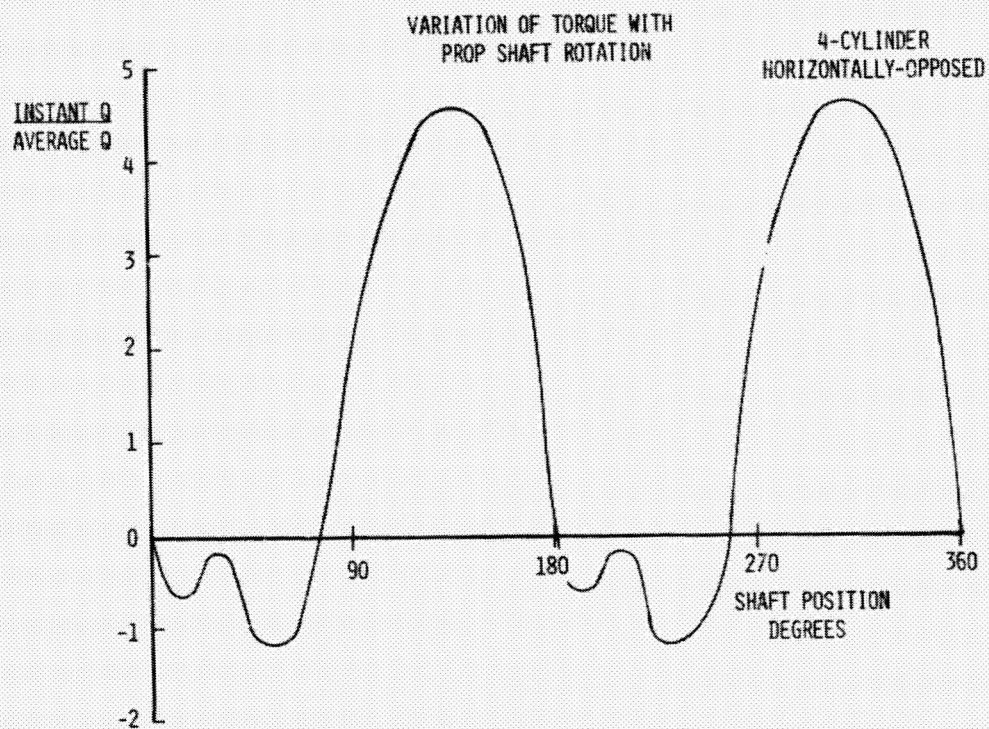


FIGURE 5

PROPELLER NATURAL FREQUENCY TEST  
HUB CLAMPED

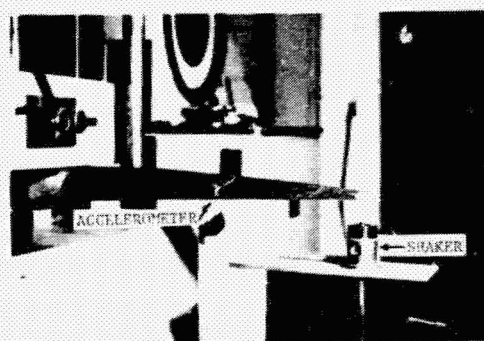


FIGURE 6

ORIGINAL PAGE IS  
OF POOR QUALITY

# PROPELLER NATURAL FREQUENCY TEST FREELY-SUPPORTED



FIGURE 7

## CAMPBELL DIAGRAM ENGINE EXCITATIONS AND PROP NATURAL FREQUENCIES

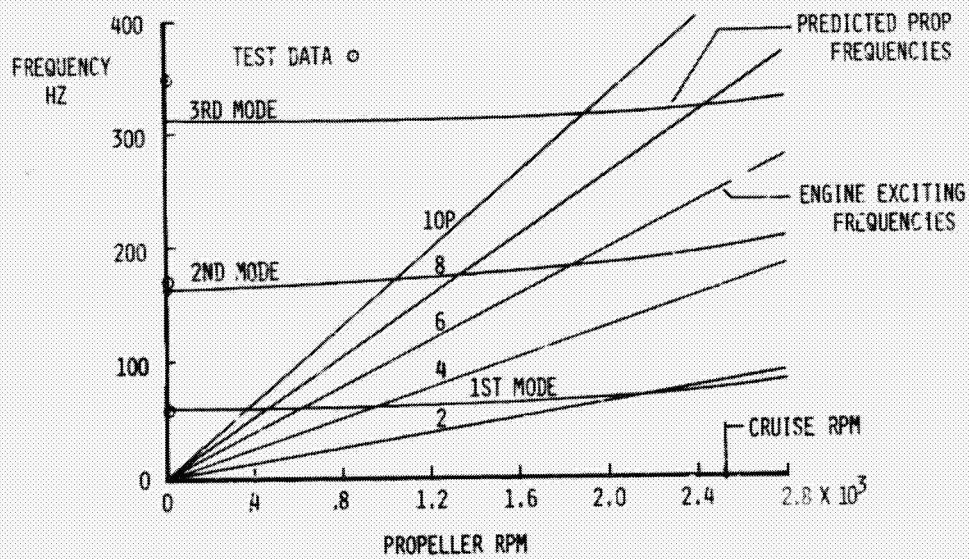


FIGURE 8

EFFECT OF MEAN INCIDENCE ANGLE  
ON MOMENT Hysteresis Loops  
(NACA 0012 AIRFOIL OSCILLATED  $\pm 6^\circ$ )

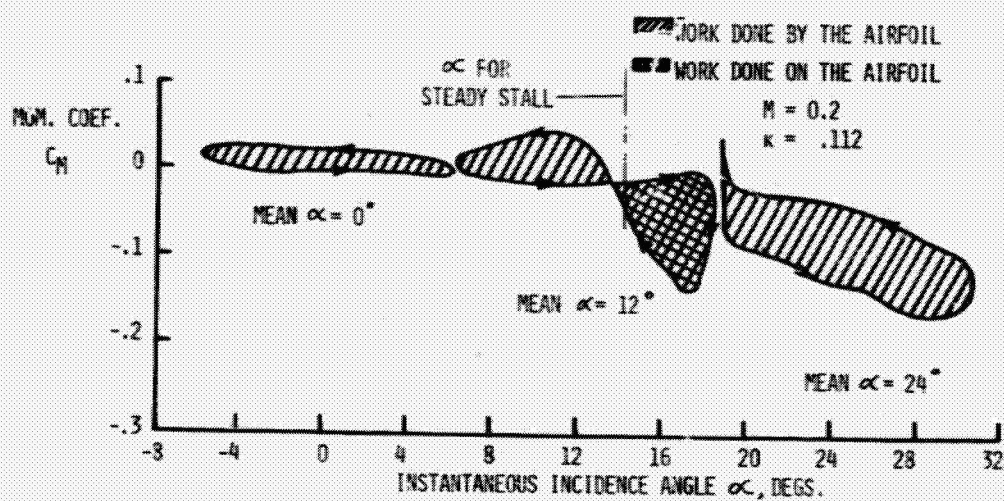


FIGURE 9

TYPICAL STALL FLUTTER CHARACTERISTICS  
 $M = 0.1$ , 3 BLADES

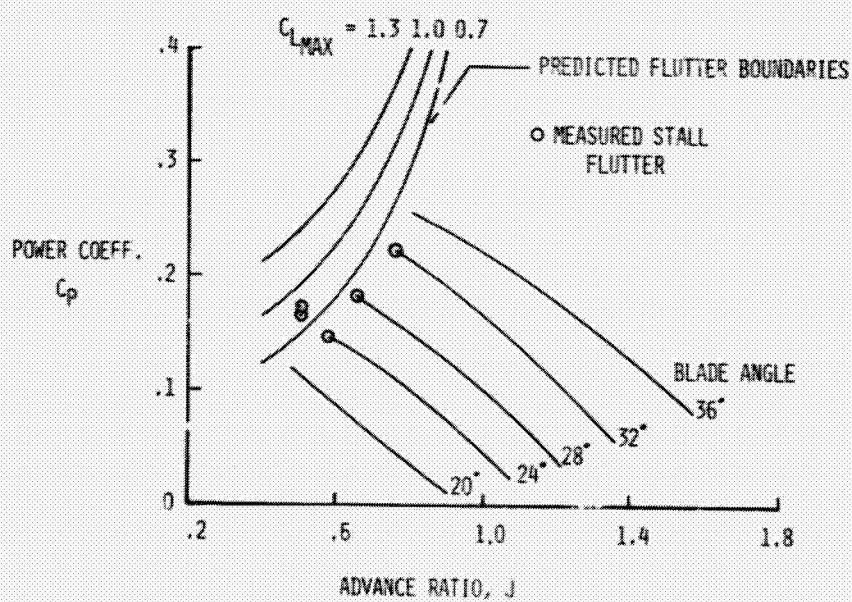


FIGURE 10

# LUMPED PARAMETER DYNAMIC MODEL

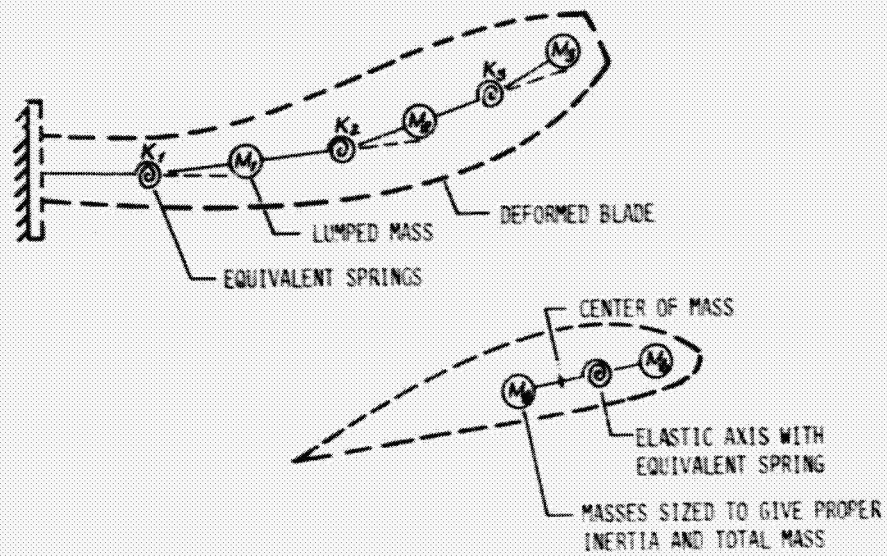


FIGURE 11. TORSION MODEL

## FLIGHT TEST APPARATUS FOR IN FLIGHT DETERMINATION OF 3 COMPONENT VELOCITY MEASUREMENT

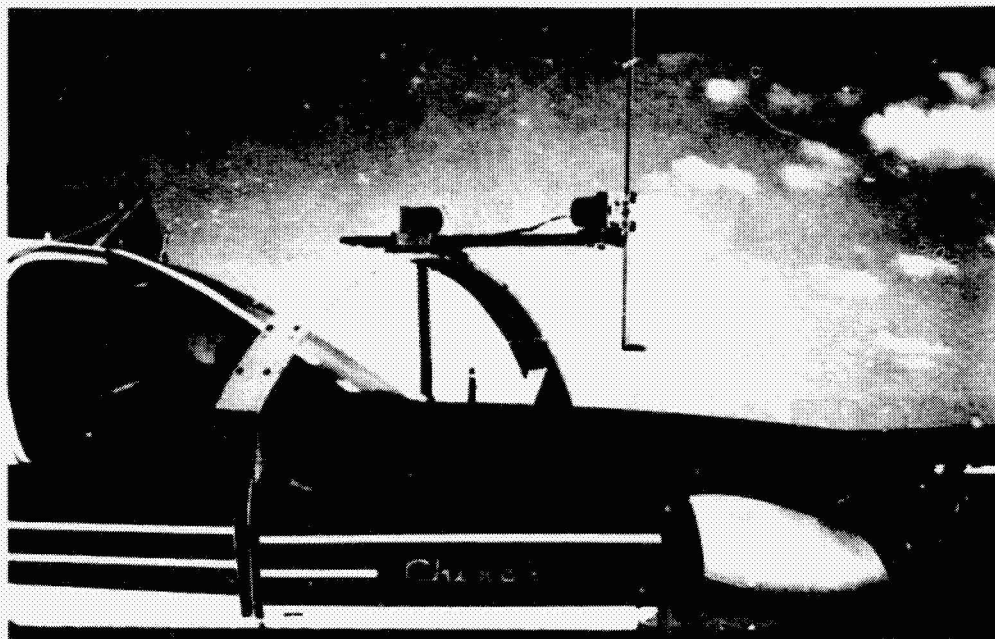


FIGURE 12.